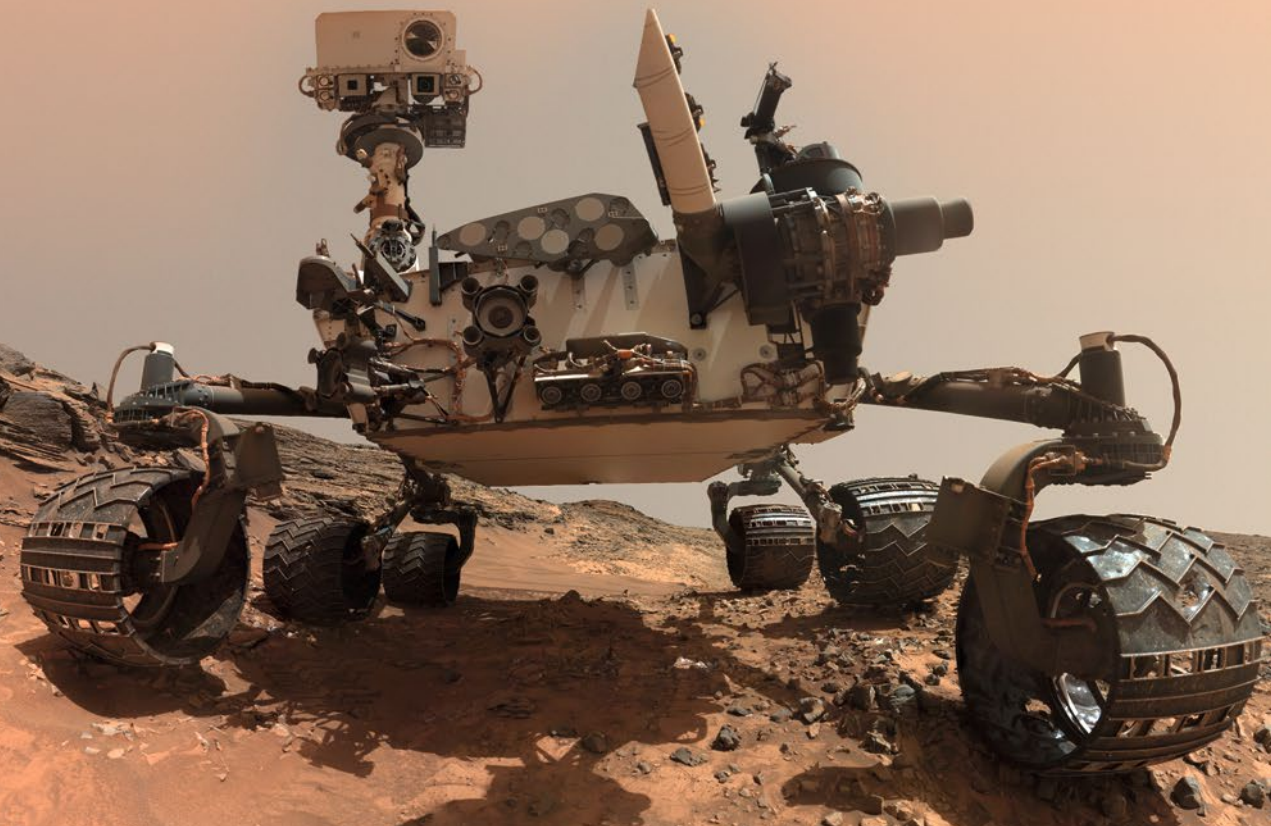


The Design and Engineering of **CURIOSITY**

How the Mars Rover Performs Its Job



Emily Lakdawalla

 Springer

PRAXIS

The Design and Engineering of Curiosity

How the Mars Rover Performs Its Job

Emily Lakdawalla

The Design and Engineering of Curiosity

How the Mars Rover Performs Its Job



Springer

Published in association with

Praxis Publishing

Chichester, UK



Emily Lakdawalla
The Planetary Society
Pasadena, CA, USA

SPRINGER-PRAXIS BOOKS IN SPACE EXPLORATION

Springer Praxis Books

ISBN 978-3-319-68144-3

ISBN 978-3-319-68146-7 (eBook)

<https://doi.org/10.1007/978-3-319-68146-7>

Library of Congress Control Number: 2017963344

© Springer International Publishing AG, part of Springer Nature 2018

This work is subject to copyright. All rights are reserved by the Publisher, whether the whole or part of the material is concerned, specifically the rights of translation, reprinting, reuse of illustrations, recitation, broadcasting, reproduction on microfilms or in any other physical way, and transmission or information storage and retrieval, electronic adaptation, computer software, or by similar or dissimilar methodology now known or hereafter developed.

The use of general descriptive names, registered names, trademarks, service marks, etc. in this publication does not imply, even in the absence of a specific statement, that such names are exempt from the relevant protective laws and regulations and therefore free for general use.

The publisher, the authors and the editors are safe to assume that the advice and information in this book are believed to be true and accurate at the date of publication. Neither the publisher nor the authors or the editors give a warranty, express or implied, with respect to the material contained herein or for any errors or omissions that may have been made. The publisher remains neutral with regard to jurisdictional claims in published maps and institutional affiliations.

Cover design: Jim Wilkie

Project Editor: David M. Harland

Printed on acid-free paper

This Springer imprint is published by the registered company Springer International Publishing AG part of Springer Nature.

The registered company address is: Gewerbestrasse 11, 6330 Cham, Switzerland

Contents

Dedication	viii
Foreword	ix
Acknowledgments	xi
Preface	xiii
1 Mars Science Laboratory	1
1.1 Introduction	1
1.2 Designing a Bigger Lander (2000–2003)	2
1.3 Becoming Mars Science Laboratory (2003–2004)	8
1.4 Preliminary Design (2005–2006)	16
1.5 The Cost of Complexity (2007–2008)	24
1.6 A Two-Year Respite (2009–2010)	39
1.7 Final Preparations (2010–2011)	42
1.8 References	54
2 Getting to Mars	57
2.1 Launch	57
2.2 Cruise	61
2.3 EDL: Entry, Descent, and Landing	66
2.4 Curiosity on Mars	101
2.5 Epilogue: Views of the Cruise Hardware	104
2.6 References	107
3 Mars Operations	110
3.1 Introduction	110
3.2 Mars' Calendar	110
3.3 Strategic, Supratactical, and Tactical Planning	114

3.4	Tactical Planning Process.....	115
3.5	Mission Summary	118
3.6	References.....	137
4	How the Rover Works.....	138
4.1	Introduction.....	138
4.2	Power System and MMRTG	138
4.3	Avionics	145
4.4	Thermal Control.....	148
4.5	Telecommunication.....	154
4.6	Mobility System.....	162
4.7	Testbeds.....	178
4.8	References.....	182
5	SA/SPaH: Sample Acquisition, Processing, and Handling.....	185
5.1	Introduction.....	185
5.2	Robotic Arm and Turret	185
5.3	The Drill.....	189
5.4	CHIMRA: Collection and Handling for In Situ Martian Rock Analysis	196
5.5	DRT: Dust Removal Tool.....	209
5.6	Organic Check Material	211
5.7	Sample Playground	213
5.8	Sam and CheMin Inlets and Wind Guards.....	217
5.9	References.....	220
6	The Mast, Engineering Cameras, Navigation, and Hazard Avoidance.....	221
6.1	Introduction.....	221
6.2	Remote Sensing Mast	221
6.3	Engineering Cameras: Navcams and Hazcams.....	224
6.4	Using the Engineering Cameras.....	227
6.5	Rover Driving.....	230
6.6	References.....	233
7	Curiosity's Science Cameras.....	234
7.1	Introduction.....	234
7.2	Mastcam.....	234
7.3	MARDI: Mars Descent Imager.....	252
7.4	MAHLI: Mars Hand Lens Imager	256
7.5	References.....	273
8	Curiosity's Environmental Sensing Instruments	275
8.1	Introduction.....	275
8.2	RAD: Radiation Assessment Detector	275
8.3	DAN: Dynamic Albedo of Neutrons	280
8.4	REMS: Rover Environmental Monitoring Station.....	285
8.5	References.....	292

9	Curiosity’s Chemistry Instruments	294
9.1	Introduction.....	294
9.2	ChemCam	294
9.3	APXS: Alpha Particle X-Ray Spectrometer	308
9.4	CheMin: Chemistry and Mineralogy	318
9.5	SAM: Sample Analysis at Mars.....	327
9.6	References.....	346
	Epilogue: Back on Earth	349
	Appendix: Curiosity Activity Summary	352
	About the Author	392
	Index	393

Dedication

For Anahita, who challenged me to be
“a writer who writes a *book*”

Foreword

On the night of August 5th, 2012, I was sitting in my room watching a video stream from JPL's Mission Control as the Curiosity rover descended toward Mars. As I watched, I sketched a comic about the Curiosity landing on my drawing tablet.

I've often anthropomorphized our space robots in my comics. In one sense, this is silly. A rover like Curiosity is a piece of hardware. It's a collection of motors, computers, and sensors. It can't think or feel. Maybe, someday, a robot will blur the line between "machine" and a "thing with feelings," but Curiosity isn't that. It's just a big, complicated car.

But in another sense, anthropomorphizing these robots feels natural. It's not that there's some magic in the circuits. It's that every single piece of hardware on Curiosity is the physical manifestation of years of planning by real people, sending it out to act on their behalf in the universe. The hardware carries with it our hopes and fears.

When Curiosity touched down on Mars, I felt so proud of our robot. I wasn't really proud of the mechanical actuators for actuating right. I was proud because I knew that each actuator, each spring, each wire, each sensor, and each line of code was lovingly crafted by someone. I knew all those people were watching along with me, all thinking, "I hope I did a good job." And they did!

While I was sitting in front of my computer that night, Emily was in the JPL press room. She had a front row seat to the action, and, through her Twitter feed, helped interpret what was going on for those of us at home.

Emily is a space enthusiast's space enthusiast and an incredible font of knowledge. A few years ago, I started wondering whether the photos taken by the new Juno spacecraft would be better than any of the ones from previous missions. After spending a few hours struggling to figure out how to compare the cameras on various spacecraft, I asked Emily for help. A moment later, she replied with an incredible spreadsheet she'd created listing every camera that had been sent into the outer solar system along with technical specifications for each. It was exactly what I was looking for. Later, when I decided to include a diagram of the Curiosity rover in one of my books, I made sure to run it by her first, to find out which parts I got wrong and which cool details I missed.



In this book, she describes how Curiosity works. She gives a window into the hopes, fears, and improbable what-if scenarios embedded in each technical decision. To tell the story, she draws on published papers, internal documents, photograph archives, and her own conversations with members of the Curiosity team over the course of the mission. For anyone curious about Curiosity – if you wonder “why was it lowered from a sky crane?” or “what’s that weird thing sticking off the side?” – then this is the book for you.

Randall Munroe
Author of *What If?*, *Thing Explainer*, and *xkcd*

Acknowledgments

This book would not exist without the generous assistance of numerous members of the Mars Science Laboratory team and the wider space science community. In particular, Ashwin Vasavada kept me updated in frequent telephone conversations, replied quickly to countless emails, and read every word of the first draft. Guy Webster and Veronica McGregor helped me access JPL and its scientists and engineers and steered the book through sometimes painful export-control review. John Grotzinger welcomed me into the mission's science team, and Jim Erickson trusted me to talk with engineers.

A huge number of people contributed to this book through interviews, email correspondence, and/or technical reviews of book sections, including Ryan Anderson, Ray Arvidson, Magdy Bareh, Paolo Bellutta, Mike Caplinger, Fred Calef, Allen Chen, Steven Collins, Nagin Cox, Joy Crisp, Mark Dahl, Lauren Edgar, Ken Edgett, Chad Edwards, Doug Ellison, Abigail Fraeman, Travis Gabriel, Matt Golombek, Javier Gomez-Elvira, Peter Grindrod, Cambria Hanson, Craig Hardgrove, Matt Heverly, Sarah Hörst, Louise Jandura, Jason Kastner, Stephen Kuhn, Danny Lam, Steve Lee, Mark Lemmon, Dan Limonadi, Maxim Litvak, Paul Mahaffy, Charles Malespin, Mike Malin, Rob Manning, Scott Maxwell, Sarah Milkovich, Andy Mishkin, Jeff Moersch, Glen Nagle, Keith Novak, Betina Pavri, the RAD team, Scot Rafkin, Rich Rainen, Elizabeth Rampe, Mike Ravine, Melissa Rice, Matt Robinson, Mariek Schmidt, Katie Stack, Dawn Sumner, Lucy Thompson, Vandi Verma, Noah Warner, David Woerner, Aileen Yingst, and Allison Zastrow. With such a long list I am sure I am missing some names. To those I have missed, please accept my apologies and gratitude for your help.

Thanks to Phil Stooke for generously sharing content of his own book in progress, particularly his frequently updated maps of the rover traverse. (The book, *International Atlas of Mars Exploration Volume 2*, complements this one.) Thanks to Mike Brown for helping me gain access to the Caltech library, which made remote research possible. Thanks to Tom Stein for supporting my use of the Analyst's Notebook and taking some of my suggestions on improving its user interface. Thanks to Ralph Lorenz for his valuable advice on book writing: "Write chaptesimalms, and eventually they will accrete into chapters."

xii Acknowledgments

The international community of space image processing enthusiasts at the online forum unmannedspaceflight.com contributed many of the beautiful mosaics you'll see in this book and helped me monitor ongoing rover activity. I want to single out Mike Howard and Joe Knapp for developing valuable software tools for browsing raw images (midnightplanets.com and curiosityrover.com); Thomas Appéré, Damia Bouic, Seán Doran, and James Sorenson for their exceptional image processing work; and Nick Previsich for singlehandedly administering the forum after I and the rest of the admins got too busy.

I'm deeply grateful to the members, staff, and board of The Planetary Society, represented by chief operating officer Jennifer Vaughn and chief executive officer Bill Nye, for their generous support of my time to perform the research and writing necessary to produce this book.

Thanks to the teachers and mentors who raised me, especially Ms. Foster, Mr. Killion, Ms. Hamilton, Dr. Aldridge, Mr. Atkison, Ms. Koeppe, Tekla Harms, Jack Cheney, Jim Head, Geoff Collins, Louise Prockter, Sasha Basilevsky, and Charlene Anderson. Finally, thanks to my husband Darius, my daughters Anahita and Sanaya, and my parents Karen Stewart, Rick and Murfy Stewart, and Rhoda and Noshir Lakdawalla for supporting my writerly ambitions – and to Concepción Peña for supporting me in supporting them, enabling this wife, mom, and daughter to be a writer, too.

Preface

The book you are holding is not quite the one I intended to write. I embarked on this project in 2013, with the working title *Curiosity on Mars - Design, Planning, and the First Mars Year of Operations*. I thought two years was a reasonable timeline, as I'd already done a lot of writing about the mission. I had been covering the Mars Science Laboratory mission as senior editor for The Planetary Society's blog since the mission's announcement, and attended most of the landing site selection meetings. Five times I had visited the gallery above the clean room where all the mission hardware came together at the Jet Propulsion Laboratory, and I returned to "the Lab" (as those in the know call it) for the landing and every press briefing. I've written three feature stories about it for *Sky and Telescope*. I'm an administrator of an online discussion forum full of armchair geologists and engineers who follow the daily motions of the rover, so I was cognizant of every twist and turn of the mission. It seemed possible that with steady work I should be able to write this book relatively rapidly.

It didn't turn out that way. I decided that understanding how the hardware worked was crucial to narrating the mission, because holey wheels, "Florida air," contaminated drill bits, and balky sampling mechanisms loomed large in the story of the rover's daily operations. I set to work researching rover engineering. The more I learned about Curiosity, the more rabbit holes I fell down. It had so many subsystems, and most had complicated histories, fascinating stories worth telling. Many of those stories hadn't been told in print, at least not in any document that the public can access. The publications that did describe Curiosity's engineering had mostly been written before launch, and contained inaccuracies that were corrected for me by helpful engineers. I came to understand that this machine was the most complicated thing ever sent beyond our planet and that no one person on Earth understands all of its parts and functions. I wrote and wrote about its design, its engineering, and its journey. Many mission engineers and scientists have contributed to making this text describe the actual spacecraft as accurately as possible.

Years passed. By 2015 Curiosity had traveled more than 10 kilometers across Mars and still the full depth of its scientific promise hadn't been realized. I changed my working title, dropping the "First Mars Year" bit, as the rover drove into its second Mars year and had only just reached the base of the mountain its science team hoped to study.

I asked my boss at The Planetary Society for permission to take a three-month sabbatical at the beginning of 2017 to finish up the project. It wasn't until the end of that sabbatical that I realized why I'd had so much trouble finishing the work. I hadn't written my book yet because I had, by now, nearly written two. I had to write a book about how the rover worked in order to be able to write the book I had intended to write about what it did on Mars. Fortunately, my editors at Springer-Praxis were amenable to splitting the project into two books. The one you're holding is the first of these: how and why the spacecraft was designed, the function of every system, and the engineering of every instrument. It's a reference work designed to answer your – and my! – questions about how the rover works and why it was built that way. It answers the same questions for all the other Mars Science Laboratory hardware, from cruise stage to Earth testbeds.

Of course, the mission has continued operating all this time, so parts of this book will be out of date immediately. It is certain to be complete as of sol 1514, and as complete as possible through sol 1800.

Now that I've written the reference book I needed, I can proceed with the second book, which will cover the mission's science, from landing site selection, through pre-landing mapping, the operational adventure, and the science results. Look for *Curiosity and Its Science Mission: A Mars Rover Goes to Work* in 2019.

1



Mars Science Laboratory

1.1 INTRODUCTION

Curiosity began in the wreckage of NASA's Mars hopes. Two spacecraft launched to Mars in 1998. Neither survived arrival. The twin disasters could have doomed NASA's Mars program – again. But the American public enthusiastically supported a NASA search for Martian life following the announcement of possible fossils in a Mars meteorite recovered from Antarctica.

NASA had enjoyed early success at Mars with the Mariners and Vikings, though the Viking landers' powerful (and expensive) life-detection experiments had failed to reveal signs of biologic activity on Mars. A lengthy hiatus in Mars exploration followed Viking in the 1980s, and the 1990s were mostly cruel to Mars missions. NASA's Mars Observer, launched in 1992, failed just days before arrival. Mars 96, a Russian mission, failed to leave Earth parking orbit. But things had been looking up at the end of the decade. Mars Global Surveyor successfully entered orbit in 1997 and began its mapping mission in 1999. And the world fell in love with a little six-wheeled robot named Sojourner that had trundled around NASA's Pathfinder lander for three months in the summer of 1997, sharing daily reports and Mars photos on the new medium of the Internet. The American public was willing to support another try at Mars.

A year after Mars Polar Lander and Mars Climate Orbiter failed, NASA announced a reformulated Mars program.¹ Their goal: to search Mars' geologic present and past for the kinds of environments that could support life. The search would require a “sustained presence in orbit around Mars and on the surface with long-duration exploration.” Joining Mars Global Surveyor in orbit would be two orbiters, 2001 Mars Odyssey (to be launched in 2001) and Mars Reconnaissance Orbiter (2005). NASA also announced two rover missions: the twin Mars Exploration Rovers (2003) and a “mobile science laboratory,” to be launched “as early as 2007,” which would eventually become Mars Science Laboratory, or MSL.

¹NASA (2000b) press release dated October 26, 2000

2 Mars Science Laboratory

From the start, MSL was an ambitious mission. It would deliver a Viking-sized suite of science instruments to the surface of Mars. But that huge science capability could move around the surface on wheels. NASA promised a precision landing, close to a very interesting geologic site on the surface of Mars. They also proposed a lifetime of two Earth years, much longer than the proposed one-month life for Pathfinder or three months for the Mars Exploration Rovers. Finally, the intent to carry analytical laboratory instruments that could ingest Martian rock required entirely new sample handling technology.

MSL occupies a pivotal position in NASA's Mars Exploration program. An advisory group stated in 2003 that MSL "both concludes the currently planned missions and... initiates the paths of exploration in the next decade." Mindful of the number of Mars missions that would be active in the years prior to its landing, NASA tasked the project with being able to respond to discoveries made while the spacecraft was being prepared for launch.² To be so flexible, the mission had to be able to achieve success at a wide variety of landing site locations: from equatorial sites to near-polar ones, and from sites where ancient geology and hard rocks would be the target, to sites where it might be possible to sample ice and search for recently habitable zones. This wide envelope of possibility meant that the spacecraft and landing system that were ultimately built had capabilities that were never used.

MSL would eventually become the most complex mission ever launched beyond Earth. Its development required a gargantuan effort spanning more than a decade. Its success depended on the invention of new technologies. Challenges in the development program forced NASA to delay the launch, at great financial cost. Originally proposed for the 2007 launch opportunity, MSL would finally depart for Mars in November, 2011.

1.2 DESIGNING A BIGGER LANDER (2000–2003)

1.2.1 "Rover on a Rope"

Chief engineer Rob Manning traces the origin of MSL's landing system to the terrible failures of 1999, particularly Mars Polar Lander. "We came to realize that we did not know how to land anything on Mars reliably, let alone something large," he wrote in a 2014 mission memoir.³ NASA's Jet Propulsion Laboratory (JPL), which had built Mars Polar Lander, formed a team to identify the technology they needed to develop in order to be able to precisely land a large rover on Mars. They began work in early 2000.

Mars is one of the hardest places in the solar system to land. The problem is its atmosphere: there is too much to ignore, and too little to slow a spacecraft for a safe landing. On bodies lacking atmospheres, like the Moon or an asteroid, spacecraft land using rockets alone. On Earth, Venus, or Titan, which have dense atmospheres, a spacecraft decelerates from supersonic speeds with a blunt-nosed heat shield, and then drops speed nearly to zero with a parachute. On Mars, a spacecraft needs all three: heat shield for high-speed

²Mars Program Synthesis Group (2003) Mars Exploration Strategy 2009-2020

³Manning and Simon (2014) *Mars Rover Curiosity*

entry, parachute for slowing during descent, and rockets for landing. The entire procedure required to land on Mars is referred to as Entry, Descent, and Landing, or “EDL” for short. (Engineers delight in abbreviating frequently-used phrases into acronyms and initialisms, turning their writing into alphabet soup. In this book I refrain from using most such abbreviations for clarity.)

All Mars landers to date have used a capsule, also known as an aeroshell, to shelter the lander during entry; the capsule is a clamshell that consists of a heat shield and a backshell. The design is similar to the capsules used by Mercury, Gemini, and Apollo astronauts to return to Earth. Astronauts in capsules usually used maneuvering rockets to guide the capsules during entry, steering them toward a landing zone where they could be picked up quickly. Mars landers, lacking human pilots, passively fell through the Martian atmosphere on a ballistic entry, like meteors. The lack of human guidance led to large uncertainty about where the spacecraft would end up landing. Achieving a precision landing required guidance, but Mars is too far away for humans on Earth to steer in real time.

To make a precision landing possible, Manning and his teammates advanced an idea that JPL had been developing since the 1990s: autonomous guidance for a Mars entry vehicle. The capsule could use accelerometers and gyroscopes to determine its position relative to its intended target as it flew. Software would command banking turns to fly the aeroshell closer to the target. Guided entry could dramatically shrink the size of a Mars landing ellipse, placing a rover closer to interesting geology.

The descent phase begins when the spacecraft has been slowed to something close to twice the speed of sound. All Mars landers have deployed a parachute for descent. Supersonic parachutes for Mars were first developed in the early 1970s for Viking, with expensive high-altitude tests. As long as the mass of a Mars lander could be kept similar to or less than that of Viking, they could stick with the same parachute design for the descent phase without performing new, expensive tests.

For the final, landing phase, JPL had successfully used two different approaches. The Vikings employed retrorockets that slowed the descent to a near-standstill, and then the spacecraft dropped to a hard landing atop three legs that crushed to absorb some of the force of the impact. Pathfinder (and, later, the Mars Exploration Rovers) worked differently (Figure 1.1). The triangular lander was folded into a tetrahedral shape and the outside of the tetrahedron fitted with airbags. This contraption dangled on a rope beneath a rocket pack that was itself connected to the parachute. At the last possible moment, a mere 100 meters above the ground, the airbags inflated, the rocket jetpack fired to zero out the downward velocity, and the rope tether cut. The lander dropped and bounced repeatedly, rolling nearly a kilometer inside its airbags, before finally coming to a rest.

Neither lander design would work for MSL. If the rover were perched atop a Viking-like lander platform, the top-heavy design would tip over in a wide variety of landing scenarios. But Pathfinder’s airbag design had a maximum payload capacity of 200 kilograms; anything larger, and the airbags would shred.⁴ Manning thought that elements of the two could be combined into a successful landing strategy. If a Viking-like descent stage could dangle a Pathfinder-like lander on a tether, the descent stage might be able to

⁴Caffrey et al (2004)

4 Mars Science Laboratory

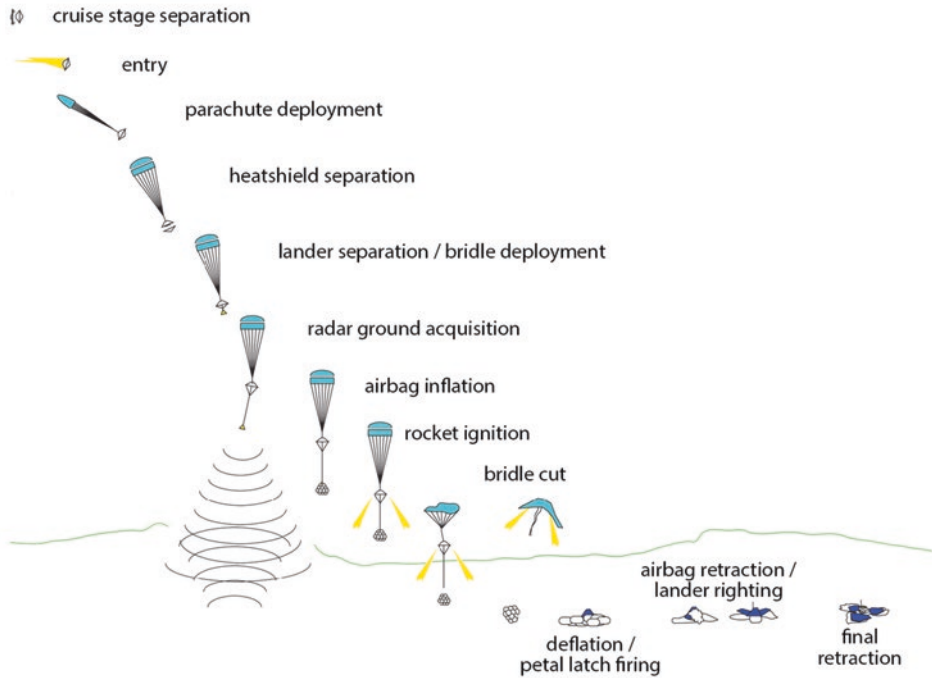


Figure 1.1. Illustration of the successful Mars Pathfinder entry, descent, and landing. Based on Golombek et al (1999).

lower the lander close enough to the ground to enable it to make a soft touchdown.⁵ In fact, they might be able to make the landing so soft that they could put a rover down directly on its wheels.⁶ Manning called this idea the “rover on a rope.” The concept became Mars Smart Lander in late 2000, when NASA announced it as part of the reformulated Mars program, with a launch “as early as 2007.”⁷

As the reformulation proceeded, Mars Global Surveyor generated a bounty of science results. Its spectrometer instrument discovered gray hematite on the surface, a mineral that probably required liquid water to form. The spectrometer also mapped dust on the surface, allowing mission planners to seek out less-dusty landing sites with good access to bed-rock. Its sharp-eyed camera proved that sedimentary rocks existed on Mars, a second line of evidence to a lengthy water-rich geologic history. And the mission generated a dramatically improved global topographic map of Mars, crucial for planning safe landings.

⁵Manning and Simon (2014)

⁶Rob Manning credits Dara Sabahi with that realization

⁷NASA (2000a) Mars Program Independent Assessment Team Summary Report

1.2.2 Mars Smart Lander

NASA chartered a Science Definition Team for the planned 2007 rover in April, 2001.⁸ The charter identified three ways in which the Mars Smart Lander concept would improve on past landers' ability to explore interesting scientific sites. Most of them related to landing precision, specified in the dimensions of a "landing ellipse."

What is a landing ellipse? Mars missions target a specific latitude and longitude spot on Mars, but a variety of factors can cause the lander to miss the target. By modeling these factors, engineers can estimate the area within which the rover is about 99% likely to land. The region is usually shaped like an ellipse with its long axis oriented in the direction of the incoming lander's trajectory.

Landing ellipses for Viking were 280 kilometers long and 100 kilometers across. Pathfinder's was smaller, but not by much, at 200-by-100 kilometers. Large landing ellipses drastically limited the locations on Mars where spacecraft could land, because there are few locations that are flat enough over such a broad area, and even fewer that are geologically interesting.

For Mars Smart Lander, the landing ellipse would be dramatically smaller: the initial directive was for an ellipse only 6-by-3 kilometers in extent, achieved using entry guidance to steer the entry capsule along its intended path. The charter also stipulated a lander with "active terminal hazard avoidance," meaning that it should be capable of detecting large rocks or steep slopes and steering around them. Finally, the rover would have "surface mobility commensurate with landing precision errors." In other words, if the landing ellipse was 6 kilometers in extent, then the vehicle should be able to drive at least 6 kilometers in its lifetime.

It's that last requirement – a roving range of the same size as the landing ellipse – that opened up the possibilities for exciting science on the proposed rover mission. The mission would not be limited to scientific exploration of sites that were also safe for landing. They could plan to explore a site with steep topography, as long as there was a safe landing zone sufficiently close by. They called these "go-to" sites, because the rover would land away from the intended scientific goal, and then go to the site before starting its scientific investigation.

NASA directed the Mars Smart Lander science definition team to set science goals consistent with the highest priorities of the Mars Exploration Payload Analysis Group, an advisory panel of Mars scientists. The number one goal of the Mars Exploration Payload Analysis Group was the search for present and past life on Mars, so the team debated whether the mission should attempt to search for extant life on Mars.

In the end, the Science Definition Team argued against Viking-like attempts at direct life detection experiments. Emboldened by the recent discovery of widespread layered sedimentary rocks across Mars by the Mars Global Surveyor camera team,⁹ they suggested an oblique approach that avoided the challenge of defining what life on Mars is expected to look like:

The most promising place to explore for evidence of life on Mars is in lacustrine or marine sedimentary rocks that accumulated rapidly under reducing conditions and where subsequent diagenesis did not obliterate the original textural and compositional

⁸NASA (2001) Mars Exploration Program Mars 2007 Smart Lander Mission Science Definition Team Report

⁹Malin and Edgett (2000)

6 Mars Science Laboratory

(isotopic, organic, and mineralogic) evidence for the environment of deposition and associated biomes...[The] strategy for searching for evidence of life on Mars is to maximize the probability of landing on sedimentary deposits in which reducing conditions have been preserved, to use mobility to explore and characterize the deposits...

Direct life detection experiments are not needed to implement this strategy for the Smart Lander Mission. Rather, positive signs of biosignatures would be used to help focus locations for sample return missions and/or follow-on missions with direct life detection experiments.¹⁰

Through all of the twists and turns of the development of the mission that followed, this strategy would remain constant. The strategy has two parts: first, search for habitable environments, places where life could thrive (now or in the past). Second, seek out rocks that have a high potential to preserve carbon-containing materials trapped within them.

The Science Definition Team responded to the charter in October 2001. Mars Smart Lander would take one of two forms. It would either be a Mobile Geobiology Explorer – a large rover that could carry a heavy instrument package beyond the confines of its landing ellipse – or a Multidisciplinary Platform with a deep drill and a small rover that could explore the site and return samples to the stationary lander.

As initially conceived, the Mobile Geobiology Explorer would carry a 100-kilogram science payload, powered either by solar panels or a radioisotope power supply, although the team argued strenuously for the latter. They suggested that in a 180-sol¹¹ primary mission, the rover should be able to traverse at least 5 kilometers and preferably 9 kilometers, to perform in-situ science at 3 locations, sampling multiple geologic units. (In hindsight, this list is comically optimistic.) The team proposed a payload consisting of up to 14 different science instruments:

- A descent imaging system.
- A mast-based remote sensing system including color cameras, infrared spectrometer, and a laser-induced breakdown spectrometer.
- Ground-penetrating radar.
- Arm-based contact science package with rock abrasion tool, elemental and mineralogical analyzers, and microscope.
- Long-duration radiation experiments (relevant to future human exploration).
- Drill/corer and sample acquisition system.
- Sample preparation and delivery system (for grinding and partitioning sample cores).
- Laboratory instruments to determine inorganic and organic chemistry, oxidation state, mineralogy, and high-resolution images of samples.
- If possible: seismology package.
- If possible: climatology package.

¹⁰NASA (2001)

¹¹A “sol” is a Martian day, about 3% longer than an Earth day

Meanwhile, JPL was in the throes of preparing the Mars Exploration Rovers for launch. To cope with the ever-increasing mass of the twin rovers, JPL added throttleable rockets to their backshells, and cameras that would take one or two pairs of images and analyze them to detect the horizontal velocity of the lander. Both of these innovations made the “rover-on-a-rope” idea more feasible.¹²

Even though it was still on the drawing board, Mars Smart Lander rapidly ran into budget problems. “The Science Definition Team had defined a mission larger than NASA could afford,” recalls Mark Dahl, who was NASA Program Executive for the mission from 2002 until 2007. In order to fit this large rover into NASA’s budget, they would need to postpone it to a 2009 launch. The mission also drifted toward a name change. When Scott Hubbard developed NASA’s “follow the water” policy in 2002, he referred to the mission in different places as Mars Smart Lander; Mobile Surface Laboratory; and Smart Mobile Lab. Eventually, NASA decided that the name of the mission should describe its goals rather than its technology, and by 2003 it was being called Mars Science Laboratory. (Conveniently, its initials, MSL, remained the same through the name change.)

1.2.3 Nuclear power

In 2002, NASA determined that MSL would be able to do better science, accessing a wider band of latitudes and surviving longer, if it were nuclear-powered. That required a radioisotope thermoelectric generator (RTG), like the ones that powered Voyager, Viking, and more recently, Galileo and Cassini. A nuclear-powered rover would have lots of advantages over the solar-powered Spirit and Opportunity. It would be able to explore a much wider range of latitudes, and it would be able to operate year-round, rather than resting through the winter. However, the nuclear power design available in 2002 – the General Purpose Heat Source RTG used for Galileo, Ulysses, Cassini, and New Horizons – was not suitable for a Mars rover. It was too massive (more than a meter long and weighing 57 kilograms). It produced more power than needed (285 watts). Most importantly, its electricity-generating thermocouples would fail if carbon dioxide from Mars’ atmosphere were to infiltrate its container.

Anticipating these problems, the Department of Energy and NASA were already in discussions to develop a new type of radioisotope power supply that would be appropriately sized for the lower mass and power of modern spacecraft, one that could also function in an atmosphere. The Department of Energy considered several designs and determined to develop two. One was the Multi-Mission Radioisotope Thermoelectric Generator (MMRTG), whose design would be based upon the RTG used on Viking lander and Pioneer missions. It would require 4.8 kilograms of plutonium dioxide fuel. The other proposed power source was a Stirling generator requiring only 1.2 kilograms of fuel. Either would deliver about 100 watts of power when first fueled. An MMRTG would throw off about 2000 watts of heat; the more efficient Stirling generator would produce about 500 watts.

¹²Manning and Simon (2014)

8 Mars Science Laboratory

NASA considered both options for MSL. They chose the MMRTG because of concern over the reliability of the Stirling generator's moving parts. Also, the relatively inefficient design of the MMRTG would benefit Mars surface operations: the waste heat could be collected and put to use to maintain the temperature of the rover against the extreme swings of the Martian environment. On June 30, 2003, Boeing Rocketdyne Propulsion and Teledyne Energy Systems announced their partnership with the Department of Energy to develop the new MMRTG, specifically naming MSL as the first mission that would use the new technology. "An MMRTG-powered rover will be able to land and go anywhere on the surface of Mars, from the polar caps to deep, dark canyons, and will safely provide full power during night and day under all types of environmental conditions," Boeing stated in a press release.

The decision to use a nuclear power supply for MSL was not yet official. It couldn't be finalized until NASA and the Department of Energy went through a process required by the National Environmental Policy Act to document the potentially harmful environmental impacts of developing the nuclear power supply, including environmental effects of a potential launch disaster. NASA dutifully analyzed both nuclear and solar options as part of the environmental documentation process. They found that MSL could accomplish its full science objectives as a solar-powered mission only at a latitude of 15° north of Mars' equator; but it could achieve minimum science objectives between 5° south and 20° north. Also, without the waste heat provided by the MMRTG, the rover would need numerous additional radioisotope heater units to maintain the rover's temperature, offsetting the environmental benefit of avoiding a launch accident with an MMRTG.

On December 27, 2006, NASA finally issued a formal Record of Decision that the mission would use nuclear power. In internal documents, however, the mission never spent much effort developing solar power as an option, because the limitations of solar power would render it far less feasible.

1.3 BECOMING MARS SCIENCE LABORATORY (2003–2004)

1.3.1 Defining the science objectives

NASA chartered a Project Science Integration Group, headed by Mars scientists Dan McCleese and Jack Farmer, to further develop possible mission scenarios for the 2009 mission. They set about defining objectives and capabilities for the mission, while keeping its development cost (that is, the cost of designing and building the rover, but not including launch, operations, or nuclear power system) under \$1 billion.

The Project Science Integration Group had a lot of new science to integrate into the mission plans. Mars Global Surveyor continued its productive mission, while 2001 Mars Odyssey arrived at Mars in February 2002. Almost immediately, its neutron spectrometer revealed that vast regions of Mars held near-surface ground ice, hidden under only centimeters of soil.¹³ Present-day ground ice led to speculation that there could be extant life surviving beneath the surface in underground aquifers.

The Project Science Integration Group advocated a mission focus on the habitability of ancient (not recent) Mars. Their proposed science objective: "Explore and quantitatively assess

¹³Boynton et al (2002)

a potential habitat on Mars.” To accomplish that objective, they proposed three scientific investigations, listed in Box 1.1. The group held open the possibility of the sampling system being used on icy targets at high latitudes in order to study a recently habitable zone on Mars. That meant the ability to access, drive on, drill into, and examine ice. It would require a landing site at a very high latitude (poleward of 60°) and a sample handling system that could handle ice without melting it, except where melting was wanted. Such a spacecraft would have to be stringently sterilized to prevent contamination of the Mars environment with Earth microbes, imposing substantial costs and complexity on the mission.

Box 1.1. Mars Science Laboratory scientific investigations.

- Assess the biological potential of at least one target environment (past or present).
 - Determine the nature and inventory of organic carbon compounds.
 - Inventory the chemical building blocks of life (C, H, N, O, P, S).
 - Identify features that may record the actions of biologically relevant processes.
- Characterize the geology of the landing region at all appropriate spatial scales.
 - Investigate the chemical, isotopic, and mineralogical composition of Martian surface and near-surface geological materials.
 - Interpret the processes that have formed and modified rocks and regolith.
- Investigate planetary processes that influence habitability.
 - Assess long-timescale (i.e., 4-billion-year) atmospheric evolution processes.
 - Determine present state, distribution, and cycling of water and carbon dioxide.

For cost and complexity reasons, the Project Science Integration Group questioned the need for “go-to” capability. Designing and verifying a system that would be capable of driving tens of kilometers would be very expensive, blowing the billion-dollar mission development cap. Also, the beginning of a go-to mission – land, and then spend months driving – would be boring. As a result of these discussions, the requirement of go-to capability went away, and so did the related verification and validation requirements for long-distance driving.

The group issued their report in June 2003, allowing a cooling-off period after the work ended so that scientists who had participated in the Group could propose instruments to the mission without a conflict of interest. In the meantime, JPL produced and released the first concept artwork of Mars Science Laboratory (Figure 1.2). It showed no instruments and appeared like a scaled-up Mars Exploration Rover, with two robotic arms and a high-gain antenna nearly a meter in diameter for direct-to-Earth communications.



Figure 1.2. Concept art for MSL, late 2003. NASA/JPL-Caltech release PIA04892.

1.3.2 The mission concept matures

Three spacecraft successfully reached Mars in January 2004: ESA's Mars Express Orbiter, and NASA's two Mars Exploration Rovers, Spirit and Opportunity. Opportunity landed within easy reach of a scientific bonanza: inside a crater, facing an obviously layered bedrock exposed in the crater's wall. A month later, the mission held a press briefing to announce that "Scientists have concluded the part of Mars that NASA's Opportunity rover is exploring was soaking wet in the past." Their mission to "follow the water" had succeeded in finding evidence for a different, wetter environment on an ancient Mars. MSL would be able to take the next step.

Mars Exploration Rover project manager Peter Theisinger shifted to the MSL project. One of his first actions was to convene an informal panel of outsiders to evaluate the proposed rover-on-a-rope design for MSL's landing. One member of the panel was a Sikorsky helicopter pilot, who "pointed out that experienced heavy-lift helicopter pilots can control both the speed and the position of their suspended loads with exquisite precision. This was a man who had extensive experience in one of the early heavy-lift helicopters, the Sikorsky sky crane," Manning wrote. From that day forward, the landing approach was often referred to as the "sky crane maneuver."

Many development challenges remained, but the mission's basic plan was fixed, and the project was ready to solicit proposals for science instruments. For flagship missions, NASA issues an Announcement of Opportunity detailing the goals of a mission, providing budget and timeline information, and seeking proposals for teams of scientists and engineers from all over the world to develop science instruments tailored to the planned spacecraft and its goals. NASA issued the MSL Announcement of Opportunity in April 2004, with proposals due in July.

To support the Announcement of Opportunity, JPL described MSL in detail for the first time in the form of a Proposal Information Package issued on April 14, 2004. To begin

with, the information package described a slightly modified primary objective for the rover mission (Box 1.2). It also detailed the design of the spacecraft components to be built at JPL (Box 1.3 and Figure 1.3), and specified the mechanisms, avionics, power, temperature conditions, and other aspects of the proposed rover design that would be available to support the instruments.

Box 1.2. Primary objective of the MSL mission.

The Mars Science Laboratory Mission will explore and quantitatively assess the habitability and environmental history of a local region on Mars. The mission has the primary objective of placing a mobile science laboratory on the surface of Mars to assess the biological potential of the landing site, characterize the geology of the landing region, investigate planetary processes that influence habitability, and characterize the broad spectrum of surface radiation. The MSL project aims to achieve this objective in a manner that will offer the excitement and wonder of space exploration to the public.

Box 1.3. Components of the MSL flight system.

- A **cruise stage** to provide power, navigational capability, and thermal control to the spacecraft for the trip from Earth to Mars.
- An **aeroshell** consisting of a heat shield and backshell with a parachute to protect the rover during its initial entry and descent in the Martian atmosphere. The aeroshell would also have the necessary hardware to provide communications during cruise, entry, and descent. The aeroshell would be able to maneuver in the air in order to reduce landing location errors caused by uncertainty in atmospheric conditions.
- A **descent stage** that would decelerate with rockets while scanning the landing area with radar, allowing the rover to generate a terrain map and identify a safe landing site. The descent stage would come to a hovering stop 5 meters above the landing site, then lower the rover on a tether to rest on its wheels. Once the rover was at rest, it would cut the tether to the descent stage, and fly away.
- A **rover** that would be capable of a mission lasting one Mars year (670 sols), driving 50 meters per sol at 5–10 centimeters per second on typical sols, with a total mission traverse capability of at least 6 kilometers. It would carry a 58-kilogram science payload, of which about 3 kg would be on an instrument arm, 9 kg on the mast, and 38 kg inside the rover. To accommodate this large payload, the rover's body would be 1.2 meters long by 0.7 meters wide by 0.35 meters deep.
- Landing accuracy would be within a 5-by-10-kilometer ellipse.
- Two instruments were already included: a meteorology package contributed by Spain, and an active neutron spectrometer contributed by Russia.

12 Mars Science Laboratory

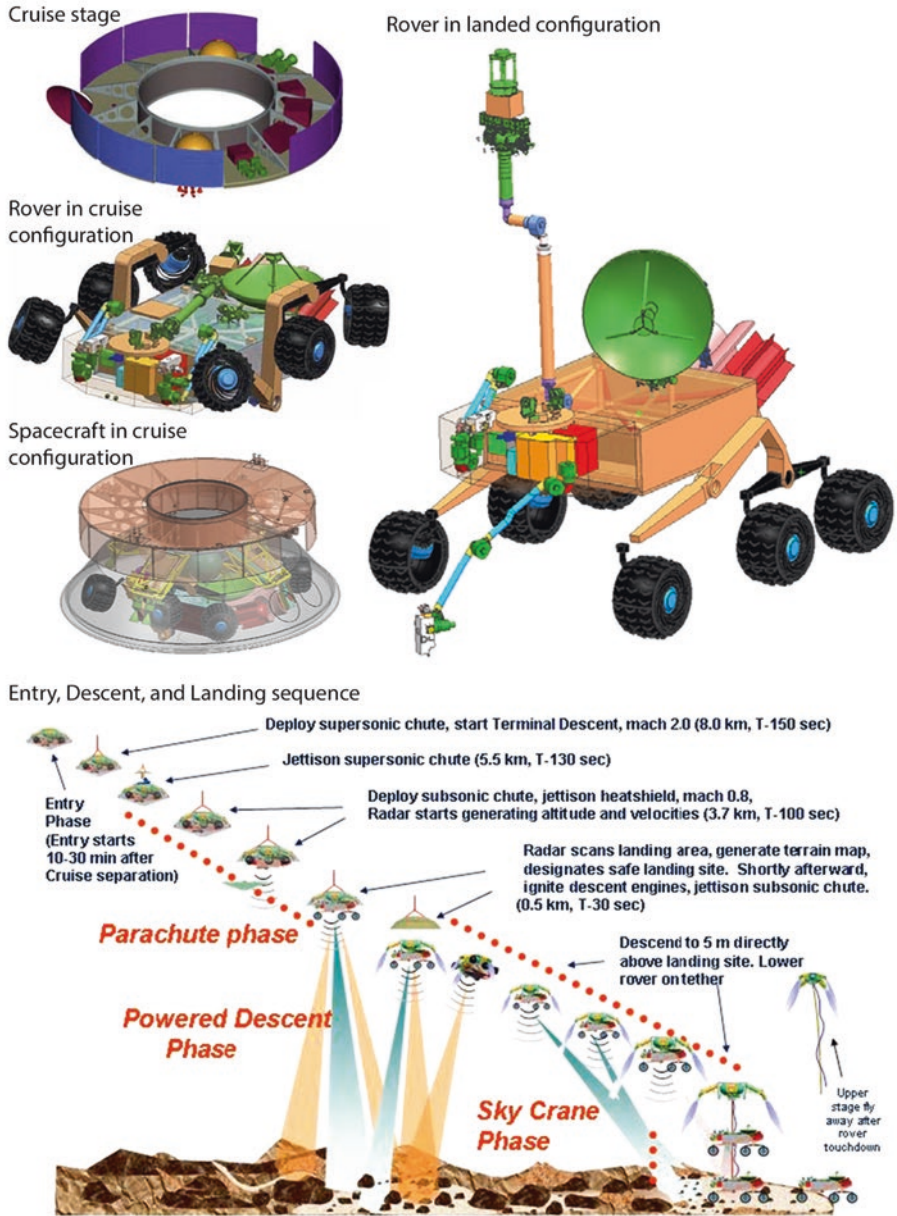


Figure 1.3. Initial design for MSL from the Proposal Information Package. Note the two arms, two RTGs, huge dish, and tall mast mounted at the center of the front of the rover. The landing sequence is substantially similar to Pathfinder's (Figure 1.1).

The design drawn in the 2004 Proposal Information Package was far from final. In actuality, the spacecraft design was in a state of extreme flux, with the mission being torn between reliability, capability, and expense.¹⁴ The 2004 rover concept differed from the final one in a number of ways. The originally planned mast was quite tall, reaching to 3.5 meters from the ground. It had a huge dish for direct-to-Earth data relay, as *Odyssey* wouldn't have the capacity to relay all of MSL's hoped-for data volume, even if the orbiter survived until the 2010 landing.

The Sample Acquisition/Sample Processing and Handling (SA/SPaH) system on the original rover design included two robotic arms, separating the heavy, rattling, dust-raising activities of drilling and retrieving rock cores and the finer tasks of scientific analysis and soil scooping onto separate arms. Both arms could deliver material to a sample processing system mounted directly to the rover body. The sample processing system would have two rock crushers to smash and sieve the rock samples into pieces smaller than a millimeter in diameter. A sample delivery system would move these samples into the analytical laboratory instruments, and an ejection system would get rid of detritus. Both arms could acquire samples in icy material, though the rock crusher would not be expected to handle ice. If the corer failed, the scoop would presumably still be available to gather loose rock samples and deliver them to the crusher.

But the biggest difference between proposed and final rovers was power. As originally planned, MSL would carry two Radioisotope Thermoelectric Generators to provide ample power and heat for operation at a wide range of latitudes.

1.3.3 Instrument selection

Teams of scientists and engineers responded to the Announcement of Opportunity by proposing 48 instruments to NASA. NASA turned around the proposals quickly, selecting eight (Box 1.4). Adding the already-accepted Russian and Spanish instruments brought the MSL mission payload to a total of ten. Some, the remote sensing instruments, would study the landscape from a distance, mostly from the top of the remote sensing mast. Others, the in situ instruments, would study rocks and soil from a turret at the end of the robotic arm, or measure the environment that the rover experienced. Finally, there were two analytical laboratory instruments buried within the body of the rover that would accept samples of rock, soil, and atmospheric gas for detailed study.

This was a huge and exciting instrument package. Some of the instruments looked familiar. Mastcam, MAHLI, and APXS all had direct parallels on the Mars Exploration Rovers (Pancam, Microscopic Imager, and APXS), but in each case the proposed MSL instrument had major improvements. Mastcam promised the possibility of color, stereo, high-definition video of rover traverses across Mars. APXS would have higher spatial resolution and speedier data acquisition than ever before.

The novel instruments were just as exciting. ChemCam would provide remote elemental analysis capability unlike anything seen on a Mars mission before, and would do it with

¹⁴Manning and Simon (2014)

Box 1.4. Mars Science Laboratory Instruments, as described in the 14 December 2004 press release announcing them.

Remote Sensing Instruments:

Mars Descent Imager (MARDI), located on the body of the rover. Principal investigator: Michael Malin, Malin Space Science Systems. The Mars Descent Imager will produce high-resolution color-video imagery of the MSL descent and landing phase, providing geological context information, as well as allowing for precise landing-site determination.

Mast Camera (Mastcam), located on the mast. Principal investigator: Michael Malin, Malin Space Science Systems. Mast Camera will perform multi-spectral, stereo imaging at lengths ranging from kilometers to centimeters, and can acquire compressed high-definition video at 10 frames per second without the use of the rover computer.

ChemCam: Laser Induced Remote Sensing for Chemistry and Micro-Imaging, located on the mast. Principal investigator: Roger Wiens, Los Alamos National Laboratory. ChemCam will ablate surface coatings from materials at standoff distances of up to 10 meters and measure elemental composition of underlying rocks and soils.

In-situ Instruments:

Mars Hand Lens Imager (MAHLI), located on the arm turret. Principal investigator: Kenneth Edgett, Malin Space Science Systems. MAHLI will image rocks, soil, frost and ice at resolutions 2.4 times better, and with a wider field of view, than the Microscopic Imager on the Mars Exploration Rovers.

Alpha Particle X-ray Spectrometer (APXS), located on the arm turret. Principal investigator: Ralf Gellert, Max-Planck-Institute for Chemistry. APXS will determine elemental abundance of rocks and soil. APXS will be provided by the Canadian Space Agency.

Radiation Assessment Detector (RAD), located on the rover body. Principal investigator: Donald Hassler, Southwest Research Institute. RAD will characterize the broad spectrum of radiation at the surface of Mars, an essential precursor to human exploration of the planet. RAD will be funded by the Exploration Systems Mission Directorate at NASA Headquarters.

Dynamic Analysis of Neutrons (DAN), located in the rover body. Principal investigator: Igor Mitrofanov. DAN will perform an in situ analysis of the hydrogen content of the subsurface.

Rover Environmental Monitoring Station (REMS), in various locations on the rover. Principal investigator: Luis Vázquez. REMS will measure temperature, pressure, wind speed and direction, humidity, ultraviolet dose, atmospheric dust, and local fluctuations in magnetic field.

Laboratory Instruments:

CheMin, located in the rover body. Principal investigator: David Blake, NASA's Ames Research Center. CheMin is an X-ray Diffraction/X-ray Fluorescence (XRD/XRF) instrument that will identify and quantify all minerals in complex natural samples such as basalts, evaporites and soils.

Sample Analysis at Mars (SAM), located in the rover body. Principal investigator: Paul Mahaffy, NASA's Goddard Space Flight Center. SAM consists of a gas chromatograph mass spectrometer and a tunable laser spectrometer. SAM will perform mineral and atmospheric analyses, detect a wide range of organic compounds, and perform stable isotope analyses of organics and noble gases.

a high-powered laser zapping rocks. RAD would make measurements that would pave the way for human exploration of Mars. DAN would bring to the surface the neutron-detection capability that had led to the Odyssey discovery of ground ice.

But the *pièce de résistance* was the analytical laboratory comprising CheMin and SAM. Geologists salivated over the prospect of performing X-ray Diffraction/X-Ray Fluorescence (XRD/XRF) on Mars with CheMin. All previous methods of mineral identification on the surface of Mars were indirect; XRD/XRF measurements are diagnostic, as long as the samples contain crystals. And SAM would sensitively study atmospheric gas isotopes, could follow up on the possible discovery of methane, and would be capable of detecting organics, dangling the possibility of finding direct evidence for Martian life.

The selected instrument package contained many items from the wish list the Science Definition Team had drawn in 2001 (see section 1.2.2). The final science package lacked a dedicated mast-mounted thermal infrared spectrometer like the Mini-TES on the Mars Exploration Rovers and significantly, a near-infrared spectrometer that could follow up on discoveries from OMEGA on Mars Express and CRISM on Mars Reconnaissance Orbiter that played a major role in landing site selection. (ChemCam can be used in a passive spectroscopic mode, but its sensitivity barely reaches into the near-infrared.) There was no arm-mounted mineralogical analyzer, no ground-penetrating radar, and no seismology package. But everything else was there.

One group was both excited and dismayed by the list of instruments: the engineers, who would have to find space, mass, and power to accommodate them all in their rover, never mind operating a machine with so many capabilities.

1.4 PRELIMINARY DESIGN (2005–2006)

A developing NASA mission faces many hurdles on the way to its destination, but there are five formal ones. First is the Preliminary Design Review, which usually takes place about four years (give or take) before launch. At the Preliminary Design Review, the mission team has to demonstrate that they have a sound concept for the mission and all its technically challenging components. Passing a Preliminary Design Review unlocks NASA's coffers, allowing a mission to spend money turning concepts into detailed designs. About a year later comes the Critical Design Review, when the mission has to present blueprints to the review panel. Passing the Critical Design Review allows a mission to transition to the third phase, Assembly, Test, and Launch Operations (ATLO), usually about two years before launch. The final hurdles are launch and arrival. MSL's Preliminary Design Review was scheduled for June, 2006. The project had a lot of work to do before then.

1.4.1 Technology development

To succeed, MSL required several new technologies for landing and surface operations.¹⁵ Guided entry required alteration of existing ballistic-entry vehicle designs into a lifting body that could fly through the Martian atmosphere. The steerable spacecraft also needed a new guidance and control system. For sky crane, they needed more powerful descent engines that could support the massive weight of the rover and descent stage, as well as a special reel for the rope that would lower the rover slowly and gently to the surface.

For surface systems, the main challenges were longevity and sample handling. In particular, the motors (also known as actuators) for all the rover's moving parts were required to survive testing 20 times longer than those developed for the Mars Exploration Rovers. The MSL mission decided to develop a new type of actuator that relied upon a dry rather than liquid lubricant. Liquid-lubricated motors must usually be heated on Mars in order for their lubricant to function, particularly at night. Dry-lubricated motors wouldn't need heaters, so would be less complex and would save the mission a considerable amount of power and complexity. Heating costs both time and energy, and scheduling time enough for heating increases the burden of tactical planning.

For sample handling, they needed to develop the arm (by now, the design included only one) and a deck-mounted rock corer, rock crusher, and sample portioning and delivery system. There was also the problem of scaling up the Mars Exploration Rover mobility system – the wheels, rocker and bogie arms, and the differential that connected them – by a factor of more than two, without scaling up their mass by a factor of eight. Because the mobility system was also their landing gear, the engineers prototyped it early, developing a physical model that they could test across a wide range of landing scenarios.

The unusual entry, descent, and landing system proposal attracted the attention and concern of NASA officials and review panels. In early 2005, NASA Administrator Mike Griffin, speaking in the context of financial pressures on NASA in general, floated the idea of delaying MSL to 2011.¹⁶ Griffin personally visited JPL in June 2005. JPL director

¹⁵Udomkesmalee and Hayati (2005)

¹⁶Cooper (2005)

Charles Elachi reportedly lobbied Griffin hard not to delay the mission. Buoyed by their confidence in the wake of the successful landings of both Mars Exploration Rovers, the JPL team assured Griffin they would be ready for 2009.

1.4.2 Shifting design, early 2006

One particular decision made early on to reduce costs would wind up haunting the rest of the mission. They decided to give the spacecraft only one main computer, located in the rover, instead of having distinct boxes for cruise, landing, and surface operations. The shift toward fewer electronics boxes was enabled by improvements in commercial electronics technology.¹⁷ High-density field-programmable gate arrays (FPGAs), in particular, allowed the rover to have less hardware, but it made the spacecraft more dependent on software development. Software could, in theory, be developed by multiple teams in parallel. But with only one main computer, all that software had to be tested in series; adding more engineers wouldn't make the test program go faster.

Late in 2005 NASA and JPL management decided to double the rover's electronic brains, giving it a complete backup system in case any of its critical electronic components failed. There was space for a second set of computers inside the rover, but it added mass, significantly set back the avionics development schedule, and added complexity to the test program. There were now two computers to test, but both were inside the same piece of hardware, and through cross-strapping, both had interfaces with many of the same pieces of equipment, increasing the number and variety of tests that were needed exponentially.

On March 10, 2006, Mars Reconnaissance Orbiter successfully entered orbit. The first new NASA orbiter since 2001 Mars Odyssey brought many capabilities to Mars that would be essential to the success of MSL. Its science payload, which would begin regular



Figure 1.4. Comparison of Mars Reconnaissance Orbiter with the two older NASA Mars orbiters. A 2010 photo of the MSL rover has been added in for scale. NASA/JPL-Caltech/Emily Lakedawalla.

¹⁷Cook (2011)

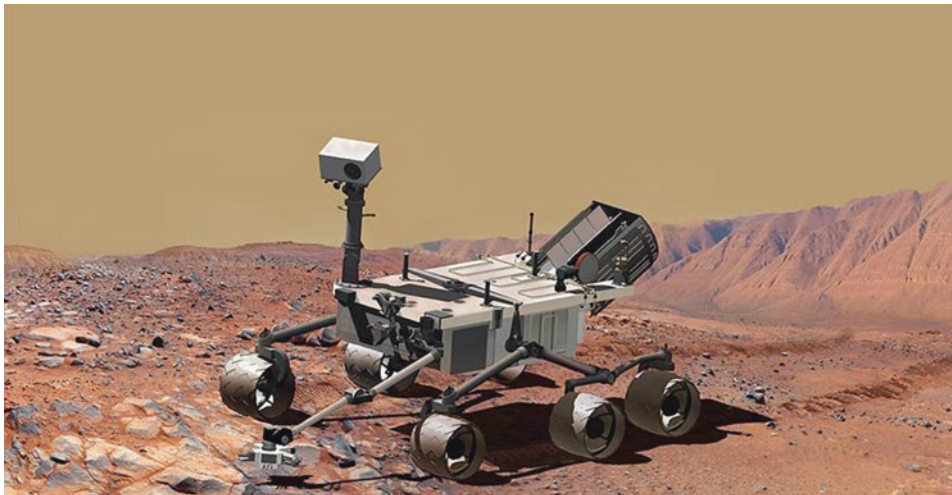


Figure 1.5. Concept art of the MSL rover prepared for the Preliminary Design Review. From Vasavada (2006).

operations in October, included a camera named HiRISE (for High-Resolution Imaging Science Experiment) that could map the surface in unprecedented detail. Perhaps more importantly for MSL, Mars Reconnaissance Orbiter carried an upgraded radio for communicating with surface missions and a 3-meter dish for high-rate communications with Earth. That dish gave Mars Reconnaissance Orbiter the ability to relay much more data to Earth than Odyssey did for the Mars Exploration Rovers (Figure 1.4). The successful arrival of Mars Reconnaissance Orbiter meant that the MSL mission could get rid of the enormous radio dish and related power requirements that had been part of the earliest design concepts.

By mid-2006, the rover concept was taking a shape that looks much more recognizable (Figure 1.5).¹⁸ Instead of two arms, there was just one, along with the sample preparation hardware bolted to the deck. The mast and arm were configured to support the instruments that had been selected in 2004. The high-gain antenna had shrunk. There was only one, rather than two, MMRTGs. (Because the environmental review process described in section 1.2.3 was not officially complete by this time, the publicly released version of the artist’s concept shown in Figure 1.5 had no MMRTG.)

The EDL concept had matured more than the rover design (Figure 1.6). The active terrain hazard avoidance that had been scoped in the initial concept was gone, replaced with a much longer powered-descent phase. The final concept of the flight system – a Dagwood sandwich of a spacecraft consisting of cruise stage, aeroshell, descent stage, rover, and heat shield – changed very little after this time (Figure 1.7). This lander would require a larger, flatter landing ellipse than had been promised for the Mars Smart Lander concept.

JPL presented these concepts at the MSL Preliminary Design Review in June 2006. Manning “thought that the team was presenting designs that were rough, much less

¹⁸Vasavada (2006)

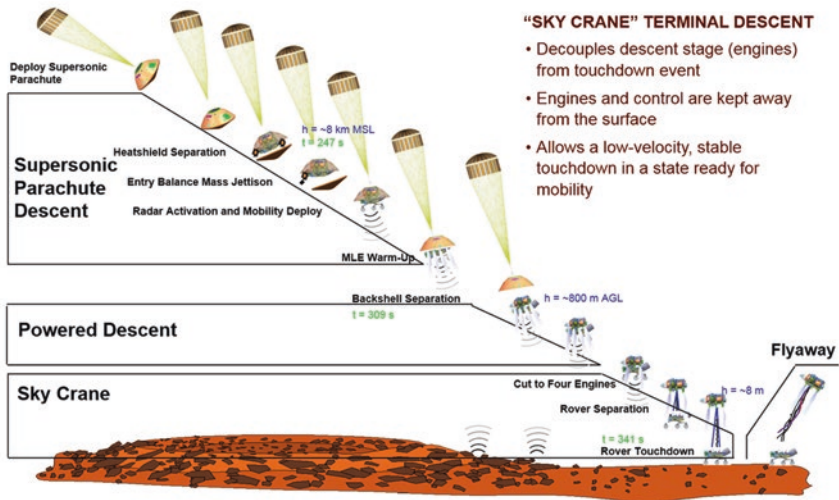


Figure 1.6. EDL timeline (top) and model of the rover (bottom) prepared for the Preliminary Design Review. Compare to Figure 1.3.

developed than they should have been at this stage.” Still, the review board voted to give MSL a passing grade, and NASA started writing checks. The biggest one was the first: NASA immediately announced a contract with Lockheed Martin for an Atlas V rocket for the fall 2009 launch, at a fixed price of \$194.7 million.

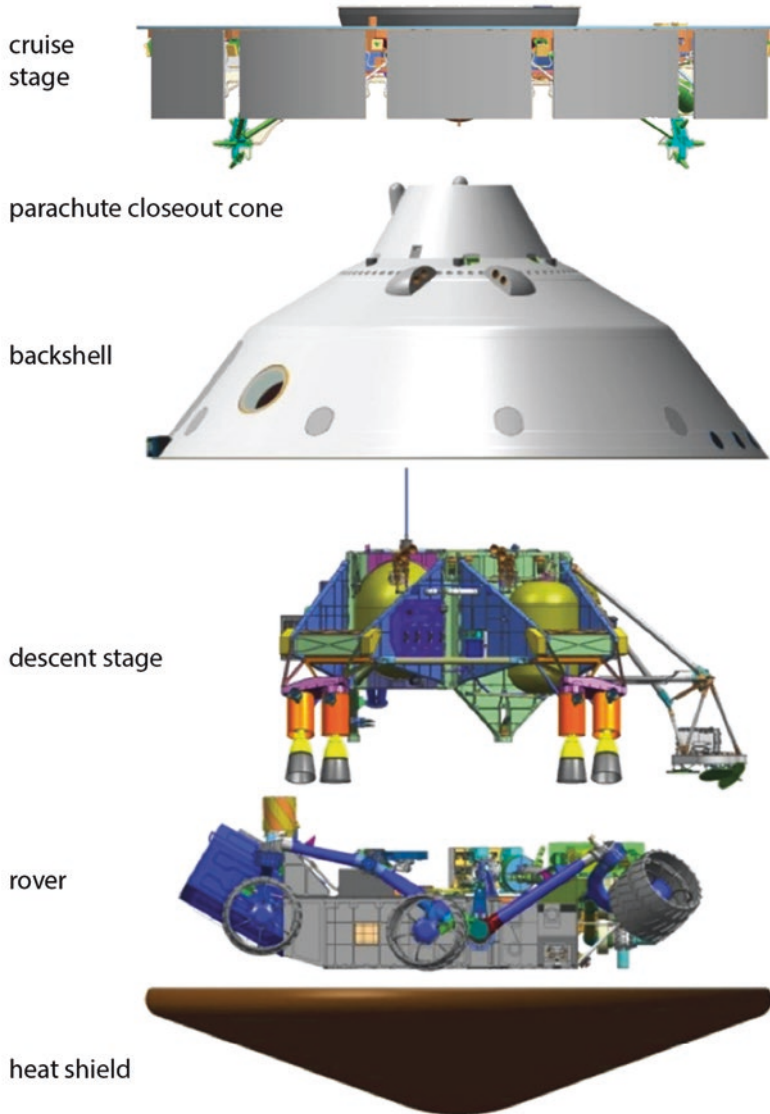


Figure 1.7. Components of the MSL flight system. NASA/JPL-Caltech.

1.4.3 First real cost estimate

Until the Preliminary Design Review, there had not been a solid cost estimate for MSL, because there had not yet been a design to price. The NASA advisory panel that had initially identified MSL as a mission worth pursuing had scoped it out as a medium-class

mission, costing under \$650 million. Internal NASA bookkeeping accounted it at \$865 million in November 2003, a number that did not include the radioisotope power source, the launch vehicle, or the cost of the focused technology program needed to bring some key landing technologies to maturity. The Preliminary Design Review revealed that, despite years of effort to find ways to keep the mission's cost down, MSL was going to be much more expensive than outsiders had anticipated. Including development costs, new technology, launch vehicle, operational costs, and reserves, project manager Richard Cook estimated a total cost of \$1634 million.

1.4.4 Where to send the mission?

At the same time as the Preliminary Design Review, the landing site selection process began. On May 31, 2006, the Landing Site Selection Committee invited the world's Mars scientists to the first in a series of community workshops. Anyone could propose landing sites, and explain how they would address the mission's science objectives. To prepare for the first landing site selection meeting, deputy project scientist Ashwin Vasavada translated the science objectives into more specific terms that would help guide the choice of landing site (Box 1.5).

Box 1.5. Curiosity science objectives.

- To assess the biological potential of at least one target environment by determining the nature and inventory of organic carbon compounds, searching for the chemical building blocks of life, and identifying features that may record the actions of biologically relevant processes.
- To characterize the geology of the landing region at all appropriate spatial scales by investigating the chemical, isotopic, and mineralogical composition of surface and near-surface materials, and interpreting the processes that have formed rocks and soils.
- To investigate planetary processes of relevance to past habitability (including the role of water) by assessing the long timescale evolution of the atmosphere and determining the present state, distribution, and cycling of water and carbon dioxide.
- To characterize the broad spectrum of surface radiation, including ultraviolet light, galactic cosmic radiation, solar proton events, and secondary neutrons.

The rover's precision landing was aimed at an unprecedentedly broad swath of Mars. Previous landers were limited by their solar power systems to regions near the equator. But MSL, with its nuclear power source, could access latitudes as far as 60° away from the equator, including regions where there is modern-day ground ice within reach of a scoop or wheel scuff. The mission also planned for the ability to reach elevations up to 2500

meters above the Martian mean, opening up Mars' southern highlands to exploration for the first time.¹⁹

MSL's ellipse was smaller than that of previous missions, so landings could be squeezed into tighter spaces (Figure 1.8). At the beginning of the landing site selection process, MSL's landing ellipse was taken to be 25 kilometers in the down-track direction, and 20 in the cross-track direction. Four main factors affected MSL's landing precision:

- *Navigational uncertainty.* The navigation of MSL and other deep-spacecraft is highly precise, but there are limits. The spacecraft could miss the target by as much as 2 or 3 kilometers both down-track and cross-track.
- *Attitude knowledge.* The mechanical alignment of MSL's gyroscope relative to the star scanner on the cruise stage might be imperfect, potentially introducing error during guided entry of as much as 4 to 6 kilometers both down-track and cross-track.
- *Atmospheric and aerodynamic variability.* The final 75 to 100 kilometers of MSL's descent would be flown without guidance, in order to maximize altitude. Variability in the atmosphere, and resulting variability in the aerodynamics of the aeroshell, can cause the spacecraft to miss by 5 to 7 kilometers in the down-track direction.
- *Winds.* Once MSL's parachute opens, guidance is no longer possible, and winds can divert the spacecraft from its intended path, resulting in as many as 1 to 2 kilometers of positional error.²⁰

More than 100 scientists attended the workshop. Scientists participated not only out of a desire to contribute to the landing site selection, but also because proposed locations would be short-listed for early scientific observations by Mars Reconnaissance Orbiter.

The outcome of the workshop was a list of 33 potential landing sites, of which 11 were voted to be top-rank possibilities. All of the favored 11 were below Martian mean elevation, and all were within 30° of the equator.²¹ The fact that no high-elevation landing sites were among the top-ranked locations presented an opportunity of some relief to the engineers developing the entry, descent, and landing systems. In July 2006, NASA's Mars Exploration Program made this relief official, setting a new requirement for the MSL landing to lie below 1000 meters' elevation.

Shortly after the workshop, on November 2, 2006, NASA lost contact with Mars Global Surveyor, and the mission was declared over on November 22. The remaining orbiters at Mars – 2001 Mars Odyssey, Mars Express, and Mars Reconnaissance Orbiter – got to work performing detailed observations of the proposed sites. The committee scheduled a second workshop for October 2007, after a year of Mars Reconnaissance Orbiter's primary science mission.

1.4.5 Plans for planetary protection

We go to Mars in part because we are interested in searching for past or present life there, so it's crucially important that we avoid forward-contaminating the planet with Earth

¹⁹ Golombek et al (2012)

²⁰ Wallace (2012)

²¹ Golombek et al (2012)

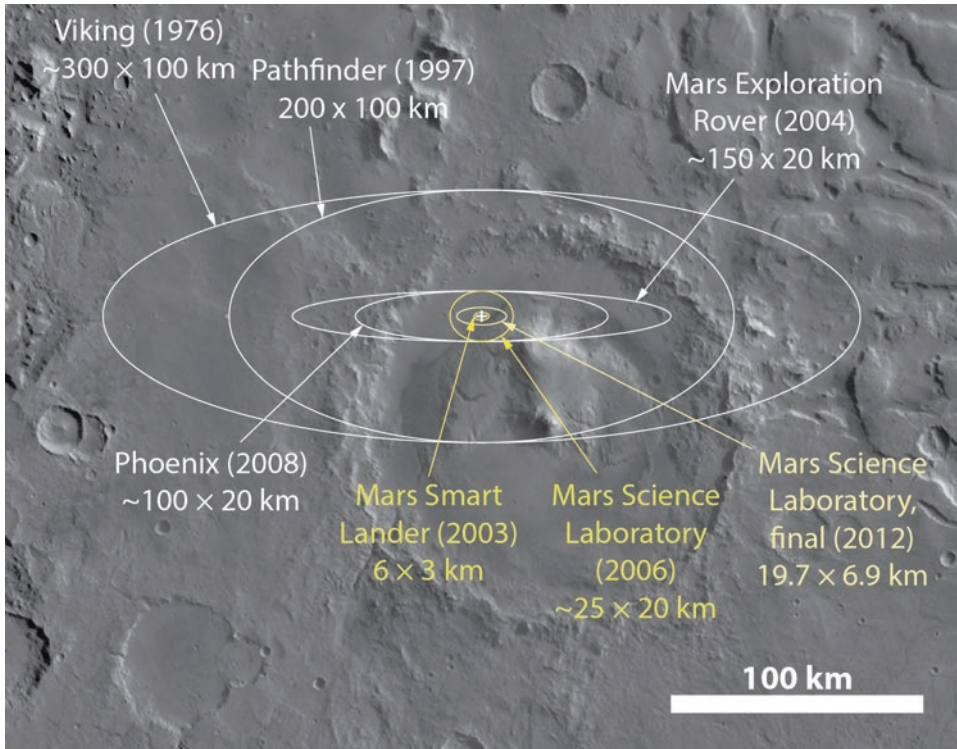


Figure 1.8. Comparison of historic Mars landing ellipse dimensions with Gale crater. Gale is about 154 kilometers in diameter. The base image is Viking orbiter data. Map by Emily Lakdawalla.

microbes. Although Mars is more clement than the rest of the planets beyond Earth, it is not a particularly kind environment to Earth microbes. It's cold, the atmospheric pressure is very low, it's incredibly arid, and it's bathed in ionizing radiation. But Earth life is tenacious. There are some places on Mars warm enough for microbial activity. There are Earth microbes that can survive very low pressures. Some scientists argue that Mars may possess limited present-day liquid water (though likely very salty); and a mere 1 millimeter of Martian soil is enough to shield microbes from damaging ionizing radiation, so life could theoretically be hiding in briny aquifers buried beneath the surface.²²

Preventing forward contamination (and also preventing the backward contamination of Earth with alien microbes) is the role of NASA's Office of Planetary Protection. One of the central concepts in planetary protection is that of "special regions." A special region is defined by the International Council for Science's Committee on Space Research as "a region within which terrestrial organisms are likely to propagate" or "a region which is interpreted to have a high potential for the existence of extant Martian life forms."²³ In

²²Rummel et al (2014)

²³Rummel (2006)

practice, there are no places on Mars that have yet been identified as having high potential for extant life, so it's the first definition that applies to planetary protection.

Because MSL is not a life detection mission, it was not planned to target a special region. However, a catastrophe on landing day could actually create a "spacecraft-induced special region." If MSL crash landed at a place with modern near-surface ground ice, the hot plutonium power source would melt that ice to water and keep it nice and warm. Any microbes that hitched a ride could potentially propagate in such an oasis.

Because MSL had the potential to create such a spacecraft-induced special region, in August 2005, NASA's Planetary Protection office classified the mission as "Category IVc". This categorization required either complete sterilization of the spacecraft, or a landing site restriction to regions where water ice is no shallower than 1 meter from the surface, plus sterilization of the parts of the rover that were expected to penetrate below the surface: the wheels and drill bits.²⁴ The 1-meter number was based on estimates of how deeply large hardware fragments could be buried upon impact.

The price tag for system-level sterilization was expected to be between \$60 and \$170 million – more than the project could afford.²⁵ The project elected to go with the cheaper option, accepting the restriction of avoiding near-surface ground ice, which Odyssey mostly mapped poleward of 45° north and south latitude. The project would sterilize the drill bits and wheels, and closely evaluate landing ellipses late in the landing site selection process to ensure that there were no hints of near-surface ground ice.²⁶ In the end, 89% of the spacecraft's surface area, and 61% of its volume, were subjected to heat sterilization, making it the cleanest NASA spacecraft launched since the Viking landers.²⁷

1.5 THE COST OF COMPLEXITY (2007–2008)

It didn't take long for the development effort to run into trouble. The main problem was schedule. Everything seemed to take longer than it should, but the 2009 launch date was fixed and immovable, and complexity cropped up everywhere. Engineers took shortcuts, moving quickly to final designs without time to test early ones, risking that problems would crop up later on, which they did.²⁸ Avionics development continued to be slowed by its complexity. A suite of sensors called the Mars Science Laboratory Entry Descent and Landing Instrument (MEDLI) – essentially another science instrument – was added to the heat shield late in 2006; the project would benefit future Mars landing efforts by supplementing models of entry with actual data, but created another interface to incorporate. The sample acquisition and handling mechanism design was completely scrapped and design effort restarted in 2007. On top of all of this, the mission suffered two particularly huge setbacks in 2007, involving the design of the motors and the heat shield. Solving these problems required massive redesigns, imposed major costs, and resulted in huge schedule delays.

²⁴ Golombek et al (2012)

²⁵ Rummel (2006)

²⁶ Golombek et al (2012)

²⁷ Benardini et al (2014)

²⁸ Manning and Simon (2014)

1.5.1 Sample handling restart

Mars Smart Lander had been initially scoped with two arms, one for coring and one for sample processing. At the time of the Preliminary Design Review, Mars Science Laboratory had had a single arm with a driller/corer and scoop, and a deck-mounted piece of sample preparation and handling hardware to crush, sieve, and portion the sampled rock. While intact cores would provide insight into near-surface layering or weathering, neither of the two analytical laboratory instruments, SAM or CheMin, needed intact cores. In fact, techniques available to crush the cores for the instruments had difficulty in achieving the fine particle sizes the instruments required.

After the Preliminary Design Review, the sample handling approach changed again. A drill would simultaneously penetrate into and powder the rock, augering it into a sample chamber. Then the drill would transfer the material from the sample chamber into a device on the arm that could sieve, portion, and deliver the right kind of sample to the waiting science instruments. The approach was simpler than the two-arm core-crushing solution, but the development effort started very late. Also, the switch from coring to percussive drilling and the addition of sample handling hardware to the end of the arm increased the weight of the turret from 15 to 34 kilograms.²⁹ The 2-meter-long arm and its 5 motors would need to be much more robust than planned to support all of that weight.

1.5.2 Motor problems

MSL's design included a total of 31 motors, not counting the ones in the science instruments: 6 to rotate the wheels, 4 to steer them, 2 for the high-gain antenna, 3 for the mast, 3 for the instrument inlet covers, 5 for the robotic arm, and 8 for the drilling, sampling, and dusting hardware in the arm turret. The MSL mission had sought to reduce the rover's power demands by using dry-lubricated motors that could operate at very low temperatures without being heated for all but 4 of these. The effort had started off well: JPL successfully developed titanium-gearred motors lubricated with powdered molybdenum disulfide that operated perfectly under Martian conditions, down to a minimum temperature of -135°C , colder than the Mars minimum of -127°C (the freezing point of carbon dioxide).³⁰ But the motors failed later lifetime tests that checked how they would cope with the demands of operating under Martian conditions for millions and millions of revolutions. Over time, the titanium gears fatigued and cracked, their teeth falling out.

With schedule pressing, they had no choice but to return to the old way of doing things: steel motors with wet lubricant, based as much as possible on the titanium motor designs that had been worked on to date. These motors could not operate under most Martian conditions without heaters. Mars Exploration Rover motors had such heaters, thin strips that were elegantly incorporated into flat surfaces planned for that purpose in the motor design. MSL motors had been designed without these interior surfaces, so there was no choice but to add them to the exteriors of the motors. Furthermore, the MSL motors were dramatically larger than the Mars Exploration Rovers', and took correspondingly longer to heat. In order to heat them up in a reasonable 1 to 2 hours, they would require larger heaters,

²⁹ Billing and Fleischer (2011)

³⁰ Novak et al (2008)

consuming more power, than they would have if they had been planned into the design from the start. In fact, they would consume so much power that they would leave the rover's battery depleted, with little power remaining to drive or do science.³¹

Steel motors were also heavier than the titanium ones would have been. The mass of the robotic arm increased by 14%, sending engineers back to the drawing board to make sure all the parts would be up to the stresses of landing and driving at their new masses.³² The motors were supplied by one vendor; the arm was being manufactured by a different vendor. Wherever the two components interacted, it took a tremendous amount of planning and work to coordinate the design efforts of the two companies. Engineers tried to minimize the mass of the heavier motors, but that meant repeatedly changing their specifications, delaying their delivery. Arm development was delayed. Meanwhile, the late redesign of the sample handling system meant that requirements for the motors in the arm kept changing even as design of the new motors had already begun.³³

The switch to wet-lubricated motors created new constraints for landing site selection. Although the rover could theoretically operate at high altitudes and high latitudes, severe winter cold would leave the rover without sufficient power to warm up its motors and drive. The Mars Exploration Rovers mostly parked in winter because shorter days without overhead sunlight limited their power. MSL could potentially suffer the same problem, if sent to a landing site more than 15° south of the equator.³⁴ (Southern winters are harsher than northern winters, due to the combination of higher average elevations, seasonal timing, and elliptical shape of Mars' orbit.) Winter immobility was acceptable for Spirit and Opportunity because the rovers had never been intended to last into the Martian winter anyway. But for MSL, which was supposed to be able to land nearly anywhere on Mars and operate for a full Martian year, cold-weather inactivity could prevent mission success.

Even the science instruments were affected. Power limitations meant that activities requiring rover motion would need to be planned for the warmest part of the Martian day. But some instruments, like ChemCam, had detectors that worked best when cold. It looked like ChemCam was stuck between a rock and a hard place, as principal investigator Roger Wiens explained in a memoir:

With the change in motor lubrication, normal operations became restricted to between 10 am and 4 pm local time to avoid excessive energy use. MSL was short on system engineering help, but eventually the combined impact of these decisions was noticed. There was an MSL leadership meeting in late 2007 in which the issue was addressed. A chart was displayed showing in one color the times of day during which ChemCam's detectors would be cool enough to meet its science requirements, with another color indicating the times of day that the rover's mast would be warm enough to point to targets. I was told that the room erupted in laughter. The two colors never overlapped. ChemCam was cool enough only at night and the mast gimbals were warm enough only in the middle of the day. It was a perfect mismatch.³⁵

³¹ Manning and Simon (2014)

³² Billing and Fleischner (2011)

³³ JPL (2014a)

³⁴ Watkins and Steltzner (2007)

³⁵ Wiens (2013) *Red Rover*

Despite a massive effort to adjust designs to cool the ChemCam detectors, it looked like the instrument might only be usable for half an hour at each end of an operational day.

1.5.3 Heat shield failure

The other disaster of 2007 involved the mission's heat shield. All NASA Mars missions to date had used a material for the heat shield called Super Lightweight Ablator, or SLA. The material consisted of a mixture of corkwood, epoxy, and gas-filled silica-glass spheres that is packed into a honeycomb structure pre-shaped into the blunt cone of the heat shield, allowing SLA to be used for heat shields of any size and shape. So MSL's larger size didn't present a manufacturing problem. But MSL was more massive and it would be arriving at Mars at a higher speed than previous spacecraft, imposing higher pressure and temperature on it, and causing air to flow around it turbulently rather than smoothly. And the heat shield would be tilted at an angle as the spacecraft performed its guided entry, heating it asymmetrically. The first great challenge of developing the heat shield was to develop new ways to test all these more-extreme conditions.

The heat shield failed these new tests "drastically."³⁶ Instead of receding slowly, the material emptied out of the honeycomb cells catastrophically, in mere seconds. The engineers couldn't figure out why, so they couldn't even attempt to modify the design to prevent failure. They had to start from scratch – and had only 18 months to find a new solution.

NASA's human exploration program came to the rescue. An alternative heat shield material had recently been developed and tested for use in a large heat shield. The material, called Phenolic Impregnated Carbon Ablator (PICA), was first used successfully on the Stardust sample return capsule, which returned to Earth in January 2006. The same year, the Orion human exploration program adopted PICA for their capsule, and subjected it to intensive tests at even more extreme conditions than MSL faced. To support the Orion effort, the manufacturer worked to double their manufacturing capacity, bringing the new capability online exactly on time to produce a heat shield for MSL.

Lockheed Martin started developing a new PICA heat shield in October 2007 on a fast-tracked schedule that had a Preliminary Design Review on February 7 and Critical Design Review on June 13, 2008. A major challenge was that PICA could not be built in large custom-shaped pieces. Individual pieces were limited to the 0.81-meter diameter of the Stardust sample return capsule. MSL's heat shield was 4.5 meters across. It would have to be tiled, like the Space Shuttle's ceramic exterior, in Stardust-capsule-sized pieces.

1.5.4 Critical Design Review

The MSL project had had its Critical Design Review in June 2007, before either the actuator or heat shield problems had fully come to light. The project passed, but the review panel noted two very serious problems. The first was that the sample handling mechanism design was not nearly mature enough. The second was that schedule pressure and

³⁶Slimko et al (2011)

development problems likely meant that the mission would need a budget increase of about \$75 million.

1.5.5 Stern descopes

The mission requested more money at an unfortunate time. There was a new Associate Administrator of the Science Mission Directorate at NASA: Alan Stern, a planetary astronomer and aerospace engineer best known for being the principal investigator of the New Horizons mission to Pluto and the Kuiper Belt. Stern had already publicly expressed frustration with cost overruns on some NASA missions harming others. In a period of 5 years, he noted, a total of \$5 billion worth of cost overruns had diverted funds from research programs and caused opportunities for other missions to be lost. Also, Stern shared with other members of the science community a concern that NASA was focusing too much of its limited resources on Mars, to the detriment of all the other compelling destinations in the solar system.

Stern told the MSL project that they could not have their requested budget increase. Rather, they had to descope their mission – remove capabilities in order to keep the mission within its original budget. Whatever savings could not be realized with descopes, they would have to take out of other missions within NASA’s Mars Exploration Program. Stern asked JPL for suggestions of what could be cut.

There were not many options. Most of the rover’s planned hardware was exactly what was needed to get the spacecraft safely to the surface. They cut a planned rock-grinding tool, replacing it with a simpler brushing tool. Richard Cook had no choice but to put science instruments on the list of things to be cut. The mission drew up a list and sent it to NASA: ChemCam, Mastcam, and MARDI. NASA accepted the cutting of ChemCam and MARDI, but pushed back on Mastcam, knowing that it would be hard to justify to the public the removal of all color photo capability from the rover. Could Mastcam be built cheaper? JPL knew that the electronics were already complete, but the optics were not, so they offered up the Mastcam optics, descoping the zoom and focus capability, leaving the rover with cameras of two different, fixed, focal lengths, and fixed focus.³⁷

The descopes were announced in a press release from NASA on September 17, 2007:

The MSL project required some focused and prudent reductions in scope in order to better ensure project success. Furthermore, because all of the funds MSL requested were not available in the Mars Exploration Program reserves pool, and because SMD did not want to impact other current or future science missions to fund these new costs, the Science Mission Directorate at NASA Headquarters has been working closely with the MSL project and the science community to identify mission scope reductions to minimize the project’s need for funds, while minimizing both technical risk and impacts to the mission’s science return.

As a result of this careful process, a combination of low-impact mission scope reductions and some new funding from the Mars Program’s reserves pool, has been

³⁷Michael Malin, personal communication, interview dated June 11, 2014

agreed upon. Together these measures effectively resolve the MSL cost increase issues identified at its [Critical Design Review].

Engineering changes to the mission include some reductions in design complexity, reductions in planned spares, some simplifications of flight software, and some ground test program changes. These changes were selected largely to help reduce mission risks. Changes in mission science content were limited to removal of the Mars Descent Imager (MARDI), the MASTCAM zoom capability from the mission, and a change from a rock grinding tool to a rock brushing tool. As noted by the science input NASA received, most of MARDI's capability can be provided by the Mars Reconnaissance Orbiter's HiRISE camera now in orbit and working successfully. Furthermore, NASA has directed that the project expend no additional funds on ChemCam, and cost-cap SAM and CheMin at their current budgets. Future budget requests for these instruments cannot be funded.

In total, the cuts would theoretically free up about \$26 million to augment mission reserves, although that number failed to account for the termination costs of the contracts with industry partners. The impact on MSL's science capability was severe. The most painful loss was ChemCam, which could not be included on the rover without further expenditure of funds. The laser instrument represented the rover's only capability to measure rock composition from a distance. Without ChemCam, the rover would need to drive up and touch with APXS every rock it might want to explore in situ, at enormous cost to operational efficiency. The loss of zoom capability on Mastcam would be detrimental to its usefulness for studying the landscape at various spatial scales. And the budget axe loomed over SAM and CheMin. The Mars science community decried the cuts as being penny-wise and pound-foolish.

At the same time, Stern directed that MSL actually add something to its design: a sample cache, a simple basket designed to hold Mars rock samples. The sample cache was intended as a first step towards Mars sample return. Stern specified that funds would come from within the Science Mission Directorate, but outside the Mars Exploration Program. Even so, members of the Mars community were angry that Stern had cut science instruments from MSL to save relatively small amounts of money, while spending for a sample cache that few people believed would ever be picked up by a future sample return mission.

Representatives of the Mars Exploration Program Analysis Group (MEPAG), led by Jack Mustard (who was not a Mars Science Laboratory science team member), met with Stern and other Headquarters personnel on September 24, 2007. In a summary of the meeting, Mustard wrote: "Almost all comments relayed to the MEPAG chair preceding the meeting were related to ChemCam, noting the loss of remote geochemical capability and the significant investments of the French science and technology communities. MEPAG relayed concerns regarding the international implications of the stop funding order for ChemCam." The group also expressed their reservations about the proposed sample cache: "The MEPAG group re-iterated the need for appropriate samples for [Mars Sample Return], and that poorly documented rock fragments in an open sieve basket will not meet the criteria for science as outlined in numerous National Academy and MEPAG reports."

1.5.6 Second site selection workshop

The landing site selection committee convened the second community workshop on October 23, 2007. The mood at the second meeting was anxious, to say the least. Scientists were still reeling from the instrument descopes. Many scientists learned for the first time about the failures in the heat shield and motor development process. The motor problems threatened to take many favorite southern hemisphere sites out of consideration.

Engineers Mike Watkins and Adam Steltzner told the scientists that higher-elevation landing sites were substantially riskier than lower-elevation sites, another blow to southern hemisphere fans.³⁸ In fact, the highest-elevation sites were so risky that Watkins and Steltzner requested that scientists proposing high-elevation sites develop a related “safe haven” site at similar latitude but much lower elevation. At the end of the workshop, the list of possible sites had formally narrowed to 11, but there was a great deal of uncertainty about whether MSL would be capable of landing at any of them, and what the quality of its science would be without ChemCam and the other cut instruments.

Just weeks later, ChemCam and MARDI were saved. The good news was announced in a letter from Alan Stern and Jim Green on November 8:

Malin Space Science Systems has agreed that there will be no additional costs to NASA for the completion of the Mars Descent Imager (MARDI). Furthermore, funds returned to the Mars Exploration Program from the unfortunate elimination of MARDI operations on Phoenix will be used to support MARDI integration on MSL. In the case of ChemCam, LANL, the French Space Agency (CNES), and even other MSL instrument team members have developed a series of descopes and support arrangements to allow instrument completion, reducing the development cost-to-go by a little over 80%; i.e., from \$2.5M to about \$400K. As a result, ChemCam will be funded another \$400K by the Mars Exploration Program, allowing them to complete development.

1.5.7 MARDI wheeling and dealing

MARDI was returned to MSL at its principal investigator Mike Malin’s personal expense, with the help of a behind-the-scenes agreement with the University of Arizona’s Peter Smith, the principal investigator of the recently-launched Phoenix Mars lander. At the moment that it was descoped, Malin says, NASA saved about \$80,000 by doing so. This was such a relatively tiny number that unusual funding sources might work to meet the shortfall. The Planetary Society, a nongovernmental organization, discussed with Malin running a fundraiser among its members to complete it. In the end, Malin decided to put up the money himself.³⁹

So MARDI was finished, but there was still no money to put it on the rover. That money came from Phoenix. MSL was not the first spacecraft with a MARDI. There had been one on Mars Polar Lander, and consequently there was one on the backup lander hardware that later became the Phoenix mission. Peter Smith had invited Malin to operate MARDI on

³⁸Watkins (2007)

³⁹The details of the impacts of the MARDI and Mastcam descopes and subsequent redesign effort of fixed-focus Mastcams are based on an interview with Michael Malin dated June 11, 2014

the Phoenix mission. But there was a problem with the interface between MARDI and Phoenix' main computer, and ultimately Phoenix MARDI was not used at all during the mission. Smith offered to give to JPL the money that he would have paid Malin to support Phoenix MARDI operations. It was enough to pay to integrate MARDI on the rover. JPL agreed, but said that the integration had to happen immediately.

By that time Malin Space Science Systems had completed assembly of MARDI, but hadn't completed the thermal testing that would be required for it to be included on MSL. It was validated enough for descent, but hadn't been tested for surface operations, a detail that would become important after landing. Delivered in July, 2008, it became the first science instrument to be integrated on the rover, and the only one to participate in every major rover test.

1.5.8 Mastcam dezoomed

The longest-lasting impact of Stern's science instrument descopes was on Mastcam. As originally conceived, Mastcam consisted of a pair of identical cameras. Each had a zoom/telephoto lens with up to 15x magnification, giving a field of view ranging from a wide 90° to zoomed 6°. They would have been capable of shooting color, high-definition, stereographic, cinematic video in stereo at a rate of 5 frames per second. For this reason, filmmaker James Cameron joined the Mastcam team as a co-investigator. The descoped version of the Mastcam consisted of two different cameras, both with narrow fields of view (one at 15°, one at 5.1°); they sacrificed same-focal-length stereo capability to maintain the ability to view the landscape at different scales. They could not capture the wide stereo video landscapes that the original design would have enabled. Cameron lost interest, because the new Mastcam was not a tool he could use for his art. The loss of public outreach value – high-definition stereo video from Mars, directed and distributed by a rich, well-connected Oscar-winning director – is incalculable.

Meanwhile, Malin Space Science Systems had to imagine, design, fabricate, test, and deliver a totally new optical design for MSL's science cameras in barely more than one year. It wasn't going to be easy, because the descoped solutions had a major oversight: fixed-focus cameras wouldn't be in focus at all the distances they were expected to cover. The Malin team considered focusing the narrower-angle camera at infinity and the wider-angle one closer to the rover, but then images in the middle ground would be out of focus for both cameras, and stereo imaging would be impossible. Mastcam engineers Mike Caplinger and Mike Ravine came up with an idea that might be cost-effective: use the already developed MAHLI instrument focus mechanism for the Mastcams. But this would not comply with the requirements of the descoped. The Project Science Group recognized that being able to focus Mastcam would be crucial, and went back to NASA Headquarters to request permission to return focus but not zoom capability to Mastcam, because the camera would not be able to achieve its science goals without a focal mechanism. NASA eventually approved the request, and design of the new Mastcam optics began in December 2007.

1.5.9 Scarecrow's debut

Back at JPL, they constructed a new outdoor Mars Yard at the top of the steep JPL campus for MSL mobility testing, and invited media to view "a parade of rovers" there on June 19,

which I attended. One of the rovers on parade was Scarecrow, a prototype for MSL (Figure 1.9). Scarecrow has a rocker-bogie suspension system, motors, and wheels, but hardly any other hardware, which allows its wheels to exert the same ground pressure on Earth that the full-size MSL's wheels would eventually do under Mars gravity. (It's called Scarecrow because, like the character in *The Wizard of Oz*, the minimally instrumented rover has no brain.) Scarecrow and the Mars Yard are still in use for mobility testing, more than a decade later.



Figure 1.9. Scarecrow rolling over enormous rocks in the newly opened JPL Mars Yard on June 19, 2007. Note the “JPL” letters machined into the wheels’ treads. Photo by Emily Lakdawalla.

1.5.10 Budget balloons

The development problems all had financial implications. In December 2007, the MSL project requested another \$91 million from NASA. Alan Stern doubted that this request reflected reality. He tasked Doug McCuistion with independently analyzing the MSL budget. McCuistion found that MSL had underestimated its likely needs by \$40 million. Stern set aside \$190 million to solve MSL's budget woes, bringing the total cost to nearly \$1.9 billion. Some of this money had newly become available with the delay of the second Mars Scout mission opportunity from 2011 to 2013. That would make 2011 the first Mars launch opportunity since 1996 to have no NASA mission slated for it.

The Mars budget had become a battleground. Mars scientists were worried about what they saw as Stern's attacks on the Mars program, and lobbied hard for more money to be moved into the program. Stern was determined to keep the MSL overruns from damaging other areas of space science. He continued to look for places in the Mars program to find funds to pay for the overruns on MSL. On March 24, 2008, the Science Mission Directorate ordered the Mars Exploration Rover mission to cut \$4 million from their \$20 million budget that year, and another \$8 million the following year. Principal investigator Steve Squyres responded that the cuts would require him to shut down Spirit. The public exploded with outrage over the threat to the charismatic rover. The next day, NASA Administrator Mike Griffin repudiated Stern's letter. Hours later, Stern resigned.⁴⁰

The public furor was symptomatic of Griffin and Stern's incompatible management visions. They fundamentally disagreed about how to handle the perennial problem of budget-busting missions. Stern fought to contain the damage within programs, and to protect the small amounts of money supporting research and analysis of NASA data. He wanted to bring an end to what he saw as irresponsible fiscal management of missions and the collateral damage they wrought on other missions. But he acted unilaterally, without the concurrence of NASA leadership. Griffin replaced Stern with Ed Weiler, who had led the Science Mission Directorate from 1998 through 2004, during the overhaul of the Mars program in the wake of the twin disasters of 1999. Weiler would remain in the position through the rest of MSL's development. Within months, Weiler delivered JPL the money they had requested. The MSL workforce increased from 700 to 800 people.⁴¹

1.5.11 Phoenix descends

On May 25, 2008, the Phoenix mission landed in Mars' high northern latitudes. Although the landing went perfectly and NASA heralded it as a success, during its short, 5-month mission Phoenix would have frustrating problems attempting to sample Martian soil and ice and deliver it to laboratory instruments (Figure 1.10). Puffs of wind blew the samples away from the instrument doors. When sampled material did fall onto the instrument, the Martian soil tended to clump and stick, failing to fall through sieves that protected the instruments from large particles, even when the sieves were vibrated.

The difficulties on Phoenix were sobering news for MSL. Sample handling hadn't yet been tested even under optimal conditions. Would wind blow away the drilled samples intended for SAM and CheMin? Would the powder stick to and clog the interior of the sample handling mechanism?

1.5.12 Assembly begins

The MSL project finally began the assembly, test, and launch operations (ATLO) phase of the mission in May, 2008. Construction on cruise and descent stages and the rover mobility hardware proceeded rapidly. They were building two nearly identical sets of rover hardware. A testbed rover, under construction in JPL's In-Situ Instrument Laboratory, would be used for testing of the rigors of landing and surface operations. The flight rover, along with

⁴⁰Lawler (2008)

⁴¹Manning and Simon (2014)

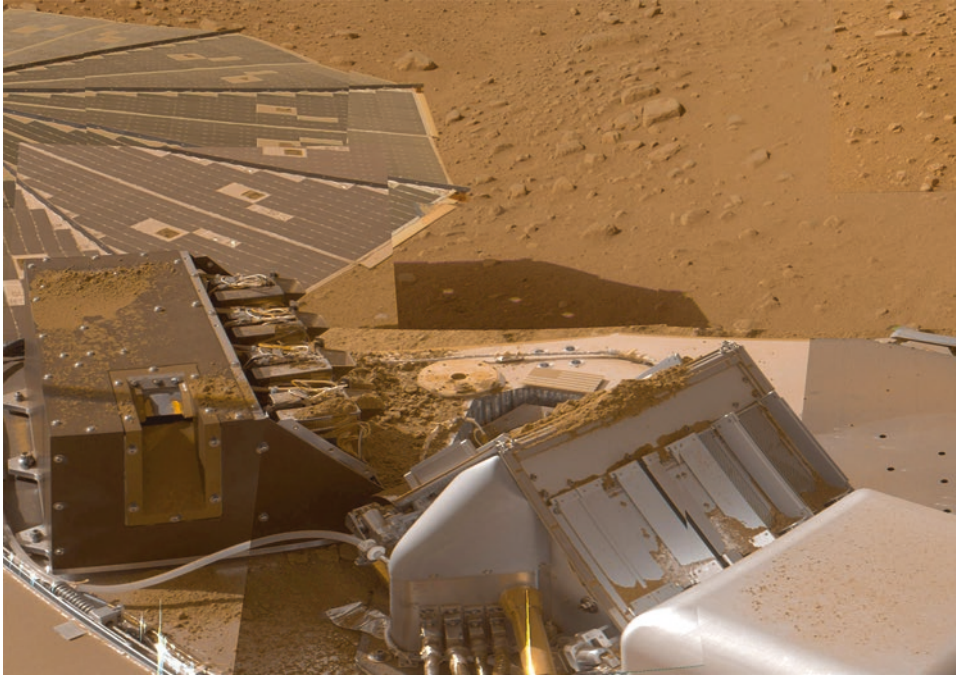


Figure 1.10. A mosaic of images of the Phoenix deck taken toward the end of the mission, after many attempts at sample delivery. The deck is covered and instrument funnels are clogged with clumpy soil. NASA/JPL-Caltech/UA/Texas A&M University release PIA12106.

the cruise stage, descent stage, and aeroshell, were all beginning to take physical form inside JPL's High Bay, the clean room where white-garmented workers methodically assembled the spacecraft (Figure 1.11, Figure 1.12, Figure 1.13, and Figure 1.14). I visited the viewing galleries of both locations several times to watch the progress of construction.

The engineers delightedly presented photos of assembly work to open the third landing site selection workshop on September 15, 2008. Watkins reported significant progress on spacecraft components, instruments, and software development, while acknowledging “lots of work to go, especially in system integration, the system level test program, and software development.” Work on incorporating heaters into the motors had relaxed the engineers’ concerns about far-southern sites. They assured workshop attendees that “All sites are currently acceptable to [the] project. Engineering [is] not a discriminator at this workshop.”

The third workshop yielded a list of four potential landing sites. Two were southern (Holden and Eberswalde craters, both of which appeared to contain ancient lake deltas). One was equatorial (Gale crater, which probably held an ancient lake and definitely had a central mountain containing layered rocks at its base). And one was northern (Mawrth Vallis, a site of uncertain geology but with fascinating chemistry). The orbiters refocused on these four locations.



Figure 1.11. Testbed rover hardware in the In-Situ Instrument Laboratory at JPL, August 25, 2008. The aluminum box at top center is the rover body. The mobility system is at left, with wheels behind red ropes at right. Arm hardware is at the bottom right. Photo by Emily Lakdawalla.



Figure 1.12. The mobility system was attached to the flight model of the rover in August 2008. NASA/JPL-Caltech release PIA11438.

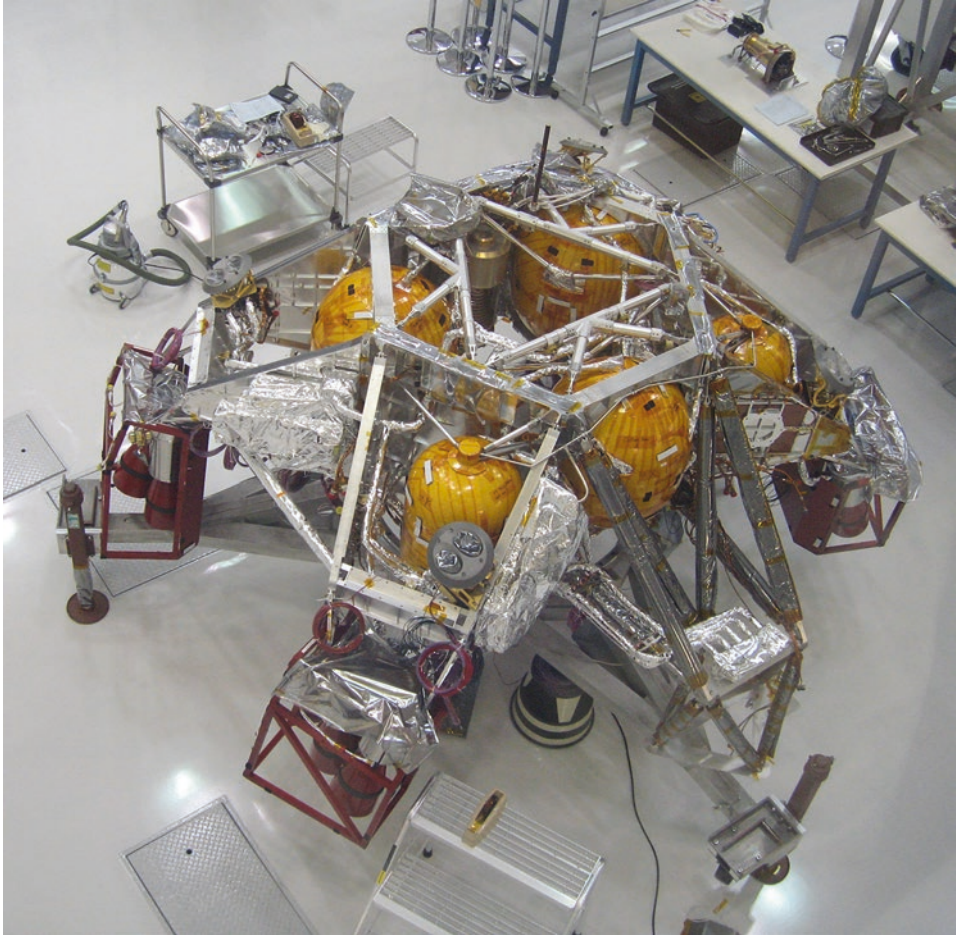


Figure 1.13. The descent stage under construction in JPL's High Bay, October 16, 2008. Photo by Emily Lakdawalla.

1.5.13 Avionics problems

Work on the avionics and software was not proceeding as well as the more visible hardware assembly. Under schedule pressure, the avionics team began integrating the subsystems together before the individual boxes had been fully tested, which only added to the number of problems that cropped up during system testing. Tests often went poorly. Bad setup, operator error, and equipment problems meant that results were unusable or tests were unrepeatable.⁴² The situation was so bad that the partially redundant system might actually be less reliable than the original, single-string system would have been.⁴³ Even

⁴²Devereaux and Manning (2012)

⁴³Cook (2011)



Figure 1.14. In the foreground, MSL's gargantuan backshell, with its human-scale access port that would later be used for MMRTG installation, covered with a custom-built aluminum platform for work access. Behind it, an enormous (and enormously expensive) rotisserie-type rig upon which the spacecraft could be stacked and inverted. In the background, the cruise stage comes together. October 16, 2008. Photo by Emily Lakdawalla.

worse, the growing complexity in the cross-strapping meant that the redundant systems might not actually be redundant:

The Rover Power Avionics Modules (RPAMs) were intended to be redundant boxes that cross-strapped power distribution as well as redundant analog and temperature telemetry across the system. As the number of spare power switches and telemetry channels eroded, adding additional cards to the RPAMs was considered. However the easily measured mass, volume, power, and cost implication of additional cards led to decision to instead make asymmetric connections amongst the existing cards. This asymmetry was justified by the use case where either string could be used for access to this telemetry and that in the event of a failure the loss of a non-redundant channel, the software or the ops team could find semi-graceful workarounds in flight base on inference from other channels and models. While feasible in principle, this asymmetric pattern was difficult to understand and led to confusion and testability shortcomings. It became very difficult to be able to say with certainty that loss of a redundant RPAM would be recoverable.⁴⁴

Having redundant computers imposed a requirement of having a lot of test duplicates in addition to the flight hardware, and late in 2008 it looked like there would not be enough hardware to go around. If it couldn't be tested, it couldn't be flown. They made the decision to redesign the avionics again so that only one of the two computer systems would run at any given time.⁴⁵ "Now the backup computer wouldn't be monitoring the prime computer, so couldn't take over immediately if the prime computer failed," Manning recalls. So they also had to redesign the fault protection systems that would protect the rover if one of the computers failed. The fault protection redesign encompassed both software and hardware, requiring internal cables to be rerouted.⁴⁶

JPL had three shifts working around the clock and on weekends to attempt to finish assembly on time. Working so many shifts was costly; the project requested another \$300 million from NASA in September, 2007. When I spoke with engineers during this period, they told me they felt up against a wall, and that no amount of money or additional staff would help.

Any of these things could have caused a mission delay. The motors finally broke the schedule. After many delays, JPL actually sent engineers on long-term detail to the supplier, Aeroflex Corporation of Long Island, to help with their development and delivery, and had both Aeroflex and JPL staff working multiple shifts to complete the work. But Aeroflex discovered new issues late in the testing process that delayed delivery of the flight units again.⁴⁷

⁴⁴ Welch et al (2013)

⁴⁵ Devereaux (2013)

⁴⁶ Manning and Simon (2014)

⁴⁷ Cook R (2009)

1.6 A TWO-YEAR RESPITE (2009–2010)

1.6.1 Launch delay

On December 4, 2008, NASA announced that MSL would miss the 2009 launch opportunity. The next planetary alignment would not come until late 2011. The round-the-clock development and testing of the spacecraft came to an abrupt halt.

The delay brought relief to MSL and made its success possible, but it cost NASA dearly: an additional \$400 million overrun brought the total price tag to \$2.3 billion. Effects of the MSL cost overruns ripple across NASA's planetary exploration program even today. Cancellations of technology development programs and lengthy delays in the announcements of new solar system mission proposal opportunities in the Discovery and New Frontiers programs, as well as NASA's withdrawal from cooperation on ESA's ExoMars project, can all be traced back to MSL's cost overruns.⁴⁸

The Department of Energy fueled the MMRTG just before NASA's announcement, on October 28, 2008.⁴⁹ They placed the MMRTG in cold storage at the Idaho National Laboratory. The plutonium was, of course, already decaying, so the rover would start Mars surface operations with less power than if it had launched in 2009.

NASA tried to minimize the budget impact of MSL's delay by allocating very little money to the project in 2009, shifting development toward 2010.⁵⁰ Richard Cook successfully fought for the project maintaining a team of engineers large enough to continue work on the major problems that had led to the delay. Motors and avionics were the two main ones, but smaller teams worked open issues on electrical systems, sample handling, test infrastructure, and software. The more visible pieces of the spacecraft, on which engineers had been laboring around the clock for months, were wrapped in plastic and moved to corners of the High Bay, not to be touched for a year (Figure 1.15). Most of the engineers who had been working on MSL were dispersed to other jobs, to be called back in mid-2010.

1.6.2 Becoming Curiosity

Despite the launch delay, NASA proceeded with a planned public contest to name the Mars Science Laboratory rover, running the contest from November 2008 to January 2009. More than 9,000 students (required to be between the ages of 5 and 18 and enrolled in a U.S. school) entered names and supporting essays into the contest. The winning entry, "Curiosity", was submitted by 12-year-old Clara Ma of Lenexa, Kansas, and announced on May 27, 2009:

Curiosity is an everlasting flame that burns in everyone's mind. It makes me get out of bed in the morning and wonder what surprises life will throw at me that day. Curiosity is such a powerful force. Without it, we wouldn't be who we are today.

⁴⁸ Green (2009)

⁴⁹ Woerner et al (2013)

⁵⁰ Manning and Simon (2014)



Figure 1.15. Panoramic view of the High Bay on March 16, 2009. The MSL hardware has been mothballed, and not an engineer is in sight. Photo by Emily Lakdawalla.

When I was younger, I wondered, ‘Why is the sky blue?’, ‘Why do the stars twinkle?’, ‘Why am I me?’, and I still do. I had so many questions, and America is the place where I want to find my answers. Curiosity is the passion that drives us through our everyday lives. We have become explorers and scientists with our need to ask questions and to wonder. Sure, there are many risks and dangers, but despite that, we still continue to wonder and dream and create and hope. We have discovered so much about the world, but still so little. We will never know everything there is to know, but with our burning curiosity, we have learned so much.

1.6.3 Problem solving

With schedule pressure reduced, the sample handling team added elements to deal with the concerns raised by Phoenix’ problems handling samples. They mounted prongs and other tools to the front of the rover to allow it to poke out stubborn gunk, and a “sample playground” with a tray, funnel, and other devices where they could dump sample for visual inspection (see section 5.7). They added wind baffles around the sample inlets and across the sample portioning device. They modified the sample portioner from a straight tube to an inverted funnel shape, to make sure sample material would not get stuck as it had on Phoenix.⁵¹

⁵¹Louise Jandura and Cambria Hanson, personal communication, interview dated June 3, 2016

The avionics team started over with one particularly challenging bit of the computer design: the asymmetric cross-strapping between the redundant main computers. They reduced the asymmetries, making the complex system slightly easier to understand and more straightforward to test.⁵²

Data on the final four landing sites poured in from the three Mars orbiters. The United States Geological Survey used overlapping pairs of high-resolution images to develop highly detailed digital terrain models of large swaths of the landing ellipses. Engineer Paolo Bellutta took algorithms developed for the Mars Exploration Rovers and applied them to the digital terrain models, making maps of the “traversability” of the terrain and estimating drive times to reach likely science targets from likely landing spots.

The delay permitted the team to solve ChemCam’s operational problems as well. Thermal engineers designed a thermo-electric cooler that could be incorporated into the ChemCam body unit and used to cool its detectors (see section 9.2.1.2). ChemCam’s spectrometers and housing had originally been built out of beryllium and magnesium rather than aluminum in order to save mass, but now mass wasn’t a factor. The addition of the coolers doubled ChemCam’s mass.⁵³ The end result was that ChemCam could actually be operated at almost any time of day, except for the hottest parts of summer afternoons.

The landing engineers worked on fiddly details of the order of events during landing, finding ways to shave off risk here and there. For example, after spending time with models and empirical tests of mobility system deployment, they shifted the event until quite late in the landing sequence, during the sky crane phase. Figure 1.16 depicts the entry, descent, and landing sequence in its final form.

Engineers on the landing team performed simulation after simulation, testing their landing system against a huge variety of landing-day scenarios, increasing their confidence in their system.

A fourth landing site selection workshop took place on September 27, 2010, to discuss the merits of the final four sites in the context of the new scientific results from Mars Reconnaissance Orbiter. All four sites remained possibilities.

Not all the development news was good. The Department of Energy measured the power output of the stored MMRTG on a quarterly basis. As of late summer 2009, the Department of Energy predicted that the MMRTG would be producing 110 watts of power on landing day, and planning proceeded according to that assumption. But the next measurement, taken in late 2009, revealed that the MMRTG was under-performing. Now they had two problems: the lower-than-predicted power levels and the mystery of why their modeling was not working.

Even before the delay, there had been insufficient power to run the rover. The delay gave them time to address the power problems by replacing the rover’s battery with one that had double the original capacity. Finding space for the new battery in the cramped interior of the warm electronics box required them to partially disassemble the rover. But the battery upgrade gave the rover about 1600 watt-hours of usable capacity, and ensured that power was rarely a limiting factor in running the rover for any but the most power-hungry activities, at least during the prime mission.⁵⁴

⁵² Manning (2014)

⁵³ Wiens et al (2012)

⁵⁴ Manning and Simon (2014)

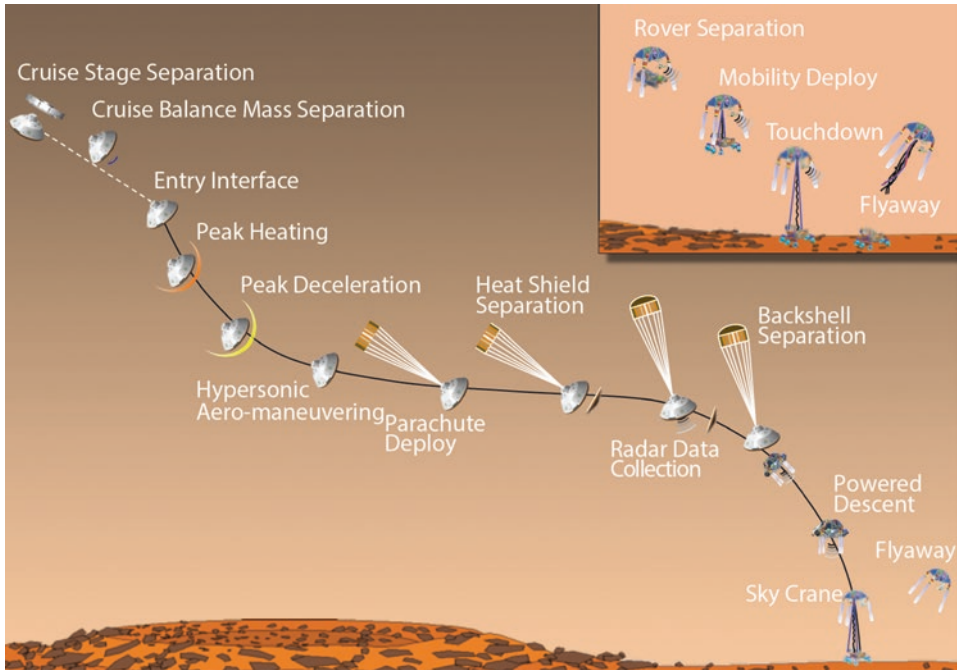


Figure 1.16. Schematic diagram of approach, entry, descent, and landing. From the Mars Science Laboratory launch press kit, November 2011. Minor changes from previous diagrams include a very late deployment of the wheels and an emphasis on the lengthy period of near-horizontal flight during the “hypersonic aero-maneuvering” phase.

1.7 FINAL PREPARATIONS (2010–2011)

1.7.1 ATLO, again

The redesigned motors finally began to arrive at JPL in 2009, with the flight models being delivered in 2010. Assembly of the rover began in June 2010 and proceeded rapidly. The legs and wheels were attached at the end of June, as was the mast with all its cameras and ChemCam (Figure 1.17). The rover first spun all six wheels on July 9, and drove on its wheels for the first time on July 23 (Figure 1.18). The arm was attached in August, and put through its paces with the rover sitting at tilts of up to 20° (Figure 1.19).

With the spacecraft finally coming together, systems engineers could begin to test how all the subsystems functioned together – and make sure that the spacecraft safely handled problems. Engineers performed a series of system tests, each focused on a different mission phase. In parallel, engineers took all components of the spacecraft into JPL’s thermal vacuum chamber to perform environmental tests. The chamber simulates the harsh environments of deep space and the Mars surface (Figure 1.20). It can be pumped down to near-vacuum, cooled with liquid nitrogen, and lit with thirty-seven 25,000-watt xenon lamps to simulate direct solar heating in deep space.⁵⁵

⁵⁵ JPL (2010)



Figure 1.17. Mobility system installation, 29 June 2010. NASA/JPL-Caltech release PIA13234.



Figure 1.18. The rover's first drive, 23 July 2010. The corner wheels are steered into position to allow the rover to turn in place. NASA/JPL-Caltech release PIA13308.



Figure 1.19. Testing out the arm's positioning from a tilted rover, 16 September 2010. NASA/JPL-Caltech release PIA13389.

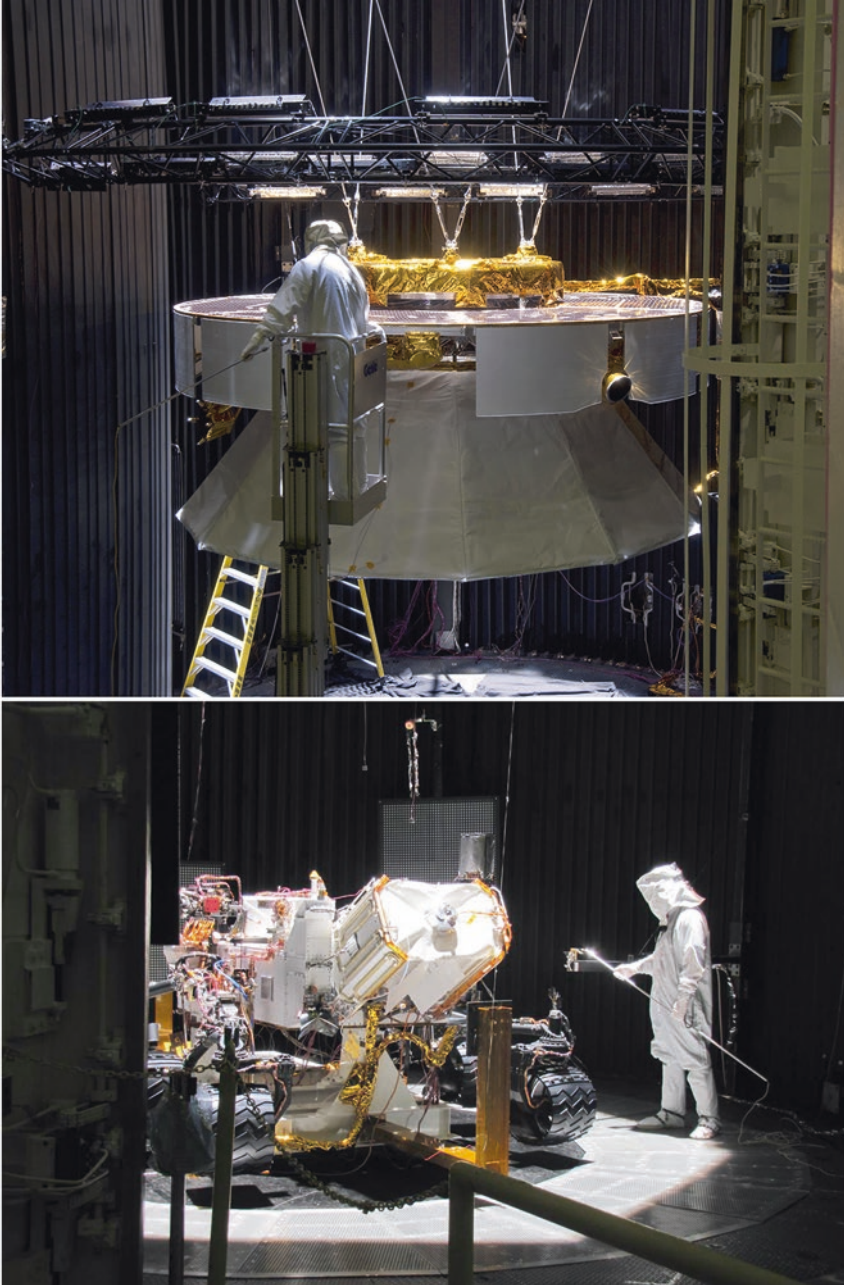


Figure 1.20. Thermal vacuum testing. Top: The cruise stage and backshell, August 24, 2010. Bottom: The rover during Surface Test 8, March 8, 2011. NASA/JPL-Caltech releases PIA13359 and PIA13806.

Despite various hiccups, the tests were mostly successful, demonstrating that the spacecraft could function through entry, descent, and landing, and in surface operational scenarios. The final system test, which took place after the spacecraft had been shipped to Florida, simulated three days of typical science activities on the surface, proving that the flight system was ready for Mars. But only just. The tight schedule and complexity of interacting systems meant that the system software was not particularly mature.

Public information officers began to stir up public interest in the mission. On June 24, 2011, NASA released a computer animation depicting the launch, cruise, and landing of the rover. The animation had been directed by JPL visualization artist Doug Ellison and produced by animator (and former JPL artist) Kevin Lane, who packed the thrilling video with accurate details of the landing sequence, informed by research and interviews with engineers (Figure 1.21).

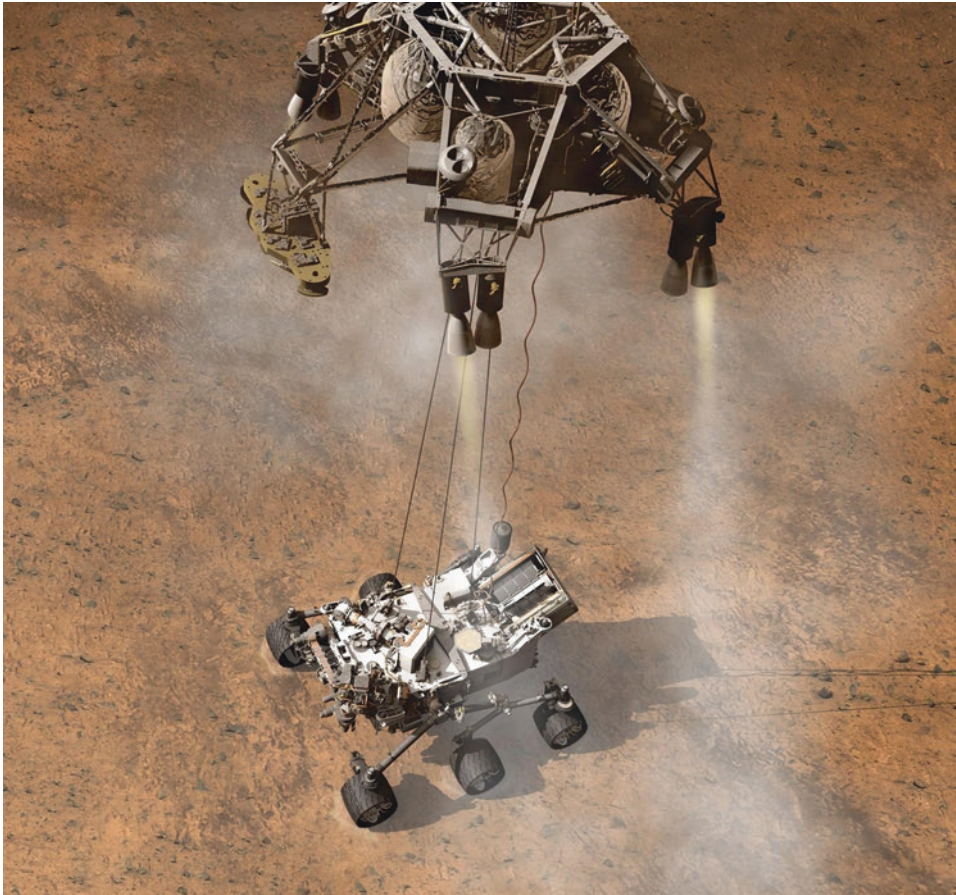


Figure 1.21. The moment of touchdown as depicted in the landing animation. NASA/JPL-Caltech release PIA14840.

1.7.2 Going to Gale

The fifth and final community workshop on landing site selection opened on May 16, 2011. Engineers remained confident that their entry, descent, and landing system could handle any of the four landing sites under discussion. Scientists pored over the data collected by Mars Reconnaissance Orbiter and Mars Express on the four sites and debated the scientific questions that could be answered at each one. The workshop produced no specific recommendation, but gave the MSL science team the background they needed to discuss the merits of the four landing sites at a team meeting on May 18.

Based on the wider community and narrower team discussions, the project science group (a committee of all of the instrument principal investigators) selected Gale crater as its top choice. In addition to its compelling scientific targets of layered rocks and alluvial fans, it was also the lowest-elevation and most equatorial of the four proposed sites, the most benign landing case. It had some possibility for science within the landing ellipse, but most of its science would be on a go-to mission, driving beyond the ellipse to reach mineral-bearing rocks at the base of the crater's central mountain (Figure 1.22).

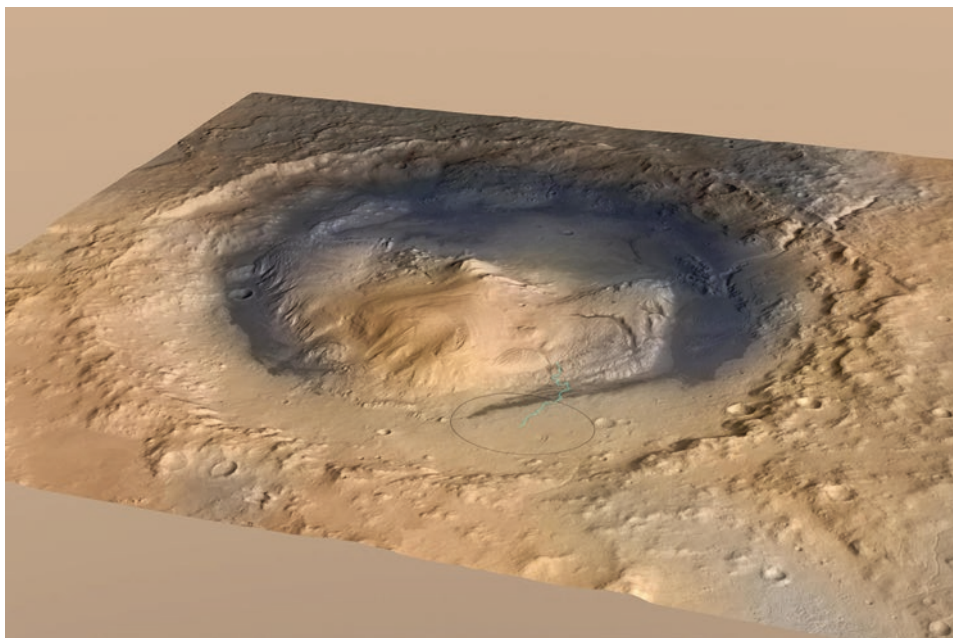


Figure 1.22. Oblique view of Gale crater. The black landing ellipse is 25-by-20 kilometers in extent. The blue line shows a possible route for Curiosity to ascend the mountain. NASA/JPL-Caltech/ESA/DLR/FU Berlin/MSSS release PIA15292.

The project science group recommended Gale and Eberswalde as potential landing sites to NASA, preferring Gale. The final decision would be made at NASA Headquarters. The landing site selection committee gave a presentation to an independent landing site certification board on June 9 and 10, 2011. The NASA Planetary Protection Office

reviewed the four sites for compliance with planetary protection provisions on June 23. The next day, the MSL project presented the four sites to NASA Headquarters representatives, who concurred with the downselection to Eberswalde and Gale. They reconvened a month later and recommended Gale. NASA announced the selection of Gale crater as Curiosity's landing site on July 22, 2011.

1.7.3 Journey to Florida

As Earth crept toward Mars on its inside track around the Sun, the once-every-26-months launch period approached. NASA had missed the intended window in 2009; they could not afford to miss the 2011 window. Between May and November 2011, all of the pieces of the interplanetary spacecraft would come together at Kennedy Space Center in Florida.

On May 12, 2011, a C-17 transport plane carried the heat shield, backshell, and cruise stage from California to Florida. A scary event happened during processing of the spacecraft on May 20. A crane operator accidentally lifted the backshell and the support cart that the backshell was attached to off of the ground, exerting unplanned loads on the backshell. There was no obvious damage, but engineers scrambled to figure out whether the weight of the cart suspended from the backshell could have damaged it. They determined that the backshell was designed robustly enough to withstand the additional load of the cart, and assembly could proceed as normal.⁵⁶ But the incident ratcheted up the tension on the launch preparations.

Meanwhile, tests continued on the rover back at JPL at a feverish pace. It was finally buttoned up and transported to Florida, along with the descent stage, on June 23. The Department of Energy delivered the MMRTG on June 30. Components of the Atlas V rocket arrived at Kennedy aboard the Delta Mariner barge a month later.

1.7.4 Planetary protection jeopardy

Problems with the drill bits dogged the mission right up until launch. Early in 2011, the project discovered that residue from oil used in manufacturing the test drill bits was contaminating drilled samples. If there was similar oil on the flight drill bits, it could invalidate SAM's attempts to search for Martian organic compounds. By March, they had figured out how to re-manufacture the drill bits, and planned to deliver them just in time for the rover to be shipped to Florida.⁵⁷

The SAM team had to know whether the flight drill bits also carried traces of hydrocarbons. In Florida, a team of contamination control engineers opened the sterile bit enclosures to check for the oil residue. They found no contamination – but in checking for oil contamination, they had broken the sterile seal on the bits, and the bits were not re-sterilized. Even if they had not checked for the oil contamination, they would have had to break the sterile containment of one of the bits to install it on the rover, because of a change in mission plan. Originally, Curiosity was to have launched to Mars with all three

⁵⁶NASA Office of Inspector General (2011)

⁵⁷Manning and Simon (2014)

bits enclosed in sterile boxes, and only break that seal upon arriving at Mars and loading the first bit in the drill. The mission decided it was too risky to launch without one bit preloaded. That bit was not in sterile wrapping throughout the rover's delivery to Florida and assembly operations, in violation of the mission's planetary protection plan.

The wheels represented another vector by which Earth microbes could contaminate Mars. They were heat-sterilized and wrapped to prevent recontamination during final assembly. But the planetary protection requirements weren't specific about when it was permissible to unwrap the wheels, with ambiguous requirements like "The flight wheels shall be mounted on the rover as late as possible and will be covered as much as possible to prevent recontamination."⁵⁸ Photos from the Kennedy Space Center show that the wheel wrappings were removed just after delivery, on June 27. The final system tests were performed in July and August with the wheels unwrapped and resting on the floor (Figure 1.23). They were re-wrapped before the spacecraft was stacked to the descent stage and back-shell in late September, and the wrappings removed for the final time before heat shield encapsulation in early October.



Figure 1.23. Engineers at Kennedy Space Center test out the rover's motor functions, July 18, 2011. NASA/KSC release KSC-2011-5919.

⁵⁸NASA Office of Planetary Protection (2014)

The lack of sterile containment of both wheels and drill bits was “a clear violation” of the mission’s planetary protection requirements.⁵⁹ The Office of Planetary Protection did not learn of the violation until less than three months before the launch, in mid-September. On September 20, Peter Theisinger formally requested permission to deviate from the requirements, and the Office of Planetary Protection rejected that request. The violation of planetary protection requirements had the potential to jeopardize Curiosity’s on-time launch.

Not enough time remained to remove, sterilize, and replace the drill bits and wheels before the launch. The only way out was a bureaucratic one: to reclassify the mission to a lower planetary protection standard. Fortunately, with its low elevation and equatorial location, Gale crater is a site where no ground ice was expected to be anywhere close to the surface, so a landing failure had no potential to create a spacecraft-induced special region (see section 1.4.5). That made it possible to reclassify the mission from planetary protection category IVc down to category IVa, reserved for “lander systems not carrying instruments for the investigations of extant martian life” that will not come into contact with any special region.⁶⁰

Catherine Conley, NASA’s planetary protection officer, formally recategorized the mission to category IVa on November 1. “Violation of NASA planetary protection requirements represents a significant risk to the MSL project,” she wrote in a letter to mission and NASA management. “Requesting a planetary protection deviation of this magnitude, so late in the project lifecycle, is improper.” She singled out the wheels as representing the greatest risk for contaminating Mars, and imposed restrictions on the rover’s future exploration activities:

The project is prohibited from introducing any hardware into a Mars Special Region, as defined in NASA Procedural Requirements document NPR 8020.12D. Fluid-formed features such as Recurring Slope Lineae are included in this prohibition. Any evidence suggesting the presence of Special Regions or flowing liquid at the actual MSL landing site shall be communicated to the Planetary Protection Officer immediately, and physical contact by the lander with such features shall be entirely avoided.

1.7.5 Final assembly

Finally, the time came to put together all the pieces of the puzzle. The rover and MMRTG met for the first time for a fit check on July 12. The MMRTG produces a prodigious amount of heat, so it wasn’t safe to install it permanently until the last possible moment. Handlers removed the MMRTG to storage in its own cavernous, climate-controlled room.

Assembly was interrupted in September by an emergency situation discovered during drill testing back at JPL. The drill percussion mechanism developed a short circuit that could damage the rover’s electronics if it occurred on Mars, jeopardizing the mission. The engineers developed a solution quickly, but implementing the solution required opening up the rover’s belly pan and adding a new wire to ground the rover’s power bus. This “battle short” wouldn’t prevent future shorts in the drill, but would protect the rover’s

⁵⁹ Stabekis (2012)

⁶⁰ United Nations COSPAR (2011) COSPAR Planetary Protection Policy

electronics if it happened again. The project agreed to take the risky step of performing surgery on the rover just weeks before launch.⁶¹ It turned out to be a wise decision, as the drill percussion mechanism has indeed experienced shorts on Mars (see section 5.3.4.2).

Stacking of the spacecraft components began inside the Payload Hazardous Servicing Facility on September 23, with the connection of the descent stage to the rover and then the backshell. They topped the stack with the cruise stage on October 10, and lifted the stack onto the base of the heat shield on October 11, completing the assembly of the spacecraft, except for the MMRTG (Figure 1.24).

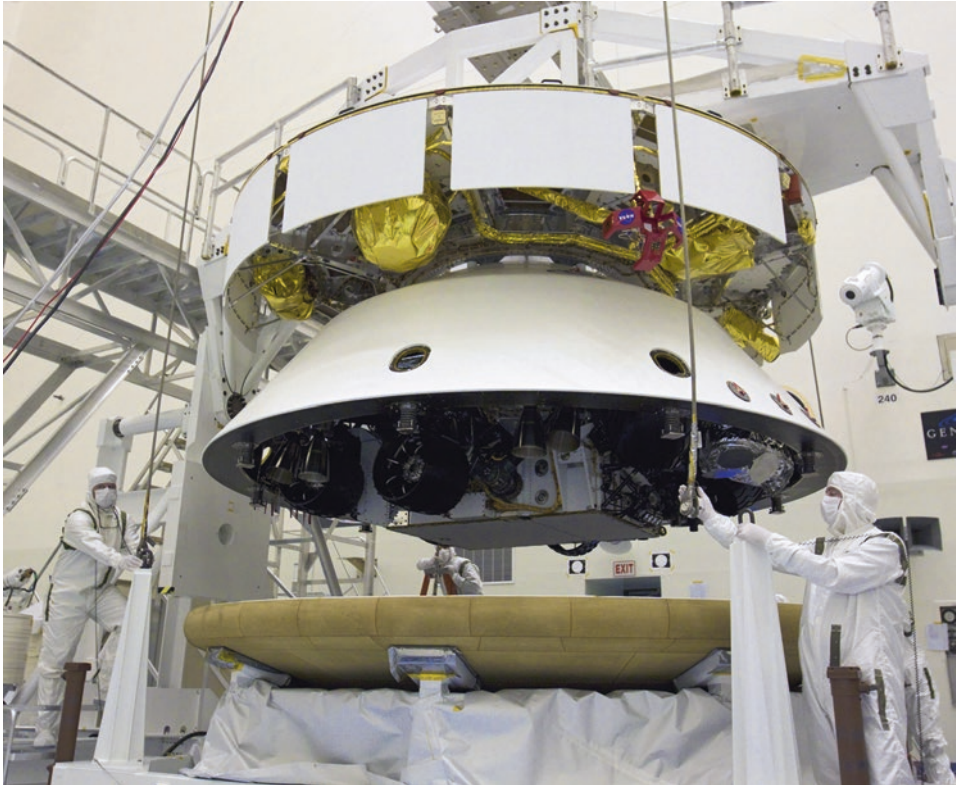


Figure 1.24. On October 11, 2011, the spacecraft stack was completed. NASA/KSC release KSC-2011-7350.

Two weeks later, with the spacecraft flipped upside down, they enclosed the saucer-shaped craft inside the fairing that would protect the spacecraft during its trip through Earth's atmosphere (Figure 1.25). MSL needed the full width of the Atlas V's largest, 5-meter fairing, but little of the length; most of the interior of the tall fairing remained

⁶¹Manning and Simon (2014)

empty. They delivered the spacecraft in its nose cone to the launch pad on November 3, then hoisted it atop the rocket (Figure 1.26).



Figure 1.25. MSL is dwarfed by its fairing, October 25, 2011. NASA/KSC release KSC-2011-7530.

The final step in assembly took place at the top of the tower just a week before launch. The MMRTG was finally installed on November 17 (Figure 1.26). A hatch in the fairing, and a matching hatch in the aeroshell, allowed technicians access to insert the MMRTG, and then to sew on the cloth windbreak over the MMRTG's cap (Figure 1.27). With the MMRTG in place, cooling the spacecraft became a top priority. An air conditioning system in the launch tower blew chilled air through an inlet in the fairing onto the cruise stage radiators, helping to dissipate the heat for the week that led up to launch.



Figure 1.26. Workers lift the MMRTG, in a protective cage, to the top of the Atlas V rocket in its launch tower on November 17, 2011. NASA/KSC release KSC-2011-7836.



Figure 1.27. Engineers work through a hatch in the rocket fairing and a second hatch in MSL's backshell to install the MMRTG onto the rover, November 17, 2011. NASA/KSC release KSC-2011-7900.

1.8 REFERENCES

- Benardini J et al (2014) Implementing planetary protection measures on the Mars Science Laboratory. *Astrobiology* 14:27–32, DOI: 10.1089/ast.2013.0989
- Billing R and Fleischner R (2011) Mars Science Laboratory Robotic Arm. Paper presented to the 15th European Space Mechanisms and Tribology Symposium, Constance, Germany, 2011
- Boeing Rocketdyne Propulsion and Power (2003) Boeing to Build Space-borne Power Generator. Press release dated 1 Jul 2003
- Boynton W et al (2002) Distribution of hydrogen in the near surface of Mars: Evidence for subsurface ice deposits. *Science* 297:81–85, DOI: 10.1126/science.1073722
- Caffrey R et al (2004) Initiating the 2002 Mars Science Laboratory (MSL) Focused Technology Program. Paper presented to the 2004 IEEE Aerospace Conference, Big Sky, Montana, USA, 6–13 Mar 2004, DOI: 10.1109/AERO.2004.1367650
- Conley C (2011) MSL deviation request. Letter to Peter Theisinger dated 1 Nov 2011
- Cook R (2009) MSL Technical and Replan Status. Presentation to the NASA Planetary Science Subcommittee meeting, Washington, DC, USA, 9 Jan 2009
- Cook R (2011) Mars Science Lab: The Challenge of Complexity. *Ask Magazine* issue 42 (Spring 2011)

- Cooper C (2005) New NASA Chief Visits JPL. La Cañada Valley Sun, 2 Jun 2005
- Devereaux A (2013) Landing Curiosity: System Engineering Challenges for NASA's Newest Martian. Presentation to the 11th Annual Conference on Systems Engineering Research, Atlanta, Georgia, USA, 19–22 Mar 2013
- Devereaux A and Manning R (2012) Challenges of MSL entry, descent and landing validation; or, '7 years of terror'. Presentation to NASA Workshop of Validation of Autonomous Systems, Pasadena, CA, USA, 20 Aug 2012
- Golombek M et al (1999) Overview of the Mars Pathfinder Mission: Launch through landing, surface operations, data sets, and science results. *J. Geophys. Res.* 104:8523–8553, DOI: 10.1029/98JE02554
- Golombek M et al (2012) Selection of the Mars Science Laboratory Landing Site. *Space Sci. Rev.* 170:641–737, DOI: 10.1007/s11214-012-9916-y
- Green J (2009) Options for Accommodating the MSL Launch Slip. Presentation to the NASA Planetary Science Subcommittee meeting, Washington, DC, USA, 9 Jan 2009
- JPL (2010) Mars Science Laboratory's Cruise Stage in Test Chamber. <http://photojournal.jpl.nasa.gov/catalog/PIA13359>. Photo released 2 Sep 2010, accessed 17 Jun 2016
- JPL (2014a) Lesson Learned: MSL Actuator Design Process Escape. <http://llis.nasa.gov/lesson/11501>. 9 Sep 2014, accessed 14 Oct 2015
- JPL (2014b) Lesson Learned: Recognize that Mechanism Wear Products May Affect Science Results. <http://llis.nasa.gov/lesson/10801>. Article dated 8 Jun 2014, accessed 14 Oct 2015
- Lawler A (2008) Space Science: NASA's Stern quits over Mars exploration plans. *Science* 320:31, DOI: 10.1126/science.320.5872.31
- Malin M and Edgett K (2000) Sedimentary Rocks of Early Mars. *Science* 290:1927–1937, DOI: 10.1126/science.290.5498.1927
- Manning R and Simon W (2014) Mars Rover Curiosity. Smithsonian Books, Washington, DC
- Mars Program Synthesis Group (2003) Mars Exploration Strategy 2009–2020
- Mars Science Laboratory Mission Project Science Integration Group (PSIG) (2003) Final Report, 6 Jun 2003
- Mustard J (2007) Summary of the meeting between Alan Stern and MEPAG representative. Letter to MEPAG stakeholders dated 5 Oct 2007
- NASA (2000a) Mars Program Independent Assessment Team Summary Report, 14 Mar 2000
- NASA (2000b) NASA outlines Mars exploration program for next two decades. Press release dated 26 Oct 2000
- NASA (2001) Mars Exploration Program Mars 2007 Smart Lander Mission Science Definition Team Report, 11 Oct 2001
- NASA (2004) Mars Program Mars Science Laboratory Mission 2009 Landed Science Payload Proposal Information Package. 14 Apr 2004
- NASA (2004) NASA Selects Investigations for the Mars Science Laboratory. Press release dated 14 Dec 2004
- NASA (2007) Mars Science Laboratory Project Changes Respond to Cost Increases, Keep Mars Program On Track. Press release dated 17 Sep 2007

- NASA (2008) Next NASA Mars Mission Rescheduled for 2011. Press release dated 4 Dec 2008
- NASA (2009) NASA Selects Student's Entry as New Mars Rover Name. Press release dated 27 May 2009
- NASA Office of the Inspector General (2011) NASA's Management of the Mars Science Laboratory Project. Report dated June 8, 2011
- NASA Office of Planetary Protection (2014) MSL Lessons Learned Presentation. Presentation to NASA Advisory Council Planetary Protection Subcommittee, Washington, DC, USA, 20 May 2014
- Novak K et al (2008) Mars Science Laboratory rover actuator thermal design. Presentation to the Spacecraft Thermal Control Workshop, El Segundo, CA, USA, 11–13 Mar 2008
- Rummel J (2006) Mars Science Laboratory Planetary Protection Landing Site Constraints. Presentation to the First Landing Site Workshop, Monrovia, CA, USA, May 31-June 2, 2006
- Rummel J et al (2014) A new analysis of Mars "Special Regions." Findings of the second MEPAG Special Regions Science Analysis Group (SR-SAG2)
- Slimko E et al (2011) MSL Heatshield Development: From Failure to Success. Paper presented to the 2011 IEEE Aerospace Conference, Big Sky, Montana, USA, 5–12 Mar 2011, DOI: 10.1109/AERO.2011.5747500
- Stabekis P (2012) Mars Science Laboratory (MSL): Planetary Protection Lessons Learned. Presentation to NASA Advisory Council Planetary Protection Subcommittee, Washington, DC, USA, 19 Dec 2012
- Stern A and Green J (2007) Announcement from Alan Stern & Jim Green, NASA Headquarters. Letter to the Mars community dated 8 Nov 2007
- Udomkesmalee S G and Hayati S (2005) Mars Science Laboratory Focused Technology Program Overview. Paper presented to the 2005 IEEE Aerospace Conference, Big Sky, Montana, USA, 5–12 Mar 2005, DOI: 10.1109/AERO.2005.1559387
- United Nations COSPAR (2011) COSPAR Planetary Protection Policy
- Vasavada A (2006) Mars Science Laboratory Project and Science Overview. Presentation to the First Landing Site Workshop, Monrovia, CA, USA, May 31-June 2, 2006
- Wallace M (2012) Curiosity: The Next Mars Rover. Presentation to the Royal Aeronautical Society, Applied Aerodynamics Group Conference, 17–19 Jul 2012, London, UK
- Watkins M (2008) MSL Project Status and Landing Site Selection Schedule. Presentation to the 3rd MSL Landing Site Selection Workshop, Monrovia, CA, USA, 15–17 Sep 2008
- Watkins M and Steltzner A (2007) MSL landing site selection: Status of Engineering Capabilities and Constraints and Plan for Site Selection. Presentation to the 2nd MSL Landing Site Selection Workshop, Monrovia, CA, USA, 23–25 Oct 2007
- Welch R et al (2013) Systems Engineering the Curiosity Rover: A Retrospective. Paper presented to the 8th International Conference on System of Systems Engineering, Maui, Hawaii, USA, 2–6 Jun 2013, DOI: 10.1109/SYSSE.2013.6575245
- Wiens R et al (2012) The ChemCam Instrument Suite on the Mars Science Laboratory (MSL) Rover: Body Unit and Combined System Tests. *Space Sci. Rev.* 170:167–227, DOI: 10.1007/s11214-012-9902-4
- Wiens R (2013) *Red Rover*. New York: Basic Books.
- Woerner D et al (2013) The Mars Science Laboratory (MSL) MMRTG In-Flight: A Power Update. Paper presented at Nuclear and Emerging Technologies for Space, Albuquerque, New Mexico, USA, 25–28 Feb 2013

2



Getting to Mars

2.1 LAUNCH

Mars launch opportunities happen about every 26 months, as Earth begins to approach Mars from behind on its faster inside track around the Sun. The earliest MSL could launch was November 25, 2011; any earlier, and it would arrive at Mars with too much speed for the entry, descent, and landing system to dissipate. The latest it could launch was December 18; any later, and the Atlas V 541 rocket wouldn't have enough thrust to deliver the spacecraft to its rendezvous point with Mars.

Within that 24-day period, no matter the launch date, MSL would arrive at Mars within a 15-minute window on August 6, 2012. That choice of timing allowed both Mars Reconnaissance Orbiter and Mars Odyssey to be in position to perform relay communications during MSL's landing without any adjustment to their orbits. The orbiter relays were crucial, because only 5 minutes after atmospheric entry, Mars would block the visibility of MSL's direct-to-Earth radio communications.

The first day of the launch period was also the day after the Thanksgiving holiday. MSL team members gathered with their families in Florida resorts and timeshares, feasting and awaiting the fireworks at Kennedy Space Center. On November 19, NASA announced a one-day delay to replace a flight termination system battery.

MSL launched at 15:02:00 UT (10:02 a.m., local Florida time) on Saturday, November 26, 2011 (Figure 2.1). The Atlas V Common Core Booster ignited first, combusting kerosene with liquid oxygen. The four solid rocket boosters lit up a split second later. The solids burned out after 90 seconds and were jettisoned 22 seconds after that. At launch plus 3 minutes 22 seconds, the clamshell of the payload fairing split open, exposing the spacecraft to space for the first time. Another minute later, the Atlas engine shut down and separated from the Centaur upper stage (Figure 2.2).¹

¹ Details of the launch and cruise events throughout this section are from Abilleira (2013)



Figure 2.1. MSL launched on an Atlas V 541 from the Eastern Test Range of Cape Canaveral Air Force Station at 15:02:00 UT (10:02 a.m., local Florida time) on Saturday, November 26, 2011. Scott Andrews/Canon.

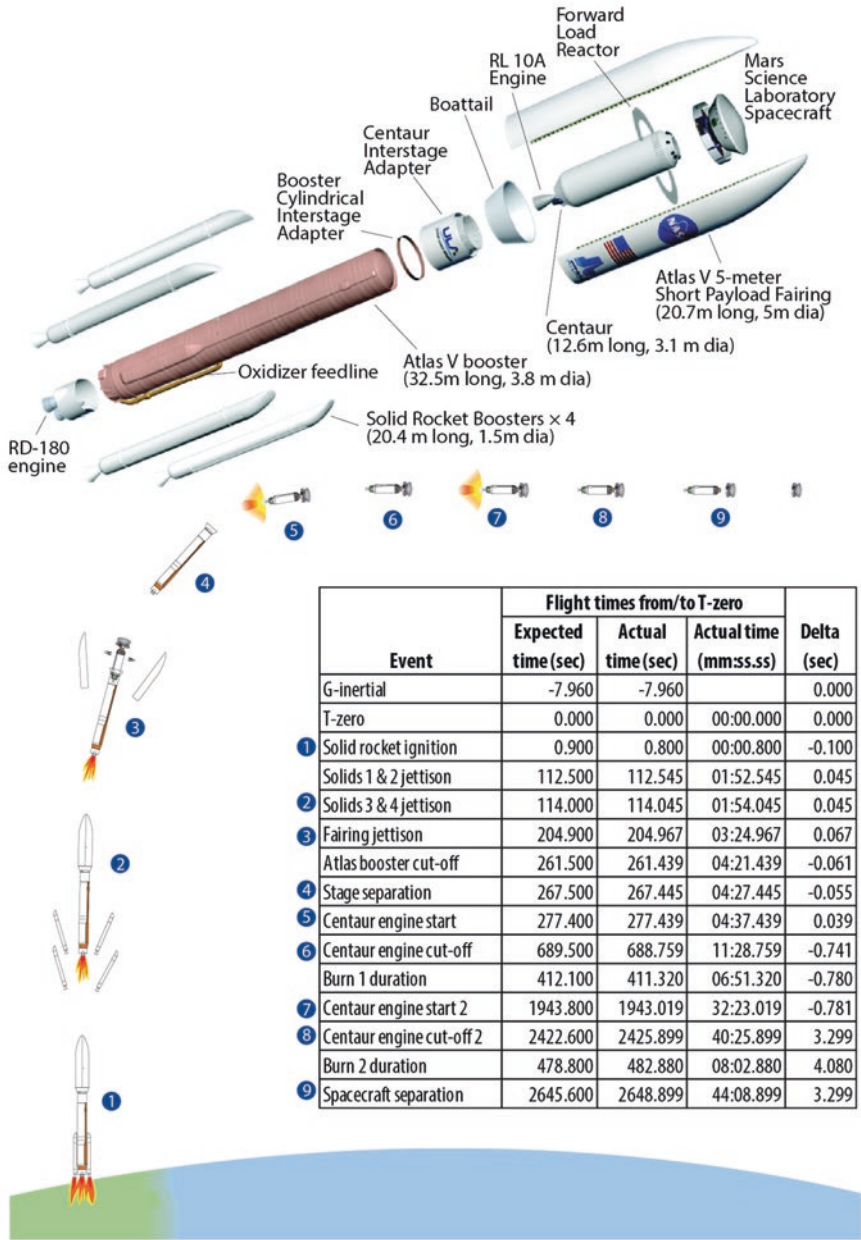


Figure 2.2. Atlas V 541 launch vehicle facts and timeline. Modified from United Launch Alliance press kit.

60 Getting to Mars

Four minutes 37 seconds after launch, the Centaur ignited and burned liquid hydrogen in oxygen for 7 minutes, placing the spacecraft into a 165-by-265 kilometer parking orbit at an inclination of 28.9°. It coasted for 20 minutes. During the coast phase, MSL was active, reporting via the launch vehicle's radio through the Tracking Data Relay System satellites to Earth that the solar cells on the cruise stage were generating power, charging the batteries.

Thirty-two minutes and 23 seconds after launch, the Centaur ignited again, burning for 8 minutes to inject MSL onto its transfer trajectory to Mars. This burn deliberately targeted the spacecraft slightly away from Mars, in order to prevent the non-sterilized Centaur upper stage from impacting the Martian surface and potentially contaminating it. With the trans-Mars injection achieved, the Centaur performed one last maneuver, spinning up the spacecraft to 2 rotations per minute. Finally, 44 minutes after launch, pyrotechnics cut the spacecraft's connection to the Centaur, and push-off springs shoved it gently away at a relative velocity of 0.27 meters per second (Figure 2.3).

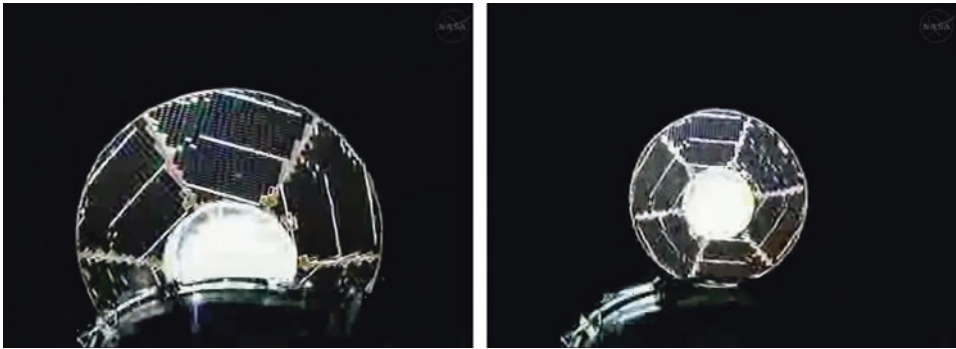


Figure 2.3. RocketCam views of the departing MSL spacecraft following separation from the Centaur upper stage. The six sets of cruise stage solar arrays are visible. Screen captures from NASA Television broadcast, November 26, 2011.

With spacecraft separation achieved, MSL was on its own. The spacecraft waited 1 minute in order to avoid interference with the Centaur's continuing radio communications. Then it turned on its amplifier, powered up the transmitter, and contacted Earth directly for the first time. As MSL zoomed away from Earth, Australia's deep-space communications dishes listened. Within 20 seconds, a ground station in Dongara, Western Australia, locked onto its carrier signal; two dishes (DSS-45 and DSS-34) in Canberra achieved carrier lock 2 seconds later. Within another 30 seconds, the stations achieved telemetry lock, successfully decoding the signal to receive MSL's reports of spacecraft health. This initial telemetry confirmed that the spacecraft was thermally stable, generating power, and was commandable. That state of affairs meant that the launch phase was over; the cruise phase had begun. Later analysis of the trajectory would reveal that "the trans-Mars injection and spacecraft separation provided by the Centaur was outstanding and set a new standard on launch vehicle performance."²

²Abilleira (2013)

2.2 CRUISE

2.2.1 The cruise stage

The cruise stage made MSL an interplanetary spacecraft (Figure 2.4). It sensed the Sun, tracked the stars, generated power, kept the rover cool, and performed trajectory correction maneuvers to steer the spacecraft's course to Mars. It did not have independent telecommunications capability. A cone-shaped medium gain antenna mounted to the cruise stage relied upon transmitting and receiving hardware buried in the descent stage. The cruise stage weighed 466.5 kilograms when dry, and carried 73.8 kilograms of propellant.³

To aid navigation, the cruise stage carried one star scanner and two sun-sensor assemblies, each of which had four sensors pointed in different directions. One sun-sensor assembly was connected to each of the rover's two computers. The cruise stage had no independent brain, relying instead on the rover's computers.

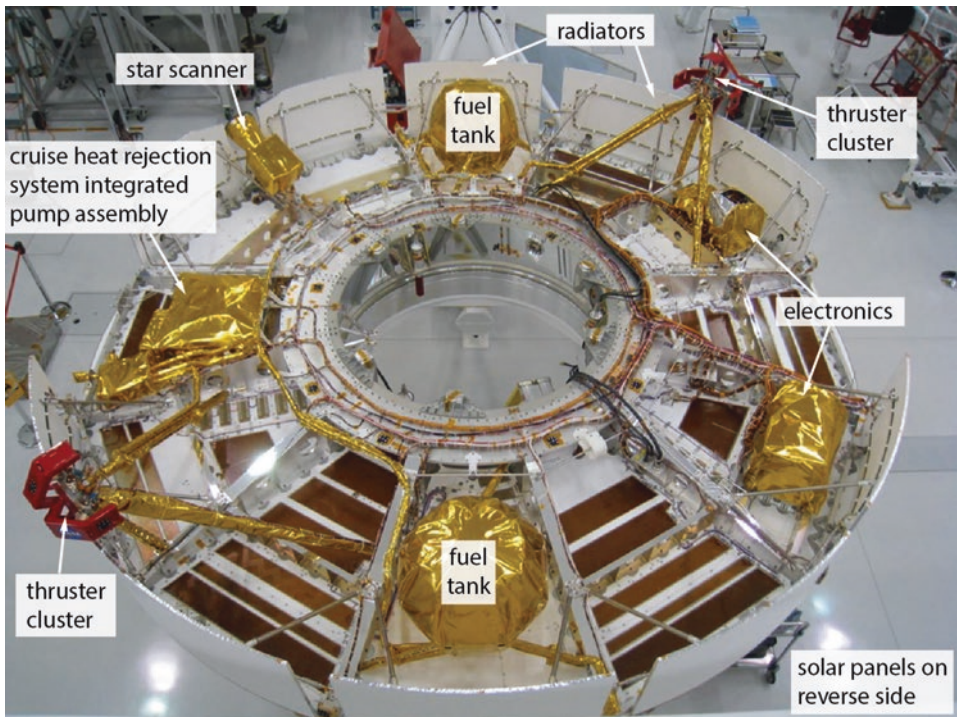


Figure 2.4. Cruise stage parts as seen at JPL in late 2008. The thruster clusters are enclosed in protective cages (red) that were removed before launch. NASA/JPL-Caltech release PIA11440, annotated by Emily Lakdawalla.

³Allen Chen, personal communication, email dated July 1, 2016, correcting numbers published before launch

MSL's power system was incredibly complex, due in part to its being controlled by the rover avionics. Although the cruise stage derived power from solar arrays, the power had to be passed through the descent stage to the rover avionics for maintenance of voltage stability and power levels. To generate power, the cruise stage had 6 arrays of solar cells (visible in Figure 2.3), capable of producing as many as 2500 watts of power at Earth's distance from the Sun. As the spacecraft approached Mars, the power output would diminish to about 1000 watts, both because of the increasing distance and because the solar panels would no longer be pointed directly at the Sun.

Keeping the interior of the interplanetary spacecraft cool was a major challenge during cruise, just as it was during the final launch preparations. Encased within the aeroshell, the MMRTG sat in close proximity to pressurized fuel tanks for the descent stage whose temperature should not rise above 30°C. The 2000 watts of waste heat that the MMRTG generated needed to be radiated to space. Using fluid running inside metal tubing, the cruise stage gathered heat from within the aeroshell. The cruise stage had a redundant pair of pumps (only one in use at a time) that moved Freon through 70 meters of tubing in the Cruise Heat Rejection System (CHRS). The flowing Freon gathered heat from the cold plates of the rover's heat exchanger and the roots of the MMRTG fins, then carried it behind the 10 cruise stage radiators (read section 4.4 for more about rover thermal control). After passing the last radiator, the tubing carried cool fluid past heat exchanger plates on electronic components of the cruise and descent stages before returning to the rover.⁴ The connections between CHRS and the rover were severed with pyros shortly before landing; the now-disused tubing is still being carried around on Mars by the rover (see Figure 2.29).

For propulsion, the cruise stage had two propellant tanks, each 48 centimeters in diameter. The tanks fed two thruster clusters, each of which consisted of four 5-newton thrusters pointed in different directions. Two of the thrusters in each cluster were "axial", and were tilted 40° away from the spacecraft's axis of rotation (one each toward the positive and negative ends of the axis). Continuously firing the axial thrusters decreased or increased the speed of the spacecraft in the direction of its rotation axis. The other two thrusters in each cluster were oriented perpendicular to the spin axis. They could be used to change the lateral speed of the spacecraft by being pulsed for 5 seconds at a time, twice per two-minute revolution.⁵

2.2.2 Cruise phase

Figure 2.5 illustrates MSL's cruise trajectory. Just three days after launch, on November 29, the spacecraft went into safe mode while attempting to use its star scanner to determine its orientation. It took weeks to track down the root cause of the problem: "a previously unknown design idiosyncrasy in the memory management unit of the MSL computer processor. In rare sets of circumstances unique to how this mission uses the processor, cache access errors could occur, resulting in instructions not being executed properly."⁶ Because the problem originated in hardware, not software, it could not be repaired, only worked around.

⁴Bhandari et al (2011)

⁵Abilleira (2013)

⁶JPL (2012a)

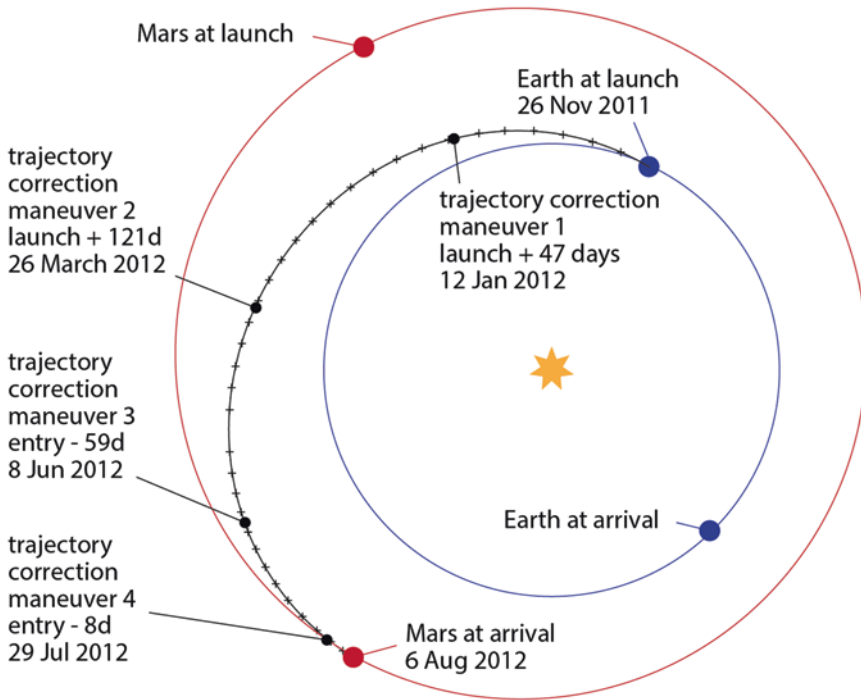


Figure 2.5. Schematic diagram of MSL cruise trajectory between Earth and Mars. Time ticks on MSL trajectory are placed every 20 days. Modified from NASA/JPL-Caltech landing press kit.

Without use of the star scanner, the spacecraft could not turn to keep its solar panels and radio antenna precisely pointed at Earth. A planned December 11 trajectory correction maneuver couldn't be performed without turning the spacecraft. Without the star scanner they couldn't determine the spacecraft's orientation and spin rate precisely, as required to time the position and duration of the multiple jet firings for the maneuver. With every passing day, the spacecraft's orientation drifted farther away from the optimal direction, so engineers rushed to develop a solution to the problem.

The mission formed a Tiger Team to try to understand the reboots triggered by the use of the star tracker. Fortunately, the initial trajectory toward Mars was so close to predictions that the mission was able to delay the necessary maneuver by a month. Still, they were unable to solve the problem before the need for the maneuver pressed. To get the orientation and spin rate information that they needed, navigators employed a trick that had been developed during a similar circumstance on Pathfinder. They measured the minute Doppler shift of the spacecraft's radio signal, caused by the spacecraft's spin; the Doppler showed up as a sine wave in the radio frequency. From the magnitude of the Doppler signal, they determined the orientation of the spacecraft. With that knowledge, they were able to command the maneuver with sufficient precision.

By far the largest of all of the deep-space course changes, the January 11, 2012 maneuver changed the spacecraft's speed by 5.635 meters per second, at a cost of about 18 kilograms of fuel. It wasn't perfectly aligned, but it was close enough for later maneuvers to clean up any errors.⁷ In early February, engineers applied a software update to avoid use of the memory functions that triggered the safe mode.

The mission used the otherwise quiet time of cruise to turn on and test all the science instruments. One of them, RAD, actually began doing mission science in December 2011, studying what human astronauts might experience on their own future cruise to Mars.⁸ The mission checked out the other nine science instruments in the middle of March; all passed.⁹ Afterward, on March 26, the spacecraft performed a second trajectory correction maneuver. The maneuver finally cleaned up the residual trajectory error and aimed MSL directly at Mars. In fact, the second maneuver was so precise that the mission was able to delay the third maneuver to accommodate a flight software update and some additional instrument checkouts.¹⁰

Throughout cruise, the navigation team tested their ability to determine the spacecraft's orientation in space with a series of commanded turns.¹¹ When test results were fed back into their landing simulations, they were able to predict the landing site more accurately: the landing ellipse could be shrunk from 20-by-25 kilometers, to only 7-by-21 kilometers. The navigators presented the opportunity to the science team, who eventually decided to shift the target closer to the mountain in the middle of Gale crater, 6.5 kilometers south and 1.3 kilometers west of the original target. On June 26, the third trajectory correction maneuver targeted MSL to the new landing ellipse. The fourth maneuver, on July 28, cleaned up residual errors.¹² During cruise, the spacecraft consumed fewer than 30 kilograms of fuel, less than 40% of the total amount available (Table 2.1).¹³

2.2.3 Approaching Mars

On June 22, six weeks before landing, NASA and JPL released a video to YouTube titled "Seven Minutes of Terror: The Challenges of Getting to Mars." Like a summer blockbuster movie trailer, with strident music accompanying disconcertingly lit appearances by lead landing engineer Adam Steltzner and others, the video presented the impending landing as seven minutes of terrifying and helpless uncertainty for the MSL team. The video struck a chord with the public. *The New York Times* reported it had already been viewed half a million times by July 10.¹⁴ By early September, the views had hit 3 million.¹⁵

⁷The story about how the navigators pulled off the first Trajectory Correction Maneuver was shared with me in an email by Rob Manning on January 8, 2015, and corrects timeline errors he made in his book, *Mars Rover Curiosity*

⁸NASA (2011c)

⁹JPL (2012b)

¹⁰Martin-Mur et al (2012)

¹¹Martin-Mur et al (2014)

¹²Martin-Mur et al (2014)

¹³Table data are from Abilleira, 2013. For a detailed accounting of the nature and reasons of all the cruise turns and calibrations, read Martin-Mur et al (2014)

¹⁴Chang (2012)

¹⁵Guy Webster, personal communication, email dated May 17, 2017

Table 2.1. Cruise performance. Based on Abilleira et al (2013).

Date	Event	Total space- craft mass (kg)	Propellant mass used (kg)	Propellant mass available (kg)	Planned velocity change (m/s)	Actual velocity change (m/s)
2011-11-26	Launch	3840.5	—	73.8	—	—
2011-11-26	Separation	3838.7	1.78	72.0	0.27	0.27
2011-11-28 to 2012-01-06	Spindown, turns, calibrations	3837.1	1.63	70.4	—	—
2012-01-11	Trajectory correction maneuver 1	3819.0	18.03	52.3	5.5071	5.6350
2012-01-25 to 2012-03-07	Turns, calibrations	3815.7	3.33	49.0	—	—
2012-03-26	Trajectory correction maneuver 2	3813.5	2.23	46.8	0.7116	0.7119
2012-03-26 to 2012-06-18	Turns, calibrations	3811.6	1.90	44.9	—	—
2012-06-26	Trajectory correction maneuver 3	3811.4	0.14	44.7	0.0414	0.0418
2012-06-26 to 2012-07-18	Turns	3811.2	0.19	44.6	—	—
2012-07-29	Trajectory correction maneuver 4	3811.2	0.03	44.5	0.0111	0.0104
2012-07-29	Turn	3811.2	0.07	44.5	—	—

The approach phase began 45 days before arrival, as the Deep Space Network collected nearly continuous Doppler and range data by monitoring MSL's radio carrier signal. The hoped-for precision landing depended upon how well navigators could determine MSL's position at entry, and how well they could communicate that information to the rover computer. Four weeks before landing, navigators began twice-daily radio tracking sessions, using widely separated ground stations as a giant interferometer to measure the spacecraft's position with incredible precision. At the same time, scientists on the Mars Climate Sounder and Mars Color Imager (MARCI) instruments on Mars Reconnaissance Orbiter delivered daily updates on atmospheric conditions over the landing site to the navigation team.¹⁶ Mars Climate Sounder couldn't see all the way to the surface at the landing site because of seasonal water-ice clouds, indicating cool weather. MARCI images showed no dust storm activity near the landing site.

By any measure, the navigational guidance of MSL to Mars was a feat of accuracy, "possibly at the limit of what is possible with current calibration and tracking measurement errors."¹⁷ The spacecraft was aimed at a target at the top of Mars' atmosphere 2.5 kilometers wide by 11.5 kilometers long and 3522.2 kilometers from the center of Mars. Following the fourth trajectory correction maneuver on July 29, 2012, navigators found the spacecraft to be aimed at a spot only 200 meters and 0.11 meters per second off of its target position and velocity. This was good enough not to risk any further maneuvering. Both of the final two trajectory correction maneuver opportunities were canceled, and the spacecraft was on its final course from six days prior to entry. When the landing was over and the navigators determined the spacecraft's actual path into the atmosphere, they found it had hit within 700 meters of its entry interface target.¹⁸

2.3 EDL: ENTRY, DESCENT, AND LANDING

On landing day, August 6, 2012 UTC (August 5, local California time), NASA aired a live television broadcast of the landing from JPL beginning about 53 minutes before atmospheric entry. The cameras were trained on a glass-walled room at one side of the main Spaceflight Operations Facility floor. The engineers seated behind monitors in that room comprised only about half of the workers monitoring the landing; the rest were holed up in an "EDL War Room" closer to the mission operations area in a separate building. On TV, EDL Operations Lead Allen Chen served as the play-by-play announcer of landing events, interpreting the X-band tones and the tersely worded, acronym-filled communications chatter for the watching world.

Forty minutes before atmospheric entry, a command shut down the rover's autonomous system fault protection. About 18 minutes before entry, the Odyssey mission reported acquisition of signal from their spacecraft. Fifteen minutes before entry, Chen reported that the flight team had run simulations of MSL's course based upon the last navigational data received, and that it looked like they were "right in the middle of the ellipse." Thirteen and a half minutes before entry, the cruise stage vented the Freon refrigerant that had piped heat from inside the capsule to the cruise stage radiators. The engineers monitoring the X-band radio signal from MSL were able to detect the minute effect that the venting of the

¹⁶Chen et al (2014)

¹⁷Martin-Mur et al (2014)

¹⁸Abilleira (2013)

Freon had on MSL's velocity. Twelve minutes before entry, the Odyssey team reported that they were "go" to serve as the communications relay for MSL's descent.

The remaining events of entry, descent, and landing unfolded very rapidly. Figure 2.6 and Table 2.2 summarize them. Figure 2.7 shows the spacecraft trajectory across Mars' surface.

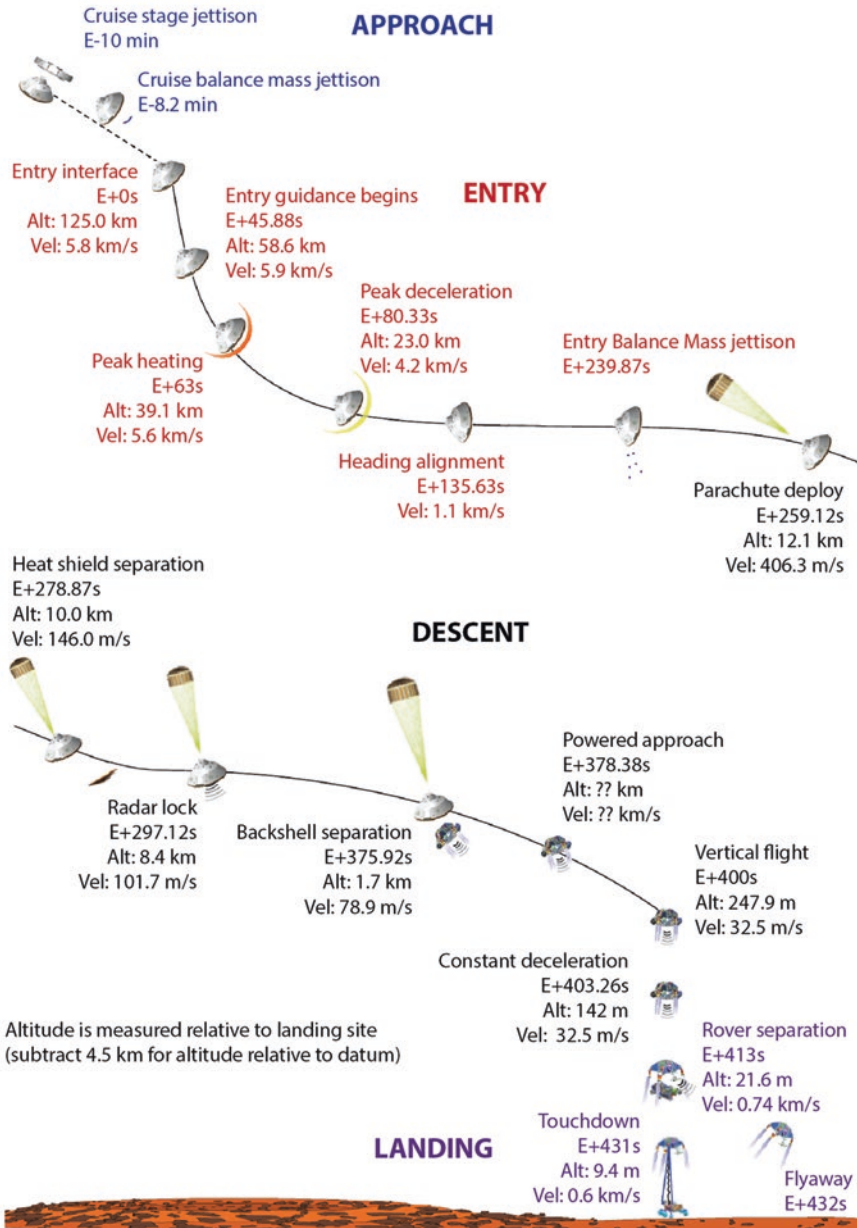


Figure 2.6. Diagram of approach, entry, descent, and landing process. Emily Lakdawalla after Kornfeld et al. 2014.

Table 2.2. *Timeline of events in entry, descent, and landing according to different ways of measuring time. Some publications refer to a “ t_0 ” that corresponds to the time that the computer updated its navigational reference point to Mars, when the spacecraft clock read 397501174.997338 seconds; others consider the entry interface time to be 540 seconds after that. AOS = acquisition of signal. LOS = loss of signal.*

Phase	Event	Time (UT, SCET)	Time (rel. to t_0)	Time (rel. to entry)	Time (MSL SCLK)	Source*
Approach	Vent Cruise Heat Rejection System	4:57:00	-286	-826	397500889.00	N2016
Approach	Cruise stage separation	5:00:46	-60	-600	397501115.00	K2014
Approach	EDL guidance & control activated	5:01:46	0	-540	397501175.00	K2014
Approach	Cruise balance mass jettison	5:02:37	50.64	-489.36	397501225.64	K2014
Approach	Mars Reconnaissance Orbiter AOS	5:02:39	53	-487	397501228.00	W2013
Wait for Guidance Start	Entry interface	5:10:46	540	0	397501715.00	K2014
Range Control	Guidance start	5:11:31	585.88	45.88	397501760.88	K2014
Range Control	Peak heating	5:11:49	603	63	397501778.00	MC2014
Range Control	Bank reversal 1	5:11:58	612.88	72.88	397501787.88	K2014
Range Control	Peak deceleration	5:12:06	620.33	80.33	397501795.33	K2014
Range Control	Bank reversal 2	5:12:19	633.88	93.88	397501808.88	K2014
Range Control	Bank reversal 3	5:12:49	663.38	123.38	397501838.38	K2014
Heading alignment	Heading alignment	5:13:01	675.63	135.63	397501850.63	K2014
Heading alignment	Mars Odyssey AOS	5:14:28	762	222	397501937.00	W2013
Straighten Up and Fly Right	Entry balance mass jettison	5:14:45	779.87	239.87	397501954.87	K2014
Straighten Up and Fly Right	Wait for parachute deployment	5:14:59	793.87	253.87	397501968.87	K2014
Parachute descent	Parachute deployment	5:15:05	799.12	259.12	397501974.12	K2014
Parachute descent	Last MEDLI measurement	5:15:14	808.86	268.86	397501983.86	K2014
Parachute descent	Heat shield separation	5:15:24	818.87	278.87	397501993.87	K2014
Parachute descent	Radar lock	5:15:43	837.12	297.12	397502012.12	K2014
Parachute descent	End direct-to-Earth transmission	5:15:45	839	299	397502014.00	Sc2014

Parachute descent	HiRISE image start	5:16:19	873.482	333.482	397502048.48	S2016
Parachute descent	HiRISE image heat shield	5:16:39	893.353	353.353	397502068.35	S2016
Parachute descent	HiRISE image lander	5:16:42	896.178	356.178	397502071.18	S2016
Parachute descent	Heat shield impact (approx.)	5:16:45	899	359	397502074.00	L2016
Parachute descent	Prime descent engine rockets	5:16:45	899.63	359.63	397502074.63	K2014
Parachute descent	Backshell separation	5:17:01	915.92	375.92	397502090.92	K2014
Powered descent	Powered approach	5:17:04	918.38	378.38	397502093.38	K2014
Powered descent	Sky crane start	5:17:38	952.89	412.89	397502127.89	K2014
Powered descent	Rover deploy	5:17:39	953.59	413.59	397502128.59	S2014
Powered descent	Rover reaches end of bridle	5:17:43	957.89	417.89	397502132.89	S2014
Powered descent	Bogie release	5:17:44	958.89	418.89	397502133.89	S2014
Powered descent	Ready for touchdown	5:17:47	961.86	421.86	397502136.86	K2014
Powered descent	HiRISE image end	5:17:57	970.9	430.9	397502145.90	S2016
Landing	Touchdown sensed	5:17:57	971.52	431.52	397502146.52	K2014
Landing	Flyaway	5:17:58	972.31	432.31	397502147.31	K2014
Landing	First rear Hazcam image	5:18:40	1014.068662	474.07	397502189.07	L2016
Landing	First front Hazcam image	5:20:37	1131.501662	591.50	397502306.50	L2016
Landing	Mars Odyssey LOS	5:23:53	1327	787	397502502.00	W2013
Landing	Mars Reconnaissance Orbiter LOS	5:23:54	1328	788	397502503.00	W2013

*Sources for the data in the table are: K2014: Karlgaard and Kutty (2014); L2016: calculated by me from MARDI image time stamps; MC2014: Mendeck and Craig McGrew (2014); N2016: Novak et al (2016); S2014: Sell et al (2014); S2016: Christian Schaller, personal communication, email dated February 17, 2016; Sc2014: Schratz et al (2014); W2013: Way et al (2013).

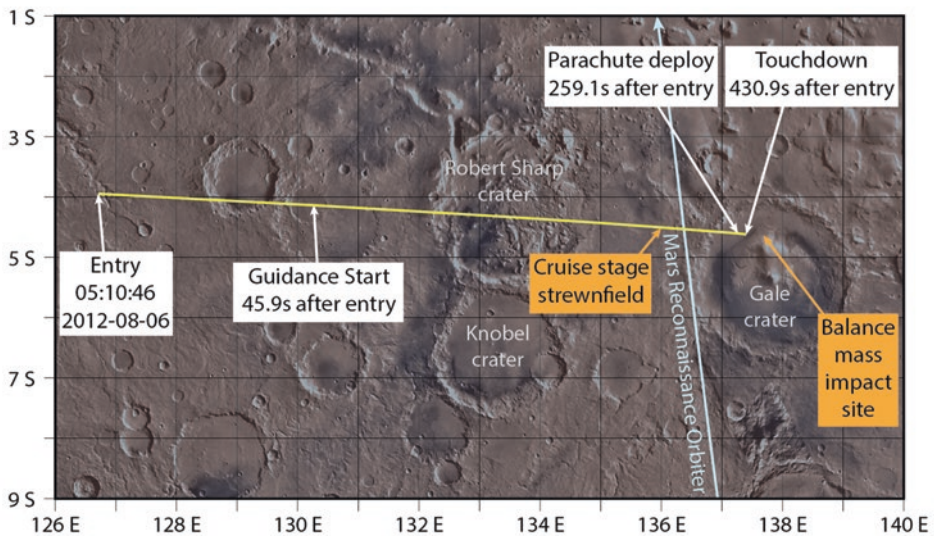


Figure 2.7. Entry, descent, and landing trajectory. Base image is from Viking global mosaic, trajectories from JPL Horizons.

2.3.1 Telecommunications during landing

Ever since the loss of Mars Polar Lander, NASA has required Mars landers to be in constant communication with Earth during the dramatic and risky events of entry, descent, and landing. On the day of MSL's landing, Mars and Earth were separated by about 248.2 million kilometers, or 828.0 light-seconds. The entire entry, descent, and landing took only 432 seconds from start to finish. There is nothing that anyone on Earth could do to rescue a mission should something go wrong; instead, any telemetry received would serve to help engineers determine the cause of a landing failure, with the goal of preventing a future one. MSL was required to transmit all highest-priority data within 3 seconds of the event it recorded. That way, some information could be salvaged from a catastrophic accident to improve future missions.¹⁹

Ideally, the spacecraft would use a single radio configuration for communications throughout entry, descent, and landing. But the MSL landing sequence had the spacecraft reconfiguring itself multiple times, throwing away hardware on which antennas were mounted. To handle communications, MSL had to switch among multiple radio systems and antennas.

There were two primary X-band radio systems for communicating directly with Earth, one within the rover (still used now for surface operations) and one attached to the descent stage. During cruise, the descent stage X-band system handled communications through a

¹⁹The details of EDL telecommunications in this section are based on Schratz et al (2014)

medium-gain antenna mounted to the cruise stage. During entry and descent, the descent stage communicated with Earth through two low-gain antennas mounted on the backshell's parachute cone, beginning with the parachute low-gain antenna and later switching to the tilted low-gain antenna (Figure 2.10). The signal from such small antennas, 112 million kilometers from Earth, was weak, so they transmitted no telemetry. Rather, they broadcast 11-second-long “tones,” signals with frequencies slightly offset from the main carrier frequency, with different frequencies signifying different events. Events during the cruise, approach, and guided-entry phases were separated far enough in time that 11-second-long signals were good enough to communicate the spacecraft's status, but after that, MSL needed higher-rate communications. When events did overlap in time, complicated logic governed which tone would play first:

If additional tone events occurred while one tone was playing, the new event was queued until the currently playing tone had completed. Then, the queued tone played. Each tone had a defined priority. Nominal tones were generally prioritized lower than tones indicating faults or specific critical events during EDL. Of the available tone events, a small subset were labeled as “stomping tones,” which interrupted a currently playing tone, causing the interrupted tone to be re-queued by flight software to replay when time permits. In the event of multiple queued tones, the highest priority tones were played first. In the event of tones with the same priority, the most recent tones were played first, because the newest information during EDL was generally favored over stale information. Because of this software logic, the time between a tone event occurring and when it actually was radiated varied by several seconds, and some tones appeared to play out of order. Although this made real-time operations more complicated, it was the preferred strategy to enhance the probability of receiving indications of off-nominal behavior in the event of a fault... Parachute deploy and touchdown tones [were] carrier-only tone, where no subcarrier modulation is used.²⁰

For transmitting telemetry during descent and landing, MSL used the Electra-Lite UHF radio within the rover, broadcasting to receivers on Mars orbiters. It transmitted through three different low-gain UHF antennas at different times: one on the parachute cone of the backshell, one mounted to the top of the descent stage, and finally the rover's helix antenna, the one that it still uses for surface operations (see section 4.5). Amazingly, during entry, descent, and landing, the Parkes radio telescope back on Earth, in Australia, was able to pick up the signal from MSL's UHF antennas. While the signal was too weak for Parkes to decode any telemetry, it did provide Doppler information as the spacecraft decelerated toward landing.

Telemetry arrived on Earth with the assistance of orbital relays. Odyssey provided the primary conduit for real-time communication. It served as a bent-pipe relay: it received MSL's signals, demodulated them, and immediately sent the decoded telemetry to Earth. The Odyssey relay arrived only seconds slower than the direct-to-Earth tones. Mars Reconnaissance Orbiter recorded MSL's UHF signals in an “open-loop” mode, without demodulating them. This recording wasn't available on Earth until hours after landing, but

²⁰ Schratz et al (2014)

would have provided more data if an anomaly happened that caused Odyssey to lose lock on the signal. The European Space Agency's Mars Express also listened for MSL's signal. It operated in an open-loop carrier-only detection mode, which didn't record telemetry but provided an alternate angle for Doppler tracking relative to that recorded from Earth.

2.3.2 The aeroshell and MEDLI

MSL's was the most challenging Mars atmospheric entry in history, for two main reasons. MSL was dramatically larger than any previous landed Mars spacecraft, and its goal was a much more precise landing than previously attempted (Figure 2.8). The aeroshell was 4.5 meters in diameter, the heat shield a 70° cone (Figure 2.9). The heat shield's shape was the same as for all previous Mars landers, but Curiosity's aeroshell was a meter larger and more than three times heavier than any previous one.²¹ In a throwback to Viking, the aeroshell was able to generate lift. Parts of the backshell and heat shield are labeled in Figure 2.10 and Figure 2.11. The backshell with parachute and balance masses weighed 576.6 kilograms.²² The heat shield weighed 440.7 kilograms.






	Viking	Pathfinder	Mars Exploration Rover	Phoenix	Mars Science Laboratory
					
Diameter (m)	3.51	2.65	2.65	2.65	4.5
Entry mass (kg)	930	585	840	602	3380
Entry velocity (m/s)	4.5	7.6	5.5	5.9	5.6
Landing mass (kg)	603	360	539	364	840 + 691
Landing altitude (km)	-3.5	-1.5	-1.3	-3.5	-4.4 (capability: -0.5)
Landing ellipse (km)	300 x 300	200 x 100	150 x 20	100 x 20	21 x 7
Lift/drag ratio	0.18	0	0	0	0.24
Entry guidance	Lift up	None	None	None	Guided
Entry control	RCS control	Spinning	Spinning	Non-spinning	RCS control

Figure 2.8. Comparison of NASA Mars aeroshells. Emily Lakdawalla after Edquist et al (2009) and Wallace (2012).

²¹Edquist K et al (2009)

²²Allen Chen, personal communication, email dated July 1, 2016, correcting numbers published before the launch

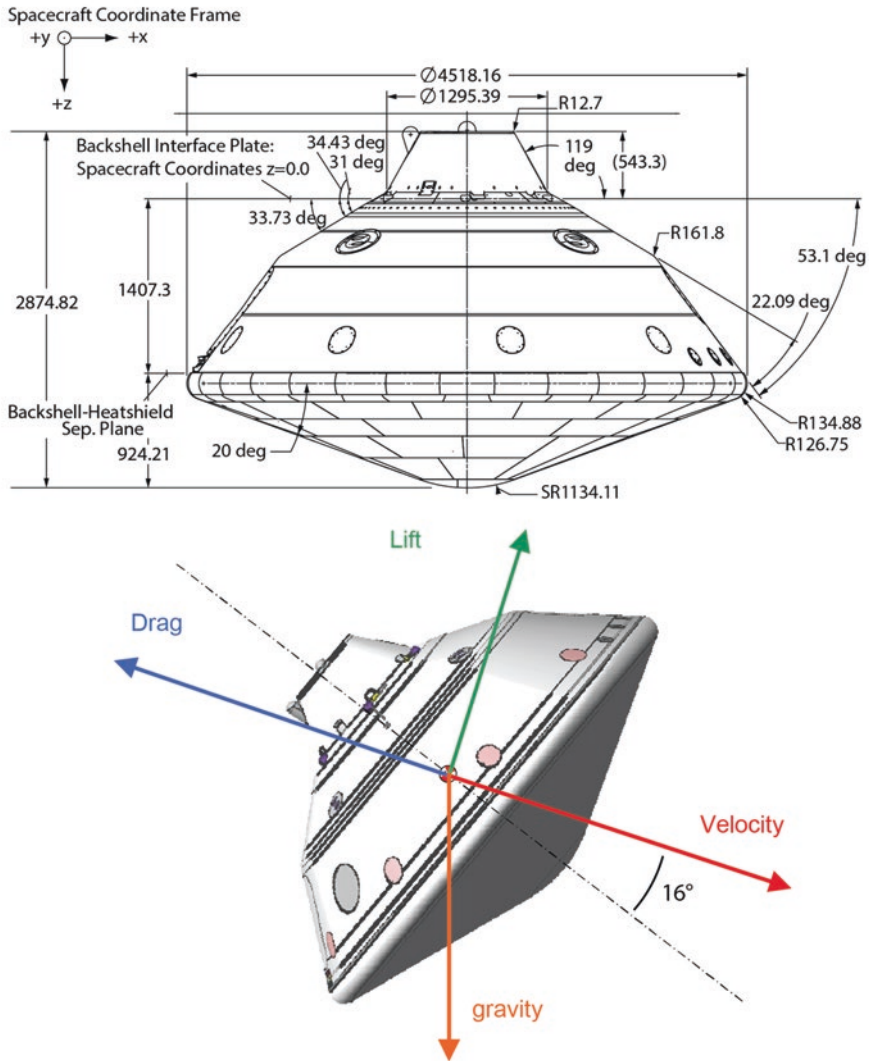


Figure 2.9. Top: Aeroshell dimensions. The aeroshell consists of the backshell and heat shield. Bottom: geometry of the aeroshell during guided flight. Images: NASA/JPL-Caltech. Top diagram based on Karlgaard et al (2014). Bottom based on Steltzner et al (2010).

The heat shield gathered an unprecedented amount of information about the descent through the Martian atmosphere, thanks to the MSL Entry, Descent, and Landing Instrumentation (MEDLI) sensors embedded within it. MEDLI had two kinds of sensors.

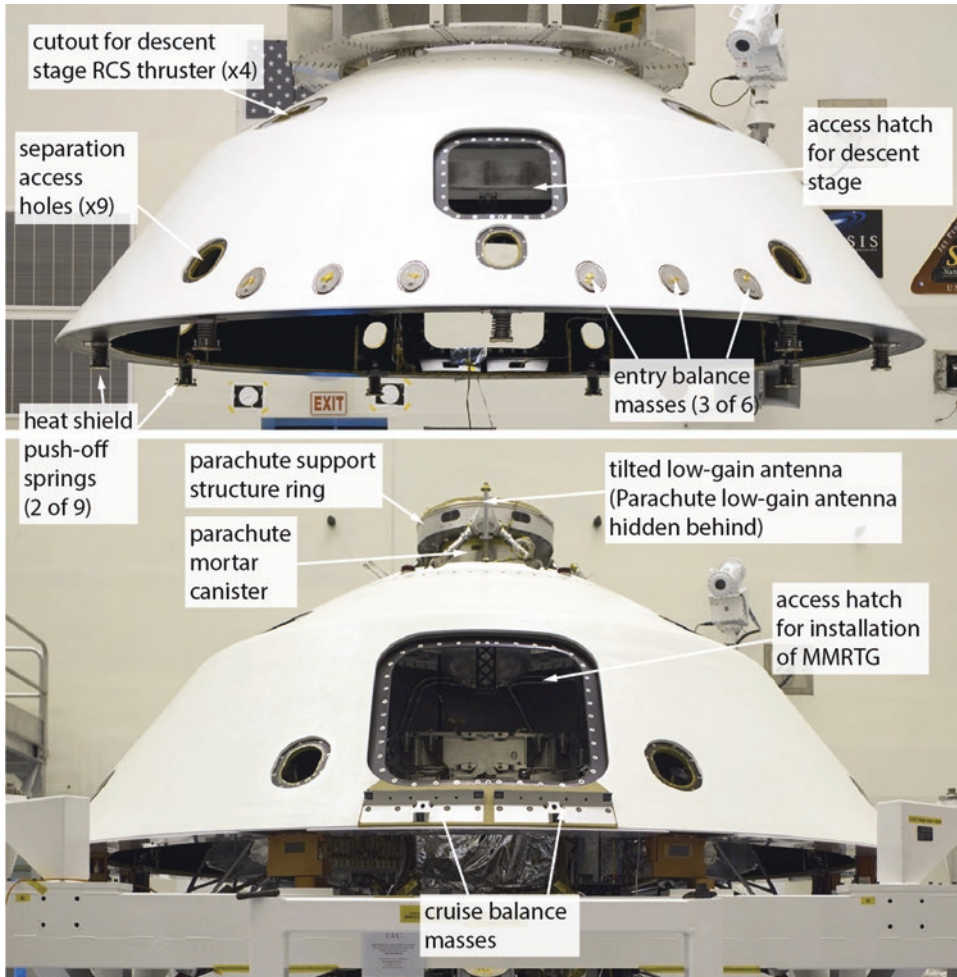


Figure 2.10. Parts of the MSL backshell. NASA/KSC image releases KSC-2011-4526 and KSC-2011-7183, annotated by Emily Lakdawalla.

Seven transducers of the Mars Entry Atmospheric Data System (MEADS) measured atmospheric pressure by tiny 2.5-millimeter through-holes in the shield. Seven MEDLI Integrated Sensor Plugs (MISP) were embedded in the heatshield within 33-millimeter-diameter plugs. They consisted of thermocouples to measure temperature and recession sensors to document how the PICA material weathered entry. Locations of the MEDLI sensors are shown in Figure 2.11 and Figure 2.12.²³

²³Little et al (2013)

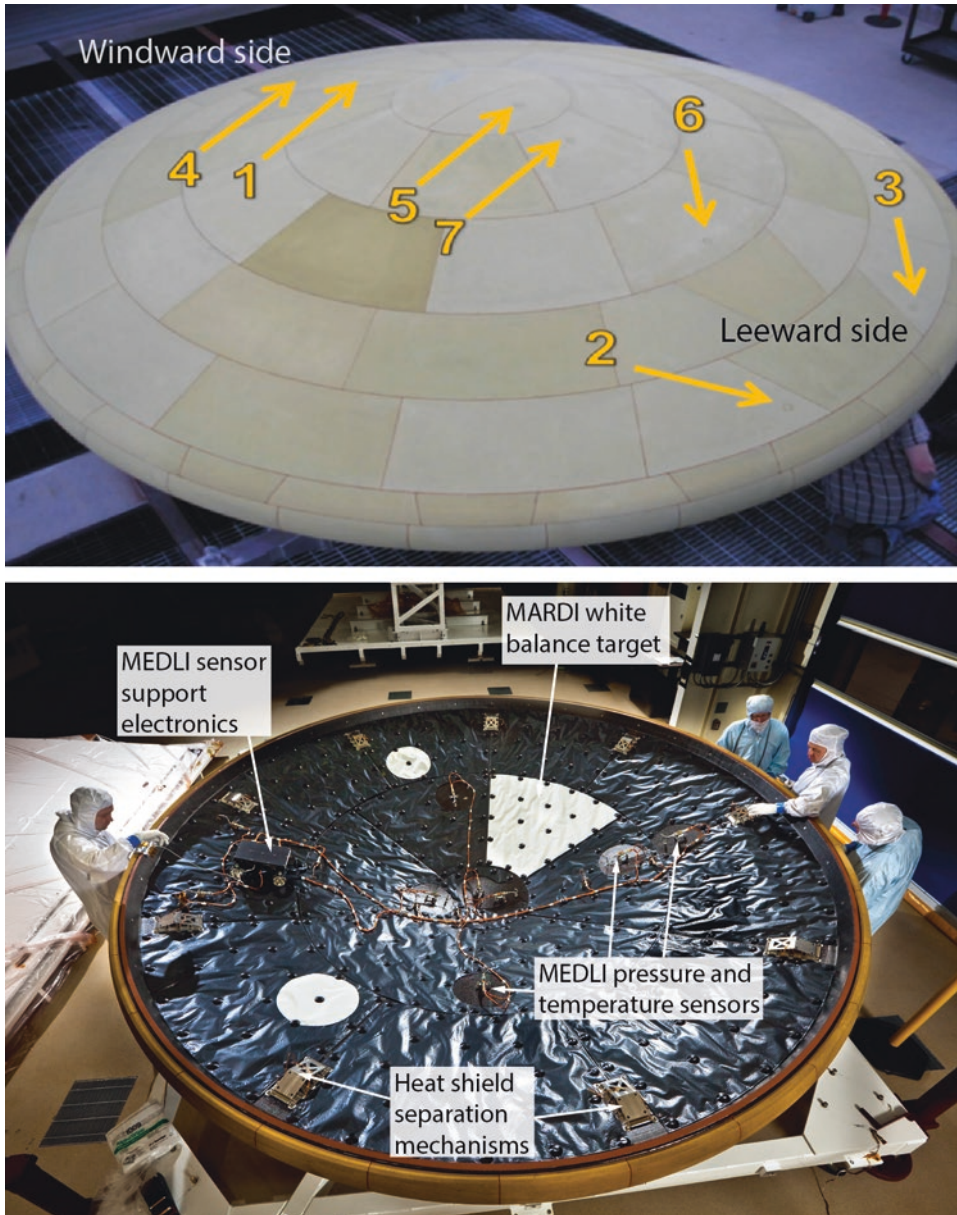


Figure 2.11. Parts of the MSL heat shield. Top: exterior surface of the heat shield, with locations of the MEDLI Integrated Sensor Plugs marked. Bottom: interior surface of the heat shield. NASA/JPL-Caltech/Lockheed Martin image release PIA14128, taken at Lockheed Martin Space Systems, Denver, in April 2011, annotated by Emily Lakdawalla.

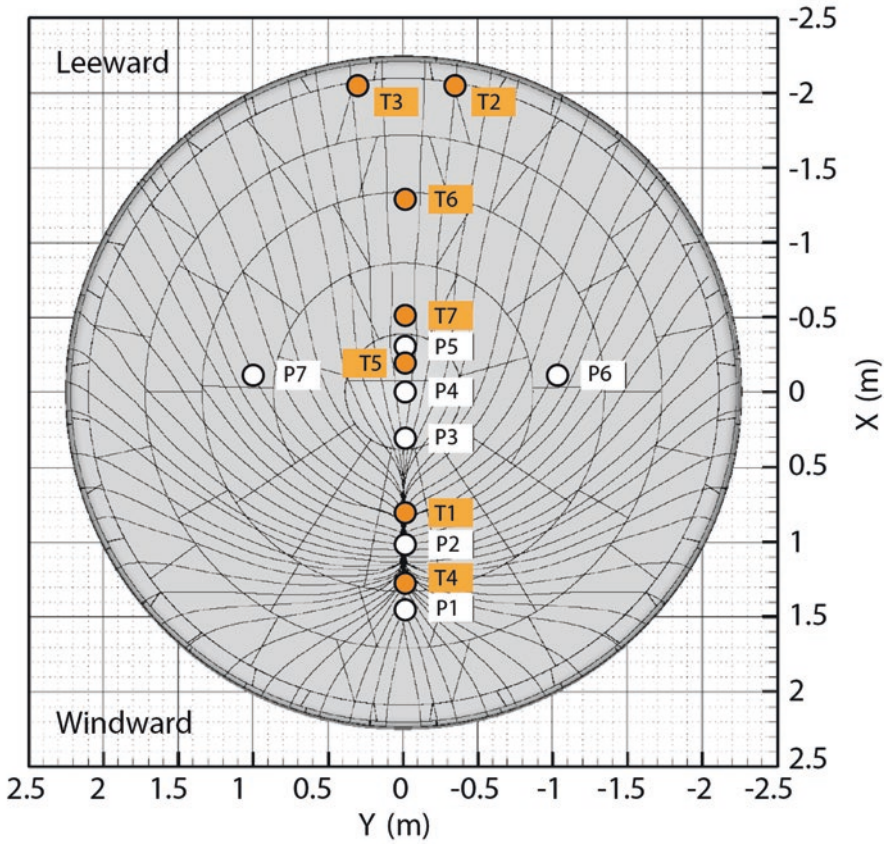


Figure 2.12. Locations of the MEDLI MEADS (orange) and MISP (white) sensors on the MSL heat shield. Flow lines show the direction of expected air flow. Based on Little et al (2013) and Beck et al (2010).

2.3.3 Final approach

Ten minutes before entry, at 5:00:46 Spacecraft Event Time on August 6, 2012, the cruise stage separated, its work complete. Later images from Mars Reconnaissance Orbiter HiRISE and CTX instruments show numerous impact craters from the cruise stage scattered over a strewnfield 12 kilometers long, indicating that the cruise stage – unprotected by an aeroshell – broke up in the atmosphere (Figure 2.13).²⁴ The cruise stage took with it MSL's star trackers. From that point on, the rover computer would maintain its sense of its own orientation by dead reckoning. MEDLI began to acquire data from the heat shield.

²⁴McEwen A (2012)

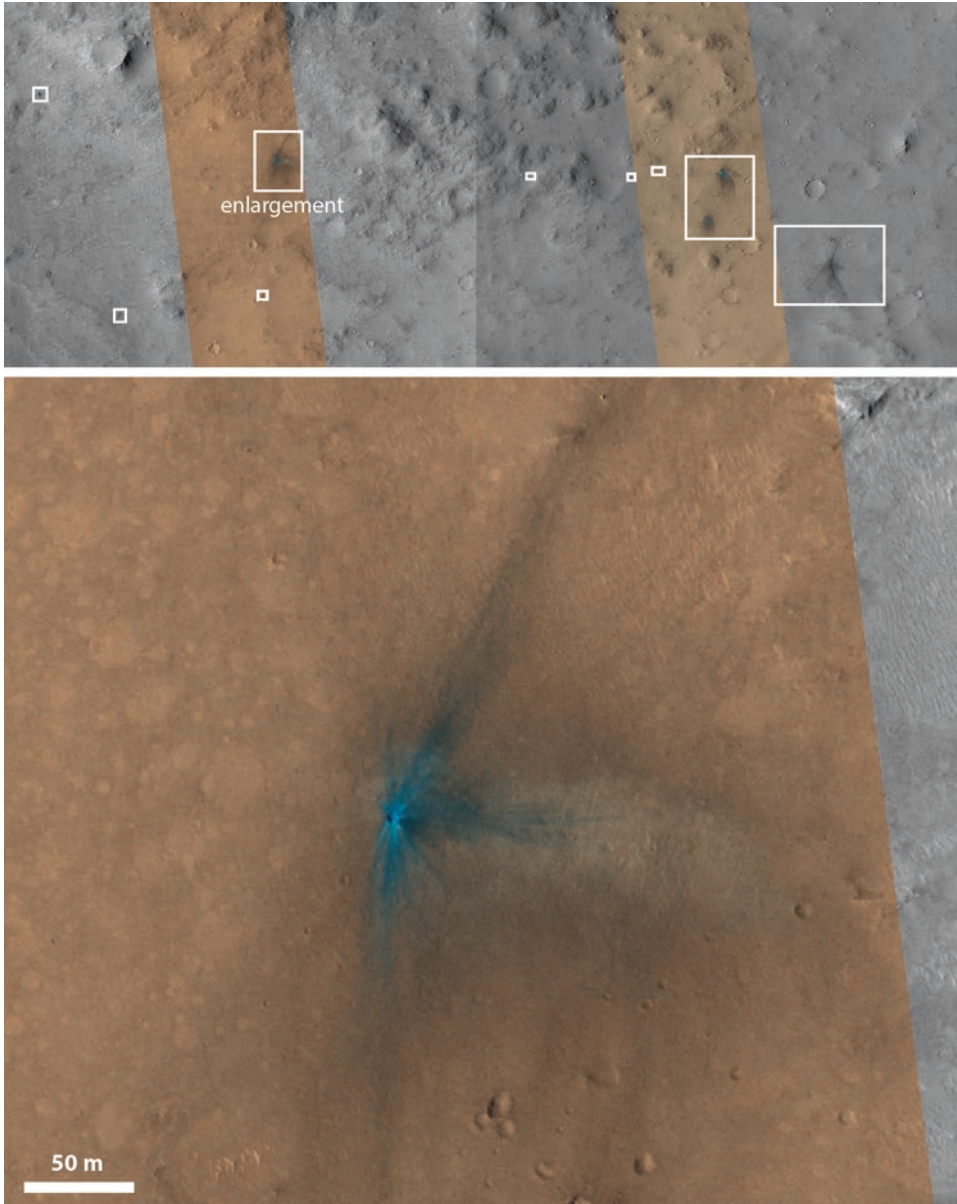


Figure 2.13. Impact sites of the cruise balance masses and fragments of the cruise stage. At about 4 meters in diameter, the two largest craters are probably the cruise balance mass impact sites. All the other, smaller impacts are likely from fragments of the cruise stage. HiRISE images ESP_029245_1755 and ESP_029601_1755. NASA/JPL-Caltech/UA.

Nine minutes prior to entry, the guidance, navigation, and control system activated, and the rover computer fed it the navigators' best estimate of the spacecraft's position and velocity. (Many publications about the landing refer to this moment, 540 seconds before entry, or 397501174.997338 seconds on the spacecraft clock, as " t_0 " for the landing phase, while others use the moment of entry as the zero point.) The spacecraft stilled its rotation and oriented to the correct angle for hitting the top of the atmosphere. It ejected two 75-kilogram blocks of tungsten, the cruise balance masses, which went on to impact the surface close to the cruise stage (Figure 2.13). The sudden loss of 150 kilograms of mass offset the capsule's center of mass away from its centerline. Once the capsule was in the atmosphere, this offset gave it a 16° angle of attack. The capsule was ready to fly in the Martian air.

MSL switched X-band antennas, now broadcasting tones from the tilted low-gain antenna, which was pointed 17.5° away from the aeroshell's axis of symmetry (Figure 2.10). The switch of antennas caused only a very brief loss of communication with the spacecraft.

As MSL approached Mars, Mars Reconnaissance Orbiter approached the equator from the south, while Mars Odyssey approached from the north (Figure 2.14). Mars Reconnaissance Orbiter's path took it across the westernmost rim of Gale crater, carrying it nearly overhead during landing, while Odyssey passed considerably to the east. That geometry would allow Odyssey to have a second communications pass with MSL later on landing day, passing to the west about two hours after landing.²⁵ Mars Reconnaissance Orbiter began its "open-loop" recording of the MSL signal at 8 minutes 7 seconds before entry.²⁶

2.3.4 Entry: 0 to 259 seconds

MSL entered the Martian atmosphere at 05:10:46 at an altitude of 125 kilometers. Traveling at a relative speed of 5.8 kilometers per second, it shed all of that velocity within the next 7 minutes. Within one minute, it had plunged to only 40 kilometers' altitude, broadcasting tones to keep Earth updated. Watching the X-band tones arrive on Earth, Allen Chen had a moment of sheer terror: a tone had arrived that indicated that the vehicle orientation was out of control, suggesting that the loss of the spacecraft could be imminent. Fortunately, it turned out to be a calibration issue with the MEADS sensors, not an actual anomaly, and the rest of the landing events happened as expected.²⁷

At 46 seconds after entry, the descent stage inertial measurement unit had begun to sense the atmosphere as a drag force of 0.2 gees, beginning the range control phase of guided entry. This was earlier than expected, because the navigation team's atmospheric model had overpredicted the temperatures there, underpredicting the pressures, although the pressures and temperatures that MSL measured were consistent with those reported by Mars Climate Sounder.²⁸ The mismatch between prediction and reality had little effect on the landing process.

²⁵ Abilleira and Shidner (2012)

²⁶ Way et al (2013)

²⁷ Allen Chen, personal communication, email dated February 24, 2016

²⁸ Martin-Mur et al (2014)

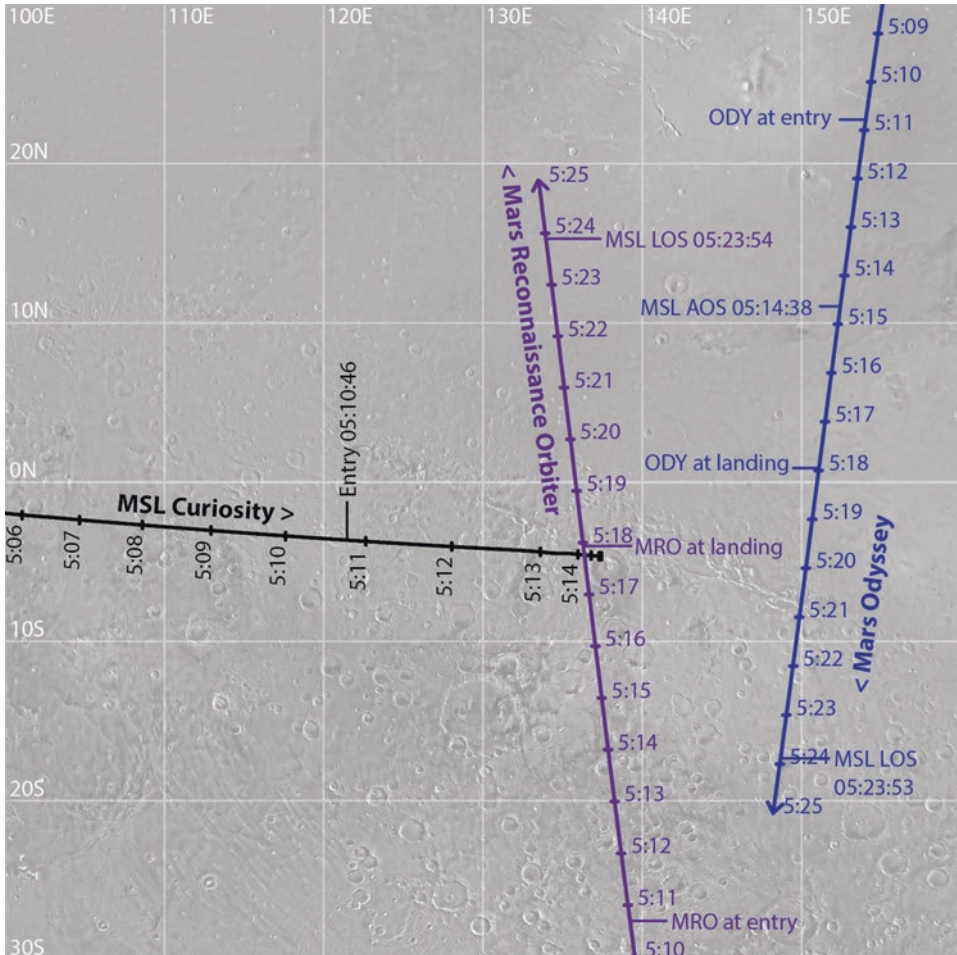


Figure 2.14. Geometry of MSL and orbiter ground tracks during entry, descent, and landing. Base image is from Viking Orbiter; spacecraft positions retrieved from JPL Horizons. ODY = 2001 Mars Odyssey; MRO = Mars Reconnaissance Orbiter; LOS = loss of signal.

During the range control phase, the rover computer predicted the downrange distance it would fly and adjusted lift as necessary in order to shoot for the correct range. Unlike an airplane, MSL had no flaps or elevators to change its angle of attack, so the way that the spacecraft adjusted its range was to perform a series of banking turns, rotating its center of gravity around the axis of its blunt nose. Its initial entry point was biased to the left (north) of the intended landing site, so it began with a banking turn to the right. The computer monitored the spacecraft's cross-range drift, and commanded a bank reversal when the drift passed a threshold. It reversed its bank angle to the left, then right, then left again. Figure 2.15 shows how the velocity, altitude, and bank angle varied with time. The first, commanded bank was at very nearly 90° (resulting in no lift being generated), so the

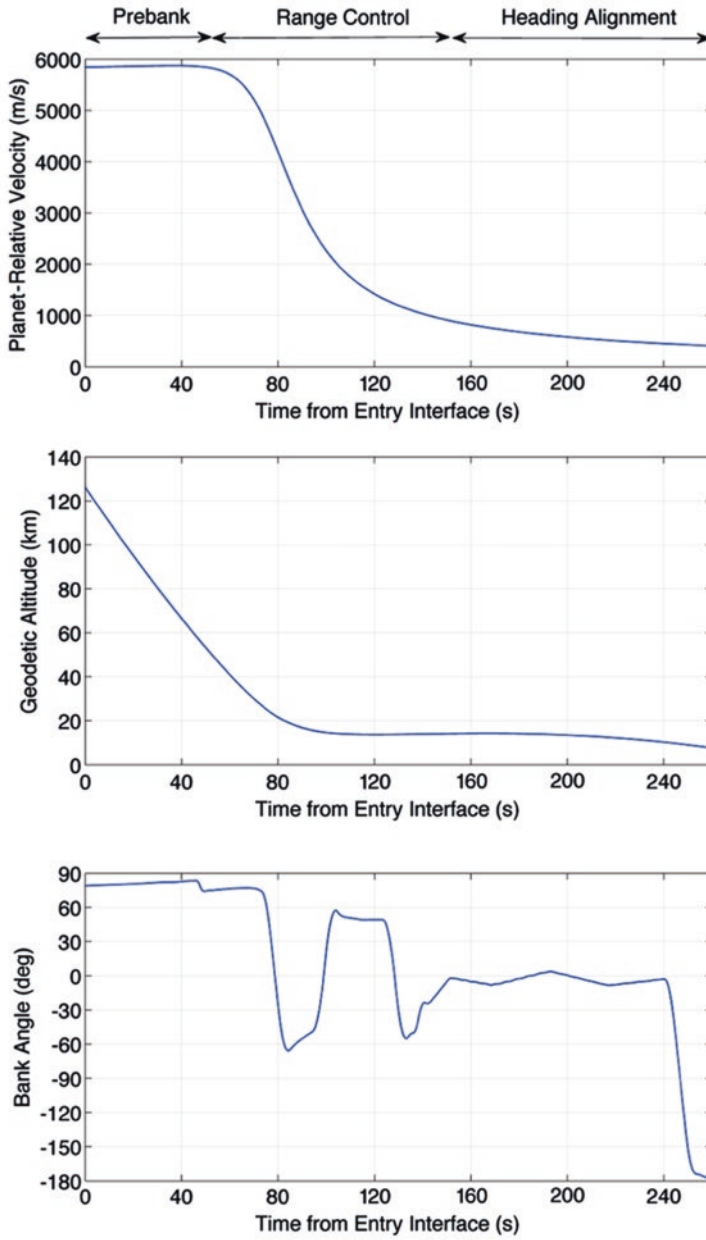


Figure 2.15. Best estimate of entry trajectory, based on spacecraft telemetry. Modified from Mendeck and Craig McGrew (2014).

spacecraft descended on an almost ballistic path. By the time of the first bank reversal, it had slowed dramatically and the spacecraft commanded less bank angle. The capsule truly began to fly in the Martian atmosphere.²⁹

All this time, the heat shield was doing its job. Initially, the spacecraft continued to lose altitude at a rate of a kilometer per second. The hypersonic entry pressurized the air in front of the capsule, creating a shock wave with temperatures as high as 4000 kelvins (Figure 2.16). At 65 seconds after atmospheric entry, the atmosphere had become thick enough that the flow of air across the heat shield abruptly transitioned from laminar (smooth) to turbulent.³⁰ The heat shield's temperature increased rapidly. At 85 seconds after atmospheric entry, the surface of the heat shield reached its peak temperature, of around 1300 kelvins (Figure 2.17). MEDLI data showed that peak heating happened at a different location and lower temperature than had been predicted during heat shield development, possibly because the flow of air over the heat shield became turbulent earlier than predicted. The PICA heat shield material withstood these forces easily, with little of it receding away: every single MEDLI thermocouple survived entry, even though some were installed just 2.54 millimeters underneath the surface.³¹

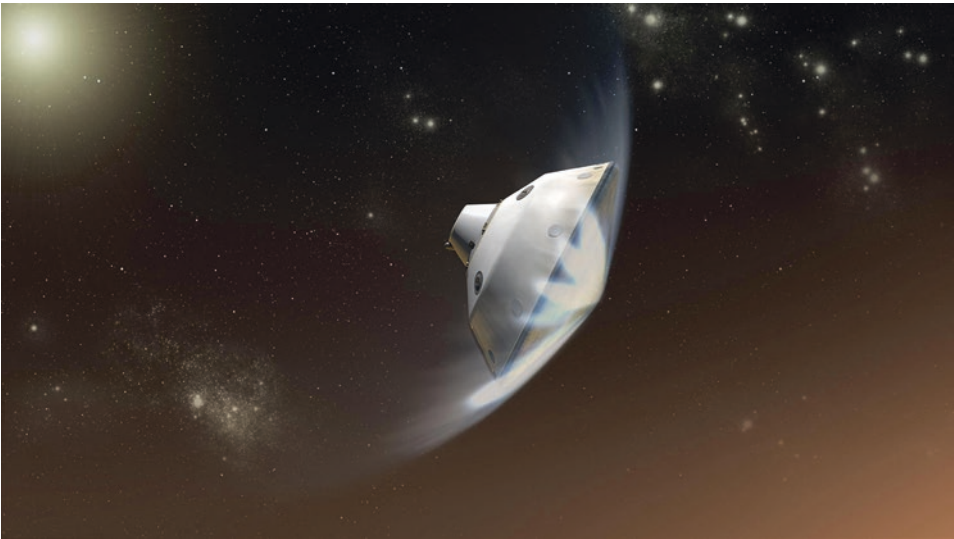


Figure 2.16. Artist's concept of the MSL aeroshell creating a shock wave during entry. NASA/JPL-Caltech release PIA14835.

²⁹ Mendeck and Craig McGrew (2014)

³⁰ Bose et al (2013)

³¹ Little et al (2013)

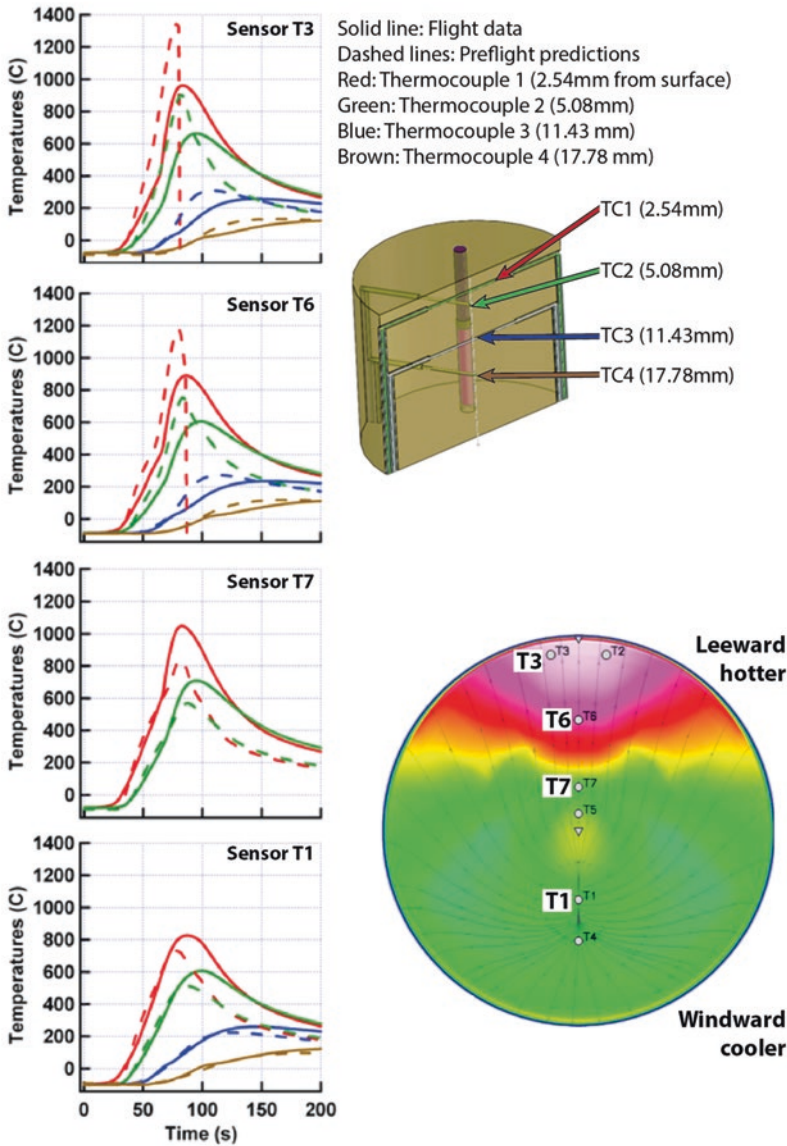


Figure 2.17. MEDLI MISP temperature flight data (solid lines) compared to preflight predictions (dashed lines), from Bose et al (2014). Each MISP sensor has four thermocouples at different depths. The colorful pattern on the heat shield shows the preflight predictions. Peak heating actually occurred closer to sensor T7 near the center of the heat shield, not at the most leeward sensor T3 as predicted.

With every second of entry, the spacecraft flew into denser air. It reached peak deceleration 80 seconds after entry, the pressure of the air decelerating it at 12.5 gees. As the spacecraft began its first bank reversal, dropping below 20 kilometers altitude, those forces began to wane, and the flying saucer entered a period of nearly level flight for two full minutes. It flew with a tailwind of about 20 meters per second, but the spacecraft's reckoning of its downrange target depended on an inertial measurement unit that wasn't affected by the wind, and the spacecraft stayed on course. The final bank reversal left it with about 1 kilometer of downrange error, well within tolerances.³²

At an altitude of 14 kilometers and speed of 1.1 kilometers per second, the spacecraft transitioned into the "heading alignment" phase of guided entry.³³ The spacecraft banked left to correct its cross-range heading, probably to compensate for a 10-meter-per-second crosswind.³⁴ It flew downrange for 100 seconds at a near-constant altitude, steering lightly to arrive at the optimal location for parachute deployment. It was during heading alignment, at 222 seconds after entry, when Mars Odyssey achieved lock on MSL's UHF signal and began relaying telemetry directly to Earth at a rate of 8 kilobits per second through the Deep Space Network station in Canberra, Australia.³⁵ Back on Earth, engineers applauded the news; the landing would occur just the same with or without Odyssey communications, but only Odyssey could give Earth real-time telemetry. "Real" time being 13.8 minutes after the events on Mars, thanks to the distance separating Mars and Earth.

MSL waited until its inertial measurement unit registered a speed of only about 400 meters per second and then changed its configuration again to prepare to deploy its parachute. MSL prepared for parachute deployment with the "straighten up and fly right" maneuver. The falling spacecraft threw away six 25-kilogram entry balance masses in pairs at two-second intervals. (You can see the entry balance masses on the backshell in Figure 2.10.) The release of the entry balance masses counteracted the off-center weight distribution that had been imparted by the release of the cruise balance masses.

The aeroshell tipped up, aligning its angle of attack to within 5° of its descent trajectory. At the same time, the reaction control system rolled the spacecraft 180° (a maneuver referred to as the "victory roll") to the desired bank angle for later radar operation purposes. Straighten up and fly right took a total of 14 seconds.³⁶ The work of the descent stage reaction control thruster system was complete. Throughout entry and descent, the reaction control thrusters had performed a total of 2256 thrust pulses, operating for a total of 110.725 seconds (Figure 2.18).³⁷ The aeroshell had dissipated 99.6% of the vehicle's kinetic energy through friction with the atmosphere.³⁸ The spacecraft was now ready to deploy its parachute. The balance masses continued along their ballistic trajectories, later impacting the ground at the northern edge of Mount Sharp, beyond the landing site to the east (Figure 2.7).

³² Mendeck and Craig McGrew (2014)

³³ Mendeck and Craig McGrew (2014)

³⁴ Martin-Mur et al (2014)

³⁵ Way et al (2013)

³⁶ Cruz et al (2014)

³⁷ Baker et al (2014)

³⁸ Way et al (2013)

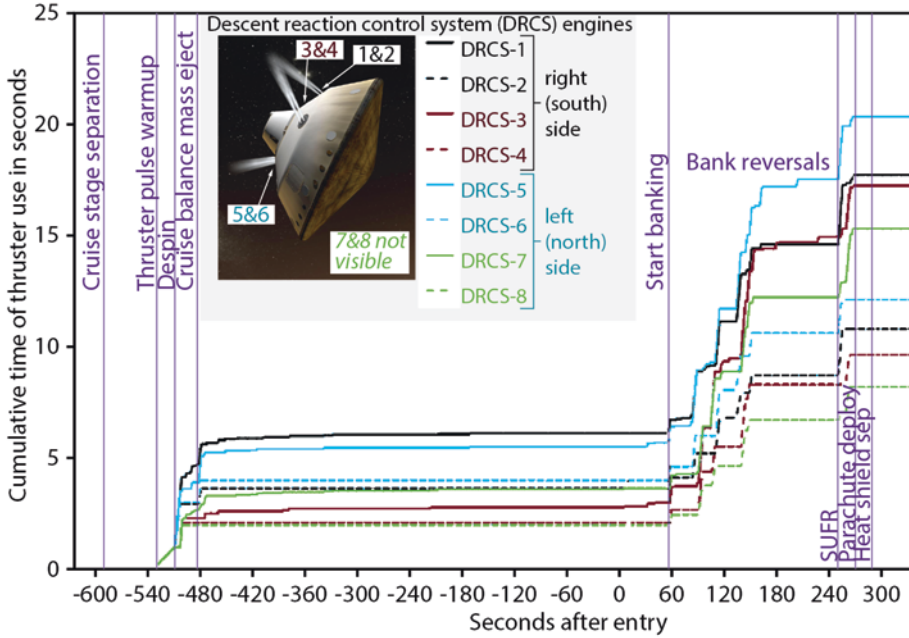


Figure 2.18. Descent reaction control system thruster use. Odd-numbered thrusters were used for all pulses; even-numbered thrusters were secondary, used only when more thrust was needed. SUFR = Straighten Up and Fly Right. Modified from Baker et al (2014).

2.3.5 The parachute

MSL’s parachute had the same shape as the Vikings’, but with a diameter of 21.35 meters it was 33% larger (Figure 2.19). Another crucial difference was the distance between the backshell and parachute: Viking’s parachute trailed by 8.5 times the parachute diameter, but MSL’s lines were longer, to separate it by 10.32 times the diameter. This increased separation was designed to reduce “area oscillations” of the parachute. The parachute was composed of orange and white ripstop nylon, except for the crown, which was made of a heavier ripstop polyester. The suspension lines were made of Technora and Kevlar, both synthetic fibers with high strength and heat resistance.³⁹

³⁹ Cruz et al (2014)

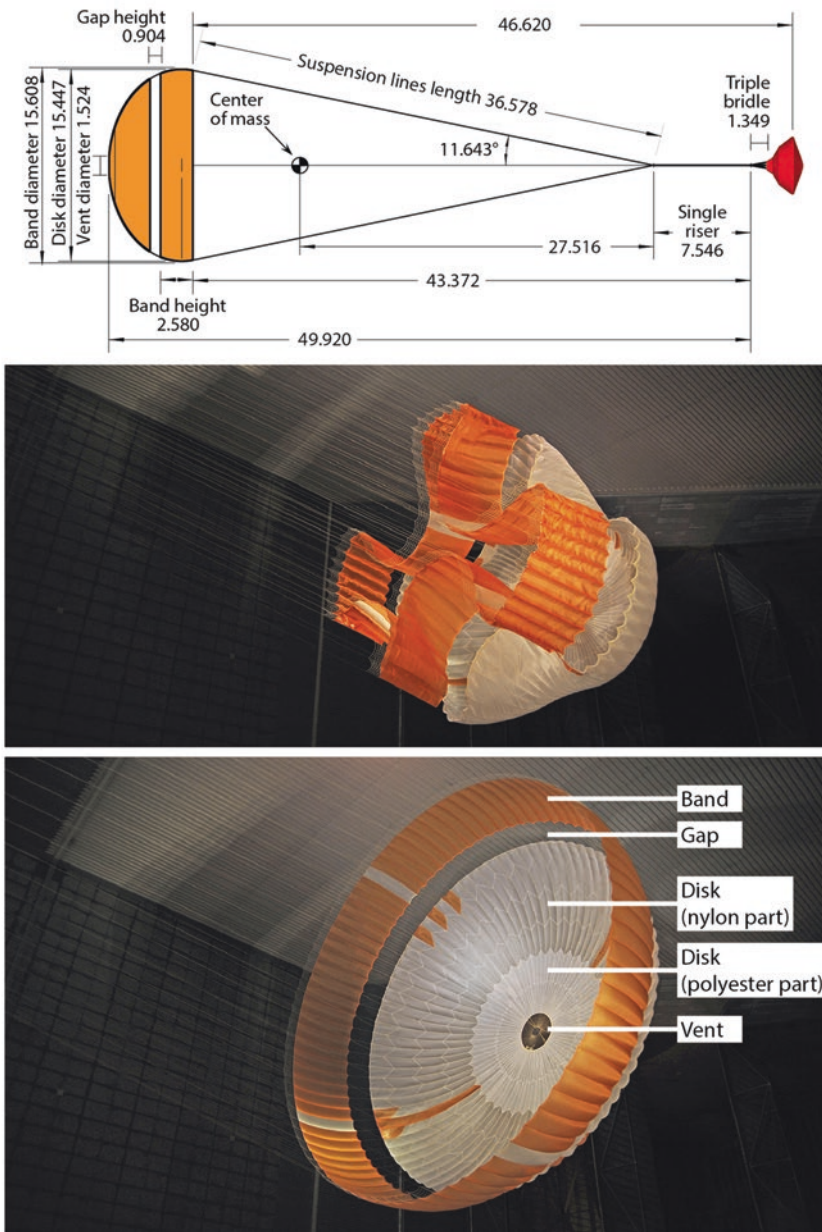


Figure 2.19. The MSL parachute. Top: dimensions, from Cruz et al (2014). The bottom two images were taken during April 2009 testing of parachute deployment in a wind tunnel at NASA Ames Research Center. NASA/JPL-Caltech releases PIA11992 and PIA11993, annotated by Emily Lakdawalla.

2.3.6 The descent stage

The descent stage was a complicated spacecraft all on its own, with a mind-boggling number of systems crammed into its open structure (Figure 2.20 and Figure 2.21). At its heart was the most sophisticated propulsion system JPL had ever built. It was actually two distinct propulsion systems that had to share components to conserve mass and volume. The descent stage also served as the structural link between all other spacecraft components, with six separation nuts each connecting the top hexagon of the descent stage to the cruise stage and backshell, and three connecting the bottom of the descent stage structure to the top deck of the rover. It weighed 1068 kilograms, of which 397 was fuel.⁴⁰

Although the rover's main computer ultimately commanded the descent stage, the descent stage contained numerous avionics of its own, including a computer to control the thruster systems; the descent inertial measurement unit, with gyroscopes that facilitated the precision flying of the guided-entry phase; an X-band radio system that was used throughout cruise, entry, descent, and landing; the Terminal Descent Sensor radar system used to measure altitude and velocity; and the bridle umbilical device used to lower the "rover-on-a-rope".

The Descent Reaction Control System (DRCS) that steered the aeroshell throughout entry and descent consisted of eight 250-newton thrusters in four pairs, one primary and one secondary. Holes cut into the backshell allowed these thrusters to protrude. MSL used the primary (odd-numbered) thrusters for small pulses; the secondary (even-numbered) thrusters came into play for larger pulses. These eight thrusters drew fuel from only one of the descent stage's three fuel tanks, the one mounted toward the rover's front. The rover's computer updated commands to the thrusters every 125 milliseconds, commanding thrusts in increments of 15.625 milliseconds.

The eight downward-pointing Mars Lander Engines (MLE) were much larger than the upward-pointing Reaction Control System thrusters, at 3300 newtons as compared to 250. The landing used only about two-thirds of the descent engines' thrust capability because the low altitude of the landing site gave MSL ample time to decelerate. They drew on three propellant tanks using a flow regulator that had been launched into Earth orbit multiple times as part of the Space Shuttle *Discovery* before being rebuilt for MSL.⁴¹ Four of the engines were canted at 5° outboard from the rover, and four were canted at 22.5°. When the descent stage was connected to the rover, the nozzles of the engines projected beyond the rover's belly pan, keeping exhaust clear of the rover (Figure 2.22).

The Terminal Descent Sensor sensed the ground with six radar beams. One beam pointed directly downward; three pointed at an elevation of 20° in different directions (one toward the rear and one each to left and right); and two, called the "headlight" beams, pointed forward and slightly left and right at elevations of 50° (Figure 2.23). Unlike other landing radar systems, MSL's was "memoryless" – measurements of range and velocity were essentially instantaneous, not relying on previous measurements or even on sharing of information between beams. It was computationally intensive, but a "bad lock" didn't propagate error forward in time, allowing the system to be robust to spurious signals.

⁴⁰Hoffman et al (2007)

⁴¹Pearlman (2017)

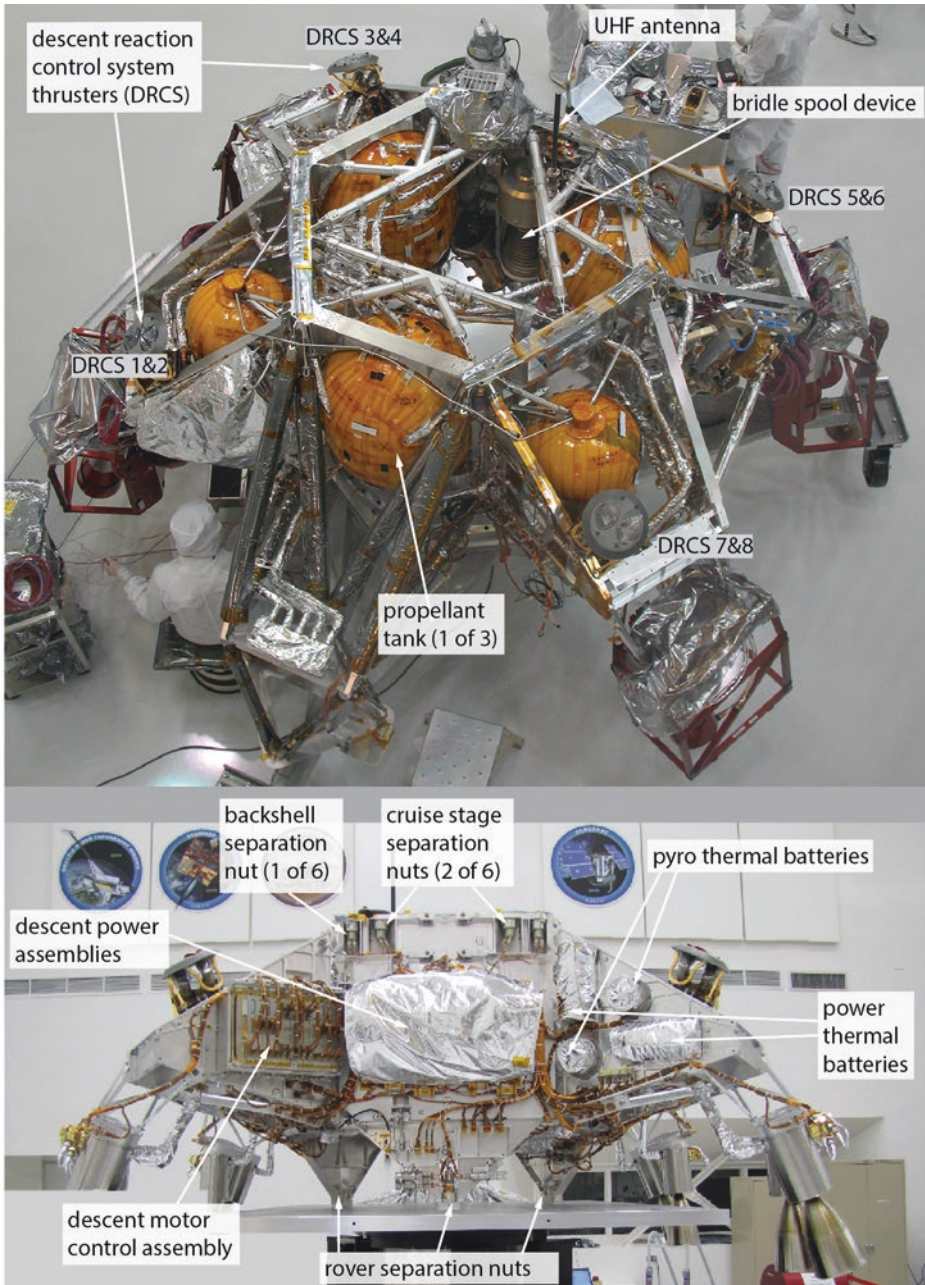


Figure 2.20. Descent stage parts (part 1). Top photo taken at JPL in early October 2008, bottom photo around November 2008. NASA/JPL-Caltech release PIA11425, annotated by Emily Lakdawalla.

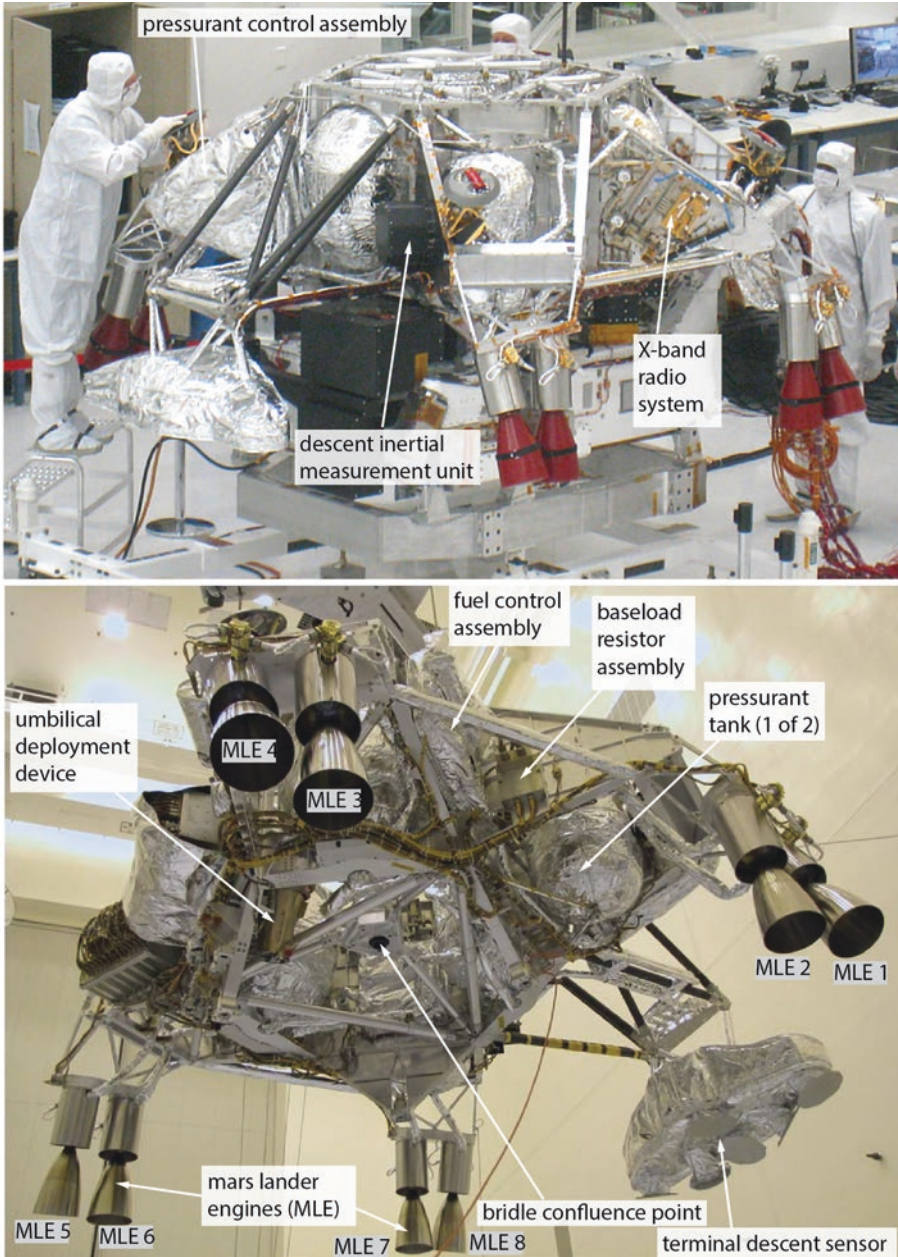


Figure 2.21. Descent stage parts (part 2). Top photo taken at JPL around November 2008. Bottom photo taken at Kennedy Space Center around November 2011. NASA/JPL-Caltech releases PIA11808 and PIA15020, annotated by Emily Lakedawalla.

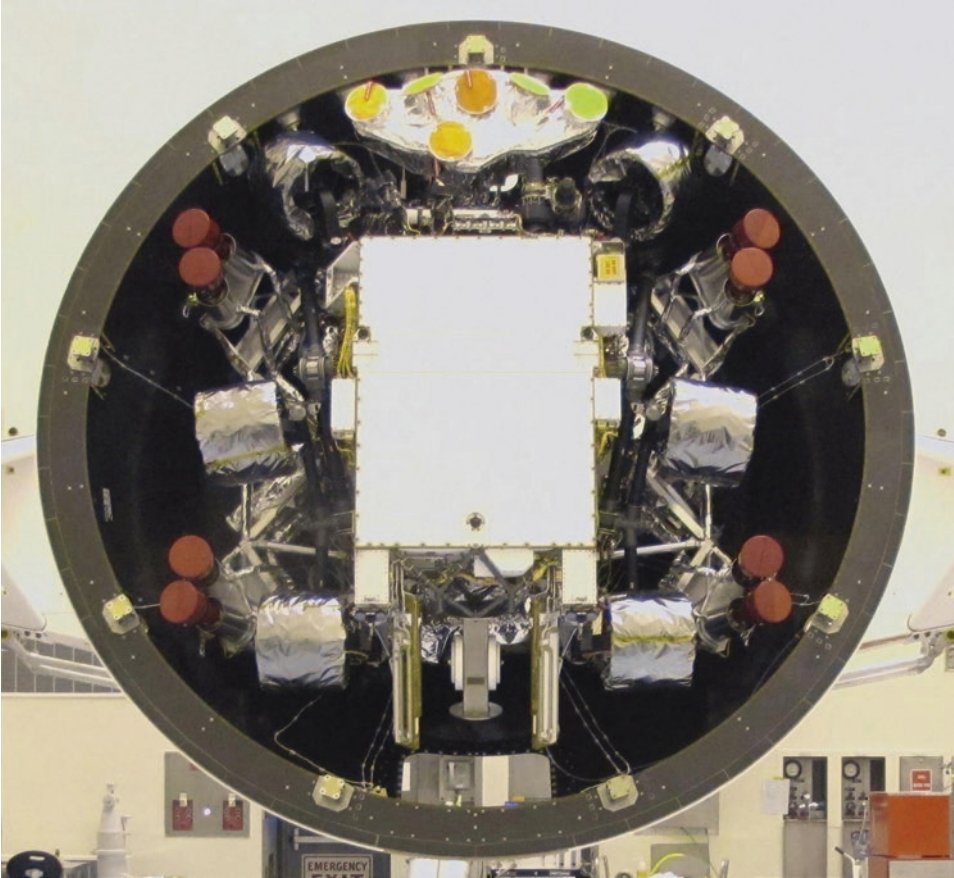


Figure 2.22. Descent stage mated to the rover and inside the backshell. The red caps on descent stage rockets, sliver wrap on rover wheels, and yellow covers on MARDI camera (square) and terminal descent sensors (round) were removed before flight. Photo taken at Kennedy Space Center in October 2011. NASA/JPL-Caltech release PIA14756.

2.3.7 Descent under parachute: 259 to 375 seconds

Still traveling at Mach 1.7, MSL fired the explosive sabot that deployed the parachute 259 seconds after hitting the entry interface, at 5:15:05 Spacecraft Event Time. The parachute filled with air, stretching its suspension lines in 1.135 seconds and fully inflating in under two seconds. In those two seconds, Mars' gravity was still accelerating the spacecraft; it sped up by 0.743 meters per second. The parachute was qualified to survive deployment at up to Mach 2.3 and able to withstand an opening force of 289 kilonewtons. In the event, it experienced only 153.8 kilonewtons. The reaction control system thrusters remained ready to work to cancel out any spinning or rocking motions, but MSL's descent was stable

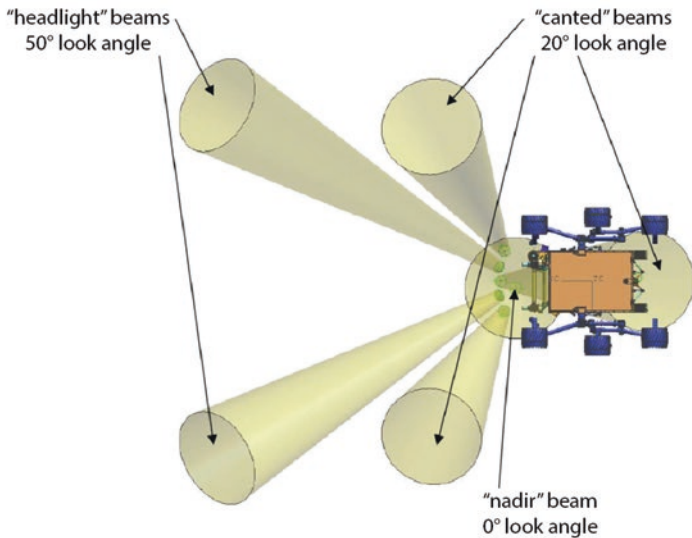


Figure 2.23. Terminal Descent Sensor beam pattern. Emily Lakdawalla after Pollard (2012).

enough for them not to be needed.⁴² With the parachute inflated, the MEDLI instrument suite shut down. Only 20 seconds after the parachute deployed, MSL had slowed to subsonic speeds, so it dropped the heat shield, exposing the rover and descent stage to the Martian air at 5:15:24.⁴³

About 6 seconds before the heat shield separated, the Mars Descent Imager (MARDI) had switched on and begun taking images at an average 3.88 frames per second. The first 26 MARDI photos were black; the next 622 documented the final 2.5 minutes of landing. As the heat shield fell away, a white-balance target on the inside of the heat shield helped MARDI's autoexposure algorithm to adjust quickly from the pitch-black interior of the capsule to the brightly lit Martian day (Figure 2.24).

Angled to the east along the descent path and with a field of view of 70-by-55°, MARDI's first images encompassed much of the eastern half of the landing ellipse. The heat shield can be clearly tracked through the first 250 of the images, and MARDI even documented the moment of its impact onto the Martian surface in image number 345, taken at 05:16:48 on the spacecraft's clock (Figure 2.25). (Note: Time stamps in MARDI image files appear to be 3 seconds later than the spacecraft clock times in the same files. The given spacecraft clock times correctly correspond to the landing timeline in Table 2.2 within a fraction of a second.)

⁴²Cruz et al (2014)

⁴³Karlgaard et al (2014)

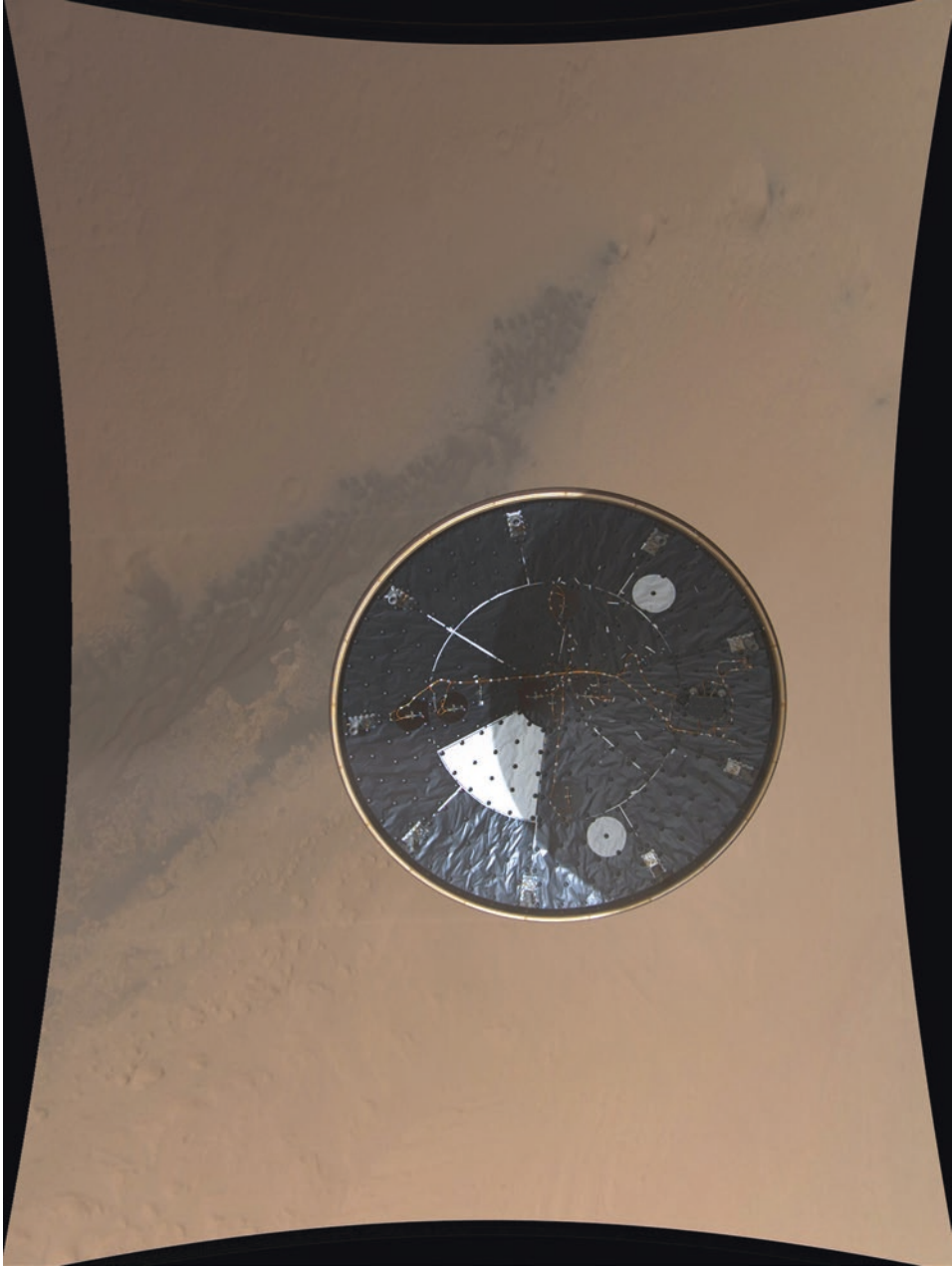


Figure 2.24. MARDI image of the heat shield taken at a spacecraft clock time of 397501995, one second after the release of the heat shield. MARDI image 0000MD0000000000100033E01. NASA/JPL-Caltech/MSSS.

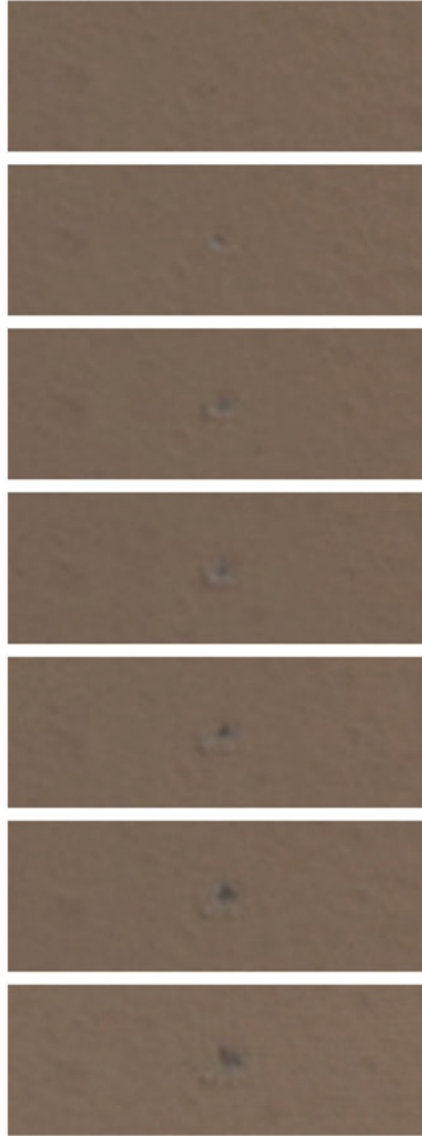


Figure 2.25. Series of MARDI images documenting the impact of the heat shield onto the Martian surface. A plume of material spread for several seconds after the impact before the MARDI field of view no longer encompassed the impact site. MARDI images 0000MD0000000000100344E01 to 0000MD0000000000100358E01, taken between 5:16:45 and 5:16:49. NASA/JPL-Caltech/MSSS.

After dropping the heat shield, MSL waited three seconds, ready to use its thrusters to cancel any rocking motion caused by the separation, but the spacecraft was steady and

needed no correction. After another two seconds, it activated the Terminal Descent Sensor radar system. The five-second delay after heat shield separation was necessary to prevent the radar system from confusing the nearby heat shield with the ground. The Terminal Descent Sensor achieved radar lock about 20 seconds after heat shield jettison. One radar beam showed a spurious measurement of the “ground” at a range of 1003.66 meters and a velocity of -47.76 meters per second about 30 seconds after dropping the heat shield. This was probably a detection of the heat shield falling toward the ground!⁴⁴

Although the Terminal Descent Sensor provided information on the distance to the ground, the instantaneous altitude of the spacecraft is not necessarily the same as its altitude relative to its final landing site some distance away; it was mainly for this reason that the landing site needed to be flat throughout the landing ellipse.⁴⁵

Shortly after dropping the heat shield, direct-to-Earth transmission of the X-band signal ceased. The MSL team was now entirely dependent upon Mars Odyssey for real-time information on the status of the landing. Odyssey performed well throughout the landing, delivering continuous updates on MSL’s health.

As MSL descended, Mars Reconnaissance Orbiter sped toward it from the south (see Figure 2.14 and look for 5:14 UTC on all three ground tracks, then follow the time forward). Less than a second after the heat shield dropped, Mars Reconnaissance Orbiter’s HiRISE camera began acquiring an image of the landing site. Like most Mars orbiting cameras, HiRISE is a “pushbroom” instrument that sweeps a long, skinny detector across the surface, taking advantage of spacecraft motion to build up an image swath about 10,000 pixels wide by as many as 126,000 pixels long. It can take as many as 100 seconds to capture a single image. Ordinarily, not much changes on the Martian surface during such a short period of time, but things were happening fast as MSL descended. HiRISE’s beam swept across the heat shield at 353 seconds after entry; it caught the backshell and then the parachute about 3 seconds later.⁴⁶ So the amazing HiRISE image actually captures different moments in time for the two pieces of hardware (Figure 2.26).

At an altitude of 3000 meters, the rover prepared its descent stage for powered descent. When the data from the Terminal Descent Sensor indicated that the spacecraft had reached a speed of 79 meters per second and an altitude of 1671 meters, 117 seconds and 10.4 kilometers’ altitude after deploying the parachute, it primed the descent stage engines, flowing fuel to them at 1% throttle, and abruptly cut the connection to the backshell and parachute.⁴⁷ For two seconds, the spacecraft plummeted, making room between it and the backshell. The parachute remained attached to the backshell, and both fell together. Lacking rockets to slow their descent further, they landed before the rover did, to the west-southwest of the rover’s landing site.

⁴⁴ Chen and Pollard (2014)

⁴⁵ Steltzner et al (2010)

⁴⁶ Christian Schaller, personal communication, email dated February 17, 2016

⁴⁷ Karlgaard et al (2014)

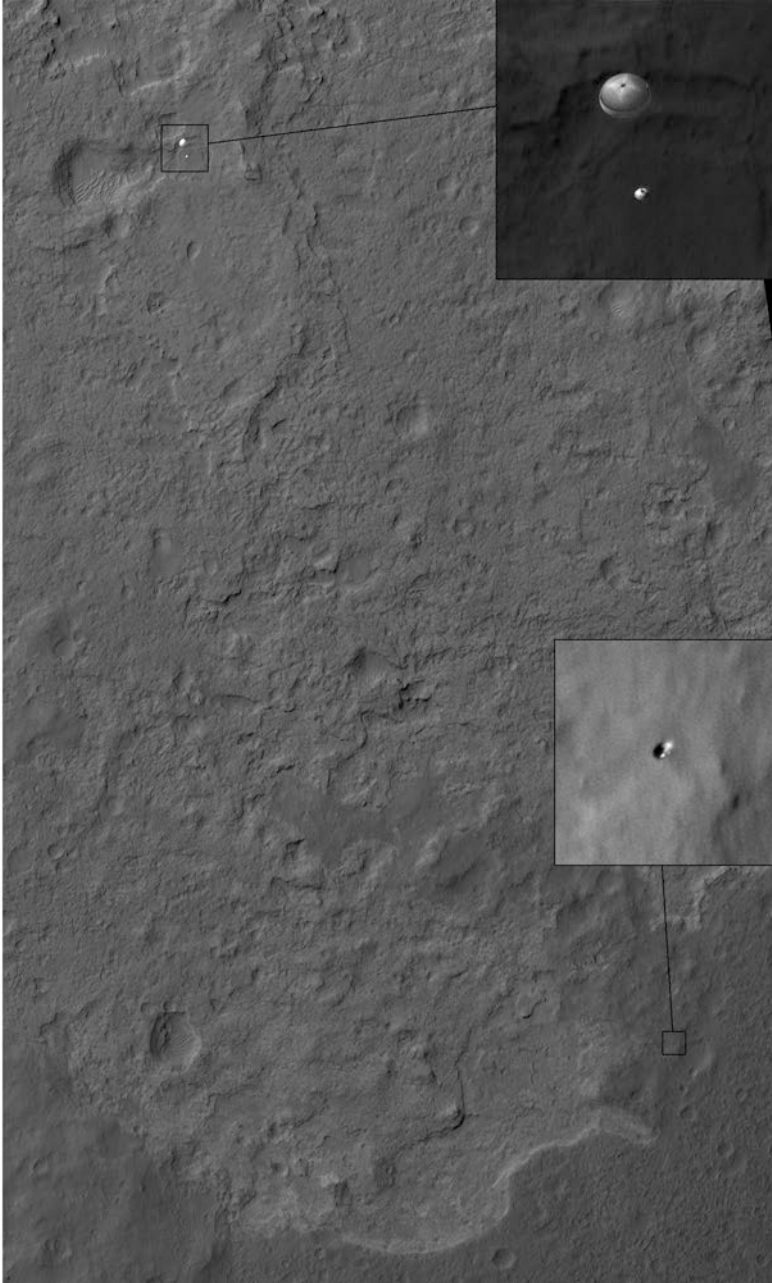


Figure 2.26. HiRISE's amazing image of MSL under parachute, its heat shield significantly below it. HiRISE image ESP_028256_9022. NASA/JPL-Caltech/UA.

2.3.8 Powered descent: 378 to 412 seconds

The Mars Lander Engines throttled up, beginning the “powered approach” phase, at 5:17:04. The rockets worked to smoothly zero out the spacecraft’s horizontal motion while bringing the vertical descent rate to 32 meters per second. Figure 2.27 summarizes the work of the landing engines. At the beginning of powered approach, the descent stage also performed a divert maneuver, shifting the spacecraft’s position 300 meters to the left of the entry trajectory, a distance sufficient to ensure that the rover’s eventual landing site would not be directly on top of the already-landed backshell and parachute.⁴⁸

Following powered approach, the spacecraft was finally directly above its eventual landing site. For the first time, the terminal descent sensor’s altitude readings directly measured the remaining distance to the surface: 247.9 meters. A brief descent phase called the “constant velocity accordion” saw the rover continuing to descend at 32 meters per second. The constant velocity accordion was intended to accommodate any mismatch between the terminal descent sensor’s measured altitude at the beginning of powered approach and the altitude of the actual landing site now beneath the rover. The constant velocity accordion could have accommodated as many as 100 meters of altitude difference; in fact, there were only 5.5 meters of altitude difference between the estimated and

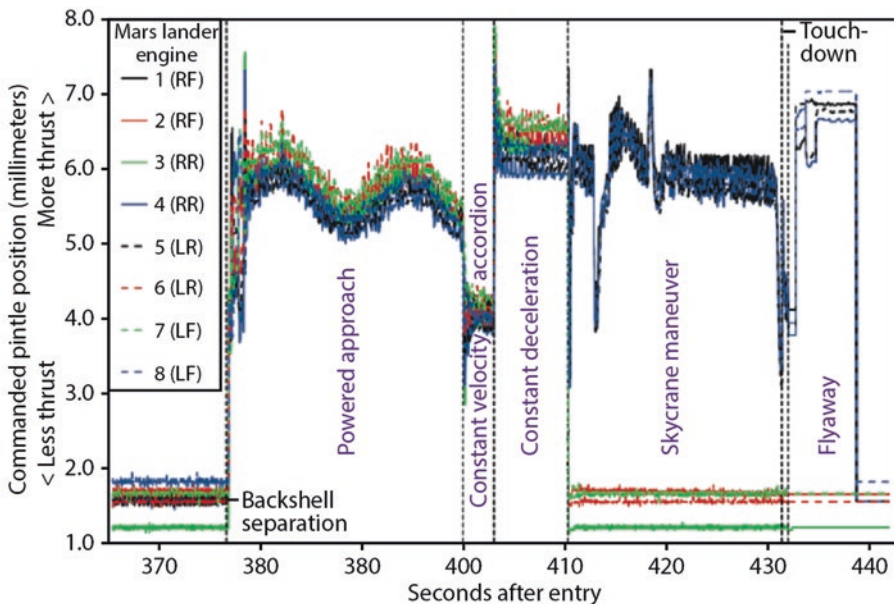


Figure 2.27. Mars Lander Engine (MLE) thruster operation during the spacecraft’s final descent. The position of a propellant injection device, called a pintle, in the throat of the rocket controlled the amount of thrust. Emily Lakdawalla after Baker et al (2014).

⁴⁸Steltzner et al (2010)

actual altitude.⁴⁹ With that out of the way, at an altitude of 142 meters, MSL entered the constant deceleration phase, smoothly slowing the spacecraft from a descent rate of 32 meters per second to 0.75 meters per second.⁵⁰ It was time to deploy the landing gear.

2.3.9 The lander

Before the MSL mission could rove Mars, its rover had to perform the functions of a lander, deploying landing legs and coming to a stable halt. Once on Mars, the landing gear had to transform into the rover's mobility system. The rocker-bogie suspension system uses a number of passive pivots to balance out rough terrain and keep the rover body as level as possible. But during landing, with the wheels not yet touching ground, the interconnected levers of the mobility system needed to be carefully restrained until the last possible moment, to keep the six wheels as close to flat as possible upon touchdown.⁵¹ The mobility system was restrained at five points: at the four corners of the rover, connecting the rockers and bogies to the rover body, and also in the center of the rover's back, holding the differential arm still. During flight, the long rocker arm connecting the front wheel to the rear bogie was folded nearly at a right angle in order to fit the mobility system within the cramped space of the aeroshell (Figure 2.28 and Figure 1.7).

Many of the devices now visible on the top deck of the rover are related to cruise, entry, descent, and landing, and several are not used in the surface mission (Figure 2.29).

2.3.10 Sky crane and landing: 412 to 432 seconds

The descent stage switched from decelerating at a constant rate to descending at a constant rate of 0.75 meters per second, so required less rocket power. Out of concern that the descent stage rocket exhaust could impinge on the rover, the four engines canted at only 5° were throttled down to 1%, the other four throttling up to compensate. The descent stage wobbled a bit in response to the sudden change in the descent engines' activity; the spacecraft allowed 2.5 seconds for those wobbles to settle out before proceeding, of which it needed only 1.25 seconds.

At 5:17:38, at an altitude of about 21 meters, with the descent stage stable and descending at 0.75 meters per second, three pyros fired to separate the rover from the descent stage. The weight of the rover pulled on three nylon/Vectran cords wrapped across a confluence point pulley and then around a spool attached to the descent stage, called the bridle umbilical device (Figure 2.30). A brake within the spool controlled the rate of descent. The rover had pulled the cords to their full length of about 7.5 meters in 5 seconds (Figure 2.31). Along with the three strings of the bridle, the bridle umbilical device also deployed an umbilical cable that allowed commands to be passed from the rover computer to the descent stage. (An artist's concept of the extended bridle and umbilical can be found in Figure 1.21.) The tapered shape of the spool made it spin at a higher angular rate as the

⁴⁹Way et al (2013)

⁵⁰Sell et al (2014)

⁵¹Jordan (2012)

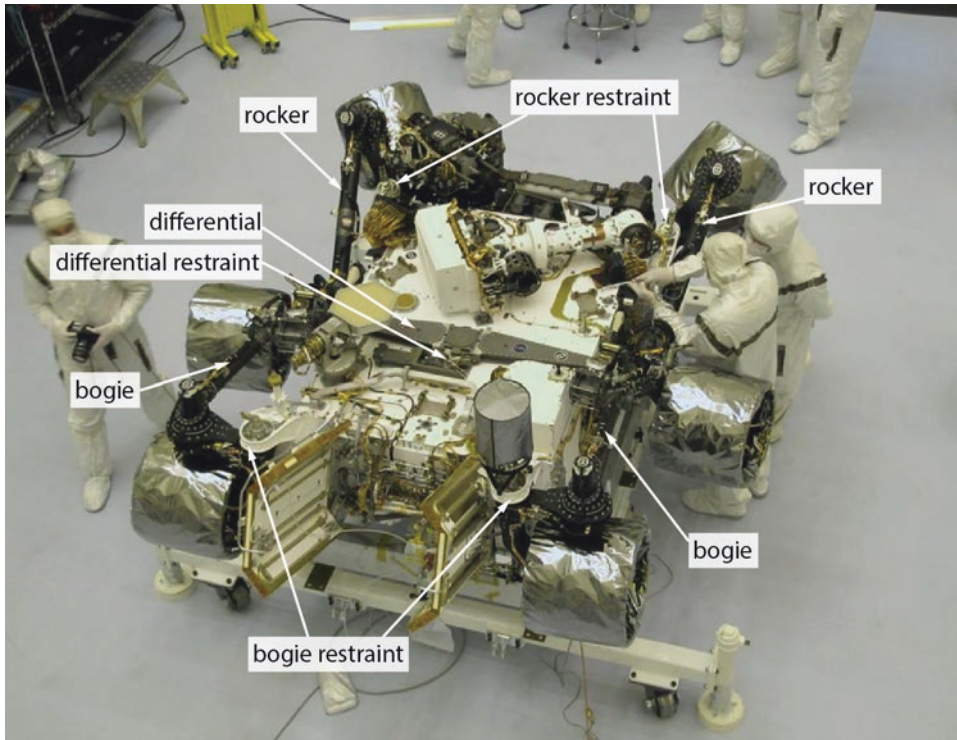


Figure 2.28. Rover mobility system in stowed configuration. Photo taken at Kennedy Space Center in November 2011. NASA/JPL-Caltech release PIA15021.

rover descended, and the faster it spun, the more the brake resisted the motion; this controlled the rate at which the rover descended under Mars' gravitational acceleration.⁵²

As the rover descended on its cables, it also deployed its landing gear. Pyros fired to separate the rear bogies from the rover body 0.7 seconds after the rover separated. The bogies fell, pulling downward on the bent rockers, and locking them into their final, straight positions. After the rover reached the end of the bridle, another pair of pyros fired to separate both rockers.⁵³ Finally, just before touchdown, one more pyro fired to release the differential restraint; waiting until the very last moment kept the wheels as coplanar as possible for touchdown, and would allow the landing gear to passively accommodate any surface roughness.⁵⁴ One thing the landing gear could not handle however, would be the presence of a rock more than 66 centimeters tall positioned to spear the rover's belly pan. HiRISE images had shown few such rocks in the landing ellipse, but bad luck could win, and MSL had no active terrain hazard avoidance capability.

⁵² Gallon (2012)

⁵³ Sell et al (2014)

⁵⁴ Jordan (2012)

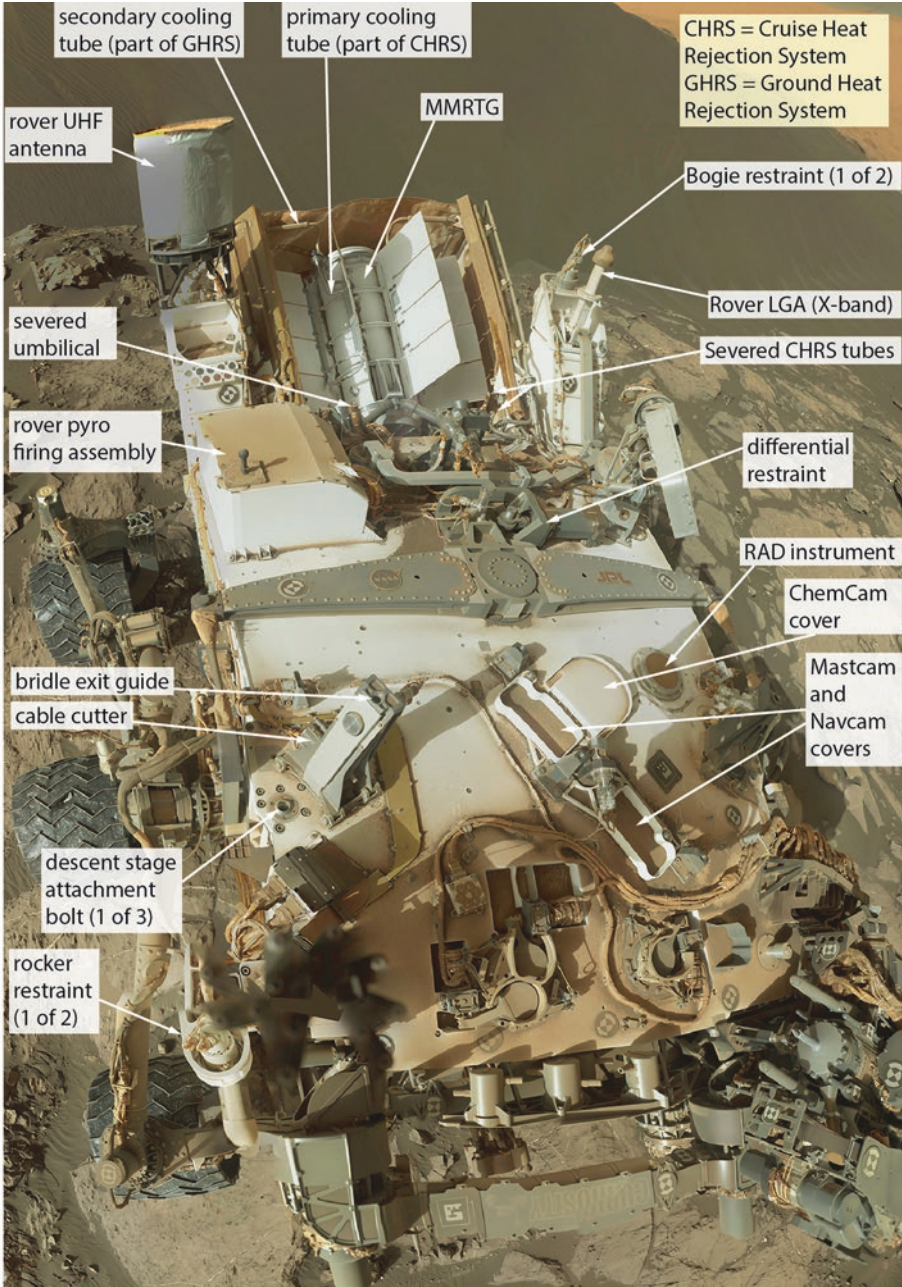


Figure 2.29. Parts of the rover relevant to cruise, entry, descent, and landing. The base image is a self-portrait taken with the Mastcam on sol 1197 (19 December 2015). NASA/JPL-Caltech/MSSS/Emily Lakdawalla.

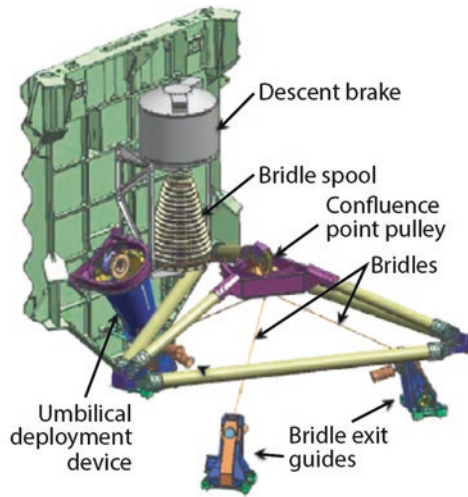


Figure 2.30. The bridle umbilical device connection to the rover. Emily Lakdawalla after Gallon (2012).

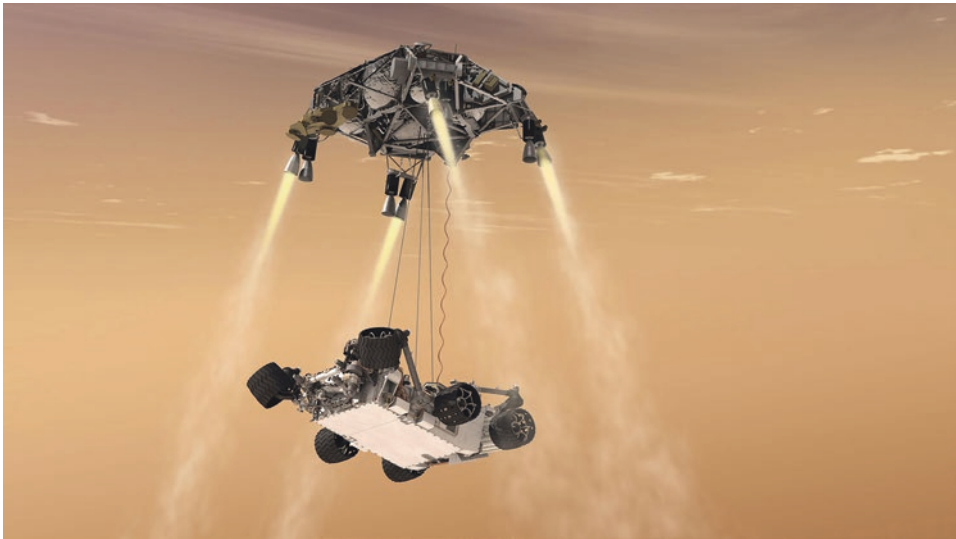


Figure 2.31. Artist's concept of the rover pulling to the end of its bridle as the Mars Lander Engines fire to maintain a steady rate of descent. NASA/JPL-Caltech release PIA14839.

Throughout, the descent stage should have continued to drop at a slow rate of 0.75 meters per second. It should then have taken 15.67 seconds for the rover's wheels to touch the ground. However, the actual time was 17.9 seconds, far longer than estimated. That is, the rover actually descended slower than planned, at only 0.6 meters per second at the

moment of touchdown. Moreover, the rover was still drifting horizontally at more than 0.1 meters per second at the moment of touchdown, more than twice as fast as expected.⁵⁵ This slower-than-expected descent, right at the moment of touchdown, was a very serious error. Rob Manning explains:

We were to discover after MSL had landed on Mars that we had missed a crucial item. The long list of variable parameters had not included one that should be obvious: gravity. In the simulations, the EDL team used a fixed value for gravity that was rather generic for that part of Mars. We failed to take into account that the shape of the surrounding terrain and hills might affect the actual gravity, and because we didn't try other values, we didn't notice just how sensitive the landing was to being slightly off with the value the team had chosen. The value for Mars gravity used in the simulation turned out to be slightly too high – *very* slightly, only 0.1 percent – but significant enough that MSL's slowest-ever landing was even slower than we expected.⁵⁶

Had the value for gravity been off by 0.1% in the other direction, the maximum design touchdown velocity could have been exceeded, potentially damaging the mobility system.⁵⁷ Fortunately, the error was in a safe direction, and the rover touched down on its wheels very gently at 05:17:57, or 431 seconds after entering the Martian atmosphere. At that moment, the rover computer stopped the descent of the descent stage, and gave command of the descent stage to the descent stage thruster system computer.⁵⁸ The rover commanded pyros within the bridle exit guides on the rover's top deck to fire guillotine-like blades that cut through the three bridle cables and the umbilical. Spring-loaded spools within the bridle exit guides retracted the cut ends of the cables attached to the rover, and a tensioned cable that had unwound with the last few meters of the umbilical lifted the cut ends of the umbilical and bridle cables dangling from the descent stage. The Curiosity rover was all by itself on the surface of Mars – but wasn't yet out of danger.

The descent stage hovered for 0.7 seconds. To avoid dragging rocket exhaust across the rover, it needed to depart the rover either forward or backward, not sideways. Because the rover was landing to the north of the eventual science target, the descent stage had been commanded to depart whichever of those two directions was the more northerly, taking it away from the likely drive direction.⁵⁹ The rover knew it had landed facing east-southeast, so the descent stage pitched backward and then burned the four canted engines at full throttle for 6 seconds, sending the descent stage on a long parabolic arc away from the rover, to a crash landing 650 meters away about 20 seconds later.⁶⁰ Throughout powered descent, it had burned 270.4 kilograms of fuel, leaving 119 kilograms of usable hydrazine in the tanks during the crash.

Back on Earth, engineers were waiting for three distinct signals to confirm that the landing had been successful and that the rover and descent stage were safely separated. Jody Davis announced the first at 05:31:45 UTC, when she noticed that the Mars Lander Engines had throttled down to half their former power, indicating that the descent stage

⁵⁵ Way et al (2013)

⁵⁶ Manning and Simon (2014)

⁵⁷ Way et al (2013)

⁵⁸ Baker et al (2014)

⁵⁹ This was explained at the August 6, 2012 post-landing press briefing

⁶⁰ Baker et al (2014)

was no longer supporting the weight of the rover: “Tango Delta nominal.” Several seconds of quiet followed that comment, because the landing would not be over safely until the descent stage had disconnected and flown safely away.

David Way announced the second positive landing signal when he noticed that the Rover Inertial Measurement Unit was no longer reporting a changing position: “RIMU stable.” The rover was therefore not being dragged by a connection to the descent stage, nor was it sliding down a slope, or tumbling off a cliff. The third announcement came from EDL communications engineer Brian Schratz, who was monitoring the strength of the UHF radio signal between rover and orbiter, which would vary (or worse, disappear) if the descent stage dragged the rover off the ground, or landed atop the rover. Eight seconds after landing, he announced “UHF strong.”⁶¹

The last two announcements collided with each other over the microphones. Adam Steltzner walked over to Allen Chen while pointing to Schratz, asking him to repeat himself; “UHF strong,” Schratz said again. Steltzner tapped Chen on the shoulder and gave him a thumbs up signal. “Touchdown confirmed,” Chen said. “Time to see where our Curiosity will take us.” The room erupted.

2.4 CURIOSITY ON MARS

It had all gone precisely according to script. Curiosity’s landing had been targeted at 4.5965°S and 137.4019°E. The actual landing location was 4.5895°S, 137.4417°E. Curiosity had arrived only 2385 meters away from its intended target, slightly downrange and to the north of the center of the landing ellipse. In computer simulations of the landing, only 24% of simulated landings got closer to the target.⁶²

Curiosity remained in contact with Mars Reconnaissance Orbiter and Odyssey for another six minutes after landing. That was long enough for Odyssey to receive the first data that Curiosity returned from the surface of Mars, and dutifully relay the images onward to Earth. As the dust settled, Curiosity snapped photos with its belly-mounted Hazcams, giving it a fish-eye view of the ground immediately around the rover. Months prior, the mission had offered the science team a choice: receive the rear Hazcam image first, or the front one first? The mission had assumed that the scientists would want to see the forward view first, because the view of Mars would be less obscured by hardware. The science team replied that the first image is not about science; it’s about seeing wheels on the dirt. They requested that the rover’s first image show a wheel in contact with the ground.⁶³

So the first image to arrive on the computer monitors of the landing engineers, two minutes after landing, was a tiny 64-pixel-square thumbnail from the rear Hazcam that was nevertheless big enough to show the horizon, the sky very brightly lit by the afternoon Sun, and in the shadows a wheel clearly sat on the surface. “We are wheels down on Mars,” an engineer stated into the microphone. The celebration on Earth for that first photo was even louder than that for the successful landing (Figure 2.32). By the time Odyssey set below the horizon, it had returned a 256-pixel-square version of the same image, as well

⁶¹ NASA (2012b)

⁶² Way et al (2013)

⁶³ John Grotzinger told me this after the end of the press briefing on August 6, 2012



Figure 2.32. MSL team members in the Mission Support Area celebrate after the successful landing and return of the first tiny Hazcam image, which is barely visible on the screen in the background. NASA photographer Bill Ingalls stood on a table and poked his camera above a similar monitor to catch the team's reaction in this photo.

as a view from the front Hazcam (Figure 2.33). The images were mottled with dust, some of it still swirling in the air, some of it stuck to the lens caps on the Hazcams.

Curiosity lost contact with both Mars Reconnaissance Orbiter and Mars Odyssey at about the same time, at 05:23:53, as both spacecraft set below the horizon. Contact with Odyssey was lost earlier than expected because the spacecraft had gone slightly long, causing Odyssey to set behind the peak of the mountain at the center of the crater. Already Curiosity was on its own, on the far side of Mars, out of contact with Earth.

Two hours later, Odyssey passed above the horizon to the west of the landing site. In the intervening time, Curiosity had stored additional Hazcam images, taken both before and after releasing their lens caps. A close look at the new rear Hazcam image revealed something astonishing: a feature visible on the horizon in the image taken immediately after landing was no longer visible in an image taken an hour later. The smudge on the horizon in the first photo returned from Mars was later determined to be the plume of dust rising from the impact site of the descent stage, 650 meters away (Figure 2.34).

The cruise stage, aeroshell, and descent stage had all done their work admirably. The rover, on Mars, still had the brains of an interplanetary spacecraft. The next major task for the mission was to teach the spacecraft to become a Mars rover.

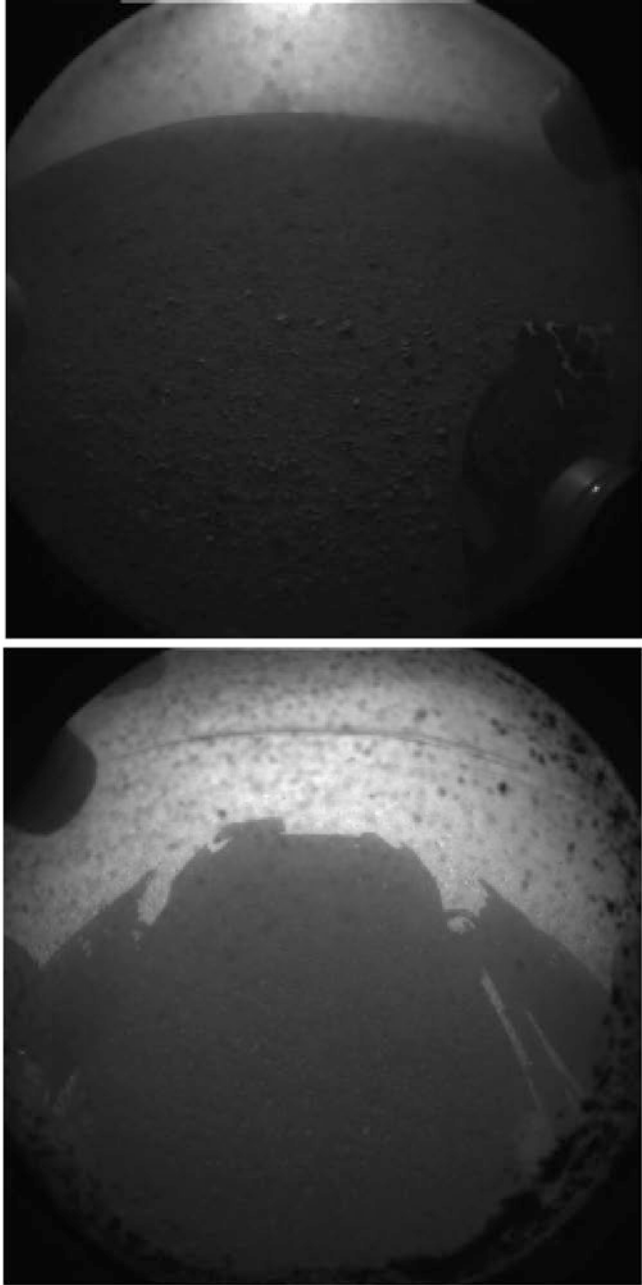


Figure 2.33. MSL's first views of its landing site. Top: Rear Hazcam (RLA_397502188EDR_D0010000AUT_04096M1), taken at 5:18:39, less than a minute after landing. Bottom: Front Hazcam (FLA_397502305EDR_D0010000AUT_04096M1), taken at 5:20:37, about 3 minutes after landing. NASA/JPL-Caltech photos.

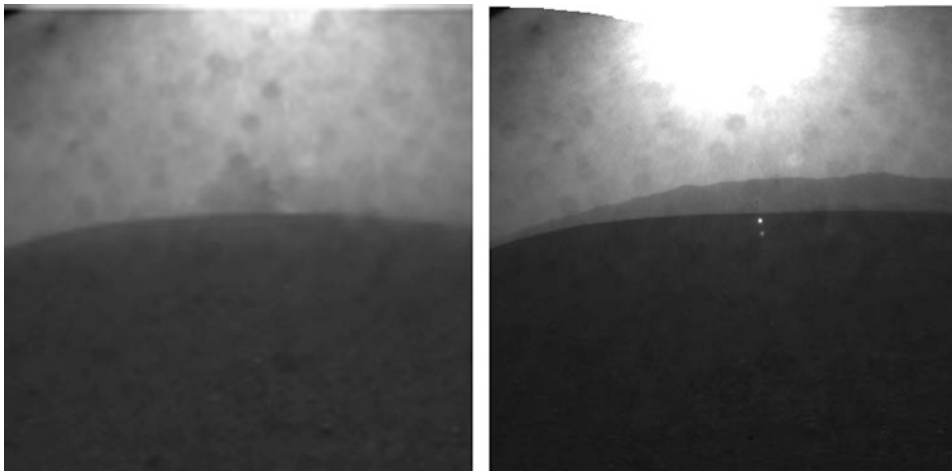


Figure 2.34. Cropped sections from two rear Hazcam images from landing day. Left: RLA_397502188EDR_D0010000AUT_04096M1, taken at 5:18:39, less than a minute after landing, includes a lumpy plume on the horizon, in the right direction to be the impact plume from the descent stage; the air appears to be cloudy with dust thrown up by the landing rockets. Right: the same region from RLA_397504876EDR_F0010000AUT_04096M1, taken about an hour later at 6:03:26, contains no such plume. Bright dots near the image center are internal reflections within the camera caused by the bright Sun being in the camera field of view. NASA/JPL-Caltech.

2.5 EPILOGUE: VIEWS OF THE CRUISE HARDWARE

The day after the landing, Mars Reconnaissance Orbiter HiRISE imaged the landing site again, catching all of the hardware on the ground (Figure 2.35). The rover was visible as a box on the surface, the descent rocket blast zone surrounding it like butterfly wings. The lighter-colored impingement zones of the four canted descent rockets looked like lighter dots on the wings (Figure 2.36). The crash sites of the heat shield, descent stage, and parachute were arrayed around the rover. The descent stage was marked with an extended spray of ejecta more than 100 meters long. Engineers suspect that its remaining fuel may have detonated on impact, blasting the spacecraft to pieces.

Since the landing, HiRISE has imaged the landing site regularly while monitoring the rover traverse, seeing the parachute blowing around over time. Post-landing HiRISE images of landing hardware are listed in Table 2.3.

Figure 2.36. Detail view of MSL landing hardware on the surface on sol 1. All scale bars are 20 meters long. Upper left: descent stage impact site. Upper right: rover. Lower left: backshell and parachute. Lower right: heat shield. HiRISE image ESP_028269_1755. NASA/JPL-Caltech/UA.



Figure 2.35. HiRISE image of the MSL landing site, sol 1 (August 7, 2012). The impact sites of the backshell, descent stage, and parachute are to the left of the blast zone that marks the rover, uprange; the heat shield is downrange, to the right. HiRISE image ESP_028269_1755. NASA/JPL-Caltech/UA.

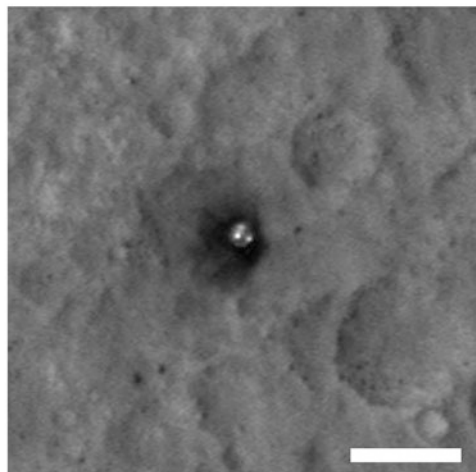
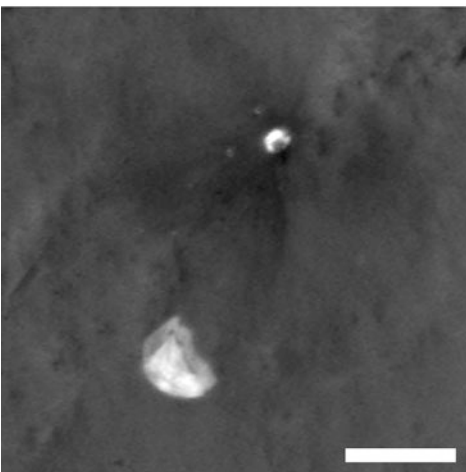
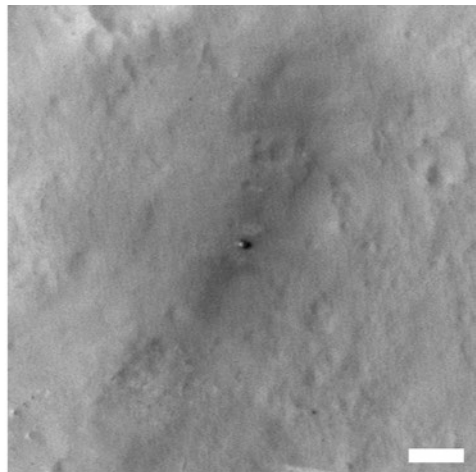
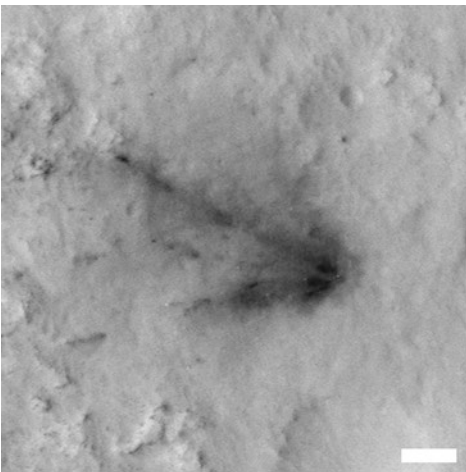


Table 2.3. HiRISE images of landing hardware. Emission angle is a measure of how directly overhead the orbiter was at the moment the image was taken. Lower emission angle is more directly overhead and produces a higher-resolution, less-distorted image. HiRISE images are grayscale except for a narrow color strip at the center; whether the hardware is visible in the grayscale only (“gray”) or color parts of the image is indicated.

Image	Date	Sol	Emission angle (degrees)	Descent stage	Backshell	Landing site	Heat shield
ESP_028269_1755	7 Aug 2012	1	45	gray	gray	gray	gray
ESP_028335_1755	12 Aug 2012	6	30	gray	gray	color	gray
ESP_028401_1755	17 Aug 2012	11	10	gray	gray	color	gray
ESP_028612_1755	2 Sep 2012	27	9	color	color	color	gray
ESP_028678_1755	8 Sep 2012	32	17	gray	gray	gray	gray
ESP_029746_1755	30 Nov 2012	113	3	gray	gray	—	—
ESP_029957_1755	16 Dec 2012	129	2	color	color	gray	—
ESP_030168_1755	2 Jan 2013	145	17	gray	gray	gray	color
ESP_030313_1755	13 Jan 2013	157	4	gray	gray	color	gray
ESP_034572_1755	11 Dec 2013	479	10	gray	gray	gray	gray
ESP_035350_1755	10 Feb 2014	538	8	gray	gray	gray	gray
ESP_036128_1755	11 Apr 2014	597	3	gray	gray	gray	—
ESP_037117_1755	27 Jun 2014	672	14	gray	gray	color	—
ESP_040269_1755	28 Feb 2015	911	2.6	gray	gray	gray	—
ESP_048774_1755	21 Dec 2016	1556	2.7	gray	gray	—	—

2.6 REFERENCES

- Abilleira F (2013) 2011 Mars Science Laboratory trajectory reconstruction and performance from launch through landing. Paper presented to the 23rd AAS/AIAA Spaceflight Mechanics Meeting, 10–14 Feb 2013, Kauai, Hawaii, USA
- Abilleira F and Shidner J (2012) Entry, descent, and landing communications for the 2011 Mars Science Laboratory. Paper presented to the AIAA Guidance, Navigation, and Control Conference, 13–16 Aug 2012, Minneapolis, Minnesota, USA
- Baker R et al (2014) Mars Science Laboratory Descent-Stage Integrated Propulsion Subsystem: Development and flight performance. *Journal of Spacecraft and Rockets* 51:4, DOI: 10.2514/1.A32788
- Beck R et al (2010) The evolution of the Mars Science Laboratory heatshield (part III). Presentation to the 7th International Planetary Probe Workshop, Barcelona, Spain, 16 Jun 2010.
- Bhandari P et al (2011) Mars Science Laboratory Launch Pad Thermal Control. Paper presented to the 41st International Conference on Environmental Systems, 17–21 Jul 2011, Portland, Oregon, USA
- Bose D et al (2013) Initial assessment of Mars Science Laboratory heatshield instrumentation and flight data. Paper presented to the 51st AIAA Aerospace Sciences Meeting, 7–10 Jan 2013, Grapevine, Texas, USA, DOI: 10.2514/6.2013-908, DOI: 10.2514/6.2013-908
- Bose D et al (2014) Reconstruction of aerothermal environment and heat shield response of Mars Science Laboratory. *Journal of Spacecraft and Rockets* 51:4, DOI: 10.2514/1.A32783
- Chang K (2012) Simulated Space ‘Terror’ Offers NASA an Online Following. *The New York Times* 11 Jul 2012, p. A14
- Chen A et al (2014) Reconstruction of atmospheric properties from Mars Science Laboratory entry, descent, and landing. *Journal of Spacecraft and Rockets* 51:4, DOI: 10.2514/1.A32708
- Chen C and Pollard B (2014) Radar terminal descent sensor performance during Mars Science Laboratory landing. *Journal of Spacecraft and Rockets* 51:4, DOI: 10.2514/1.A32641
- Cruz J et al (2014) Reconstruction of the Mars Science Laboratory Parachute Performance. *Journal of Spacecraft and Rockets* 51:4, DOI: 10.2514/1.A32816
- Edquist K et al (2009) Aerothermodynamic design of the Mars Science Laboratory heatshield. Paper presented to the 41st AIAA Thermophysics Conference, 22–25 Jun 2009, San Antonio, Texas, USA, DOI: 10.2514/6.2009-4075
- Edquist K et al (2009) Aerothermodynamic design of the Mars Science Laboratory backshell and parachute cone. Paper presented to the 41st AIAA Thermophysics Conference, 22–25 Jun 2009, San Antonio, Texas, USA, DOI: 10.2514/6.2009-4078
- Gallon J (2012) Verification and validation testing of the Bridle and Umbilical Device for Mars Science Laboratory. Paper presented to the 2012 IEEE Aerospace conference, 3–10 Mar 2012, Big Sky, Montana, USA, DOI: 10.1109/AERO.2012.6187289
- Hoffman P et al (2007) Preliminary design of the Cruise, Entry, Descent, and Landing Mechanical Subsystem for MSL. Paper presented at the 2007 IEEE Aerospace Conference, 3–10 Mar 2007, Big Sky, Montana, USA, DOI: 10.1109/AERO.2007.352826

- Jordan E (2012) Mars Science Laboratory differential restraint: The devil is in the details. Paper presented at the 41st Aerospace Mechanisms Symposium, May 16–18, 2012, Pasadena, California, USA
- JPL (2012a) Spacecraft Computer Issue Resolved. <http://mars.jpl.nasa.gov/news/whatsnew/index.cfm?FuseAction=ShowNews&NewsID=1206>. Status report dated 9 Feb 2012, accessed 7 Jan 2015
- JPL (2012b) Mars-Bound NASA Craft Adjusts Path, Tests Instruments. <http://mars.nasa.gov/msl/news/whatsnew/index.cfm?FuseAction=ShowNews&NewsID=1211>. Status report dated 26 Mar 2012, accessed 11 Feb 2016
- Karlggaard C et al (2014) Mars Science Laboratory Entry Atmospheric Data System Trajectory and Atmosphere Reconstruction. *Journal of Spacecraft and Rockets* 51:4, DOI: 10.2514/1.A32770
- Kornfeld R et al (2014) Verification and validation of the Mars Science Laboratory/Curiosity rover entry, descent, and landing system. *Journal of Spacecraft and Rockets* 51:4, DOI: 10.2514/1.A32680
- Little A et al (2013) The Mars Science Laboratory (MSL) Entry, Descent, and Landing Instrumentation (MEDLI): hardware performance and data reconstruction. Paper presented to the 36th AAS Guidance and Control Conference, 1–6 Feb 2013; Breckenridge, CO, USA
- Manning R and Simon W (2014) Mars Rover Curiosity. Smithsonian Books, Washington, DC
- Martin-Mur T et al (2012) Mars Science Laboratory Navigation Results. Paper presented at the 23rd International Symposium on Space Flight Dynamics, 29 Oct–2 Nov 2012, Pasadena, CA, USA
- Martin-Mur T et al (2014) Mars Science Laboratory interplanetary navigation. *Journal of Spacecraft and Rockets* 51:4, DOI: 10.2514/1.A32631
- McEwen A (2012) Impacts from MSL tungsten blocks and cruise stage. http://www.uahirise.org/ESP_029245_1755, image caption dated 5 Dec 2012, accessed 7 Jan 2015
- Mendeck G and Craig McGrew L (2014) Entry guidance design and postflight performance for 2011 Mars Science Laboratory mission. *Journal of Spacecraft and Rockets* 51:4, DOI: 10.2514/1.A32737
- NASA (2011a) Mars Science Laboratory Launch. Press kit dated Nov 2011
- NASA (2011b) NASA Ready for November Launch of Car-Size Mars Rover. Press release dated 19 Nov 2011
- NASA (2011c) NASA Mars-Bound Rover Begins Research In Space. Press release dated 13 Dec 2011
- NASA (2012a) Mars Science Laboratory Landing. Press kit dated Jul 2012
- NASA (2012b) First words of safe landing on Mars - Tango Delta Nominal. http://www.nasa.gov/mission_pages/msl/news/msl20120821f.html posted 21 Aug 2012, accessed 23 Feb 2016
- Novak K et al (2016) Thermal response of the Mars Science Laboratory spacecraft during entry, descent, and landing. Paper presented to the 46th International Conference on Environmental Systems, 10–14 Jul 2016, Vienna, Austria
- Pearlman R (2017) From space plane to sky crane: How part of a space shuttle landed a rover on Mars. <http://www.planetary.org/blogs/guest-blogs/2017/0804-from-space-plane-to-sky-crane.html> article dated 5 Aug 2017, accessed 27 Oct 2017.

- Pollard B (2012) Radar Terminal Descent Sensor (TDS). Presentation given to the JPL Section 334 Forum, 3 Aug 2012, Pasadena, CA, USA
- Schratz B et al (2014) Telecommunications performance during entry, descent, and landing of the Mars Science Laboratory. *Journal of Spacecraft and Rockets* 51:4, DOI: 10.2514/1.A32790
- Sell S et al (2014) Powered flight design and performance summary for the Mars Science Laboratory mission. *Journal of Spacecraft and Rockets* 51:4, DOI: 10.2514/1.A32682
- Steltzner A et al (2010) Mars Science Laboratory entry, descent, and landing system overview. Revised version of Steltzner A et al (2006) Mars Science Laboratory entry, descent, and landing system. Paper presented at the 2006 IEEE Aerospace Conference, 4–11 Mar 2006, Big Sky, Montana, USA
- United Launch Alliance (2011) Atlas V MSL Mission Overview. Press kit.
- Wallace M (2012) Curiosity: The Next Mars Rover. Presentation to the Royal Aeronautical Society, Applied Aerodynamics Group Conference, 17–19 Jul 2012, London, UK
- Way D et al (2013) Assessment of the Mars Science Laboratory entry, descent, and landing simulation. Paper presented at 23rd AAS/AIAA Space Flight Mechanics Meeting, 10–14 Feb 2013, Kauai, Hawaii, USA

3



Mars Operations

3.1 INTRODUCTION

Operating a lander is quite different from operating an orbiter or flyby craft. Navigators steer orbiters' paths long in advance, so scientists can plan observations months ahead. Rovers don't have the luxury of predictability. Each day's activities can't be planned until controllers back on Earth have received data that tell them the condition and state of the spacecraft, and the lay of the landscape surrounding it. A team can do strategic planning – make a list of top-level science goals – in advance, but to accomplish the strategic plan, the team has to develop a new tactical plan each Martian sol. To make things more complicated, Martian sols are not quite the same length as Earth days.

NASA performed tactical planning for the first time on another world with the Surveyor lunar landers, and later with the Viking and Pathfinder landers, but tactical planning was elevated to an art form with the Mars Exploration Rovers. Over a decade of mission operations, the Spirit and Opportunity teams perfected a way of planning the daily operations of a rover on another world, beginning by working on “Mars time,” then switching to an Earth time schedule.¹ Curiosity followed in their tracks, but the complexity of its instrument package required some changes to the Spirit and Opportunity way of doing things.

3.2 MARS' CALENDAR

3.2.1 Mars sols and seasons

Mars missions are bound to the same kinds of celestial cycles that dictate Earth's 24-hour days, 365-day years, and four seasons. When it comes to days and seasons, Mars has some coincidental similarities to Earth. Mars' solar days are just 3% longer than Earth days, being 24 hours 39 minutes 35.244 seconds long, on average. To differentiate Earth days from Mars days, one Mars solar day is called a “sol”, a term coined during the Viking

¹ Bass et al (2005)

missions.² Because of the similarity in day length, Mars landed mission time can be run on a 24-hour clock, with hours split into 60 minutes of 60 seconds each, just like on Earth. Mars seconds are 1.0275 Earth seconds long.

Mars' axial tilt is also similar to Earth's at 25.2° , resulting in Earth-like seasons of spring, summer, fall, and winter. Curiosity landed 4.6° south of the equator, so the southern hemisphere seasons are relevant. Scientists measure the seasons on Mars using solar longitude, abbreviated L_s (pronounced "ell sub ess"). L_s is 0° at the southern autumnal equinox (beginning of northern spring), 90° at southern winter solstice, 180° at southern vernal equinox, and 270° at summer solstice.

Mars' years last 687.9726 Earth days or 668.5921 Mars sols. Because Mars' orbit is eccentric, Mars' distance to the Sun varies over the course of a year: it is 206.62 million kilometers from the Sun at perihelion, but 249.23 million kilometers away at aphelion. The difference in distance means the Sun is 45% brighter at perihelion than at aphelion. Aphelion happens at $L_s=70^\circ$, just before southern winter solstice (Figure 3.1).

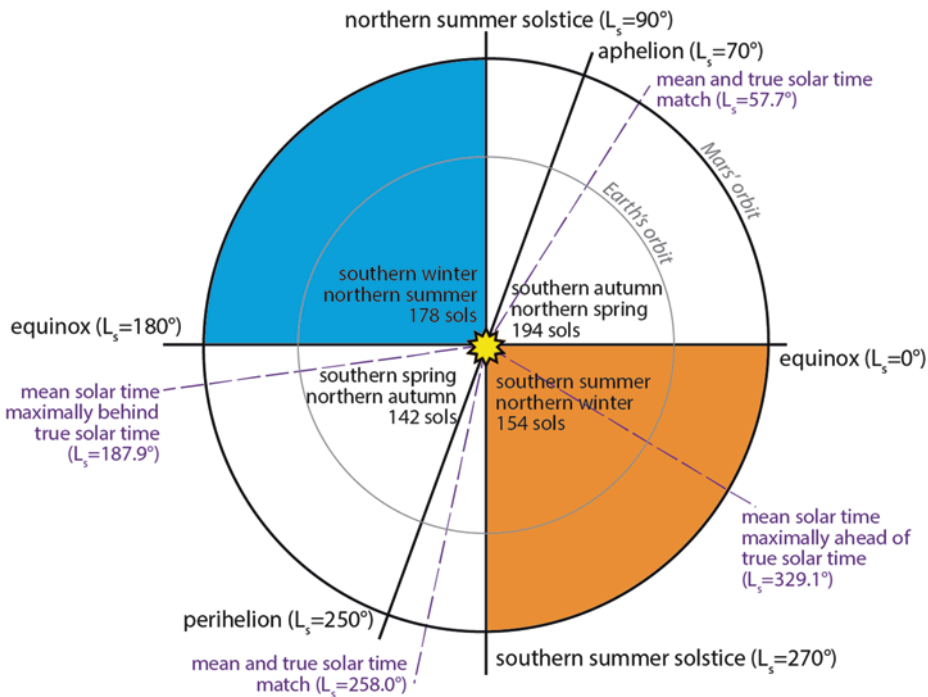


Figure 3.1. Geometry of Mars' orbit. See text for discussion.

²Reichardt (2015)

Table 3.1. Mars seasons relevant to the Curiosity mission. Data from Cantor et al (2010).

Mars year	Northern spring/ southern autumn equinox ($L_s = 0^\circ$)	Northern summer / southern winter solstice ($L_s = 90^\circ$)	Northern autumn / southern spring equinox ($L_s = 180^\circ$)	Northern winter/ southern summer solstice ($L_s = 270^\circ$)
31	Sep 13 2011	Mar 30 2012	Sep 29 2012 / sol 53	Feb 23 2013 / sol 196
32	Jul 31 2013 / sol 350	Feb 15 2014 / sol 543	Aug 17 2014 / sol 722	Jan 11 2015 / sol 865
33	Jun 18 2015 / sol 1019	Jan 03 2016 / sol 1212	Jul 04 2016 / sol 1390	Nov 28 2016 / sol 1533
34	May 05 2017 / sol 1687	Nov 20 2017 / sol 2059	May 22 2018	Oct 16 2018
35	Mar 23 2019	Oct 08 2019	Apr 08 2020	Sep 02 2020
36	Feb 07 2021	Aug 25 2021	Feb 24 2022	Jul 21 2022
37	Dec 26 2022	Jul 12 2023	Jan 12 2024	Jun 07 2024
38	Nov 12 2024	May 29 2025	Nov 29 2025	Apr 25 2026
39	Sep 30 2026	Apr 16 2027	Oct 17 2027	Mar 12 2028
40	Aug 17 2028	Mar 03 2029	Sep 03 2029	Jan 28 2030

Planets move faster when close to perihelion than they do when near to aphelion, and the difference is stark for Mars. Winters in Mars' southern hemisphere, which begin near aphelion, are long and cold under a fainter, distant Sun. Summers are short and hot, with a big Sun overhead. Autumn is the longest season in the southern hemisphere, at 194 sols; winter has 178 sols; spring has 142 sols; and summer has 154 sols.

To discuss the passage of years, Mars atmospheric scientists have settled upon a convention first defined by Bruce Cantor, Philip James, and Wendy Calvin in a 2010 paper. Mars years begin at $L_s=0^\circ$, and the beginning of Mars year 1 on April 11, 1955. The choice of year 1 is, of course, arbitrary, but it is about one Mars year before the Space Age began with the launch of Sputnik in 1957.³ Curiosity landed at $L_s=151^\circ$ of Mars year 31, after the coldest part of winter had passed, headed into spring. Years and seasons relevant to the Curiosity mission are listed in Table 3.1.

3.2.2 Mars solar time

Curiosity may be nuclear-powered but needs sunlight to take photos and warm its motors, so solar time rules its activities. Keeping track of sunrise and sunset times has to take into account Mars' orbital eccentricity, which makes the solar day length vary slightly over the course of the year. To simplify timekeeping, there is a defined convention of local mean solar time (LMST), counting time in evenly advancing increments. It approximates local true solar time (LTST). Mean and true solar time are identical close to aphelion and perihelion, at $L_s=57.7^\circ$ and 258.0° . They are most dissimilar at $L_s=187.9^\circ$, when mean solar time runs behind true solar time by 39.9 minutes, and at $L_s=329.1^\circ$, when mean solar time runs ahead of true solar time by 51.1 minutes (Figure 3.2).⁴ Curiosity (like all landed Mars missions) operates according to a mean solar time clock so that every sol is of the same

³Allison (1997)

⁴Allison (1997)

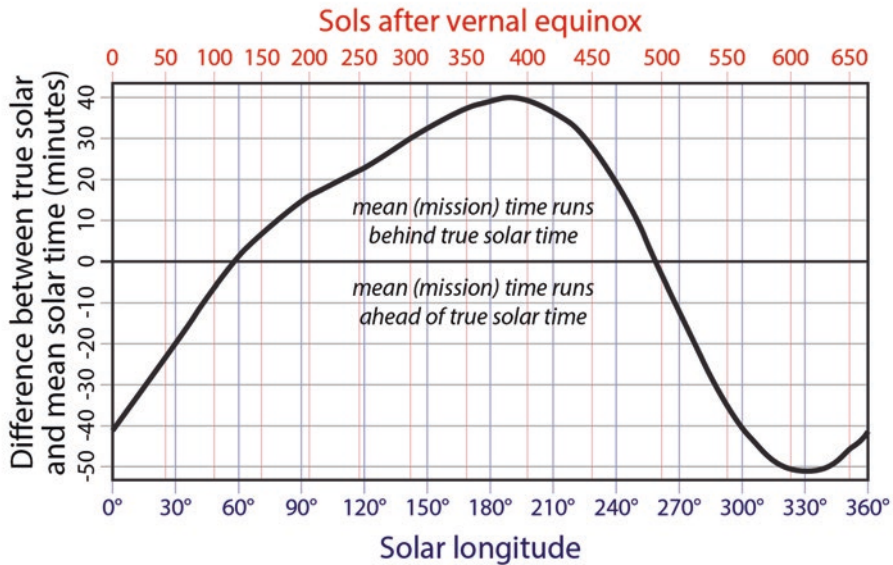


Figure 3.2. Difference between mean and true solar time as a function of solar longitude. Emily Lakdawalla after Allison (1997)

length, but tracking local true solar time is very important for thermal control and camera systems.⁵ In this book I'll generally refer to the two interchangeably as “local time,” differentiating between local mean and local true solar time only if the situation requires it.

3.2.3 Rover timekeeping

One way the mission measures time is with the spacecraft clock, which counts time in seconds. Landing happened at a spacecraft clock time of 397502503. The mission calendar is reckoned in sols, counting up from landing day on sol 0.

The rover motion counter (RMC) is another way of ordering rover activities, including science, in time. The rover motion counter comprises 10 integer indices, keeping track of when various rover motors have operated. In order, the 10 indices are site, drive, pose, arm, CHIMRA, drill, mast, high-gain antenna, brush, and inlet covers. The site index

⁵Local Mean Solar Time is defined for a fixed longitude on the surface. For Curiosity, that longitude was defined before landing to be 137.42°E. Curiosity's mission time does not shift with Curiosity's changing longitude. For every 246 meters that Curiosity drives west of the initial landing position, the Sun rises 1 second later than it does at the longitude of the landing site. Curiosity actually landed at 137.441635°E, which meant that there was about a 4-second difference between Curiosity mission time and the Local Mean Solar Time – not enough of a difference to make it worth it to adjust the software, especially because this tiny difference is swamped by the variations in sun rise/set times caused by the difference between True and Mean Solar Time.

increments every time the rover updates its knowledge of its geographic location, so has been counting up since the beginning of the mission. Curiosity increments the site index when it updates its knowledge of its orientation by sighting the Sun with the Navcam (see section 6.5.1); incrementing the site index sets all other indices to 0. The drive index increments every time the rover rolls or steers its wheels. Incrementing the drive index sets all other indices except site to 0. All science data with the same site/drive index is from the same geographic location. The rest of the indices increment whenever the relevant motor is operated, and help to place activities in order at a specific site/drive location.

3.3 STRATEGIC, SUPRATACTICAL, AND TACTICAL PLANNING

Curiosity is far more capable than its predecessors, especially when it comes to drilling and sampling, but there are no more hours in the day for Curiosity operations to be planned than there were for Spirit and Opportunity. There are 10 science instruments, and more than 400 scientists, and planning has to be mindful of the needs of multi-sol campaigns. Performing daily operations with a complex rover while keeping eyes set on long-term goals is difficult for such an unwieldy team.

Many different factors limit what the rover can accomplish in a given sol. Power is one: most activities draw power from the batteries at a faster rate than the MMRTG can replenish it, but for safety reasons the tactical team is usually required to leave the rover batteries nearly fully charged at the end of each sol's plan. Communications are another serious bottleneck: the rover can capture far more data than there is capacity to transmit it to Earth. But at the beginning of the mission, the most stringent limit on Curiosity's activities was imposed by the sheer complexity of the machine.

To make it all work, Curiosity mission operations are planned on four different timescales, with all four working in parallel:

- The Project Science Group (PSG), a committee consisting of the project scientist (John Grotzinger at landing, and later Ashwin Vasavada), NASA Mars Program Scientist Michael Meyer, and the principal investigators of the science instruments, establishes the overarching scientific questions motivating Curiosity's mission, and determines the very long-term driving destinations. The goals, questions, and destinations were established in the mission proposal and subsequent extended-mission proposals.
- The *strategic or long-term planning* process addresses development and testing of first-time activities, planning science and sampling campaigns, and long-term management of rover resources. Long-term planners map out a "sol path" covering several sols, a high-level list of activities that directs the mission toward accomplishing the Project Science Group's goals. Strategic planning works on week- to months-long time scales, and is mostly conducted on Earth time.
- The plans needed to implement the strategic plans are developed first in a "*supratactical*" planning process. One to several sols ahead of time, the supratactical team sequences the "look-ahead plan", beginning to sketch out the actual list of commands to be sent to the rover. At the beginning of the mission, the supratactical process was conducted on Mars time.

- Finally, the *tactical* team produces each sol’s plan. The supratactical team hands the tactical team an outline of the activity plan for that sol, called a skeleton plan, along with guidelines for what the rover needs to accomplish to stay on the look-ahead plan. Each skeleton plan contains science blocks, periods of time during which the tactical team can add in science observations, resource limitations permitting. The tactical team responds to data downlinked from the rover each sol, fleshes out the plan handed to them by the supratactical team, and generates commands to uplink to the rover for the next sol. Tactical planning was conducted on Mars time when the mission began, with the tactical planning timeline taking 1 sol, operating every day of the Earth week, around the clock.⁶

Curiosity differs from its predecessors Spirit and Opportunity in having the supratactical planning process, which is necessary because of Curiosity’s complexity and the intensive resource demands of its analytical instruments, CheMin and SAM. In parallel with strategic planning, the supratactical process takes care of the negotiations among different instruments for rover resources, assigning activities to different sols to balance out demands.

3.4 TACTICAL PLANNING PROCESS

3.4.1 Mars time operations

Since the rover needs a plan for each sol that responds to what happened the previous sol, the ideal way to operate Curiosity is to begin planning the next sol at the end of each active sol on Mars. When the mission operated on Mars time, the planners worked over the rover’s night to deliver a new tactical plan at around 10:00 local time each rover morning.

Late in the afternoon (between 3:00 and 6:00 p.m. local time), both Mars Odyssey and Mars Reconnaissance Orbiter fly over the landing site. (Read more about rover telecommunications in section 4.5.) Colloquially, a communications session is referred to as a “pass”, because the orbiter is passing across the rover’s sky as the rover uplinks its data. The orbiters relay the data onward to Deep Space Network radio dishes on Earth. The last orbiter communications session before Earth planning begins is called the “decisional data pass” because it is the last pass containing data that Earth planners can use to make decisions about rover activities. Decisional data includes telemetry on the health and safety of the rover, and Hazcam and Navcam images that can be used to build a terrain mesh, a 3D map of the terrain around the rover.

The rest of the data comes down in priority order. The tactical team carefully assigns priority to every data product that they command the rover to produce. They assign highest priority to science data that is beneficial for planning – such as Mastcam images of the area that the arm instruments can reach, or ChemCam can zap; these usually arrive quickly. Other data may come down days later. The Mastcams, in particular, generate huge volumes of data and can store it for months inside large flash memory drives within each instrument’s electronics. Low-priority Mastcam data can easily sit on the rover for a year

⁶Chattopadhyay et al (2014)

before downlink. The mission always tries to keep some volume of data in memory so that if an onboard anomaly prevents new activities, all available downlink sessions can be used to downlink science data. The team makes all these priority assignments during tactical planning, but can also reprioritize data still on the rover to force it to return to Earth sooner or later, as appropriate.

On Earth, a downlink team of instrument scientists and rover engineers studies the downlinked data to assess rover health and suggest a set of activities. Responsibility shifts to an uplink team, which includes representatives of every science instrument as well as rover planners (also known as rover drivers). The uplink team generates a command sequence and sends it to the rover. Usually the Deep Space Network transmits the sequence directly to the rover's steerable high-gain antenna around 10:00 a.m. local solar time, after the Sun has warmed the rover slightly, in time for it to begin its next sol of operations on Mars.

Operating on Mars time presents two main challenges. One: the full cycle from data downlink to sequence uplink has to be completed within about 16 hours, over the rover's night; if the sequence doesn't get prepared by the end of that time, they miss their uplink window and lose a whole sol of activity on Mars. Two: Mars time and Earth time are not the same. To work on Mars time is to begin the planning day 39 minutes later each day. In 38 Earth days, there are 37 Mars sols. If the Earth and Mars schedules are perfectly aligned one day, then, 19 days later, the two schedules are perfectly out of sync, and operating on Mars time requires working through the Earth night.

For the first 90 sols after landing, the mission operated on Mars time, through nights and weekends, with the whole science team co-located with the engineers at the Jet Propulsion Laboratory (JPL) in Pasadena, California. Mars time helped the engineers maintain a tight connection with the rover as they commissioned all its instruments and tools, and permitted them to use all of the 16-hour rover night to prepare each sol's worth of activities. But Mars time is grueling for humans, whose circadian rhythms and private lives still run on Earth time.

3.4.2 Slide sols, restricted sols, and solidays

After sol 90, the science team members returned to their home institutions and the mission transitioned to Earth time. They had increased planning efficiency to the point that one sol's worth of activities could be developed in a 9-hour planning day. Earth time operations are permitted to take place between the hours of approximately 6:00 a.m. to 10:00 p.m. California time. So in a day where uplink needed to take place no later than 4 p.m. California time, they could begin the planning day at 7 a.m., an "early slide sol." In this way the team could operate as though they were on Mars time for about half of the sols, as long as they could fit a 9-hour planning period in work-permissible hours within the 16-hour window between the receipt of end-of-sol data from Mars and the time of the next sol's uplink.

As days and sols turn over, the beginning of Curiosity's Mars sol creeps later and later in the tactical team's Earth day. If decisional data arrives on the team's computers after the planned start of work, they don't have time to analyze the data from Mars before they need to plan the next day's activities. For a couple of sols, they can slide the Earth planning

timeline a little later in the day – starting, say, at 11:00 in the California morning and finishing at 8:00 in the evening – but these “late slide sols” only buy a couple of days on Mars-like time.

An Earth planning day comes when the decisional data arrive from Mars too late for an Earth time schedule, in the middle of the day in California. On these “restricted sols,” the team has to plan the rover’s activities without any knowledge of whether the previous sol’s activities executed successfully. If the previous sol included arm work or driving, further motion is usually precluded until the planners can assess the success of the activities, so restricted sols following arm work or driving are heavy with remote sensing. (The engineers do consider it safe to move the mast head to perform imaging and ChemCam operations despite not knowing the state of the rover.) If the previous sol included a drive, the team has no way of knowing what the immediate landscape looks like around them. Therefore, they can’t conduct science work with the arm or target remote sensing. When the mission is in restricted sols, drives can only be commanded at most every other day. The mission’s first restricted sol was sol 92.

Common restricted-sol activities include untargeted remote sensing in which cameras or spectrometers shoot in the blind. Some remote sensing observations don’t actually require detailed position information, like 360° panoramas, or imaging of distant targets whose positions don’t change much with one drive, like targets on the crater rim, the Gale central mountain, or sky objects like the Sun, clouds, Mars’ moons, stars, and comets. The team may also use restricted sols for SAM or CheMin analyses of samples already inside the rover. Sometimes restricted sols include little activity at all, an opportunity to let the batteries recharge. The restricted-sol period continues until the Mars clock drifts far enough with respect to the Earth clock for the 9-hour planning cycle to fall within the 16-hour window again. There is a “soliday” – an Earth day in which there is no need to plan for Mars, one every 38 Earth days – and then the mission comes in for two or three days of early slide sols to begin a couple of weeks of unrestricted planning. Whenever possible, the mission tries to plan solidays to fall on weekends.

3.4.3 Weekends, holidays, and surge sols

Even after the transition to Earth time, daily Mars operations imposed difficult demands on the lives of mission personnel. Operating through weekends was especially hard on workers with families. Knowing that the mission could continue for years, Curiosity management worked to reduce the mission planning schedule.

As of sol 180, the mission ended routine Sunday tactical planning, planning two sols every Saturday instead. During restricted sols, the rover could be commanded to drive on Saturdays, to allow Mondays and Wednesdays to be used for planning driving sols, with Tuesdays and Thursdays used for untargeted remote sensing. Fridays could then be given over to arm activities and/or targeted operations with remote sensing instruments. Sundays were often used for time- and power-intensive SAM and CheMin analyses and/or untargeted weather observations.

As of sol 270, the mission ended routine Saturday planning. From then on, Friday tactical planning covered three sols, or two with a soliday. And very rarely, the mission reactivated Saturday planning in order to take advantage of unrestricted sols for driving or drilling, but the project ended this practice in May 2015.

For a few months beginning sol 515 and again on sol 635, in order to maximize the use of unrestricted sols, the mission employed the concept of “surge sols”. These are engineer-only (no formal science activity) sols with only a 6-hour planning period. They allow the team to begin planning very early or late in the Earth day and eke out another day or two of unrestricted drive sols before flipping over into restricted-sol operation. The project also performed surge-sol planning on weekends during unrestricted-sol periods, again without formal science team participation.

After the end of the prime mission, around sol 765, the mission reduced planning days further, producing two-sol plans only three weekdays a week when in restricted sols. Nowadays, a typical 38-day/37-sol period begins with two or three early slide sols, then two or three weeks of 5-day-a-week unrestricted sol-planning, followed by two or three late slide sols, then two or three weeks of 3-day-a-week restricted-sol planning, then a soliday. At the start of Earth time planning, operations were more often in restricted than in unrestricted sols. As the team has become more experienced and the planning period has been shortened (to 8 hours), the mission now enjoys slightly more days in unrestricted sols.

The mission has always reduced the intensity of planning during major United States holidays like Thanksgiving, Christmas/New Year, and Independence Day. They prepare multi-sol plans to tide the rover through these periods, usually focusing on routine environmental observations. Holiday plans don’t usually generate as much data as regular plans, so routine orbiter communications (which the rover handles autonomously according to a schedule delivered months in advance) during holidays are periods of catching up on data downlink.

3.5 MISSION SUMMARY

Recounting the daily operations of the rover is beyond the scope of this book. The following broad overview is intended to provide context for the discussion of how the rover’s systems and instruments work in the rest of this book.⁷ Appendix 1 contains a list of the official mission summaries of each sol of activity. A brief overview of mission activities is in Table 3.2.

3.5.1 Site context

Curiosity landed in the northern floor of Gale crater, at 4.5895°S, 137.4417°E and an elevation of 4501 meters below the Martian datum (Figure 3.3). One of the deepest holes on Mars, Gale is located at the boundary between Mars’s southern highlands and northern lowlands. Gale displays clear evidence for water having once flowed from the highlands surrounding the crater through gaps in the rim and then depositing overlapping alluvial fans of sediment on the crater floor. One such channel and fan is Peace Vallis, to the

⁷This section is based upon my years of reporting for planetary.org on the ongoing adventures of the Curiosity mission. That reporting is based upon mission images, press releases and team blog entries on the JPL and United States Geologic Survey websites, roughly monthly interviews of Ashwin Vasavada, and occasional conversations with numerous other team members

Table 3.2. Brief summary of major phases of the Curiosity mission.

Sol	Site/drive	Date (UTC)	Event
0	1/0008	6 Aug 2012	Landing
21	3/0100	27 Aug 2012	Drive toward Glenelg
57	5/0000	3 Oct 2012	Arrive at Rocknest
102	5/0388	19 Nov 2012	Depart Rocknest, drive toward Glenelg
166	6/0000	23 Jan 2013	Arrive at John Klein in Yellowknife Bay
272	6/0068	12 May 2013	Arrive at Cumberland, Yellowknife Bay
324	7/0000	5 July 2013	Depart Cumberland, begin Bradbury traverse
392	16/0050	12 Sep 2013	Arrive at Darwin (Waypoint 1)
402	16/0328	23 Sep 2013	Depart Darwin, continue Bradbury traverse
439	21/1572	31 Oct 2013	Arrive at Cooperstown (Waypoint 2)
453	22/0484	14 Nov 2013	Depart Cooperstown, continue Bradbury traverse
535	26/0366	6 Feb 2014	Cross Dingo Gap
574	30/0740	18 Mar 2014	Arrive at the Kimberley (KMS-9)
634	32/0204	19 May 2014	Depart the Kimberley
753	42/1020	18 Sep 2014	Arrive at Pahrump Hills
923	45/0558	12 Mar 2015	Depart Pahrump Hills
992	48/1194	22 May 2015	Arrival at Marias Pass
1072	49/0294	12 Aug 2015	Depart Marias Pass, travel south to cross the Stimson unit
1172	51/0592	23 Nov 2015	Approach Bagnold Dunes for first campaign
1248	52/0722	9 Feb 2016	Traveling west toward the Naukluft plateau
1281	53/1284	14 Mar 2016	Climb onto Naukluft plateau
1369	54/2508	12 Jun 2016	Turn south to cross the Bagnold dunes
1427	56/1326	11 Aug 2016	Approach Murray buttes
1454	57/2582	8 Sep 2016	Depart Murray buttes, drive south
1508	59/0936	2 Nov 2016	Enter southern Bagnold dunes
1601	60/3162	6 Feb 2017	Begin second Bagnold Dune campaign
1671	62/1140	19 Apr 2017	Exit dunes, traverse south to Vera Rubin Ridge (formerly known as Hematite Ridge)
1726	64/0000	14 Jun 2017	Arrive at Vera Rubin Ridge, turn east along ridge base
1812	66/0000	11 Sep 2017	Reach top of Vera Rubin Ridge

northwest of the landing site. But there were many other such channels and fans all around the rim; Peace Vallis was just one of the last to form, so is the most prominent today.

At the center of Gale crater is a 5-kilometer-tall central mound of layered sediments formally named Aeolis Mons. The science team refers to the mountain as Mount Sharp, after Robert Sharp, a pioneering Caltech planetary geologist. Researchers studying orbital data before the landing were divided on how the mountain formed, but it did seem clear that different styles of geology prevailed at different times. In particular, the lowermost elevations of the mountain were made of nearly horizontally layered rocks, whereas the upper, brighter slopes lacked such obvious layering. NASA's Mars Reconnaissance Orbiter had spotted spectral signs of clays, sulfates, and hematite in Gale's lowermost layered rocks, all of which form in different kinds of wet environments. Reaching the lowermost slopes of the mountain to study those rocks was a major goal for the science team. Then they hoped to climb up through the layered rocks to study the history preserved in them. They never intended or expected to summit the mountain; at best, they hoped to reach the

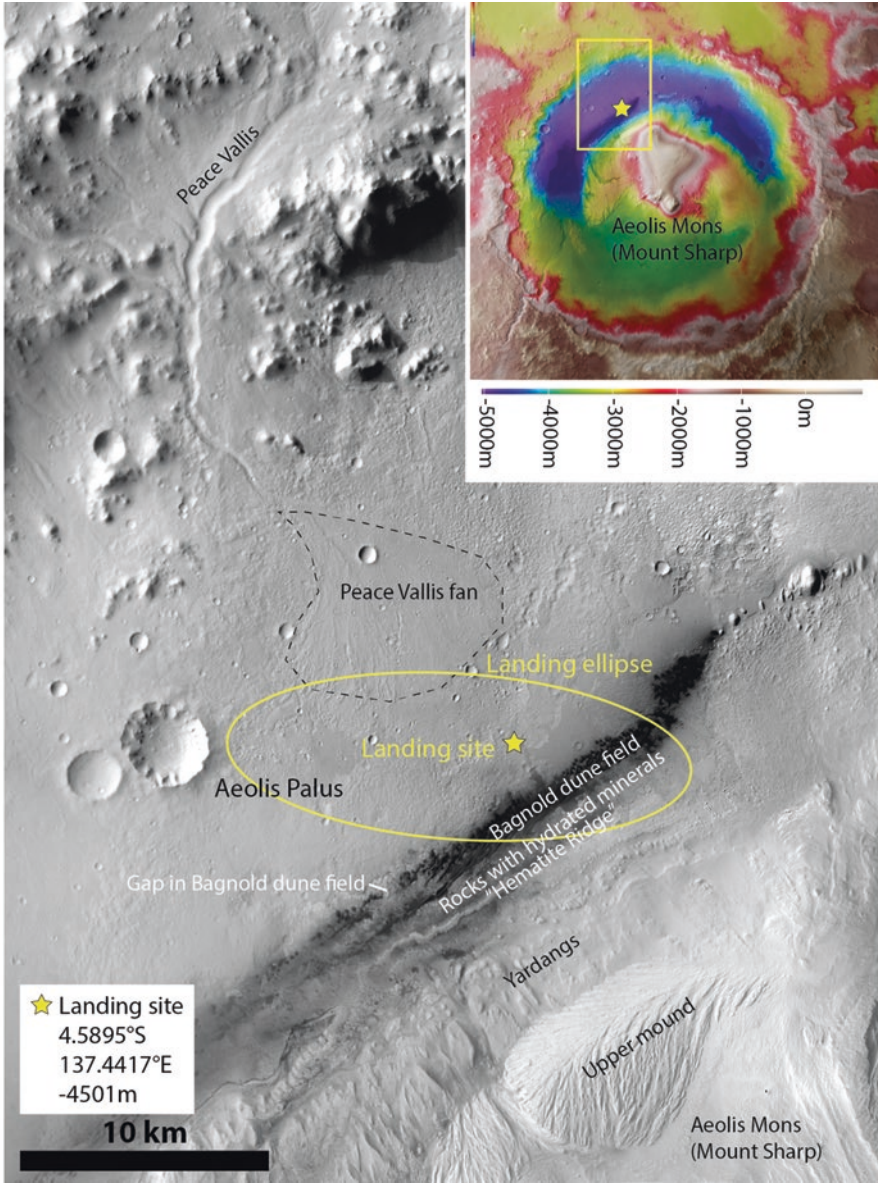


Figure 3.3. Context map of the landing site. Inset: topographic map of Gale crater from Mars Express. Gale is about 150 kilometers in diameter. Yellow rectangle shows location of main map. Elevation scale is in meters relative to Martian datum. Main map: major landmarks at the landing site. Base image is the Mars Odyssey THEMIS daytime infrared mosaic. NASA/JPL-Caltech/ASU/Emily Lakdawalla.

boundary between the lower mound and the upper mound in order to understand what happened in Mars' history to change the style of sediment deposition so abruptly.

During the cruise, members of the science team had carefully mapped the geology of the landing ellipse using orbital images, so they were prepared with a good understanding of the regional geology and their likely drive route before the landing. The landing placed them several kilometers to the southeast of the end of the Peace Vallis fan. Between the rover and the mountain lay a linear swath of black sand dunes, later called the Bagnold dune field, named for Ralph Alger Bagnold, a pioneer in the study of sand's behavior in deserts. Most of the dune field was considered hazardous to the rover. However, southwest of the landing site, the dunes thinned out near a cluster of steep-sided buttes that the mission named the Murray buttes after Bruce Murray, a Mars geologist and early leader in NASA's Mars exploration. To reach the interesting rocks at the base of the mountain, Curiosity faced a lengthy drive – more than 9 kilometers as the orbiter flies, much longer for a wheeled rover dodging obstacles. At Murray buttes, the rover could cross the dune field and finally reach the lower mound's layered rocks. Figure 3.4 is a visual summary of the rover's route.

3.5.2 Yellowknife Bay campaign and the sol 200 anomaly

The first order of business upon landing was to establish the basic functions of the rover, like raising the mast, establishing routine telecommunications, and making sure that the rover's power and thermal systems were operating as expected. Then the rover stood down for four sols for an upgrade of its operating system, reprogramming the main computer from an interplanetary spacecraft into a surface rover. Figure 3.5 provides an overview of the major external Curiosity rover systems relevant to the surface mission.

Initially, the engineering side of the tactical team had more control over Curiosity than the science team did. Curiosity required a commissioning activity phase to work it through its engineering and science functions. Even after commissioning ended, there was a long list of first-time activities that engineers methodically paced through: first drive, first contact science target, first scooping, first use of different driving modes, first drill site, and so on.

Rather than immediately beginning the journey southwest across nondescript-looking terrain, the project science group decided to start the mission with a drive of about 500 meters east to a location they named Yellowknife Bay, where three distinct rock types occurred together. While working through its first-time activities, Curiosity would be able to perform productive science there.

Curiosity used all the environmental and remote sensing instruments for the first time on Mars at the landing site. RAD measured the radiation environment. DAN detected neutrons from the ground (and also from the MMRTG). Mastcam took photos, testing out its focal mechanism. ChemCam lasered a rock. REMS took weather data. In the very first days of operations, the REMS team discovered that one of their wind sensor booms had been damaged, likely by gravel launched into the air by the force of the descent engines impinging upon the surface. The wind experiment on REMS has never functioned fully, but the rest of the REMS sensors have been active since landing.



Figure 3.4. Route map for the mission to sol 1800. Bold text denotes drill or scoop sites. Map by Emily Lakdawalla on a base image of Mars Reconnaissance Orbiter CTX mosaic colorized with Mars Express HRSC image.

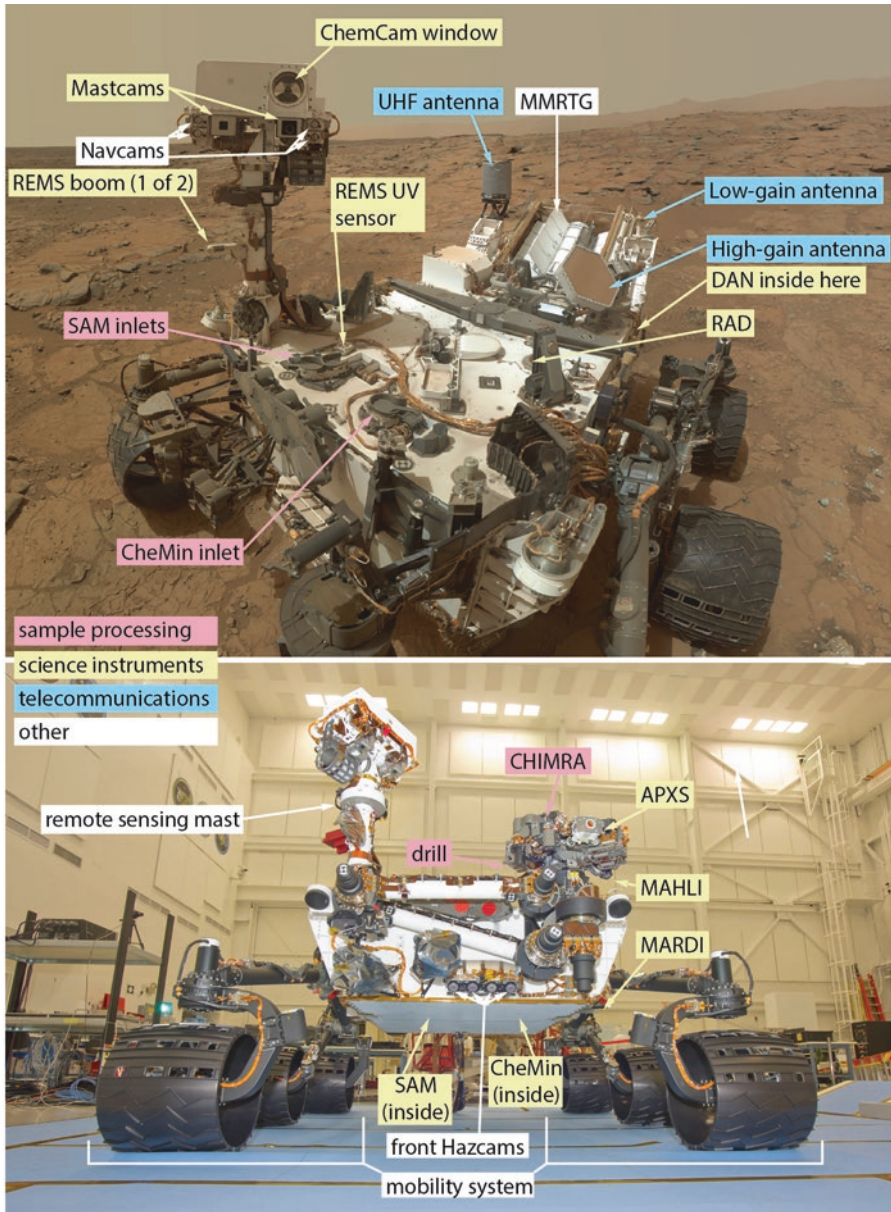


Figure 3.5. Science instruments and major external systems of the Curiosity rover. Top image is a rover self-portrait taken at John Klein on sol 177. NASA/JPL-Caltech/MSSS image release PIA16764. Bottom image taken June 3, 2011 during mobility testing. NASA/JPL-Caltech image release PIA14254, annotated by Emily Lakkawalla.

The rover drove for the first time on sol 16. During the next few weeks the rover drivers slowly increased its driving autonomy, beginning with blind drives, later adding in visual odometry to increase drive accuracy (see section 6.5 for more on the different driving modes). SAM ingested its first atmospheric sample on sol 18. The SAM team initially thought they had detected abundant methane in the air, but it turned out to be contamination from the leak that had happened before launch (see section 9.5.1.3).

Scientists selected a rock they named Jake Matijevic for the first contact science observations (APXS compositional info and MAHLI photos) on sol 46. The engineers commanded the arm to reach out and scoop a sample of sand for the first time at the Rocknest sand drift on sol 61 (Figure 3.6). They shook the sample inside the Collection and Handling for In situ Martian Rock Analysis (CHIMRA) sample handling mechanism on the arm in order to scrub the apparatus of any remaining manufacturing residue.⁸ They scooped again



Figure 3.6. Left Mastcam photo 0061ML0003060000102375E01 documenting the first day of scooping at Rocknest. CHIMRA acquired a full scoop from the site at lower right, then shook out some of the sample to reduce the amount in the scoop, leaving a fresh pile of dark sand on the ripple surface. NASA/JPL-Caltech/MSSS.

⁸CHIMRA is pronounced “chimera”

and delivered the first Martian samples to the laboratory instruments CheMin and SAM for the first times on sols 71 and 93.

MAHLI captured the first full rover self-portraits at Rocknest on sols 84 and 85 (see section 7.4.3.5 for more on how MAHLI captures self-portraits). In order to continue analyzing the Rocknest sample while proceeding toward Yellowknife Bay, the rover planners developed and quickly deployed the ability to drive with cached sample held inside the CHIMRA mechanism (see section 5.4.5).

Curiosity acquired its first drilled sample on sol 176, at John Klein (Figure 3.7). Analyses of the first drill samples were interrupted by a major anomaly – arguably the scariest event of the mission after landing – on Wednesday, February 27, sol 200. The event is now known as “the sol 200 anomaly.” The routine morning uplink revealed that the rover was behaving strangely, returning real-time telemetry but not performing commanded activities. Engineers quickly diagnosed an issue with the rover’s onboard memory. Later in the day, their concern elevated when more telemetry from Curiosity indicated that it had not gone to sleep as commanded, so was depleting its batteries.

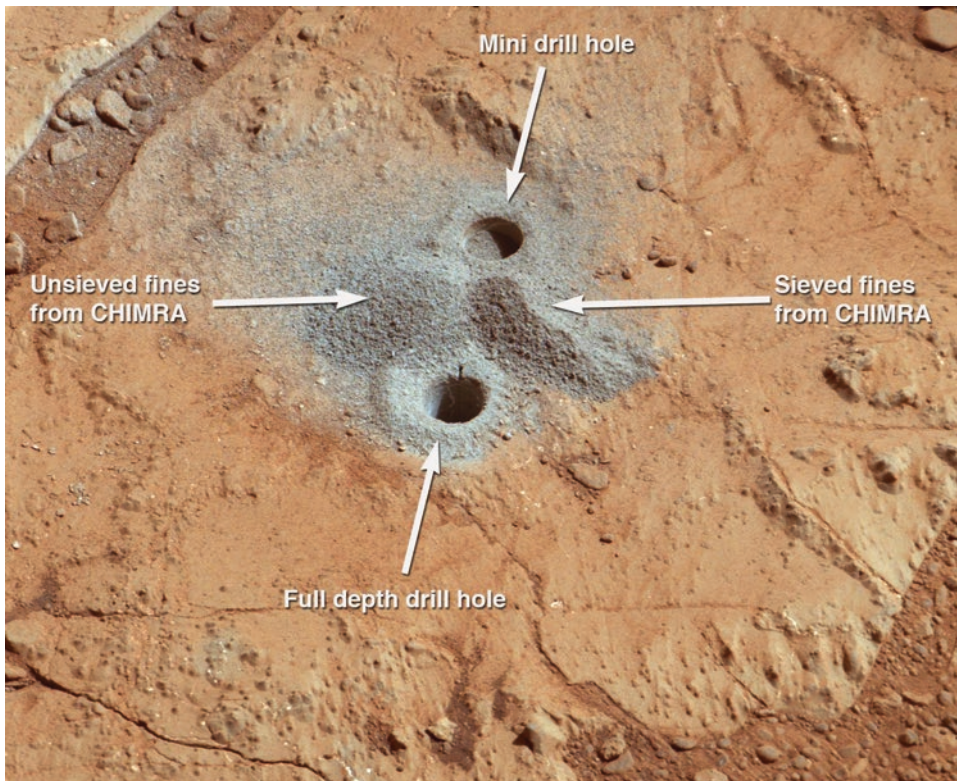


Figure 3.7. John Klein drill site after drilling activities were completed. Mastcam acquired this photo on sol 229, after CHIMRA dumped the remaining drilled sample in two piles. NASA/JPL-Caltech/MSSS release PIA16815.

Unlike the smaller Spirit and Opportunity rovers, Curiosity has an entire spare computer system available for the rover to switch to. On sol 201, the mission uplinked commands to swap from the A-side computer, with its corrupted memory, to the B-side computer. Commissioning of the instruments on the B-side computer was completed as of sol 223 (23 March 2013). The rover has operated on the B-side computer ever since.

As a consequence of the swap to the B-side computer, the rover switched eyes. It has two pairs of each of its engineering cameras (the Navcams and front and rear Hazcams, see section 6.3), with complete sets connected to each computer. The switch from A-side to B-side computers moved its Navcam point of view down by 4.8 centimeters. Similarly, the front Hazcam view of the world shifted to the rover's left by 8.2 centimeters. The rear Hazcam view shifted to the rover's left by about a meter, from one side to the other of the MMRTG. Because the rover's autonomous hazard-finding software had been trained on Mars only with A-side images, the project was forced to repeat some of the commissioning activities using the rover's new eyes.

During recommissioning of autonomous driving modes, the engineers made the unpleasant discovery that the pointing of the B-side Navcams shifted very slightly over the course of a sol, likely because their mounting bracket warped with daily extremes of Martian temperature, enough to confuse the onboard rangefinding software. Over the ensuing weeks, they had to perform calibration activities to understand the temperature-dependent behavior. Only after this investigation was complete were they able to test autonomous navigation capability.

After recovering from the sol 200 anomaly, rover operations almost immediately stood down again because of solar conjunction. When the Sun is within 3° of Mars in Earth's sky, radio communications can be affected by solar radio emissions. Mars landers and orbiters aren't directly affected, but because communications aren't reliable, Earth controllers avoid any activities that might place the spacecraft at risk of needing intervention. During solar conjunction, from sol 235 to 260, the rover performed only background environmental science observations and transmitted a daily "beep" to Earth. After conjunction, the rover drilled for a second time at a nearby site named Cumberland, on sol 279.

Early impressions of the drilled material suggested that Curiosity had accomplished its science objectives (listed in Box 1.5). The mission had successfully explored the biological potential of at least one target environment (using SAM to inventory organic compounds) and had gathered the data needed to conclude that the environment was a biologically relevant one (the still water of a lake bottom). The mission had characterized the regional geology of the landing site before landing, and followed that up with successful chemical, mineralogic, and isotopic analyses with the science instruments. The isotopic measurements of water in the ancient Mars rocks had corroborated orbital science results indicating that Mars has lost much of its atmosphere. And RAD's successful operation had hit Curiosity's last goal of characterizing surface radiation. With all the crucial first-time activities complete and minimum mission success achieved, the science team could go on their driving adventure.

3.5.3 The Bradbury traverse

On sol 295, Curiosity departed Cumberland, investigating a few outcrops close to Yellowknife Bay. Then the rover embarked on a 13-kilometer journey across the floor of the crater to the southwest, toward Murray buttes and the gap in the Bagnold sand dune field that would allow the rover to cross it safely and reach the base of the mountain.

During the time at Yellowknife Bay, engineer Paolo Bellutta had led the effort to map out a “rapid transit route” for the rover using the traversability algorithms he had developed during the landing site selection process (see section 1.6.3). It was not the shortest possible path, but sought to minimize drive time by keeping the rover to relatively flat terrain with good visibility, which would maximize single-sol drive distances. (Being able to see far ahead permits longer blind drives, which is the fastest driving mode; see section 6.5 for more about the different driving modes.) The traverse was across a region of low, hummocky plains with rare outcrops of rock. From orbit it appeared largely similar to the terrain Curiosity had already traversed. The rover would be permitted to perform science observations as opportunities came up, but driving was a higher priority than science. They used autonav for the first time to extend a planned drive on sol 347, and quickly racked up record-breaking drive distances, including one of 141 meters on sol 385.

Long drives also used up time and energy, limiting resources available for science. The science team selected three locations along the proposed path where orbital images suggested that there was more coherent outcrop, worthy of brief stopovers for science. Curiosity reached the first site, Darwin, on sol 390, staying until sol 402. On sol 426, the rover passed from terrain that the science team had mapped as “hummocky plains” to a new landscape, called “rugged terrain” (Figure 3.8). Rugged terrain featured more bedrock in the form of sharp blocks of rock protruding from the plains. The rougher terrain slowed down autonav, making drive distances shorter. On sol 439, Curiosity approached a site called Cooperstown to characterize the rugged-terrain rock.

The months after Cooperstown were full of problems. An unsuccessful flight software update (see section 4.3.2.2) delayed them at Cooperstown until sol 453. On sol 456, the rover experienced a “soft short” in its MMRTG, later determined to have been caused by part of the electrical power circuit touching its metal housing (see section 4.2.3).⁹ The short spontaneously resolved itself on sol 461 and didn’t recur for a year. On sol 463, the rover drivers commanded a set of MAHLI images of the wheels, which revealed a huge hole in the left front wheel. They started commanding wheel images after every drive to monitor the development of the wheel damage. Wheel imaging slowed down driving and revealed rapidly progressing damage (Figure 3.9 and section 4.6.4).

The mission appointed a Tiger Team led by Rich Rainen (who had managed the rover’s mechanical team during its construction) to answer three questions: What was causing the damage? How could the mission reduce or prevent further damage? And what was the life expectancy of the wheels?¹⁰ Following experiments in the Mars Yard, the Tiger Team quickly determined that the rugged terrain was a factor. Sharp-pointed rocks that were embedded in the ground did not shift when the rover passed over them; instead, they pierced the wheels. No rover had encountered such embedded, sharp rocks before.

The project directed the engineers to avoid pointy rocks to the best of their ability, take one set of wheel images on every drive, and perform full wheel imaging (five sets of images interspersed with 60-centimeter drives, in order to present all surfaces of the wheels to the cameras) once every 100 meters. This effectively ended the use of autonav for some time, which dramatically slowed the rover’s progress. Moreover, every

⁹JPL (2013)

¹⁰Interview of Rich Rainen and James Erickson conducted September 18, 2014



Figure 3.8. Top: typical hummocky terrain. Part of a mosaic of left Mastcam images from sol 412. Bottom: typical rugged terrain. Part of a mosaic of left Mastcam images from sol 437. NASA/JPL-Caltech/MSSS.

full-wheel-imaging sol advanced the rover only 2 meters toward the destination at the cost of a precious drive sol. One consolation was that sequencing arm activities for wheel imaging permitted more opportunities for APXS and MAHLI use than the science team had previously been able to justify. The project began to employ surge sols (see section 3.4.3) in order to make the most of every opportunity to drive.



Figure 3.9. Development of damage to the left front wheel. MAHLI images taken on sols 177, 411, 463, and 469. NASA/JPL-Caltech/MSSS.

As the engineers performed further tests on wheel damage, a group of scientists and engineers led by John Grotzinger and Matt Heverly mapped the terrain ahead and drove a virtual rover through digital terrain models to develop plans for a feasible future long-term drive path that would avoid wheel-damaging terrain. Unfortunately, the previously planned rapid transit route, which had preferred high ground for visibility, coincided with the worst terrain. In between high ground were depressions filled with sand, which would be kinder to the wheels, but the valleys had their own problems: driving in depressions meant less long-distance visibility; required a slightly longer drive distance in order to detour around highlands; and had potential issues with “pinch points” where the rover would have to pass through relatively narrow and/or steep gaps in order to exit one valley and enter another.

On sol 524, the rover departed the rapid transit route to enter sand-filled valleys. The rover had to pass over a relatively high sand ripple blocking Dingo Gap in order to enter the first of the valleys (Figure 3.10). It successfully made the crossing on sol 535.

Driving in valleys provided far more opportunities to study rock layers from the side, and the science observations improved. On sol 574, the rover approached the third and final Bradbury traverse science stop, named the Kimberley, where three distinct rock units came together (Figure 3.11). They spent nearly two months at the Kimberley, drilling at Windjana on sol 621. While working at Windjana, the MAHLI instrument experienced and recovered from its first anomaly, which put the instrument out of service from sols 615 through 626.

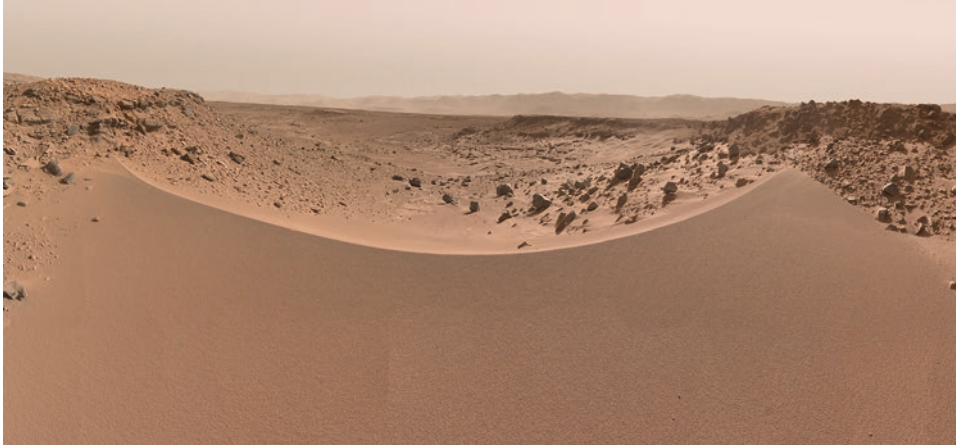


Figure 3.10. Dingo Gap, where a tall sand ripple obstructed Curiosity's progress westward into the safer valleys. In the distance is the rim of Gale crater. Left Mastcam mosaic from sol 530. NASA/JPL-Caltech/MSSS.



Figure 3.11. View from the Kimberley, a mosaic of many left Mastcam images taken on sol 590. In the foreground are layered rocks, the lowest of the three distinct units exposed at the Kimberley. Two more units make up the lower and upper slopes of Mount Remarkable, the mound at middle right. Curiosity drilled near the toe of that mound at Windjana on sol 621. In the distance on the left are the lower foothills of Mount Sharp, Curiosity's eventual destination. In the distance on the right is the rim of Gale crater. NASA/JPL-Caltech/MSSS.

The pause at the Kimberley allowed the wheel damage Tiger Team to complete their work. See section 4.6.4 for details on the wheel investigation and results. Wheel imaging at every drive proved that damage was progressing only slowly and at a rate predicted from Earth experiments. So sol 636 was the last time that the engineers sequenced single sets of wheel images before every drive; after that, they continued doing full wheel imaging approximately every 500 meters.

Instrument teams began preparing for extended-mission operations. CheMin, for instance, tested whether they could re-use sample cells. On sol 640 the rover delivered a Windjana sample to a CheMin cell that had previously held Cumberland material. They detected no cross-contamination of the Windjana sample by Cumberland and cleared future deliveries of samples to previously used cells.

On May 30, 2014 (corresponding to sol 645) the team selected a new future traverse that diverted the rover to the south around a large region of potentially wheel-damaging caprock called the Zabriskie plateau. The new route had the advantage of leading the rover to rocks that represented the base of Mount Sharp earlier than originally planned, before crossing over the dune field. They would need to cross a short stretch of the Zabriskie plateau in order to reach those rocks. The rover climbed onto the plateau on sol 691.

They started using surge sols again in order to make the most of unrestricted drive sols. They tested a new “sidewalk mode” of MARDI imaging on sol 651 (see section 7.3.2) and used it for science purposes on the drive onto the plateau. As the rover approached the dune field, it encountered more sand ripples and some valleys filled with rippled sand. The rover bogged down in sand twice, once at Sourdough on sol 672 and again at Hidden Valley on sol 711. The team backed out of Hidden Valley and modified the path slightly to avoid valleys containing obvious sand ripples, sticking to places where the sand seemed to be a thin coating over rock. On the way out of Hidden Valley, they noticed a bit of Mount-Sharp-related rock that appeared suitable for drilling, but a drill attempt at Bonanza King on sol 733 resulted in the fracturing of the rock, halting drilling. The team elected to abort the sample attempt and drive onward to a better-looking outcrop.

3.5.4 Mission to Mount Sharp

Curiosity arrived at basal Mount Sharp rocks at a site called Pahrump Hills on sol 751, just after the first extended mission began. The Zabriskie plateau had ended, and Curiosity left the rock units of the Bradbury plains behind. The bright-colored Pahrump Hills outcrop contained material that the mission had referred to as the “paintbrush unit” when mapped from orbit, but it was renamed the Murray formation as Curiosity approached. It consisted of very finely laminated mudstone. Across a distance of 150 meters, the outcrop rose 15 meters of elevation, a convenient vertical slice through hundreds of rock layers. Curiosity drilled into the lowest-elevation spot on the outcrop, at Confidence Hills, on sol 759.

The rover proceeded to walk the Pahrump Hills outcrop three times. On the first circuit (sols 780 through 799) the focus was remote sensing. On the second circuit (sols 800 through 862) there was more contact science work with APXS and MAHLI to characterize the rock (Figure 3.12). Finally, on the third trip, Curiosity drilled at two locations, Mojave near the base of the outcrop on sol 882, and Telegraph Peak near the top on sol 908.

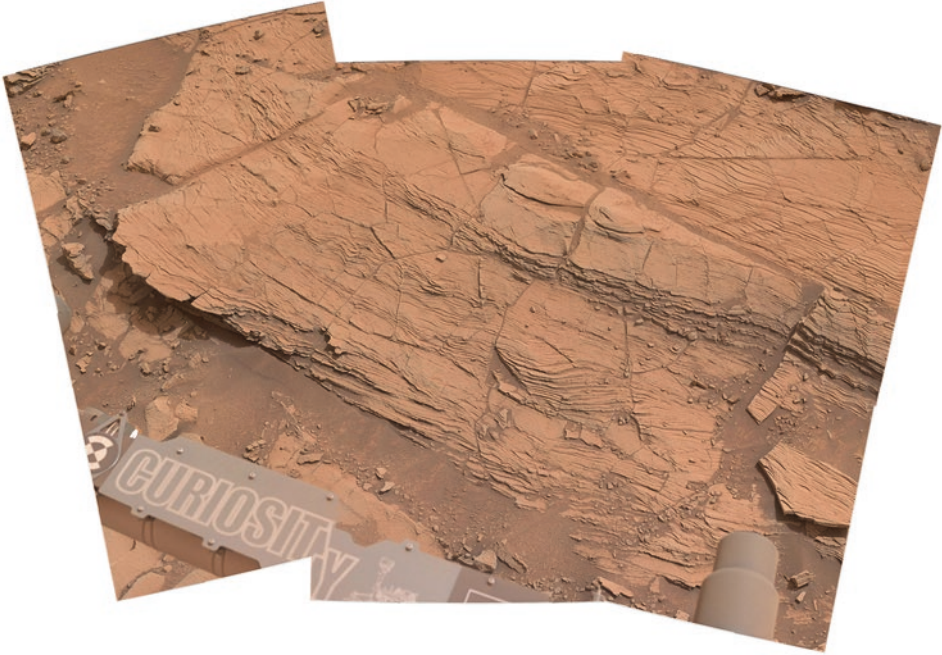


Figure 3.12. Left Mastcam panorama of the “work volume” in front of the rover after a drive to an outcrop named Chinle on sol 826, during the second circuit of Pahrump Hills. These kinds of mosaics are used to plan contact science with MAHLI and APXS. Curiosity surveyed the outcrop to study trends in sedimentology and composition up the outcrop. NASA/JPL-Caltech/MSSS.

Unfortunately, as the rover prepared for the second circuit on sol 801, the autofocus laser on the ChemCam instrument failed. By sequencing many observations at slightly different focal depths the ChemCam team could continue to gather science data, but less efficiently, and large arrays of shot points were no longer possible. With prodigious effort the team developed a new autofocus capability using the ChemCam imager, but not until sol 983, so autofocus was not available for the entire Pahrump Hills campaign (see section 9.2.3).

Another persistent problem began at the Telegraph Peak site: the drill experienced a soft short in the percussion mechanism on sol 911 that has recurred intermittently on a number of occasions (see section 5.3.4.2).

Curiosity departed Pahrump Hills on sol 949 to drive around the northern edge of the Bagnold dune field through sand-floored valleys. It proceeded across the Murray formation, among ridges of a new capping rock, initially called the “washboard unit” and later named the Stimson formation. The scenery was especially fine during this traverse, because the Stimson erodes into steep buttes.

The ChemCam team recovered autofocus capability as the rover was preparing to travel from primarily Murray valley bottoms to primarily Stimson higher plains, at a site called Logan Pass. When Logan Pass proved too sandy for safe travel, the rover turned around and headed to a new location, Marias Pass, where the newly capable ChemCam serendipitously found some silica-rich rock. After standing down for the mission’s second solar

conjunction from sols 1005 through 1026, the rover drilled into this silica-rich rock at Buckskin on sol 1060.

Curiosity turned south, aiming directly toward the dunes. The path took it repeatedly across the boundary between the Stimson and Murray formations. The team observed interesting cracks with bright alteration haloes around them all over the Stimson unit. They drilled into both unaltered and altered Stimson unit at Big Sky (unaltered) and Greenhorn (altered) on sols 1119 and 1137.

On sol 1174, the rover arrived at the northern edge of the Bagnold dune field. After some initial reconnaissance, the rover scooped samples at Gobabeb beginning sol 1224. Unfortunately, the sample processing activities were cut short by an anomaly on sol 1231. One of the four motors in the CHIMRA sample handling mechanism, the primary thwack actuator, stalled. Investigation proved that it still worked, but out of caution the engineers modified sample processing activities to rely less on the affected motor (see section 5.4.6.3 for more detail).

Curiosity left the first dune site behind on sol 1248, now traveling west to skirt around the extreme northern edge of the dunes. On sol 1281 the rover again ascended a steep boundary between the Murray and Stimson formations to reach a highland called the Naukluft plateau, where the wind had eroded the sandstone into fantastic shapes. Since the Naukluft plateau would be the last time Curiosity drove on the Stimson unit, the team decided to drill again into an alteration halo (at Lubango, on sol 1321) and into unaltered Stimson (at Okoruso, on sol 1332) (Figure 3.13). On sol 1353, the rover descended from the plateau, placing wheels on the Murray formation again. The team drilled at Oudam, the lowest-elevation site of a long future traverse across the Murray formation.

On sol 1369, they turned south to finally cross the dunes among the Murray buttes. The rover would remain on Murray formation rocks for many kilometers, with well-exposed bedrock everywhere, rapidly ascending in elevation. It gave the science team the opportunity to systematically read the layers of the rock to see how the environment changed over time. To do that, they changed their approach to selecting drill sites. The team began to drill every time the rover gained 25 meters of elevation. Three such regular drill intervals followed. Marimba, on sol 1422, was just north of the buttes; Quela, on sol 1464, was just to their south; and Sebina, on sol 1495, was another 25 meters above. Conveniently, the new regular-interval style of traverse roughly coincided with the start of the second extended mission on September 1, 2016, corresponding to sol 1448.

Unfortunately, the regular intervals of drilling came to a halt on sol 1536, when Curiosity attempted to drill at a site named Precipice. A problem had developed in the drill that was unrelated to the intermittent drill percussion problem that first appeared on sol 911. Now the drill feed mechanism would not advance reliably. As of sol 1800, the rover has not drilled since. It has collected one more sample, a scoop of sand at a site named Ogunquit Beach at the southern edge of the Bagnold dunes on sol 1651, but did not deliver the sample to CheMin prior to sol 1800 because of concern about the drill.

The rover continued to advance southward to approach the interesting-chemistry rocks first seen from orbit, doing science on the way with its other instruments while engineers investigated the problem with the drill. As of this writing, the rover had climbed onto Vera Rubin Ridge, formerly known as Hematite Ridge. Engineers began testing on Mars a new mode of drilling without using the drill feed on sol 1848.

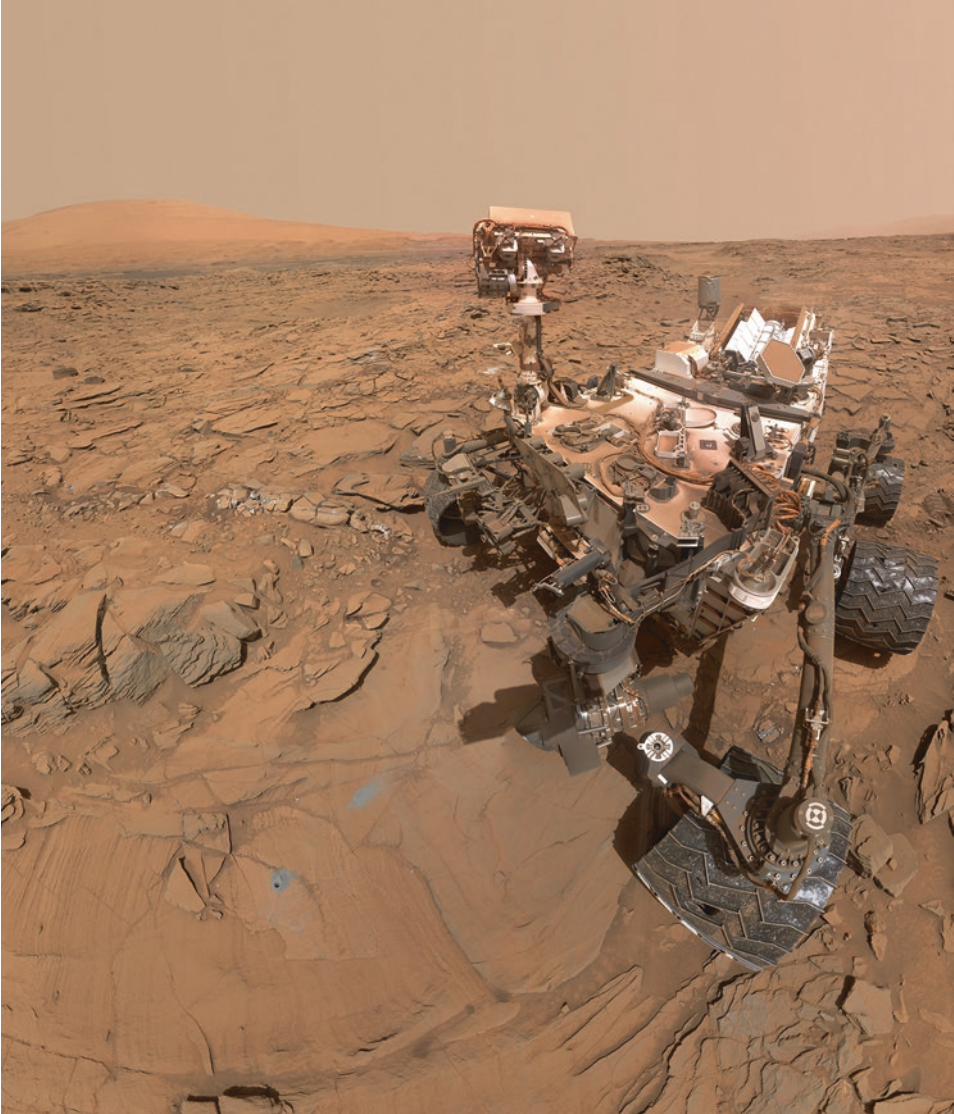


Figure 3.13. Curiosity MAHLI self-portrait at the Okoruso drill site. In the foreground is Okoruso. In the middle ground, just below the REMS boom, a bright spot marks the location of the Lubango drill site. Lubango was in an altered halo, Okoruso in unaltered Stimson rock. NASA/JPL-Caltech/MSSS.

As of sol 1800, Curiosity had attempted sampling in 20 locations, of which 17 resulted in the successful acquisition of sample and subsequent delivery to SAM and CheMin. Sample processing related to these 16 drill sites and 2 of the sand scooping sites is summarized in Figure 3.14 and Table 3.3.

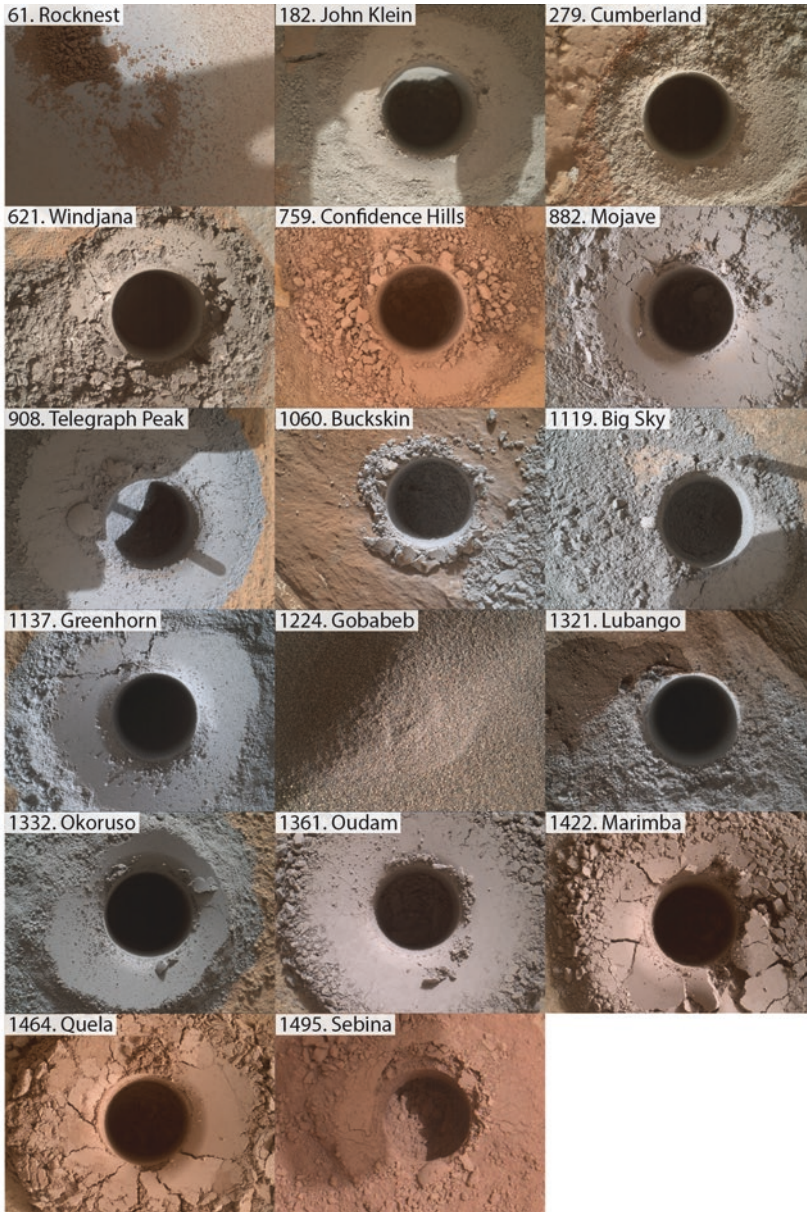


Figure 3.14. Seventeen Curiosity sample sites on Mars. Each is a MAHLI focus stack taken from a standoff distance of 5 centimeters, except for Rocknest (a photo of 150-micrometer sample on the observation tray from a standoff distance of 5 centimeters) and Sebina (a zoom in on a single image from a 25-centimeter standoff distance). As of sol 1800, there was no close-up photo of material sampled from Ogunquit Beach. NASA/JPL-Caltech/MSSS.

Table 3.3. Summary of Curiosity drill and scoop campaign activities through sol 1800. As of sol 1800, Ogunquit Beach sample remained inside CHIMRA. For explanations of the activities listed in the leftmost column, read Chapter 5.

Activity	Rocknest	John Klein	Cumberland	Windjana	Bonanza King	Confidence Hills	Mojave	Telegraph Peak	Buckskin	Big Sky	Greenhorn	Gobabeb	Lubango	Okoruso	Oudam	Marimba	Quelea	Sebina	Precipice	Ogunquit Beach
Mini-Drill	Scoops: 174, 176, 180	615	726*	756	867*, 881	1059	1116	1134	1224, 1224,	1320	1332	1361	1422	1464	1495	1536*	1651			
(*=unsuccessful)	61, 66, 182	279	621	759	882	908	1060	1119	1137	1228, 1231	1320	1332	1361	1422	1464	1495				
Full drill	70, 76, 77, 78, 95	284, 289	-	-	-	-	-	-	-	-	-	-	-	-	-	-	-	-	-	-
O-tray dropoff	79	193, 194	279, 464	623	-	762	884	922	1061	1121	1139	1224, 1228	1323	1334	1362	1425	1465, 1495,	1466	1496	1651
Pre- and post-sieve sample volume inspection																				
Drill wall survey with MAHLI	-	270	279, 283, 292	628	-	768	883	910	1064	1123	1142	-	1324	1337	1364	1426	1466	1496	-	-
Pre-sieve (coarse fraction) dump	64, 67, 73, 81, 128	229	486	704	-	765	889	930	1064	1123	1142	1226, 1228, 1251	1324	1337	1364	1426	1466	1496	-	-
Post-sieve (fine fraction) dump																				
MAHLI self-portrait (stereo)	84, 85	177, 270	-	613, 627	-	868, 882, 884	-	1065	1126	-	1228, 1241	-	1338	-	1463,	1466	-	-	-	-
CheMin delivery	71, 77, 94	195	282	623, 640	-	765	884	922	1061	1121	1139	1226	1323	1334	1362	1425	1466	1496	-	-
SAM delivery	93, 96, 98, 116	196, 199, 224, 227	281, 286, 290, 353, 367, 381, 414, 463, 464	624, 653, 694	-	773	887, 891, 892	928, 954	1075	1129	1147, 1178	1224, 1230	-	-	1382	1443, 1484	1484	-	-	1651

Even if the mission were to end tomorrow, scientists would be working on interpreting Curiosity's data for decades. Of course, the mission hopes for much longer survival than that.

3.6 REFERENCES

- Allison M (1997) Accurate analytic representations of solar time and seasons on Mars with applications to the Pathfinder/Surveyor missions. *Geophys. Res. Lett.* 24(16):1967–1970, DOI: 10.1029/97GL01950
- Bass D, Wales D, and Shalin V (2005) Choosing Mars time: Analysis of the Mars Exploration Rover experience. Paper presented at IEEE Aerospace Conference, 5–12 March 2005, Big Sky, MT, USA, DOI: 10.1109/AERO.2005.1559722
- Cantor B, James P, and Calvin W (2010) MARCI and MOC observations of the atmosphere and surface cap in the north polar region of Mars. *Icarus* 208:61–81, DOI: 10.1016/j.icarus.2010.01.032
- Chattopadhyay D et al (2014) The Mars Science Laboratory supratactical process. Paper presented at SpaceOps 2014 Conference, 5–9 May 2014, Pasadena, USA
- JPL (2013) Rover Team Working to Diagnose Electrical Issue <http://mars.nasa.gov/msl/news/whatsnew/index.cfm?FuseAction=ShowNews&NewsID=1559> Status report dated 20 Nov 2013, accessed 15 Aug 2016
- Reichardt T (2015) The man who named the Martian day. <http://www.airspacemag.com/daily-planet/man-who-named-martian-day-180957350/>. Accessed 2 Mar 2016

4



How the Rover Works

4.1 INTRODUCTION

Curiosity may look superficially like the Mars Exploration Rovers and Sojourner (Figure 4.1), but its redundant systems, powerful science suite, and complicated sample manipulation make it a different beast entirely. The rest of this book describes all the components that enable Curiosity to do science on Mars, how they are supposed to work, and how things have occasionally gone wrong.

Figure 4.2 shows Curiosity's external parts, Figure 4.3 its internal ones. Its basic dimensions are outlined in Figure 4.4. The aluminum rover body, also known as the warm electronics box (WEB) is a block 163-by-117-by-46 centimeters in size. It is painted white for thermal control and to reduce the glint of reflected sunlight into cameras. The warm electronics box supports the other external components and keeps the avionics and science instruments inside it within a controlled temperature range.

4.2 POWER SYSTEM AND MMRTG

Curiosity draws its power from a Multi-Mission Radioisotope Thermoelectric Generator (MMRTG).¹ The MMRTG trickles the power that it generates into two rechargeable 42 amp-hour large-cell lithium-ion batteries. The MMRTG generates power using the heat from radioactive decay of 4.8 kilograms of plutonium dioxide (a ceramic form of plutonium-238), of which about 69% of the mass was radioactive plutonium-238 when it was first fueled on October 28, 2008. Plutonium-238 has a half-life of 87.7 years. Power production will decline over time, reducing rover activity. Once the MMRTG no longer generates enough power for survival and communications, the mission will end, probably by 2030, if nothing else ends it earlier. The MMRTG weighs 40 kilograms.

¹The description of Curiosity's MMRTG in this section is based on NASA (2013), Jones et al (2013), and Woerner et al (2012)

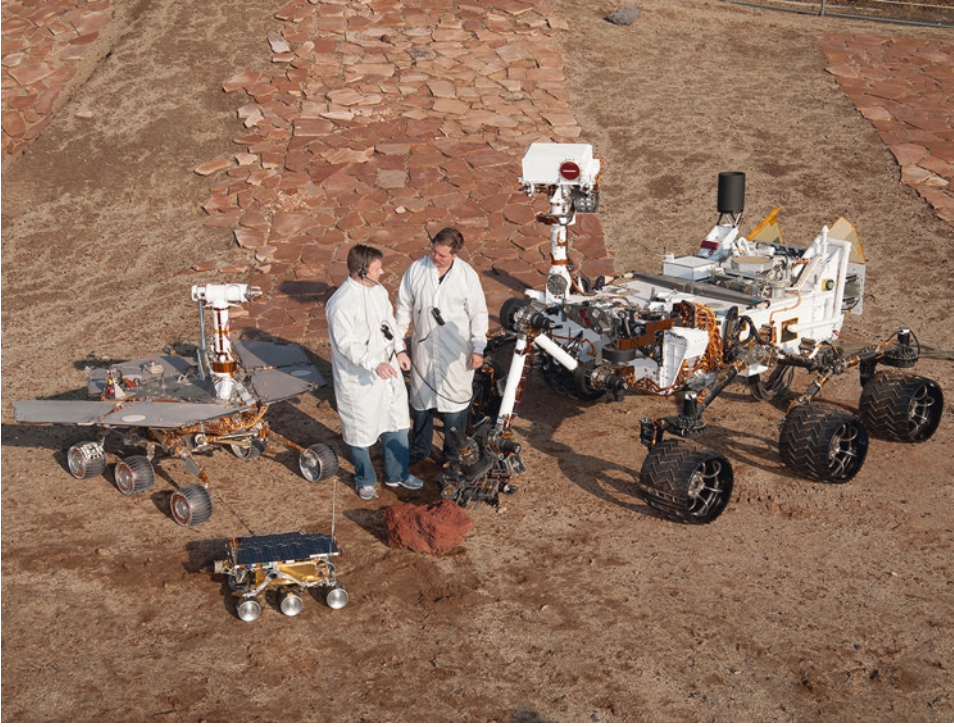


Figure 4.1. Family portrait of the three JPL Mars rovers. In front is Marie Curie, the flight spare of the Sojourner rover, now a museum piece. At left is the Surface System Test Bed for the Mars Exploration Rover mission. At right is the Vehicle System Test Bed for the Curiosity mission. NASA/JPL-Caltech release PIA15279.

4.2.1 How the MMRTG works

A radioisotope thermoelectric generator converts heat into electricity with no moving parts by taking advantage of the thermoelectric effect. Holding two different electrically conductive materials at different temperatures and joining them in a closed circuit generates current. A pair of conductive materials joined in this way is called a thermocouple. A thermocouple has a “hot shoe” and a “cold shoe.” In Curiosity’s MMRTG, the decaying plutonium heats the hot shoes of the thermocouples. External fins splaying out into the Martian air chill the cold shoes.

The plutonium dioxide ceramic is split into 32 pellets, each weighing 150 grams. Each pellet is clad in iridium. The iridium cladding is a safety feature that blocks the alpha particles emitted by the plutonium pellets. It also has a high melting temperature (2400°C), in case the cooling system fails.

The MMRTG was carefully designed to survive a launch accident, like a launch pad explosion or a midair breakup, without releasing radioactive material into Earth’s atmosphere or oceans (Figure 4.5). Two pellets go inside a graphite impact shell.

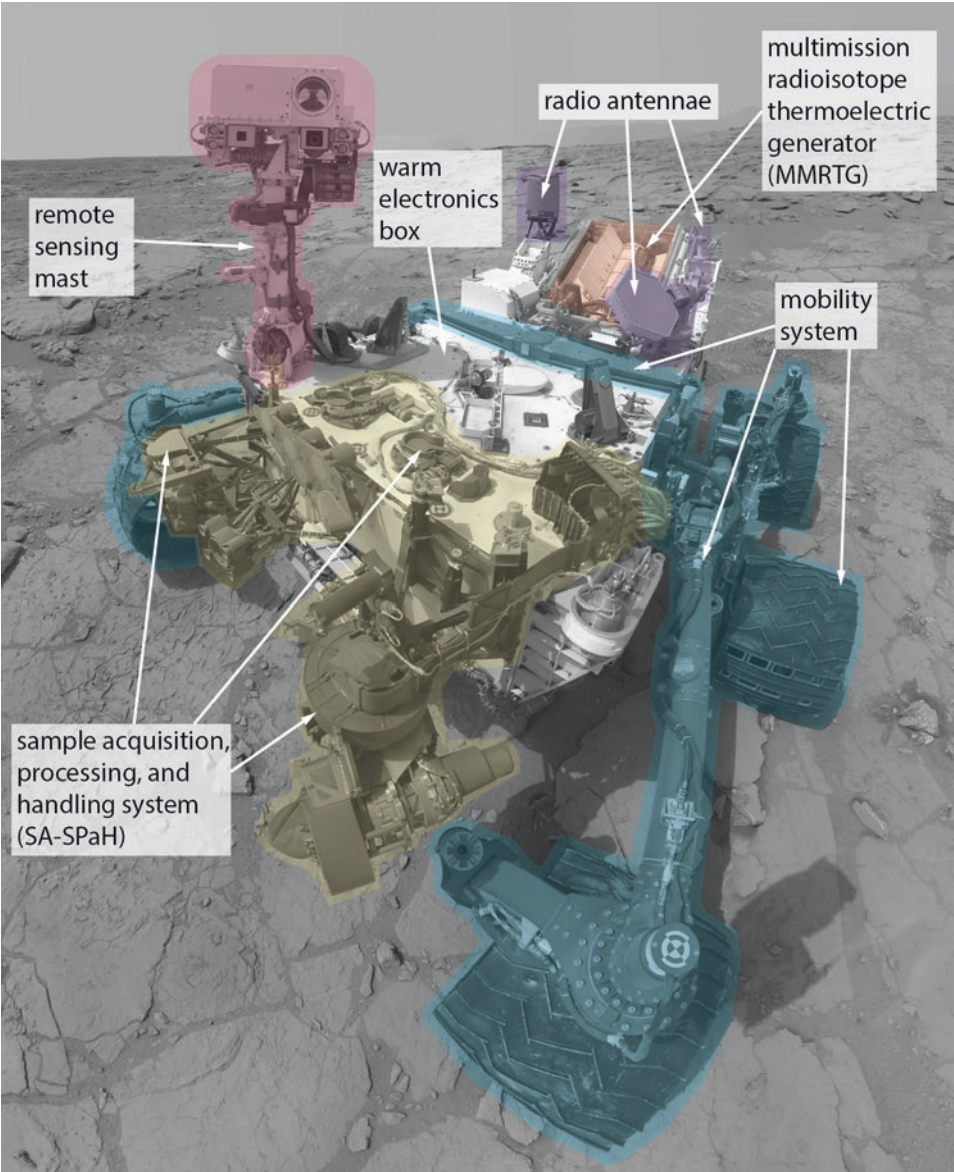


Figure 4.2. Overview of external components of rover systems. Not all of the robotic arm is visible in this photo because it was taken with MAHLI, which is mounted on the arm. Base image is the MAHLI self-portrait taken at John Klein on sol 177. NASA/JPL-Caltech/MSSS/Emily Lakdawalla.

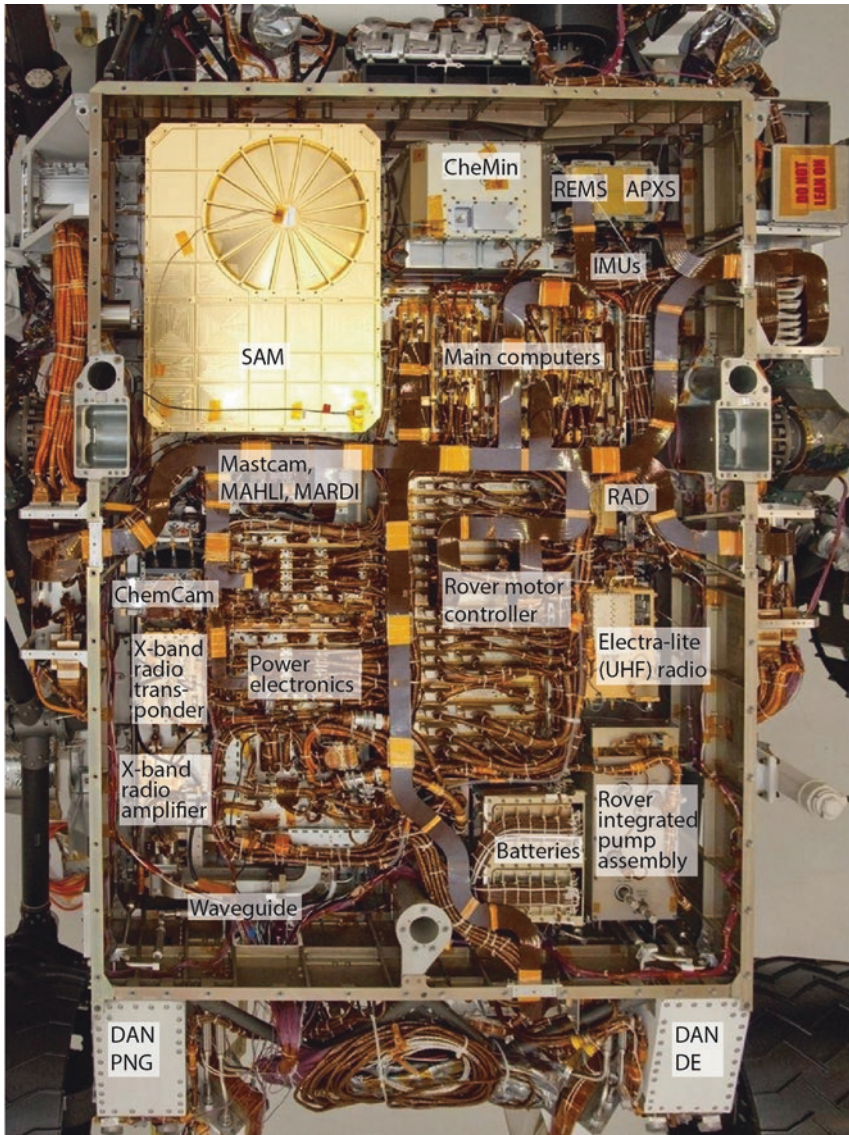


Figure 4.3. Interior of the rover; looking up from below. SAM, CheMin, REMS, APXS, Mastcam, MAHLI, MARDI, RAD, ChemCam, and DAN PNG and DE are all science instruments. IMUs (inertial measurement units), rover motor controller, and power electronics are all part of the rover avionics. Telecommunications components include the Electra-lite (UHF) radio and X-band transponder, amplifier, and waveguide. Batteries are part of the power system, and the rover integrated pump assembly is part of the thermal control system. NASA/JPL-Caltech/Emily Lakdawalla.

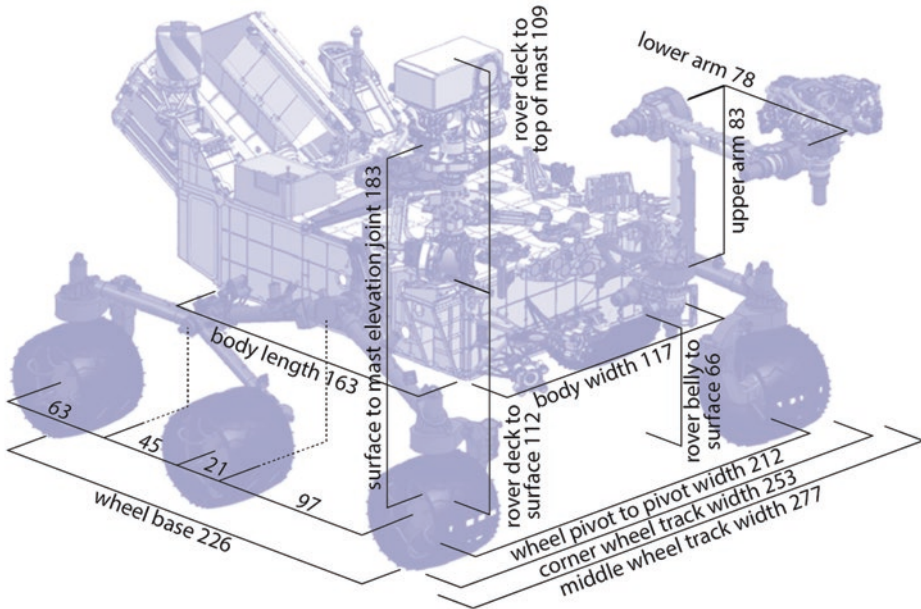


Figure 4.4. Dimensions of some large elements of the rover in centimeters. NASA/JPL-Caltech/Emily Lakdawalla.

A carbon-bonded carbon-fiber sleeve encases the impact shell. Two such sleeves are inside each general-purpose heat source module. The core of the MMRTG is a stack of eight of these modules, and the core is surrounded by an aluminum alloy housing. In the event of a launch accident at high altitude, the aluminum housing would melt, which would scatter the eight modules. Those lower-mass modules would have lower terminal velocities than the whole MMRTG. At their lower velocities, the carbon fiber aeroshells wouldn't melt upon reentry. Even if the pellets are subjected to large enough forces to break them, their ceramic form means they'll break into large chunks rather than a dust that could be inhaled.²

To turn the heat from the MMRTG core into power, the safely constructed, hot core is encased in a graphite heat distribution block. Then comes a layer of thermoelectric modules, their hot shoes in contact with the heat distribution block and their cold shoes touching the outer shell of the MMRTG and its heat-radiating fins. The hot shoes operate at a temperature of 520°C, the cold shoes at a still-toasty 75°C during cruise and 150–185°C on Mars, depending on the season.³

²NASA Science Mission Directorate (2006)

³Woerner et al (2013), Woerner et al (2012)

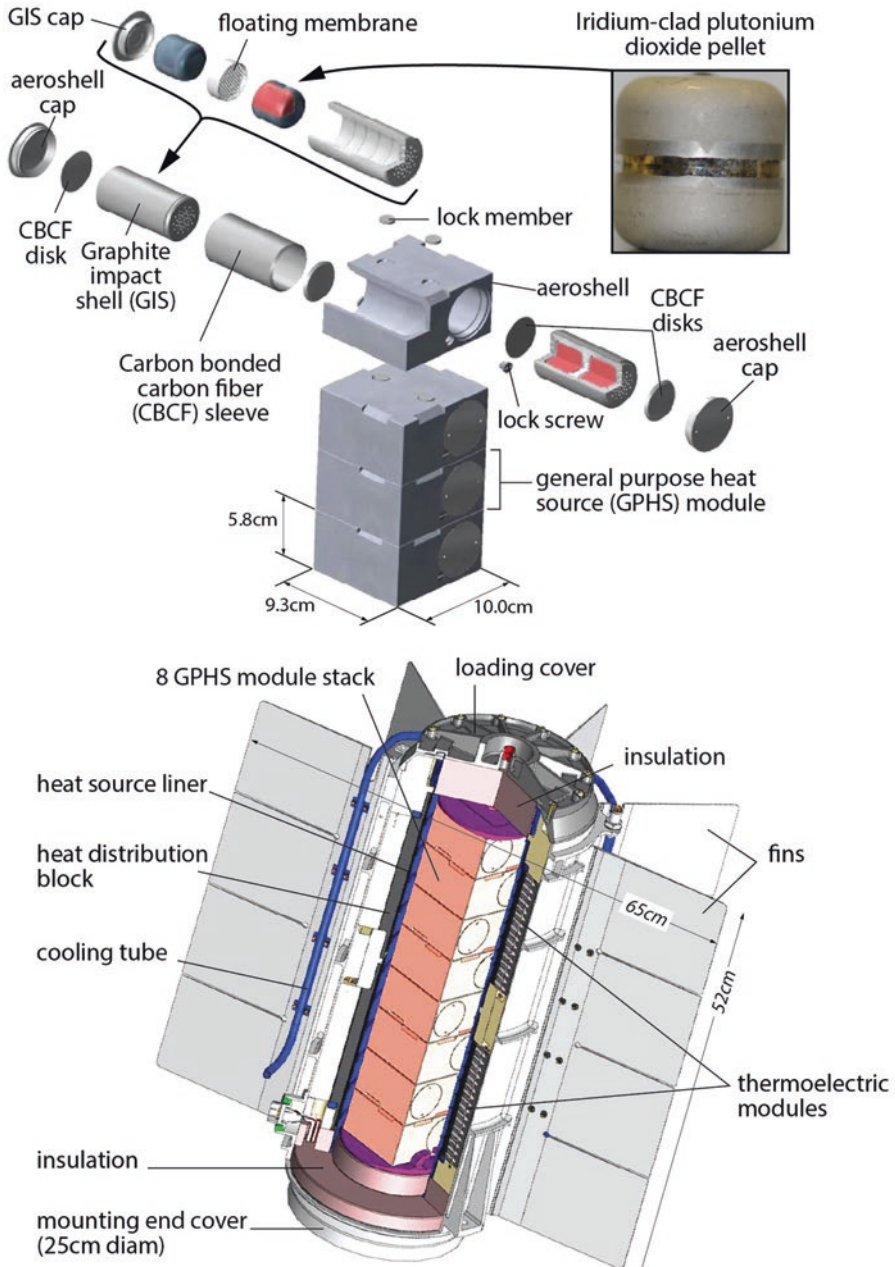


Figure 4.5. Parts of the Multi-Mission Radioisotope Thermoelectric Generator (MMRTG). Emily Lakdawalla after Woerner et al (2012).

The MMRTG is not very efficient at turning heat into electricity. When first fueled, the thermocouples converted about 110 watts to electricity. The rover's heat rejection system uses some of the remaining 1900 watts of heat to keep the warm electronics box warm (more on that in section 4.3); the rest of the heat radiates away into the Martian air.

The rover requires 45 to 70 watts of that power at all times while sleeping.⁴ It consumes at least 150 watts whenever it is awake, and up to 500 watts while driving. Therefore, the rover is completely dependent upon its batteries and spends most of its time asleep and recharging. It is active for about 6 hours of each Martian day, on average.⁵

4.2.2 Performance on Mars

Upon landing, the MMRTG generated about 114 watts, ranging from 109 to 119 watts over the course of the sol. You might have noticed that this is more power than it generated when it was first fueled, while on Earth. The MMRTG was designed to operate at the lower ambient temperature on Mars, where there is a higher contrast in temperature between the hot and cold shoes of the thermocouples. It generates more power at night, when ambient temperatures are lowest.

Over time, the performance of the MMRTG decays at a rate of roughly 1 watt per 80 sols. The plutonium decay is exponential – it declines more slowly as time goes on – but the MMRTG performance decay is close to linear. That's because the thermocouples are also degrading, but unlike the plutonium they degrade faster with age. At the beginning of the mission, engineers estimated that the MMRTG would still be producing 54 watts 17 years after was fueled, on October 28, 2025, which would correspond to sol 4702.⁶ Even with efficiency improvements, the rover's activity will be increasingly energy-constrained with time.

4.2.3 Anomalies

On sol 456 (November 17, 2013), the rover experienced a partially conductive “soft short” in the MMRTG, apparently caused by a part of the electrical power circuit touching the aluminum housing.⁷ The Cassini spacecraft had MMRTGs of the same design, and experienced similar shorts. As a result of the short, the voltage difference between the rover's power bus and chassis changed (from 11 volts to 4 volts on that particular sol). The rover's power system is robust to such changes in voltage, having been designed with a floating bus. The mission halted activity for 6 sols to investigate the problem, which had spontaneously disappeared by sol 461.⁸ It occurred again on sols 816, 1084, and 1158, and has been happening more frequently since. The soft short is annoying because it halts operations, but it does not threaten the health of the rover.⁹ Table 4.1 lists all the soft shorts to sol 1582.

⁴Gross and Cardell (2011)

⁵Welch et al (2013)

⁶Woerner (2014)

⁷JPL (2013a)

⁸JPL (2013b)

⁹David Woerner, personal communication, email dated June 16, 2016

Table 4.1. Dates and effects of Curiosity MMRTG soft shorts to sol 1582. Courtesy Steven Lee.

Sol	End Sol	Sols Since Prior Short	Character of Short
456	461	n/a	Intermittent, then Constant
816	835	355	Intermittent
1084	1090	249	Intermittent
1158	1166	68	Constant
1173	1181	7	Constant
1187	1191	6	Intermittent
1204	1221	13	Intermittent, then Constant
1233	1239	12	Constant
1247	1256	8	Constant
1257	1269	1	Intermittent, then Constant
1284	1288	15	Intermittent, then Constant
1288	1289	1	Constant
1338	1362	50	Intermittent
1373	1422	11	Intermittent
1445	1461	23	Intermittent
1473	1495	12	Intermittent
1530	1582	35	Intermittent, then Constant

4.3 AVIONICS

The rover has two redundant sets of avionics controlling all of its functions, referred to as the A-side and B-side.¹⁰ Each side has three main processor units. Two redundant rover power analog modules (RPAMs) function like the rover's cerebellum, controlling all of its essential life support functions: power distribution, system fault protection, and wakeups/shutdowns. The rover compute elements (RCEs) are like the rover's cerebrum, controlling its higher functions. The rover motor control assembly (RMCA) is like the rover's motor cortex, controlling all motion of wheels, arm, turret, antenna, mast, and instrument covers. Both A-side and B-side power modules are interconnected with both A-side and B-side computers, as are the two cooling system pumps, two radio transceivers, two inertial measurement units, and individual science instruments. It's easy to see why testing of the avionics was so time-consuming and challenging: just those four pairs of redundant components yield 16 possible configurations.

Because the rover spends most of its time asleep in order to conserve power, it performs wakeups and shutdowns several times per sol. Before the computer shuts down, it sets a countdown timer in the power module; when the timer expires, the power module turns on the main computer again. One function that is partially available even while the rover is asleep is communications. An orbiter can hail Curiosity through a transceiver, requesting the sleeping rover to wake up. This capability would only be needed if the rover lost its clock timing, so did not know when communications passes would occur.¹¹

¹⁰Lee and Donaldson (2013)

¹¹Makovsky et al (2009)

4.3.1 The sol 200 anomaly

On sol 200 (February 27, 2013), the rover sent telemetry to Earth indicating problems in its flash memory on the rover compute element. The memory problems had caused several software tasks to hang, preventing the rover compute element from performing the planned shut down for that day. The software should have handled the memory loss gracefully: onboard fault protection watchdog timers should have caught the issue and placed the rover in a safe state. But the watchdogs were being pacified without actually triggering a safe mode. Without the ability to shut down, the rover could have drained its batteries in three to six days.¹² As the anomaly investigation continued that afternoon, Earth testing revealed that the next time the rover attempted to communicate with Earth, that process would hang, and the computer would shut off the radio, which could leave operators without the ability to command the rover.¹³

The mission asked for emergency time on the Deep Space Network to send a series of commands to the rover to swap to the backup computer, just in time before the rover's radio would be powered off. After 2:00 in the morning in California, or about 8:00 in the morning local time for Curiosity, after both the engineers and the rover had had totally sleepless nights, the signal was sent. Curiosity sent a signal back indicating that the computer swap had been successful, but the signal arrived a heart-straining 3 minutes later than expected.

Subsequent investigation revealed that the problem originated in a single bad chip in the A-side computer's flash memory array. They worked around the problem by instructing the A-side computer not to use half of its flash memory. Fortunately, there was plenty of margin available. The software was updated to handle these conditions more gracefully. The rover has used the B-side rover compute element as its primary computer ever since. Engineers patched the flight software to return the A-side computer to service as a reliable backup after sol 772.

4.3.2 Flight software

Each of the rover compute elements has a 133 megahertz RAD750 processor running the VxWorks operating system, 256 megabytes of RAM, and 4 gigabytes of flash data storage. (Smartphones in common use at the time of launch operated at about four times the speed with four times the storage.)¹⁴ The rover's flight software includes many autonomous functions to reduce the workload of daily tactical planning. For example, communications windows are scheduled long in advance; an occasionally updated table in rover memory keeps track of all such windows, and the rover automatically executes communications passes within those windows, even if it has to wake itself up to do so.

The rover's autonomy has increased over time, thanks to several flight software upgrades. It takes many sols to uplink new software to the rover, and then a minimum of four sols to verify, install, and commit the new software on both of the rover computers. Each of the instruments also has its own flight software, which can be upgraded independently of the main flight software.¹⁵

¹²JPL (2014)

¹³Magdy Bareh, personal communication, August 28, 2017

¹⁴Davis (2012)

¹⁵Danny Lam explained the upgrades to me in an email on April 4, 2017

4.3.2.1 *Flight software version R10.5.8 (sol 8)*

The rover landed running version R9 of its flight software (specifically, version R9.4.7). Immediately after landing, the rover upgraded to version R10.5.6, which removed many of the cruise functions and added in many surface operations functions. When they transitioned to version R10.5.6, they followed by patching the new software to fix a potential problem with the X-band radio transponder, and the rover ran version R10.5.8 for some time.

4.3.2.2 *Flight software version R11.0.4 (sol 484)*

A bit more than a year after landing, as the rover was traveling between Cooperstown and the Kimberley, the engineers began to uplink version R11.0.4. The upgrade actually failed to complete on the first attempt, but finished successfully on sol 484 (see section 3.5.3). Version R11 had a number of improvements, new features, and bug fixes that increased operational efficiency:

- New autonomy to track certain types of unsuccessful data transmission attempts, allowing it to reattempt transmission without being commanded to, saving time for tactical planners.
- Dramatic improvements to data compression, allowing more data to be downlinked in a given pass.
- Improvements to fault protection logic in the event of multiple sequential switches between A and B side computers.
- “Dream mode” ability to initiate heating of rover motors while still asleep.
- Temperature-dependent camera models for the Navcams (necessary for visual odometry and autonomous navigation, see sections 3.5.3 and 6.5) became part of onboard rover software rather than being sequenced from the ground each time.
- Improvements to multi-sol driving capability, including the ability to save on-board terrain maps during sleep so the rover can use the same one to continue a drive the next day without regenerating it, allowing the rover to spend more time driving.
- Several improvements intended for drilling while parked on a slope: new ability to steer wheels one at a time, improving steering stability on slopes; visual odometry during arm operations, allowing slip checking (see section 6.4.3) when drilling on slopes.
- Lots of efficiency, fault protection, and system robustness improvements for sample operations, making both Mars operations and ground planning more efficient.
- Added ability to adjust ChemCam focus position to produce Z-stacks as a single command, making sequencing less onerous.

“Dream mode” was an especially important improvement to the rover’s efficiency during colder winter months.¹⁶ The first activity of the day often requires preheating motors before they can be used, which can take up to two hours. To have the rover computer

¹⁶Lee and Donaldson (2013)

powered on and waiting for motor warmup consumes precious energy that would otherwise be available for driving or science. Dream mode solved this problem. To prepare for dream mode, before shutdown, the rover computer delivers a heater schedule to the power analog module. If any preheating is scheduled to begin before rover wakeup, the power analog module can command the heater to turn on while the rover is otherwise asleep. In dream mode, the rover is also capable of checking temperature sensors once an hour while asleep. Although it was in development since before landing, dream mode wasn't actually used operationally until sol 1180, shortly before the rover's second winter solstice.

4.3.2.3 Flight software version R11.0.5 (sol 772)

In October 2014, engineers patched R11.0.4 to R11.0.5 to permanently resolve the problem with the A-side computer that had existed since the sol 200 anomaly. The patch, applied only to the A-side computer, instructed it not to read its bad memory cells, and gave the rover a fully functional backup computer again.

4.3.2.4 Flight software version R12.0.3 (sol 879)

In January 2015, they upgraded to version R12. Its improvements were more modest than R11's:

- Ability to use inertial measurement units to sense slipping during drilling operations on slopes.
- Other improvements to driving that made the guarded mode easier to sequence.
- Added “hooks” into the flight software that made it easier to add a new ability in the future without a complete flight software upgrade. The hooks were for software added in 2017 that permitted traction control, in which wheels can be driven at different speeds when certain conditions are met, in order to allow wheels going over obstacles to travel faster than other wheels.

4.4 THERMAL CONTROL

Maintaining the temperature of a spacecraft's components within allowable ranges presents challenges for any mission. Space is cold; the Sun is hot; a vacuum doesn't conduct heat. Mars has a thin atmosphere that mitigates the temperature swings that would occur in a vacuum, but not as well as Earth's does.

Curiosity's external parts can handle temperatures as high as 50°C and as low as -128°C, and can cope with wide temperature swings from day to night every sol. In fact, the rover was designed to handle more extreme weather than it needs to, because the landing site hadn't been chosen when the rover design was finalized. Located close to the equator and at low elevation, Gale's weather is relatively benign. The REMS instrument has measured overnight lows in the air just above the ground averaging around -75°C (ranging from -85°C to -65°C), and daytime highs averaging around -10°C (ranging

from -30°C to $+5^{\circ}\text{C}$) (see section 8.4.3). Ground temperatures have been as warm as 15°C and as cold as -100°C .¹⁷

Different parts of the rover have different thermal requirements. The warm electronics boxes inside the rover's body and head keep their interiors warmer than -40°C and cooler than 50°C , although their contents won't fail as long as temperatures stay between -55°C and $+70^{\circ}\text{C}$.¹⁸ But some instruments, particularly ChemCam's body unit, don't like running hot. Other instruments, like SAM, have components that generate a lot of heat. These instruments have integrated coolers to keep their electronics at safe temperatures.

4.4.1 Rover avionics mounting panel

All the temperature-sensitive electronics and systems are bolted to a rover avionics mounting panel (RAMP). The panel is, in turn, attached to the top deck of the rover with titanium structures designed not to conduct heat from the interior to the exterior of the rover. Martian atmosphere occupies the small amount of space inside the rover that is not filled with electronics. The mostly carbon dioxide gas inhibits the transfer of heat between the internal hardware and the rover's sides and belly panel.

4.4.2 Sensors and survival heaters

A total of 221 temperature sensors monitor conditions all over the rover, though only about half are in use at any given time, since there are redundant sensors for the rover's A- and B- side electronics. A few critical components (such as the batteries) have their own survival and warm-up heaters controlled by a total of 8 mechanical thermostats.

Curiosity's 17 cameras and 32 motors can survive all expected ambient temperatures outside the rover's body, but have minimum operating temperatures between -55°C and -40°C . When they are too cold (as they always are overnight and early in the morning, and can be during the day, depending on the season), they have to be warmed before use. The rover's main computer switches these warm-up heaters on and off as commanded.

4.4.3 Rover heat rejection system

The rover heat rejection system (RHRS) pumps Freon (trichlorofluoromethane, CFC-11) through tubing that loops near the MMRTG to pick up waste heat and then into the rover body to warm the electronics (Figure 4.6). The heat rejection system contains a total of 60 meters of aluminum and stainless-steel tubing. The rover integrated pump assembly (also visible in Figure 4.3) acts like the rover's heart, pumping Freon near all the parts of the rover that need to be warmed and cooled. It contains a large accumulator, or tank, that gives the Freon room to expand when it warms. Peak temperatures in the system have never risen above 72°C ; the system can handle Freon temperatures as high as 90°C .¹⁹

¹⁷Keith Novak, personal communication, email dated February 28, 2017

¹⁸The description of the heat rejection system in this section is based on Novak et al (2013)

¹⁹Keith Novak, personal communication, email dated February 28, 2017

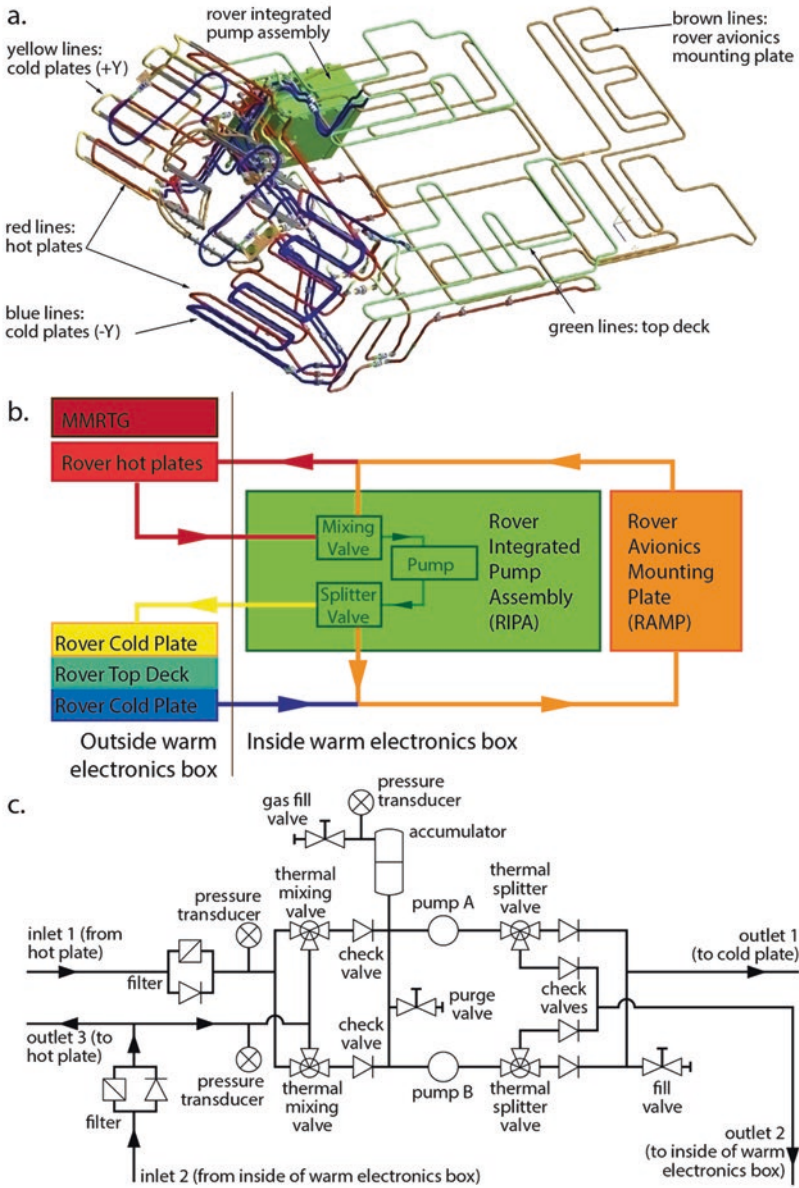


Figure 4.6. Rover heat rejection system. (a) Layout of the tubing. (b) Schematic diagram of the system, color coded to match (a). (c) Pumps, valves, filters, and manifolds that make up the interior of the pump assembly. Emily Lakdawalla after Novak et al (2013).

There are two heat exchangers on the back of the rover, one on each side of the MMRTG (Figure 4.7). The heat exchangers have tubing bonded to both sides. There is a hot plate on the inward-facing side of each heat exchanger, where the fluid picks up waste heat from the MMRTG and returns to the pump. On the outward-facing side of each heat exchanger is a cold plate, where fluid flowing through the tubing radiates heat away. Aerogel fills the honeycomb core of the heat exchangers, thermally separating the hot inner face from the cold outer face. If the interior of the rover needs to be heated, the pump sends fluid warmed by the MMRTG through the tubing connected to the rover avionics mounting plate. When the rover runs hot, the pump can send fluid from the rover avionics mounting plate to the cold plates on the outside of the heat exchangers and just underneath the rover's top deck.

The MMRTG is exposed to the Martian elements, including wind. During the coldest winter months, high winds could rob the rover of heat necessary to survive. The heat exchangers and body of the rover shield the MMRTG from winds blowing from the front or sides of the rover, but the back is unprotected. A fabric windbreaker (Figure 4.7) bridges the cold plates on the back of the rover, dramatically reducing the wind's chilling effect.

Because the heat rejection system is absolutely essential to rover health, there are two redundant pumps and two redundant mixer valves and splitter valves (Figure 4.6c). The mixer and splitter valves allow the heat rejection system to selectively heat or cool the Freon as needed. For rover safety, they work independently of any computer, operating passively in response to the temperature of the fluid flowing through them.

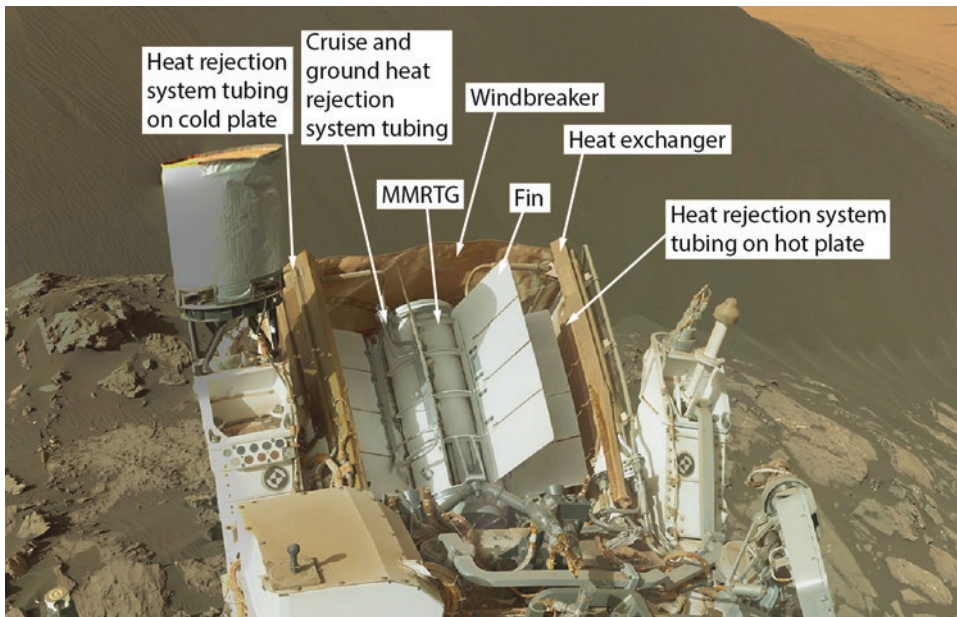


Figure 4.7. External parts of the rover's heat rejection system. Cruise and ground heat rejection system tubing in direct contact with the MMRTG is not used on Mars; it was for cooling the MMRTG on Earth and during cruise (see section 2.2.1). The base image is the Mastcam self-portrait taken on sol 1197. NASA/JPL-Caltech/MSSS/Emily Lakdawalla.

The mixer valve controls the amount of flow across the rover's hot plates. If the mixer valve falls below a temperature of -10°C , it opens all the way, sending 97% of the fluid through the hot plates. If the mixer valve measures a temperature of 10°C , it closes to its minimum setting of 55%, which runs just enough fluid in the hot plates to keep the fluid temperatures below 90°C . The splitter valve controls the flow to the cold plates and top deck. When its temperature rises above 35°C , it opens all the way to 96%; it closes to its minimum setting of 4% at 15°C .²⁰

4.4.4 Heater tables

All of Curiosity's components have minimum allowable operating temperatures. Some components would spend too much time at those temperatures without assistance, so have built-in heaters. The most heat-demanding components are the motors. Curiosity's motors do not operate well at temperatures below -55°C because the wet lubricant inside the gearbox is highly viscous at that temperature. All the motors have heaters to permit their operation when ambient temperatures are lower than that. Heating requires both power and time, two limited resources, so during tactical planning it is imperative to predict how long and how much power it will take to prepare motors for use. Time of day, season, wind speeds, and rover orientation (potentially causing shadowing) all have strong effects on the start temperatures of rover hardware. With so many variables involved, engineers can't predict exactly how much heating will be necessary for a given motor on a given sol to be operated at a given time. Instead, they budget enough power to heat the motors as much as necessary for a predicted worst-case scenario.

Prior to landing, thermal engineers prepared two "heater tables" that laid out the energy requirements for motor heating for the worst-case environments for every motor for each hour of the day for two representative days in the Martian year: landing day, which was on L_s 151 (approaching the southern hemisphere vernal equinox), and the coldest day, winter solstice, L_s 90. The landing-day table would allow conservative budgeting of energy expenditures for heating throughout the rest of spring and most of summer until fall started to bring cooler temperatures, when they would have to switch to the winter table.

The heater tables stipulate, for each heater, for each hour of the day:

- *Warmup period.* This varies with the mass of the motor. The largest motors that drive and steer the wheels weigh 6 kilograms and can take up to 2 hours to preheat when they are coldest.
- *Target temperature of the temperature sensor.* The sensors and heaters are on the outside, not inside, the motors. But it's the deep interior of the gearbox that has to be brought to -55°C . This unfortunate arrangement results from the late switch to wet-lubricated motors (see section 1.5.2). To drive in the morning, the outside of the motor and its temperature sensor may be heated as high as -5°C in order to generate a big enough pulse of heat to bring the interior to temperature within a reasonable amount of time.

²⁰Novak et al (2013)

- *High and low set points for temperature cycling during the maintenance heating period.* Once the motor preheats, the exterior temperature is allowed to fall to a lower set point before the heater turns on again and continues to oscillate within a small temperature range. For some motors, after preheating, the heater turns on when needed to maintain the exterior temperature of the motor between -49°C and -44°C .
- *Duty cycle prediction.* The amount of time during the maintenance heating period that the heater will be turned on.
- *Timeout period.* How long to wait for the target temperature to be reached before giving up, shutting down the heater, and aborting the day's plan. If this happens, the rover will continue performing remote sensing activities, but will not proceed with any drives or arm work.
- *Energy* (in watt-hours) associated with warmup and maintenance heating of the motor. This is taken out of the power budget in the day's plan.

Fortunately, it isn't always necessary to preheat motors. Even on the coldest winter days, Gale crater heats up to about -25°C , well above the motors' minimum operating temperature. The biggest motors take the longest to heat, and are the ones that enable Curiosity to drive. During the winter, there is a 3-hour period when the rover can drive without spending time or energy preheating, from about 14:40 to 17:50 local true solar time each day. (Heater tables are a case where it is necessary to employ true rather than mean solar time; see section 3.2.2.) During the spring and summer this is a 6-hour period, but still in the afternoon, from about 12:30 to 18:30 each day.

Therefore, waiting for the motors to preheat naturally requires waiting until the afternoon to drive. However, the mission would often prefer to move the rover in the morning in order to allow sufficient time for driving and post-drive imaging to complete before the afternoon orbiter relay. Rover planners compromise by usually starting drives between 11:00 and 12:30, which means motors usually need to be preheated, but for a relatively short time.

4.4.5 Performance on Mars

Curiosity's thermal control systems have operated flawlessly.²¹ The temperature of the interior of the electronics box has varied within acceptable limits, ranging from lows near 5°C to highs of 17°C in winter and 37°C in summer. The rover's temperature profile has been reliably the same, day after day, making it easy for rover planners to decide when to operate the instruments that need cool ambient temperatures. The battery survival heaters have never been turned on and likely never will be.

There were several surprises after the spacecraft landed on Mars. While REMS measured ground temperatures that were in good agreement with predictions, it found air temperatures to be much higher than predicted: 25°C warmer than predicted during the day, and 10°C warmer at night. The team now uses current REMS data on atmosphere temperatures to help them predict rover temperatures (see section 8.4.3).

²¹Cucullu et al (2014)

The rover operated using the L_s 151 or spring-summer heater table until sol 434, when some of the wheel motors got cold enough that the thermal team switched to the L_s 90 (winter) heater table. The sudden switch to preheating for winter solstice temperatures dramatically reduced available power and drive time, and was, of course, overly conservative. It also added complexity, because sometimes heating had to happen in one sol's plan for the subsequent sol's activities. The worst impact was on drive time, because increased preheat time imposed a limitation on drive time at a point in the mission when they were attempting to extend drives to cover more distance.

The team briefly tried a hybrid approach (using the spring-summer heater table for some systems and winter table for others), but this was operationally complex, and couldn't last long in any case because of rapidly cooling temperatures. They switched all of the mobility system completely to the winter table on sol 456, and all remaining subsystems to the winter table on sol 463. Because the stepwise switch to winter heating requirements dramatically affected rover activities, the thermal team began the process of developing an intermediate set of tables, optimized for L_s 130, covering early spring and late fall seasons.

4.5 TELECOMMUNICATION

Curiosity receives commands directly from Earth, but returns more than 99% of its data through an orbital relay. Telecommunications bandwidth is one of the primary limitations on the science return from Curiosity (or any other deep-space mission). Curiosity typically returns about 500 megabits per sol. Actual volumes in any given transmission depend on many factors, especially the geometry of an orbiter's communications pass (range, elevation, and duration of the pass).

Curiosity's operational schedule is dictated by communication opportunities, scheduled months in advance. The sol begins at about 10:00 a.m. local time, when Curiosity usually receives the day's command sequence directly from Earth via an X-band transmission between a Deep Space Network dish and Curiosity's high-gain antenna. Curiosity warms up and performs the commands – driving, arm operations, and/or remote sensing – and typically wraps up work in time for the afternoon communications passes. Overnight, Curiosity usually rouses from sleep to return more data. Whichever communications pass is the last one before the next sol's tactical planning shift begins is called the “decisional” data pass (see section 3.4 for more about tactical planning).

4.5.1 The Deep Space Network

For more than 50 years, Earth has listened to faint signals from distant spacecraft with the giant radio antennas of NASA's Deep Space Network (DSN). The DSN consists of three ground stations positioned approximately 120° of longitude apart from each other, so that at least one station can “see” a spacecraft at all times. The three stations are Goldstone, located near Barstow, in California; Madrid, in Spain; and Canberra, Australia. Each station has multiple dishes, including one 70-meter dish and several 34-meter dishes (Figure 4.8). The 34-meter dishes can be arrayed to create a single aperture comparable to



Figure 4.8. Dishes of the Canberra Deep Space Network pointed at Mars. In this photo, taken on November 18, 2013, two 34-meter dishes (DSS-34 at center and DSS-45 at right) were listening to signals from the MAVEN orbiter as it arrived at Mars. At the same time, at left, the 70-meter DSS-43 simultaneously received data from Mars Odyssey and Mars Reconnaissance Orbiter. Photo courtesy Glen Nagle, Canberra Deep Space Communication Complex.

a single 70-meter dish. For Mars, which is nearby, this usually isn't necessary. In fact, a single antenna can receive signals from multiple Mars spacecraft simultaneously. The DSN provides support for European and Indian Mars missions as well as NASA ones.

4.5.2 Curiosity hardware

Figure 4.9 details external parts of Curiosity's telecommunications hardware; refer to Figure 4.3 for locations of internal parts.²² Curiosity has three antennas. Two X-band antennas can communicate directly with Earth. A UHF antenna links Curiosity with orbiters. There is one high-gain and one low-gain X-band antenna. X-band communications happen through one of two redundant Rover Small Deep Space Transponders (RSDST). The transponders are an improved version of the design used for the Mars Exploration Rovers.

4.5.2.1 High-gain antenna

The high-gain antenna is hexagon-shaped, 28 centimeters in diameter, and is steerable in both azimuth and elevation. It can both receive commands from and transmit telemetry to Earth, but it has to be aimed properly. It has a 5° pointing accuracy, limited in part by the accuracy of the rover's knowledge of its own orientation. It can provide a downlink of 160

²²Curiosity's telecommunications hardware is described in Makovsky et al (2009)

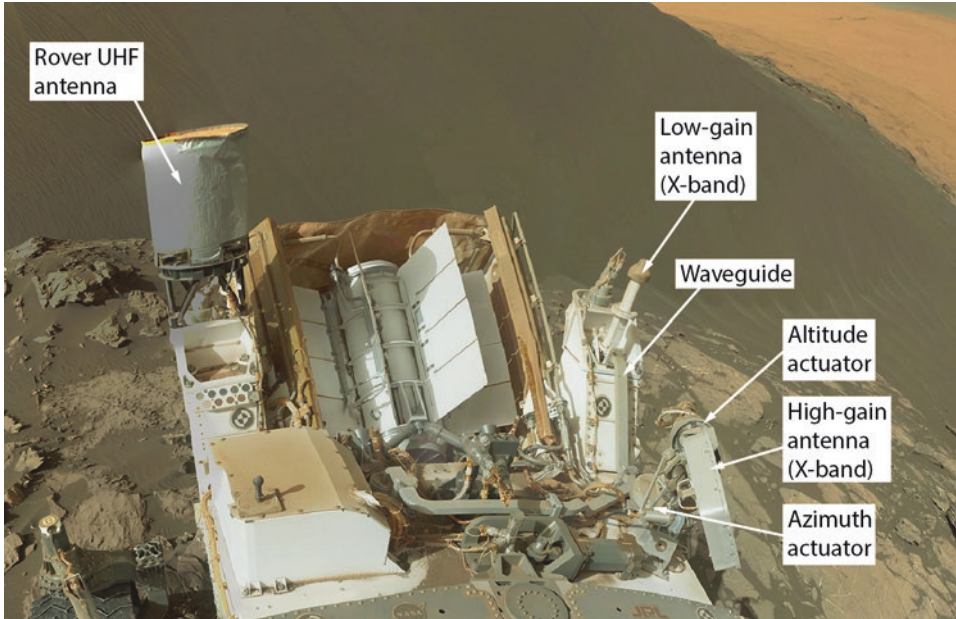


Figure 4.9. External parts of Curiosity's telecommunications hardware as seen in the sol 1197 Mastcam self-portrait. NASA/JPL-Caltech/MSSS/Emily Lakdawalla.

bits per second to a 34-meter Deep Space Network radio antenna, or 800 bits per second to a 70-meter antenna. Running in the other direction, the high-gain antenna can receive uplinked commands at a rate of 1 or 2 kilobits per second. A typical command load is about 225 kilobits. Planners schedule 15 minutes for communication sessions to allow sufficient margin.

Curiosity's daily commanding is scheduled for approximately 10:00 a.m. local time because Earth is always above the horizon at that time. The high-gain antenna sits above the rover's deck, but its view of Earth can be blocked by the rover mast or the hardware that sticks up from the back end of the rover (see Figure 4.7). To avoid this problem, rover drivers sometimes finish a drive with a turn designed to provide the high-gain antenna an unobstructed view of Earth for the next morning's uplink window.

At some times, Earth can be quite low on the eastern horizon during the usual communications window. This happens a few months before Earth-Mars opposition, when Earth is at its maximum elongation in Mars' sky and rises long after the Sun does in the morning (Figure 4.10). During these times, local topography and/or rover tilt can block the high-gain antenna's view of Earth. For instance, when the rover crossed Dingo Gap around sol 535 – a time when Earth was already rising late – the rover finished the drive tilted downhill to the west, causing the RTG to obscure the high-gain antenna's view of Earth. The mission rescheduled their morning command windows later in the day, when Earth was higher in the sky, compressing the time they had available for the day's activities.²³

²³ Ashwin Vasavada interview, February 6, 2014

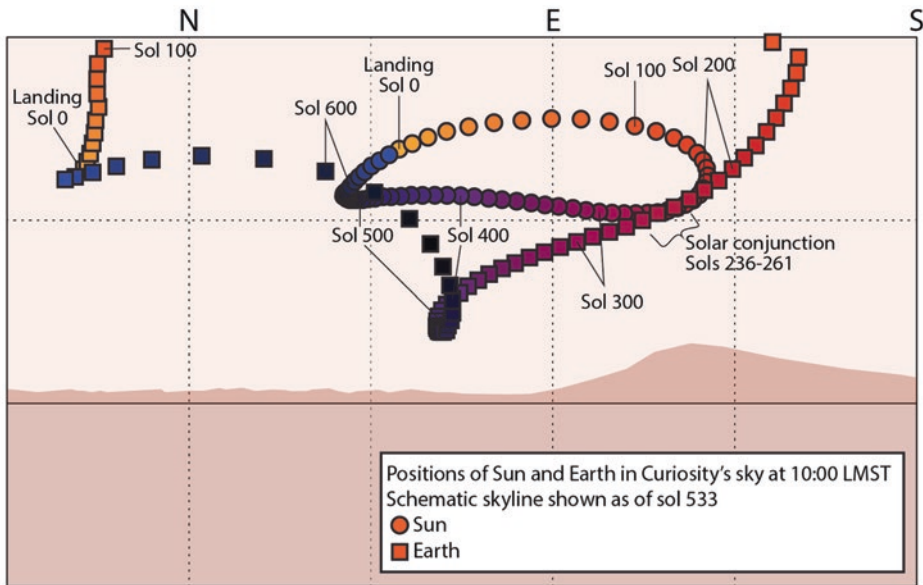


Figure 4.10. Positions of Sun (colored circles) and Earth (squares) in Curiosity's sky at 10 a.m. local time during the first Martian year of operations. Diagram by Emily Lakdawalla using Sun positions from the NASA GISS "Mars24" software.

4.5.2.2 Low-gain antenna

The low-gain antenna provided direct-to-Earth information on rover status throughout the landing. Since landing, it is used every rover morning when Curiosity finishes execution of its master sequence and starts execution of the next master sequence, an event called "hand-over." At the start of the new master sequence, the rover sends a "beep" from its low-gain antenna; receipt of that beep on Earth indicates that all's well with the new sequence. Other than that, Curiosity has only used its low-gain antenna when it is in safe mode. Because the rover may not know Earth's position well enough to point the high-gain antenna, it awaits instruction from Earth through the low-gain antenna at a rate of 15 bits per second. One of the first actions in a safe mode recovery is to tell the rover where to point the high-gain antenna in order to increase data transmission rates.

4.5.2.3 UHF antenna

The single UHF quad-helix antenna is connected to redundant Electra-Lite transceivers, whose design is based upon the Electra transceiver in Mars Reconnaissance Orbiter. There are also Electra transceivers on NASA's MAVEN and ESA's ExoMars Trace Gas Orbiter. The NASA Odyssey and ESA Mars Express orbiters use older types of transceivers. Compared to the orbiter Electras, Curiosity's Electra-lite is less capable, but it is also less

massive and consumes less power. When Earth visibility is limited, the UHF system can also be used to receive commands. The UHF link can operate on one of three frequencies, but in practice Curiosity almost exclusively uses 401.585625 megahertz, the same as the fixed frequency of the Mars Exploration Rover and Phoenix radios.

4.5.3 Orbiter relays

Characteristics of all the Mars orbiters capable of communicating with Curiosity are listed in Table 4.2.²⁴ Almost all of Curiosity's data has passed through two of them, Mars Odyssey and Mars Reconnaissance Orbiter. When Curiosity landed, both orbiters traveled in near-polar, sun-synchronous orbits, with local time on the ground beneath the orbiter being about 3:00 a.m. and p.m. for Mars Reconnaissance Orbiter, and 4:00 a.m. and p.m. for Odyssey. On February 11, 2014 (sol 540), Odyssey began an orbit adjustment that would shift its orbit to 6:00 a.m. and p.m. The orbit shift was complete on November 10, 2015 (sol 1160).²⁵

Curiosity's communications system was designed to a goal of an average 75 megabits of data per sol through Odyssey and 250 megabits per sol through Mars Reconnaissance Orbiter. Particularly favorable passes can achieve 150 megabits through Odyssey and more than 500 megabits through Mars Reconnaissance Orbiter. In its slower orbit, MAVEN can relay even more data in a single pass, though less frequently.

Electra is a software-defined radio, which means that modifications to its programming can introduce new capabilities. After Mars Reconnaissance Orbiter launched, software engineers upgraded its radio to support adaptive data rate capability, where the transceiver monitors the signal-to-noise ratio of Curiosity's transmission in real time, and commands the rover's radio to increase the data rate when possible, making the most of every contact.

Because Odyssey and Mars Reconnaissance Orbiter are in sun-synchronous orbits, Curiosity can rely upon the availability of communications sessions with both of them twice a day, once before sunrise and once in the afternoon. The actual time of a communications pass depends on how far to the east or west of the rover the ground track passes. Successive Odyssey ground tracks are separated by about 29.5°, while Mars Reconnaissance Orbiter ground tracks are separated by about 27°. So the best ground track on any given sol may be as much as about 14° east or west of the zenith, which pushes the center of the contact time earlier or later in the day by nearly an hour. Passes that are not overhead are also of lower quality because of the greater distance separating the rover and orbiter and because the orbiter is above the horizon for a shorter duration. Some days may have two useable passes, both with poor data rates. There is a roughly 5- to 6-day cycle for each orbiter, affecting the quantity of data that Curiosity can deliver and the time of day at which the rover must be prepared to deliver the data.

Odyssey is an old orbiter, and its communication rate with Curiosity is limited to 256 kilobits per second. Conservative use of Odyssey's remaining fuel should keep it going until around 2020. However, one of its four reaction wheels failed in 2012. If a second

²⁴ Edwards et al (2013a and 2013b) describe orbiter relay support for Curiosity

²⁵ Lakdawalla (2016)

Table 4.2. Telecommunication capabilities of Mars orbiters. After Edwards et al 2013a and 2013b.

	Mars Odyssey	Mars Express	Mars Reconnaissance Orbiter	MAVEN	ExoMars Trace Gas Orbiter
Agency	NASA	ESA	NASA	NASA	ESA
Launch/arrival dates	7 Apr 2001 24 Oct 2001	2 Jun 2003 25 Dec 2003	12 Aug 2005 10 Mar 2006	18 Nov 2013 22 Sep 2014	14 Mar 2016 19 Oct 2016
Orbit	400 km circular 93° inclination sun- synchronous 118 min period ~4:00 a.m. ascending node later moved to~6:00 a.m. ascending node	330 × 10,530 km 86.9° inclination non-sun- synchronous 7.5 hr period	225 × 320 km 93° inclination sun-synchronous 112 min period ~3:00 p.m. ascending node	150 × 6200 km 75° inclination non-sun- synchronous 4.5 hr period	400 km circular 74° inclination non-sun-synchronous 118 min period
HGA diameter	1.3m	1.65m	3m	2m	2.2m
UHF Transceiver	CE-505	Metacom	Electra	Electra	Electra (dual-string)
Forward link:	437.1 MHz	437.1 MHz	435–450 MHz	435–450 MHz	435–450 MHz
Frequency Data rate	8, 32 kbps	8 kbps	8, 32, 128 kbps	8, 32, 128 kbps	8, 32, 128 kbps
Return link:Frequency	401.585626 MHz	401.585626 MHz	390–405 MHz	390–405 MHz	390–405 MHz
Data rate	8, 32, 128, 256 kbps	2, 4, ..., 128 kbps	1, 2, 4, ..., 2048 kbps adaptive data rates	1, 2, 4, ..., 2048 kbps adaptive data rates	1, 2, 4, ..., 2048 kbps adaptive data rates

reaction wheel fails, it will have to transition to thruster-only attitude control, which will burn fuel at a much more rapid rate, ending the mission in 1 to 3 years. Its new, later orbit is less convenient for mission planning, because data relay comes much later in Curiosity's day, limiting the time available to prepare sequences before they need to be uplinked.

Mars Reconnaissance Orbiter's fuel could last until 2035 at current usage rates. But it has had important equipment failures. One of the two redundant traveling wave tube amplifiers for its radio system failed early in the mission, and it had to switch to its backup inertial measurement unit in 2013. The lifetime of Mars Reconnaissance Orbiter is likely to be limited to the lifetime of one or the other of these backups.

ESA's Mars Express demonstrated relay capability several times early in its mission, on sols 13, 24, 30, and 59. They now test relay capability four times per Earth year.²⁶ However, Mars Express is also aging. It has experienced some serious anomalies with its solid state memory and is running very low on maneuvering fuel. It could do emergency backup communication but is not likely to ever become a major participant in Curiosity data relay.

NASA's MAVEN demonstrated Curiosity relay using adaptive data rates on November 6, 2014 (sol 800). The two missions began formally testing regular communications on April 3, 2016 (sol 1301) with a 10-part plan testing both forward and return links between the two spacecraft.²⁷ As of 2017, MAVEN performs routine relay passes roughly once every other week. Exercising the relay communications between MAVEN and Curiosity is a high priority for JPL and NASA, because the future Mars 2020 rover has to plan to rely on MAVEN for telecommunications.

ESA's ExoMars Trace Gas Orbiter carries two NASA-provided Electra radios. It performed a data relay test at a fixed rate with Curiosity on 22 November 2016. The orbiter will begin testing adaptive data rates and forward linking in 2018.

NASA is in discussions with the Indian Space Research Organisation (ISRO) to include Electra hardware on India's second Mars orbiter, currently planned for launch in 2022.²⁸

4.5.4 Issues affecting communications

During solar conjunction, when the Sun lies directly between Earth and Mars, reliable uplink can't be counted on, so all Mars spacecraft are placed into a low-activity mode. Solar conjunction does not affect their ability to function, but if an activity placed a spacecraft in danger, Earth engineers couldn't reliably uplink commands to resolve the problem. Solar conjunctions happen once every 26 months (roughly 760 sols), and the period of uplink blackout lasts for 3 to 5 weeks. Table 4.3 lists conjunctions during the Curiosity mission so far. During the 2013 conjunction, orbiters did not relay data to Earth. However, in 2015 and 2017, Curiosity spent conjunction uplinking data to orbiters, and the orbiters successfully relayed much of it to Earth.²⁹

²⁶ Ashwin Vasavada, personal communication, email dated January 11, 2017

²⁷ Ashwin Vasavada, personal communication, email dated January 11, 2017

²⁸ Bagla (2017)

²⁹ Lakdawalla (2015)

Table 4.3. List of solar conjunctions during the Curiosity mission to date.

Sols	Date	Location
236–261	April 2013	Yellowknife Bay
1005–1026	June 2015	Marias Pass
1759–1779	July-August 2017	Base of Vera Rubin Ridge

Occasionally, an Earth weather-related issue affects uplink or downlink; these problems are infrequent, but expected. However, the DSN has been embattled during the rover’s time on the Martian surface, with budget cuts stressing maintenance and staffing.³⁰ The DSN has continued to meet its official targets of 95% uptime, but is suffering compared to historically overachieving performances of more than 99% uptime. For Curiosity, lost data is usually recoverable, but lost communications sessions can result in lost opportunities to acquire new data. If an uplink session is lost, Curiosity sits idle for at least a day, and the team has to choose whether to retry the same plan the next day. The loss of Friday uplinks results in the loss of two or three sols of activity. If there is a problem with the downlink of images after a drive, Curiosity can’t point at specific targets, drive, or use its arm in the next sol’s plan because the engineers don’t know the rover’s position. (Effectively, an unrestricted sol is turned into a restricted sol when a downlink session is lost.)

4.5.5 Performance on Mars

Mars Reconnaissance Orbiter returns the lion’s share of Curiosity’s data, though not as much as it might, because of interference from a spurious 400 megahertz tone generated by the orbiter’s CRISM instrument. When the rover landed, the orbiter shut off its science instruments temporarily in order to test the communications link.³¹ For the first two weeks, they tested varying frequencies and fixed data rates. Curiosity achieved a transmission rate of 2048 kilobits per second overnight on sol 17.

In the early morning of sol 18, they tested a new capability of adaptive data rate transmissions, in which Mars Reconnaissance Orbiter diagnosed the strength of the signal it detected from the Curiosity radio link, and commanded the rover to the optimal data rate as the signal strength changed. The pass had a maximum elevation angle of only 36° – not the best geometry – but the orbiter was able to command Curiosity to return data at high enough rates to receive 479 megabits of data, the largest-ever amount of data returned in a single communications pass from the surface of Mars by a wide margin.³² They began using adaptive-data-rate transmissions for all Mars Reconnaissance Orbiter passes on sol 22. With the new transmission protocol, Curiosity routinely exceeded predicted downlink volumes by factors of 2.³³

³⁰Voosen (2016)

³¹Edwards et al (2013a)

³²Sol 18 Mission Manager’s report, MSL Curiosity Analyst’s Notebook

³³Sol 17 Mission Manager’s report, MSL Curiosity Analyst’s Notebook

From sol 27 through 62, they powered on the orbiter's science instruments one at a time to assess the impact of interference on the quality of the signal. Operating CRISM introduces interference that mostly prevents Curiosity from achieving 500-megabit relay sessions, reducing the maximum nearer to 400 megabits. The effect is most pronounced at higher elevation angles. Nevertheless, the link still averages 225 megabits per downlink.³⁴

Periodically, one or the other orbiter experiences an anomaly that sends it into safe mode, interrupting relay communications. As of this writing, there has never been a sol when both Odyssey and Mars Reconnaissance Orbiter were in safe mode. Should one of these two orbiters fail, MAVEN will be called upon to do more frequent communications sessions in order to ensure the Curiosity mission continues with as little interruption as possible.

4.6 MOBILITY SYSTEM

Curiosity's mobility system comprises the wheels, their motors, and a system of linkages called a rocker-bogie suspension (Figure 4.11).³⁵ The rocker-bogie suspension system permits the rover to traverse obstacles more than one and a half times the height of one wheel, while keeping all six wheels firmly in contact with the ground, distributing the weight of the rover evenly among the wheels, and limiting the tilt of the rover body.

The suspension system is connected to ten motors, which drive and steer six wheels. (The middle wheels do not steer.) Ongoing damage to the wheels has been a source of trouble for the mission, but careful driving has reduced the rate of damage, and Earth testing has verified that the rover will be able to complete planned mission extensions – all the way onto the highest unit that Curiosity can reasonably be expected to reach on Mount Sharp – even with the ongoing rate of damage.

4.6.1 Rocker-bogie suspension system

The front wheels attach to a long rocker arm. The middle and rear wheels are linked together to form a bogie, which connects to the back end of the rocker arm through a passively rotating pivot that can tilt forward and back by as much as 45°. The rocker arm is connected to the rover body at another passive pivot, which can tilt forward and back by about 20°. (In practice, much tighter limits are usually set on these pivots such that the rover will autonomously stop driving if unexpectedly higher angles are reached.) If that were the end of it, the rover body would flop forward or backward on the two rocker pivots, but a differential mechanism connects the left and right sides of the rocker-bogie suspension system to keep the rover body nearly level. A vertical swingarm connected to the rocker rises above the rocker pivot and connects through a link assembly to a

³⁴Edwards et al (2013a)

³⁵There is no publication by an engineer that describes the rocker-bogie suspension system in detail. Sources for description of the mobility system include Heverly (2012) and Arvidson et al (2017)

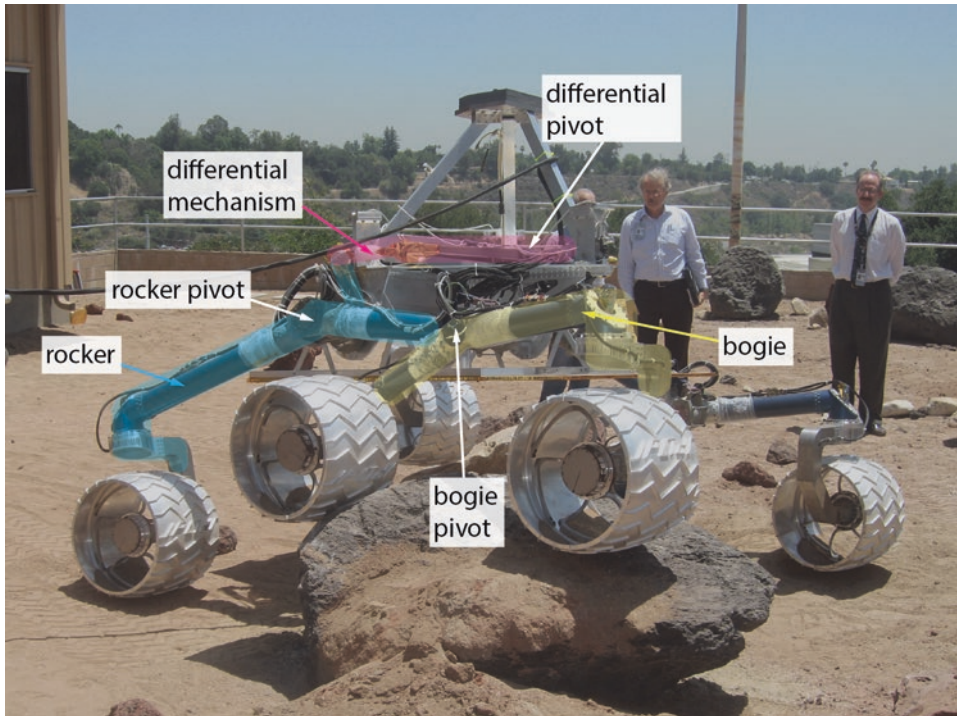


Figure 4.11. Engineers demonstrate the obstacle-climbing capability of the rocker-bogie suspension system on the “Scarecrow” test bed rover, June 19, 2007. Scarecrow is a stripped-down model designed to exert the same force on Earth’s surface that the actual rover does on Mars under lower Martian gravity. Note that Scarecrow’s body is nearly level and all wheels are in contact with the ground despite the fact that three of the wheels are scaling obstacles similar in height to a wheel. Photo by Emily Lakdawalla.

horizontal swingarm that crosses the back of the rover. The horizontal swingarm is attached to the rover body at the center differential pivot, another passive pivot.

If one front wheel climbs an obstacle, it pushes the horizontal swingarm backward on that side, resulting in an equal and opposite downward motion of the front wheel on the other side. The opposing vertical motions of the front wheels ensure that they maintain contact with the ground, and the rover body stays level. Meanwhile, the passive bogie pivot allows the middle wheel on the same side as the obstacle to drop, staying on the ground, as the front wheel climbs.

The rover is robust to local tilt, designed to be stable on a slope of up to 45° . For safety, rover drivers set tight limits on rover tilt based upon their expectations for the terrain. They rarely set limits above 7° of tilt for the rockers and 17° for the bogies, which are the angles they expect when traversing a 40-centimeter-tall obstacle sitting on flat terrain.³⁶

³⁶Matt Heverly, personal communication, email dated March 11, 2017

The rocker-bogie suspension system actually performs better rolling bogie-first than rocker-first. Curiosity, the Mars Exploration Rovers, and Sojourner have all been designed to drive rocker-first so that if a forward drive gets the rover into a hazardous situation, it is more likely to be able to back straight out of the problem terrain. Curiosity sometimes drives backwards, but when facing backward the MMRTG obstructs the Navcams' view of the nearby terrain, preventing the rover drivers from obtaining the images they need to plan future drives. So backwards drives have to finish with a turn or at least a wiggle to one side or the other to allow the Navcams to see the terrain ahead.

4.6.2 Motors

Curiosity's actuators consist of a motor, a gearbox, a brake, and an encoder; in this book, "motor" typically applies to a whole actuator assembly (Figure 4.12). The motors are very powerful. A single drive motor has enough torque to drive the rover up a vertical wall. The rover's top speed, 4.2 centimeters per second (151 meters per hour), is so slow that the motion is quasi-static. There is no freewheeling, and all wheel rotation is commanded wheel rotation. When the wheels aren't rolling, they are braked.

Because only the four corner wheels are steerable, the rover can't "crab" (drive sideways), but it can turn in place, allowing it to pick its way safely among a field full of obstacles provided that the obstacles are separated by more than the width of the rover. The

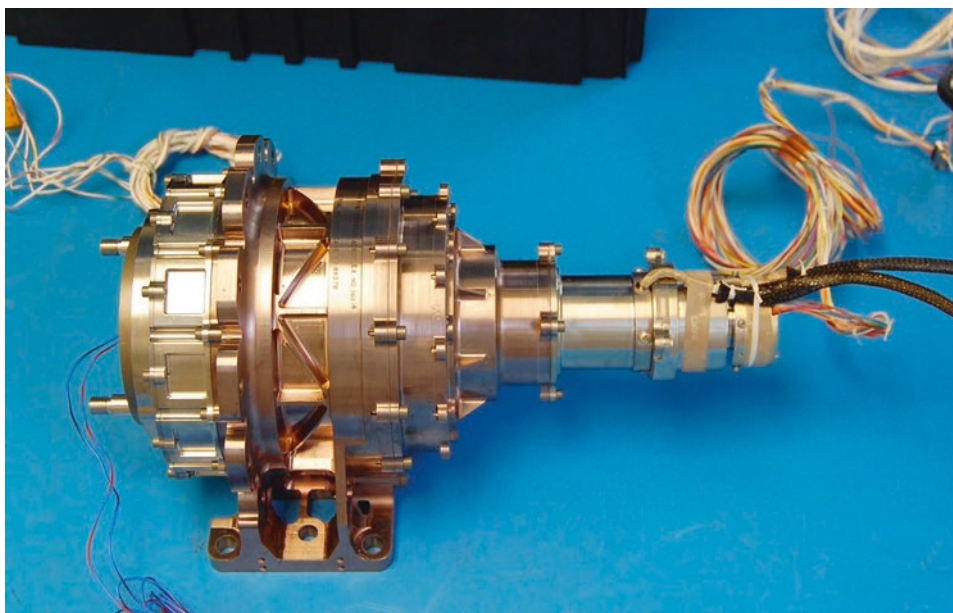


Figure 4.12. One of the high-torque drive motors for Curiosity's mobility system. The motor end is at the right side; its output passes into a four-stage gearbox that rotates the plate at left. From Cook (2009).

steering motors are positioned above the wheel's centers, connected by U-shaped brackets to the motorized wheel hubs, so that the wheels steer in place about a vertical axis. A turn in place of 60° or more draws a complete circle of wheel tracks on the ground, leaving telltale “donuts” about 2.75 meters in diameter along the rover's tracks (Figure 4.13).

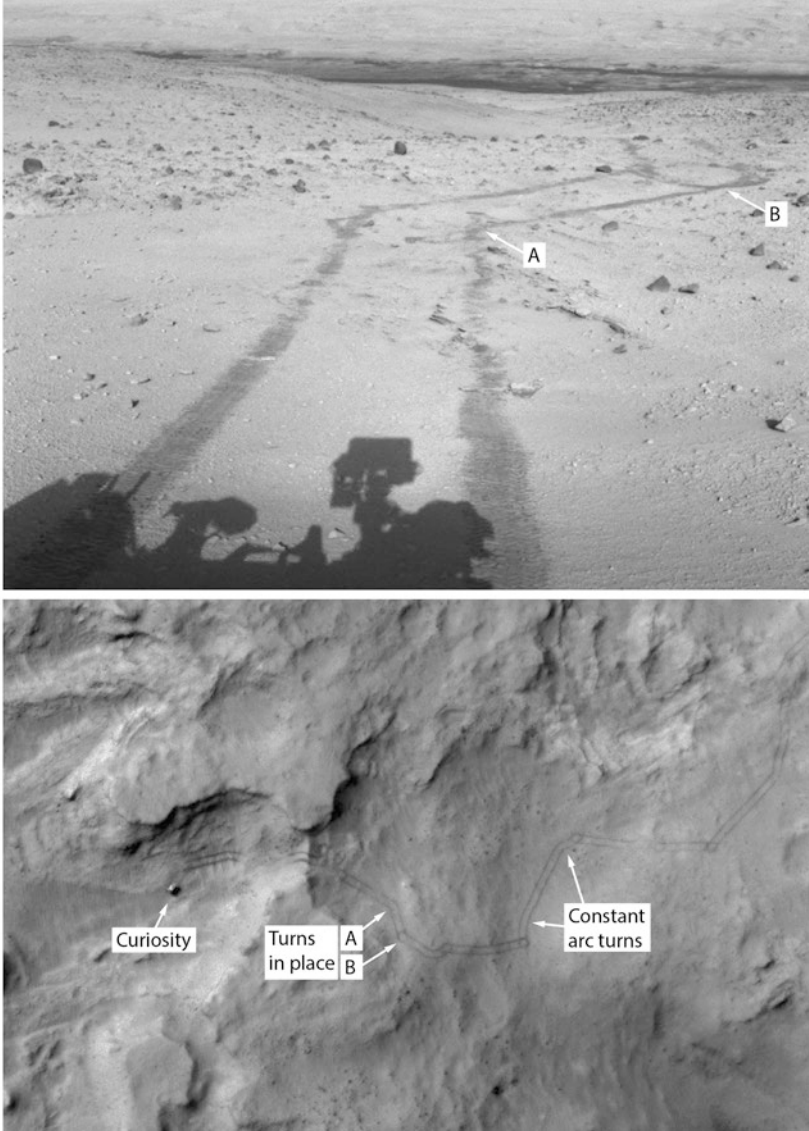


Figure 4.13. Donuts along tracks document rover turns. Top: Right Navcam photo taken after a drive on sol 527 (NRB_444289916RADLF0260000NCAM00252M1) showing marks of two turns in place: “B” is a complete donut, and “A” is not. Credit: NASA/JPL-Caltech. Bottom: Mars Reconnaissance Orbiter HiRISE image ESP_035350_1755 taken sol 538, including donuts A and B as well as tracks of several arcing turns. NASA/JPL-Caltech/UA/Emily Lakdawalla.

The rover's motor controller can only run eight motors at a time, so the rover cannot steer and drive simultaneously. Thus drives alternate between straight drive segments and arcing turn segments. Wheel rotation rates are adjusted for arcing turns so that the wheels on outer edges of turns rotate faster than inner wheels.

4.6.3 Wheels

Curiosity's wheels presented a design challenge because they had to serve as both landing gear and running gear.³⁷ As landing gear, they had to absorb the mechanical shock of touchdown, protecting the wheel motors from harm. After landing, the wheels needed to provide good traction over Martian terrain, including floating the heavy rover over sand. They needed to be as lightweight as possible, and to fit within the narrow confines of the aeroshell. The final design represents a compromise among all these competing requirements. Surviving the landing trumped all other requirements, and most of the design effort focused on ensuring Curiosity could drive away from any imaginable landing scenario. Unfortunately, that proved shortsighted.

The wheels are 50 centimeters in diameter at their centers (including the height of the treads), with a crowned profile such that they are 46.5 centimeters in diameter at their outer edges (Figure 4.14). They are 40 centimeters wide. They consist of an aluminum tire and a titanium hub-and-spoke assembly. The spokes have a complex shape that makes them springy in all directions, allowing them to do their job of absorbing a landing jolt even if they landed on slopes or rocks.

Each wheel was machined from a single block of aluminum. The wheel skin is incredibly thin – at just 0.75 millimeters, as thin as it was possible to machine – in order to limit the wheels' total mass. The wheels are stiffened by three circumferential rings: two at the inner and outer edges, and a third ring located about a third of the way inside the outer ring to provide a place for the spokes to attach. Together, all these design elements enabled the wheels to deform dramatically under the force of a landing and return to their original shape (Figure 4.15).

Other design elements had to do with surface operations. A black anodized coating prevents the wheels from throwing glints into camera images. For traction, the wheels have treads or "grousers". The height and spacing of the grousers represent a compromise among several factors. The grousers had to be spaced close enough that they would cog with features on rock faces, about 65 millimeters apart. Their height is relatively short. Through laboratory tests of different tread designs, the mobility team found that most of the improvement in wheel traction came with treads whose height was comparable to the particle size of the material the wheel drove on. They settled upon a tread height of about 3% the wheel radius, or about 7 millimeters. After the challenging Opportunity experience of driving a rover across sloping crater walls, in which the rover tended to skid downslope, they added a chevron pattern to the wheel treads in order to prevent the same from happening to Curiosity.

³⁷Haggart and Waydo (2008)

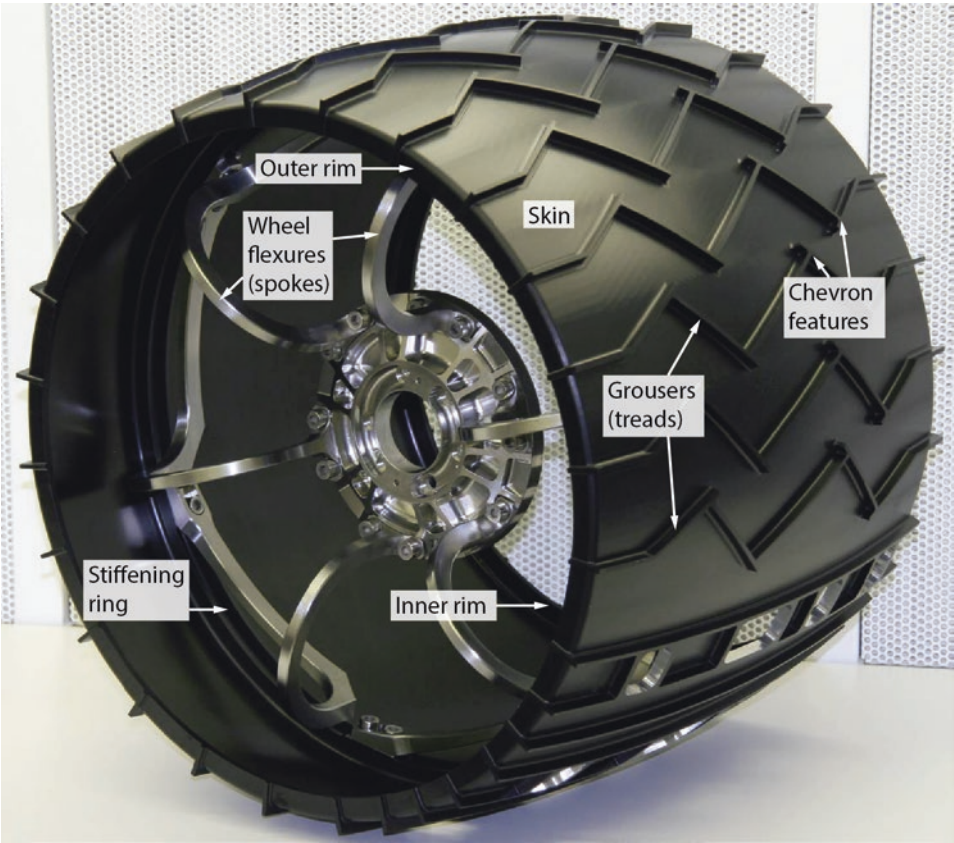


Figure 4.14. Parts of Curiosity's wheel. Curiosity wheels are crowned, 50 centimeters tall at center, 46.5 centimeters diameter at sides, and 40 centimeters wide. NASA/JPL-Caltech/Emily Lakdawalla.



Figure 4.15. Spring-like deformation of a rover wheel during testing. In this test, two of the spokes have “bottomed out” on the inside surface of the wheel. After this test, the wheels sprang back to their original shape. From Lee (2012).

If the ground were perfectly flat and rigid, the crowned shape of the rover wheels would touch it only at one point. In reality the weight of the rover drives it in to the ground, so to approximate the ground pressure of rover wheels on the surface, engineers defined the contact area as being the wheel width times the wheel radius. (This effectively assumes that 57° of the wheel's full circumference is in contact with the surface.) In operation, the wheels do not generally touch the ground over so much of their radius (Figure 4.16).

The wheels have twelve holes cut into them, part of an asymmetric tread feature that interrupts the otherwise regular pattern of the wheel treads (Figure 4.17). This feature makes marks at regular intervals (about 1.5 meters apart) in rover wheel tracks. The track markings can be directly compared to the expected distance traveled in order to measure

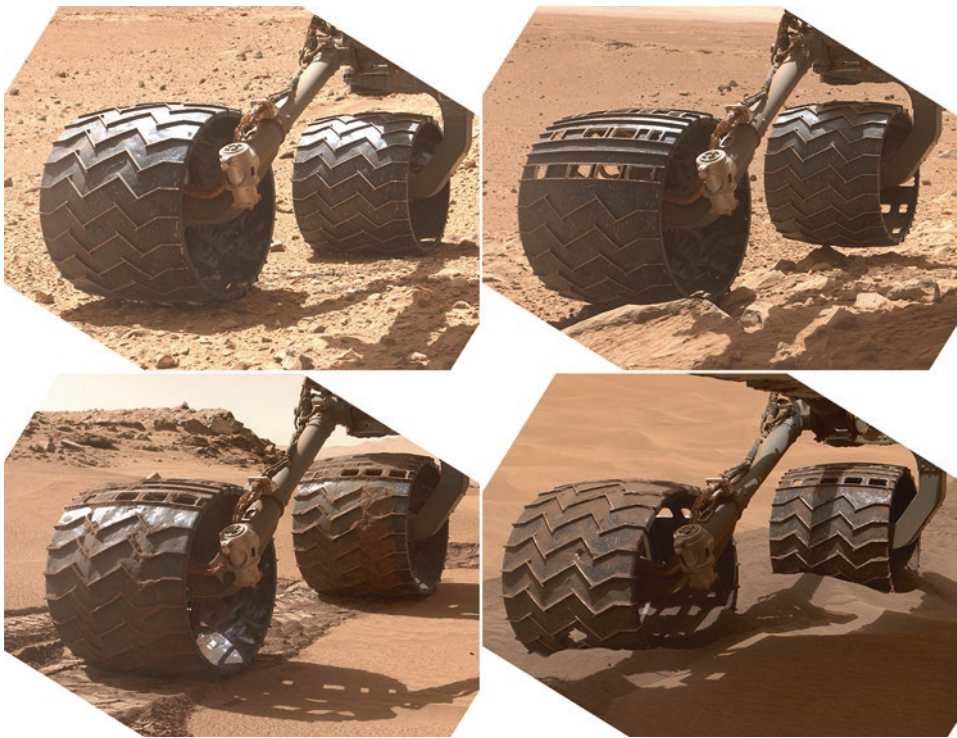


Figure 4.16. Wheel performance on different substrates. Upper left: small rocks over regolith, the substrate encountered by most previous missions. The wheels dig slightly into the surface, but only a small area of the wheel is in contact. Upper right: a jagged, rocky surface. At times, the rocks contact the surface at only one point, as the right rear wheel does here. The wheel skin is thick enough that the rover's weight merely resting on a pointy rock does not puncture a wheel. Lower left: a well-packed sand ripple on which the wheels are getting good traction, similar to that in the upper left image. Lower right: a ripple made of fluffier sand into which the wheels are embedding as they slip. MAHLI images 0504MH0002610000200627E01, 0506MH0002610000200672E01, 0529MH0002610000201142E01, and 0711MH0002610010204346E01, NASA/JPL-Caltech/MSSS.

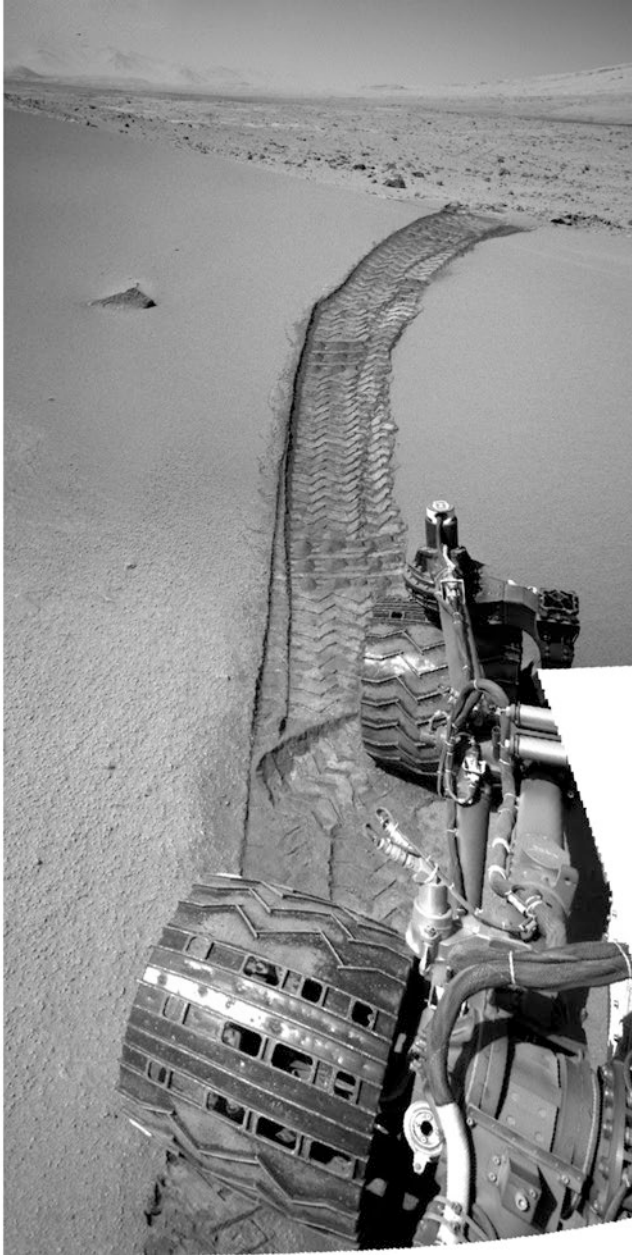


Figure 4.17. Asymmetric tread features in the rover wheels mark the rover's tracks every time the wheel has rotated once, about once every 1.5 meters. They also spell out "J P L" in Morse code. J is · - - - ; P is - · - - ; L is · - · · . Mosaic of two left Navcam images taken on sol 535. NASA/JPL-Caltech.

how much the rover wheels have slipped during a traverse. In initial wheel designs, these features were the letters “J P L” machined into the pattern of the treads (see Figure 4.11), but NASA objected to JPL labeling the wheels in this way. So the design was changed to one that incorporated bland rectangular holes. Mischievously, the wheels’ designers made those holes spell out “J P L” in Morse code in the tracks.

4.6.4 Wheel degradation

The wheels performed perfectly upon landing; the only visible damage from the landing event was a tiny crack in the left middle wheel. During the first 500 meters of the rover traverse from Bradbury Landing to Yellowknife Bay, the wheels suffered little additional damage. The team surveyed the wheels with MAHLI on sol 411, noticing a puncture in the left front wheel. Re-imaging the wheels on sol 463, they observed that the tear had grown dramatically worse. From that sol forward, the team commanded numerous wheel-imaging sequences, shooting photos of all wheels with the MAHLI camera and the right-side wheels with Mastcam in between every drive. Periodically, they would devote an entire drive to full surveys of the wheels by driving the rover short distances between four or five wheel surveys in order to image the entire wheel surface. Wheel imaging is summarized in Box 4.1.

Box 4.1. Sols with MAHLI and ChemCam RMI wheel imaging to sol 1800.

Sols in bold indicate full wheel imaging. Sols in italic indicate ChemCam RMI imaging. Sometimes the full wheel imaging included images taken on multiple consecutive drive sols.

34	527	589	744	1260
60	528	591	803	1269
177	529, 532	595	834	1287
275	537	597	840	1313, 1315
411	540	601	842	1355
463	542	605	939, 940	1380
469	546, 547	631	955	1386
472	548	633	958	1403
476	549	635	962, 963	1407
488, 490	552	636	971	1416
493	553	637	989	1434, 1435
502	554, 555	640, 641	1046	1444
504	559	646	1057	1459
506	560	653	1065	1471
508	561	660	1076	1482
510	562, 563	667	1087	1512
512, 513, 515	564	679	1102	1591
518	566, 568	695	1127	1681, 1682
519	569	706	1157	1729, 1730
520	571	708	1178, 1179	1798
521	574	711	1182	
524	587	713	1214	
526	588	729	1245	

Over time, more punctures and tears appeared in the middle and front wheels, while the rear wheels remained relatively unscathed. Figure 4.18 through Figure 4.22 document the condition of all six wheels at three points in the mission. As of sol 513, the rover had driven 4.7 kilometers; as of sol 708, 8.7 kilometers; and as of sol 1513, 15.1 kilometers. Improved understanding of how to save the rovers’ wheels slowed the progression of



Figure 4.18. MAHLI survey of right front wheel on sol 513 (left column), 708 (middle), and 1313–1315 (right). See text for discussion. NASA/JPL-Caltech/MSSS.

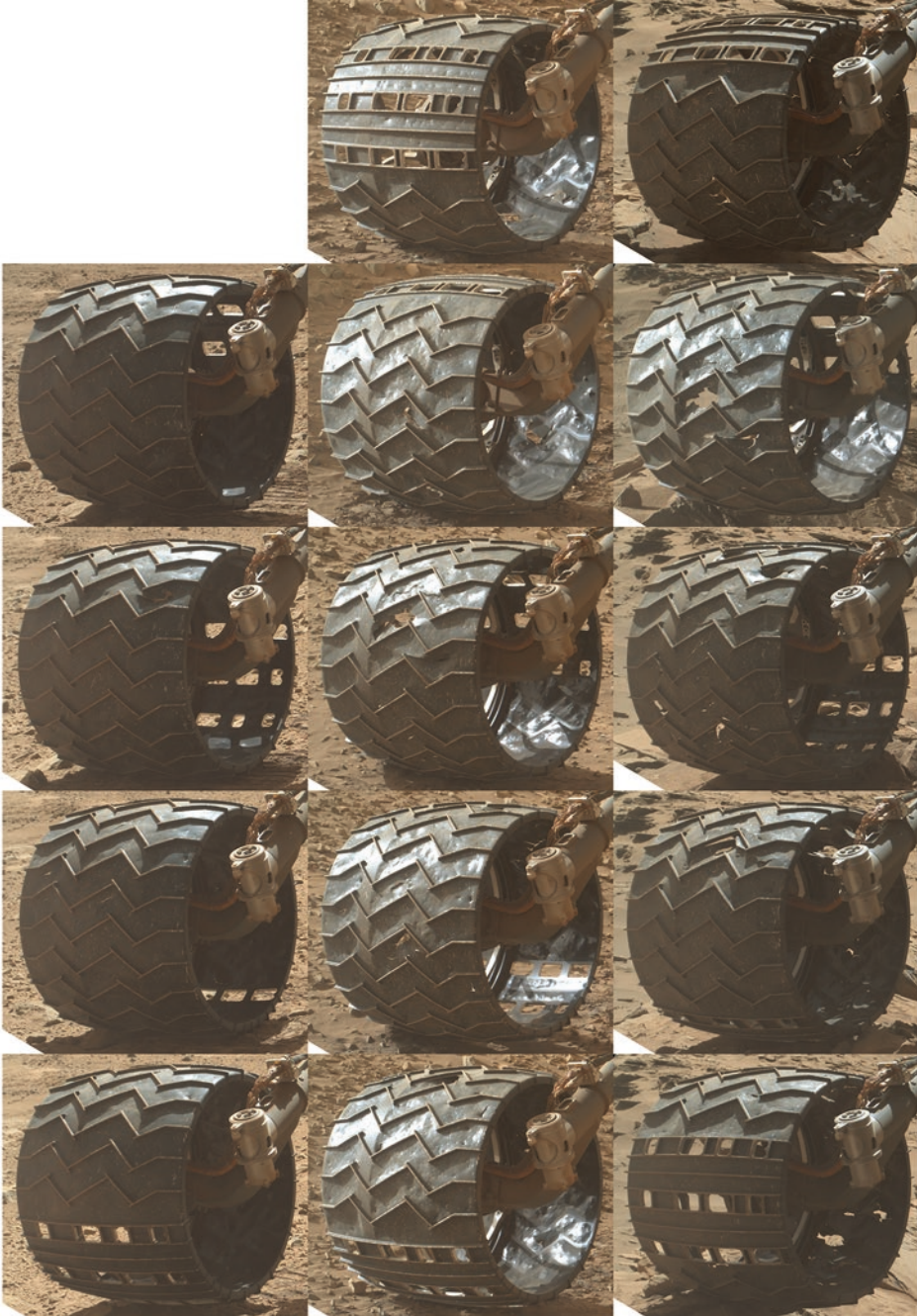


Figure 4.19. MAHLI survey of right middle wheel on sol 513 (left column), 708 (middle), and 1313–1315 (right). See text for discussion. NASA/JPL-Caltech/MSSS.



Figure 4.20. MAHLI survey of rear wheels on sols 513 and 1313–1315. See text for discussion. NASA/JPL-Caltech/MSSS.

damage after sol 708. Fewer new punctures formed, but dents and cracks progressed. The first wheel images to reveal broken grousers, on the left-middle wheel, were taken on sol 1641, after about 16 kilometers of driving. As of sol 1800 the rover has driven 17.5 kilometers, with no further broken grousers.

The punctures were caused by two factors: metal fatigue and forces intrinsic to the rocker-bogie suspension system.³⁸ Fatigue is a consequence of the flexibility of the wheels.

³⁸The investigation of causes of wheel damage is described in Arvidson et al (2017)



Figure 4.21. MAHLI survey of left middle wheel on sol 513 (left column), 708 (middle), and 1313–1315 (right). See text for discussion. NASA/JPL-Caltech/MSSS.



Figure 4.22. MAHLI survey of left front wheel on sol 513 (left column), 708 (middle), and 1313–1315 (right). See text for discussion. NASA/JPL-Caltech/MSSS.

They flex back and forth with each wheel rotation. Stress concentrates at the tips of the chevron shapes in the grousers. Eventually the skin cracks near chevron points, and over time the cracks grow and merge. Once the cracks propagate entirely across the width of the wheel, the grousers are unsupported by skin stretching between them, so they flex even more with each wheel rotation. Eventually, repeated flexing fatigues the grousers and they also begin to snap.

At first, it was difficult to understand why only the left and middle wheels seemed to be getting damaged. When at rest on level ground, the front, middle, and rear wheels on each side bear weights of 564, 636, and 458 newtons, respectively. Experiments in the Mars Yard showed that wheels were robust to punctures at these forces. It takes 800 newtons for a sharp metal cone to puncture wheel skin, and 1500 newtons for sharp rocks collected from the Mojave Desert to do so.

How could such high forces on wheel surfaces be generated? Earth tests revealed that the answer lay in kinematics of the full rocker-bogie suspension system. The motors drive all six wheels at fixed rotation rates. When one wheel encounters an obstacle that does not move aside or press into the ground under the weight of the rover, that wheel must travel a longer distance than the other wheels as it rolls over the obstacle. But its motor drives it at the same fixed rate as the other wheels. So the wheel encountering the obstacle is dragged as it travels.

Additionally, when the rover drives forward, four of its six wheels are on forward-projecting legs. If one of these wheels climbs an obstacle, some of its rotation rate goes toward vertical motion, and its horizontal motion is slowed. The remaining wheels continue moving horizontally at full speed, shoving the blocked wheel on its forward-projecting leg toward the obstacle with considerable force. If the obstacle is strongly cemented into the ground and pointy, it can open a hole. Consider a rolling suitcase: when you drag it behind you, you exert an upward force as you pull on the wheels, helping it to climb an obstacle. When you push it in front of you, you exert a downward force as you push, and the suitcase's motion is easily and often stopped by small obstacles, jarring your arm. In tests in the Mars Yard of driving forward over sharp cones, the front and middle wheels punctured easily, while the rear wheels remained whole.

The mission dramatically reduced the rate of damage by:

- Picking local drive paths carefully among potentially damaging rock, consequently ending the use of autonav (which would blithely drive the rover over pointy rock patches).
- Mapping the terrain ahead using orbital data (including HiRISE images and Odyssey THEMIS thermal inertia maps) and seeking out less “pointy” terrain during long-term traverse planning.
- Avoiding turns on sharp terrain.
- Sometimes driving backwards.

After sol 660, the engineers decided that the turns-in-place required at the ends of backwards drives in order to do drive-direction imaging held more potential for wheel damage than was saved through backwards driving.

As of the mission's second landing anniversary, when the rover had driven about 8 kilometers, the engineers estimated the following remaining lifetime for the wheels:³⁹

- Bedrock with lots of rocks: 8 kilometers.
- Lots of rocks, not on bedrock: 13–14 kilometers.
- Bedrock with few rocks (like flagstones): 30–40 kilometers or more.
- Smooth or sandy, with few or no rocks: indeterminate (causes no damage).

Furthermore, Mars Yard testing suggests that, on average, once three grousers have broken on a wheel, about 60% of its life has been consumed.⁴⁰ The rover's wheels are now expected to survive as long as the mission does, although they may look much the worse for wear by the time the mission ends. Curiosity should be able to achieve at least 28 kilometers total mission odometry unless there is a dramatic change in the terrain.

On sol 1646, in response to the observation of broken grousers on sol 1641, the mission tested new traction control ability for the first time.⁴¹ Traction control was turned on by default on sol 1678. The rover senses when a wheel is climbing an obstacle by monitoring tilts of rockers and bogies. The rover responds by slowing the turn rate of the wheels that are not climbing obstacles, allowing the climbing wheel to rotate faster, thereby reducing the likelihood of punctures and widening cracks.

Even with “failed” wheels the rover may continue to be able to drive. The wheels fail when all the grousers have snapped, leaving the inner two-thirds of the wheel diameter flapping, connected to the rest of the wheel only at the locations of the asymmetric tread features (Figure 4.23). This is hazardous to the rover, because sharp edges on the broken wheels can scrape against the cable that runs to the wheel motors. Slicing into a cable could not only jeopardize the functioning of that wheel's motors, it could also potentially cause a short circuit that would risk the motor controller – which also controls the motion of all other moving parts on the rover. Driving the rover with a wheel in this condition on Mars could be hazardous, but it would still be better than not driving at all. In the Mars Yard, driving on such wheels has been tested; eventually the inner two-thirds of the wheel snaps off completely, and the rover is able to drive quite effectively on the remaining third of the wheel surface that is still attached to the inner stiffening ring.⁴²

³⁹Lakdawalla (2014)

⁴⁰Steve Lee, personal communication, review dated August 13, 2017

⁴¹Herkenhoff (2017)

⁴²James Erickson, personal communication, interview dated September 18, 2014



Figure 4.23. Wheel tested to failure. The rover can still drive effectively on this wheel, but the sharp edges of the broken grousers and webbing present a hazard. Photo taken in the JPL Mars Yard on October 13, 2014 by Emily Lakdawalla.

4.7 TESTBEDS

4.7.1 The Mars Yard

A rover as large as Curiosity requires a large area for testing purposes. The JPL Mars Yard is 66-by-36 meters in size, located at the top of the steep Pasadena campus (Figure 4.24).⁴³ Most of it is flat and level, with the surface material made of beach sand, decomposed granite, brick dust, and volcanic cinders. There are also lots of basalt rocks of different sizes that engineers can move around to simulate different driving conditions. One side of

⁴³ JPL (2008)



Figure 4.24. Panoramic view of the Mars Yard at JPL. NASA/JPL-Caltech.

the Mars Yard is sloped at a range of angles for testing driving and arm operations on sloping surfaces. At one end is a small building that garages test rovers, associated equipment, and engineers (Figure 4.25).

4.7.2 The Vehicle System Testbed

The Vehicle System Testbed (VSTB), also known as “Maggie,” is the highest-fidelity copy of the rover and is housed in the shed at JPL’s Mars Yard.⁴⁴ It is used for testing driving, arm movements, and drilling using the same software and electronics that are on Mars, on a suspension system that will put the rover in similar positions as experienced on Mars.⁴⁵ It has the same body, suspension system, arm, sample handling system, mast, and other motorized elements as the flight rover. Initially, it had the same wheels as the flight rover, but after degradation they were eventually replaced with wheels twice as thick as those on Mars. (Their rapid degradation resulted in part from bearing nearly the full Earth weight of the full-scale rover.)

The Vehicle System Testbed’s avionics are similar to those of the flight rover, but are housed on a rack outside the rover’s body and connected to the rover’s body with an umbilical to facilitate testing. There is no RTG, so the same umbilical carries power. The umbilical is long enough to stretch the entire length of the Mars Yard. Like the flight rover, there are two complete main computer systems. While there is a cooling system, it is different from the one used on Mars. Because it’s on Earth, there is flexibility to reconfigure the VSTB as needed to accommodate tests. For example, prior to landing, the arm was removed and operated separately on a tiltable stand to allow engineers to do driving and arm testing simultaneously.

⁴⁴A sign in the Mars Yard shed states that MAGGIE stands for “Mars Automated Giant Gizmo for Integrated Engineering,” but that is likely a backronym for the name, the original source of which is lost to history

⁴⁵Vandi Verma, personal communication, email dated February 9, 2017

The VSTB has a full complement of engineering cameras, but does not have many flight-like science instruments. There is a flight-like MAHLI, which took the self-portrait in Figure 4.25. The APXS instrument is similar to the flight one but does not usually have its radioactive source (though the APXS team did once install a source for testing).

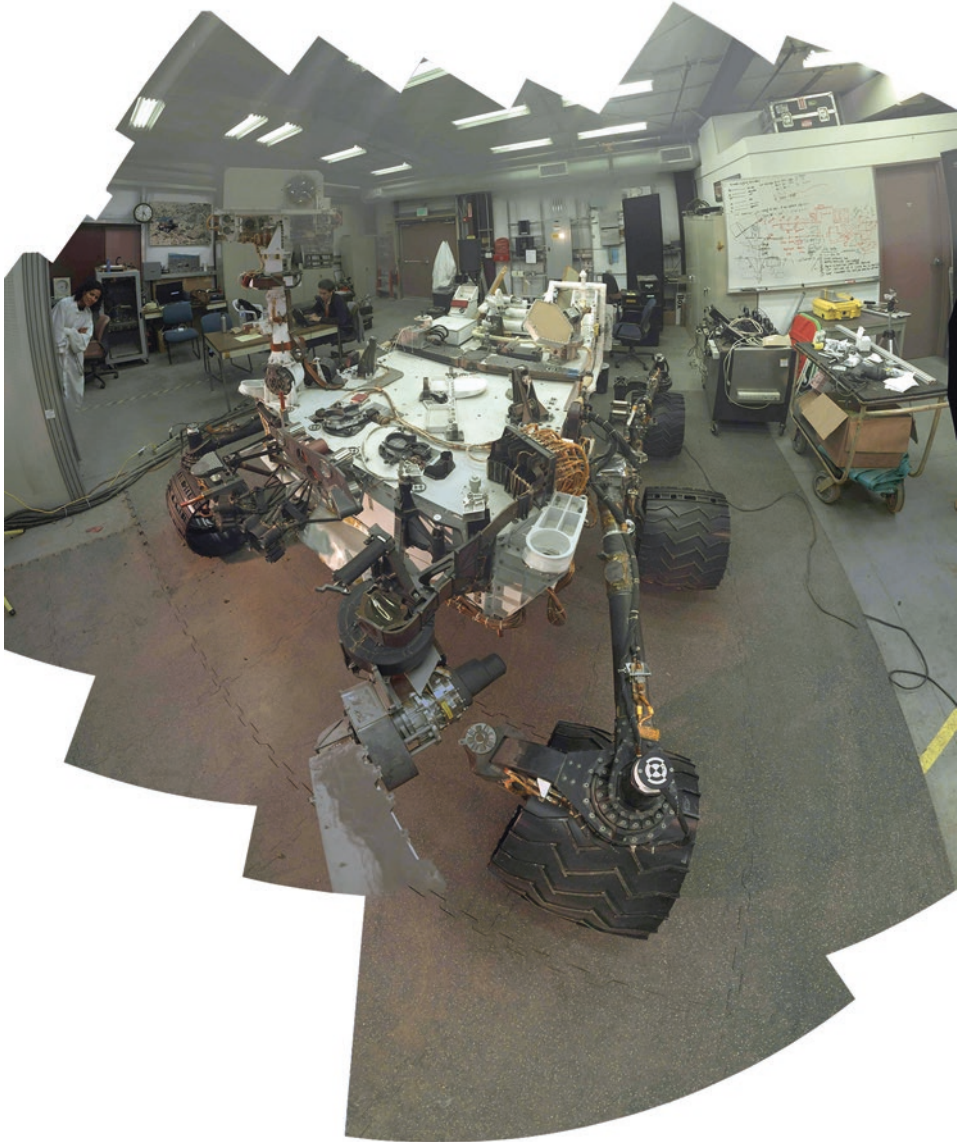


Figure 4.25. MAHLI self-portrait of the vehicle system testbed taken inside the Mars Yard shed, August 1, 2012. NASA/JPL-Caltech/MSSS.

Substitutes take the place of the ChemCam imager and Mastcams. There is no MARDI or CheMin. SAM electronics are present, but not the rest of the instrument. However, there are functioning SAM and CheMin inlet covers, and the engineers can collect sample material dropped through them in order to measure volume.

4.7.3 Scarecrow

Scarecrow is a second engineering model of the rover. It consists of a full-scale mobility system connected to a small body containing batteries and electronics. The whole model has a mass of 340 kilograms, or 3/8th of the mass of the flight rover, so that it exerts the same ground pressure on Earth that Curiosity does on Mars. Its name derives from the character in *The Wizard of Oz*: Scarecrow doesn't have a brain. It does have force and torque sensors in its axles to measure wheel loading under Mars gravity. It can report motor current as well as roll, pitch, and yaw using onboard inertial measurement unit, much as the actual rover can. It has ultrasonic range finders on each wheel to measure sinkage.⁴⁶ It is used primarily to test how well the rover traverses different types of terrain (Figure 4.26).



Figure 4.26. Scarecrow descending a slope in the Mars Yard, October 2007. NASA/JPL-Caltech image release PIA10014.

⁴⁶Heverly et al (2013)

4.7.4 The Qualification Model Dirty Testbed

Before and shortly after landing, the tricky operations of drilling and sample preparation were worked out in the Qualification Model Dirty Testbed (QMDT). This had a non-flight-like arm with a high-fidelity duplicate of drill and sampling system. It was operated in a thermal vacuum chamber to mimic the Mars environment.

4.8 REFERENCES

- Arvidson R et al (2017) Relating geologic units and mobility system kinematics contributing to Curiosity wheel damage at Gale crater, Mars. *J. Terramechanics* 73:73–93, DOI: 10.1016/j.jterra.2017.03.001
- Bagla P (2017) India eyes a return to Mars and a first run at Venus. *Science* DOI: 10.1126/science.aal0781
- Cucullu G et al (2014) A curious year on Mars – Long-term thermal trends for Mars Science Laboratory rover’s first Martian year. Paper presented to the 44th International Conference on Environmental Systems, Tucson, Arizona, 13–17 Jul 2014
- Davis J (2012) Curiosity sol 4: EDL updates, rover ready for software upgrade <http://www.planetary.org/blogs/guest-blogs/jason-davis/2012-08-10-curiosity-sol-4-edl-updates.html> Article dated 10 Aug 2012, accessed 26 Feb 2016
- Edwards C et al (2013a) Relay support for the Mars Science Laboratory Mission. Paper presented to the 2013 IEEE Aerospace Conference, 2–9 Mar 2013, Big Sky, Montana, USA, DOI: 10.1109/AERO.2013.6497325
- Edwards C et al (2013b) Replenishing the Mars relay network. Paper presented to the 2013 IEEE Aerospace Conference, 2–9 Mar 2013, Big Sky, Montana, USA, DOI: 10.1109/AERO.2014.6836354
- Gross M and G Cardell (2011) An overview of NASA’s Mars Science Laboratory. Paper presented at the 9th European Space Power Conference, Saint Raphael, France, 6 Jun 2011
- Haggart S and J Waydo (2008) The mobility system wheel design for NASA’s Mars Science Laboratory Mission. Paper presented at the 11th European Conference of the International Society for Terrain-Vehicle Systems, Nov 2008, Torino, Italy
- Heverly M (2012) Introduction to mobility for MSL. General Release for MSL Science Community and General Public, Sep 2012, Pasadena, California, USA
- Heverly M et al (2013) Traverse performance characterization for the Mars Science Laboratory rover. *J Field Robotics* 30:835–836, DOI: 10.1002/rob.21481
- Jones L, Moreno V, and Zimmerman R (2013). The F1 multi-mission radioisotope thermoelectric generator (MMRTG): A power system enabler for the Mars Science Laboratory (MSL) mission. Presentation to Nuclear and Emerging Technologies for Space, 25–28 Feb 2013, Albuquerque, New Mexico, USA.
- JPL (2008) The Mars Yard III. <https://www-robotics.jpl.nasa.gov/facilities/facility.cfm?Facility=14> accessed 21 Jun 2017

- JPL (2013a) Rover Team Working to Diagnose Electrical Issue. <http://mars.nasa.gov/msl/news/whatsnew/index.cfm?FuseAction=ShowNews&NewsID=1559> Status report dated 20 Nov 2013, accessed 15 Aug 2016
- JPL (2013b) Curiosity Resumes Science After Analysis of Voltage Issue, <http://mars.nasa.gov/msl/news/whatsnew/index.cfm?FuseAction=ShowNews&NewsID=1560> Status report dated 25 Nov 2013, accessed 15 Aug 2016
- JPL (2014) Lesson learned: MSL sol-200 anomaly <http://llis.nasa.gov/lesson/11201> Article dated 29 Apr 2014, accessed 14 Oct 2015
- Lakdawalla E (2014) Curiosity wheel damage: The problem and solutions. <http://www.planetary.org/blogs/emily-lakdawalla/2014/08190630-curiosity-wheel-damage.html> Article dated 30 Jun 2014, accessed 11 Jan 2017
- Lakdawalla E (2015) Curiosity update, sols 978–1011: Into Marias Pass; ChemCam back in action; solar conjunction <http://www.planetary.org/blogs/emily-lakdawalla/2015/06101727-curiosity-update-sols-978-1011.html> Article dated 10 Jun 2015, accessed 30 Jan 2017
- Lakdawalla E (2016) A new angle on Mars for Mars Odyssey. <http://www.planetary.org/blogs/emily-lakdawalla/2016/04190923-a-new-angle-on-mars-for-odyssey.html> Article dated 19 Apr 2016, retrieved 9 Jun 2016
- Lee D (2012) The Mission Loads Environment and Structural Design of the Mars Science Laboratory Spacecraft. Presentation to University of California Irvine, 17 Feb 2012.
- Lee G and J Donaldson (2013) Dreaming on Mars: How Curiosity performs actuator warm-up while sleeping. Paper presented to the 8th International Conference on System of Systems Engineering, Maui, Hawaii, 2–6 Jun 2013
- Makovsky A et al (2009) Mars Science Laboratory telecommunications system design. Article in Deep Space Communications and Navigation Systems Center of Excellence (DESCANSO) Design and Performance Summary Series
- Manning R and Simon W (2014) Mars Rover Curiosity: An Inside Account from Curiosity's Chief Engineer. Smithsonian Books, Washington DC
- NASA (2003) NASA Facts: Multi-mission radioisotope thermoelectric generator (MMRTG). Fact sheet published online October 2013.
- NASA Science Mission Directorate (2006) Final Environmental Impact Statement for the Mars Science Laboratory Mission.
- Novak K et al (2013) Thermal performance of the Mars Science Laboratory rover during Mars surface operations. Paper presented at the 43rd International Conference on Environmental Systems, International Conference on Environmental Systems (ICES), Vail, Colorado, 14–18 Jul 2013
- Voosen P (2016) Deep Space Network glitches worry scientists. Science DOI: 10.1126/science.aah7362
- Welch R et al (2013) Systems Engineering the Curiosity Rover: A Retrospective. Paper presented at the 8th International Conference on System of Systems Engineering, Maui, Hawaii, 2–6 Jun 2013
- Woerner D et al (2012) The Mars Science Laboratory's MMRTG: A mission's perspective. Presentation to AISS/ASME/SAE/ASEE 48th Joint Propulsion Conference & Exhibit and 10th International Energy Convers, Atlanta, Georgia, 29 Jul-Aug 1, 2012

- Woerner D et al (2013) The Mars Science Laboratory (MSL) MMRTG in-flight: A power update. Paper presented to Nuclear and Emerging Technologies for Space 2013, Albuquerque, New Mexico, 25–28 Feb 2013
- Woerner D (2014) An enhanced MMRTG for Exploration of the Outer Planets. Poster presented at the July 2014 Outer Planets Assessment Group meeting, Bethesda, MD, 23–24 Jul 2014

5



SA/SPaH: Sample Acquisition, Processing, and Handling

5.1 INTRODUCTION

Curiosity has unprecedented capability for interacting with the Martian surface using a collection of hardware called the Sample Acquisition, Processing, and Handling (SA/SPaH, pronounced “saw-spaw”) system (Figure 5.1). SA/SPaH includes the robotic arm and turret, the drill, and the sample scooping/sieving/portioning apparatus called Collection and Handling for In situ Martian Rock Analysis (CHIMRA, pronounced “chimera”). Also included in SA/SPaH are the Dust Removal Tool (DRT, but usually just called the “brush”), a variety of immobile hardware bolted to the front of the rover that supports sampling and drilling activities called the “sample playground,” and motorized inlet covers and spring-loaded wind guards for the SAM and CheMin instruments.

5.2 ROBOTIC ARM AND TURRET

Curiosity’s arm is huge. It measures 2.2 meters long from its base to the center of the turret. The arm weighs 101 kilograms; the turret alone is 34 of that.¹ Curiosity’s arm has five degrees of freedom, provided by individual motors. The motors power five joints, in order of their position along the arm: the shoulder azimuth joint; shoulder elevation joint; elbow joint; wrist joint; and turret joint. The operation of most of these joints mostly mimics the flexibility of a human arm, except that Curiosity’s elbow is fully double-jointed. Curiosity’s arm was designed to be strong enough that an Earth copy, under Earth gravity, could support its own weight without any additional help, which makes testing motions using the testbed rover substantially easier than it might otherwise be.

¹The arm is described in detail in Billing and Fleischner (2011)



Figure 5.1. Parts of Curiosity's Sample Acquisition, Processing, and Handling (SA/SPaH) system. Top image is the John Klein self-portrait from sol 177 (NASA/JPL-Caltech/MSSS); bottom image was taken during testing at Kennedy Space Center on August 13, 2011 (NASA release KSC-2011-6470), annotated by Emily Lakdawalla.

5.2.1 Arm mounts

The arm exerts significant loads on the rover whether it is extended or stowed. While stowed, caging mechanisms restrain the arm's motion. On the top of the shoulder bracket are three mechanisms that securely hold the turret when the rover is driving (and held it during launch and landing). A forward-projecting (“+X”) parapet captures the turret, and then the turret rotates 50°, pushing two hooks on the turret into two “duckbill” clamps on the bracket, whose flaring mouths guide the hooks into place. See Figure 5.1 for the locations of all these components.

Although the turret is tightly restrained to the rover's left shoulder when stowed, the arm's elbow joint only rests passively on its tripod-shaped bracket on the rover's right side. The elbow has to be able to slide back and forth along the bracket because the front panel of the rover is made of aluminum and the arm's tubular structure is titanium. Aluminum's coefficient of thermal expansion is almost three times higher than that of titanium, so the front panel expands and contracts by millimeters more than the arm does over the 180°C range of temperatures that Curiosity experiences over the Martian seasons. The aluminum shoulder bracket that supports the arm incorporates flexures that allow the bracket to accommodate the differing thermal expansion of the bracket and the titanium shoulder motor.

5.2.2 Cabling

Running all the signals needed to monitor and control the arm's motors and instruments to the rover's computer was a major challenge. There are 920 different signals being monitored on the robotic arm, of which 555 are at the very end of the arm on the turret, including 300 within CHIMRA. The signals travel to the avionics through 10 meters of flex cable, 63 millimeters wide and 5 millimeters thick, strapped to the outside of the rover arm. To allow freedom of motion, the flex cable wraps several times around each of the five actuators in large spools. The flex cable from the arm debouches into a rover bulkhead on the rover's left shoulder, where its signals transfer to a huge bundle of Kapton-wrapped round wires.

5.2.3 Turret

The turret is about 60 centimeters in diameter. The centerpiece of the turret is the drill. Attached to it are CHIMRA, the dust removal tool (brush), MAHLI, and APXS (Figure 5.2). The science instruments are separated from the drill by vibration isolator mounts to mitigate the effects of vibration from CHIMRA and drill percussion.

5.2.4 Using the arm

The arm was tested and qualified to be able to reach targets within a cylinder-shaped region called the “primary workspace” (often referred to as the “magic cylinder”), shown in Figure 5.3.² But it can readily reach targets beyond that, in a wider region called the

²Use of the arm for sample collection is described in Anderson et al (2012)

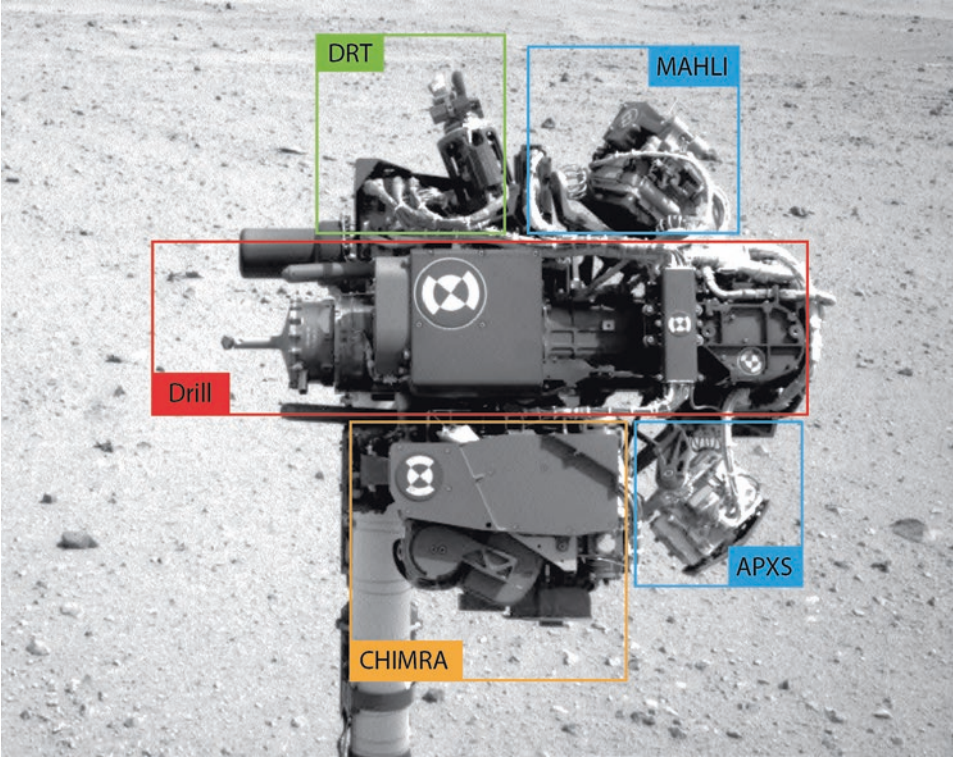


Figure 5.2. Parts of Curiosity's robotic arm turret, including the drill, dust removal tool or brush (DRT), Collection and Handling for In situ Martian Rock Analysis (CHIMRA), and two science instruments, the MAHLI camera and APXS elemental analyzer. Navcam image NLA_400335692EDR_F0040000NCAM00107M, taken during the first turret checkout on sol 32. NASA/JPL-Caltech/Emily Lakdawalla.

“work volume.” The arm functions slowly and deliberately, its tip moving at a maximum speed of 1 centimeter per second. The arm's heft imposes limits on the accuracy of its placement: gearbox backlash, thermal expansion and contraction, and the massive weight of the turret combine in difficult-to-predict ways with the tilt of the rover to make its position in space uncertain within about a centimeter.³ The uncertainty is slightly larger for the instruments because the amount and direction that they sag on their wire rope vibration isolators depends on the orientation of the turret.

Once the arm has been deployed to a location, it can be repositioned to the same pose over and over again with surprising precision. The precision holds even when a different tool is selected on the turret. Rover planners take advantage of this precision to get closer to targets than the arm's initial placement inaccuracies allow. The rover planners commonly use the contact plate on APXS to test exactly where a target is, by advancing APXS toward the target and waiting for the contact plate to record contact. In circumstances where the APXS can't be used in this way (soils, loose rocks, or very uneven

³Kuhn (2013)

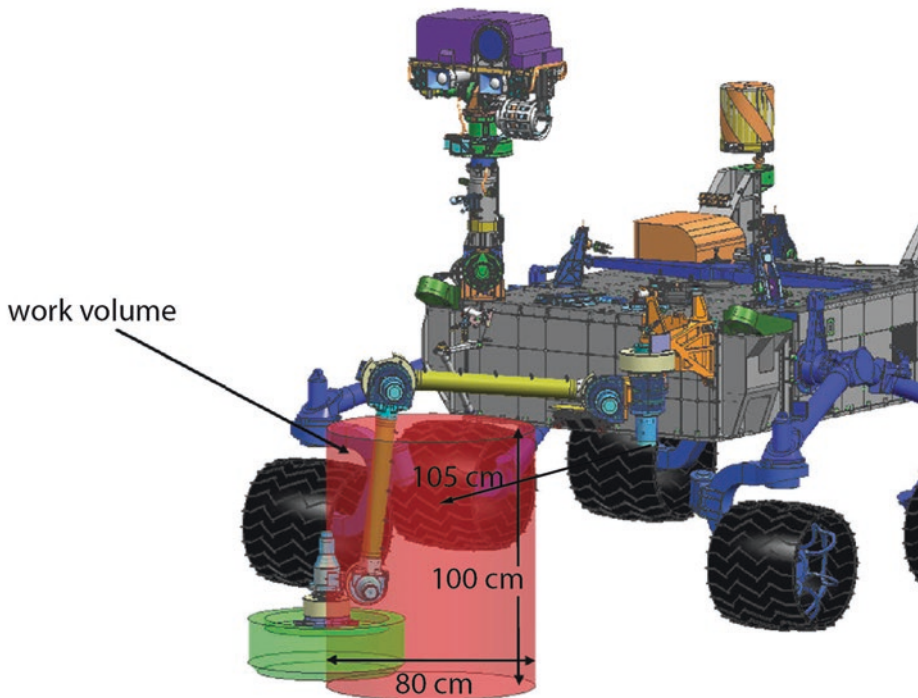


Figure 5.3. The “magic cylinder” is centered 105 centimeters in front of the rover body, 100 centimeters tall and 80 centimeters in diameter. If the rover is on a level surface, the workspace extends 20 centimeters below the surface. Modified from Billing and Fleischner (2011). The CAD model of the rover shown here predates several design changes.

surfaces), they can use MAHLI. MAHLI’s autofocus distance is very sensitive to the distance to the target, so arm engineers can use the MAHLI autofocus distance to upgrade their knowledge of the position of the target to get closer on a later sol. Rover planners can even use APXS in “proximity mode” (see section 9.3.2) as a test of where the surface lies.

5.3 THE DRILL

Curiosity’s drill is a percussion instrument that hammers its rotating bit, boring holes 1.6 centimeters wide and up to 6.5 centimeters deep.⁴ The drill has four motors: a drill feed mechanism for moving the drill bit up and down; a drill spindle mechanism to rotate the bit; a percussion mechanism; and a drill chuck mechanism that can release the drill bit assembly and exchange it for a new one from one of two bit boxes located on the front of the rover (Figure 5.4).

⁴The drill is described in detail in Okon (2010)

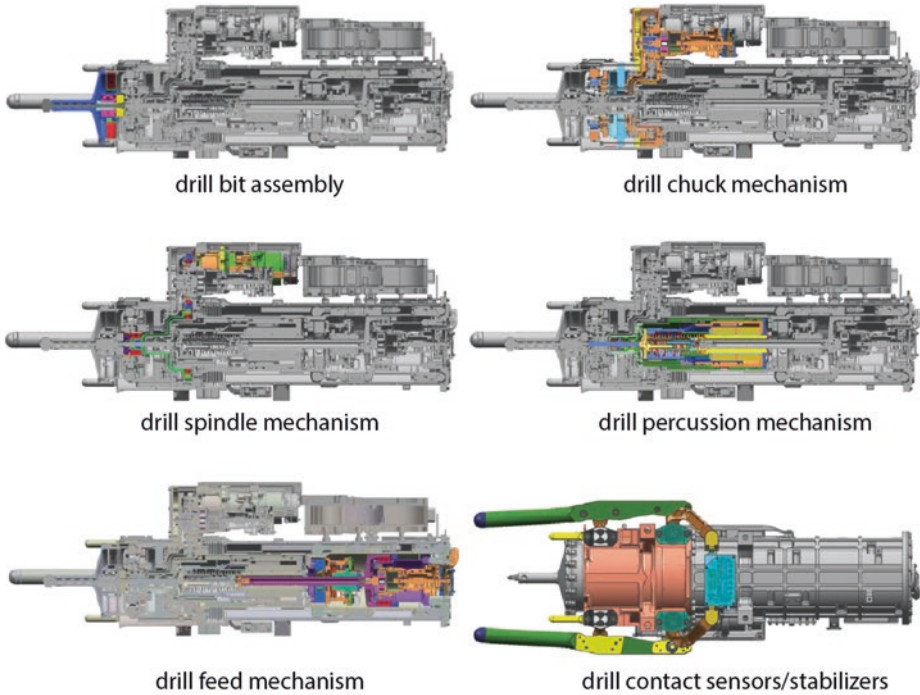


Figure 5.4. Parts of the drill. Images from Okon (2010), annotated by Emily Lakdawalla.

5.3.1 Drill bit assembly

The drill bit assembly consists of a drill bit, collection sleeve, and sample chamber (Figure 5.5). The spade-shaped steel bit is a commercial off-the-shelf component that has been modified, with two deep flutes machined into it to help move powdered rock up the collection sleeve and into the sample chamber (Figure 5.6). The steel collection sleeve covers all but the last 1.5 centimeters of the drill bit. After 16 drill sites, Curiosity is still using the original drill bit. Although it is not as shiny as it once was, it has not dulled dramatically (Figure 5.6).

5.3.2 Drilling

To prepare to drill, Curiosity places two projecting contact sensors against the rock, and then continues to drive the arm motors even after the contact sensors are in contact with the rock target (Figure 5.7). This is called “preloading”; the arm can press onto the rock with up to 300 newtons of force. Front Hazcam images taken before and after preloading usually document a tiny upward motion of the rover body as the arm pushes against the rock. Once the arm is placed and preloaded for drilling, the arm doesn’t move; all drilling motion is performed by the drill itself using the drill feed mechanism.

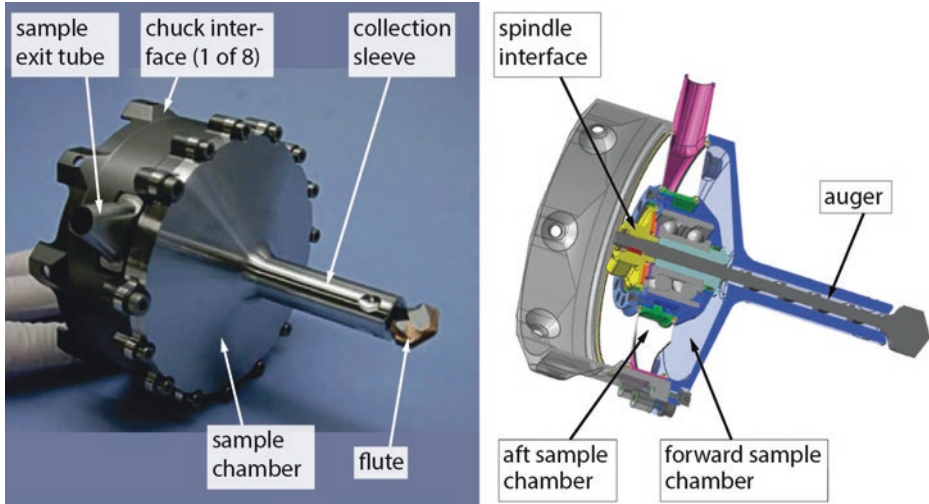


Figure 5.5. Parts of the drill bit assembly. Photos from Anderson et al (2012), annotated by Emily Lakdawalla.

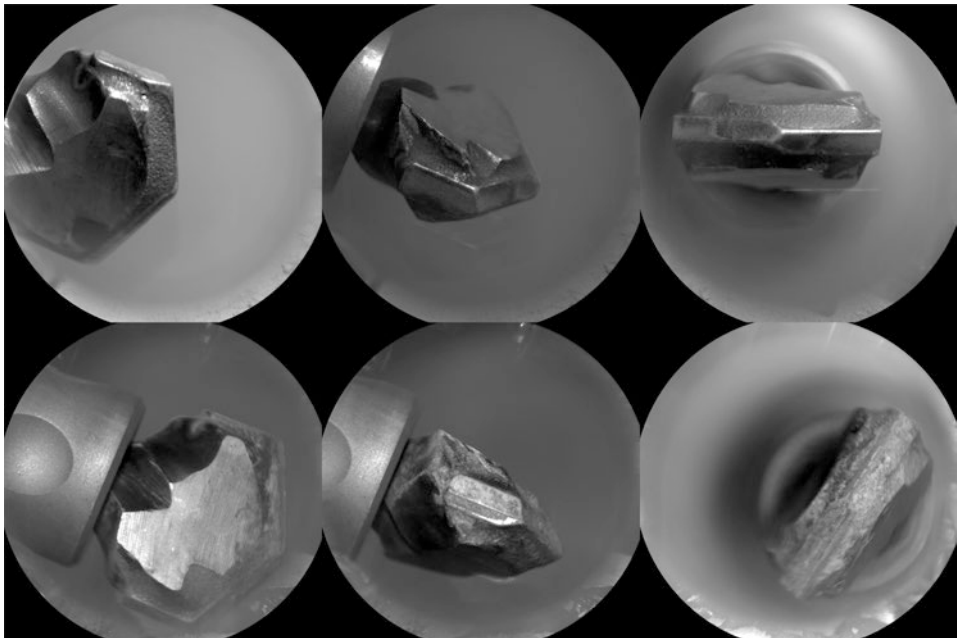


Figure 5.6. Condition of Curiosity's drill bit over time as observed using ChemCam RMI. Top row: sol 172, before the first drill site at John Klein. Bottom row: sol 1528, after drilling at Sebina. NASA/JPL-Caltech/CNES/CNRS/LANL/IRAP/IAS/LPGN.

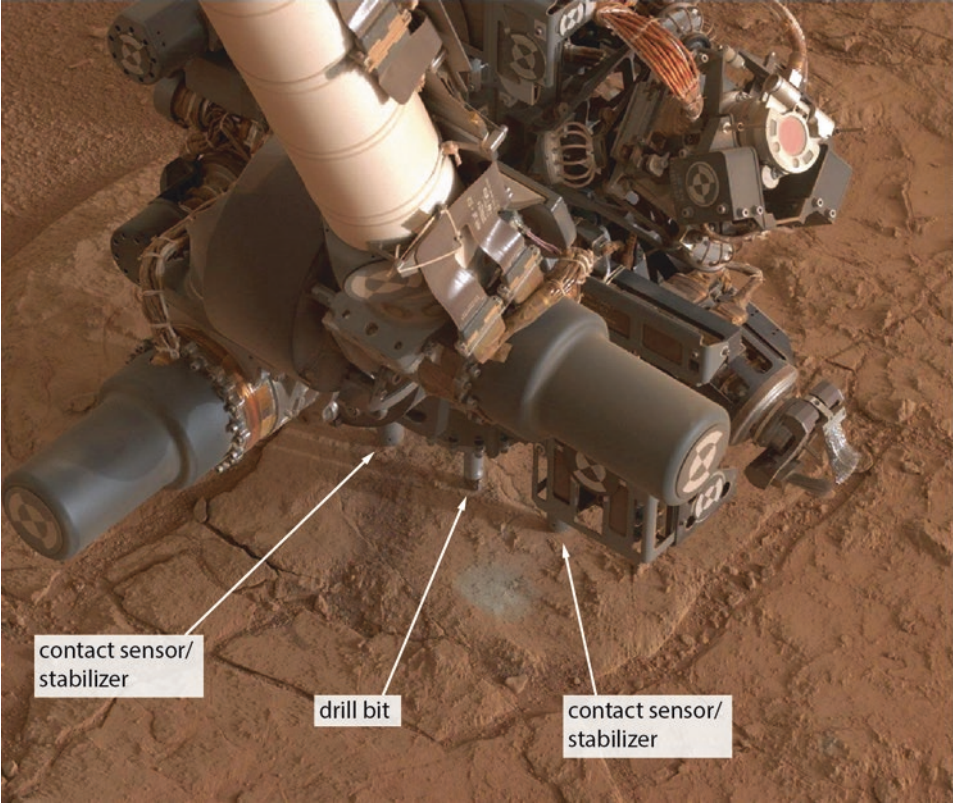


Figure 5.7. Drill use on Mars. The two contact sensors/stabilizers are pressed against a rock, and the drill feed has extended to place the drill in contact with the ground. Mastcam image 0174ML0006380000105184E01, NASA/JPL-Caltech/MSSS/Emily Lakdawalla.

Once the drill feed mechanism has advanced the drill bit to contact the rock, drilling begins with percussion from a 400-gram mass striking a spring-loaded anvil rod 30 times per second. The team can select the initial energy of the blows within a range from 0.05 to 0.81 joules. At first, the drill uses no rotation, only percussion, to strike a small asterisk-shaped divot in the rock at the location of the desired drill hole – like a carpenter using a nail or awl to set the starting location for their drill. These initial taps dig no more than 0.8 millimeter into the rock.⁵

For the first 1.5 centimeters of drilling, the powdered material piles up around the drill hole, making a tailings pile. After the first 1.5 centimeters, the collection tube contacts the surface, and powdered material that passes by the spade tip of the bit climbs up the auger into a two-chambered sample collection area within the drill bit assembly. After drilling, the feed retracts and the arm lifts the drill off the rock. The rover then photographs the drill bit with Mastcam to verify that it is none the worse for wear after the drilling activity.

⁵Supplementary material to Grotzinger et al (2014)

At many sites, Curiosity performs a “mini-drill” test before the full drill, penetrating less than the unsleeved 1.5 centimeters into the rock, in order for the tactical team to assess rock and rock powder properties before committing to gathering powdered rock sample. A rock with an extremely unusual water-rich mineral composition could liquefy under the vibration of the drilling mechanism, which would be catastrophic for the ability to acquire samples. The team can choose to skip mini-drilling to save time if they determine from a rock’s appearance (from Mastcam, MAHLI, and ChemCam RMI) and composition (from ChemCam LIBS and APXS) that it is similar to previously drilled rocks.

5.3.3 Drill bit assembly replacement

What if the drill bit gets worn out, or worse, stuck in a rock? If the rover slips during drilling, it could leave the drill bit stuck. To avoid the situation, before drilling, the rover drivers make sure that the rover is in a stable position, with all wheels firmly in contact with the ground, and no small rocks under the wheels. If there is any question of wheel stability, they may sequence a set of MAHLI wheel images in order to be sure the wheels are stable. If the rover should slip, binding the drill bit, the drill feed mechanism is capable of pulling upward with a force of nearly 10,000 newtons.⁶ If the drill remains stuck, they can try pulling the feed while percussing and/or rotating, which would reduce the friction between the drill and the rock but could also result in the loss of the acquired sample. If the drill bit remains stuck after that, they can try motion of the arm to counteract whatever motion of the rover had caused the drill bit to bind.

If all of these efforts fail, the rover can detach its bit and leave it behind in the rock, exchanging it for one of two more bits located in bit boxes on the front of the rover (Figure 5.8; another good view of a drill bit box is in Figure 5.18). Because the drill bit has not yet needed swapping, the drill chuck mechanism has not been used since a brief test wiggle in the first weeks after landing.⁷

5.3.4 Drill problems

Several issues have affected the drill both before and after launch. One was the potential contamination of the drill bit that caused the reclassification of MSL’s planetary protection status (see section 1.7.4). The others are: the possible presence of Teflon debris in drilled samples; a short in the percussion mechanism; and a serious problem with the drill feed mechanism. A new problem was diagnosed in the drill chuck mechanism as this book was going to print around sol 1800. It is similar in character to the drill feed problem. It will not be further discussed here.

5.3.4.1 Teflon debris

Shortly before launch in November 2011, engineers doing testing of drilling operations found that seals inside the engineering model of the drill bit assembly were slipping during

⁶Limonadi D (2012b)

⁷Ashwin Vasavada, personal communication, email dated February 9, 2017

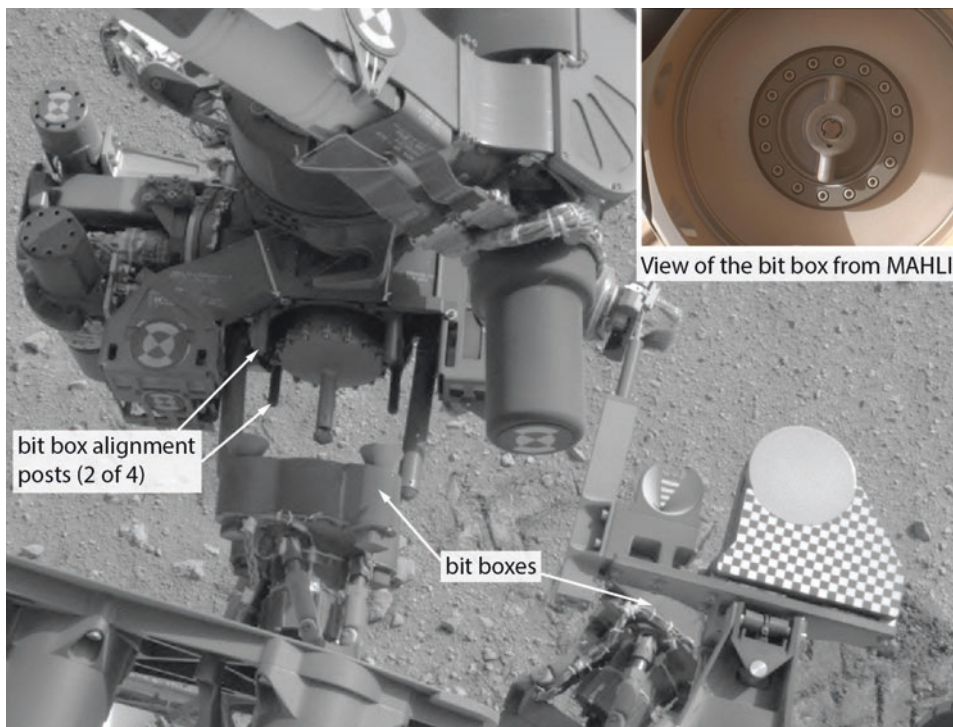


Figure 5.8. A test of the positioning of the turret for drill bit replacement. If the drill bit really were being replaced, Curiosity would already have used the drill chuck mechanism to release the drill bit it is holding. Four round-tipped posts surrounding the drill bit assembly would advance into four funnels at the corners of the bit box, aligning the drill with the replacement drill bit assembly. To the right of the turret is the sample playground. Navcam image NLA_400696022RAS_F0040000NCAM00110M1 taken sol 34. Inset: a view of the interior of the bit box taken by MAHLI from a similar position. Image 0036MH0000490010100065E01. NASA/JPL-Caltech/MSSS/Emily Lakdawalla.

drilling, which generated Teflon debris that mixed with the drilled rock powder.⁸ This was a potentially serious source of contamination that could compromise SAM's ability to detect organic materials within Mars' rocks. Although the possibility of Teflon contamination of the drilled material had been recognized early in development, when the drill was actually tested, it generated more debris than expected. It was too late in the process to effect any kind of design change, of course. The mission ultimately determined that the amount of contamination was small enough that it would not likely affect SAM results, and suggested that the mission avoid using the drill in a way that generated the most debris – “minimizing the low-rate-of-penetration operations.” No sign of Teflon contamination has been noticed in drilled samples since landing.

⁸JPL (2014) Lesson Learned: Recognize that Mechanism Wear Products May Affect Science Results <http://llis.nasa.gov/lesson/10801>. Article dated June 8, 2014, accessed October 14, 2015

5.3.4.2 *Battle short and the sol 911 percussion anomaly*

Another potentially serious problem was discovered during Earth testing of a testbed version of the drill mechanism in 2011. A broken bushing caused a short circuit in the test drill that could have fried the rover’s motor controller if engineers had not acted swiftly. The consequences of such an event happening on Mars would be dire. It was too late to make any changes to the flight drill. Engineers in Florida opened the belly pan of the rover to install a “battle short” that would route half of the excess current to ground if such a short circuit developed in flight.⁹

On sol 911, sensors detected current flowing through the battle short as Curiosity was using drill percussion to transfer sample from the drill to CHIMRA, halting the operation.¹⁰ There is no way to know if the cause is the same as the problem discovered on Earth, but the effect is similar. The shorts have recurred since sol 911, but are intermittent and extremely brief. If they remain that way, the battle short adequately protects the electronics. The engineers have instructed the rover to tolerate very brief shorts without faulting and terminating the drilling process.¹¹ At the same time, the mission has shifted to relying less on the percussion mechanism. They now avoid using drill percussion for sample transfer, relying on CHIMRA vibration. They have also changed the way they operate the drill: originally, they began drilling with a medium percussion level and made adjustments according to the penetration rate, but they now begin with very light percussion and only increase the rate as needed. Engineers have also developed a new rotary-only drilling technique, made possible by the softness of the rocks within Gale crater, but rotary-only drilling has not yet been used on Mars because of a different drill anomaly.

5.3.4.3 *Sol 1536 drill feed anomaly*

On sol 1536, the engineers attempted rotary-only drilling at a site called Precipice. The operation did not complete, because the drill feed mechanism stalled immediately. Current flowed to the drill feed motor, but the motor produced no motion. Like the problem with the percussion mechanism, it is intermittent, so has been difficult to troubleshoot, but it appears to reside in the drill feed brake mechanism. As of sol 1800, the rover hasn’t done any drilling.

The drill feed motor has a power-off brake: when no electricity is flowing to the brake, a disk (the “moveable brake”) is pressed against another disk (the “fixed brake”) by a set of springs. The pressure holds the drill feed firmly in position even when percussion, vibration, and rotation mechanisms are operating. Energizing a solenoid pulls the moveable brake away from the fixed brake, allowing the drill feed motor to spin a worm drive that slowly translates the drill feed out or in. The brake has two solenoids for redundancy.¹²

⁹Manning and Simon (2014)

¹⁰James Erickson, interview dated April 10, 2015

¹¹Ashwin Vasavada, interview dated May 1, 2015

¹²Steve Lee, interview dated September 1, 2017

Engineers troubleshooting the issue found that energizing either solenoid with the normally commanded current failed to produce any feed motion. Commanding with tweaked parameters (like higher current, energizing both solenoids instead of one, multiple attempts to disengage the brake, and so on) produced some motion, but not reliably. The team strongly suspects that a displaced component or piece of foreign debris is interfering with motion of the movable brake, preventing it from fully disengaging when commanded.

From December 2016 through March 2017, engineers tested and performed diagnostics in an attempt to recover the full use of the drill feed. After developing several innovative techniques, they achieved the full range of feed motion, albeit at speeds too high to drill into rocks. However, after using CHIMRA to sieve a sand sample at Ogunquit Beach on sol 1651 (March 29, 2017), engineers found that the behavior of the drill feed had deteriorated.

As of this writing, the engineering team is pursuing a new drilling and sample delivery approach that does not require using the drill feed. They successfully extended the feed to its full 110-millimeter distance on sol 1780. On Earth, they are working on developing the ability to perform feed-extended drilling (FED), using arm motion instead of feed motion to advance the drill bit into the rock. Initial testing of feed-extended drilling began on Mars on sol 1848. While this can recover the ability to drill, not using the feed also prevents transfer of sample material to CHIMRA (see section 5.4.2.1). Future feed-extended sample transfer (FEST) may involve reverse augering material from the sample chamber out through the bit and directly into SAM and CheMin.

5.4 CHIMRA: COLLECTION AND HANDLING FOR IN SITU MARTIAN ROCK ANALYSIS

CHIMRA (pronounced “chimera”) is a labyrinth of chambers that can sieve and portion out samples for delivery to the science instruments.¹³ The main parts of CHIMRA are shown in Figure 5.9. There are two main paths by which sample moves around inside CHIMRA: one with a 150-micrometer sieve, and another with a 1-millimeter sieve.

Curiosity can acquire sample material either through drilling or through scooping loose material with the CHIMRA scoop. CHIMRA uses a combination of gravity and vibration to move sample around: the rover rotates the turret into a direction where the desired direction of sample motion is downward, and then uses its vibration mechanism to encourage the powder to move. CHIMRA’s labyrinthine interior is difficult to imagine even for the engineers who interact with it on a regular basis. Four 3D-printed models of CHIMRA located throughout mission operations enable engineers to twist and turn it and open and close its doors to simulate its movements physically.

¹³The main published source for information on CHIMRA is Sunshine (2010). Cambria Hanson and Louise Jandura explained its intricacies and some last-minute design changes to me in great detail in an interview on June 3, 2016

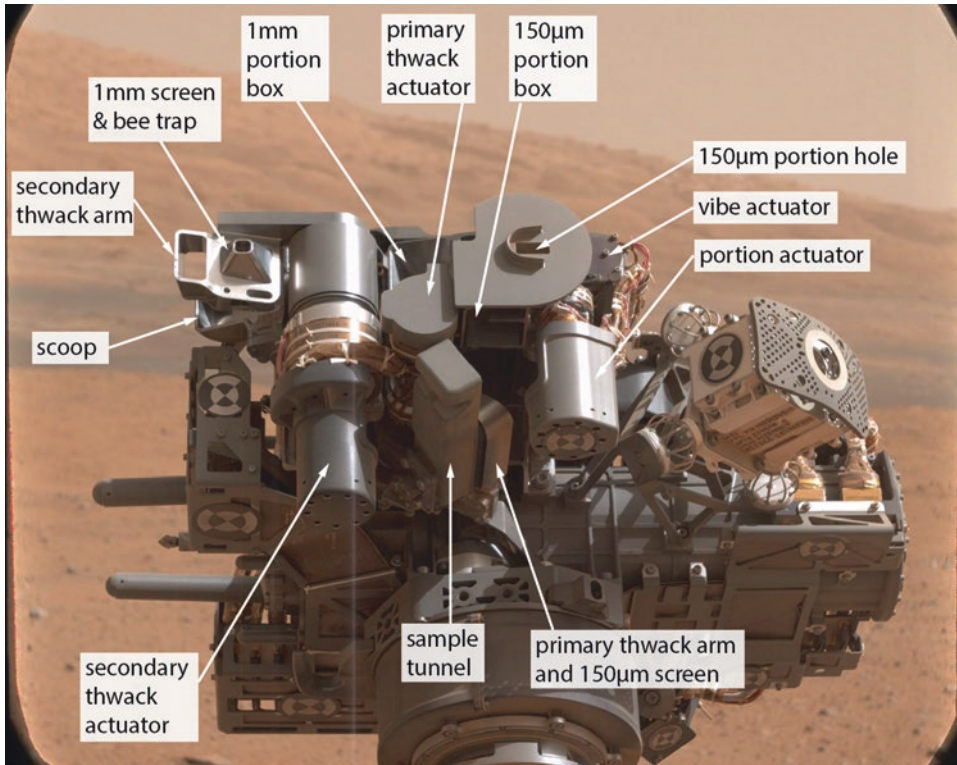


Figure 5.9. Parts of CHIMRA. Left Mastcam image 0032ML0000830000100870E01 of turret from initial checkout on sol 32. NASA/JPL-Caltech/MSSS/Emily Lakdawalla.

5.4.1 CHIMRA tour

Engineers designed CHIMRA to avoid clogging. Its interior spaces are as wide open as possible, without sharp corners. Wherever possible, the design avoids forcing sample to move through a narrower space than it has already passed through. The mechanism was also designed to allow engineers to visually inspect every surface within CHIMRA repeatedly over the course of the landed mission.

CHIMRA has four motorized mechanisms: the vibration actuator, the portion door actuator, and the primary and secondary thwack actuators. The vibration actuator is a self-contained mechanism that rotates an off-center tungsten mass to generate vibrations. It generally vibrates at a speed that encourages the CHIMRA mechanism to resonate, which efficiently shakes the 8-kilogram CHIMRA on its mount while not wasting much energy vibrating the rest of the 34-kilogram turret. The portion door mechanism is a very small motor that rotates a lever that presses up against the open end of the hole out of which CHIMRA drops 150-micrometer-sieved portions. The thwack mechanisms both serve multiple functions. Each of the two thwack mechanisms is connected to a door that opens up CHIMRA for inspection, sample dumping, and cleaning, and a “thwack arm” that

carries a sieve. The primary thwack mechanism is connected to parts of the 150-micrometer sieve path (section 5.4.2). The secondary thwack mechanism is connected to parts of the 1-millimeter sieve path, including the scoop (section 5.4.3). Both can be wound up with a spring to slam the sieve against the rest of the mechanism to clear stuck sediment, hence the “thwack” moniker (section 5.4.4).

5.4.2 CHIMRA 150-micrometer sample pathways

This pathway can generate individual sample aliquots amounting to about 75 cubic millimeters each for delivery to SAM or CheMin, or a single “portion plus” aliquot of (very approximately) three times that size.

5.4.2.1 Drill to CHIMRA reservoir

After Curiosity has drilled a sample, the sampled powder sits in the forward sample chamber, immediately above the drill bit. The drill reservoir is two-chambered so that the drill can be used at angles of up to 20° without sample spilling out of the sample exit tube prematurely, regardless of drill orientation. Once the drill feed is fully retracted, the drill bit assembly sample exit tube aligns with the CHIMRA sample inlet tube. In the aftermath of the drill feed anomaly described in section 5.3.4.3, this is an important detail. If the drill feed is not available, the only way to transfer material from the drill to CHIMRA will be by dumping the drilled material somewhere and picking it up again with the scoop, a difficult or perhaps impossible proposition.

To move the sample into CHIMRA, the rover tilts the drill and uses either drill percussion or CHIMRA vibration to shift the powder from the forward sample chamber to the aft sample chamber. Then CHIMRA vibration and a rolling motion of the arm guides the sample from the aft sample chamber out the sample exit tube on the drill and into the sample inlet tube on CHIMRA (Figure 5.10). With a combination of vibration and back-and-forth rocking motions, the sample moves through the sample inlet tube, past an elbow in the tube, and into the CHIMRA sample reservoir.

The CHIMRA reservoir is divided in two by an internal partition, called the thin wall, which has a slot on one side. When sample enters the reservoir, it pools in the corner of the upper half of the reservoir, away from that slot. To visually inspect the drilled material before it is sieved, rover planners can tilt toward the slot and use vibration to transfer the material to the lower half of the reservoir. From there it can be slid through the rabbit hole on the secondary thwack arm and into the scoop. Then they can open the scoop and take photos of the sample with the Mastcams, close the scoop, and tilt to return the sample back through the rabbit hole and into the reservoir.

5.4.2.2 Scoop to CHIMRA reservoir

To acquire a scooped sample, the rover opens the scoop and positions it over the sample site. The secondary thwack actuator closes the scoop, dragging it through the sand to a depth of about 35 millimeters, usually acquiring a big mound of sand in the scoop.

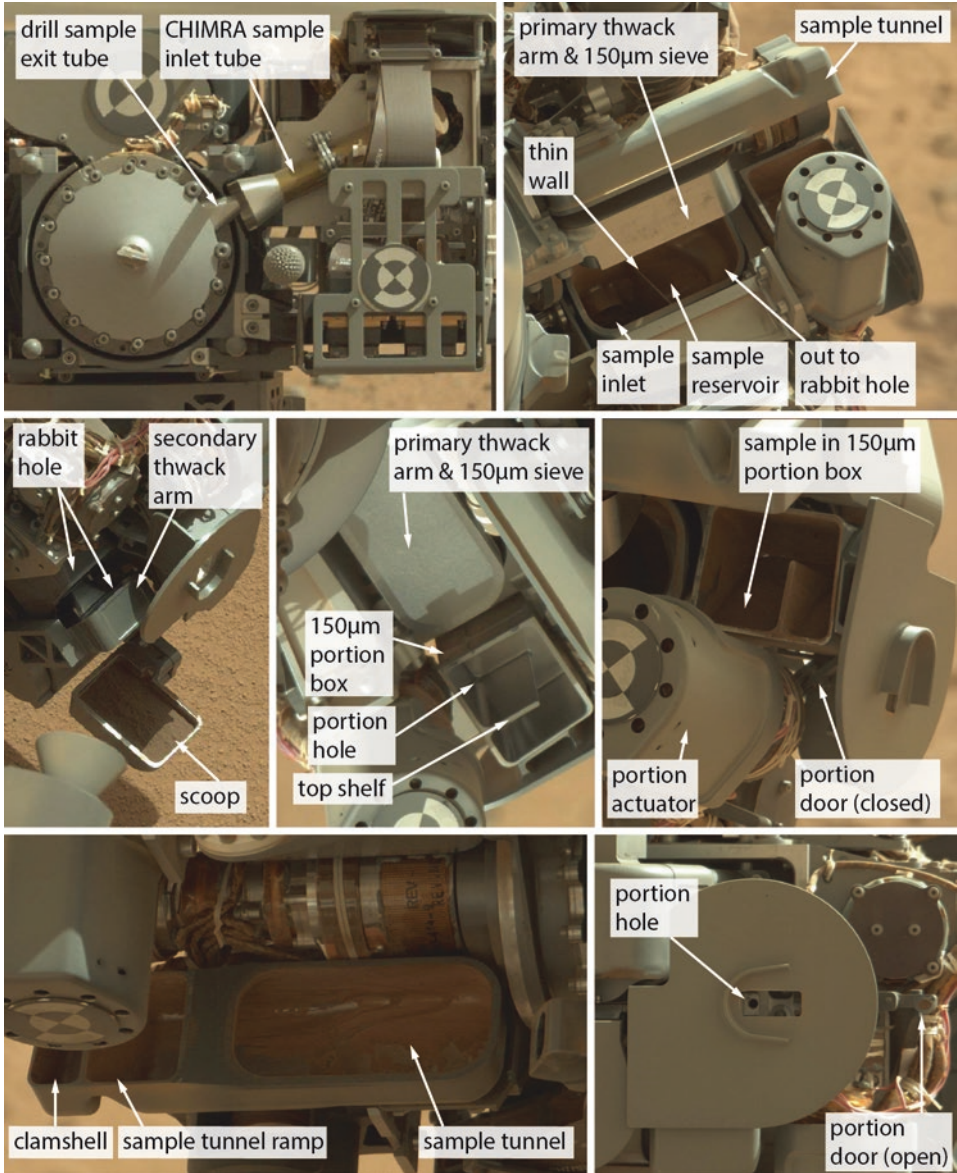


Figure 5.10. Parts of the 150-micron sample pathway within CHIMRA. Photos from turret checkout before and after scooping at Rocknest on sols 64 and 65. NASA/JPL-Caltech/MSSS/Emily Lakdawalla.

The secondary thwack actuator can apply a huge amount of torque to overcome resistance from buried pebbles, if they exist. After acquiring the sample, the scoop tilts slightly downward and CHIMRA vibrates in order to spill material from the scoop until it has reached a level that corresponds to the desired 12 cubic centimeters of sample (see Figure 3.6). Then the scoop can optionally be leveled out and vibrated within view of the Mastcams, which can take movies to watch the particles move around inside the scoop, performing a search for very large particles. Because this requires human inspection, the rover has to wait at least one night (until the next tactical planning sol) to proceed. If the sample passes muster, the scoop is closed and the material in it gets transferred through the rabbit hole to the CHIMRA sample reservoir.

5.4.2.3 150-micrometer sieving

To sieve, engineers rotate the turret to turn the reservoir topside down, which places the sample on the 150-micrometer sieve. Then CHIMRA vibrates and the arm wrist rocks the turret gently back and forth to encourage the sample to spread out across the sieve. Initially, engineers expected it to take as much as an hour to produce enough sieved sample, but experiments on Earth and Mars have yielded a standard 20-minute time of sieving operations to produce approximately 12 cubic centimeters of sieved material. The post-sieve (fine) material accumulates in the sample tunnel, while pre-sieve (coarse) material remains in the sample reservoir.

5.4.2.4 Inspecting sieve efficiency

Once sieving is complete, CHIMRA rotates and vibrates to move the sieved sample down the sample tunnel ramp and into the 150-micrometer portion box. This motion also moves the coarse pre-sieve material (the sample that did not pass through the 150-micrometer sieve) through the rabbit hole and into the scoop. At this point, engineers can peek into the portion box to assess how much material passed through the sieve, and can open the scoop to see how much material did not pass through the sieve. Comparing the two volumes gives an estimate of sieving efficiency.¹⁴ The engineers changed this behavior following the development of a problem with the primary thwack arm on sol 1231 (see section 5.4.6).

5.4.2.5 150-micrometer portioning

To prepare a portion, CHIMRA uses a series of small rotations and vibrations to walk the sieved sample around the interior of the portion box until it is all piled up on top of the portion hole. (These motions may also move the coarse pre-sieve material that was in the scoop through the 1-millimeter sieving pathway, where it stays until it is dumped.) A very small amount of vibration encourages sample to enter the portion hole – not much, to

¹⁴Steven Kuhn, personal communication, email dated August 14, 2015

avoid packing the hole and potentially clogging it. The hole has an inverted funnel shape, opening wider toward the outside, to prevent clogging. For a single 75-cubic-millimeter aliquot, the rover tilts CHIMRA again to move the extra sample away from the portion hole, back under the “top shelf” of the interior of the portion box. For a “portion plus” aliquot (used only for dropping a larger sample to the observation tray), CHIMRA skips the step of sliding the excess material off of the top shelf.

5.4.2.6 *Delivering a 150-micrometer portion to SAM or CheMin*

Before delivery, Mastcam turns and takes photos of the sample inlet. Then the mast head rotates 180° away from the sample inlet, to keep any blowing dust away from the cameras. The rover moves the turret over a sample inlet, opens the inlet cover, moves the turret to within about a centimeter of the inlet, opens the portion door, and vibrates to make sure the portion drops. The portion door closes, the arm moves away, the sample inlet closes, and CHIMRA can repeat the sample preparation and drop-off process again. After all of the sample dropoffs have been completed, Mastcam takes another picture of the sample inlet to document successful closure of the inlet door.

5.4.3 CHIMRA 1-millimeter sample pathways

This pathway generates a single aliquot with a volume of 45 to 130 cubic millimeters; all the rest of the sample is lost during the portioning activity. Therefore, the mission hasn’t used the 1-millimeter pathway on precious drilled sample, only with scooped samples, although it is theoretically possible to create a 1-millimeter-sieved portion from a drilled sample. Only SAM can accept this coarser sample size; it’s unsafe for delivery to CheMin.

5.4.3.1 *1-millimeter sieving*

Figure 5.11 shows parts of CHIMRA relevant to the 1-millimeter grain-size sample pathway. To pass material from the scoop through the 1-millimeter pathway, the turret tilts in the opposite direction to the one it uses to move material from the scoop into the reservoir. The material lands on the 4-millimeter grate, and whatever passes through lands on the 1-millimeter sieve behind the grate. Whatever passes that sieve falls into the bee trap, a funnel that opens into the 1-millimeter reservoir. Anything that passes the 4-millimeter grate but not the 1-millimeter sieve exits the space between the two through a slot, returning to the scoop. Curiosity dumps remaining coarse material before proceeding. The shape of the bee trap prevents the sieved material from being lost as any coarse stuff is dumped.

5.4.3.2 *1-millimeter portioning*

To prepare a 1-millimeter aliquot, the arm tilts so that the material in the bee trap piles up on the 1-millimeter portion tube. This portion tube, unlike the 150-micrometer portion hole, is a blind tube, closed at one end. With the portion tube filled, CHIMRA cracks open the scoop

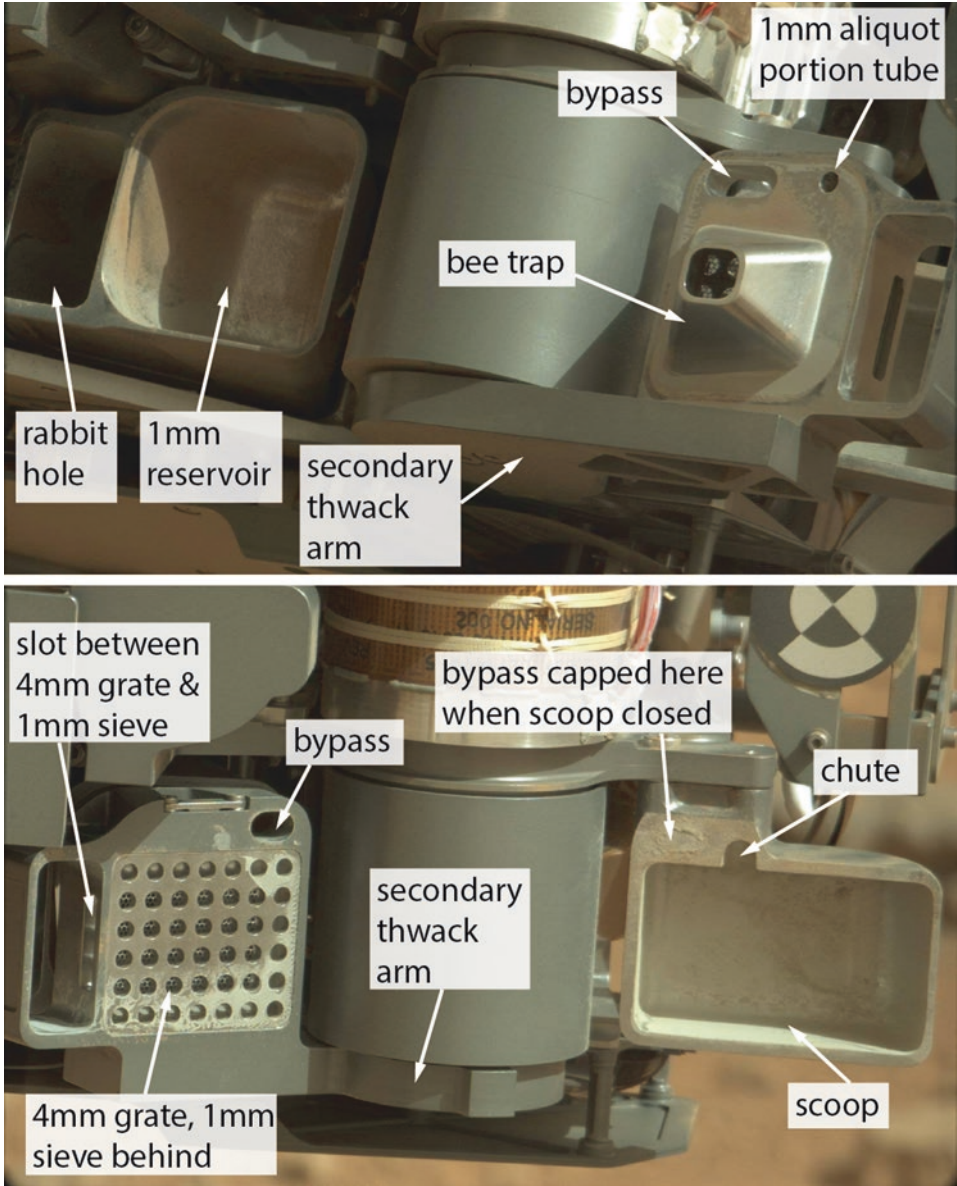


Figure 5.11. Parts of the 1-millimeter CHIMRA sample pathway. Photos from turret checkout on sol 229. NASA/JPL-Caltech/MSSS/Emily Lakdawalla.

and secondary thwack arm. All the remaining sieved sample that was in the reservoir slides out of it and onto the ground, leaving behind the material collected in the 1-millimeter portion tube. Then CHIMRA closes up the scoop again, tilts to spill the material that was in the portion tube back into the reservoir, and then angles the aliquot into a bypass hole on the secondary thwack arm. While CHIMRA is closed, the bypass hole is closed at one end by a wide lip on one side of the scoop. Then CHIMRA angles the scoop like a cup and cracks the scoop open slightly, allowing the material to spill out of the bypass and into the scoop. A little chute cut into the side of the scoop encourages material to fall neatly from the bypass into the scoop. Once the portion is in the scoop, it can be inspected before delivery.

Because this process drops all of the rest of the 1-millimeter-sieved material that had been held in CHIMRA, only one portion can be created from each sample. To get the double or triple portion that SAM now prefers (see section 9.5.2.5), Curiosity has to start over with a new scoop of sand for each portion.

5.4.3.3 *Delivering a 1-millimeter sieved aliquot*

Dropping the sample is a delicate operation because the width of the scoop is similar to the width of the sample inlet. To deliver a 1-millimeter sieved aliquot to an instrument, the scoop is tilted and vibrated to slide the portion into one of the corners of the scoop's tip. Then a SAM sample door is opened and the scoop tip placed over the sample inlet. As the scoop opens, the rest of the turret rotates in order to keep the position of the scoop tip motionless, dumping the sample into the inlet.

5.4.3.4 *Medium-grain-size fraction portioning*

The 150-micrometer and 1-millimeter pathways can be combined to create a single aliquot with an intermediate sample size. This capability was first used at Namib dune on sol 1228 (Figure 5.12). CHIMRA acquired a scooped sample, passed it to the reservoir, and sieved it through the 150-micrometer sieve. Then Curiosity dumped the post-sieve sample and sent the pre-sieve sample through the 1-millimeter pathway. CHIMRA created a single aliquot as described above, and then delivered it to SAM.

5.4.4 **Cleaning and thwacking**

After the first drill at Yellowknife Bay, scientists expressed a desire to use the contact science instruments (particularly APXS) to examine the drilled sample, and the rover planners quickly developed a way to oblige them, dumping the sample in neat piles for APXS analysis (see Figure 3.7). If the pre-sieve material is not dumped before 150-micrometer portioning, it can end up in the 1-millimeter sample reservoir. Material dumped from there drops less neatly than material dumps from the scoop, because it falls off the secondary thwack arm around the bee trap on all sides, which tends to disperse it over a broader area. A tighter pile is better for APXS, because then it is more likely that the APXS field of view will contain only sample material and not “windows” of whatever material the pile was

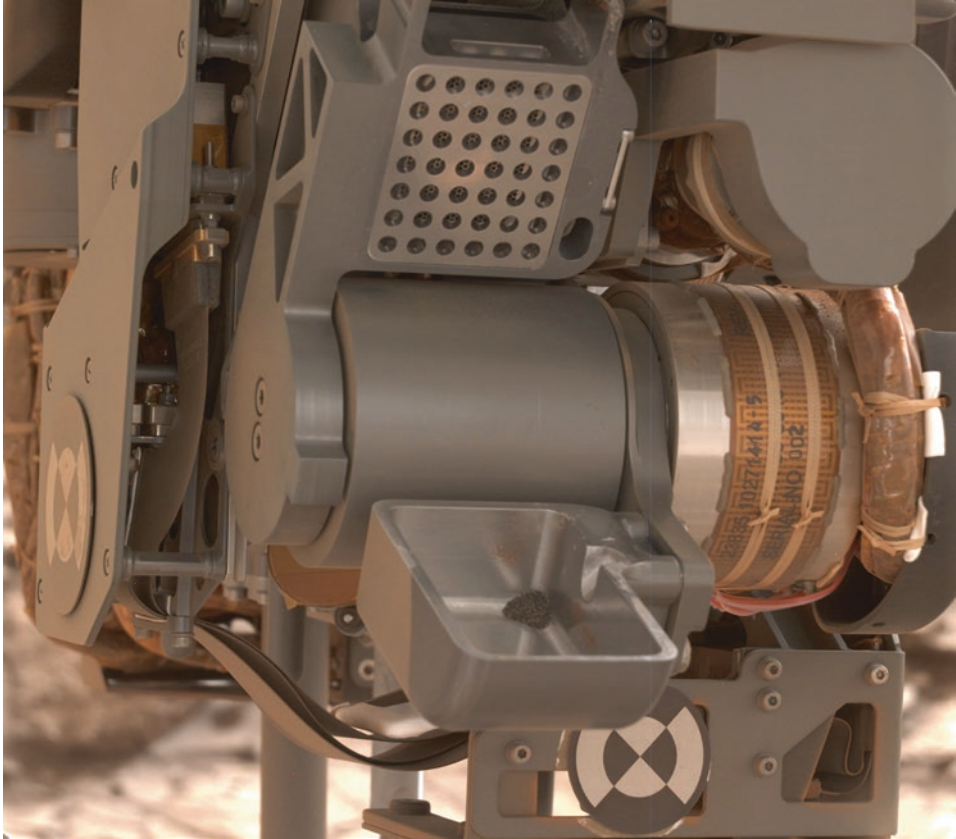


Figure 5.12. A medium-grained (150-micron to 1-millimeter) aliquot in the scoop, ready for delivery to SAM. Left Mastcam photo 1228ML0036640000503705E01. NASA/JPL-Caltech/MSSS.

dumped on. Pre-sieve (coarse) material is most often dumped before departing a sample site, while post-sieve (fine) material is usually held for longer as cached sample.

To prepare for a new sample, CHIMRA goes through a process to make the interior as clean as possible. First, it dumps any remaining pre-sieve sample by opening up the scoop wide, then rocking and vibrating to encourage very last bit of sample that may have been lurking within the reservoir to exit the scoop. Then it opens the sample tunnel and 150-micrometer sieve and uses rocking and vibration to empty all of the loose material from that side. At that point, it's time for thwacking.

During ordinary operation of the primary thwack actuator, the sample tunnel opens on its own for the first few degrees. After 5° of opening, a cam inside the mechanism engages the primary thwack arm, which holds the 150-micrometer sieve. As the sample tunnel continues to open, the primary thwack arm follows it, maintaining the 5° separation and winding a spring. Toward the end of its range of motion, continued opening of the sample tunnel door passes a "point of no return," shortly after which its continued motion

disengages the latch holding the primary thwack arm to the sample tunnel. The coiled spring unwinds, slamming the primary thwack arm against the sample reservoir at very high speed, dislodging any material that may have been stuck in the holes of the sieve. The force of the thwack also dislodges material that was stuck to other interior surfaces of CHIMRA. CHIMRA follows a primary thwack with vibration and rocking to encourage any loosened material to exit out through the open scoop.

Secondary thwack works similarly. As the secondary thwack actuator opens the scoop, the secondary thwack arm follows the scoop for its first 10° of motion. Then a latch engages, holding the secondary thwack arm in place while the scoop continues to open, winding a spring. As the scoop reaches the end of its range of motion, the latch disengages, and the thwack arm slams against the scoop, dislodging any material that may have been stuck in its sieve and grate. Further rocking and vibrating activity cleans out any powder dislodged by the secondary thwack.

Note that the two thwack operations are designed to encourage material that may be wedged in a sieve to exit the sieve in the direction from which it arrived.

Before and after primary and secondary thwacks, the rover uses Mastcam to examine the interior surfaces of CHIMRA (Figure 5.13). Table 5.1 lists Mastcam images documenting the interior and exterior of CHIMRA. The only times that the cameras can get a clear look at the back sides of the two sieves, or of the interiors of the sample tunnel and bee trap, are after primary and secondary thwacks. After photographing the sieves and other parts, the primary and secondary thwack actuators close up CHIMRA, re-engaging the latches that hold the thwack arms close to the CHIMRA doors, and CHIMRA is ready to accept a new sample.

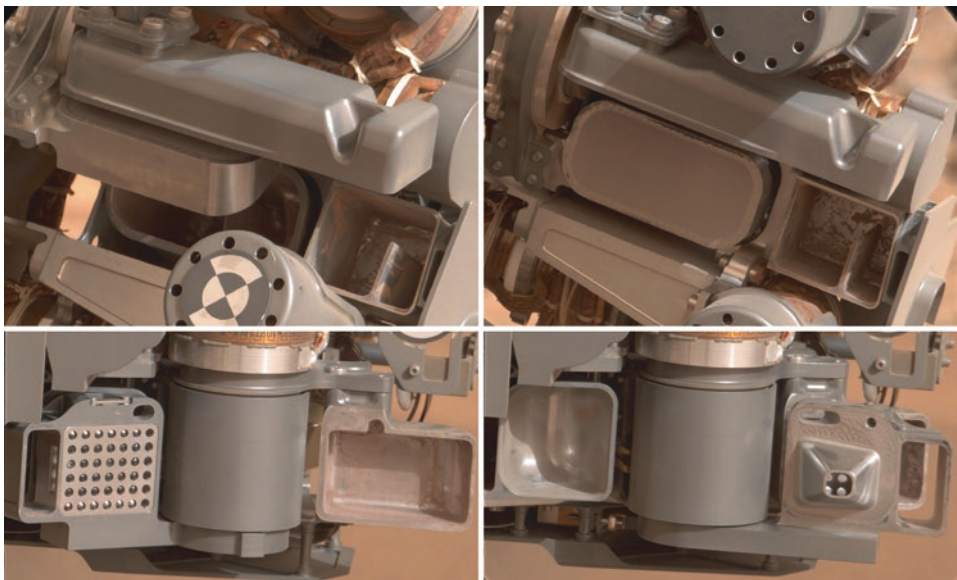


Figure 5.13. Pre-thwack (left column) and post-thwack (right column) views of the primary (top) and secondary (bottom) thwack mechanisms. Photos taken by Mastcam on sol 840. NASA/JPL-Caltech/MSSS.

Table 5.1. Sols of Mastcam and ChemCam RMI photos documenting CHIMRA activities to sol 1800. Images were taken with Mastcam unless ChemCam is specified.

Turret checkout	Sieve checkout	ChemCam RMI sieve checkout	Scooping activity	Pre- and post-sieve volume inspection	Drill bit assembly checkout
32 (all)	576	172 (partial)	61	79	128 1321
51 (all)	840	564 (focus test)	64	193	173 1327
65 (all)	1064		66	194	180 1332
73 (all)	1123	578	67	279	182 1359
81 (all)	1133	704	69	464	229 1361
128 (thwackless)	1142	840	70	623	486 1418
173 (thwackless)	1293	894	73	762	581 1419
486 (thwackless)	1535	1048	74	884	617 1420
576 & 578 (all)		1089	93	922	621 1422
581 (thwackless)		1133	411	1061	704 1457
704 (all)		1202	1224	1121	726 1459
781 (thwackless)		1293	1228	1139	756 1460
840 (all)		1327	1231	1224	759 1464
894 (all)		1359	1651	1228*	762 1491
954 (thwackless)		1419		1323**	781 1493
1048 (all)		1460		1334**	840 1494
1089 (all)		1494		1362**	867 1495
1132 (thwackless)				1425**	881 1533
1133 (all)				1465,1466***	882 1534
1202 (all)				1495,1496***	894 1535
1226 (secondary thwack only)					908 1536
1231 (secondary thwack only)					954 1537
1293 (primary thwack only)					1048 1541
1327 (all)					1059 1542
1359 (all)					1060 1543
1418 (thwackless)*					1089 1757
1419 (all)					1116 1780
1457 (thwackless)*					1119
1459 (secondary thwack only)					1132
1460 (all)					1133
1491 (thwackless)*					1134
1493 (secondary thwack only)					1137
1494 (all)					1202
1533 (thwackless)*					1226
1534 (secondary thwack only)					1231
1535 (all)					1293

Turret checkout: Photos of the interior and exterior of CHIMRA taken in initial checkout or after sample dumping. “All” indicates both primary and secondary thwacks were performed, and CHIMRA components imaged before and after each. Where only primary, only secondary, or no thwacking was performed, some components will not be visible. *After the primary thwack actuator anomaly on sol 1231, “thwackless” inspections performed after post-sieve sample dumping did not include motion of the primary thwack arm. **Scooping activity** includes scooping and manipulation of sample within the scoop. **Pre- and post-sieve volume inspection:** After sieving, the pre-sieve material (coarse fraction) is directed to the scoop for visual inspection, and the tunnel ramp cracked open to view the post-sieve material (fine fraction) in the portion box. *Sol 1228 includes inspection of a medium-size fraction). **After the problem with the primary thwack arm at Namib dune, they switched to examining both fractions in the scoop. ***Near Murray buttes, wind blew the dumped pre-sieve sample before APXS had a chance to examine it. They switched to dumping the sample and immediately performing an overnight APXS observation, following up with examination of the post-sieve sample in the morning.

5.4.5 Cached sample operations and doggie bagging

At Rocknest it quickly became apparent that if the rover couldn't drive while CHIMRA held sample, the mission could be stuck with a prolonged delay. The SAM team wanted to take many deliveries of sample, running their experiment in different ways each time. One option would be to perform many dropoffs to SAM sample tubes before driving away, a procedure called "doggie bagging." Curiosity does doggie-bag samples, but not many; the SAM team has to strike a balance between holding options open for future analyses and consumption of clean sample tubes.

The engineers came up with a workable solution: driving with cached post-sieve sample in the stowed turret. The clamshell happens to be positioned perfectly for long-term sample storage (with its opening upward) when the turret is stowed. There is sufficient room in the clamshell for 12 cubic centimeters of sample without spilling, provided that the rover's tilt does not exceed 20°. The limitations exist because sieved sample must not be allowed to fall onto the back side of the 150-micrometer sieve. Thwacking is a one-way operation designed to motivate particles out of the sieve toward the reservoir. Any particle that falls on the back of the sieve and clogs a hole would be further embedded by thwacking and likely stuck forever. After performing any cached-sample contact science with the arm, CHIMRA does a recovery sequence of rocking and vibrating to ensure that any sample that may have escaped the clamshell returns to it before the arm is stowed.

The limits for cached sample operations were developed very quickly, early in the mission, with many time pressures on the engineering team. Cached-sample operations required lots of extra arm motions to move the sample to different locations depending on the desired orientation of the turret, always preventing the sample from falling on the back side of the sieve. Later, the engineering team developed a new set of operational rules called evolved cached sample operations, which they first used on Mars on sol 1064. While protecting the safety of the CHIMRA system, the new rules allow some sample to fall on the back side of the sieve, requiring fewer arm motions and therefore less energy and time to run. This increases the flexibility of cached-sample operations.¹⁵

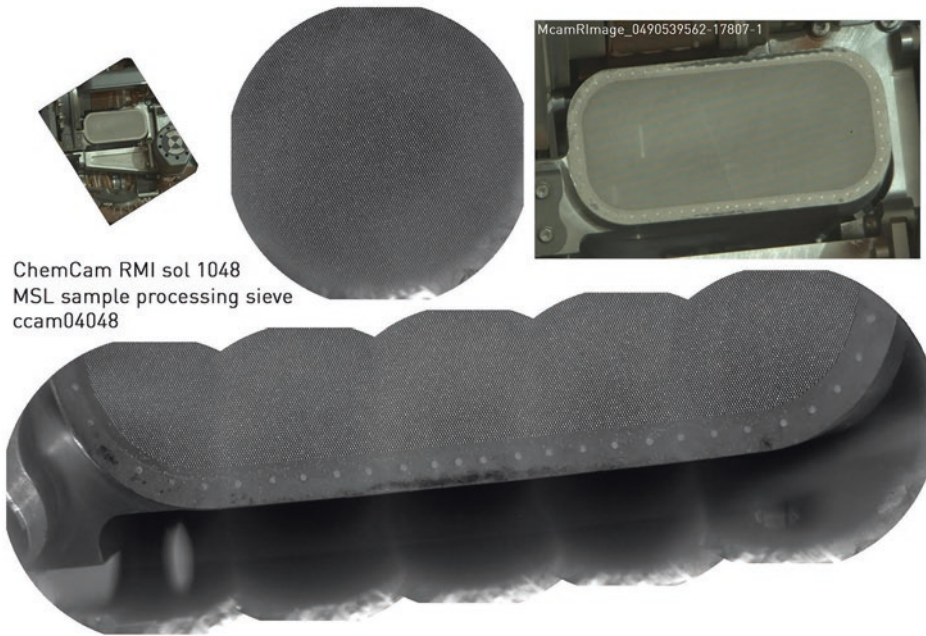
5.4.6 CHIMRA concerns and anomalies

CHIMRA has mostly functioned as designed – quite a coup for such a complicated piece of equipment, the likes of which has never before been sent to another planet. There are two issues affecting its use: concern about its 150-micrometer sieve, and a problem with the primary thwack actuator.

5.4.6.1 150-micrometer sieve edge weld separation

Originally, three identical CHIMRA devices were built. One is now on Mars, one is on the testbed rover, and one was tested to failure on Earth in the Qualification Model Dirty Testbed (see section 4.7.4). After performing about 130 primary thwacks with the test unit, the edge

¹⁵Vandi Verma, personal communication, email dated April 1, 2017



ChemCam RMI sol 1048
MSL sample processing sieve
ccam04048

Figure 5.14. ChemCam RMI inspection of the 150-micrometer sieve performed on sol 1048. NASA/JPL-Caltech/CNES/CNRS/LANL/IRAP/IAS/LPGN/mosaic by William Rapin.

welds that hold the 150-micrometer sieve onto the primary thwack arm began to pop apart, creating a gap through which larger particles could leak into the sieved sample.¹⁶

To prevent the degradation of the edge welds on the flight unit of the 150-micron sieve, engineers now command primary thwacks only when preparing for a new sample. After some primary thwacks, they use ChemCam to perform a detailed inspection of the edge welds and the sieve, including angling the sieve to direct a specular reflection at the cameras in order to search for any deformation (Figure 5.14). Table 5.1 lists all sols on which ChemCam inspection of the sieve was performed.

5.4.6.2 Drill sample cross-contamination

Transfer of material from drill to CHIMRA was originally intended to be done with some drill percussion. Following the sol 911 drill percussion anomaly (section 5.3.4.2), engineers developed a method to perform sample transfer with limited percussion. However,

¹⁶Dan Limonadi, personal communication, email dated February 2, 2013

continued testing suggested that this new method did not empty the drill sample chamber as effectively as before, increasing the risk that sample material from a previous site might cross-contaminate a new sample. Indeed, CheMin results suggest Buckskin sample cross-contaminated the Big Sky sample, although there could be other explanations (section 9.4.4). Engineers experimented with a new non-percussion sample transfer method on Mars on sols 1460 and 1494 to reduce cross-contamination risk.¹⁷

5.4.6.3 Primary thwack actuator anomaly

On sol 1231, during routine sample processing, the primary thwack arm stalled. After sieving, Curiosity typically cracks open the primary thwack arm to peek into the portion box to estimate how much sample is inside. This time, it stalled after opening only 1°. Cautious testing since then has seen the actuator operate fairly normally without stalling. (They tested cautiously because if the primary thwack arm were to fail in a wide-open position, it would no longer be possible to sieve a fine fraction, making it difficult to prepare samples for delivery to CheMin.) Testing included extra imaging of primary thwack arm motion on sols 1237–1243.

Engineers have reduced use of the primary thwack arm in order to avoid faults. They no longer crack open the primary thwack arm to inspect the post-sieved sample. Since Lubango (drilled sol 1324), they drill, inspect the pre-sieve (coarse) fraction of the sample in the scoop, immediately dump this fraction, transfer the post-sieve (fine) fraction to the scoop, and visually inspect it there, thereby shifting the workload to the secondary thwack actuator rather than the primary thwack actuator.

5.5 DRT: DUST REMOVAL TOOL

The dust removal tool is a brush for cleaning rock surfaces before they are studied with MAHLI, APXS, or Mastcam’s narrowband filters. It consists of two wire brushes, driven by a single motor (Figure 5.15).¹⁸ When Curiosity landed, functions related to the use of the brush had not yet been tested on Earth, so its first use was on sol 150. Initially, rover planners inspected the brush only after brush operations. On sol 291, following the third brushing operation, at Cumberland, they discovered that one set of bristles was bent (Figure 5.15, middle row), leading to concern that the bent wire bundle could wrap around the brush’s central spindle during brush operations. The mission halted use of the brush and began a period of extensive Earth testing. The brush was not cleared for use on Mars until arrival at the next drill site, Windjana, and didn’t see routine use until arrival at Pahrump Hills. Since then, they have imaged the brush both before and after each operation, and no further degradation in the brush bristles has been observed (Figure 5.15, bottom row). Table 5.2 lists all brush sites up to sol 1514.

¹⁷Ashwin Vasavada, personal communication, email dated November 17, 2017

¹⁸There is no published paper about the DRT hardware. Information in this section comes from a paper mentioning the DRT software by Kim (2013) and personal communication with Ashwin Vasavada (email dated February 9, 2017).

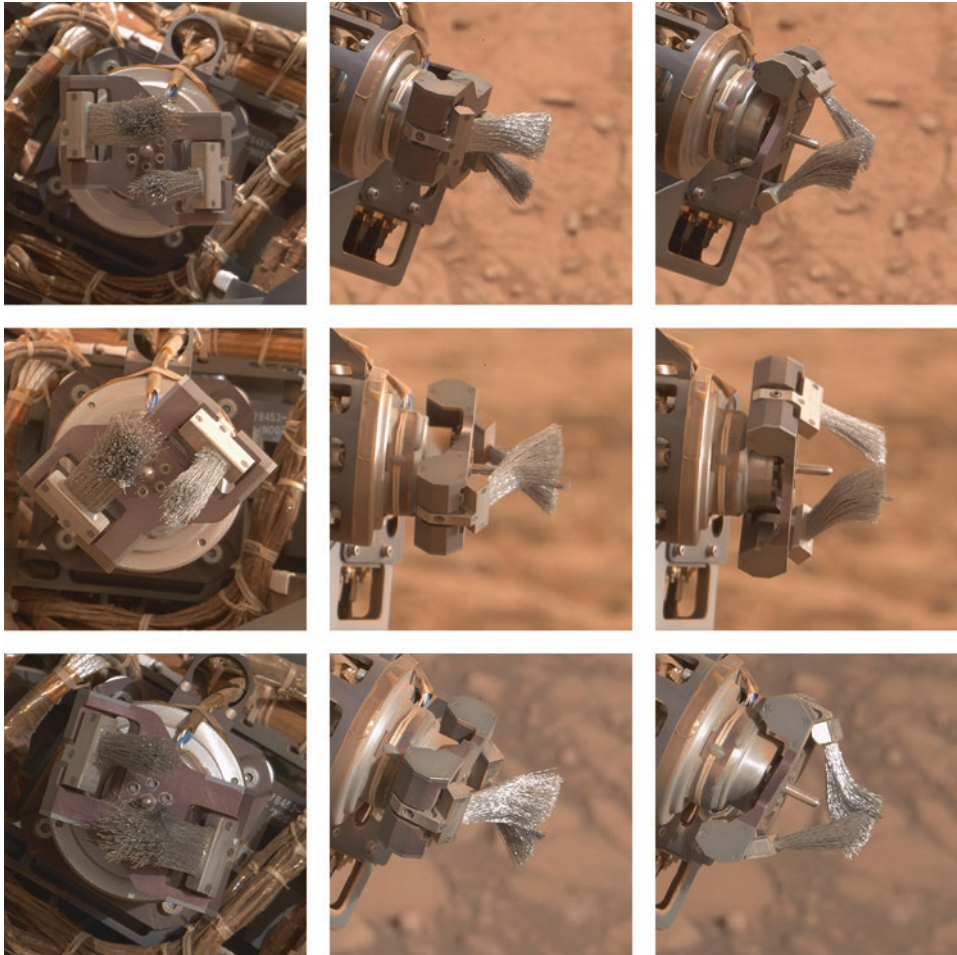


Figure 5.15. Condition of the dust removal tool (DRT) over time, as seen in standard right Mastcam engineering support imagery. Top row: after its first use on sol 150. Middle row: after the third use, at Cumberland, when one wire bristle was discovered to be bent. Bottom row: after more than 50 uses, on sol 1416, at Chibia. NASA/JPL-Caltech/MSSS.

The motor speed can be changed during a single brush operation, and the robotic arm can be moved while the brush is running to sweep an elongated area. If Curiosity were to hold the brush in one position during use, the brushing action would leave an unbrushed spot in the center. So Curiosity moves the arm while brushing to sweep out the center, creating an oval spot. The entire brushed area is contained within a 60-millimeter circle.

Figure 5.16 shows two different kinds of brushed spots. The size of the brushed spot depends upon how close the brush gets to the surface. Originally, Curiosity brushed at a height of 1 centimeter, which produced a brushed spot about 46 millimeters in diameter. Concern that the bristles could wrap around the center post following the discovery of the bent bristles led them to use a higher standoff of 1.5 centimeters thereafter, which

Table 5.2. Summary of dust removal tool (brush) to sol 1806. List courtesy Ken Edgett.

Bradbury Group	Pahrump Hills	North of the dunes	Among the dunes	South of the dunes
150 Ekwir	722 Bonanza	975 Albert	1358 Oudam	1681 Duck Brook
169 Wernecke	King	998 Ronan	1366 Auberes	Bridge
291 Cumberland	755 Maturango	999 Wallace	1380 Koes	1695 Mason Point
612 Windjana	758 Moenkopi	1057 Buckskin	1416 Chibia	1702 Fern Spring
	767 Morrison	1092 Ledger	1418 Marimba	1710 White Ledge
	805 Pelona	1105 Winnipeg	1436 Conda	1715 Timber Point
	806 Ricardo	1109 Cody	1444 Ganda	1736 Winter Harbor
	808 Rosamond	1114 Big Sky	1474 Jwaneng	1744 Mingo
	809 Mojave	1119 Big Sky 2	1477 Catumbela	1806 Robinson Rock
	813 Punchbowl	1130 Greenhorn	1484 Serowe	
	814 Afton	1157 Augusta	1491 Sebina	
	Canyon	1166 Swartkloofberg	1511 Penobscot	
	815 Topanga	1245 Kudis	1523 Sutton	
	819 Mescal	1251 Kuiseb	Island	
	824 Puente	1259 Gorob	1531 Precipice	
	828 Pickhandle	1266 Stockdale	1586 Belle Lake	
	830 Goldstone	1273 Schwarzrand		
	844 Santa Ana	1275 Mirabib		
	853 Tecoya	1279 Khomas		
	880 Mojave 2	1287 Sesriem		
	905 Telegraph	Canyon		
	Peak	1293 Brukkaros		
	936 Hyrum	1300 Bero		
		1318 Lubango		
		1330 Okoruso		
		1341 Kwakwas		
		1348 Meob		
		1355 Inamagando		

produces a brushed spot about 40 millimeters in diameter. Either way, the cleared area is slightly wider than the field of view of APXS, so even with positioning uncertainty, APXS's field of view will be entirely in the brushed area.

When the brush interacts with very soft rocks, the wire bristles may scratch the surface. If the rock is extremely soft, wires near the center can get hung up on a protuberance and actually drill into the rock (see Figure 5.17 for an example).

5.6 ORGANIC CHECK MATERIAL

A palette on the front center of the rover contains 5 cylinder-shaped bricks of hermetically sealed organic check material provided by the SAM team (Figure 5.18).¹⁹ It is intended to check the cleanliness of the whole SAM sample processing pathway, to ensure that any

¹⁹Conrad et al (2012)



Figure 5.16. Moenkopi (left), brushed on sol 758, was a raised feature. Maturango (right), brushed sol 755, was a flat spot, and the brush was moved during brushing. The Confidence Hills drill site is in the background. Drill holes are 16 mm across; brushed spots are at least 45 mm across. Left Mastcam image 0758MH0001900010204611C00. NASA/JPL-Caltech/MSSS.

organic materials detected by SAM in Martian material really do come from Mars and are not Earthly contamination left behind on the external parts of the sample processing chain: the drill, CHIMRA, and sample inlets. The five bricks are identical. They are composed of a ceramic that has been doped with a minute amount of fluorinated hydrocarbon chemical that can be detected by SAM. Each brick is covered with a foil seal. It can be drilled and sampled just like a rock, and the sample dropped into SAM. Drilling it breaks the seal, so each brick can be used only once. Figure 5.19 shows how the rover would position the drill on one of the bricks for sampling.

The organic check material has not yet been used. (For more information, see 9.5.1.12.) The team tested the process of positioning the drill to sample the organic check material on sols 34 and 1076, taking images with MAHLI to document turret positioning (Figure 5.19). They also performed imaging of the organic check material with the MAHLI cover closed on sol 1416.

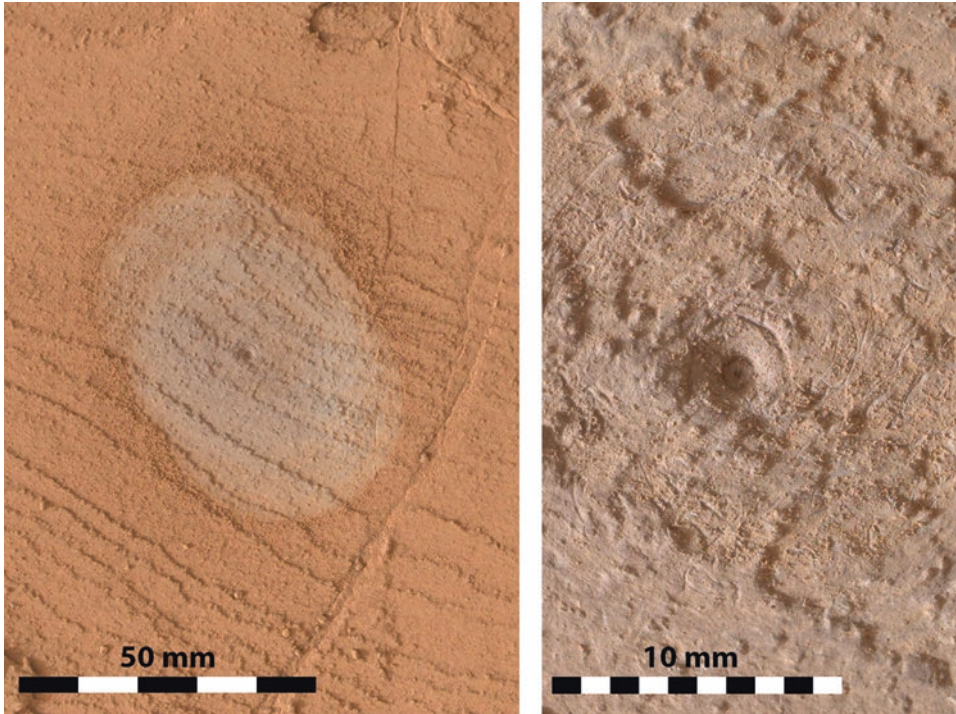


Figure 5.17. Scratches and drilling near the center of a brushed spot at Pelona, at the Pahrump Hills site, sol 805. MAHLI images 0805MH0001900010300492C00 and 0805MH0003070010300514C00. NASA/JPL-Caltech/MSSS.

5.7 SAMPLE PLAYGROUND

Immediately in front of the mast is a suite of tools intended to allow the rover to study the properties of drilled or scooped sample. This “sample playground” was a late addition to the rover design, added after the experience of the Phoenix mission, which had a difficult time handling clumpy Martian materials (see section 1.5.11).²⁰ The sample science team looked at how their mature design might be vulnerable to clumpy soil, and developed a set of tools to help them investigate sampled material before committing to delivering it to CheMin and SAM.

The sample playground comprises the science observation tray, engineering tray, CheMin surrogate funnel and soil capture plate, dust removal tool scratching post, and two portion pokers (Figure 5.20). Sols in which science cameras were used to image parts of the sample playground are listed in Table 5.3, but the playground is also often captured in Mastcam and Navcam views of the work volume, and in MAHLI self-portraits.

The science observation tray, also known as the “O-tray”, is a circular titanium plate 75 millimeters wide. The rover can drop portions of drilled or scooped sample onto it for

²⁰Anderson et al (2012)

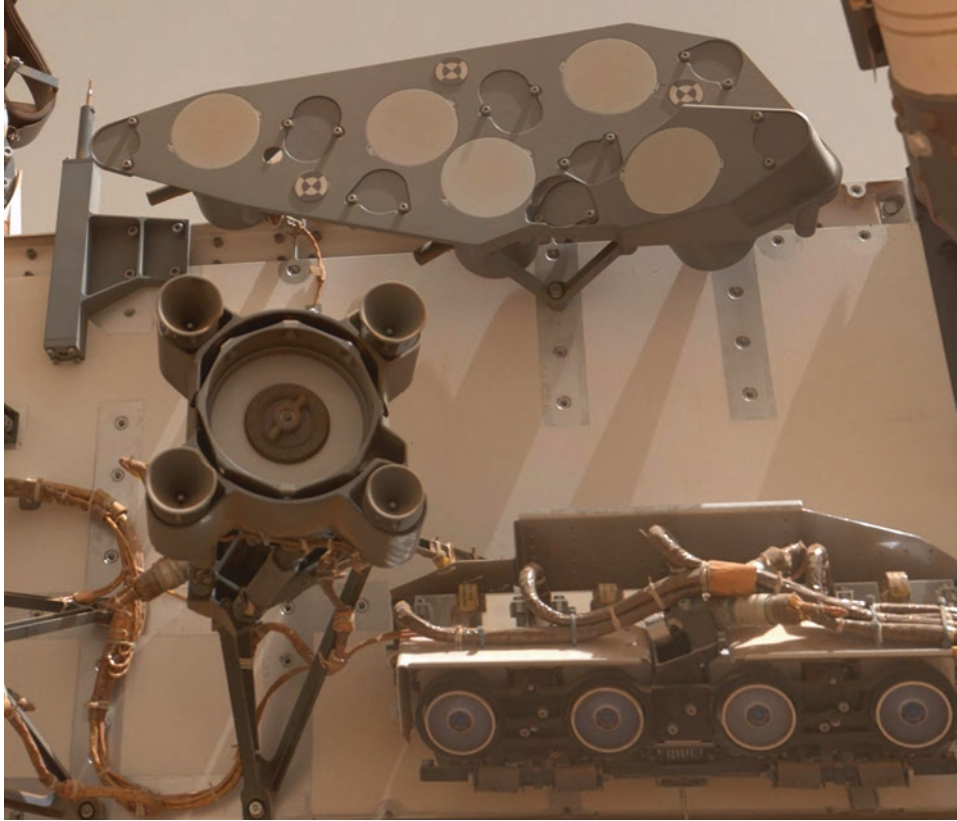


Figure 5.18. The organic check material mounting plate bolted to the front center of the rover contains five foil-capped cylinder-shaped bricks of ceramic material. Between the five bricks are smaller drill positioning pads, places for the drill contact stabilizers to press during drilling. Below the mounting plate is one of the two spare drill bit boxes and the four front Hazcams. Mosaic of four MAHLI self-portrait frames taken on sol 1065. NASA/JPL-Caltech/MSSS.

investigation with APXS, MAHLI, and mast-mounted cameras. It was intended to provide a surface of known composition on which to perform APXS observations of sampled material. Unfortunately, vibration from CHIMRA, necessary for portion delivery, appears to transfer through the rover arm to the body and cause delivered portions to “walk” off of the sample tray (see Figure 5.20 for an example). This behavior, which is much worse on Mars than it was in the Earth testbed, has prevented much use of the observation tray for science. The APXS team has developed a different method of measuring the composition of drilled materials by studying the composition of pre- and post-sieve dump piles. The APXS team has also occasionally taken advantage of the vibration-induced cleaning of the observation tray to perform measurements of the composition of airfall dust.

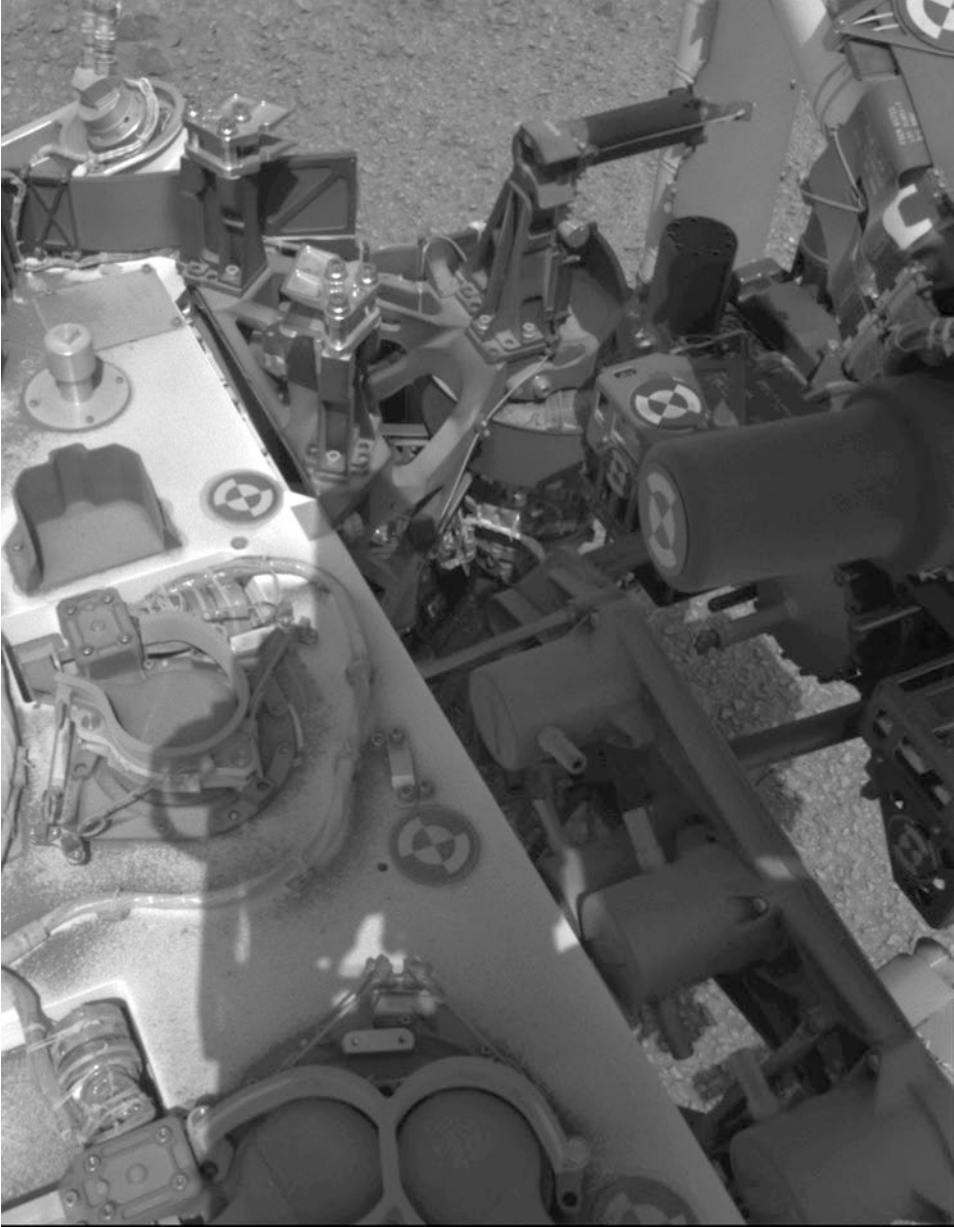


Figure 5.19. A test of the drill's positioning on one of the organic check material bricks. From this point of view, you can see the tubular inlet and outlet ports that allowed the SAM team to dope the ceramic bricks with a fluorinated compound after they were sealed in their can-shaped housings. Navcam image NLB_493020688RAD_LF0490814NCAM00467M1, sol 1076. NASA/JPL-Caltech.

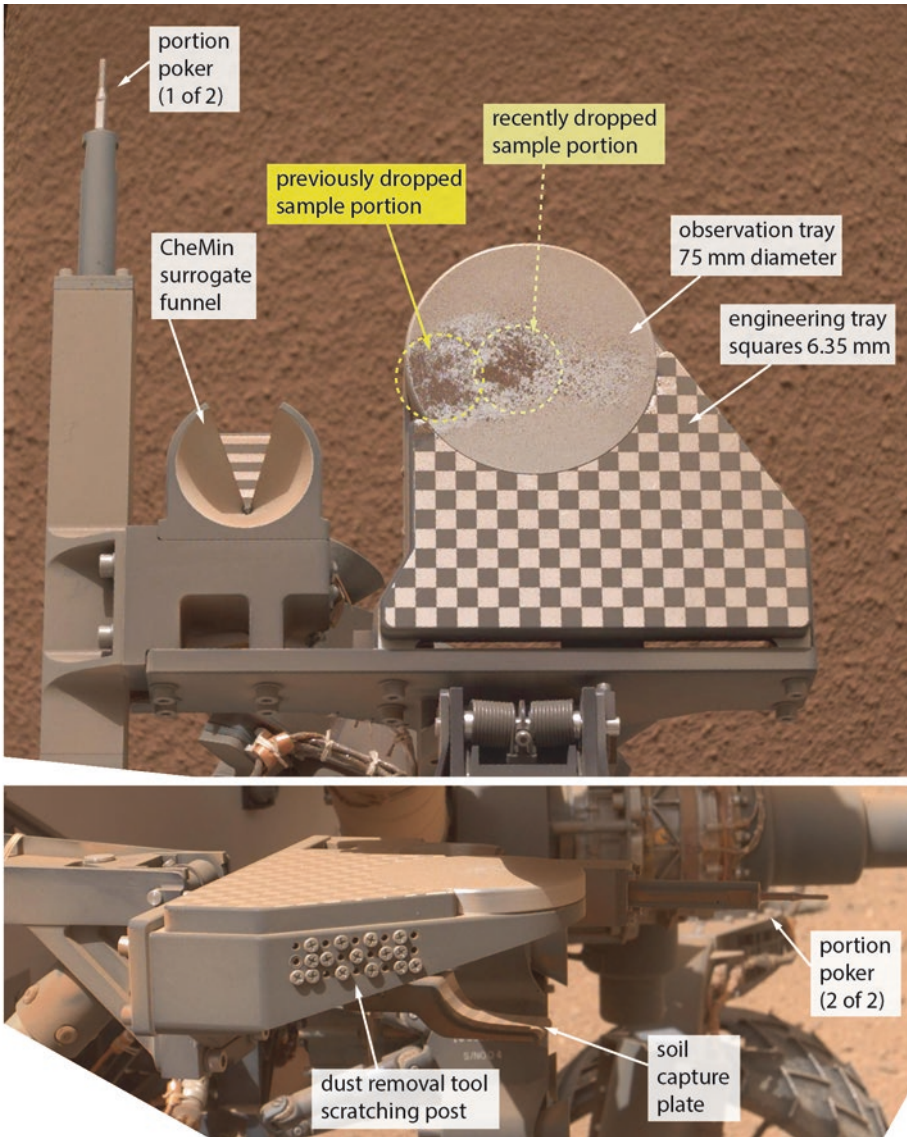


Figure 5.20. Parts of the sample playground seen from above by Mastcam and from the right side by MAHLI. In the top image, two portions have been dropped to the center of the observation tray. CHIMRA vibration transferred through the arm to the rover body has caused the first portion to “walk” off the tray during delivery of the second portion. Delivery of both portions has also shifted some of the accumulated dust off of the tray. Mastcam image ML0005780000102730E01 and MAHLI image 0544MH0003460000201460C00. NASA/JPL-Caltech/MSSS/Emily Lakdawalla.

Table 5.3. Sols with targeted imaging of the sample playground (mostly of the observation tray).

Mastcam	MAHLI
70	37
76	73
77	93
78	95
79	177
81	544
95	571
284	572
289	

The rest of the sample playground elements have not been used on Mars. The engineering tray, located closer to the rover body than the observation tray, has a checkerboard pattern made of 0.25-inch (6.35-millimeter) squares. It was intended for use in estimating the volume of portions dropped to SAM and CheMin. To the left is the CheMin surrogate funnel and soil capture plate. If there are concerns about soil clumping and potentially clogging the CheMin inlet funnel, the drop can be tested with the surrogate funnel. On the right side of the engineering tray, a palette of screw heads provides a place to clean off the DRT in the event that Martian material clings to its brushes. Finally, two portion pokers, one pointing vertically and one horizontally, provide Curiosity with the capability to poke out the CHIMRA portion hole if it should become clogged with material. However, the inverted funnel shape of the CHIMRA portion hole makes it very unlikely that material could pass all the way through CHIMRA and then clog the portion hole; the portion pokers have not been used and hopefully never will be.

5.8 SAM AND CHEMIN INLETS AND WIND GUARDS

The final elements in the sample delivery chain are the motorized sample inlets on the top of the rover deck. Three flaps (two for SAM's inner and outer carousel rings, and one for CheMin) open and close to allow CHIMRA to deliver portions. Mastcam shoots photos of the inlets before and after each delivery in order to check whether wind blew the sample away from the inlet and deposited it on the deck nearby. The rover also uses MAHLI to image the fine mesh grate over the open CheMin sample inlet from time to time, often at night, when the MAHLI LEDs can be used as flashlights to evenly illuminate the interior. The goal of this imaging is to check for clogging by excessively large particles. All these imaging activities are summarized in Table 5.4.

An amusing side effect of the repeated imaging of the sample inlets is that it has been possible to track the motions of bits of gravel on the rover deck over the course of the landed mission (Figure 5.21). This gravel was tossed onto the deck during landing and has rattled around the top surface ever since, occasionally drawing squiggly lines in accumulated deck dust.

The difficult experiences of sample delivery in the Phoenix mission caused engineers to be concerned about wind blowing Curiosity's tiny sample portions away. To mitigate against this possibility, they added spring-loaded collars around the sample inlets, and a corresponding plate over the CHIMRA portion hole. In the event that wind dispersal of

Table 5.4. Imaging of the CheMin and SAM inlet ports by Mastcam and MAHLI to sol 1800.

CheMin inlet (Mastcam)	CheMin inlet (MAHLI)	SAM inlets (Mastcam)	SAM inlet (MAHLI)
14	36	14	93
51	74	90	96
71	81	93	282
94	94	96	
195	195	114	
282	282	116	
623	411	117	
765	558	196	
884	564	224	
922	666	227	
1061	774	281	
1121	895	286	
1139	1028	290	
1226	1064	353	
1323	1091	367	
1334	1123	381, 382	
1362	1136	413, 415	
1375	1142	463, 464	
1425	1184	624	
1466	1259	653	
1496	1287	694	
	1324	773	
	1337	887, 888	
	1348	891	
	1364	892	
	1375	928	
	1402	954	
	1427	1075	
	1438	1129	
	1459	1147	
	1466	1178	
	1470	1224	
	1477	1230	
	1484	1231	
	1489	1233	
	1496	1382	
		1409	
		1443	
		1456	
		1651	

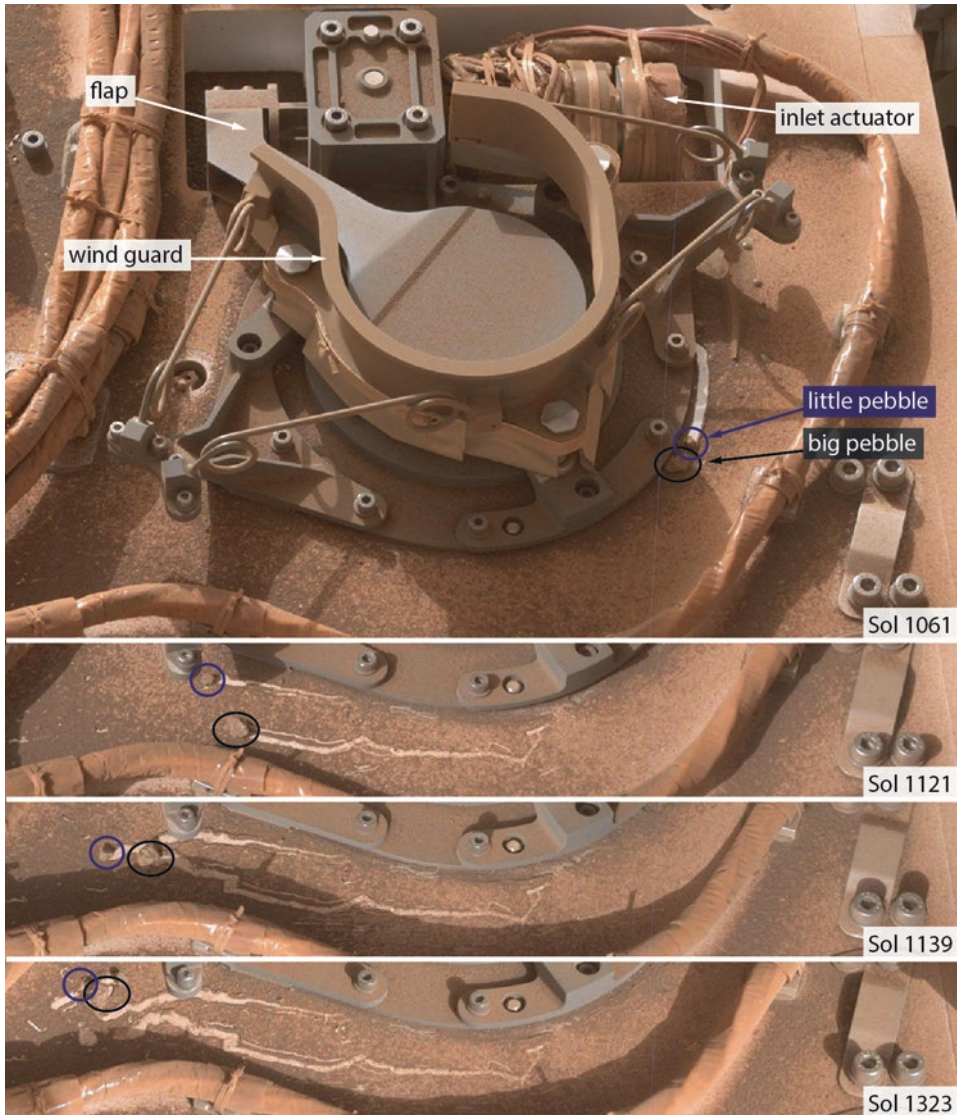


Figure 5.21. CheMin inlet and wind guard as seen from Mastcam. Pebbles that have been on the deck since landing leave tracks as the rover's motion vibrates them across the deck. NASA/JPL-Caltech/MSSS/Emily Lakdawalla.

sample is found to be a problem, the engineers can deliver sample with the portion plate pressed against a wind guard. This capability has not been used. Mastcam videos of portion delivery recorded on sols 64, 78, 284, and 289 showed the portions dropping straight down for a distance longer than the few centimeters separating the portion hole and sample inlets. The mission has also taken advantage of REMS wind data to select times of day for sample delivery when winds are expected to be minimal.

5.9 REFERENCES

- Anderson R et al (2012) Collecting samples in Gale crater, Mars: an overview of the Mars Science Laboratory Sample Acquisition, Sample Processing and Handling System. *Space Sci Rev* 170:57–75, DOI: 10.1007/s11214-012-9898-9
- Billing R and Fleischner R (2011) Mars Science Laboratory robotic arm. Paper presented to the 14th European Space Mechanisms and Tribology Symposium, 30 Sep 2011, Constance, Germany
- Conrad P et al (2012) The Mars Science Laboratory organic check material. *Space Sci Rev* 170:479–501, DOI: 10.1007/s11214-012-9893-1
- Grotzinger J et al (2014) A habitable fluvio-lacustrine environment at Yellowknife Bay, Gale Crater, Mars. *Science* 343, DOI: 10.1126/science.1242777
- Kuhn S (2013) Curiosity’s scoop campaign, a summary. <http://www.planetary.org/blogs/guest-blogs/curiositys-scoop-campaign-kuhn.html> Article dated 8 Jan 2013, accessed 6 May 2016
- JPL (2014) Lesson Learned: Recognize that Mechanism Wear Products May Affect Science Results. <http://llis.nasa.gov/lesson/10801>. Article dated 8 Jun 2014, accessed 14 Oct 2015
- Kim W et al (2013) Mars Science Laboratory CHIMRA/IC/DRT flight software for sample acquisition and processing. Paper presented to the 8th International Conference on System of Systems Engineering, 2–6 Jun 2013, Maui, Hawaii, USA
- Lakdawalla E (2017) Curiosity update, sols 1548–1599: Serious drill brake problem as Curiosity drives through Murray red beds. <http://www.planetary.org/blogs/emily-lakdawalla/2017/02031109-curiosity-update-sols-1548-1599.html> Article dated 3 Feb 2017, accessed 9 Feb 2017
- Limonadi D (2012a) Sampling Mars, part 1: The hardware. <http://www.planetary.org/blogs/guest-blogs/20120816-limonadi-sampling-mars-1-tools.html> Article dated 16 Aug 2012, accessed 26 Feb 2016
- Limonadi D (2012b) Sampling Mars, part 3: Key challenges in drilling for samples. <http://www.planetary.org/blogs/guest-blogs/20120821-limonadi-sampling-mars-3-drilling-challenges.html> Article dated 21 Aug 2012, accessed 6 May 2016
- Manning R and Simon W (2014) *Mars Rover Curiosity: An Inside Account from Curiosity’s Chief Engineer*. Smithsonian Books, Washington DC
- Novak K et al (2008) Mars Science Laboratory rover actuator thermal design. Presentation to the Spacecraft Thermal Control Workshop, 11–13 Mar 2008, El Segundo, California, USA, DOI: 10.2514/6.2010-6196
- Okon A (2010) Mars Science Laboratory Drill. Paper presented to the 40th Aerospace Mechanisms Symposium, 12–14 May 2000, NASA Kennedy Space Center
- Sunshine D (2010) Mars Science Laboratory CHIMRA: A device for processing powdered Martian samples. Paper presented to the 40th Aerospace Mechanisms Symposium, 12–14 May 2010, NASA Kennedy Space Center

6



The Mast, Engineering Cameras, Navigation, and Hazard Avoidance

6.1 INTRODUCTION

The Curiosity mission navigates Mars using a combination of human and artificial intelligence. Both methods rely upon a suite of engineering cameras for situational awareness. The twelve engineering cameras are in six pairs: two redundant pairs each of Navcams, front Hazcams, and rear Hazcams. A remote sensing mast lifts the four Navcams nearly two meters above the Martian surface, while the eight Hazcams are mounted at belly height, four facing forward and four to the rear. The Hazcams and Navcams are flight spares or build-to-print copies of the engineering cameras of the same names on the Mars Exploration Rovers; this not only saved money in hardware, but made it significantly easier to use a modified version of the same rover driving software for Curiosity as for Spirit and Opportunity. The mast also carries the Mastcams and parts of the ChemCam and REMS instruments. Both Navcams and Hazcams are routinely used to gather data for environmental science purposes.

6.2 REMOTE SENSING MAST

Curiosity's vantage point is a bit higher than most humans'. From the Navcams' position at 1.9 meters above the Martian surface, Curiosity can see quite far: if the landing site were perfectly flat, the horizon would be 3.6 kilometers away. Of course, Curiosity sits inside a crater, and topography rises above the horizon as far as the rover can see. The nearest foothills of Gale crater's central mound were about 5 kilometers from Curiosity on landing day. The nearest point on Gale's rim was 20 kilometers to the north; to the east and west, the visible rim is more like 40 kilometers away. All of this topography is usually visible in Curiosity images of the horizon, although the crater rim and sometimes even the central mountain disappear and reappear over time as the amount of dust in the air waxes and wanes.

The Remote Sensing Mast (RSM) has three motors, of which one, the mast deploy actuator, was used only once to lift the mast permanently to its vertical position.¹ The mast's azimuth and elevation actuators are mechanically capable of panning 362° horizontally and tilting 182° vertically in order to point cameras at every possible target within Curiosity's view. The elevation mandrel and azimuth twist cap allow the cabling to flex as the mast tilts and rotates. Software prevents the mast from rotating to hard stops, limiting it to panning 360°. Software also limits how far down it can tilt, preventing it from pulling on the cable bundle that runs up the mast to the mast head, reducing its tilt limit by 4°. Thus its tilt can be commanded from -87 to $+91$ °. Two booms containing REMS instrument components are mounted to the mast below the actuators, so their positions are fixed (Figure 6.1).

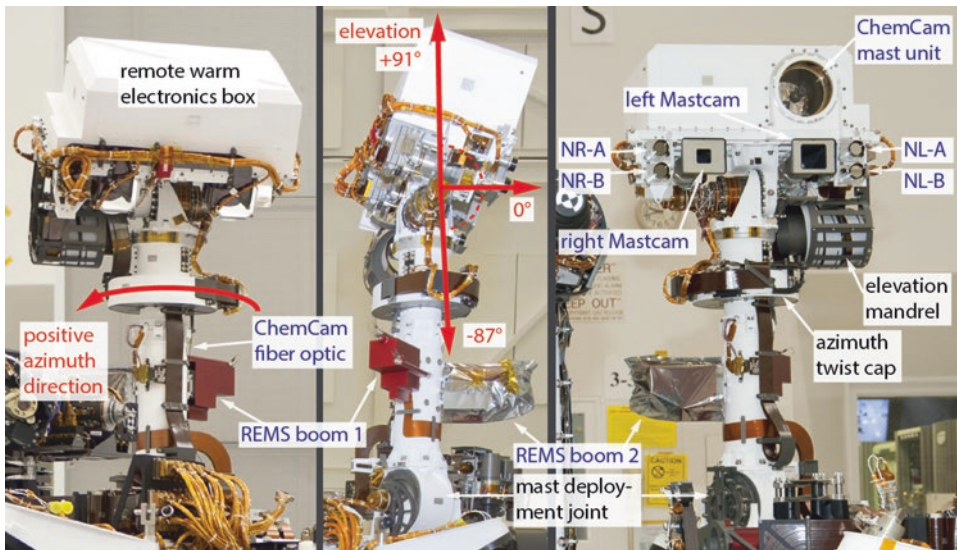


Figure 6.1. Parts of the remote sensing mast as seen in photos taken during assembly at JPL in 2011. The mast is about one meter tall. In this photo, the two REMS booms are covered for their protection; the covers were removed before flight. NR-A, NL-A, NR-B, and NL-B refer to the right and left Navcams connected to the A-side and B-side computers. NASA/JPL-Caltech/Emily Lakdawalla.

¹The mast and engineering cameras are described in Maki et al. (2012)

The mast has to be able to point incredibly precisely in order for ChemCam to zap targets selected within Navcam images. The mast's absolute pointing accuracy is 0.25° (4.6 milliradians), or about 6 Navcam pixels; but its pointing is repeatable to less than a single Navcam pixel. This pointing precision has enabled Curiosity to perform sharp-shooting feats like profiling down the side of drill holes (Figure 6.2).



Figure 6.2. ChemCam laser shots are spaced using minute motions of the remote sensing mast. Here, ChemCam laser shots are spaced 1.4 mm apart horizontally in rasters marching down the wall of the Okoruso drill hole. Drill holes are 1.6 centimeters in diameter, and this one was 2.6 meters away from the mast head when the shots were fired. Corresponding mast shot-to-shot angular motion was 0.03° (0.5 milliradians). MAHLI image 1338MH0005880000501506R00, taken at night with LEDs on. Contrast in the image has been increased to emphasize the laser shot points. NASA/JPL-Caltech/MSSS/Emily Lakdawalla.

6.3 ENGINEERING CAMERAS: NAVCAMS AND HAZCAMS

The Navcams are located approximately 1.9 meters from the ground when the rover is level, but their precise elevation depends upon the tilt of the mast head. They are spaced a very wide 42.4 centimeters apart, which gives them depth perception out to a distance of 100 meters. That helps engineers plan long blind or visual odometry drives, the most time-efficient driving modes, as long as the Navcams have a good view of the path ahead. Figure 6.1 shows the positions of all the Navcams. The switch from A-side to B-side cameras after sol 200 moved the rover's Navcam vantage point downward by 4.8 centimeters.

The fish-eye Hazcams provide Curiosity with situational awareness of the terrain both forward and aft of the rover and in between the wheels, particularly in areas not visible to the Navcams. The Hazcams are hard-mounted to the rover so have fixed fields of view. Figure 6.3 shows the locations of all the Hazcams. They are boresighted 45° below the horizon, with 120° field of view vertically, and 180° corner-to-corner. Because of the wide view, raw Hazcam images are very distorted. The front Hazcams are mounted near the middle of the front of the rover, with the A-side and B-side cameras interleaved, each offset from the next by 8.2 centimeters, giving a stereo separation of 16.4 centimeters for each pair. The front Hazcams provide detailed stereo maps of the area within reach of the robotic arm.

When Curiosity switched to the B-side computer, the front Hazcam view of the world shifted to the rover's left by 8.2 centimeters, resulting in a view that is more obscured (primarily by the shoulder elevation actuator) than the previous view was (Figure 6.4). The rear Hazcams are mounted on either side of the RTG in two pairs spaced 10 centimeters apart, with the A-side rear Hazcams on the rover's left side and the B-side rear Hazcams to the rover's right, separated by 1 meter. So when Curiosity shifted to the B-side computer, the rear view seemed to shift left by 1 meter. The new rear view is not substantially different in quality from the old view.

The Navcams and Hazcams have identical detectors, 1024 pixels square. It takes 5.4 seconds to read out a single full-frame image. Rover planners can improve that speed by binning the images or by reading out partial, "windowed" (cropped) images. The cameras are sensitive to light in the 600 to 800 nanometer range – slightly longer-wavelength than human color vision, and similar to the red filter on the Mastcams (Figure 6.5). Only two of the six cameras can be powered simultaneously. So stereo pairs are usually taken at the same time, but front and rear Hazcam pairs have to be taken sequentially.

Navcam images of the path ahead and arm workspace are decisional data, required to plan later sols (see section 3.3). It can be tricky to squeeze all the necessary data into the first available downlink, especially if a drive happens late in the sol after the Mars Reconnaissance Orbiter communications pass so only an Odyssey pass is available. Compressing the images reduces file sizes, which allows more images to be returned to Earth. But lossy compression reduces data quality, potentially affecting the quality of the range information that rover drivers use to plan driving and arm positioning. So images that are used for generating range maps are compressed very little, while other images taken only for documentation purposes (for instance, to verify the placement of the robotic arm) are compressed much more.

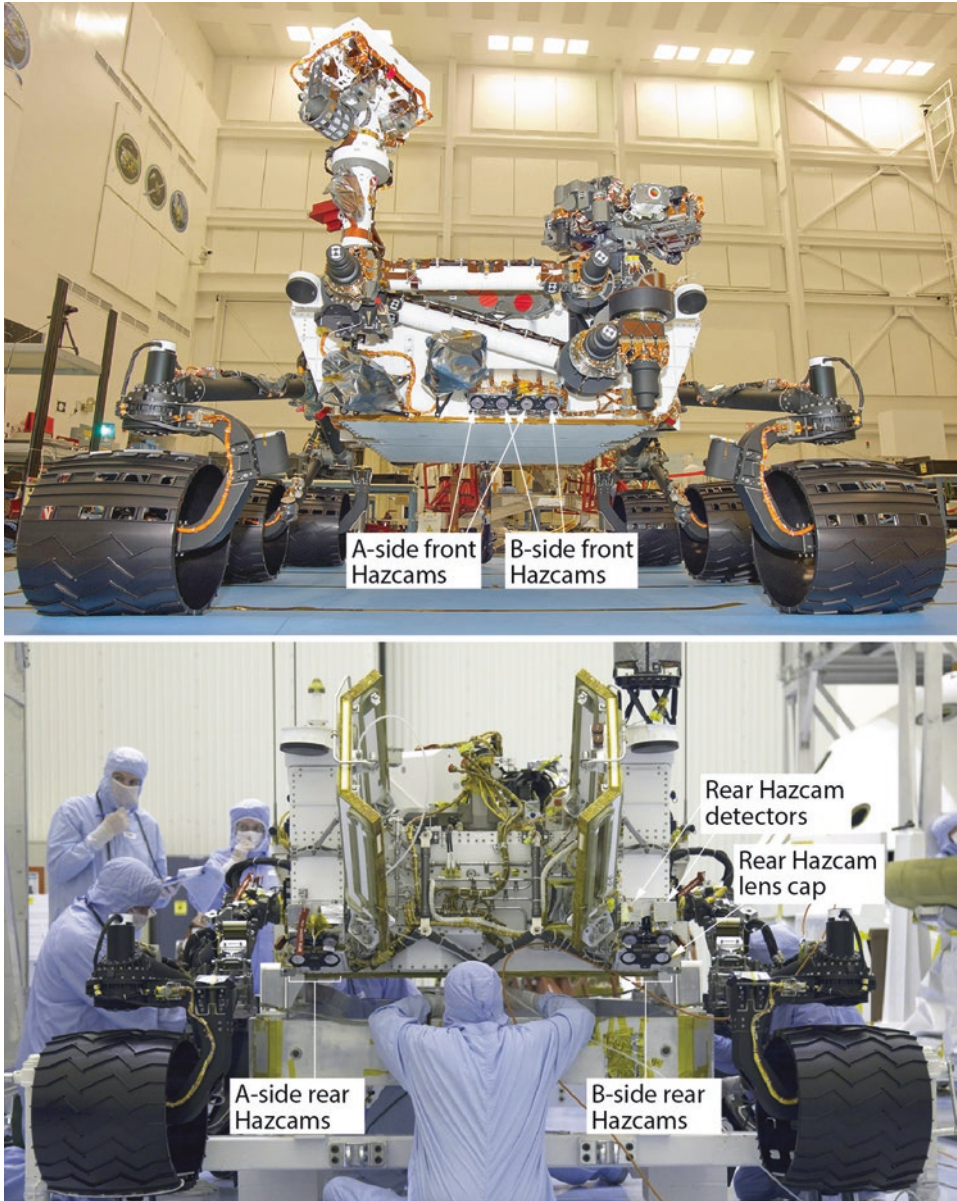


Figure 6.3. Locations of the Hazcams. Top image taken during JPL mobility testing on 3 June 2011. NASA/JPL-Caltech image release PIA14254. Bottom image taken at arrival of the rover at Kennedy Space Center. Credit: NASA/Frankie Martin, release KSC-2011-5909.

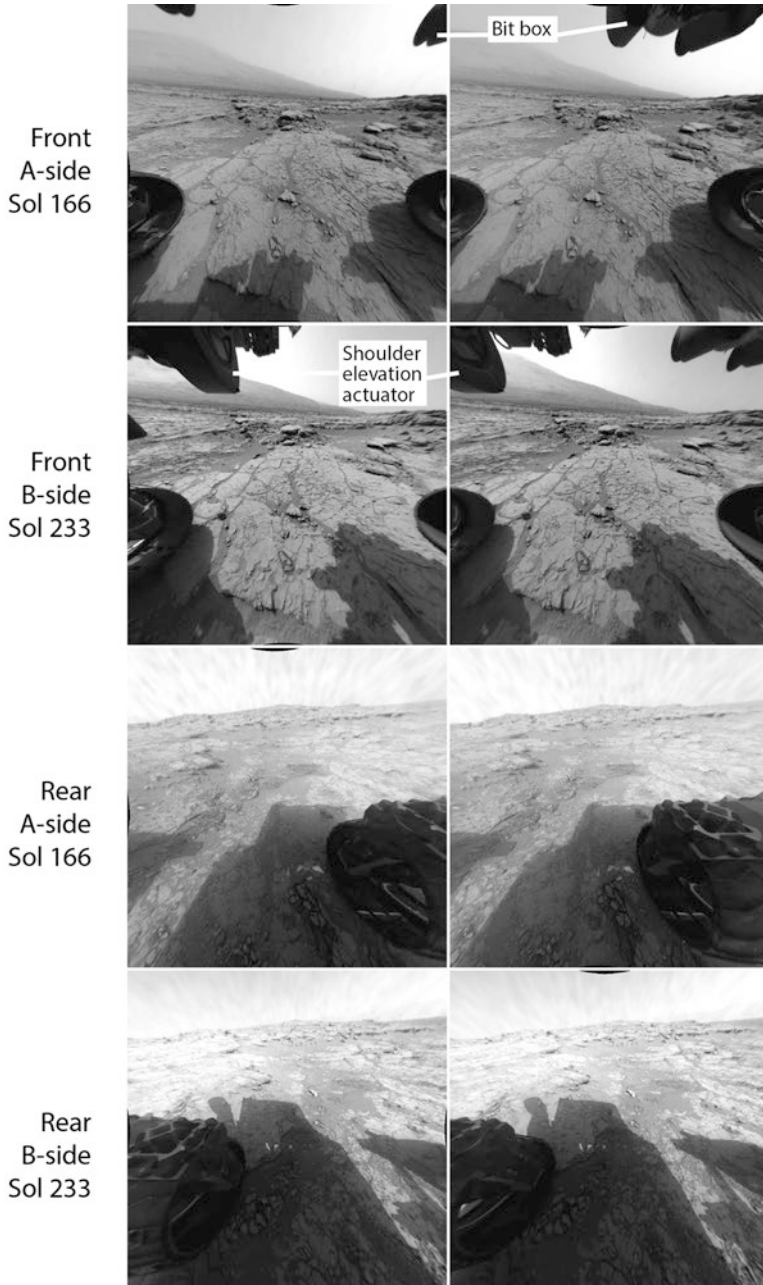


Figure 6.4. Shifting Hazcam points of view between sol 166, on the A-side cameras, and sol 233, on the B-side cameras. The rover did not change position in the time between these two sets of images. The images have been reprojected to correct for the fish-eye distortion of the Hazcams. NASA/JPL-Caltech.

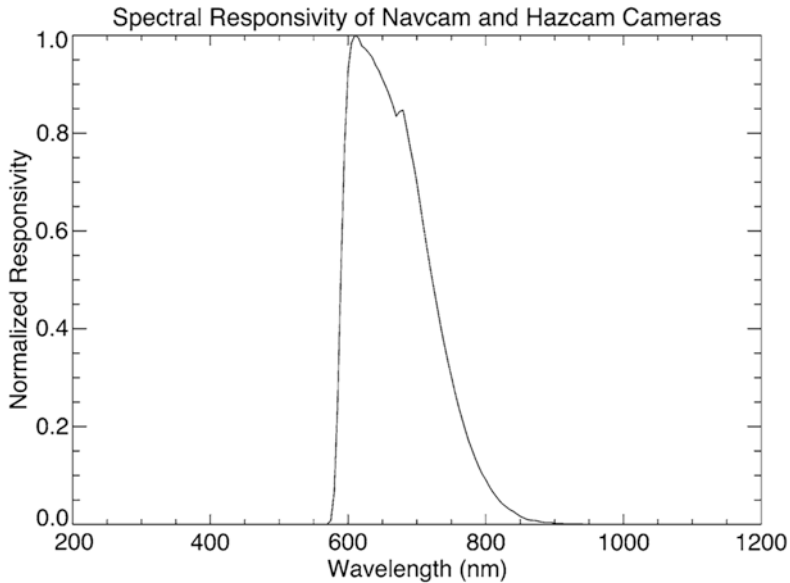


Figure 6.5. Spectral responsivity of Navcams and Hazcams. From Maki et al. (2012).

6.4 USING THE ENGINEERING CAMERAS

6.4.1 Navcam panoramas

With the Navcams' 45° field of view, it technically takes only eight pairs of Navcam images to cover the complete 360° in stereo around the rover. But to generate good stereo range information for planning, it's necessary to have substantial overlap between adjacent image tiles, so most 360° Navcam panoramas contain 12 image footprints (where a footprint includes one each of left- and right-eye images) in any tier. Curiosity requires so much overlap because the wide spacing of Curiosity's Navcams translates into a 21-centimeter offset from their pan axis. Rotating the mast shifts the camera position, making edges of adjacent Curiosity Navcam frames match poorly, particularly close to the rover.

Occasionally, particularly at drill sites, the rover takes a complete lower tier Navcam panorama to image the deck. The top of Mount Sharp is usually cut off in standard Navcam panoramas, but occasionally the team commands an upper tier to fill Mount Sharp in. When the rover is traveling in valleys among ridges or buttes, the team may command partial or complete upper tiers (often just half of the Navcam field of view) to capture topography above the horizon.

6.4.2 Drive imaging

Most drives end with two high-priority Navcam panoramas, crucial for planning the next sol's activities. One is a 5-by-1 array of stereo pairs that covers the likely future path of the rover, up to and just above the horizon: the "drive-direction panorama." Another is a 5-by-1 array pointed off the front right corner and right side of the rover, one tier down from the drive-direction panorama: the "ChemCam targetable region." When data volume permits, the rover acquires a complete 12-frame, 360° panorama after a drive by adding in left and right "wings" of two frames each and then the rear view, comprising the last three frames. Because much of the rear Navcam view is occluded by the RTG and UHF antenna, the rear view isn't very useful for drive planning, so the rear-view images have much lower down-link priority than all the rest. As a result, they are often not returned to Earth until many hours after the rest of the panorama. On sols when resources are limited, the rear-view portion of the panorama may be deferred until the next sol, or not taken at all.

When the rover uses Navcams and Hazcams for visual odometry or autonomous navigation, it takes them in a 4-by-4 summation mode, producing images only 256 pixels square. Visual odometry frames look like the view out the window of a moving vehicle, with rocks and other features slowly tracking across the field of view. Autonomous navigation adds Hazcam frames to the mix, interleaved with the Navcam images. If mid-drive Hazcam images are full resolution (1024 pixels rather than 256 pixels square), that's usually a sign of mid-drive use of the DAN instrument in its active mode, rather than autonomous navigation (see section 8.3).

6.4.3 Slip checks

Even if engineers don't plan to move the rover, they usually command Hazcam imaging as the first activity of the day, to make sure that thermal contraction during the overnight chill hasn't caused any shift in the rover's position. Slip-check images are also useful after arm activities, because the arm's substantial weight can cause the rover's position to shift slightly.

6.4.4 Environmental observations

The meteorology science theme group frequently uses Navcam movies for routine observations of atmospheric dynamics. There are two main types: zenith movies and Mount Sharp movies (technically called supra-horizon movies).² Both require only rover-relative pointing so can be performed on restricted sols. They are simple to command and produce low volumes of data, so can be captured during periods when the rover needs to be relatively inactive (e.g. over conjunction and lengthy Earth holidays).

The team takes zenith movies to search for high-altitude clouds. To capture zenith movies, the Navcam points at an elevation of 85°, almost directly overhead. A Navcam shoots 8 images at intervals of about 13 seconds, observing for a total of 91 seconds. The images are downsampled by a factor of two, producing 512-pixel-square images. To analyze the

²Kloos et al. (2016)

images, the atmospheric science team averages the 8 images together and then subtracts the average frame from all 8 original frames to search for faint ghosts of clouds in each image. If the Sun were in the field of view, it would overwhelm the Navcams' ability to see clouds. Therefore, the rover never takes zenith movies within 3 hours of local noon; and takes most in the late afternoon. To further avoid the Sun, the Navcam points north to take photos during the winter (L_s 0–180) and south during the summer (L_s 180–360). On average, the mission acquires these observations about once every 6 sols.

Mount Sharp movies are to search for orographic clouds over Mount Sharp. They can also reveal lower-altitude clouds because they look at a lower angle through the atmosphere than zenith movies. To take them, a Navcam points southeast, at 135° , at an elevation of 38.5° . To avoid the Sun, these movies have to be taken after 10:00 a.m. local solar time. Initially, they were taken the same way as the zenith movies (eight frames, 512 pixels square, at intervals of 13 seconds), but after sol 594 the sequence and pointing was changed to cover more of the mountain and ground in a swath 1024 pixels tall by 512 pixels wide. To keep the data volume the same, they reduced the movies to only 4 frames captured at intervals of 13 seconds.

There are also dust devil movies, in which the rover gazes to the north to search for the motion of dust devils across the plains.³ The northward direction was chosen because it offered Curiosity the longest-distance view in which dust devils might be visible. Dust devils were observed in only two of 250 dust devil movie observations. As it turned out, dust devils were happening, but the Navcams were pointed in the wrong direction to see them. On sol 1520, a dust devil was fortuitously spotted in a Mastcam multispectral observation aimed at Mount Sharp. Since then, the environmental science theme group has aimed dust devil movies toward Mount Sharp at the south and observed lots of them marching across the lower slopes of the mountain.⁴

A particularly pretty type of Navcam observation is Navcam sunset movies, to determine scattering properties of the atmosphere.

6.4.5 Anomalies

The switch from A-side to B-side cameras after the sol 200 anomaly should have been a relatively minor event. Unfortunately, the rover planners found after the switch that the terrain meshes derived from A-side and B-side cameras did not match. Engineering camera team lead Justin Maki figured out that the camera bar to which the Navcams are mounted warped with temperature change.⁵ The engineers had to develop a temperature-dependent camera model and upload it to the rover before they could use autonomous navigation capability.

Images from the rear Hazcams often appear significantly noisier than those from the front Hazcams. The rear Hazcams run much warmer than the front ones due to their proximity to the hot MMRTG radiator fins. The high temperature increases the cameras' dark current, amplifying the brightness of hot pixels.

³Moores et al. (2014)

⁴Lemmon et al. (2017)

⁵Justin Maki, personal communication, review dated September 22, 2017

6.5 ROVER DRIVING

The rover drivers plan rover motion using a variety of local coordinate systems. They can instruct the rover to use various amounts of artificial intelligence to complete a drive. From less to more autonomous, the rover driving modes include blind driving, visual odometry (“visodom”), and autonomous navigation (“autonav”). Another mode, “guarded motion,” is a hybrid of visodom and autonav. Rover autonomy has a trade-off, because the greater the rover computing power required to drive safely, the slower the rover moves. To drive for distance, a drive may include segments of blind driving, then visodom, then autonav until reaching a time limit.

6.5.1 Coordinate systems

Placing the rover’s scientific observations in geographic context is crucial to interpreting them. The rover has inertial measurement units to dead-reckon its position and orientation. Ideally, all rover measurements would be tied precisely to a latitude/longitude/elevation spatial frame, but this can’t happen automatically because of imprecise instantaneous knowledge of the rover’s location.

The quality of the rover’s position information degrades with time, for two reasons. First, the wheels slip. This means that the amount of distance the rover has traveled is never quite the same as the distance commanded. If wheels on one side slip more than those on the other side, slip results in unexpected rotation as well as distance. And second, the bumping and jostling of the rover as it travels over rough terrain accelerates the inertial measurement units in ways that can be incorrectly interpreted as distance traveled.

To help manage the uncertainty in rover position and to compartmentalize the errors, the mission keeps track of several different spatial reference frames.⁶ The two most commonly used ones are the rover frame and the site frame. The rover frame is fixed relative to the rover. The rover frame origin is at a spot on the ground between the middle wheels (assuming the rover is perfectly level). In the rover frame, +X is forward, +Y is to the right, and +Z is down. A site frame has its origin at a fixed point on the surface of Mars. The rover performs operations like camera pointing, arm activities, and drives relative to the site frame. The site frame has +X pointing north, +Y pointing east, and +Z pointing downward in a direction perpendicular to the map. Over time, error accumulates in the rover’s reckoning of its motion relative to the site origin. Periodically, the team declares a new site origin and increments the site number. By keeping careful track of where measurements were made in the rover frame, and precisely determining the geographic location of each site frame, science measurements can be precisely geolocated.

When the mission declares a new site origin, the spatial position is determined by comparing Navcam photos to orbital image data, but it’s harder to precisely identify the rover’s orientation in space. Curiosity’s inertial measurement units provide continuously up-to-date pitch (front-to-back tilt) and roll (side-to-side tilt) information, but the rover’s

⁶The various reference frames are described in detail in Alexander and Deen (2015).

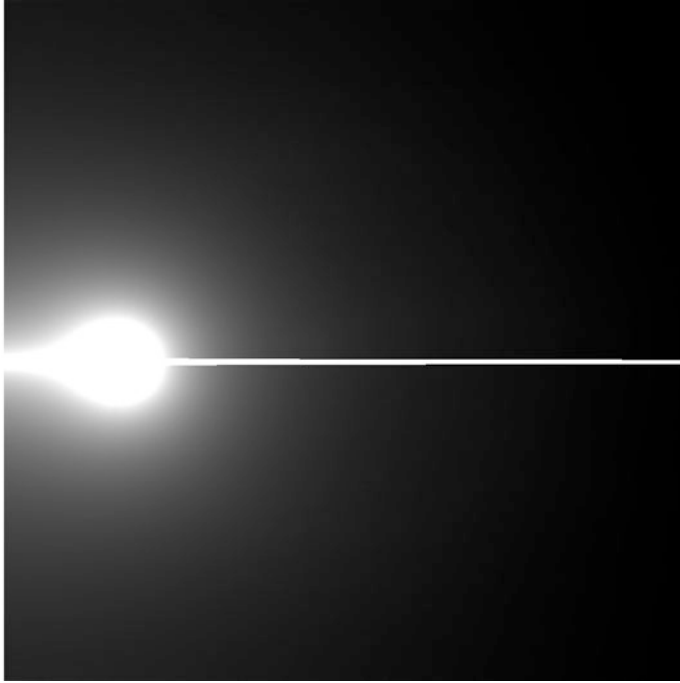


Figure 6.6. A typical right Navcam image of the Sun, taken to support a new site frame declared after a drive on sol 324. The horizontal line is pixel bleeding caused by overexposure. Image NRB_426264304EDR_F0060864SAPP07612M. NASA/JPL-Caltech.

knowledge of its yaw (compass orientation) degrades over time. Curiosity periodically updates its yaw knowledge by shooting a mid- to late-afternoon photo of the Sun with the right Navcam. Even with pixel bleeding, the rover can identify the location of the Sun precisely enough to identify its yaw relative to the local coordinate system (Figure 6.6).

6.5.2 Driving modes

6.5.2.1 Blind driving

In a blind drive, the rover doesn't employ any onboard intelligence to look at the landscape during the drive. Instead, the rover planners examine a 3D model of the landscape or "terrain mesh" calculated from Navcam and Hazcam images, and command the rover to roll its wheels a certain distance, turn through a specific number of degrees, and so on. The lengths of blind drives are limited to the distance that the rover can see well enough with the Navcams to develop a terrain mesh, usually no more than 50 meters. Blind drives can be longer than 50 meters if the terrain slopes upward and is benign. If the terrain is slippery (as it may be if it's sandy or sloping), blind driving can be inaccurate. Blind driving is the fastest mode, achieving speeds of roughly 100 meters per hour.

When executing a blind drive, the rover doesn't perform any checks to make sure it is on course. It does always perform checks to make sure that the mobility system is operating within safety limits, and will stop the drive short if (for example) there is too much tilt or too much resistance to the motion of a wheel. The rover planners may set these limits differently for each and every drive: a drive over smooth terrain should result in little rover tilt, so they'll set tilt limits lower than they would for a drive over rockier terrain.

6.5.2.2 *Visual odometry*

Visual odometry, or “visodom”, helps the rover maintain the course that the rover drivers set. During a drive, the rover looks to the side with its Navcams, taking stereo images at specified intervals (ranging from 50 to 150 centimeters). The rover computer compares pairs of images, matching features between image pairs, to determine how far the rover actually moved. The rover can then re-plan its path based upon its determination of how far it judges it has actually traveled, or can stop its travel if it is not making sufficient progress due to wheel slippage. Visual odometry slows the rover to roughly 50 meters per hour.

6.5.2.3 *Autonomous navigation and guarded motion*

Autonomous navigation, or “autonav”, is an even more sophisticated autonomous driving capability that allows the rover to drive beyond its terrain mesh. The rover drivers identify a goal, specified as a position in the local site frame coordinate system. The rover moves a short distance of 50 to 150 centimeters. It snaps Hazcam images and processes them into 3D information to update the terrain mesh. It identifies obstacles exceeding 50 centimeters in height and slopes steeper than 20°. The rover charts the “traversability” of a square of nearby terrain extending 5 meters around the rover, divided into a 20-centimeter grid. Each grid cell is assigned a “goodness” and “certainty” estimate that rolls together the rover's determination of the safety of that patch of terrain. The rover fits models of itself into this map to find the safest path. It rolls forward by another increment of 50 to 150 centimeters depending on how safe it perceives the terrain to be, then repeats the Hazcam imaging and evaluation process. Because of all the calculation, autonav is slow: a top speed of about 50 centimeters per minute, or about 30 meters per hour.

A related form of driving is “guarded motion,” where the rover planners give the rover a specific path to follow using visual odometry, but then instruct the rover to use autonav to verify that the path is indeed safe as it moves forward.

The use of autonav was ended following discovery of the wheel degradation problem (see section 4.6.4); mitigating wheel damage required rover planners to avoid hazardous terrain on a scale finer than the 20-centimeter grid used by autonav. It was re-enabled as of sol 1780, and planners have discretion to choose whether the local terrain is benign enough to enable autonav.

6.5.2.4 *Multi-sol driving*

When Curiosity landed, it could not save the terrain maps generated one sol and use them on the next sol. As part of a set of improvements included in flight software version R.11, implemented on sol 484, engineers added the ability to save on-board terrain maps during sleep to enable the rover to use the same one to continue a drive the next day, increasing the drive distances achieved during traverse periods.

6.6 REFERENCES

- Alexander D and Deen R (2015) Mars Science Laboratory Project Software Interface Specification: Camera & LIBS Experiment Data Record (EDR) and Reduced Data Record (RDR) Data Products, version 3.5.
- Kloos J L et al (2016) The first Martian year of cloud activity from Mars Science Laboratory (sol 0–800). *Adv Space Res* 57:1223–1240, DOI: 10.1016/j.asr.2015.12.040
- Lemmon M T et al (2017) Dust devil activity at the Curiosity Mars rover field site. Paper presented at the 48th Lunar and Planetary Science Conference, The Woodlands, Texas, 20–24 Mar 2017
- Maki J et al (2012) The Mars Science Laboratory engineering cameras. *Space Sci Rev* 170:77–93, DOI: 10.1007/s11214-012-9882-4
- Moore J E et al (2014) Update on MSL atmospheric monitoring movies sol 100–360. Paper presented at the 45th Lunar and Planetary Science Conference, The Woodlands, Texas, 17–21 Mar 2014

7



Curiosity's Science Cameras

7.1 INTRODUCTION

Curiosity has five science cameras. The color Mastcams view the rover's world in color at two different resolutions. The Mars Hand Lens Imager (MAHLI, pronounced "Molly") on the turret at the end of the arm, is a wide-angle color camera that can be held close to a target or perform distance imaging. The Mars Descent Imager (MARDI) is fixed to the rover body, pointing down, with a view of the surface as it passes under the rover. Together, these three instruments are often referred to as the "MMM" cameras. They have common detector and electronics and software design and differ only in their optics. Finally, there is the laser-equipped ChemCam, which measures elemental compositions of nearby rocks and also possesses the camera with the highest angular resolution on the rover, the Remote Micro-Imager (RMI). It will be described in Chapter 9 with the other composition analysis instruments.

Figure 7.1 shows the locations of camera instruments and related hardware on the rover. The engineering cameras (Navcams and Hazcams, section 6.3) serve science functions as well. They provide context for science observations and perform remote sensing science observations, particularly atmospheric science. Table 7.1 compares all of Curiosity's imaging capabilities.

7.2 MASTCAM

The Mastcam instrument consists of two camera heads located on the mast, an electronics assembly located in the belly of the rover, and a calibration target on the rover deck. With the Mastcams, the science team investigates geomorphology, stratigraphy, and texture of the landscape, rocks, and sediments around the rover. They also monitor atmospheric and even astronomical phenomena. They support the rover's engineering activities and provide

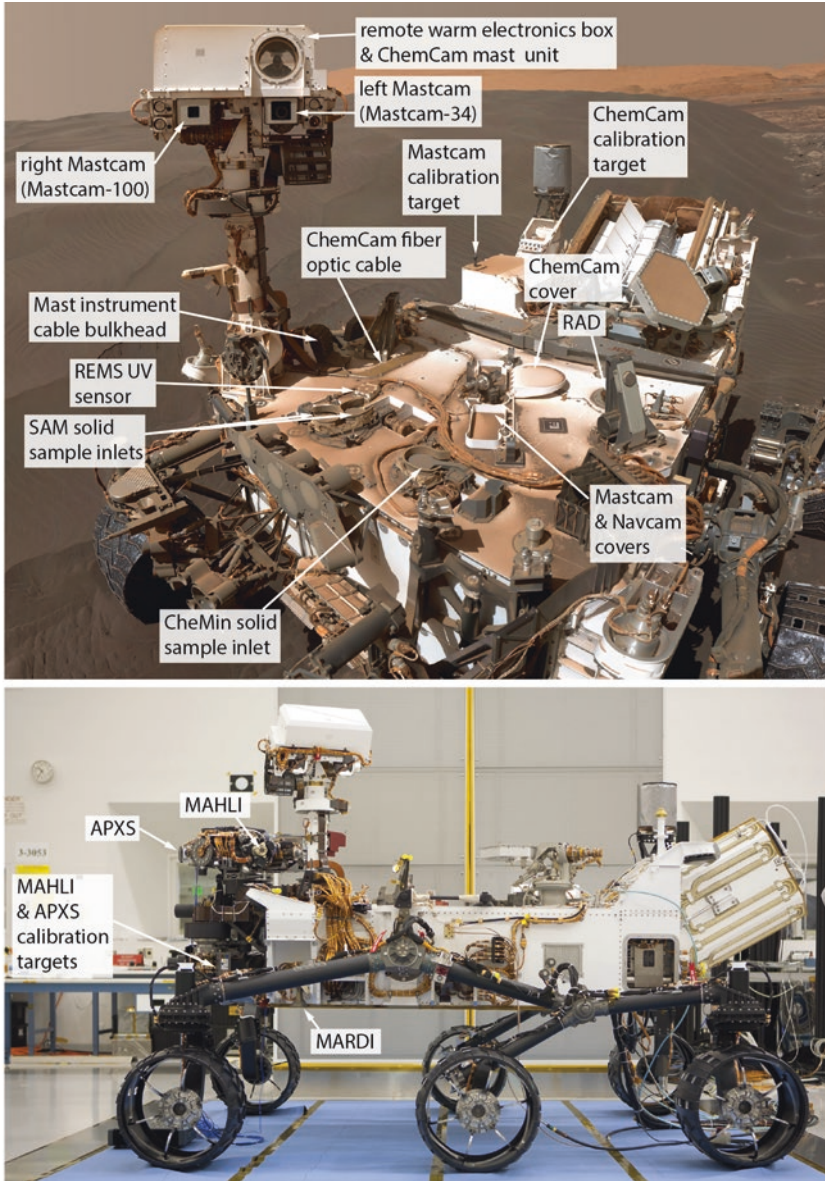


Figure 7.1. Locations of camera instrument components on the rover, as well as some devices often imaged with Mastcams. Mastcam, Navcam, and ChemCam covers in top image were used only during cruise and landing. Top image is cropped from the Gobabeb MAHLI self-portrait mosaic, sol 1228. Bottom image taken at JPL during assembly. NASA/JPL-Caltech/MSSS/Emily Lakedawalla.

Table 7.1. Comparison of the capabilities of Curiosity's cameras.

	FHaz	RHaz	Nav	ML	MR	RMI	MAHLI	MARDI
CCD Detector (pixels)	1024 × 1024	1024 × 1024	1024 × 1024	1600 × 1200	1600 × 1200	1024 × 1024	1600 × 1200	1600 × 1200
FOV (°)	124 × 124	45 × 45	20 × 15	6.8 × 5.1	1.3	34.0–38.5	70–52	70–52
Ifov at center (mrad/pixel)	2.1	0.82	0.22	0.074	0.022	0.402–0.346	0.76	0.76
Stereo?	yes	yes	yes, but with different resolution/FOV in each eye	no	yes, with arm movement	no	yes, with arm movement	yes, with rover movement
Stereo separation (cm)	16.7	10	42.4	24.5	–	arbitrary	arbitrary	arbitrary
Depth information from focal depth?	no	no	yes	yes	yes	yes	yes	no
Height above surface (m)	0.68	0.78	1.9	1.9	2.1	arbitrary	0.66	0.66
Spectral bandpass (nm)	600–800	600–800	395–1100	450–950	420–690	420–690	420–690	420–690
Filters	monochrome	monochrome	8 plus Bayer	8 plus Bayer	monochrome	Bayer color	Bayer color	Bayer color

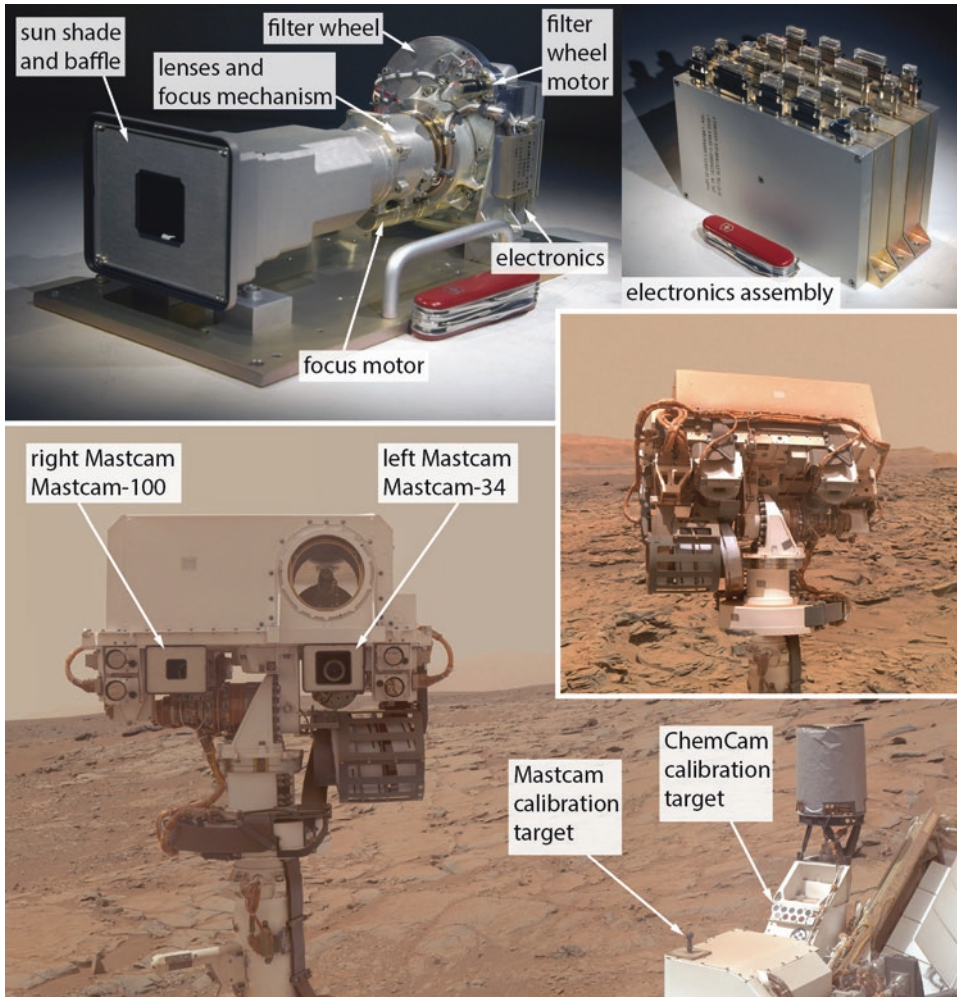


Figure 7.2. Parts of the Mastcam instrument. Photos of the Mastcam-100 camera head and digital electronics assembly were taken at Malin Space Science Systems before their delivery to JPL for assembly. Bottom self-portrait taken at the John Klein drill site on sol 177 by MAHLI. Inset self-portrait showing the back of the camera heads and their wire harnesses taken at Okoruso drill site, sol 1338. NASA/JPL-Caltech/MSSS/Emily Lakdawalla.

context images for data from other science instruments. The Mastcams were built by Malin Space Science Systems, San Diego, California. The principal investigator for the Mastcam experiment is Michael Malin of Malin Space Science Systems.

The Mastcams differ from previous lander cameras in two significant ways. First, nearly all Mastcam views are in full, human-vision-like color. Second, the two camera “eyes” have different focal lengths, which makes stereo imaging more complex than for previous missions. (Read section 1.5.8 for the history of the development of Mastcam that

Table 7.2. *Mastcam facts.*

	Mastcam-34 (Mastcam-L)	Mastcam-100 (Mastcam-R)
Boresight height above bottom of wheels	1.97 m	
Elevator actuator axis height above bottom of wheels	1.91 m	
Stereo separation	24.64 cm	
FOV (horizontal 1600 pixels)	20.6°	6.8°
FOV (vertical 1200 pixels)	15°	5.1°
instantaneous field of view (IFOV)	218 μ rad	74 μ rad
Pixel scale at a distance of 2 meters	450 μ m	150 μ m
Pixel scale at a distance of 1 kilometer	22 cm	7.4 cm
focal ratio	f/8	f/10
effective focal length	34 mm	100 mm
in-focus range	0.4 m to infinity	1.6 m to infinity
exposure range	0 to 838.8 s in 0.1 ms increments	
video frame rate	5.9 to 7.7 fps at 720p (1280-by-720) 3.9 to 4.7 fps for full frame	

led to the flight of a pair of Mastcams with different focal lengths.) The left Mastcam or Mastcam-34 has shorter focal length, lower angular resolution, and wider field of view. The right Mastcam or Mastcam-100 has longer focal length, higher angular resolution, and narrower field of view.

7.2.1 How Mastcam works

7.2.1.1 Camera heads

The Mastcams are 2-megapixel color cameras with focusable lenses and filter wheels.¹ The heads contain electronics, a detector, a filter wheel assembly, a focus mechanism, and a sunshade/baffle that also serves as a mount (Figure 7.2). Each head contains two stepper motors, one to drive the filter wheel and one to drive the focus mechanism. The two Mastcams have boresights separated by 24.64 centimeters, and they are angled inward by 2.5° (1.25° each) in order to ensure that the smaller field of view of the Mastcam-100 is entirely contained within the wider field of view of the Mastcam-34 for any target located farther than 1.4 meters away from the rover. The boresights cross at a distance 2.8 meters

¹Prior to landing, there was no peer-reviewed paper describing Mastcam or MARDI. Mastcam was described in two Lunar and Planetary Science Conference abstracts: Malin et al. (2010) and Bell et al. (2012). Also useful is Alexander and Deen (2015). Two peer-reviewed articles were in preparation as this book was being written: Bell et al. (2017) and Malin et al. (2017). Because Mastcam shares its electronics, detector, and focal mechanism design with MAHLI, the Edgett et al. (2012) MAHLI paper is also informative.

away from the cameras, at a spot on the ground 2 meters away from the rover. The detector is capable of capturing 720p high definition video (1280-by-720 pixels) at a rate of 5 frames per second. Further facts are summarized in Table 7.2.

The Mastcams have the same detectors as MAHLI and MARDI and use the same focus mechanism as MAHLI. The detector is a Kodak KAI-2020CM Charge-Coupled Device (CCD), which is 1640 pixels wide by 1200 pixels high. The sides and corners of the images are partly occluded by the baffle and are affected by vignetting. The vignetting exists because the filter wheels, and specifically the shapes of their openings, were built before the descope of zoom capability, at a time when Mastcam only planned to produce 1200-by-1200-pixel subframes. Most images taken for science purposes crop away the sides to an image width of 1344 or 1200 pixels, operationally called a “full frame” (Figure 7.3). On sol 1589, the Mastcam team switched to using 1328-by-1184-pixel “full frames” for more efficient memory management.² The original full-frame image size used 12.3 blocks in flash memory; the slightly smaller subframe uses just under 12 blocks at virtually no cost to the usefulness of the image.

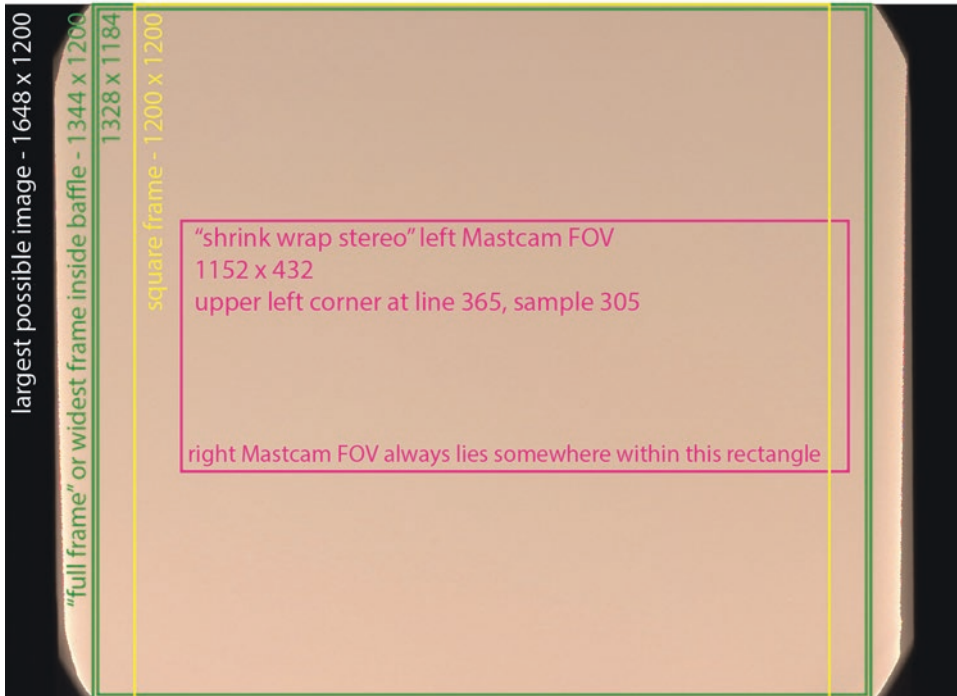


Figure 7.3. Size of the left Mastcam frame and common subframe areas. Mastcam image 320ML0010520330107781E01. NASA/JPL-Caltech/MSSS/Emily Lakdawalla.

²Michael Malin, personal communication, email dated April 14, 2017

7.2.1.2 Color imaging

Unlike most space cameras, the Mastcams, MAHLI, and MARDI take natural color images like consumer digital cameras. Each pixel is covered with a red, green, or blue filter in a Bayer pattern. A Bayer pattern is a checkerboard of colored pixels; in every 2-by-2 array of pixels, two corner pixels are covered by green filters, one is covered by a red filter, and one by a blue filter. Color comes from interpolating among the pixels to generate complete red, green, and blue images. Interpolation can happen onboard the spacecraft or on Earth.

Each Mastcam eye is equipped with an 8-position filter wheel. It may seem odd to add a filter wheel to a camera that already has color filters over its detector, but fortunately for spectroscopists, the Bayer color filters on the Mastcam detectors are “leaky” in infrared wavelengths. During normal color imaging, a broadband filter blocks these infrared wavelengths (Figure 7.4). But the Mastcams can operate like other filter-wheel-equipped space cameras in the near-infrared with six narrowband science filters in each eye, used for spectroscopic imaging (Figure 7.5). The science filters were distributed between the two cameras so that, if one camera fails, the other will still be able to accomplish some of the science objectives. Three of the filters are essentially identical between the two eyes, and three differ, so a total of nine distinct science filters is available for multispectral imaging. Each eye’s filter wheel also has one filter with a neutral-density coating that blocks most light and permits the Mastcams to directly image the Sun through a blue (right eye) and infrared (left eye) filter.

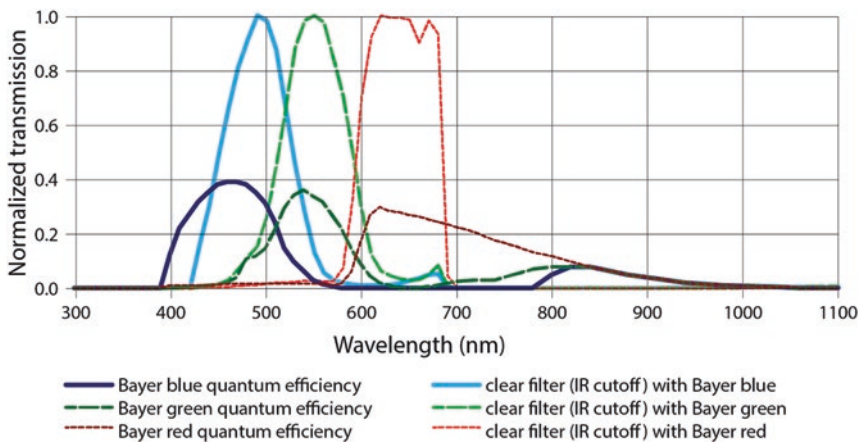


Figure 7.4. Mastcam detector Bayer filter bandpasses without and with the “clear” infrared cutoff filter. Dark lines show the quantum efficiency of the optics and detector; at wavelengths beyond about 850 nanometers, all three Bayer filters allow an equal amount of light to pass. Brighter lines show the normalized transmission of the three Bayer filters with the clear filter in the optical path, which allows only visible wavelengths (420–690 nanometers) to pass. Data courtesy Jim Bell.

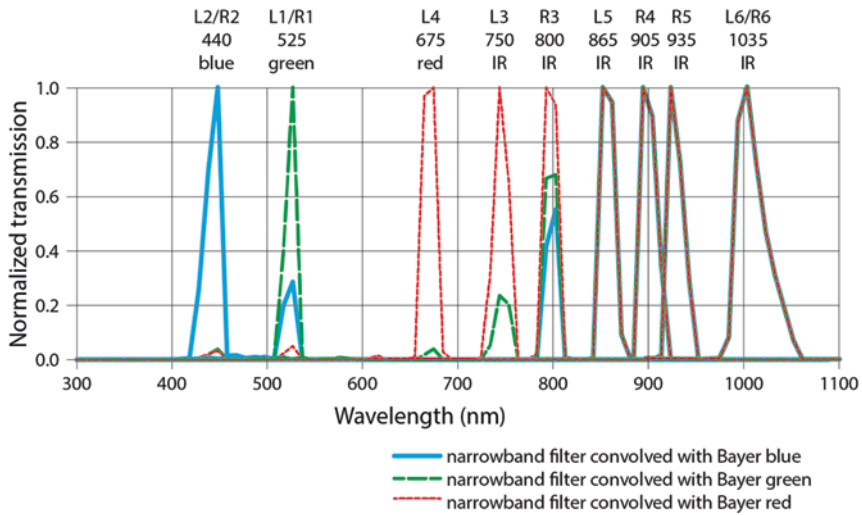


Figure 7.5. Mastcam narrowband filter transmission. Data courtesy Jim Bell.

The narrowband filters are usually named by their filter wheel positions (L0, L1, etc...) or referred to using the wavelengths that were requested from the Mastcam filter supplier (440, 525, 675, etc...), but their actual center wavelengths are slightly different from those values. The as-built center wavelengths of the filters on the cameras on Mars are listed in Table 7.3.

Table 7.3. Mastcam spectral filters and bandpasses as built. Data from Bell et al. (2012).

Filter Position	Left Eye Wavelength± Bandwidth (nm)	Nickname	Right Eye Wavelength ± Bandwidth (nm)	Nickname
0	590 ± 88	Clear	575 ± 90	Clear
	640 ± 44	Bayer red	638 ± 44	Bayer red
	554 ± 38	Bayer green	551 ± 39	Bayer green
	495 ± 37	Bayer blue	493 ± 38	Bayer blue
1	527 ± 7	525, green	527 ± 7	525, green
2	445 ± 10	440, blue	447 ± 10	440, blue
3	751 ± 10	750	805 ± 10	800
4	676 ± 10	675, red	908 ± 10	905
5	867 ± 10	865	937 ± 10	935
6	1012 ± 21	1035	1013 ± 21	1035
7	880 ± 10 ND5	880, solar	440 ± 20 ND5	440, solar

As a consequence of the convolution of Bayer and narrowband filters, some narrowband images contain less spatial information than others. In particular, an image taken through L2/R2 (440), L3 (750), R3 (800), L4 (675), or R7 (440 ND) has good signal only

in one out of every four pixels (the red ones or blue ones), while L1/R1 (525) has signal in only one of every two pixels (the green ones). JPEG-compressing the full-size versions of these images before transmitting them to Earth would have very strange results. So before converting the shorter-wavelength narrowband images to JPEG, the camera electronics throw out data from the relatively unresponsive pixels and do bilinear interpolation to fill in data from the missing pixels. As an example, for the L2/R2 (blue) images, the electronics throw out the data from the red and green pixels and fill in with values interpolated from the blue pixels. Narrowband filter images that have been JPEG-compressed are returned to Earth as grayscale, with only the luminance (brightness and darkness) channel; the chrominance (color variation) information isn't provided. Because the longer exposures required to take narrowband filter images accentuate the effects of bad pixels and because the images have intrinsically less spatial information, they tend to look noisier than the broadband color images.

7.2.1.3 Focus

The Mastcam focal mechanism uses a stepper motor with 16100 discrete motor positions. To autofocus, a Mastcam starts at a commanded motor position and then takes a set of images, incrementing the motor count by a specified step each time. Usually, the autofocus images are subframes of the full scene. The camera then JPEG-compresses the photos. The file size of the photos measures the complexity of the scene; an out-of-focus scene will be blurrier, so will compress to a smaller file size. The camera considers the motor count as a function of JPEG file size and fits a parabola to the sizes of the three largest files. The vertex of the parabola is taken to be the best-focus motor count, and Mastcam moves the focus to that position and takes one more image.

When a scene has a lot of depth, the autofocus algorithm doesn't always select the focal depth that scientists want, so it can be better to specify the focal depth for those observations. To save time when capturing landscape mosaics, the Mastcams can be commanded to autofocus one frame and then use the same focus setting for subsequent frames that are expected to be in focus at the same position.

The motor count associated with an in-focus image is a function of the range to the best-focus features in the image. For the Mastcam-100, the temperature of the instrument also affects the focus. To determine range from motor count, use the following equations:³

$$\text{Mastcam - 34 : range} = 363.64 / (2427.50 - (\text{motor count}))$$

$$\frac{\text{Mastcam - 100 : range} = 3322.3}{(3491.9 - 2.58 * (\text{instrument temperature}) - (\text{motor count}))}$$

³Bell et al. (2017)

7.2.1.4 Electronics

Each Mastcam, MAHLI, and MARDI has its own board in the electronics assembly. The following discussion therefore applies to MARDI and MAHLI as well as each Mastcam.

Each electronics board has a computer, 128 megabytes of SDRAM, and 8 gigabytes of flash memory for each camera, which can accommodate about 4000 total images. The electronics assembly determines autofocus and autoexposure parameters and sends this information to the camera heads. The camera detector captures 12-bit images. After it acquires an image, a camera head sends the data to the RAM inside the digital electronics assembly for further processing and storage. For all images, the camera head electronics create thumbnails 1/8th the size of the originals as they are transferred to the electronics board. (The electronics aren't capable of downsampling images by any factor other than 8.) Mastcam converts the images from 12- to 8-bit depth to reduce file size. Most commonly, the team commands the instrument to use a square-root look-up table to do the 12-to-8-bit conversion. This allots more of the limited 256 values in the 8-bit image to darker areas, preserving detail in shadows that would otherwise be lost. Images are usually stored raw, without compression (in which case each full-size image takes about 2 megabytes of space, on average).

The main rover computer maintains a list of the files in storage, and copies requested images to its own memory as commanded before transmitting them to Earth. Thumbnail images get returned to Earth very soon after acquisition, supplying the Mastcam team a visual index to the image data collected on the rover. When the rover computer requests an image from Mastcam, it requests that the image be compressed before transmission, either losslessly or lossily. The electronics board has a lot of options for lossy compression. Mastcam can use Bayer interpolation⁴ to convert pictures to color, then save them in JPEG format. Usually, the JPEG images are compressed using a method that preserves more detail in an image's brightness and darkness (luminance) but downsamples the detail in the color variation (chrominance) by a factor of two. Such images are referred to as "JPEG 422", while JPEG-compressed images that preserve full-resolution chrominance information are referred to as "JPEG 444".

Returning space science data in lossy JPEG format is somewhat unusual, although it's getting more common as camera detector sizes outstrip our ability to transmit all that data to Earth. Even slight JPEG compression produces large savings in file sizes. A JPEG quality of 90 (measured on a scale from 1, lowest, to 100, highest quality) generally produces images with less than half the file size of an uncompressed image (Figure 7.6).⁵ The team selects less compression (typically JPEG quality 85) for images intended to support science, and more compression (typically JPEG quality 65) for images taken for documentation purposes.

The cameras' large flash memory volume makes it possible to keep raw data onboard and return science images months or even years after they were originally taken. At times when the rover is not capable of doing much science (like during holidays, solar conjunctions, or

⁴Onboard interpolation uses the Malvar-He-Cutler linear interpolation algorithm

⁵Bell et al. (2017)

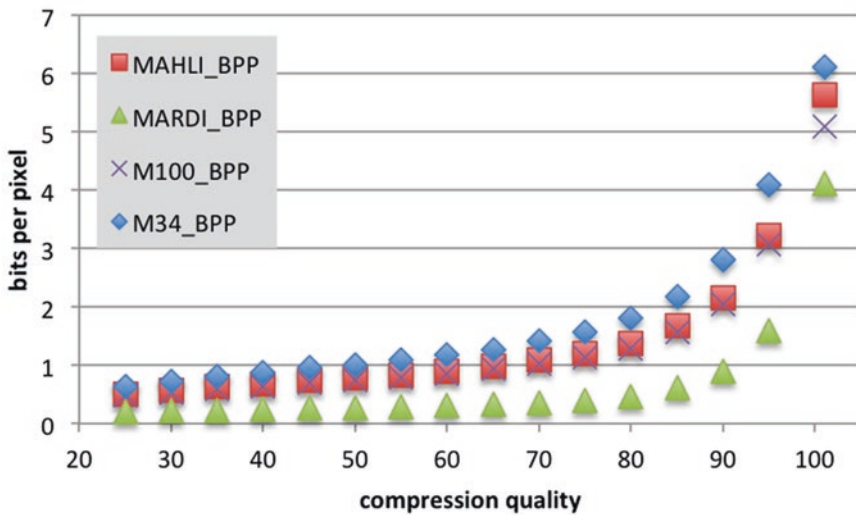


Figure 7.6. Relationship between JPEG compression quality and file size for all four Curiosity color cameras. Mastcam-34 images have the largest file sizes because they are usually in focus over most of the image so have high amount of detail, which compresses poorly. MARDI, by contrast, is out of focus, so compresses much more readily. An uncompressed image has 8 bits per pixel. Compression quality 101 refers to losslessly compressed images. Figure from Bell et al. (2017), based on analysis by Jason Van Beek and Michael Malin.

anomalies that restrict mobility) but is still capable of sending data to orbiters, daily downlinks can be packed with Mastcam data that has been idling on the rover for months, usually losslessly compressed versions of images that had previously been returned lossily.

7.2.1.5 Artifacts and blemishes

Several types of artifacts can affect the quality of Mastcam images. Some of these are intrinsic to the camera, some have to do with the way the data are stored or transferred, and some result from how the images are processed either within the camera or on Earth. Each camera has some (but very few) bad pixels: hot pixels that make bright spots, dead pixels that make dark spots, and gray pixels that don't respond as well as others around them to incoming light. Occasionally, a new hot pixel appears on a camera detector, likely caused by an energetic particle flying from the MMRTG or from space. One such hot pixel appeared on the center right of the right Mastcam on sol 392, and had disappeared again by sol 710. A particularly bright one appeared near the top right of the left Mastcam on sol 834 and has remained ever since (Figure 7.7).

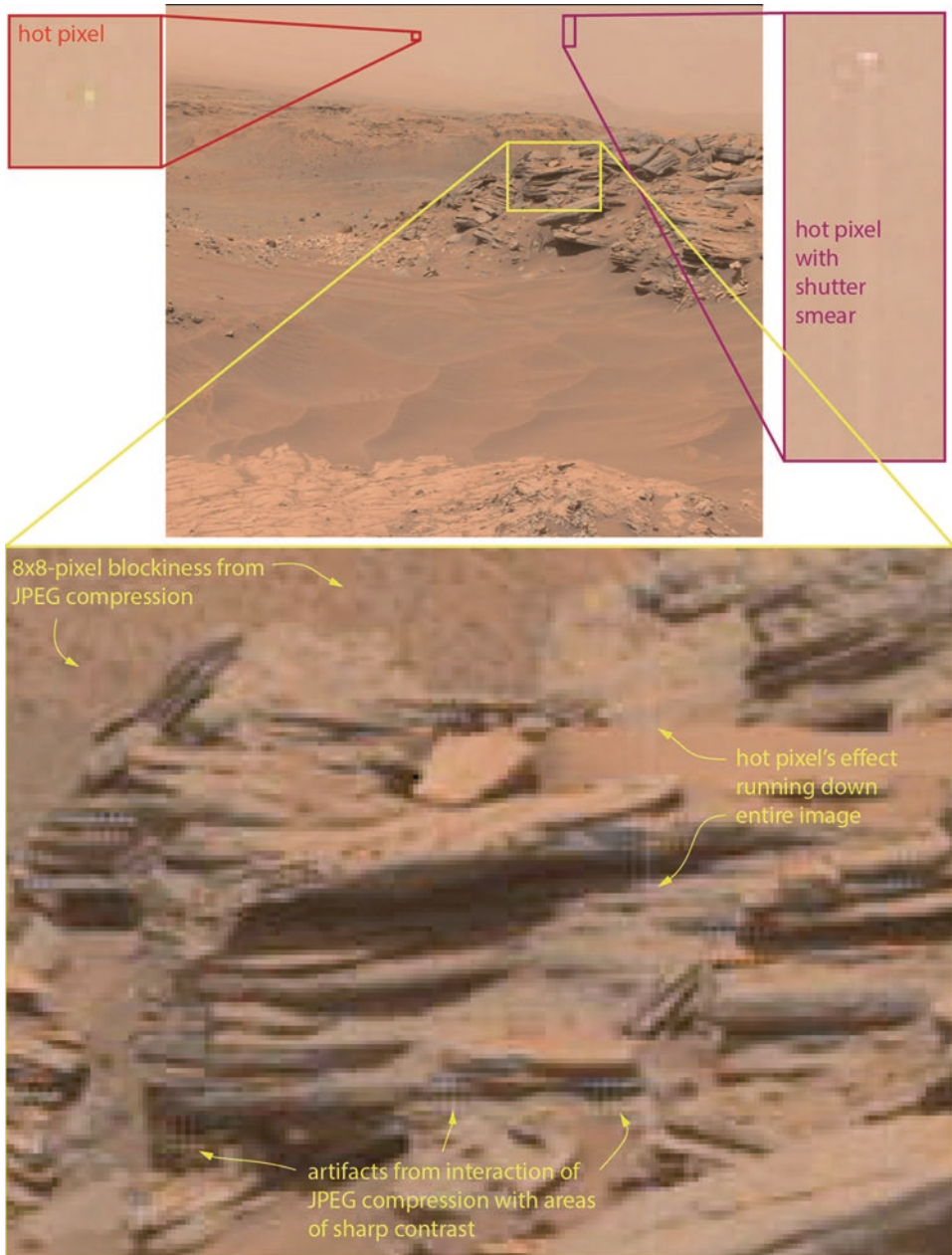


Figure 7.7. How hot pixels, shutter smear, and JPEG compression can reduce Mastcam image quality. Taken as part of a drive direction panorama, this Mastcam image was returned to Earth with fairly high JPEG compression (quality 65). Mastcam image 1030ML0045010040305530E01. NASA/JPL-Caltech/MSSS/Emily Lakdawalla.

Images containing particularly bright objects – such as parts of the rover, or hot pixels – can be affected by shutter smear. The Mastcams have no physical shutters. Instead, once the camera has exposed the detector for the requested length of time, it shifts the charge out of the exposed area and into a shielded area called the transfer cell, one line at a time. All the rest of the lines in the image are shifted upward as each line is moved into the transfer cell and read out. While this is all happening, the detector is still being exposed to the scene. As long as the readout of the image happens quickly relative to the exposure time, it's hard to notice the effects of shutter smear. But if the scene is bright enough that the exposure time is short – or if the scene contains a very bright pixel – there may be a vertical bright smear streaking the image, running down from bright pixels. The hot pixel that appeared on the left Mastcam on sol 834 is bright enough to create such a streak on all left Mastcam images acquired since it appeared (Figure 7.7). Fortunately, the Mastcam CCDs are large enough that, although cosmetically annoying, the blemishes are not harmful to science.

The JPEG compression means that most images have some compression artifacts. JPEG compression works on 8-by-8-pixel blocks, and the boundaries of those blocks are often visible. JPEG compression is more effective in places with smooth variations in color and brightness, but can introduce strange artifacts in areas of high contrast. Areas where there is high contrast or a lot of variation also tend to be areas of scientific interest – for instance, in an area of very finely laminated rock layers in alternate Sun and shadow (Figure 7.7, bottom). Where the compression artifacts make it difficult to interpret the geology, the team can choose to re-transmit the image with less compression, or even losslessly – as long as the original image is still stored in the camera's flash memory. As of early 2017, not quite half of all of the Mastcam data had been returned a second time with lossless compression. At that time, the mission switched to returning all non-time-critical Mastcam science data losslessly, accepting delayed data return in exchange for a larger proportion of losslessly compressed data and a reduction in the complexity of data curation.⁶

7.2.1.6 *Calibration target*

The Mastcam calibration target is a flight spare of the ones flown on the Mars Exploration Rovers whose design was modified by the addition of magnets. It is mounted on the rover deck, 1.2 meters away from the cameras, on top of the box that houses the rover pyro fire assembly (Figure 7.8).

Unfortunately, because of the location of the hardstop on the azimuth actuator of the remote sensing mast, it is not possible to image the calibration target through both Mastcam eyes with a single pointing. The mast head has to rotate almost 360° in order to image the calibration target through both Mastcams. (This problem will be solved for Curiosity's successor, Mars 2020, by moving the calibration target just a few centimeters toward the center line of the rover.) The right Mastcam is somewhat farsighted, with a minimum

⁶Michael Malin, personal communication, email dated April 14, 2017

in-focus range of 1.6 meters, so its images of the calibration target are not in focus, but that doesn't affect the calibration target's usefulness.

Like the Earth sundials that the calibration target resembles, the Mastcam calibration target has art and text embellishments. Most of these are inherited from the Mars Exploration Rover Pancam calibration target, but there is a new motto: "Mars 2012" at the top of the dial (the year is usually hidden from view behind the gnomon as seen by Mastcam, but it's visible to MAHLI), and "to Mars to explore" at the bottom. On the four vertical sides the following text is engraved:

For millennia, Mars has stimulated our imaginations. First we saw Mars as a wandering red star, a bringer of war from the abode of the gods.

In recent centuries, the planet's changing appearance in telescopes caused us to think that Mars had a climate like the Earth's.

Our first space age views revealed only a cratered, Moon-like world, but later missions showed that Mars once had abundant liquid water.

Through it all, we have wondered: Has there been life on Mars? To those taking the next steps to find out, we wish a safe journey and the joy of discovery.

The calibration target is 8 centimeters square and has 7 regions useful for calibration, including 4 color chips at the corners and 3 grayscale rings around the black gnomon (central post). Ring-shaped "sweep" magnets underneath the color chips and the lighter two of the grayscale rings attract Martian dust to them, keeping the centers of the magnets less dusty than the rest of the calibration target.⁷ The top of the rover pyro fire assembly has, unfortunately, turned out to be one of the dustiest spots on the rover. The Mastcams image the calibration target whenever they do multispectral imaging, using the same set of filters as were used for the science observation. Although the dust is obscuring the areas intended to be used for calibration, the dust affects the brightness and color of the calibration target in a way that is straightforward to model, so it remains a useful calibration tool.

7.2.2 Using Mastcam

As with the Navcams, Mastcam imaging can either be targeted, or "blind." To do targeted imaging, the Mastcam team needs Navcam images to provide spatial information. Targeted imaging doesn't just happen at drive stops: Curiosity can perform targeted Mastcam imaging in the middle of a drive as long as the drive has not taken Curiosity beyond the terrain mesh calculated at the last drive stop. Blind imaging doesn't require Navcam context. Blind observations include 360° panoramas, Sun and horizon observations (since the position of the Sun and of distant landscape features don't measurably change over the course of a short drive), and observations in rover-relative locations, like the arm work volume and ChemCam targetable region.

⁷Kinch K et al (2013) Dust on the Curiosity mast camera calibration target. Paper presented at the 44th Lunar and Planetary Science Conference, The Woodlands, Texas, March 18-22, 2013

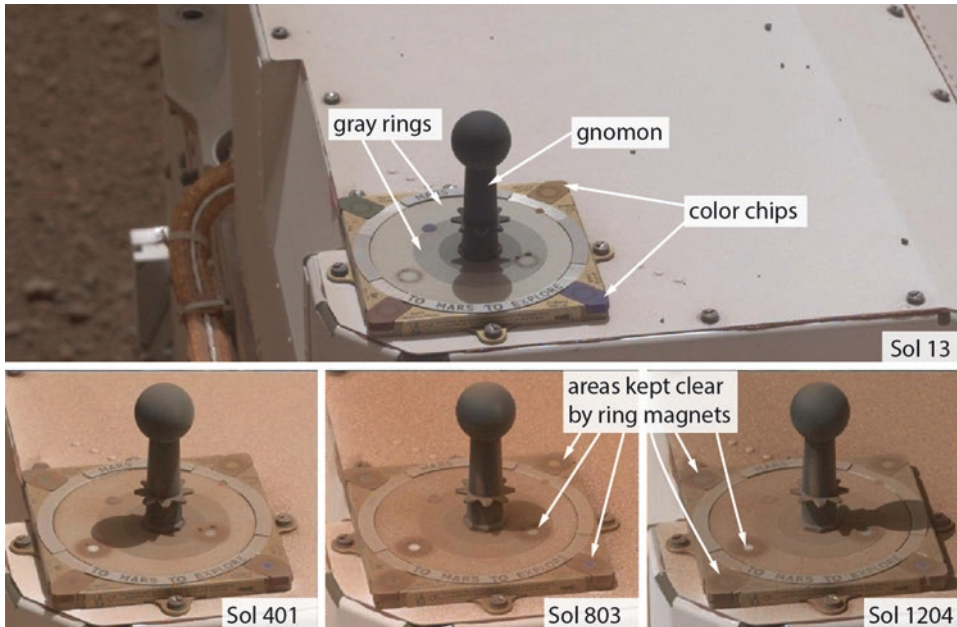


Figure 7.8. Mastcam calibration target as seen over time. NASA/JPL-Caltech/MSSS/Emily Lakdawalla.

7.2.2.1 360° panoramas

The rover acquires 360° panoramas with the wider-angle left Mastcam in interesting science locations and also roughly every 250 to 300 meters along long traverses in order to document the landscape. Full panoramas need no specific targeting (except coarsely, to include the top of Mount Sharp), so they are often taken on restricted sols when the rover's precise state isn't known. It takes 23 left Mastcam frames to complete a single tier over the full azimuth range of 360°, at about 8 minutes per tier, and roughly an hour for a typical complete panorama. One tier is centered near the horizon; each subsequent tier drops by 12°; and a partial tier covers the predicted location of the peak of Mount Sharp.

To save on time and bandwidth, the tiers below the horizon are usually incomplete, with areas including the rover deck skipped. This is a source of frustration to mission team members and the public alike, who would like to see a Mastcam self-portrait of the rover on the Martian surface including the robotic arm (which can't be imaged in MAHLI self-portraits). To date, only one Mastcam panorama has included all of the rover deck; it was taken on sol 1197, at Namib dune.

The higher-resolution right Mastcam requires 9 times as many images to cover the same amount of terrain as the left Mastcam, so has only taken a 360° terrain panorama once, in imaging sessions conducted from sols 172 to 198, while at John Klein.

7.2.2.2 *Tactical support imaging*

The left Mastcams are often used to take 5-by-1 “drive direction” mosaics to survey distant terrain in more detail. Unlike Navcam drive direction panoramas (section 6.4.2), the Mastcam panoramas don’t include right-eye imaging, so do not contain depth information of tactical value. They can be shot blind as long as the rover drivers have a good estimate of the direction they will want to travel. They are useful for helping rover drivers avoid rocks that could damage the wheels. Other tactical planning products include mosaics of the work volume in front of the rover to prepare for in-situ work (see Figure 3.12), and mosaics of the region targetable by the ChemCam laser in front of and to the right side of the rover, to improve ChemCam target selection. The Mastcams are also used to inspect the turret before and after drilling and sampling operations, to image instrument inlet covers before and after sample delivery, and occasionally to capture movies of sample handling events. They are used to document the health of the wheels, but due to the position of the mast on the rover’s right shoulder, the Mastcams can only see the wheels on the right side of the rover.

7.2.2.3 *Mastcam science imaging*

Most science imaging is done through the clear filter (producing RGB color images, with infrared light cut off) unless otherwise noted.

Science images and mosaics. Both Mastcams are used to obtain targeted observations of areas of scientific interest. The images may be used for science in and of themselves for study of geomorphology, or may provide valuable context to other types of science data. If a region of interest is larger than a camera’s field of view, the Mastcam team will sequence a mosaic made of slightly overlapping images that can be assembled on Earth later.

Stereo images. The overlapping fields of view of the two Mastcams allow stereo imaging. For single observations, the Mastcams usually acquire one full frame through each eye, but mosaics require a different strategy. Because of the different fields of view of the two cameras, it would be wasteful in data bits to capture and return to Earth full images in both eyes for each spot in a stereo mosaic. So they subframe (that is, crop) Mastcam-34 images taken as part of a stereo mosaic, returning one subframed Mastcam-34 left-eye image for every Mastcam-100 right-eye image. Operationally, the team refers to these sequences as “shrinkwrap stereo,” because the field of view of the Mastcam-34 image has been shrunk to some size that contains (“wraps”) the entire Mastcam-100 image. But because the two cameras’ boresights are toed in by 2.5° (1.5° each), the horizontal position of a Mastcam-100 image within a corresponding Mastcam-34 image depends on the target’s distance from the rover. This complicates the efforts of mission planners to determine how to subframe the images. In practice, most shrinkwrap stereo observations are cropped to match the vertical extent of the Mastcam-100 image (which is the same regardless of the distance to the target), but the horizontal image dimension encompasses all possible positions of the Mastcam-34 field of view, trading slightly higher data volume for a major reduction in planning complexity. Figure 7.3 illustrates the location of the shrinkwrap stereo subframe on the left Mastcam field of view.

Focus stacks. Mastcam has the capability to take many images at different focal depths and merge them onboard into a single best-focus image and range map. This capability exists because it was required for the shallow-depth-of-field MAHLI and has only been used on Mars by Mastcam on two sets of observations: one on sol 193 and another on sol 1051/1052. For more on focus stacking, see section 7.4.2.3.

Clast surveys. After drives, the Mastcams often take a stereo pair of images of the terrain to the right of the rover. These photos are shot blind and cover the field of view of the ground temperature sensor of REMS boom 1 (see section 8.4.2.1).

ChemCam documentation. Mastcam stereo images usually provide context for ChemCam laser shot points, especially blind targets and AEGIS targets (see section 9.2.2.2). The ChemCam team has developed a method to automatically colorize ChemCam images with lower-resolution right Mastcam color information, helping them interpret their data.

Multispectral imaging for mineralogy. When a target is expected to have interesting spectral content, the team uses all or some of the science filters to image it. ChemCam laser targets, brushed spots, and areas associated with drilling, scooping, or sample dumping are usually hit with all fourteen science filters. Where the team expects to see minerals that may contain water – most often found in calcium sulfate veins crosscutting the rocks – they may perform a “hydration survey” using right-eye filters 0, 3, 4, 5, and 6, or just 0, 5, and 6, to differentiate among more-hydrated or less-hydrated forms of calcium sulfate. The smaller number of filters and use of just the right-eye camera diminishes the data volume and simplifies the planning relative to fourteen-filter observations, so hydration surveys can be small mosaics without generating a prohibitively large data volume.

When Mastcam takes multispectral images, nothing in the file names indicates which filter was used, but the filters are almost always used in order, e.g. [L0, L1, L2, ... , L6]. If it is a multi-position mosaic, the filter wheel may be spun backwards on every other footprint in order to reduce total wheel rotation, e.g. [R0, R5, R6, shift position, then R6, R5, R0, shift position, repeat].

Photometry. Multispectral observations taken with the left camera filters 1, 2, 3, and 6 of the same spot several times over the course of a day allow scientists to study surface properties of the Martian soil. Photometry surveys are often performed when the rover is parked for some period, over holidays or during anomaly investigations. They can sequence photometry observations two or three days in a row, performing them at different times of day to build up dense temporal coverage.

Atmospheric studies. The Mastcams routinely image the Sun through the solar filters, using the Sun's known brightness to probe the optical depth (which is related to how much dust is in the atmosphere). Sun images are usually subframed to 256 pixels square. At the same time, photos of the sky are usually taken in a direction away from the Sun with left-eye filters 2 and 5, which have similar bandpasses to the solar filters, to measure aerosol scattering properties. On occasion, Mastcam sky surveys span the sky from horizon to zenith, with or without multispectral observations. Beginning on sol 939, they also began to take routine images pointed due north at the distant crater rim as a way to observe the dustiness of the atmosphere within the crater.

Astronomical imaging. Astronomical imaging has a variety of scientific goals. At night, capturing movies of Phobos and Deimos passing through the field of view at the same time, or of moons occulting bright stars like Aldebaran, can help constrain the moons' orbital positions. During the day, the Mastcams can observe Phobos and Deimos transit the Sun for the same purpose (and can even image large sunspots, from a different perspective than solar spacecraft, particularly in the Sun images from sol 1000–1047, when a very large group was visible). Mastcam has also watched Phobos enter Mars' shadow, probing for dust in the upper atmosphere. It has targeted other bright sky objects, including Jupiter, Saturn, Ceres, Vesta, and stars like Regulus, and achieved a detection of Comet Siding Spring. Mastcams have even watched the Sun set, justified for atmospheric science purposes but mostly to produce evocative images of a sunset on another planet. Box 7.1 summarizes Mastcam imaging of astronomical targets.

Box 7.1. Astronomical imaging with Mastcam to sol 1800.

Sunset: 587, 956

Transits of the Sun by Phobos: 37, 42, 363, 368, 369, 713, 1032; 1692; by Deimos: 42; by Mercury: 650, 956.

Photography of Phobos: 45, 635, 662, 964; Deimos: 772, 777, 1732, 1738; 1742.

Sequence of images of Phobos entering or exiting eclipse: 393, 964, 970, 979, 987, 998, 1002; 1730; 1736; same by Deimos: 995.

Phobos over Mount Sharp at sunset: 613.

Phobos and Deimos mutual events, 351, 378, 393, 964.

Siding Spring: 772; with Earth, Phobos, and Deimos, 782; with Deimos 783; with Phobos 784.

Other: Jupiter 378; Phobos occultation of Aldebaran 387; Jupiter & moons & Phobos & Deimos 393; Phobos & Jupiter & Deimos & Ceres & Vesta & Saturn & Regulus 606, Regulus 662.

7.2.3 Anomalies

The Mastcams have worked well on Mars, with the first puzzling problem appearing early in 2017. On sol 1576, atmospheric scientist Mark Lemmon first noticed seeing large differences between the zenith atmospheric opacity measurements computed from left and right Mastcam solar images. Yet images from the two cameras do not have different brightnesses when the rover was looking in other directions through different filters. Whatever caused this change in behavior happened at some time between sol 1490 and sol 1576.⁸ At the time of writing, the best explanation appears to be that sand has blown into the right camera baffle, which flows onto the cameras' front windows when the rover looks up. The Mastcam team is working on testing this hypothesis, taking some images looking inside the Mastcam sunshade on sol 1749.

⁸Mark Lemmon, personal communication, email dated June 15, 2017

7.3 MARDI: MARS DESCENT IMAGER

The Mars Descent Imager (MARDI)'s intended purpose was to help the science team rapidly identify the location of Curiosity's landing site. The images would also bridge the gap between the orbital coverage of the site and the Mastcam view from the ground. MARDI functioned as designed, taking 622 images between heat shield separation and touchdown, and many more after (see section 2.3.7). By the time Curiosity was launched, the sharp eyes of the HiRISE camera on Mars Reconnaissance Orbiter had made MARDI's landing-site-localization function mostly redundant, but the video that MARDI returned during the descent provided engineers invaluable information on the dynamics of the landing, and provided rover fans with a thrilling movie.

MARDI was not required to operate after landing, so was never tested on Earth for survival through Mars day/night temperature cycles. It has no heaters. However, it also has no moving parts, so there is no reason to expect it to suffer from Martian conditions any more than MAHLI and the Mastcams do. Since landing, MARDI has been used to image the ground beneath the rover, documenting the rock fragments and outcrops along rover traverses.

Curiosity's MARDI was built by Malin Space Science Systems, who had also built MARDI instruments for Mars Polar Lander (which crashed) and 2001 Mars Surveyor (which was canceled). The principal investigator is Michael Malin. The Surveyor MARDI later flew to Mars on Phoenix, but was not actually used during the landing because of late-appearing concerns about the spacecraft computer's interface with the instrument. Although Curiosity's MARDI bears the same name as these predecessors, it is a wholly different instrument. It has a successor instrument already in space, the JunoCam aboard NASA's Juno orbiter mission to Jupiter. (Interestingly, JunoCam launched a few months before MARDI on Curiosity.)

7.3.1 How MARDI works

MARDI is mounted to the left front side of the rover, pointed straight downward (Figure 7.9).⁹ It uses the same detector, electronics, and software as MAHLI and the Mastcams (see section 7.2.1), with much simpler optics. It is in focus at any distance beyond 2 meters. It obtains color 1600-by-1200-pixel images over a wide field of view of 70-by-55°. Images taken after landing, from an elevation 66 centimeters above the ground, are slightly out of focus, and MARDI's ability to resolve ground features since landing is the same as it was from a height of 2 meters. On the ground, the MARDI field of view covers an area about 92 centimeters across the driving direction and 66 centimeters along the driving direction. The fixed MARDI view includes part of the left front wheel and the area immediately behind it and next to it, underneath the rover. Further MARDI facts are summarized in Table 7.4. Figure 7.10 shows examples of MARDI images taken under different conditions. They have been projected to correct for the distortion caused by its wide-angle lens.

⁹The MARDI instrument is described in Malin et al. (2009) and Malin et al. (2017)

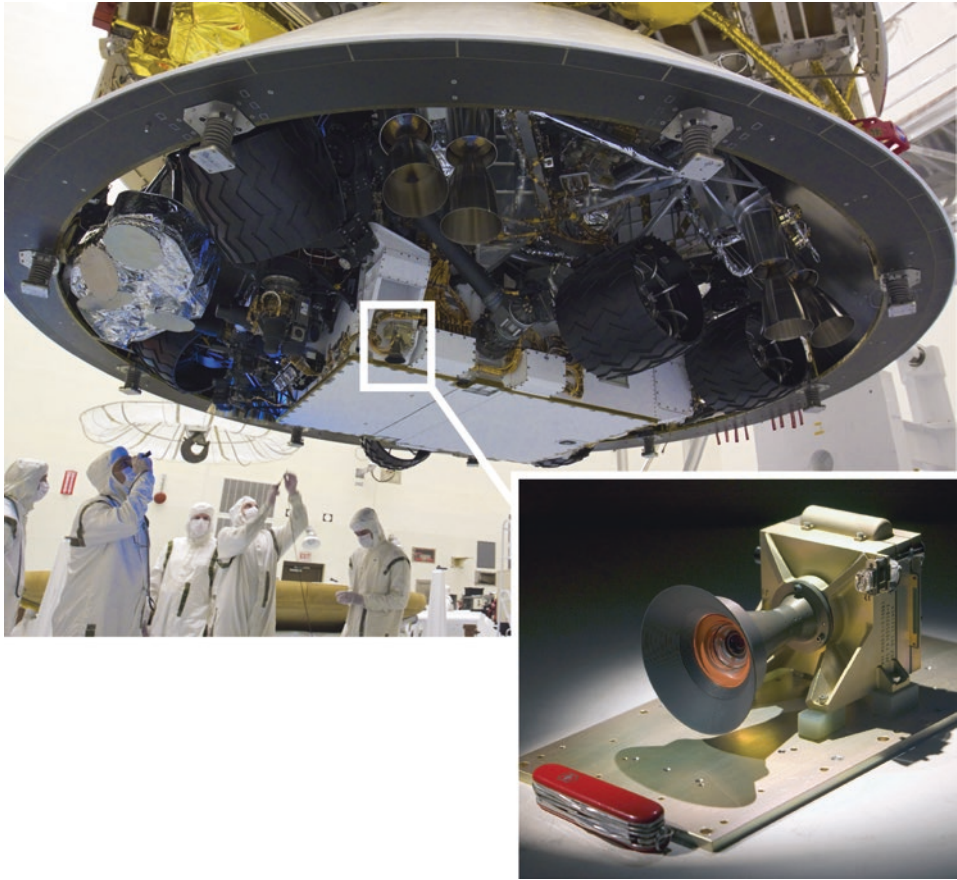


Figure 7.9. Location of the MARDI instrument on the rover. Inset photo taken at Malin Space Science Systems; large photo taken during final assembly at Kennedy Space Center, showing MARDI's point of view beneath the rover in descent configuration. NASA/JPL-Caltech/MSSS.

Table 7.4. MARDI Facts.

	2 km elevation	2 m elevation	66 cm elevation
depth of field	2m - infinity		
angular resolution	0.76 mrad/pixel		
field of view (FOV)	70° x 55°		
spatial resolution	1.5 m/pixel	1.5 mm/pixel	0.5 mm/pixel at image center (out of focus)

7.3.2 Using MARDI

Landing video. On landing day, MARDI switched on about 6 seconds before heat shield separation and took 1504 images at an average 3.88 frames per second with exposures of 0.9 milliseconds. The first 25 were black, seeing the inside of the heat shield; the next 622



Figure 7.10. Examples of MARDI images. Top: View of the heat shield during descent. Middle: sol 45 image under daylight conditions, showing reduced contrast. Bottom: sol 738 image under twilight conditions, which improves contrast. Images 0000MD000000000100035C00, 0045MD0000300000101520E01, and 0738MD0003120000102267E01. NASA/JPL-Caltech/MSSS.

chronicled the final 2.5 minutes of landing, from heat shield separation to touchdown; and the final 857 were taken on the surface. The MARDI descent images not only captured the dynamics of the spacecraft's descent, they also documented large gravel being propelled toward the rover as the rockets impinged on the surface, quickly providing an explanation of how the rover deck came to be salted with gravel.¹⁰ Unfortunately, the front element of the MARDI lens was coated with dust during the landing. The dust coating scatters sunlight, which has the effect of reducing the contrast of MARDI images taken since landing.

Clast surveys. At parking spots between traverses, MARDI shoots a photo to document the sizes and shapes of rock fragments on the surface. Since sol 310, MARDI clast survey images have mostly been taken at twilight (around 18:30 local true solar time), which reduces the light scattering off of the dusty front window, producing much higher quality images (see Figure 7.10).¹¹ Beginning on sol 488, MARDI has also sometimes been used before and after short “bumps” to obtain 4 or 5 overlapping images for analysis of the three-dimensional shapes of rock clasts.¹²

Sidewalk mode. MARDI can take movies during drives, acquiring mosaics along drive paths.¹³ In sidewalk mode, MARDI takes an image every 3 seconds, but only saves the image if onboard software determines that the new image is significantly different from the previous one. The saved images have more than 75% overlap. Returning every third image to Earth allows the construction of a mosaic, but if all images are returned, the team can generate a digital elevation model in addition to the mosaic. Sidewalk mode was tested on sol 651 and has since been used to document terrain thought to be hazardous to rover wheels as well as science stops like Pahrump Hills. A complete list of sidewalk mode observations to sol 1647 is in Table 7.5.

Table 7.5. MARDI Sidewalk Mode sequences to sol 1800.

Sol	Description
651	Test of sidewalk mode
691	Characterize terrain thought to be hazardous to rover wheels
739	Characterize terrain thought to be hazardous to rover wheels
780	Stratigraphy of Pahrump Hills outcrop
785	Stratigraphy approaching Book Cliffs
787	Stratigraphy between Book Cliffs and Gilbert Peak
790	Stratigraphy to Alexander Hills
792	Stratigraphy to Chinle outcrop
794	Stratigraphy to Whale Rock
797	Stratigraphy between Whale Rock and scuff test site
1181	Document sediment interaction with the wheels at Bagnold Dunes
1281	Document drive across knobby Stimson contact

¹⁰ Schieber et al. (2013)

¹¹ Garvin et al. (2014)

¹² Garvin et al. (2015)

¹³ Minitti et al. (2015)

7.4 MAHLI: MARS HAND LENS IMAGER

7.4.1 Introduction

The Mars Hand Lens Imager (MAHLI, pronounced “Molly”) functions as it is named: it works like the hand lens that any field geologist carries in order to examine the grain size and structure of rocks. But it’s capable of many other tricks. Located on the turret on the end of the robotic arm, MAHLI can work very close to targets, taking photos with microscopic detail, like its predecessor, the Microscopic Imager (MI) on the Mars Exploration Rover mission. Unlike MI, MAHLI is focusable, from 2.04 centimeters to infinity. When held at its minimum working distance, MAHLI can take images with resolutions of 13.9 microns per pixel, enough to resolve the finest grains of sand. But its wide (~35°) field of view makes it a useful tool for imaging large and distant objects, too. It can acquire detailed mosaics of interesting outcrops with arm motions, and obtains 3D information from stereo pairs or its focal depth.¹⁴ Figure 7.11 shows parts of the MAHLI camera, and Table 7.6 summarizes MAHLI facts.

Its position on the end of the robotic arm allows MAHLI to examine Curiosity itself, so the mission often commands it to document the condition of the wheels, remote sensing mast, and instruments. And it’s taken some of the most iconic photos of the whole mission: self-portraits of the rover at drill sites, such as the one on the cover of this book. MAHLI was built and is operated by Malin Space Science Systems, San Diego, California. The principal investigator is Ken Edgett of Malin Space Science Systems.

7.4.2 How MAHLI works

MAHLI components include a camera head mounted on the turret at the end of the rover arm, an electronics assembly located inside the body of the rover, and a calibration target mounted on the “shoulder” of the rover arm, its azimuth actuator. The camera head detector and other electronics and internal electronics assembly are identical to those of Mastcam (see section 7.2.1). Its optics, calibration target, and usage are different.

7.4.2.1 Camera head and electronics

MAHLI’s optics include a sapphire window in front of a group of stationary elements (refractive lenses). Behind the sapphire window and stationary elements is a movable group of three elements, operated by a single motor.¹⁵ Because the sapphire window has a long wave cutoff filter and the lens elements filter out ultraviolet light, only light with wavelengths ranging from 394 to 670 nanometers reaches the detector.

Various design elements help MAHLI survive extreme temperatures, exposure to dust, and sampling-related vibration. MAHLI was designed to operate between –40°C and +40°C,

¹⁴The paper of record for MAHLI is Edgett et al. (2012); two other valuable resources are Edgett et al. (2015) and Yingst et al. (2016)

¹⁵Ghaemi (2009)

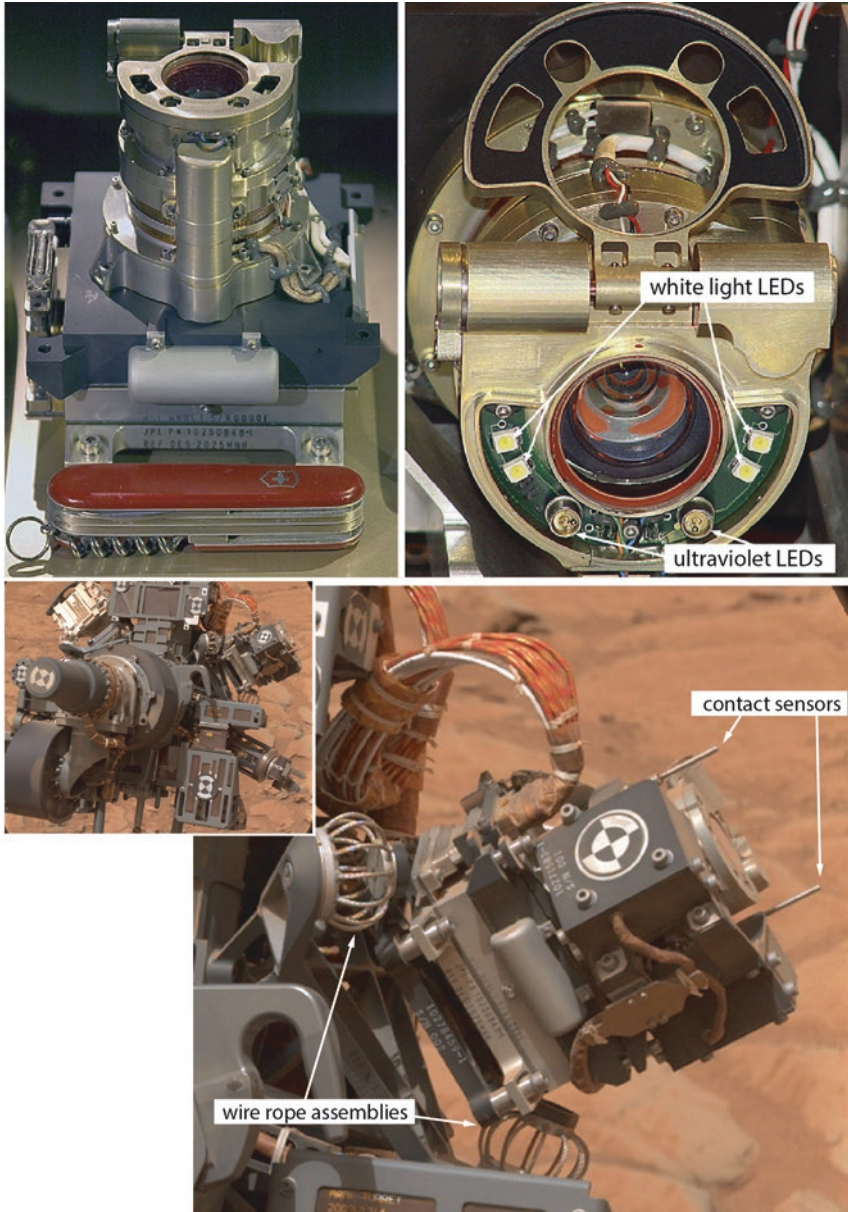


Figure 7.11. Upper left: MAHLI camera head with 89-millimeter-long pocket knife for scale. Upper right: MAHLI camera head with dust cover open. From Edgett et al, 2012. Bottom: MAHLI on Mars as viewed from the right Mastcam, Curiosity sol 128. Image 0128ML0006510000103943E01. NASA/JPL-Caltech/MSSS/Emily Lakdawalla.

Table 7.6. MAHLI Facts.

	Target located 25 cm away from front window	Target at infinity
depth of field	1 mm	–
field of view (FOV, diagonal)	34°	38.5°
FOV (horizontal 1600 pixels)	26.8°	31.1°
FOV (vertical 1200 pixels)	20.1°	23.3°
instantaneous field of view (IFOV)	402 μ rad	346 μ rad
focal ratio	f/9.8	f/8.5
effective focal length	18.4 mm	21.4 mm

but because it is outside the rover it must be able to survive far more extreme temperatures when it is powered off. It has a movable lens cover to keep the dust out. The dust cover includes a transparent Lexan lens window in order to permit imaging with the cover closed. Unfortunately, as with MARDI, a thin film of dust covered the window during landing, and photos taken with the cover closed have very low contrast and an orange-colored cast. A contact sensor assembly with two probes protects the camera against contact with the surface, causing the forward motion of the arm to stop when it has brought MAHLI's sapphire window within 17 millimeters of a hard surface. A vibration isolation platform, which connects MAHLI to the turret through a set of three springy wire rope assemblies, isolates MAHLI somewhat from the intense vibration of the drill and CHIMRA.

MAHLI carries six light-emitting diodes (LEDs) on a ring around the outside of the front lens element in order to illuminate science targets from different directions and with ultraviolet light. Windows on the dust cover allow light from the LEDs to be visible even with the cover closed. Four of the LEDs emit white light, positioned in two pairs on either side of the lens. The white-light LEDs can be commanded to operate together or independently (with either one side or the other sides or both sides lit), to simulate the way a geologist tilts a rock while examining it with a hand lens to catch glints of sunlight off of crystal facets. Nighttime white-light LED imaging also allows scientists to directly compare the colors of rock targets at different locations without having to account for differences in solar illumination.

Two ultraviolet LEDs that emit light at a wavelength of 365 nanometers are intended for identifying minerals that are fluorescent or phosphorescent, and are usually used overnight. They do leak some light in short visible wavelengths, so white surfaces appear blue in MAHLI nighttime ultraviolet images. So far there has been no unambiguous detection of fluorescent or phosphorescent minerals. It would have helped to equip MAHLI with shorter-wavelength LEDs, but no such LEDs were available when MAHLI was being designed (no flight-qualified ones, anyway).

MAHLI's camera head is connected to the electronics through an astonishing 12.7 meters of cable harness. As with Mastcam, MAHLI images are usually stored onboard the instrument in raw 8-bit form without compression or Bayer interpolation. Full MAHLI frames can be acquired at a maximum rate of about 1 frame per second, slower than the maximum rate for Mastcam. MAHLI has video capability because of its shared electronic design with Mastcam and MARDI, but it has rarely used this ability. Table 7.7 lists the few video observations with MAHLI. A rare, spectacular MAHLI video observation happened

Table 7.7. Summary of all MAHLI video mode observations to sol 1800. “ATLO” = Assembly, test, and launch operations, i.e. images taken before launch.

Date or Sol	Target Name	Day/Night
30 Nov 2010	rover deck	ATLO
2 Dec 2010	MAHLI cal target	ATLO
3 Feb 2011	infinity focus position	ATLO
26 May 2011	ATLO	ATLO
165	Sayunei	Night
166	Sayunei	Day
282	CheMin inlet	Night
687	Nova	Day

on sol 687, when MAHLI took video of the target Nova as ChemCam lasered it. MAHLI was able to see the flash of the plasma excited by ChemCam, and saw motion of dust as ChemCam blasted the target.

7.4.2.2 Focusing MAHLI

MAHLI’s focusing ability means it can point at targets from working distances as close as 2.04 centimeters from the sapphire window, and also focus at infinity. MAHLI can focus on targets with the cover in either the open or closed position. MAHLI focuses using the same motor that opens and closes the dust cover. It is a stepper motor with up to 16100 step positions (Figure 7.12). From steps 0 to 5100, the cover is closed. Then the motor engages the dust cover. Beyond a motor count of 12000, the cover is fully open. From motor steps 0 to 1480, MAHLI is in focus at its minimum working distance of 2.04 centimeters with the cover closed. With the cover still closed, it is in focus at infinity at a motor count of about 4523.

To work with the cover open, the MAHLI team commands it to fully open to a motor count of 15504, then steps to the desired focus position. MAHLI is in focus at infinity at a motor count of 12552, and in focus at its minimum distance of 2.04 centimeters at a motor count of 15600. The stepper motor moves at 150 motor steps per second, so it takes less than 2 minutes to open the cover and focus the camera. The dust cover sweeps through a space about 5 centimeters beyond the camera. To be sure of ample space to operate the dust cover safely, it is never articulated with the camera head less than 10 centimeters from a target.

Like the Mastcams, MAHLI can either be manually focused (commanded to a specific motor count position) or autofocused. The MAHLI team manually focuses images when the scene will contain a wide depth range, such as during rover wheel imaging or wide views of outcrops. Autofocus is more commonly used for hand-lens imaging where it is crucial because of MAHLI’s shallow depth of field. The depth of field ranges from about a millimeter at a working distance of 2 centimeters, to about 8 millimeters at a working distance of 12 centimeters, and continues increasing toward infinity. In fact, MAHLI focus is so sensitive to distance from the target that MAHLI autofocus distance is a tactically useful measure of the distance between a commanded turret position and a target. Ordinarily, rover planners nudge a target with the APXS contact

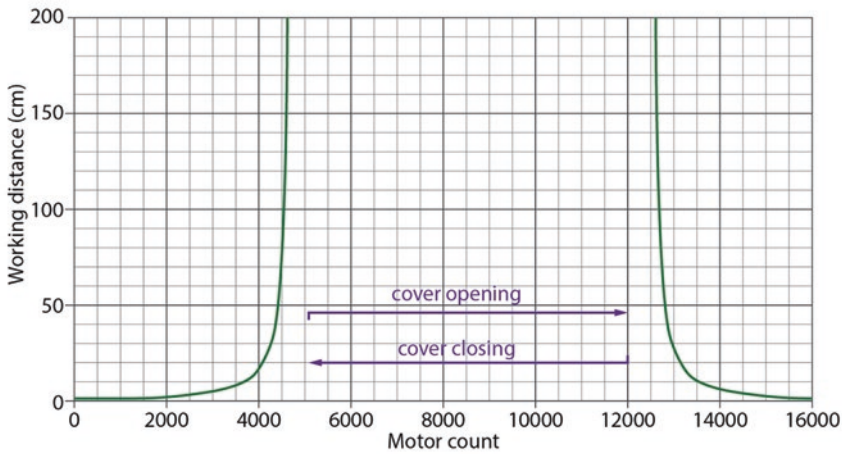


Figure 7.12. Relationship between MAHLI motor count, behavior of the lens cover, and working distance at which the target is in focus. By Emily Lakdawalla after Edgett et al. (2015).

sensor to precisely determine its range from the rover (see section 9.3). But when the APXS contact sensor isn't available for ranging (when a surface is especially rough or when it is composed of loose materials), MAHLI autofocus distance works as a measure of the distance to the target.

7.4.2.3 Z-stacks

MAHLI can obtain “z-stack” images in order to compensate for its shallow depth of field. To obtain in-focus images over a greater distance range, MAHLI can be commanded to acquire several (typically 8 or 16) images at different motor count positions. Later, using a different set of commands, onboard software will locate the best-focus parts of each image, and merge them into a single data product, called a focus-merge image product or a z-stack. As a byproduct of the focus merge process, MAHLI also creates another data product called a range map – essentially, a digital elevation model of the target. Returning a single, color-interpolated z-stack and its associated grayscale range map requires less data volume than returning the 8 images used to produce them, so it functions as a kind of data compression.

MAHLI z-stacks are usually not made until later in the sol, or even one or many sols after the original images were taken. The resulting focus-merge data products have file names and time stamps that reflect the date and time that they were produced, not the date and time of the original data, which can make them difficult to track down. Recognizing this issue, the MAHLI team has released an open-source “Principal Investigator’s

Notebook” for each of the public releases of MAHLI data, and information about which sol’s data contributed to z-stack images is included in metadata delivered to the PDS.¹⁶

7.4.2.4 Figuring out MAHLI image scale

Both the field of view and the pixel scale depend upon the working distance between MAHLI and a target. To the MAHLI team, working distance is measured from the front of the sapphire window to the target. For rover planners, the zero point is located at the minimum distance they can safely command MAHLI to take a photo, 19 millimeters in front of the sapphire window. This is usually – but not always – called the “toolframe distance”, “standoff distance” or “RP [rover planner] distance,” which distinguishes it from MAHLI instrument “working distance.” Unfortunately, rover planners sometimes refer to this as the “working distance,” which gets confusing. To convert rover-planner distances into MAHLI instrument working distances, add 19 millimeters. If you are not certain of the convention being used, you can unambiguously determine the range to the in-focus parts of an image using the motor count.

The pixel scale of a MAHLI image can be derived from the working distance (instrument team convention) using the following formula:¹⁷

$$\text{Pixel scale}(\mu\text{m} / \text{pixel}) = 6.9001 + [3.5201 \times \text{Working Distance}(\text{cm})].$$

The MAHLI team has derived an empirical relationship between motor count and working distance, based upon measuring objects of known size and distance on both Earth and Mars.¹⁸

$$w = (am^{-1} + b + cm + dm^2 + em^3)^{-1}$$

in which

w = working distance (instrument team convention)

m = motor count

$a = 0.576786$

$b = -11.8479$

$c = 2.80153 \times 10^{-3}$

$d = -2.266488 \times 10^{-7}$

$e = 6.26666 \times 10^{-12}$.

¹⁶The MAHLI Principal Investigator’s Notebooks are available for download from Ken Edgett’s page on Researchgate: https://www.researchgate.net/profile/Ken_Edgett/publications

¹⁷Mars Science Laboratory (MSL) Software Interface Specification for Camera & LIBS Experiment Data Record (EDR) and Reduced Data Record (RDR) Data Products version 3.5, August 5, 2014

¹⁸Yingst R A et al (2014) Cameras on Landed Payload Robotic Arms – MAHLI and Mars and Lessons Learned from One Mars Year of Operations. Paper presented to the International Workshop on Instrumentation for Planetary Missions (IPM-2014), 4-7 Nov 2014

Table 7.8 is a lookup table relating motor count to working distance, pixel scale, and image size. The last three columns provide a guide to the size of sediment grains that can be resolved in images taken at different distances, according to the classic Wentworth (1922) sediment classification scheme. It takes at least 2 pixels across an object to be able to detect it, so sand grains are resolvable from MAHLI standoff distances under about 1 meter, while silt grains are only resolvable at the very closest standoff distances, and then only the coarsest silt grains that have good contrast against the background. As a rule of thumb, if you can see individual grains in a sedimentary rock in a Mastcam image, you're looking at a conglomerate; if you can see individual grains in a MAHLI image but not in a Mastcam image of the same target, it's a sandstone; and if you can't detect grains even with MAHLI, it's a siltstone or mudstone.

7.4.2.5 *Calibration target*

MAHLI's calibration target is attached to the robotic arm shoulder azimuth actuator (Figure 7.13). A preflight photograph of the calibration target is shown in Figure 7.14. The calibration target contains red, green, blue, and gray color swatches made from the same material used in the Mastcam calibration target, leftover materials from the Mars Exploration Rover Pancam calibration target. There is also a fluorescent chip made of a material called SpectraFluor Red that glows red (at a wavelength of 626 nanometers) when illuminated with the MAHLI ultraviolet LEDs (365 nanometers). An opal glass bar target has a chart modeled on the US Air Force 1951 Resolution Test Chart, designed to monitor camera focus and resolution performance over time. The calibration target is mounted vertically on the rover, which was intended to discourage dust settling and keep it relatively clean. Unfortunately, the calibration target was coated with a thin film of dust thrown up during landing, but the calibration target functions adequately for its primary purpose of checking that there is no drift in camera focus. The calibration target has been imaged on sols 34, 165, 179, 322, 411, 591, 825, 989, 1091, 1157, 1340, 1519, 1632, and 1696. MAHLI has imaged the Mastcam calibration target on sols 544, 707, and 1028. MAHLI also images the Mastcam and ChemCam calibration targets in nearly every self-portrait.

There are several quirky elements in the MAHLI calibration target. A cartoon of "Joe the Martian" is meant as a thank-you to the public for the opportunity to conduct the MAHLI investigation and as an invitation for children to follow the Curiosity mission. The Greek letters " $\gamma\delta\beta\gamma$ " are printed within the "0" of the "1.0" text on the bar target. A 1909 United States penny is embedded in the bottom of the calibration target. It is intended as an homage to field geologists' practice of placing a coin or other small object on a rock outcrop to provide scale before taking a photo, and the MAHLI team often includes a picture of it in public releases of MAHLI images (Figure 7.15). 1909 was the first year that the Lincoln cent was issued, and would have been a century before the year of Curiosity's launch; unfortunately, the launch delay to 2011 obscured the significance of the date on the 1909 coin. The coin is 19 millimeters in diameter.

Table 7.8. MAHLI image dimensions and pixel scale with respect to motor count. Lines in bold represent very common motor counts for MAHLI, near standard target standoff distances of 25, 5, and 2 centimeters.

Motor count (cover closed)	Motor count (cover open)	working distance from MAHLI front window (cm)	toolframe or standoff distance (cm)	pixel scale (μm)	Width of 1600-pixel image (cm)	Depth of field (near, mm)	Depth of field (far, mm)	width of 10mm scale bar (pixels)	Max diameter of a granule (4mm) (pixels)	Max diameter of a grain of sand (2mm) (pixels)	Max diameter of a grain of silt (62.5 μm) (pixels)
4475	12600	231	229	819	131	-891	4531	12	4.9	2.4	<1
4375	12700	84.0	82.1	302	48.4	-155	261	33	13	6.6	<1
4275	12800	50.7	48.8	185	29.7	-60.9	83.2	54	22	11	<1
4175	12900	35.9	34.0	133	21.3	-31.7	39.4	75	30	15	<1
4075	13000	27.6	25.7	104	16.6	-19.1	22.4	96	38	19	<1
4061	13014	26.7	24.8	101	16.1	-18.0	20.9	99	40	20	<1
3975	13100	22.2	20.3	85.1	13.6	-12.7	14.2	117	47	23	<1
3875	13200	18.5	16.6	71.9	11.5	-8.9	9.7	139	56	28	<1
3775	13300	15.7	13.8	62.1	9.94	-6.6	7.0	161	64	32	1
3675	13400	13.5	11.6	54.6	8.73	-5.1	5.2	183	73	37	1.1
3575	13500	11.9	10.0	48.6	7.78	-4.0	4.0	206	82	41	1.3
3475	13600	10.5	8.6	43.8	7.00	-3.2	3.2	229	91	46	1.4
3375	13700	9.3	7.4	39.7	6.36	-2.7	2.6	252	101	50	1.6
3275	13800	8.4	6.5	36.4	5.82	-2.2	2.2	275	110	55	1.7
3175	13900	7.5	5.6	33.5	5.36	-1.9	1.8	299	119	60	1.9
3077	13998	6.9	5.0	31.0	4.97	-1.6	1.6	322	129	64	2.0
3075	14000	6.8	4.9	31.0	4.96	-1.6	1.6	323	129	65	2.0
2975	14100	6.2	4.3	28.8	4.61	-1.4	1.4	347	139	69	2.2
2875	14200	5.7	3.8	26.9	4.31	-1.2	1.2	371	148	74	2.3
2775	14300	5.2	3.3	25.3	4.04	-1.1	1.1	396	158	79	2.5
2675	14400	4.8	2.9	23.8	3.81	-1.0	1.0	420	168	84	2.6
2575	14500	4.4	2.5	22.5	3.59	-0.9	0.9	445	178	89	2.8
2475	14600	4.1	2.2	21.3	3.41	-0.8	0.8	470	188	94	2.9
2411	14664	3.9	2.0	20.6	3.29	-0.8	0.8	486	194	97	3.0
2375	14700	3.8	1.9	20.2	3.24	-0.7	0.7	495	198	99	3.1
2275	14800	3.5	1.6	19.3	3.08	-0.7	0.7	519	208	104	3.2
2175	14900	3.3	1.4	18.4	2.94	-0.6	0.6	544	218	109	3.4
2075	15000	3.0	1.1	17.6	2.82	-0.6	0.6	568	227	114	3.6
1975	15100	2.8	0.9	16.9	2.70	-0.5	0.6	593	237	119	3.7
1875	15200	2.6	0.7	16.2	2.59	-0.5	0.5	617	247	123	3.9



Figure 7.13. Photo of the rover taken during assembly at JPL, showing the location of the calibration target. NASA/JPL-Caltech release PIA14289. Insets: two images of the calibration target, taken before departing Earth using a DSLR camera (left) and after landing on Mars, by MAHLI (right). Image 0034MH0000460010100041E01. NASA/JPL-Caltech/MSSS/Emily Lakdawalla.

7.4.2.6 Bad pixels and blemishes

MAHLI has a few dozen dark specks in all images. These have been constant throughout the mission, and are caused by microscopic particles on the detector. The MAHLI team is more concerned about the possibility that operating the camera close to the surface will invite dust to settle on the optics when the cover is open, especially when operating near freshly drilled rocks and their piles of fine drill tailings. They try to take flat-field images of the sky about once every 180 days, in part to watch for new dust particles affecting their images. One dust particle was detected on the sapphire window in a Mastcam image of MAHLI taken on sol 617.

Like the Mastcams, MAHLI is susceptible to shutter smear (see section 7.2.1.5). In fact, MAHLI experiences shutter smear at longer exposures than Mastcam and MARDI because it takes longer for MAHLI to read out its images. However, it doesn't affect science data and is mostly only noticeable in self-portrait photos, when white surfaces of the rover can appear smeared. Hot pixels often cause streaks running down images due to shutter smear. MAHLI landed with a number of hot pixels, and new ones have appeared during the course of the mission; some heal, but others have persisted. While these are cosmetically annoying, they don't affect the quality of the data for science.

7.4.3 Using MAHLI

Because using MAHLI almost always requires using the arm, there are fewer opportunities for MAHLI science than for Mastcam science. A substantial portion of the MAHLI data set is engineering support imaging and rover self-portraits. Various types of MAHLI

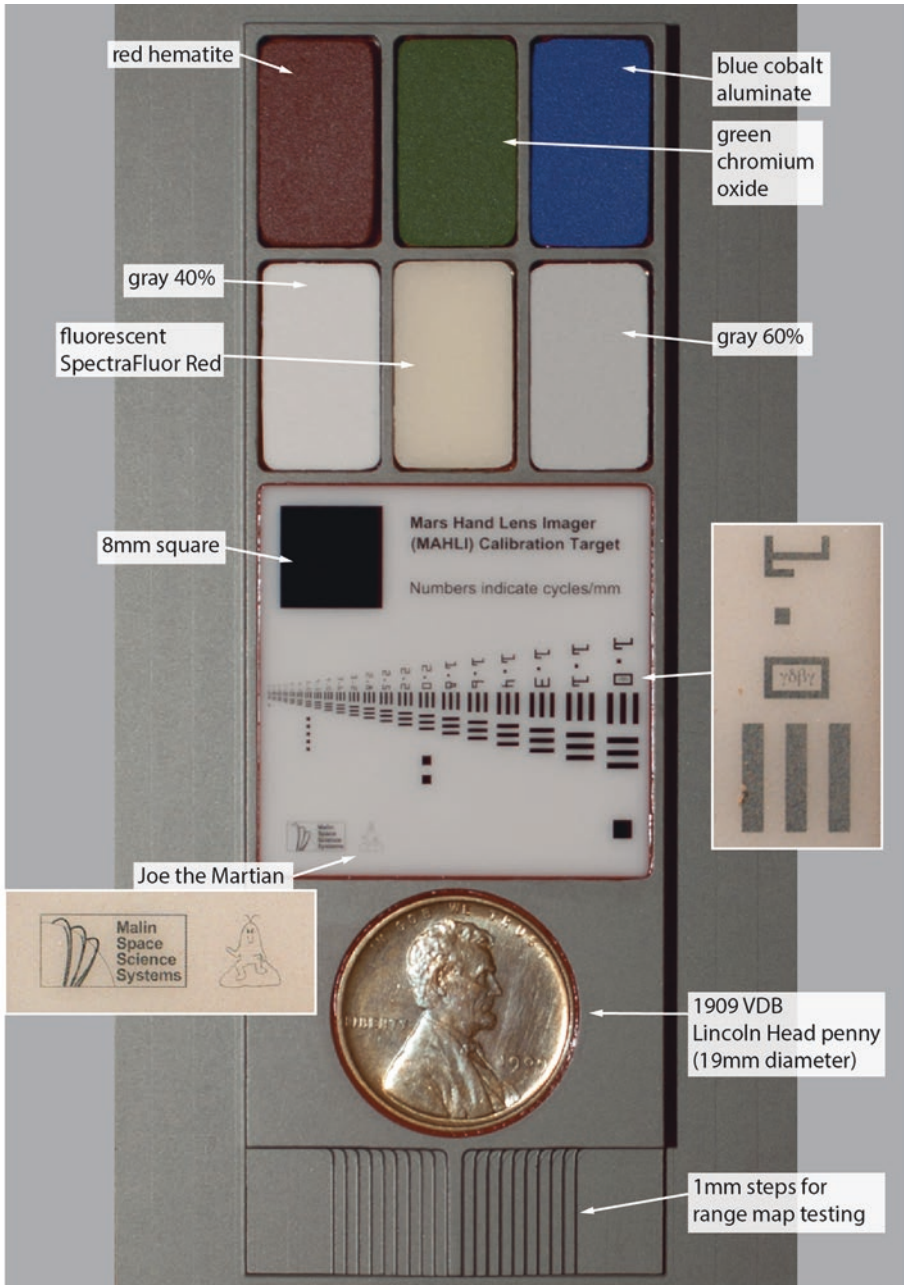


Figure 7.14. MAHLI calibration target, taken during spacecraft assembly. Inset images are from Mars, images 0034MH0000440010100031C00 and 0034MH0000450010100C00. NASA/JPL-Caltech/MSSS/Emily Lakkawalla.



Figure 7.15. A mosaic of nine MAHLI images on a conglomerate target taken at the Darwin waypoint, sol 400. The penny is 19 millimeters in diameter. NASA/JPL-Caltech/MSSS image release PIA17362.

imaging also provide context and support for drilling, scooping, sample dumping, and APXS activities, helping to build a multi-instrument data set. When MAHLI can reach them, it's often pointed at ChemCam shot points. Occasionally, MAHLI captures large mosaics, allowing detailed study of the sizes, shapes, colors, and distributions of grains within a rock for sedimentology studies.

7.4.3.1 MAHLI nested target imaging

A major use of MAHLI is to capture sets of nested images of targets that are usually also APXS targets, including drill sites. Usually, MAHLI takes a single context image from a standoff distance of 25 centimeters, achieving a scale of about 100 microns per pixel. Then it moves to a standoff distance of 5 centimeters and takes a z-stack at about 31 microns per pixel, often repeating the observation from a slightly different position for stereo imaging purposes. This image scale is the same as that of MI images taken by the Mars Exploration Rovers, making it simple to compare close-up data from Spirit or Opportunity APXS and MI with Curiosity APXS and MAHLI. For some observations, MAHLI acquires an observation from a standoff distance of only 1 or 2 centimeters, with a “best” resolution of 16 to 21 microns per pixel (Figure 7.16). To capture these, the MAHLI team asks the rover planners to get MAHLI as close as possible to the target, which varies depending upon the target’s topography and reachability. Sometimes MAHLI will do these observations at night, so that the LEDs can illuminate the target with light of a well-known intensity, allowing the team to directly compare the color of one target to another imaged at another location. Sometimes MAHLI will take nested images of targets both before and after brushing.

7.4.3.2 Mosaics

It takes close cooperation between the rover planners and MAHLI team to produce a MAHLI mosaic, so there have not been many, but they are scientifically productive on sedimentary targets with varying grain size (e.g. Figure 7.16). It’s also fun and educational to use MAHLI to image a vertical rock face from a low angle not accessible by Mastcam; these “dog’s eye” views are often expanded into mosaics. A list of MAHLI mosaics is in Table 7.9.

7.4.3.3 MAHLI Landscape Imaging

When the zoom capability was descopeed from the Mastcams, the rover lost its ability to capture wide views of the Martian landscape in color using a single frame. MAHLI is now the widest-angle color camera on the rover that can do landscape imaging, so soon after landing the team planned to use MAHLI during traverses to take single pre- or post-drive images to document the changing landscape. MAHLI takes these images from its stowed position, so they can be captured on sols when available resources restrict use of the arm. When stowed, the camera looks over the rover’s left shoulder (measured about 110° to the left of the rover’s forward direction), and images are rotated about 150° counterclockwise from horizontal. MAHLI performed its first infinity-focus test on sol 274, just before leaving Yellowknife Bay. The experiments determined the best-focus motor position for landscape imaging (a motor count of 12552), and throughout the drive to Mount Sharp MAHLI took a single photo at this motor count after most drives. An example of a MAHLI landscape image is shown in Figure 7.17. The last such routine landscape image was on sol 1112, but the team continues to occasionally request such photos when they’re expected to show a subject of scientific or engineering interest.

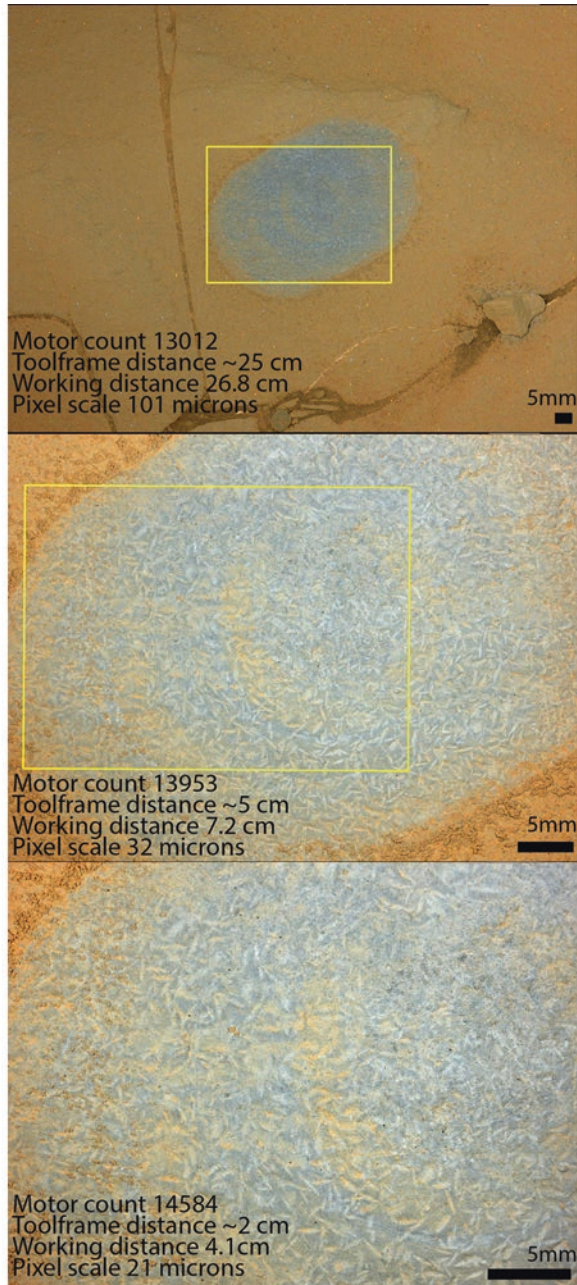


Figure 7.16. MAHLI images of target “Mojave” taken at night on sol 809 under LED illumination at three different working distances, after the target had been brushed. Images 0809MH0004440010300853C00, 0809MH0004450010300857C00, and 0809MH0004460010300905C00. NASA/JPL-Caltech/MSSS/Emily Lakdawalla.

Table 7.9. Sols and names of MAHLI mosaics as of sol 1648.

Bradbury Group	Pahrump Hills	North of the Dunes	South of the Dunes
66 Rocknest Scoop 1 Trough	802 Garlock	974 Bigfork	1407 Robotic arm workspace
	805 Pelona	998 Ronen	1407 Boulder with targets
67 Rocknest Scoop 2 Trough	805 Ricardo	1028 Big_Arm	named Tumba and Funda
	808 Rosamond	1031 Dog's eye of	1409 Funda
84 Self Portrait	809 Mojave	Missoula Area	1418 Marimba
85 Self Portrait (stereo)	810 Potatoe	1032 Clark	1457 Quela
154 Persillion	813 Punchbowl	1057 Buckskin	1463 Self Portrait
158 Tindir	814 Anaverde	1065 Rover	1463 Ombomboli
168 JK/YKB Drill	814 Afton_Canyon	Undercarriage	1474 Utuseb
Candidate Site	815 Topanga	inspection	1474 Jwaneng
177 Self Portrait	819 Mescal	1092 Lebo	1482 Cassongue
230 John Kllein Hole and Cuttings	824 Puente	1105 Sacajawea	1491 Sebina
	828 Chinle Oblique	1105 Winnipeg	1504 Thrumcap
270 McGrath	868 Self Portrait	1114 Big_Sky	1504 Wonderland
283 Cumberland Drill Site	869 Mojave Chunk	1126 Self Portrait	1514 Southwest_Harbor
	882 Self Portrait	1157 Augusta	1518 Folly_Island
291 Narrows_3	Extension	1166 Swakop	1523 Seawall
292 Narrows_3	905 Telegraph_Peak	1182 track_wall	1531 Precipice
303 Point Lake	930 Coalville	1182 Weissrand	1552 The_Anvil
322 Ailik_RP	935 APXS vein material	1202 Greenhorn Sieved	1566 Old_Soaker Workspace
324 Fleming	raster	Sample	1566 Old_Soaker
387 Ruker	937 Back of Coalville	1228 Gobabeb Scoop 1	1566 Bar_Island
398 vein_mosaic	938 APXS vein material	1228 Self-portrait	1570 Valley_Cove (and
400 vein_mosaic	raster extension	1241 Self Portrait	Gilley_Field)
400 conglomerate mosaic_left	946 Kern_Peak	Supplemental frames	1581 Smalls_Falls
	946 Vein Material	1254 Kuiseb	1589 Cape_Elizabeth
400 conglomerate mosaic_right	T-shaped	1275 Palmhorst	1591 Munsungun
	948 Vein Material Stereo	1275 Palmwag	1593 Misery
442 Cooperstown	mosaic	1277 Sperrgebiet	1611 Patch_Mountain
487 Cumberland Dump Pile		1277 Klein_Aub	1614 Chain_Lakes
		1278 Sperrgebiet	1614 Spider_Lake
550 Bungle Bungle		1279 Khomas	1634 Canada_Falls
583 Square_Top		1325 Lianshulu	1668 Morancy_Stream
584 Square_Top		1327 Lubango	1675 Lookout_Point
Dogseye		post-sieve discard pile	1679 Maple_Spring
585		1330 Okoruso	1702 Fern_Spring
right of Square_Top		1338 Self Portrait	1714 Prays_Brook
585 Square_Top		1341 Kwakwas	1715 Old_Mill_Brook
585 Rock face right of Square_Top		1341 Okoruso Site	1727 Jones_Marsh
		1344 Impalila	1734 Pecks_Point
591 Tickalara Trough		1351 Dog's eye of	1749 Ile_Damour
605 Lagrange		Nauaspoort	1788 Dumplings_Island
612 Windjana		1371 Berg_Aukas	1811 Mount_Ephraim
613 Self Portrait		1380 Koes	1865 Barberton
615 Windjana			
627 Windjana Drill Hole Cuttings			
629 Stephen			
722 BonanzaKing2			
722 BonanzaKing1			
726 BonanzaKing2			

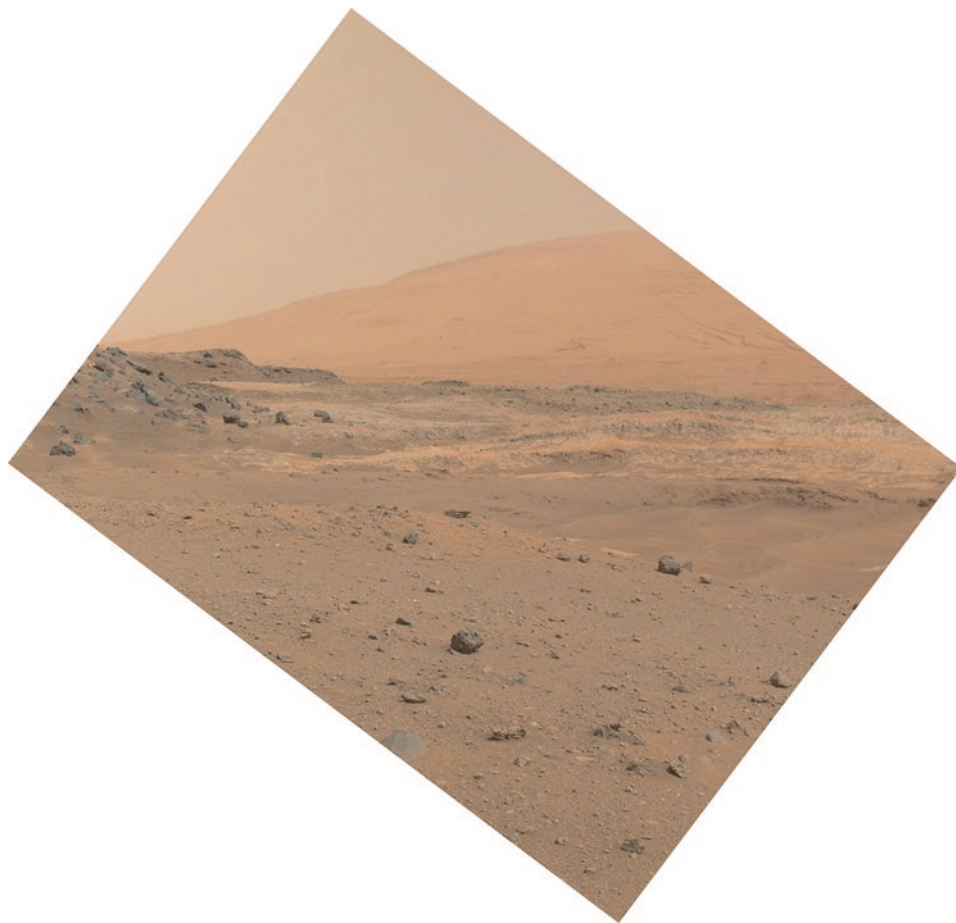


Figure 7.17. A MAHLI stowed-position landscape image from sol 952, in “Artist’s Drive” beyond Pahrump Hills. Image 0952MH0003250050304147E01. NASA/JPL-Caltech/MSSS.

7.4.3.4 MAHLI engineering support images

MAHLI is regularly used to examine hardware on the rover, in particular the rover’s wheels, because the mast-mounted cameras can only see the right side wheels partially and the left side wheels not at all. MAHLI documented the first visible puncture in a rover wheel on sol 411, and has monitored wheel condition since then (see section 4.6.4). MAHLI also monitors dust accumulation on the REMS ultraviolet sensor and has been used as a diagnostic tool for the condition of the REMS wind booms, dust accumulation on the ChemCam and ChemCam windows, and interior of the CheMin inlet.

7.4.3.5 MAHLI self-portraits

Self-portraits are a special rover self-examination product. They are mosaics of more than 50 MAHLI images, taken with the arm held out and in front of the rover. A MAHLI self-portrait has become part of the standard set of documentation activities performed at sample sites, though the mission forgoes the self-portrait if pressed for time.

The rover usually holds MAHLI about 2 meters above the bottoms of the rover wheels (that is, at “eye level”) for self-portraits. To capture the images for the mosaic, the arm rotates the camera in such a way as to keep MAHLI fixed in one location with only its optical axis pivoting. MAHLI takes images for the upper half of the mosaic first, then repositions the arm to keep it from blocking the camera’s view and takes the photos for the lower half. Rover planners time the mosaic carefully to keep not only the arm but also its cast shadows out of view as much as possible, because the moving arm shadows make assembly of the mosaic difficult.

At the Buckskin drill site on sol 1065, the rover planners implemented a special position for the self-portrait, with MAHLI held in nearly the same position as it is for wheel imaging. The low perspective gives the impression of the rover looming over the observer. Figure 7.18 shows some of the MAHLI frames used to create the Buckskin self-portrait, which also graces the cover of this book.

Table 3.3 documents all sampling activities, including self-portraits at sample sites. At John Klein, Windjana, Confidence Hills, and Quela, the MAHLI team took a full self-portrait on one sol, before drilling, and then supplemented the self-portrait with extra frames taken on subsequent sols to document the change at the site after sampling activities were complete. Two self-portraits have included imaging of the mast head in more than one position. At Windjana, MAHLI imaged the head both facing the camera and looking down at the drill site. At Okoruso, MAHLI imaged the head both facing the camera and facing away, looking at Mount Sharp.

7.4.4 Anomalies and precautions

Through sol 1800, MAHLI has had no hardware issues apart from the dusting of the originally transparent lens cover during the rover’s descent to the surface. However, on one occasion, a MAHLI problem caused a robotic arm fault, and on another, a MAHLI issue required a 2-week recovery including 8 sols in which the dust cover was open.

The first of these anomalies occurred on sol 615. MAHLI was imaging the recently drilled Windjana mini-drill hole when the camera head faulted, causing the arm to be unable to move while the rover awaited analysis and further instruction from Earth. During the 2-sol wait, MAHLI was held just 5 centimeters above the fresh drill cuttings, with its cover open. The fault had to do with real-time MAHLI image compression producing unexpectedly large image files. MAHLI was returned to normal operation on sol 627.

The second anomaly occurred on Sol 1619. In this case, the MAHLI cover failed to open completely. As in the previous fault, the arm didn’t move, pending further instruction from the ground. The dust cover stayed open for 8 sols. Inspection using the Mastcams, Navcams, and Hazcams, followed by careful testing of the dust cover on

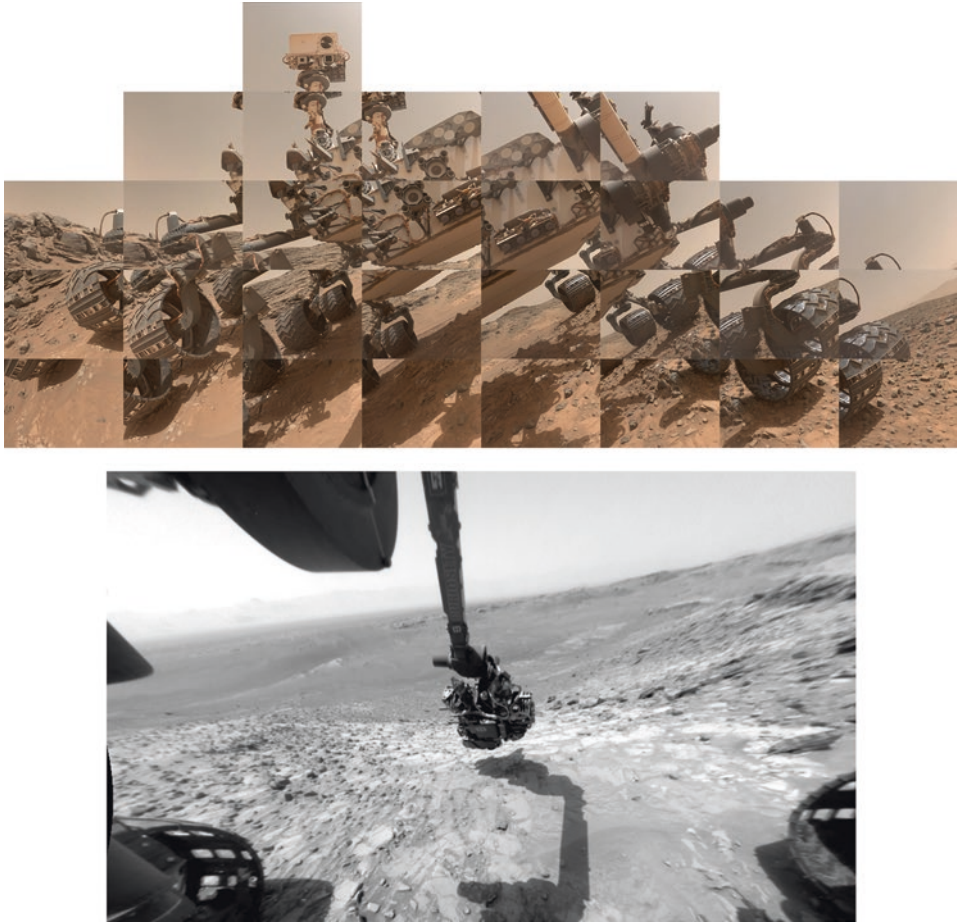


Figure 7.18. Top: A subset of the MAHLI frames used to produce the mosaic printed on the cover of this book, taken at Buckskin on sol 1065. Bottom: View of the turret taken from the left front Hazcam during the Buckskin self-portrait sequence. A small local low in topography allowed the rover planners to create this unusual low-angle view. MAHLI is located on the upper right side of the turret in this view. NASA/JPL-Caltech/MSSS/Emily Lakdawalla.

subsequent sols, showed normal operation. Investigation revealed that while MAHLI was operating within its allowable temperature range, the fault occurred at a temperature lower than MAHLI had ever been commanded to operate before. Flight rules were modified to require MAHLI operation at higher temperatures, with the low-temperature limit set at -20°C .¹⁹

On sols 764, 774, and 1575, the arm has faulted during MAHLI imaging, leaving the MAHLI cover open for a few sols during recovery. To avoid long periods of the MAHLI

¹⁹Ashwin Vasavada, interview dated March 10, 2017, and Ken Edgett, email dated April 10, 2017

cover being left open as a result of an arm fault, MAHLI now requires the cover to be closed for all imaging performed within a few sols before holiday or conjunction periods. That leaves enough time for recovery and cover close before a command moratorium.

Toward the end of September 2016, as Curiosity cleared the Murray buttes and re-entered the Bagnold dune field and its sand transport corridor, repeat imaging of sandy spots showed dramatic wind-induced sand motion. Blowing sand presents little hazard to MAHLI (sand grains are too heavy to stick to the window), but finer materials like drill tailings could be a concern. If blowing sand grains strike dust or drill cuttings on the ground, the fine material can be lofted into the wind and then stick electrostatically to MAHLI's sapphire window. Between the Sebina, Precipice, and Ogunquit Beach sample sites in late 2016 and early 2017, the MAHLI team performed all close-up imaging with the cover closed. And as a precaution while driving across windy sand transport corridors, the MAHLI team modified their operations procedures to open the dust cover with the camera aimed down, so that any sand particles that do strike the front of MAHLI's optics will (hopefully) bounce or roll off.

7.5 REFERENCES

- Alexander D and Deen R (2015) Mars Science Laboratory Project Software Interface Specification: Camera & LIBS Experiment Data Record (EDR) and Reduced Data Record (RDR) Data Products, version 3.5
- Bell J et al (2012) Mastcam multispectral imaging on the Mars Science Laboratory rover: Wavelength coverage and imaging strategies at the Gale crater field site. Paper presented at the 43rd Lunar and Planetary Science Conference, The Woodlands, Texas, 19–23 Mar 2012
- Bell J et al (2017) The Mars Science Laboratory Curiosity rover Mast Camera (Mastcam) instruments: Pre-flight and in-flight calibration, validation, and data archiving. *Earth and Space Sci*, DOI: 10.1002/2016EA000219
- Edgett K et al (2012) Curiosity's Mars Hand Lens Imager (MAHLI) investigation. *Space Sci Rev* 170:259–317, DOI: 10.1007/s11214-012-9910-4
- Edgett K et al (2015) Curiosity's robotic arm-mounted Mars Hand Lens Imager (MAHLI): Characterization and calibration status. In: MSL MAHLI Technical Report 0001, Version 2, DOI: 10.13140/RG.2.1.3798.5447
- Garvin J et al (2014) Sedimentology of Martian gravels from MARDI twilight imaging: Techniques. Paper presented at the 45th Lunar and Planetary Science Conference, The Woodlands, Texas, 17–21 Mar 2014
- Garvin J et al (2015) Terrain analysis of Mars at cm-scales from MARDI stereo imaging. Paper presented at the 46th Lunar and Planetary Science Conference, The Woodlands, Texas, 16–20 Mar 2015
- Ghaemi F T (2009) Design and fabrication of lenses for the color science cameras aboard the Mars Science Laboratory Rover. *Optical Engineering* 48:10, DOI: 10.1117/1.3251343

- Kinch K et al (2013) Dust on the Curiosity mast camera calibration target. Paper presented at the 44th Lunar and Planetary Science Conference, The Woodlands, Texas, 18–22 Mar 2013
- Maki J et al (2012) The Mars Science Laboratory engineering cameras. *Space Sci Rev* 170:77–93, DOI: 10.1007/s11214-012-9882-4
- Malin M et al (2009) The Mars Science Laboratory (MSL) Mars Descent Image (MARDI) Flight Instrument. Paper presented at the 40th Lunar and Planetary Science Conference, The Woodlands, Texas, 23–27 Mar 2009
- Malin M et al (2010) The Mars Science Laboratory (MSL) mast-mounted cameras (Mastcams) flight instruments. Paper presented at the 41st Lunar and Planetary Science Conference, The Woodlands, Texas, 1–5 Mar 2010
- Malin M et al (2017) The Mars Science Laboratory (MSL) Mast cameras and Descent imager: Investigation and instrument descriptions. *Earth and Space Sci*, DOI: 10.1002/2016EA000252
- Minitti M et al (2015) Mapping the Pahrump Hills outcrop using MARDI sidewalk mosaics. Paper presented at the 46th Lunar and Planetary Science Conference, The Woodlands, Texas, 16–20 Mar 2015
- Schieber J et al (2013) The final 2 1/2 minutes of terror – what we learned about the MSL landing from the images taken by the Mars Descent Imager. Paper presented at the 44th Lunar and Planetary Science Conference, The Woodlands, Texas, 18–22 Mar 2013.
- Wentworth C (1922) A scale of grade and class terms for clastic sediments. *J Geol* 30:377–392, DOI: 10.1086/622910
- Yingst R A et al (2014) Cameras on Landed Payload Robotic Arms – MAHLI and Mars and Lessons Learned from One Mars Year of Operations. Paper presented to the International Workshop on Instrumentation for Planetary Missions (IPM-2014), 4–7 Nov 2014
- Yingst R A et al (2016) MAHLI on Mars: Lessons learned operating a geoscience camera on a landed payload robotic arm. *Geosci Instrum Method Data Syst* 5:205–217, DOI:10.5194/gi-5-205-2016

8



Curiosity's Environmental Sensing Instruments

8.1 INTRODUCTION

Environmental sensing instruments include the Rover Environmental Monitoring Suite (REMS), a package of several meteorological instruments, and the Radiation Assessment Detector (RAD), which measures the radiation dose at the surface. Dynamic Albedo of Neutrons (DAN) straddles the boundary between remote and environmental sensing; in passive mode it detects ambient neutrons, and in active mode it can also bombard the surface with neutrons to explore for subsurface water and light elements.

The environmental instruments operate mostly in the background, quietly taking data at routine intervals. Sequencing them mostly involves commanding when to retrieve the data from Mars. They can operate during periods like holidays and conjunctions when the rover is otherwise inactive, and some components operate even while the rover is asleep.

8.2 RAD: RADIATION ASSESSMENT DETECTOR

The Radiation Assessment Detector (RAD) is an energetic particle analyzer, performing the first-ever direct radiation measurements on the surface of Mars.¹ It is funded by NASA's Exploration Science Mission Directorate – the human exploration side of NASA. A major goal of the RAD investigation is to assess the hazard that energetic particles pose to future human astronauts. RAD was already detecting them while Curiosity cruised toward Mars, so RAD produced some of the first scientific results of the Curiosity mission. The RAD principal investigator is Donald Hassler of Southwest Research Institute, Boulder, Colorado.

¹RAD's design and function is described in Hassler et al. (2012); two post-landing summaries of RAD performance and results are Matthiä et al. (2016) and Zeitlin et al. (2016)

8.2.1 Scientific background

Most of the energetic particles that RAD detects on the surface of Mars are galactic cosmic rays, except during solar events. Galactic cosmic rays are high-energy particles that probably originate in supernovae. Most of them (85–90%) are protons, and most of the rest are helium nuclei; electrons and heavier nuclei account for 1% each. The flux of galactic cosmic rays varies with solar activity: there are fewer cosmic rays near solar maximum, when the heliosphere pushes outwards and provides the solar system more protection from cosmic rays.

Solar energetic particles originate in the solar corona along with flares and coronal mass ejections. Solar events can produce 10,000 times more particles than the normal background rate. During big solar events, solar particles can overwhelm galactic cosmic rays as the primary source of energetic particles at the surface of Mars, but only for brief periods of a few hours to a few days. Mars and Earth will usually not see the same fluxes of solar particles, because they usually see the Sun from different directions.

Mars' thin atmosphere shields the surface from lower-energy solar energetic particles but presents almost no barrier to cosmic rays. Mars lacks any significant magnetic field, so can't deflect incoming charged particles, as Earth can. Almost all of the cosmic rays that hit the atmosphere reach the surface, producing a radiation dose 1000 times that experienced at the surface of Earth. As the incoming particles strike atoms in the Martian atmosphere and surface (and in rovers), the collisions generate secondary particles like neutrons and gamma rays, so the number of energetic particles at the Martian surface is actually greater than it is above the atmosphere. However, this increase in energetic particle flux doesn't result in an increased radiation dose, because the heaviest, most damaging ions – such as iron nuclei – fragment into smaller nuclei as they experience collisions in the atmosphere, with only 25% of them reaching the surface. So Mars' atmosphere does provide a small amount of protective shielding, but many protons still reach the surface unimpeded, and the breakup of larger nuclei results in more protons than in space.

Mars' surface has presumably been exposed to this bombardment from energetic particles for many millions (perhaps billions) of years. Ionizing radiation has likely changed the chemistry of the Martian surface. It could be one cause of the weathering rinds that have formed on Martian rocks. Mars is the inverse of Mercury in terms of its experience of space weathering: Mars suffers ionizing radiation but not micrometeorite impacts, while Mercury (which has a weak magnetic field but no atmosphere) suffers micrometeorite impacts but little ionizing radiation. The Moon withstands both; Earth, little of either.

8.2.2 How RAD works

RAD is located within the body of the rover. It looks upward through a thin Kapton window on the rover deck that allows particles to pass into the instrument (Figure 8.1). The sensor has a view cone 65° wide. The size of the cone represents a trade-off between observing as wide a portion of the sky as possible and keeping the mass and volume of the instrument as small as possible. Its sensor head contains multiple silicon detectors in a vertical stack. Depending on their energy, charged particles may penetrate none, some, or all of the detectors. Besides charged particles, RAD can also detect neutrons and gamma rays. RAD accumulates about 400 kilobytes of data in an ordinary sol. It has 16 megabytes of RAM.

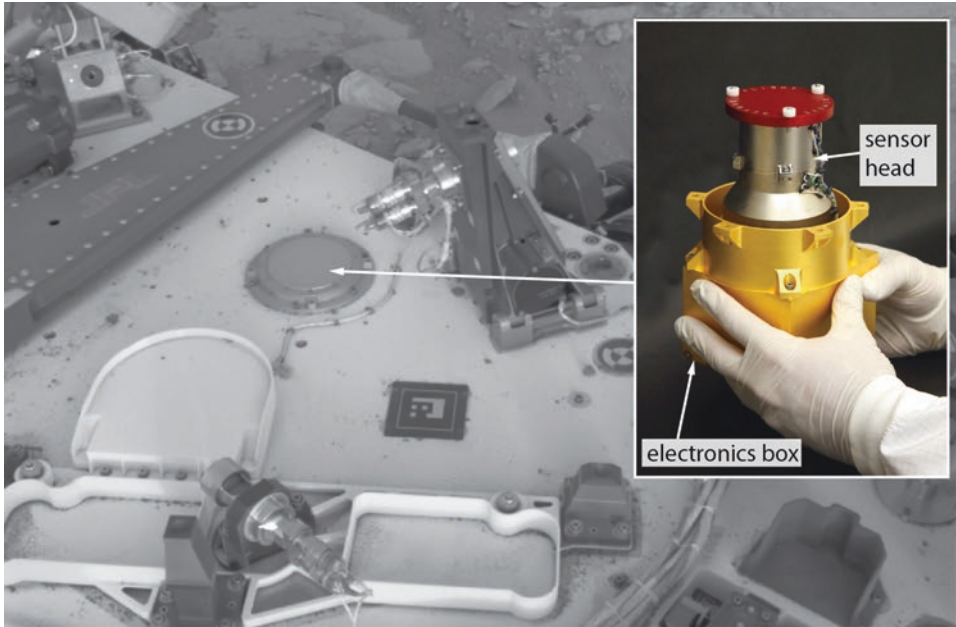


Figure 8.1. Top: The top of the RAD sensor head is visible as a circular plate on Curiosity's deck in this Navcam photo (NRA_409403780RADLF0051858) from sol 134. The plate covers the cylindrical instrument (inset). NASA/JPL-Caltech/Emily Lakdawalla. Bottom: schematic diagram of the RAD detectors. Colored lines show possible paths of charged and neutral particles that RAD can detect. Diagram modified from Rafkin (2014).

In order to measure the energy, mass, and charge of incoming particles, RAD examines how many of the stacked detectors a particle passes through and how much energy the particle loses as it passes through the detectors. At the top of the stack are three solid-state silicon detectors (labeled A, B, and C in Figure 8.1). Then comes a thick cesium iodide scintillator (D) and a plastic scintillator (E). Finally, another plastic scintillator (F) encloses D and E. Neutral or charged particles interacting with scintillators D, E, and F cause the scintillating material to emit orange light which is, in turn, detected with photodiodes. In order to make sure that all the detectors are looking at the same population of particles, the planar A, B, and C detectors have different widths, and D has a pyramid shape, defining a viewing cone about 65° wide.

Charged particles with very high energies can penetrate the entire instrument (purple line in Figure 8.1). Lower-energy ones may get stopped part of the way through (blue lines). Charged particles must pass through at least the top (A) detector and register in the B detector in order to be counted as an “event.” If a charged particle strikes only detector A, or any other lower detector without hitting the upper ones, it will be rejected from analysis (red lines). The role of the anticoincidence shield (detector F and outer rings on detectors B and C) is to detect the charged particles coming from the “wrong” directions and allow the RAD team to reject events triggering detections in D and E that did not enter from the direction of the viewing cone. If particles stop within the detector stack, RAD can determine their charge, mass, and energy. Some particles will pass all the way through, but will be dramatically slowed, and will deposit much of their energy in detector E. In this case, RAD can determine the charge and energy of these particles, but not their mass.

For neutral particles like gamma rays and neutrons, the viewing cone doesn't matter; RAD detects them coming from all directions as events detected in D and E but not any of the other detectors. Curiosity's own MMRTG generates lots of gamma rays and neutrons, but most of them are at low energies. RAD can detect these particles, but threshold parameters are set to reject them so as not to saturate the processing electronics, which are optimized to measure naturally occurring particles. The high atomic mass of the cesium iodide composing scintillator D makes it effective at detecting incoming gamma rays. The plastic in scintillator E makes it poor at detecting gamma rays, but good at detecting neutrons. Neutrons striking hydrogen nuclei produce recoil protons that may, in turn, produce an event in detector D. (For more about the interactions between fast-moving neutrons and hydrogen, read section 8.3 about DAN.)

RAD was originally planned to operate continuously in the background, around the clock. Unfortunately, constraints on the power system were initially quite conservative. As a result, RAD was first proposed to operate on a one-hour cycle, awake part of the time and asleep part of the time. The one-hour cycle was chosen in order to allow RAD to notice the onset of solar particle events soon after they begin, and change its observation cadence without any commands from Earth.

8.2.3 Using RAD

RAD works independently of the rover's other activities. RAD began the mission taking observations once per hour for 16 minutes, and sleeping for the other 44 minutes. Over the course of the mission, RAD operations have become nearly continuous. As of sol 1800, a

typical cadence is 16 minutes 10 seconds of observations, followed by only 27 seconds of sleep. During its sleep period, RAD bundles its ongoing observations and resets the instrument.² RAD operates even when the rover's main computer is asleep, gathering and storing data until the rover main computer requests it in preparation for downlinking it to Earth, originally about twice per week, but now at the start of every UHF communications pass. Each time RAD wakes up, it performs a 10-second "pre-observation" measurement. If it detects a high particle flux during the pre-observation measurement, it automatically shifts into a solar event mode, in which it makes more frequent observations. In solar event mode, RAD flags the data as high priority, so that the next time the rover communicates with Earth, the mission will learn of the solar event. This has happened only about 5 times since landing because of the unexpectedly low activity of the most recent solar maximum.³

One interesting finding from RAD is that diurnal changes in atmospheric pressure have an effect on the number of energetic particles reaching the surface, and the effect was large enough (and RAD sensitive enough) for RAD to detect it.⁴

Figure 8.2 shows some sample RAD data. RAD has been operating almost continuously since sol 9. The only hiccup in RAD operations came early in the mission, with an outage from sol 29 to 34 caused by an unexpected problem in the way that RAD and the main rover computer communicated with each other. Once the problem was understood,

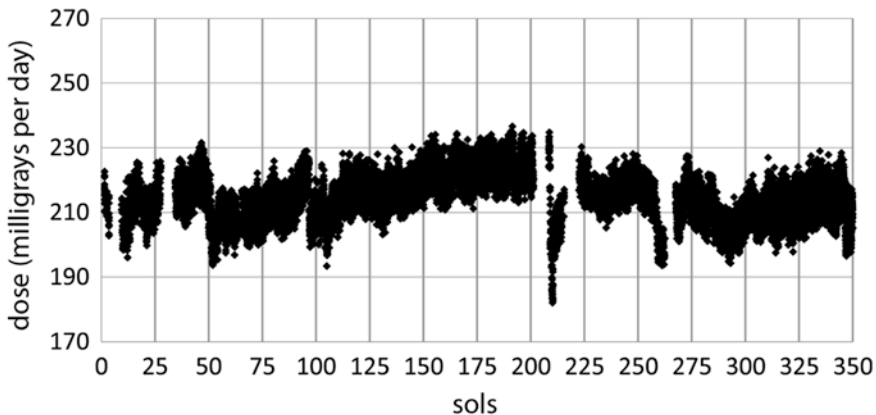


Figure 8.2. Dose rate measured by the RAD E detector during the first 350 sols of the mission. An astronaut would experience daily doses of roughly 200 milligrays. For context, medical X-rays and CT scans typically impart from 0.01 to 10 milligrays, depending on the type. From Rafkin et al. (2014).

²Betina Pavri, personal communication, September 22, 2017

³Hassler et al. (2013); Don Hassler, personal communication, email dated November 10, 2017

⁴Rafkin et al. (2014)

the rover engineers developed a workaround, and the problem hasn't happened since.⁵ Other gaps in RAD data have causes external to the instrument, such as rover software updates, the sol 200 anomaly, and conjunctions.

Unlike any of the rest of Curiosity's instrument data, RAD data are archived at the Planetary Plasma Interactions node of the Planetary Data System.

8.3 DAN: DYNAMIC ALBEDO OF NEUTRONS

Dynamic Albedo of Neutrons (DAN) surveys the ground up to a meter underneath Curiosity's traverse for chemically unusual spots and for the presence and abundance of subsurface hydrogen. The Federal Space Agency of Russia contributed DAN to the Curiosity project. Its Principal Investigator is Igor Mitrofanov of the Institute for Space Research (IKI). DAN comes from a long line of in-space neutron detectors going back to the Luna and Apollo missions. Its design is based upon the High Energy Neutron Detector (HEND), part of the Gamma Ray Spectrometer on Mars Odyssey. HEND and other neutron detectors flown to Mars, the Moon, Mercury, and asteroids have mapped water ice and mineral-bound water across the inner solar system.⁶

8.3.1 Scientific background

How do neutrons reveal the presence of subsurface hydrogen to these instruments? It begins with the same galactic cosmic rays and high-energy solar particles, that RAD detects (section 8.2.1). Curiosity also constantly emits neutrons from the plutonium decaying in its MMRTG. They bombard Mars' surface, colliding with atoms in the rocks and soils surrounding the rover (Figure 8.3). The impacts have so much energy that they can excite atomic nuclei into higher-energy states. The nuclei emit neutrons and other nuclear particles as they return to their lower-energy states. This process creates a constant source of high-energy neutrons. The neutrons lose energy with each collision, until they reach an equilibrium (or "thermal") energy. If neutrons escape before experiencing enough collisions to be "thermalized," they are "fast" neutrons. Slower neutrons are "epithermal," and the slowest, "thermal."

Neutrons are low in mass compared to most atomic nuclei; the neutrons bounce off most nuclei with nearly the same energy they began with. But when a neutron collides with the nucleus of a small atom, the atom's nucleus recoils from the collision, and the incoming neutron loses speed. In the limiting case, an incoming neutron collides with a hydrogen nucleus – a proton – which has the same mass as the neutron. Therefore, the presence of hydrogen in soil dramatically slows neutrons, and there are more thermal and fewer epithermal and fast neutrons emitted from the surface above soil that is hydrogen-rich.

⁵ Scot Rafkin, personal communication, email dated March 5, 2017

⁶ The paper of record for DAN is Mitrofanov et al. (2012). A post-landing summary is in Mitrofanov et al. (2014).

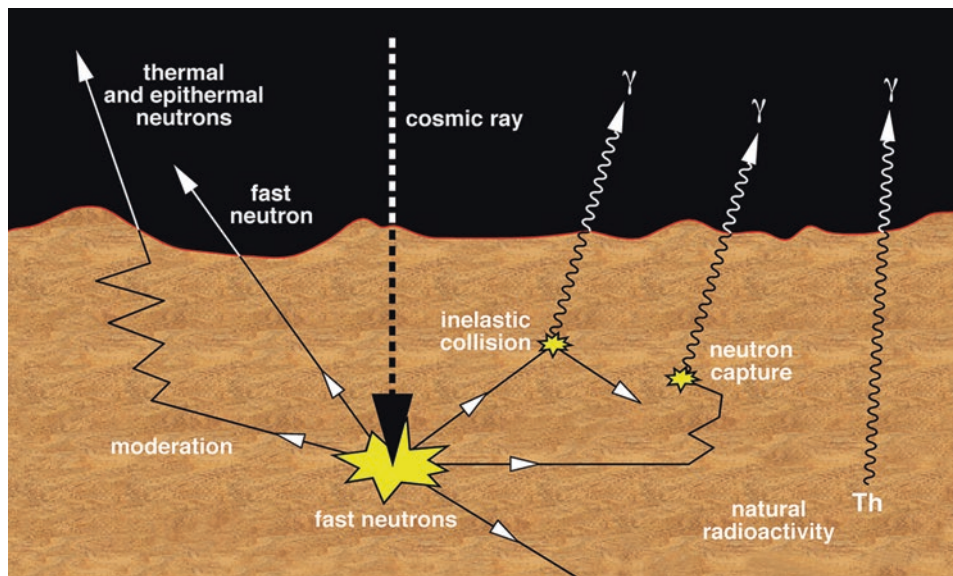


Figure 8.3. Cartoon showing the various sources of nuclear radiation from a planetary surface. Most result from incoming cosmic rays. NASA/JPL-Caltech/UA.

Another way that neutrons interact with soil atoms is by neutron capture. Nuclei with relatively large cross sections, like iron and chlorine, are more likely to capture neutrons; they're especially likely to capture the slowest (thermal) neutrons. By measuring the relative abundances of epithermal and thermal neutrons – that is, measuring the static albedo of neutrons – a neutron spectrometer can constrain the abundance of hydrogen and neutron-absorbing elements (not individually, but in bulk) in the subsurface.

Curiosity's Dynamic Albedo of Neutrons instrument goes a step further than this static measurement. DAN includes an active neutron source, a Pulsing Neutron Generator (PNG). By actively bombarding the surface with neutrons and then counting how the flux of epithermal and thermal neutrons vary with time, the DAN team can infer the distribution of hydrogen (or other neutron-slowing or -absorbing species) with depth beneath the surface, for the upper meter of soil. DAN is the first spaceborne neutron detector to have an active neutron source. Active neutron experiments are more commonly used in oil exploration geology on Earth, where neutron detectors and generators are lowered into boreholes to scan for the presence of hydrogen-rich hydrocarbons in subsurface rocks. DAN's neutron source is similar to Russian industrial instruments.

8.3.2 How DAN works

DAN has two components, a module with the detector and electronics, and the neutron generator (Figure 8.4). The detector is located in the left rear corner of Curiosity, and the neutron generator is in the rover's right rear corner (Figure 8.5). The rear Hazcams are mounted to the outside of the corner boxes containing DAN.

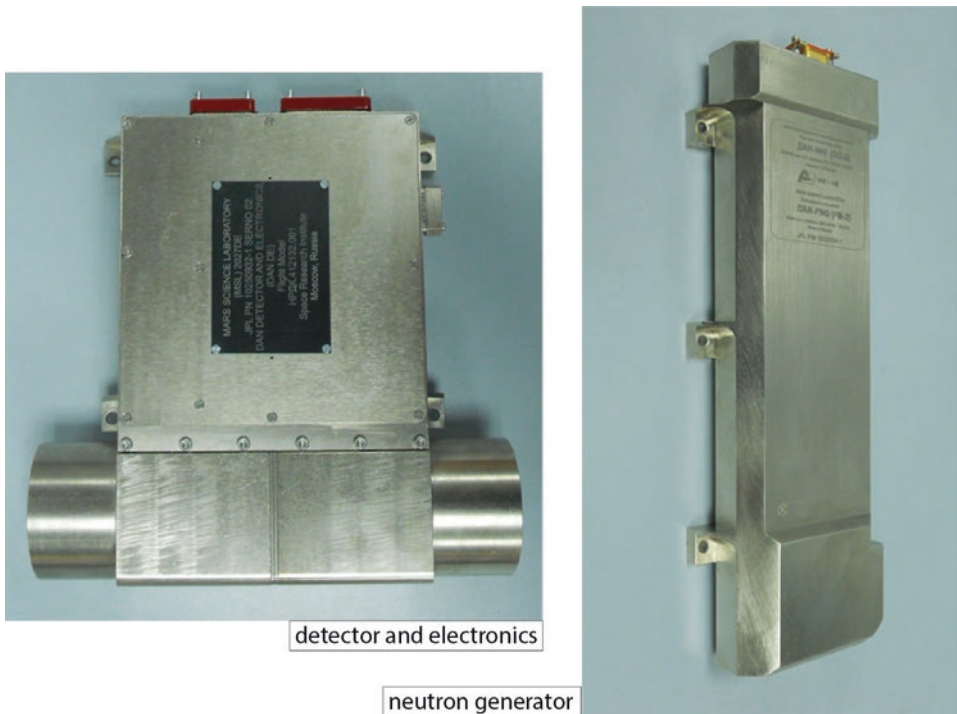


Figure 8.4. Components of the DAN instrument. Photos from IKI Laboratory for Space Gamma Spectroscopy.

The detector has two counters, both of which are filled with helium-3 at a pressure of 300 kilopascals. Detection happens when a neutron is captured by a helium-3 nucleus, which produces a proton and a triton (a hydrogen-3 nucleus). The two counters differ in their shielding. One is enclosed in a shield made of lead, and the other in a shield made of cadmium. Both lead and cadmium screen out X-rays, but the cadmium also shields out low-energy (thermal) neutrons. The cadmium-shielded one detects only epithermal neutrons and is called the Counter of Epithermal Neutrons (CETN), while the lead-enclosed detector is called the Counter of Thermal Neutrons (CTN). The lead-enclosed detector will always count more neutrons, and subtracting the counts of the cadmium-shielded detector from those of the lead-shielded detector will yield a count of thermal neutrons.

DAN can perform passive neutron detection continuously, but can also be commanded to operate in an active mode. Curiosity must be sitting still to perform a DAN active observation. The generator is a compact ion accelerator that steers deuterium ions into a tritium-enriched target to generate neutrons with energies of 14.1 MeV. (For comparison, incoming galactic cosmic rays have energies ranging from about 10 to 20 MeV.) It generates 13.4 million neutrons with each pulse, all within a period of about 2 microseconds. It can be operated with a single pulse, but usually generates 10 pulses per second.

After an active pulse it can take several milliseconds for neutrons of different energies to leak out of the surface. The detectors count up the arriving neutrons over time, producing a “die-away curve,” a graph of the number of counts with respect to time since the

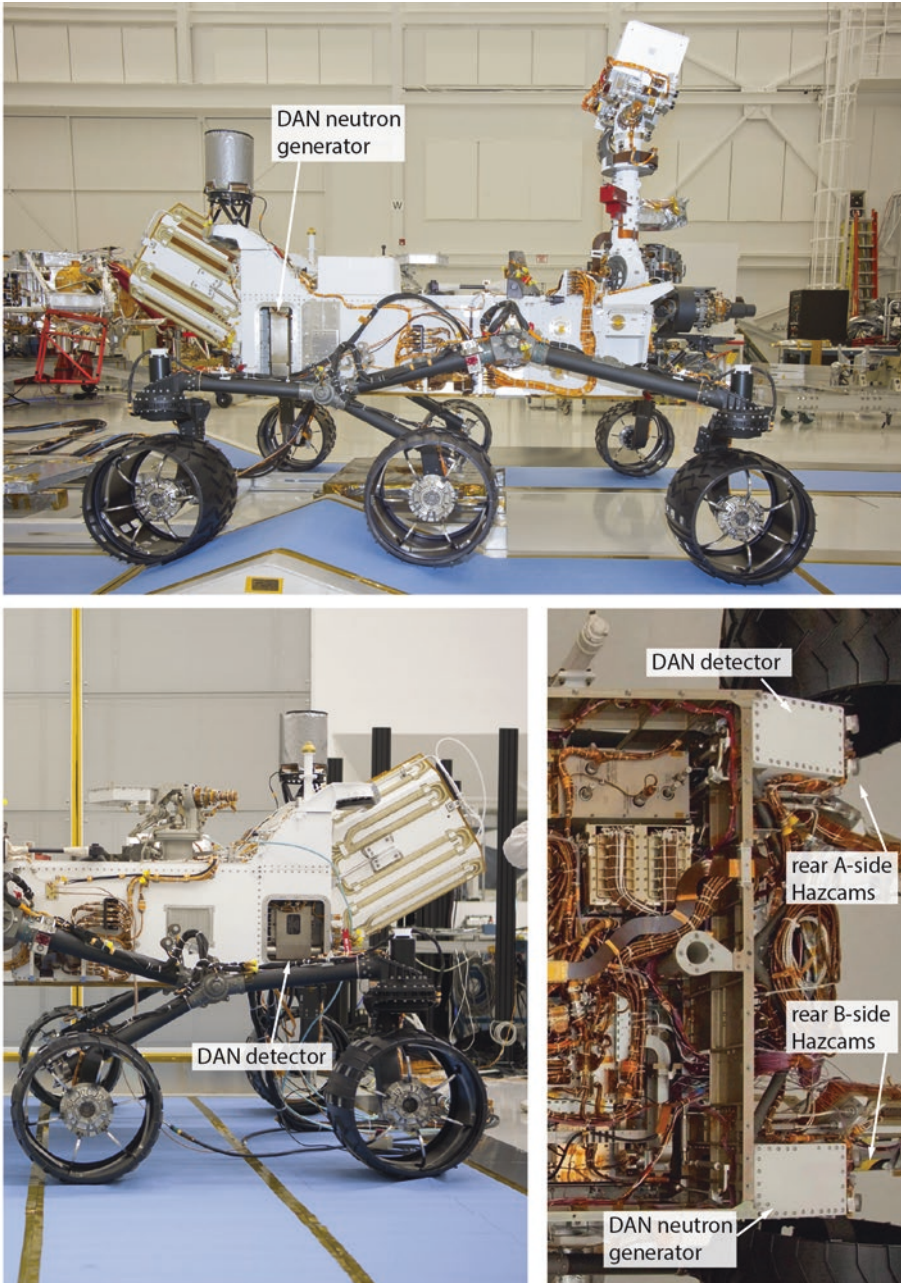


Figure 8.5. Location of the DAN instrument components on the rover. Top photo: NASA/JPL-Caltech release PIA14257. Lower left: PIA15181. Lower right view with belly pan removed: NASA/JPL-Caltech, annotated by Emily Lakdawalla.

pulse for each detector. Stacking die-away curves from many pulses improves the signal-to-noise ratio of the DAN data. The most commonly used DAN active observation includes 20 minutes of 10-hertz pulsing, or about 12,000 total pulses. The rover usually takes rear Hazcam images during a DAN active observation to document the kind of material underneath the DAN instrument at the time.

The detector is expected to count roughly 10 neutrons returning from each pulse, or about 100 counts per second during 10-hertz pulsing. The amount of neutrons that leaks varies by a factor of a few, depending upon how much hydrogen and other neutron absorbers are present in the surface. For comparison, the continuous neutron emission from the MMRTG produces about 25 and 10 counts per second in the lead- and cadmium-shielded detectors, respectively. During cruise, DAN detected higher counts of 35 and 15 per second as a result of exposure of the spacecraft to galactic cosmic rays. Once on Mars, the background increased even further because of the response of the surface of Mars to galactic cosmic rays. Thus the background is comparable in magnitude to the dynamic contribution from the neutron generator. The DAN team uses the tenth-of-a-second delay between pulses to measure the background, which can be removed from the results of active surveys.

Turning DAN active neutron counts into estimates of subsurface hydrogen abundance requires mathematical modeling. The DAN team performs simulations with a large set of models for the subsurface. The models all begin with a typical Martian soil composition (based on APXS measurements from the Mars Exploration Rover mission). They also assume a rate of incoming cosmic radiation, which is dependent upon the density of the atmosphere above the rover at the time of the measurement, so they incorporate REMS data on the atmospheric pressure at the time of the active DAN measurement. They allow other model parameters to vary. Some models are homogeneous ones, in which the total abundance of hydrogen and chlorine are allowed to vary. Other models are two-layer ones, in which chlorine is held constant but the amount of hydrogen is allowed to vary in upper or lower layers, and the layer thickness also allowed to vary. The models spit out die-away curves, and then the DAN team performs a least-squares analysis to find which set of model parameters best fits the observed die-away curve.

Two things limit the lifetime of the active scanning capability of the DAN experiment. The pulsing neutron generator has a warranted lifetime of 10 million pulses, so Curiosity can expect to perform about 1000 typical active observations over its lifetime. It is not likely that Curiosity will hit this limit, though, because DAN's neutron generator also has a clock time limit of about 3 years after launch. Helium generated by the neutron-generating pulses and the decay of its tritium target eventually ruins the vacuum inside the ion accelerator. Similar hardware on Earth has lasted anywhere from 2 to 6 years, with a median lifetime of 3 years, before failing. If the neutron generator fails, DAN will be less capable of estimating the depth of any subsurface layering that might be present, but it can still be used in passive mode to watch for subsurface variations.

8.3.3 Using DAN

DAN operates most of the time in a passive mode, its two detectors counting up neutrons any time the rover's computer is awake. The counts are typically binned every 20 seconds, producing a nearly continuous record of the number of neutrons hitting the detectors, including along rover traverses.

Because of the neutron generator's limited lifetime, the DAN team desired active scans to be performed frequently during rover traverses. Initially, most drives of any length included two to four mid-drive DAN active scans. But the 15-minute length of each DAN observation traded directly against drive distance, so the strategy of frequent DAN observations was abandoned after sol 403. Instead, there is most commonly one DAN active observation per drive sol. The observation may be performed after the end of a drive sol, between drive sols (its most typical location during restricted-sol periods), or before the next sol's drive. DAN cannot be used in active mode at the same time as some other rover activities because of the neutrons it generates. Examples include ChemCam observations, CheMin analyses, and driving or arm motion.

There were nearly 500 DAN active experiments performed over the course of the mission up to sol 1417. DAN has operated throughout the mission with no significant gaps in coverage; nearly every rover stop is documented with a DAN active measurement. DAN active measurements have fed back into tactical planning. DAN measurements of abundant thermal neutrons on sol 991, combined with unusual ChemCam measurements of rocks in the same area, led to the drilling of the high-silica target Buckskin below Marias pass on sol 1060. DAN had the opportunity to experiment on silica-rich materials at the Greenhorn and Lubango sites on sols 1144 and 1329.

8.3.4 Anomalies

The three-year expected lifetime of DAN's neutron generator ran out at the end of 2014, but DAN continues to operate normally. In October 2016, it showed the first signs of degradation. To the relief (and surprise) of the DAN team, the instrument returned to nominal operations afterward. Still, the generator can be expected to fail any day. The DAN and rover operations teams have collaborated on a workaround to allow DAN to continue operations as the neutron generator ages, and they monitor its health regularly.

8.4 REMS: ROVER ENVIRONMENTAL MONITORING STATION

One of the signal accomplishments of NASA's Mars program has been the continuous monitoring of Martian weather and climate since the beginning of Mars Global Surveyor's science mission in 1998. The data set permitted scientists to develop general circulation models for Mars' atmosphere like those that have been developed for Earth. But moving from global to smaller-scale models depends on surface meteorological data that has been historically scarce. REMS is designed to gather the wind, temperature, moisture, and pressure data necessary to constrain small-scale weather models for Mars. It also studies the ultraviolet radiation that penetrates Mars' atmosphere, which can have harmful effects on organic molecules.⁷

⁷The main paper describing REMS is Gómez-Elvira et al. (2012). Post-landing articles summarizing REMS performance and results are Pla-García et al. (2016), Smith et al. (2016), and Vasavada et al. (2017)

The principal investigator of the REMS experiment is Javier Gómez-Elvira of the Centro de Astrobiología (CSIC-INTA) in Spain. Most of the REMS components were provided by the Centro de Astrobiología, except for the pressure sensor located within the rover body and humidity sensor on Boom 2. They were provided by the Finnish Meteorological Institute, who also contributed the pressure sensors on the Viking and Phoenix landers.

8.4.1 Introduction: Gale weather

Gale is in a complicated weather regime, where global, regional, and local weather patterns are all important, and the patterns change on daily and seasonal timescales.⁸ There are three main global wind patterns. In the “daily thermal tide,” the Sun heats air on half of Mars, making the atmosphere expand and so decreasing its surface pressure, while cooling air on the night side has higher pressure. Air flows from the high to low pressure areas, generating a current that wants to flow perpendicular to the terminator, toward the sunlit side and away from the night side of Mars. In the “hemispheric dichotomy slope flow,” Mars’ global topographic dichotomy also drives winds, which flow upslope (north to south) during the day and downslope (south to north) overnight. Finally, there is a seasonal pattern driven by the heating and cooling of Mars’ poles: air rises at the hot pole and sinks at the cold pole near the solstices, and rises from the equator and sinks at the poles near the equinoxes. All of these effects combine to make complex patterns of winds that change diurnally and seasonally.

Where is Gale in all of this? It’s close to the equator and has high elevations to the south but also has Elysium Mons to the north. At some times of year (like the southern autumnal equinox at $L_s=0$), all the different circulations add up to produce practically no predicted wind in the Gale region. By contrast, near southern summer solstice at $L_s=270$, Gale is predicted to experience strong winds blowing from north to south all day and night.

However, Curiosity may feel few of these global currents. Gale is a deep hole in the ground, surrounded by high walls and containing a tall mountain in its center, and generates its own weather. During the day, wind blows upslope, toward the crater walls and the mountain peak. At night, winds flow downslope. Curiosity landed near the deepest part of the crater, and over the course of the mission it has moved from a wind regime controlled by the crater walls to one controlled by the mountain.

Martian calendar information relevant to the REMS experiment is summarized in Table 8.1. For more information on the Martian calendar, see section 3.2.

Table 8.1. Mars seasonal events and correspondence with Earth dates and Curiosity sols.

Mars year	Spring equinox ($L_s = 0^\circ$)	Summer solstice ($L_s = 90^\circ$)	Autumnal equinox ($L_s = 180^\circ$)	Winter solstice ($L_s = 270^\circ$)
31	Sep 13 2011	Mar 30 2012	Sep 29 2012 / sol 53	Feb 23 2013/sol 196
32	Jul 31 2013 / sol 350	Feb 15 2014 / sol 543	Aug 17 2014 / sol 722	Jan 11 2015/sol 865
33	Jun 18 2015 / sol 1018	Jan 03 2016 / sol 1212	Jul 04 2016 / sol 1390	Nov 28 2016/sol 1533
34	May 05 2017 / sol 1687	Nov 20 2017 / sol 2059	May 22 2018	Oct 16 2018

⁸Rafkin et al. (2016)

8.4.2 How REMS works

REMS consists of four units: two booms mounted on the mast, an ultraviolet sensor mounted on the deck, and an electronics box located inside the rover (Figure 8.6). The electronics box contains a pressure sensor. Both Boom 1 and Boom 2 have wind and air temperature sensors. Boom 1 has a ground temperature sensor, and Boom 2 has a humidity sensor. REMS is a relatively autonomous instrument, gathering data 10 times per second for the first 5 minutes of every hour, all the time. The science team also inserts several longer periods (an hour or more) of continuous 10-times-per-second data collection into every sol of activity, rotating the periods around the Martian clock to cover all times of day over a period of several sols. MAHLI is routinely used to monitor the condition of the ultraviolet sensor, and occasionally to view the booms.

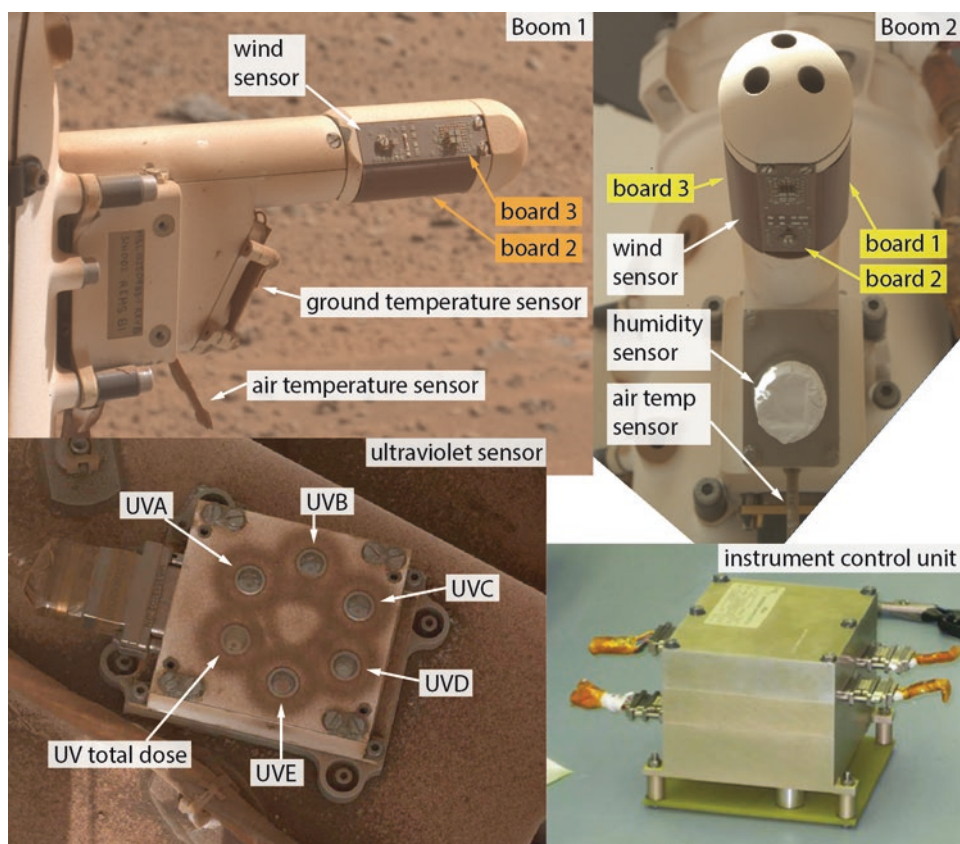


Figure 8.6. REMS components. Top left: Boom 1 as seen by MAHLI (0526MH0003430000201119C00). Top right: Boom 2 as seen by MAHLI (1572MH0006620020601062C00). Boards 2 and 3 of the Boom 1 wind sensor (orange) failed upon landing. All three boards of the boom 2 wind sensor (yellow) failed around sol 1500. Bottom left: Mastcam mosaic of the ultraviolet sensor, imaged in the sol 1197 Mastcam self-portrait. The individual labels identify the different photodiodes. Bottom right: REMS instrument control unit located in the body of the rover, which also contains the pressure sensor. NASA/JPL-Caltech/MSSS/Emily Lakdawalla.

8.4.2.1 *REMS booms*

The two booms are located 1.6 meters above the surface, sticking out from the mast, on a part of the mast that does not rotate, so their orientations are fixed. Boom 2 projects directly forward, while Boom 1 is oriented 120° clockwise from it, pointing back and to the right side of the rover (see Figure 7.1 for their locations). The 120° separation was intended to make sure that one boom would always experience wind that did not lie in the wake of the mast.

The wind sensors use hot film anemometry. By recording the amount of power it takes to keep tiny titanium resistors at a constant temperature, the science team can figure out how effective the wind is at cooling the resistors, and use that to determine how fast the wind has to be moving past the resistors. Because hot film anemometry depends upon the temperature of the instrument, it's best to have the resistors separated from the hot rover as much as possible. It's also best to have the resistors located as far as possible from anything that could obstruct the flow of the wind. The mast does disturb the motion of the wind, so there were two booms to measure the wind blowing at different points with respect to the mast. To keep the resistors disconnected from the boom structure, they were mounted on little pedestals and attached to their electronics boards with extremely thin wires. Unfortunately, two of the three boards on the wind sensor on Boom 1 were damaged during landing, so the wind experiment has never operated as designed.

The air temperature sensor consists of two thermistors on each boom, one at the middle and one at the tip of the boom. The one at the tip is intended to record air temperature; the one at the middle helps to calibrate out any heating of the thermistor by heat conducted through the boom itself. The electronic circuits that run the two booms, located at the base of each boom, must be kept above -70°C . When a sensor detects that the temperature falls below that, it turns on its heater.

The ground temperature sensor uses three thermopiles to measure the infrared brightness temperature of the ground. It detects the temperature from an area to the right of the rover. Mastcam “clast survey” images, taken at the end of drives, cover the area of the REMS ground temperature sensor field of view (see section 7.2.2.3). The MMRTG and its 2000 watts of waste heat are an important source of error in the REMS temperature measurements. There was concern that it might heat the air and ground around the rover, including some of the ground within the view of the ground temperature sensor. However, the data show little evidence of the MMRTG's heat affecting air or ground temperature measurements.⁹

The humidity sensor employs a polymer film whose electrical properties change as temperature and humidity change. The polymer film constantly responds to changes in the environment, but humidity can only be read once the sensor receives power. Supplying power to the sensor warms it, so the most accurate humidity measurements are the ones made immediately after it has been powered on.¹⁰ Mars has little water in its air, but at night

⁹Pla-García et al. (2016)

¹⁰Gómez-Elvira et al. (2012)

the temperature drops low enough that relative humidity can reach as high as 70%. In places where the ground gets exceptionally cold at night (dusty places with low thermal inertia), it's possible that the near-ground air gets cold enough for water frost to precipitate in a very thin layer on rock surfaces.¹¹ Curiosity has periodically looked for ground frost in the early morning after winter nights, but has so far not observed it.

8.4.2.2 REMS Ultraviolet sensor

The ultraviolet sensor has six photodiodes sensitive to different ultraviolet wavelengths. Five of them (named UVA, UVB, UVC, UVD, and UVE and labeled in Figure 8.6) look at narrower slices of the ultraviolet spectrum, and the sixth (UVABC or UV total dose) looks at the full ultraviolet range (Figure 8.7). By measuring the amount of light falling on the photodiodes and correcting for the solar elevation angle and amount of dust that has accumulated on the diodes, the REMS team can derive the aerosol optical depth, a measure of how much sunlight has been blocked from reaching the ground by particulate matter in the atmosphere. Mastcam photos of the Sun can make the same measurement more

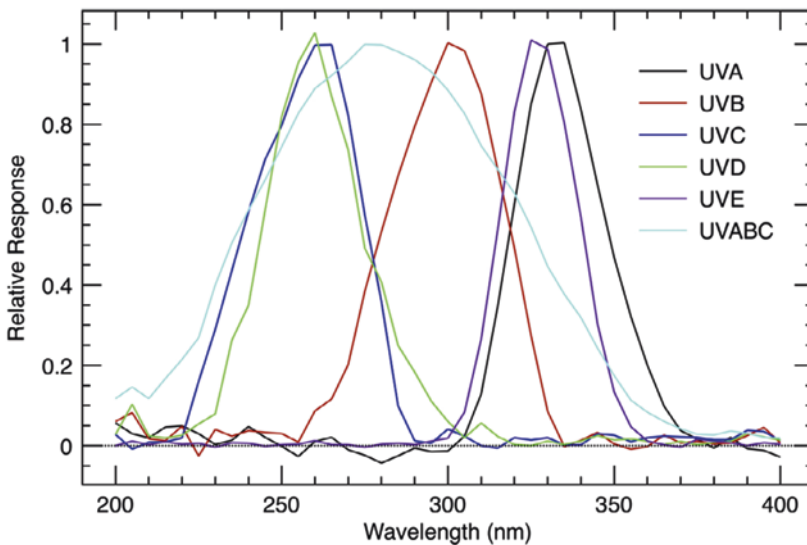


Figure 8.7. Spectral response of the REMS UV photodiodes. “UVABC” is also known as “UV total dose.” UVA, UVB, and UVE have provided the highest-quality data. From Smith et al. (2016).

¹¹Martínez et al. (2016)

precisely than REMS, but the REMS UV sensor measurements are far more frequent (multiple times per day, as opposed to the Mastcam cadence of roughly once per week). The sensors are covered about 10% of the time by shadows (mostly from the rover mast), but they spend most of their daytime unobstructed, and data taken in shadow are easy to remove from the data set.

Dust is an obvious concern to an upward-pointed light sensor, therefore each of the photodiodes is surrounded by a ring-shaped magnet that prevents Martian dust from falling in its center, working to keep the photodiodes clean. MAHLI takes a photo of the sensor roughly every two months in order to monitor dust deposition on it (see Figure 8.8). Although a lot of dust has accumulated on the magnets over time, the windows over the sensors have remained relatively clean over the course of the mission, and have become cleaner when the rover has paused in windy areas, particularly during the Pahrump Hills investigation from sol 800–900 and while driving through the Murray buttes around sol 1400 and following. Empirically, the REMS team has found the UVA, UVB, and UVE sensors to provide the best estimates of optical depth.¹²

8.4.2.3 *REMS Pressure sensor*

The pressure sensor is located inside the REMS electronics box, itself inside the belly of the rover. Although it is thermally isolated from the environment, the rover warm electronics box has vents that allow its interior to be filled with Martian atmosphere at ambient pressure. The pressure sensor has two transducers, one of which is designed to be more stable, and the other of which is designed to be more responsive to rapid pressure changes. Either provides good measurements, though, so the two transducers provide redundancy in the experiment design. Each has two electrodes, with the distance between the electrodes changing as a result of changes in pressure. That changes the capacitance of the transducer, providing a sensitive measure of pressure changes. The pressure sensors provide better readings after warming up, so measurements toward the end of the 5-minute window of each hour are considered more accurate than those recorded in the beginning.¹³

8.4.3 **REMS on Mars**

The loss of two of the wind sensor boards on Boom 1 (identified with orange tags in Figure 8.6) during landing was catastrophic to the wind experiment. REMS recorded data from the forward-facing wind sensor on Boom 2 since landing, but because the rover has been facing primarily south throughout the surface mission, and the prevailing wind has come mostly from the north, virtually all of the wind measurements have been

¹²Smith et al. (2016)

¹³Gómez-Elvira et al. (2012)

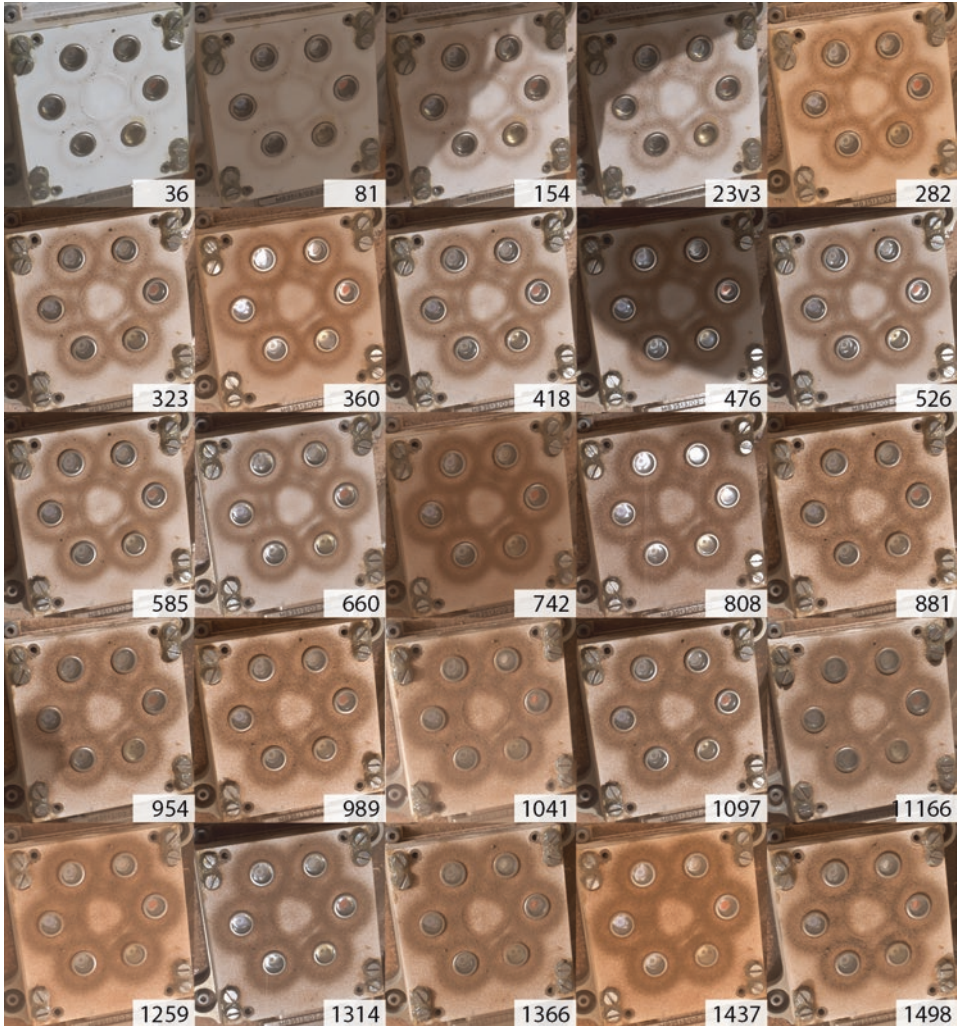


Figure 8.8. All MAHLI images of the REMS ultraviolet sensor to sol 1500. More images were taken on sols 1552, 1614, and 1675. NASA/JPL-Caltech/MSSS.

contaminated by rover hardware being in the way. The first board on Boom 2 failed on sol 1485, and the other two on sols 1491 and 1504.¹⁴

Apart from the issues with the wind sensor, the REMS instrument package has been performing reliably, sol after sol, recording measurements of Mars' weather. Figure 8.9 summarizes some of the REMS data for most of the mission, sols 0–1514.

¹⁴Ashwin Vasavada, personal communication, email dated April 17, 2017

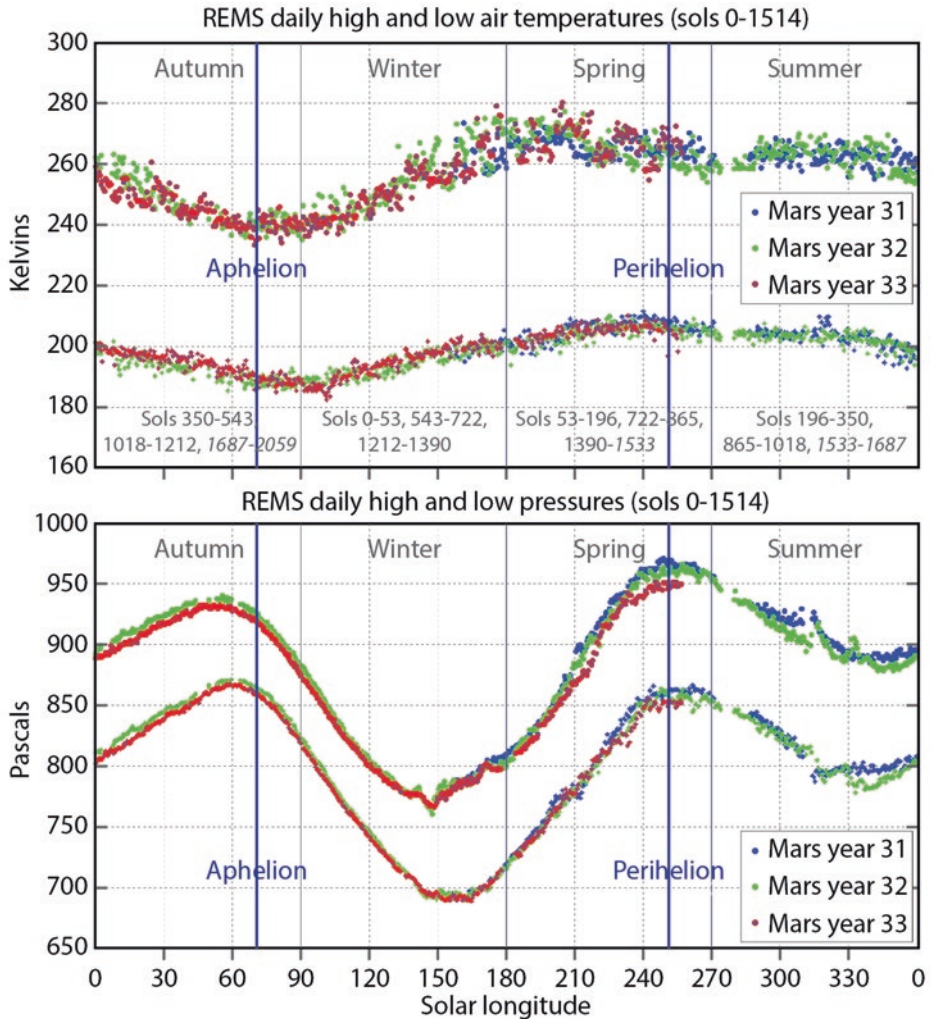


Figure 8.9. REMS air temperature and pressure minima and maxima for sols 0–1514 give an illustration of the continuity and density of the data set. The air temperature repeats reliably (within a narrow band of variation) year over year. Seasonal pressure variations have been consistent, with a notable secular decrease in pressure with time, caused by Curiosity's increasing elevation. Seasons (gray text) refer to the southern hemisphere, where Curiosity landed. Note that sol numbers for each season go a bit into the future, beyond the data set. Graphs courtesy Javier Gómez-Elvira.

8.5 REFERENCES

- Hassler D et al (2012) The Radiation Assessment Detector (RAD) investigation. *Space Sci Rev* 170:503–558, DOI: 10.1007/s11214-012-9913-1
- Hassler D et al (2013) Mars' surface radiation environment measured with the Mars Science Laboratory's Curiosity rover. *Science*, DOI:10.1126/science.1244797

- Gómez-Elvira J et al (2012) REMS: The environmental sensor suite for the Mars Science Laboratory rover. *Space Sci Rev* 170:583–640, DOI: 10.1007/s11214-012-9921-1
- IKI Laboratory for Space Gamma Spectroscopy (2011) Russian neutron detector DAN for NASA's Mars Science Laboratory landing rover. <http://1503.iki.rssi.ru/DAN-en.html>. Accessed 21 May 2014.
- Martínez G et al (2016) Likely frost events at Gale crater: Analysis from MSL/REMS measurements. *Icarus* 280:93–102, DOI: 10.1016/j.icarus.2015.12.004
- Matthiä K et al (2016) The Martian surface radiation environment – a comparison of models and MSL/RAD measurements. *J Space Weather Space Clim* 6:A13, DOI: 10.1051/swsc/2016008
- Mitrofanov I et al (2012) Dynamic Albedo of Neutrons (DAN) experiment onboard NASA's Mars Science Laboratory, *Space Sci Rev* 170:559–582, DOI: 10.1007/s11214-012-9924-y
- Mitrofanov I et al (2014) Water and chlorine content in the Martian soil along the first 1900 m of the Curiosity rover traverse as estimated by the DAN instrument, *J. Geophys. Res. Planets* 119:1579–1596, DOI: 10.1002/2013JE004553
- Pla-García J et al (2016) The meteorology of Gale crater as determined from rover environmental monitoring station observations and numerical modeling. Part I: Comparison of model simulations with observations. *Icarus* 280:103–113, DOI: 10.1016/j.icarus.2016.03.013
- Rafkin S C R et al (2014) Diurnal variations of energetic particle radiation at the surface of Mars as observed by the Mars Science Laboratory Radiation Assessment Detector, *J. Geophys. Res. Planets*, 119:1345–1358, DOI: 10.1002/2013JE004525
- Rafkin S C R et al (2016) The meteorology of Gale Crater as determined from Rover Environmental Monitoring Station observations and numerical modeling. Part II: Interpretation. *Icarus* 180:114–138, DOI: 10.1016/j.icarus.2016.01.031
- Smith M et al (2016) Aerosol optical depth as observed by the Mars Science Laboratory REMS UV photodiodes. *Icarus* 180:234–248, DOI: 10.1016/j.icarus.2016.07.012
- Vasavada A et al (2017) Thermophysical properties along Curiosity's traverse in Gale crater, Mars, derived from the REMS ground temperature sensor. *Icarus* 284:372–386, DOI: 10.1016/j.icarus.2016.11.035
- Zeitlin C et al (2016) Calibration and Characterization of the Radiation Assessment Detector (RAD) on Curiosity. *Space Sci Rev* 201:201–233, DOI: 10.1007/s11214-016-0303-y

9



Curiosity's Chemistry Instruments

9.1 INTRODUCTION

Curiosity has four instruments that study the chemistry of Martian materials. Two of them focus on elemental abundances. ChemCam is a remote sensing instrument, able to detect the elemental composition of a rock or soil from a distance of up to 7 meters by shooting it with a laser, a technique deployed in space for the first time on Curiosity. The Alpha Particle X-Ray Spectrometer (APXS) is a contact science instrument to examine the compositions of rocks and soils reached by the arm, and has a long Martian heritage.

The other two composition instruments form Curiosity's analytical laboratory, ingesting samples directly. CheMin is an X-ray fluorescence/X-ray diffraction instrument for determining crystalline mineralogy, the first instrument of its kind sent beyond Earth. Sample Analysis for Mars (SAM) is a fiendishly complex machine with an oven for heating samples to drive off gases. SAM's manifolds and pumps can direct gas from oven or atmosphere to a gas chromatograph mass spectrometer and a tunable laser spectrometer for measuring molecular and isotopic gas composition.

9.2 CHEMCAM

ChemCam employs a process called laser-induced breakdown spectroscopy (LIBS) to measure the elemental composition of the targets it zaps (Figure 9.1). When it fires its laser, it converts some of the target into plasma. A telescope gathers the light emitted by the plasma and sends it to a spectrometer. The wavelengths of the emitted light are diagnostic for some elements. ChemCam also uses its telescope to capture high-resolution context images of the LIBS targets using its camera, the Remote Micro-Imager (RMI). Nothing like ChemCam has been sent to Mars (or any other planet) before. Table 9.1 lists facts about the ChemCam instrument.¹

¹Two papers published before the mission described ChemCam: Maurice et al. (2012) and Wiens et al. (2012)

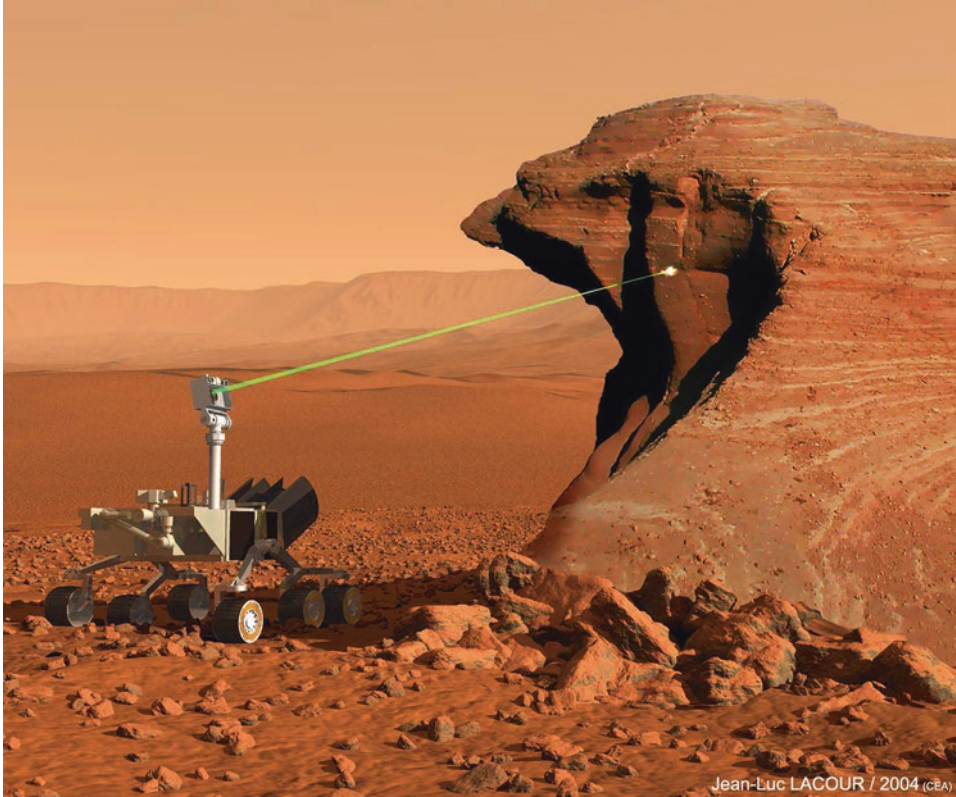


Figure 9.1. In fanciful artwork created for the ChemCam instrument proposal in 2004, ChemCam zaps a rock. By Jean-Luc Lacour for the ChemCam team.

Table 9.1. ChemCam facts.

Mast unit mass	5778 g
Mast unit dimensions	384 x 219 x 166 mm
Body unit mass	4789 g (of which 2344 g is thermo-electric cooler)
Body unit dimensions	197 x 238 x 154 mm
Fiber optic cable mass	63 g
Fiber optic cable dimensions	5753 mm x 1.4 mm diameter
Calibration target mass	161 g
Calibration target dimensions	146 x 51 x 16 mm; 1.56 m from ChemCam window
RMI CCD	1024 x 1024 pixels
RMI FOV	22.5 mrad
RMI IFOV	78 to 85 μ rad vertical, 87 to 105 μ rad horizontal
Autofocus laser wavelength	785 nm
LIBS laser wavelength	1067 nm

Table 9.2. Major and minor elements detected by ChemCam and APXS.

	Major elements	non-metallic elements	halogens	minor and trace elements
ChemCam only (lighter elements)	oxygen	hydrogen carbon	fluorine	lithium rubidium strontium barium
ChemCam and APXS	sodium magnesium aluminum silicon potassium calcium titanium iron	phosphorus sulfur	chlorine	chromium manganese nickel zinc
APXS only (heavier elements)			bromine	copper

Like APXS, ChemCam can only sense elemental composition; it isn't able to tell how the elements are arranged into minerals. Many rocks on Mars have essentially the same elemental composition (the same as basalt) but completely different mineralogy and geologic histories. Still, ChemCam is valuable for searching for targets for follow-up contact science. Also, ChemCam is able to detect lighter elements that aren't accessible to APXS. Table 9.2 lists the major and minor elements detectable by ChemCam and APXS.

ChemCam is one of Curiosity's international instruments. The Principal Investigator for ChemCam is Roger Wiens of the Los Alamos National Laboratory. The Deputy Principal Investigator is Sylvestre Maurice at the Institute de Recherche en Astrophysique et Planétologie. Part of it (the mast unit) was built at the Centre National d'Etudes Spatiales (CNES) in Toulouse, France, while Los Alamos built the body unit. ChemCam is operated out of Los Alamos and CNES, alternating every other week, and holding a hand-over phone meeting every Monday. The French ChemCam team must work very late into their local evening, on clocks usually 9 hours ahead of those in Curiosity mission operations at JPL.

9.2.1 How ChemCam works

ChemCam consists of four distinct pieces of hardware: the mast unit, body unit, the electrical and optical cables connecting them, and a calibration target. The mast unit contains the LIBS laser, telescope, and camera, as well as electronics. The body unit contains the spectrometer.

9.2.1.1 The ChemCam Mast Unit

Remote warm electronics box. Figure 9.2 shows the mast unit. The mast unit is located inside the remote warm electronics box, the large "head" of the mast. The mast unit must be kept to between -40°C and $+35^{\circ}\text{C}$ for instrument health. Thermostats inside the

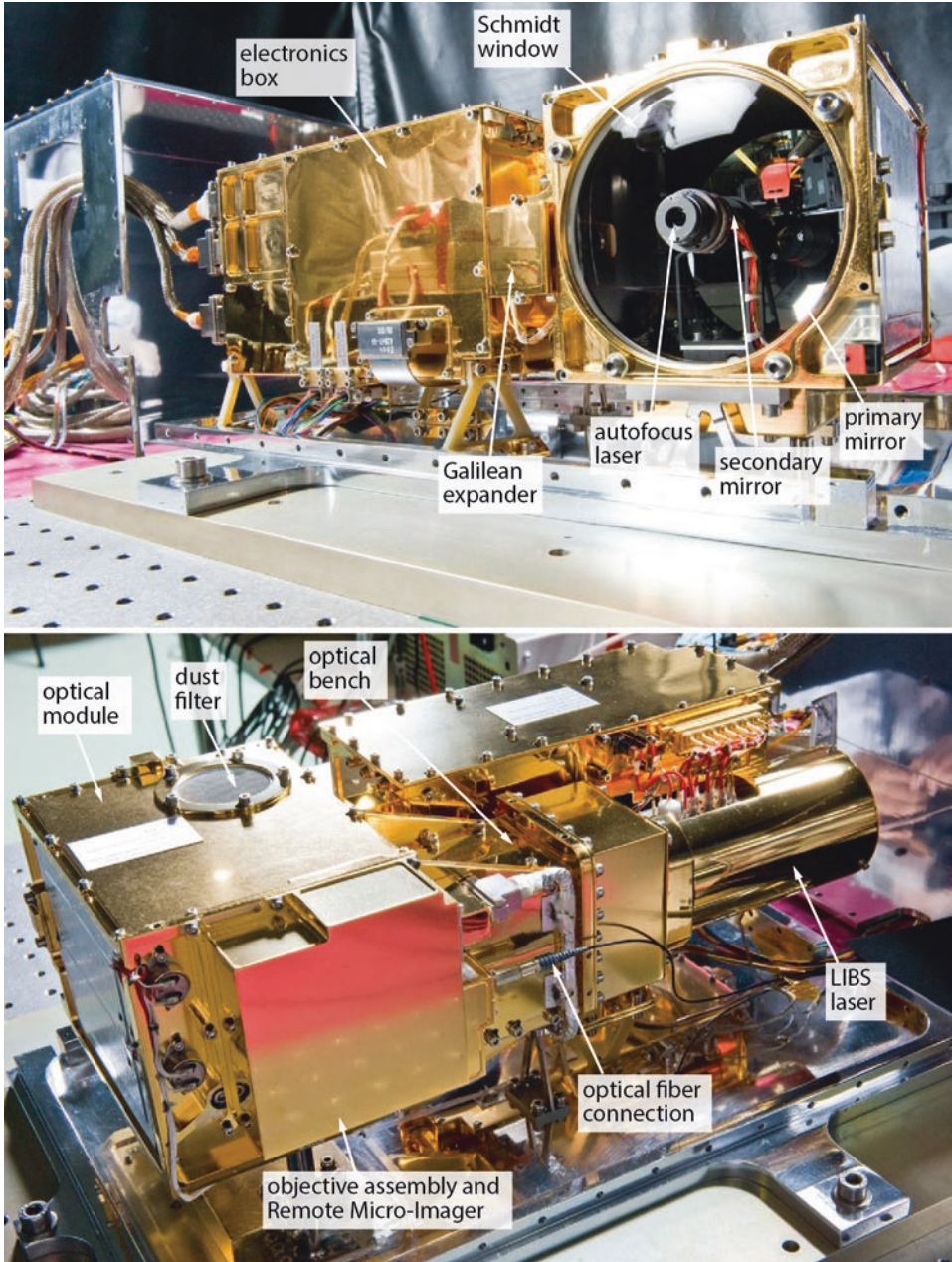


Figure 9.2. ChemCam Mast Unit (front and back). Images courtesy Roger Wiens.

electronics box trigger survival heaters every night, when the temperature falls below -35°C . The instrument is designed to be used at temperatures between -20°C and $+20^{\circ}\text{C}$, so when ambient temperatures are cold, it is warmed to -15°C in order to be used. Any warming is performed at a maximum rate of 5°C per minute.

LIBS laser. The LIBS laser is based upon a commercial laser, but was redesigned to reduce its mass by a factor of 10 and to make it reliable under the rigors of spaceflight. Its wavelength is 1067 nanometers, in the near-infrared. It should be able to sustain at least 20 million shots over its lifetime. Individual pulses last 5 nanoseconds, and it can fire up to 10 times per second. The laser fires through a telescope that focuses the beam diameter to between 0.25 and 0.35 millimeters.

Remote Micro-Imager. The Remote Micro-Imager is a flight spare from the camera system developed for the Philae lander on ESA's Rosetta mission. (Other flight spares of the same instrument were used on the ill-fated Phobos Grunt mission.) RMI has a 1024-pixel-square CCD and captures black-and-white images using wavelengths of light from 450 to 950 nanometers. It has an auto-exposure feature. It can repeatedly capture images as fast as 1 frame per second. The RMI is intended to provide context imaging for LIBS shot points at a resolution finer than is achievable with the right Mastcam. It has also turned out to be useful for long-distance imaging.

Autofocus laser. To focus the laser on a target, ChemCam employs a second laser, with a wavelength of 785 nanometers, for an autofocus operation. The autofocus laser is mounted to the back of the secondary mirror. To prepare for a ChemCam LIBS operation, the team would estimate the distance to the target using Navcam stereo ranging, passing that value to ChemCam as a part of the instrument's commands. The autofocus laser illuminated the target at 638 different test focus steps around that estimated distance, and a photodiode recorded how the intensity of the reflected light varied with focus. The intensity followed a generally bell-shaped curve. These data were sometimes noisy and the top of the curve sometimes flat, so electronics determined the best-focus position for LIBS and imaging by finding the axis of symmetry of that intensity curve.

Autofocus using RMI. Unfortunately, the autofocus laser failed on sol 801. The ChemCam team implemented a quick workaround within 15 days. ChemCam was commanded to perform nine sets of LIBS observations for each observation point at a range of focal distances around the best-guess distance determined from Navcam images; only one of these would turn out to be in focus.² This process generated results but was wasteful in terms of time and data, and the team worked quickly in parallel to develop a new autofocus method using the RMI. The new autofocus capability was uploaded to Mars on sol 980 and used for the first time on sol 983. The RMI takes nine to eleven images, and performs a simple algorithm to measure image contrast, selecting the highest-contrast image to determine the in-focus distance and then proceeding with LIBS analysis. The method is similar to that employed by the Mastcams and MAHLI, except that the color cameras measure image complexity rather than image contrast to find the best-focus position. Regardless of the method, it takes the RMI about two minutes to autofocus.

²Peret et al. (2016)

LIBS operation. Once the instrument has determined the best-focus position for LIBS, it is ready to fire. The LIBS laser beam passes through two sets of lenses, expanding it from 3 millimeters to 90 millimeters in diameter. The beam bounces it off of a secondary mirror and then off of a curved primary mirror and out the instrument’s front window. The window is 3 millimeters thick and made of silica glass to protect the optics from dust and temperature changes. The 90-millimeter-wide beam converges at the target distance, vaporizing rock into plasma. The same primary mirror collects the light from the plasma and bounces it off of the secondary mirror. But the collected light doesn’t go back from the secondary mirror toward the laser, because of a special “dichroic” lens in the optical path that reflects the 1067-nanometer laser light but is transparent to all the shorter wavelengths. Then most of the light gathered from the plasma bounces off a second dichroic mirror; the dichroic passes about 20% of the light to a different optical path for taking context images with the Remote Micro-Imager, sending the rest toward the fiber optic cable, to be used for spectroscopy.

9.2.1.2 *The ChemCam Body Unit*

The body unit is located inside the rover, on its right side (see Figure 9.3). Light from the mast unit travels down a fiber optic cable 5.743 meters long, wrapping three times around a mandrel connected to the mast’s elevation actuator, and another three times around a spool connected to the azimuth actuator. Then it runs down the mast, where it winds once around the mast deployment joint. It splits off from the rest of the bundle of cables from mast-mounted instruments, traveling across the top of the deck to a point close to the interior location of the body unit; it drops over the top edge to the side of the rover and then plugs in to the body unit (Figure 9.3).

ChemCam spectroscopy. Once it reaches the interior of the rover, the light transmitted down the fiber optic cable enters a demultiplexer (a device that splits the light into different-wavelength portions). The demultiplexer splits off first the ultraviolet and then the violet range with dichroic lenses and finally employs an ordinary mirror to deliver the rest of the light to the longest-wavelength spectrometer. The three spectrometers are called ultraviolet (UV, from 240.1–342.2 nanometers), violet (VIO, 382.1–469.3), and visible and near infrared (VNIR, 474.0–906.5). The light passes through a slit to enter a spectrometer and then bounces off a collimating mirror and a grating that spreads the light out by wavelength. Then another collimating mirror delivers the rainbow of light to a CCD that is 2048 pixels wide. Because the ultraviolet and violet spectrometers cover narrow wavelength ranges, there is higher spectral resolution at shorter wavelengths: 20 pixels per nanometer in the ultraviolet and 23 pixels per nanometer in the violet. The wider wavelength range of the VNIR spectrometer produces a lower spectral resolution of 4 pixels per nanometer.

ChemCam thermal management. The body unit resides inside the warm body of the rover, but its detectors have to be actively cooled. This was not the original plan; the ChemCam spectrometers were developed based on earlier information from the mission that specified a cooler rover interior (see section 1.5.2 for more on the unpleasant discovery of this issue).

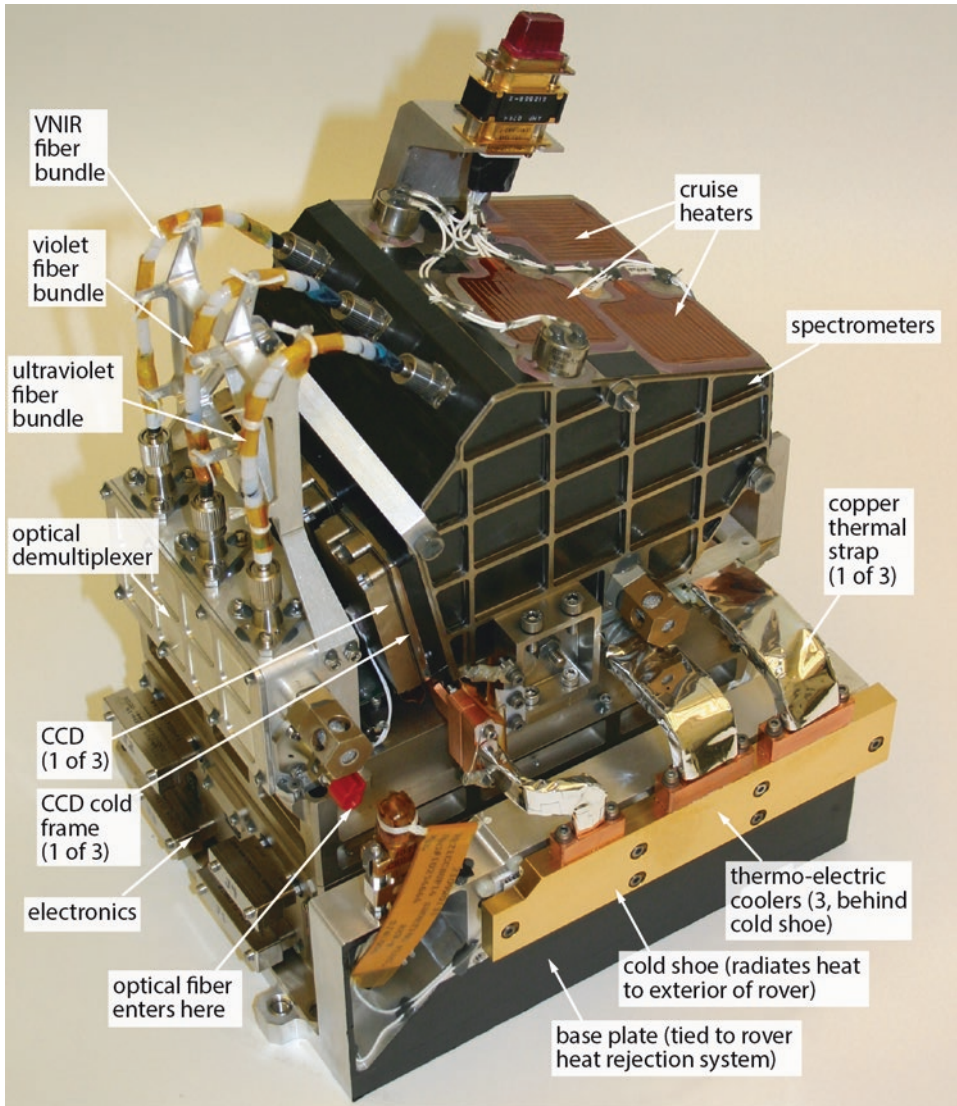


Figure 9.3. The ChemCam body unit. After Wiens et al. (2012).

Solving this problem required a redesign of the ChemCam body unit. They thermally isolated the CCDs from the spectrometers, connecting them with copper thermal straps to three thermo-electric coolers located next to the rover exterior wall. The coolers radiate heat away from the CCDs across two paths: through the wall of the rover to the outside, and via a base plate to the rover avionics mounting panel to the rover's heat rejection system (see section 4.4). Because of the rover's selected equatorial landing site, summer heating is not as extreme as in the worst-case scenario, and the thermo-electric coolers permit ChemCam to be operated nearly the entire day, year-round.³

³Roger Wiens, personal communication, email dated March 14, 2016

9.2.1.3 The ChemCam Calibration Target

A variety of factors can affect LIBS calibration, so ChemCam includes a calibration target using ten samples of well-studied composition (Figure 9.4). Four of the samples are basaltic glass of different types (macusanite, norite, picrite, and shergottite), and four are ceramic mixtures of basalt, anhydrite (a sulfate mineral), and clay minerals in different proportions. Glass and ceramics have grain sizes that are very small, so are homogeneous even at the fine scale of the ChemCam LIBS laser shot. One sample is graphite, serving as a reference for carbon, and there is a titanium metal plate for wavelength calibration. The edge of the titanium plate is painted black, making a high-contrast edge against the white-painted calibration target plate, useful for checking the focus and resolution of the RMI. The calibration target is mounted on the back of the rover, tilted 37.9° away from vertical. The mast points 28.5° downward in order to target the center of the target. The target is 1.56 meters from ChemCam. It is less dusty than the Mastcam calibration target, and has been imaged by both Mastcams (sols 14, 718, and 838) for cross-instrument calibration purposes. Unlike the Mastcam calibration target, it is far enough from the mast that the right Mastcam can view it in focus.

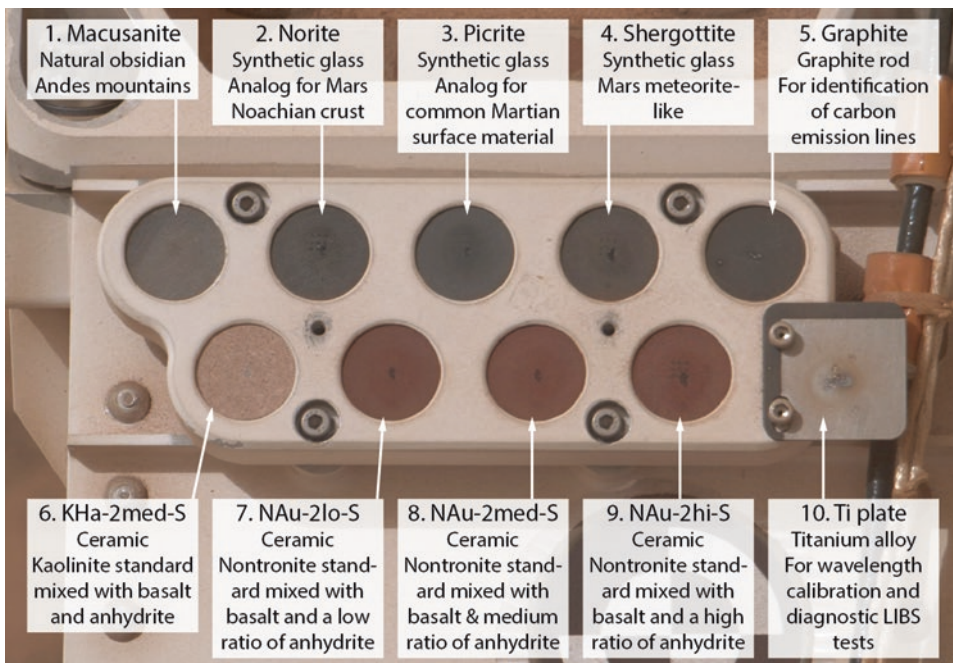


Figure 9.4. The ChemCam calibration target as seen by the right Mastcam on sol 838. Many laser shot points are visible. Image 0838MR0036830000500777E01. Credit: NASA/JPL-Caltech/MSSS.

9.2.2 Using ChemCam

9.2.2.1 Sun-safety

The mast points some of the instruments (Mastcams and Navcams) at the Sun regularly for navigation and science, but the ChemCam instrument is sensitive to the Sun, so there are many restrictions on mast motion in order to protect ChemCam. Depending on the focus position of ChemCam, it is either “sun-safe” (in which case it can tolerate the Sun passing through its field of view) or “sun-unsafe” (in which case the Sun passing through the field of view could seriously damage the instrument). During tactical planning, engineers check mast pointing to make sure that ChemCam will always be sun-safe before approving a sequence.⁴

Even when ChemCam is sun-safe, the Sun shining into its window can heat the instrument, so engineers have to plan sequences to make sure that the Sun will not shine directly into the ChemCam window for longer than 3 minutes. They do this by defining a cone spanning plus or minus 16° around the ChemCam boresight, and modeling how long the Sun stays within it. Obviously, ChemCam observations will always be sun-safe if the instrument is pointing below the horizon. Adding 4° to the 16° cone to account for the curvature of Mars' horizon yields 20° below the horizon as an always sun-safe pointing direction for the mast that requires no further checking. Also, slews of the mast to move to a new pointing position happen quickly enough that they don't need to be checked for ChemCam warming as long as ChemCam is sun-safe.

When ChemCam is being used and so is in a sun-unsafe focal range, the Sun must never be permitted to shine into its window. This has to hold true even if a rover anomaly happens in the middle of a ChemCam observation, an anomaly that may take several sols to resolve. The rover planners define a “keepout cone” 17° away from the ChemCam boresight. Sweeping this cone across the sky along the path of the Sun during a given sol produces a “keepout band”, a region in which ChemCam must never be allowed to perform an observation.

With onboard fault protection software, the rover checks to ensure that mast pointings will be sun-safe before performing them. The rover even checks sun-safety once per second as it drives, and will stop a drive if sun-safety will be violated. (This has never actually happened.)

Targets located 2 meters away present a different kind of hazard to ChemCam. The problem is that the “antireflection” coating on the front window is good at allowing sunlight and LIBS-produced plasma illumination to pass through it, but is not quite as antireflective at the 1067-nanometer wavelength of the laser. Some laser light bounces back from the front window on every laser pulse. For two distance ranges, 1.20 to 1.36 meters and 1.942 to 2.217 meters, the reflected laser light can be focused by the primary mirror onto the secondary mirror, possibly causing some damage to the secondary mirror at the spot of the laser hit. The ChemCam team has stated that the instrument can perform about 100,000 shots in these ranges without risking serious damage. The shorter of the two distance ranges is never needed, because it is even closer to ChemCam than the calibration target; ChemCam

⁴Described in detail in Peters et al. (2016)

is likely never to be so close to a rock, because it would have to be next to a nearly vertical cliff. (The artwork in Figure 9.1 notwithstanding, it is an unlikely situation for Curiosity to be so close to such a steep cliff.) The longer of the two distances covers ranges extremely close to the rover, and only a few hundred such shots have been made.

9.2.2.2 *Types of Observations*

The ChemCam team divides their operational history into three seasons. Season 1 covers sols 0 to 800. Season 2, when ChemCam had no autofocus capability, lasted from sols 801 to 980. Season 3, in which ChemCam uses its RMI for autofocus, is from 981 to the present.⁵ See section 9.2.1.1 above for a description of the different autofocus modes.

LIBS observations. To perform a LIBS observation, the science team looks at Navcam and Mastcam images that were taken on a previous sol and selects a target. Navcam stereo images provide geometric information, while higher-resolution Mastcam images can be used to fine-tune target selection. The farthest target that ChemCam has attempted LIBS on was Mell, on sol 530, at a distance of 7.45 meters, but 90% of targets are much closer, within 4.5 meters; the team restricts quantitative analyses to targets within 5 meters.⁶ Before ChemCam can begin an observation, the autofocus and LIBS lasers may need pre-heating. The telescope autofocuses on the target and collects a “before” RMI image. The instrument collects a passive spectrum to be used later, for subtraction from the LIBS spectrum. Then the LIBS laser fires many laser pulses, usually 30 but occasionally some other number. It can collect a maximum of 150 spectra at 3 per second (referred to as a “burst”) before having to pause to transfer data. After the LIBS operation is complete, RMI takes an “after” image, then moves to the next target or returns the focus to the sun-safe position. The experimental result is a spectrum whose peaks imply the presence of different elements.

Depth profiling. Most of the time, the ChemCam team averages the data from many LIBS shots at each point to improve the signal-to-noise ratio of LIBS data. However, by analyzing shots individually, it is possible to perform depth profiles for elements. Each LIBS shot ablates approximately 1 micrometer of material, and ChemCam has occasionally found composition to change at that scale. For example, in the rock Bathurst Inlet, lithium, rubidium, sodium, and potassium concentrations decrease with depth, possibly “due to aqueous alteration processes (i.e. frost deposition, followed by melt and evaporation or sublimation) that have preferentially mobilized the alkalis.”⁷ Another rock had a thin layer of manganese on the surface, thin enough for ChemCam to penetrate through.⁸ ChemCam has performed depth profiles of up to 1000 shots.⁹

⁵Maurice et al. (2016)

⁶Maurice et al. (2016)

⁷Ollila et al. (2014)

⁸Lanza et al. (2016)

⁹Maurice et al. (2016)

Rasters. ChemCam commonly performs several observations in a “raster” or array. Rasters can be of any size, but 1-by-5, 1-by-10, and 3-by-3 arrays are the most common. It takes about 30 minutes to perform a 1-by-5 raster, 40 for a 3-by-3, and an hour for a 1-by-20. The most common spacing between points is 2 milliradians (giving approximately 1-millimeter point-to-point spacing at locations close to the rover) but the spacing may be wider or narrower.¹⁰ The pointing accuracy of the mast is such that ChemCam has been able to perform rasters within drill holes (Figure 9.5). RMI images are taken at the beginning and end of the raster observation. When necessary for large rasters, additional images are taken in the middle. During season 2 (sols 801 to 980), when ChemCam had no autofocus capability, there were few rasters (see section 9.2.1.1). Unfortunately, this coincided with virtually all of the time spent at the first major field site after arrival at Mount Sharp, Pahrump Hills.

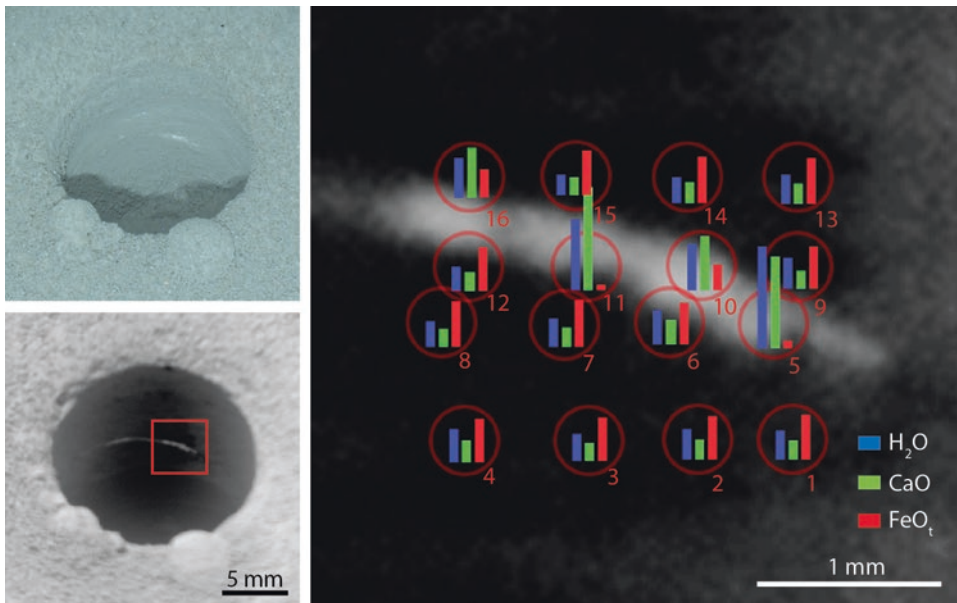


Figure 9.5. Example raster data within a drill hole, Telegraph Peak. Top left: MAHLI image 0911MH0004750000303057R00 of the drill hole under nighttime illumination. A tiny white vein is visible in the drill hole wall. Bottom left: ChemCam RMI image CRM_479251063_CCAM03921 of the drill hole; red square shows the region of a 4x4 raster targeting the vein and the area around it. Right: Zoom in on the vein and the raster of ChemCam measurements showing how hydrogen, calcium, and iron content vary among the different observations. Within the vein there is an increase in calcium and hydrogen and a decrease in iron, thought to indicate that the vein is composed of a hydrated calcium sulfate, likely bassanite. This set of observations was performed during ChemCam Season 2. Courtesy William Rapin.

¹⁰Roger Wiens, personal communication, email dated March 26, 2016

Passive mode. As a part of every observation, the spectrometers first gather spectral information using reflected sunlight without firing the LIBS laser. Such “passive” observations can also be gathered without taking any LIBS data, useful on distant targets. Passive spectra have helped the team identify iron oxidation states, diagnosing the mineralogical shift from less-oxidized magnetite to more-oxidized hematite in bedrock along the rover’s traverse after it reached the Bagnold dune field. The team also identified the presence of iron sulfates from their 430-nanometer absorption feature in passive spectra taken of rocks around Pahrump Hills. ChemCam passive sky observations investigate the abundance of water vapor and oxygen in the atmosphere, useful for comparison to REMS and SAM measurements of local humidity and oxygen abundance.¹¹

Blind targeting. The rapid pace of drive campaigns means that there is often not time to receive the Navcam data needed for targeting ChemCam images before the rover drives away. Beginning on sol 318, to gather some ChemCam data during drives, ChemCam performed blind-targeted measurements of a patch of ground directly to the right of the rover at the end of drives, at a distance that would be 3 meters away if the ground were level. Initially, they performed only single-point analyses, but they added blind line scans with multiple shot points beginning on sol 386.¹² Blind targeting was performed only during ChemCam season 1 (until sol 801), because the new autofocus algorithm requires a distance seed derived on Earth from analysis of Navcam images.¹³ Blind targeting was eventually replaced by AEGIS targeting.

AEGIS targeting. AEGIS stands for Automated Exploration for Gathering Increased Science.¹⁴ It is a set of artificial-intelligence algorithms to enable a rover to autonomously select and/or refine observation targeting, first used on the Opportunity Mars Exploration Rover. For Curiosity, AEGIS permits ChemCam target selection without waiting for instructions from the ground. It runs on the rover’s main computer, acquiring Navcam images, identifying potential targets, filtering them based on criteria supplied by the ChemCam team, and then ranking the targets. The ChemCam team can adjust the target selection criteria each time an AEGIS sequence is planned, prioritizing outcrop, dark or light rocks, or other kinds of targets. On Mars, the whole process takes only 4 to 8 minutes and can be performed immediately after the end of a drive. AEGIS can also refine the pointing of ChemCam LIBS shots, running on RMI images to select bright veins or grains for targeting. Adding AEGIS capability to Curiosity began in summer 2015; uplink was spread out over many weeks. The code was installed into flight software on sol 1141. Checkouts were complete in February 2016, on sol 1237. AEGIS was used for routine operations for the first time on sol 1343.¹⁵ The Navcam mode has been used more often than the RMI mode.

¹¹ Roger Wiens, personal communication, email dated March, 26, 2016

¹² Cousin et al. (2014)

¹³ Roger Wiens, personal communication, email dated March 26, 2016

¹⁴ Francis et al. (2016)

¹⁵ Francis et al. (2017)

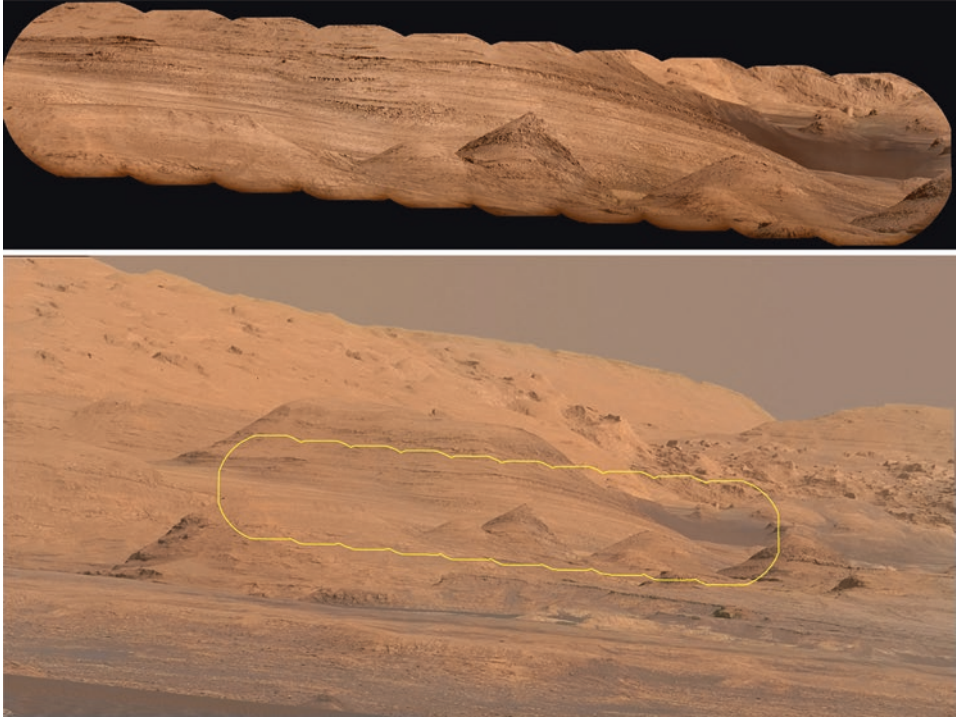


Figure 9.6. ChemCam RMI long-distance observation of Mount Sharp, sol 1283. Credit: NASA/JPL-Caltech/LANL/MSSS/James Sorenson.

Long-distance imaging. The RMI is Curiosity's highest-resolution camera, and is often pointed at very distant targets. For instance, the team used the RMI in a long-distance campaign to monitor sand ripple motion on the backs of the Bagnold dunes, to study the upper part of Peace Vallis where it enters the crater from the northwestern rim, and to get a look at possible future science locations on Mount Sharp (Figure 9.6). Long-distance imaging has dramatically better quality in season 3, after sol 981, now that the RMI can autofocus on distant targets.

Dusting. The rapid expansion of air around the superheated plasma generated by ChemCam shots can very effectively remove very fine Martian dust from rock surfaces (Figure 9.7). A typical 30-shot observation blasts aside dust for a 6-to-9-millimeter diameter around the shot point.¹⁶ Although ChemCam hasn't yet been used for this purpose deliberately its accidental use as a remote dust removal tool improves the value of Mastcam multispectral imaging on rocks, and the MAHLI team likes to image LIBS pits to see the color of dusted-off rocks.

¹⁶Maurice et al. (2016)



Figure 9.7. Two ChemCam raster targets at Windjana, “Stephen” (top) and “Neil” (bottom), were dusted off by ChemCam, revealing the dark color of the rock beneath the bright dust. MAHLI image 0627MH0001900010203555C00, NASA/JPL-Caltech/MSSS.

9.2.2.3 Calibration

Transforming ChemCam spectra into elemental abundances requires comparing the data to ChemCam measurements of samples of known composition. Initially, the ChemCam team’s calibration library contained 66 samples with compositions expected to be found on Mars that had been shot with the flight model of ChemCam under Earth ambient conditions. The original library performed well for common Mars materials like dust and basalt, but relatively poorly for more unusual materials like calcium sulfate veins and feldspars.¹⁷ Two laboratory copies of ChemCam (one each at Los Alamos and CNES) operate under Mars-like temperature and pressure conditions. The Los Alamos laboratory expanded the data set to 450 different types of rocks, covering a wider range of compositions than in the initial 66. The team began testing a new calibration model on ChemCam data during the mission’s second conjunction period, beginning on sol 1004, and delivered recalibrated versions of earlier major-element data to the Planetary Data System on December 3, 2015.

¹⁷Roger Wiens, personal communication, email dated December 17, 2015

9.2.3 Anomalies

The main anomaly encountered by ChemCam on Mars was the loss of the autofocus laser on sol 801 (section 9.2.1.1), which resulted in no autofocus capability until sol 983, when the new RMI-based autofocus algorithm was put into use. One drawback is that relying on the RMI means that autofocus doesn't work at night or even, sometimes, in areas of deep shadow. ChemCam rarely performed observations at night before the anomaly because of the high energy cost of heating the mast actuators at night, so that restriction has had little effect, but the issue of rover shadowing has occasionally affected target selection.¹⁸ The new method also scans a shorter range of possible focal distances than the old method, so it requires a good-quality distance seed, meaning that shooting in the blind is no longer possible. On the plus side, laser autofocus didn't work at distances longer than 18 meters, so the new autofocus method performs much better at imaging at infinity.

9.3 APXS: ALPHA PARTICLE X-RAY SPECTROMETER

APXS measures the elemental composition of rocks and soils by emitting alpha particles and X-rays at a surface and counting the X-rays that return. Curiosity's APXS is the third in a line of similar instruments carried to Mars on Pathfinder and the Mars Exploration Rovers, with improvements that make it more sensitive, faster, and able to operate over a wider range of the Martian day.¹⁹ The APXS team uses measured elemental abundances to group observed targets into classes of similar composition, often comparing rocks across rover landing sites. The principal investigator is Ralf Gellert of the University of Guelph, Canada, and APXS was provided to the mission by the Canadian Space Agency.

APXS is located on the turret and has to be deployed to close proximity or in contact with a rock or soil (Figure 9.8). Because it requires the arm and several hours for a high-quality measurement, it gets used less frequently than the remote sensing instruments. It sees heavy use at sample sites and significantly less frequent use at stops during traverses. APXS measurements also assist the team in selecting drill targets. By analyzing drill tailings, APXS can help the CheMin team constrain the composition of the component of the drilled rock that is amorphous and therefore not accessible to CheMin mineralogical analysis. APXS measurements of potassium in drill tailings combined with SAM measurements of argon gas evolved from a sample have been used to measure the exposure ages of outcrops through potassium-argon dating.²⁰ Elements that APXS can detect are listed in Table 9.2.

¹⁸William Rapin, personal communication, email dated April 5, 2016

¹⁹There is no peer-reviewed publication describing the APXS as there is for most other instruments; there is only an LPSC abstract: Gellert et al. (2009); two other good sources of information on the instrument and its performance on Mars are Gellert et al. (2015) and Campbell et al. (2012)

²⁰Farley et al. (2014)



Figure 9.8. APXS deployed onto the John Klein drill target. Mosaic of four Mastcam images taken on sol 168. Credit: NASA/JPL-Caltech/MSSS.

9.3.1 How APXS works

APXS has three main elements: a sensor head located on the end of the robotic arm; an electronics unit located in the front left corner of the body; and a calibration target that is mounted below the MAHLI calibration target attached to the shoulder azimuth actuator. Just like MAHLI, the APXS sensor head is separated from the turret by a set of three springy wire rope assemblies to isolate the instrument from vibrations caused by drilling and CHIMRA sample processing. Parts of APXS are shown in Figure 9.9.

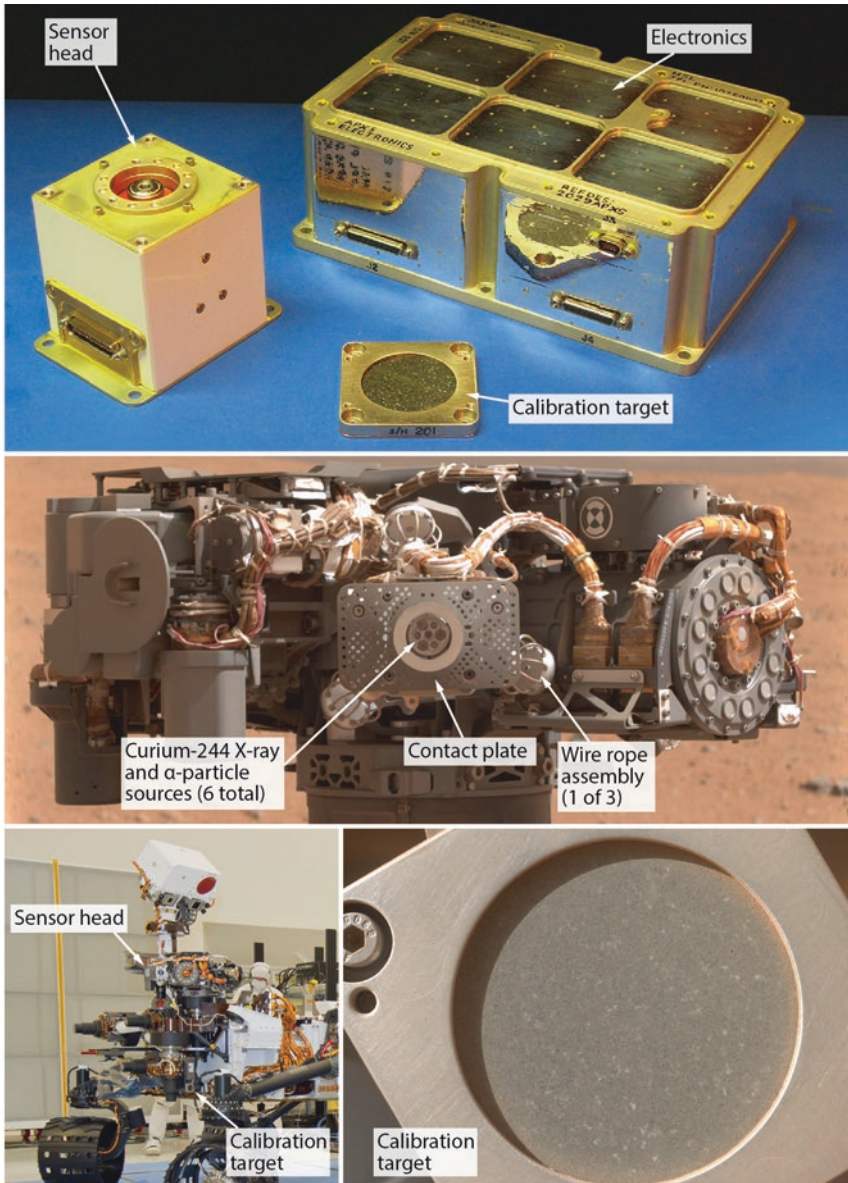


Figure 9.9. Parts of APXS. Top: flight hardware (NASA/University of Guelph). Middle: photo taken during initial turret checkout (MAHLI image 0032ML0000620000100855E01, NASA/JPL-Caltech/MSSS). Lower left: photo showing location of calibration target (NASA/JPL-Caltech release PIA14255). Lower right: MAHLI photo of the APXS calibration target taken during initial checkout on sol 34 (0034MH0000480010100038E01, NASA/JPL-Caltech/MSSS).

The sensor head contains six curium-244 sources. Three of them are covered in a titanium foil and emit both alpha particles and X-rays, while the other three are more thoroughly sealed and emit only X-rays. A cutaway drawing of the internal workings of the sensor head is shown in Figure 9.10. When the alpha particles impinge on atoms in the upper tens of micrometers of the target, they cause the atoms to eject inner-shell electrons, which emit X-ray photons as they fall back to their ground state, a process called particle-induced X-ray emission (PIXE). Impinging X-rays can have the same effect, in X-ray-induced fluorescence (XRF). Particle-induced X-ray emission is a more efficient process for small-mass atoms (sodium to titanium), while X-ray-induced fluorescence is more effective for larger atoms (chromium to strontium). APXS uses a silicon drift detector to detect and count these emitted X-rays. The half-life of curium-244 is 18.1 years, more than the anticipated lifetime of Curiosity's power supply, so degradation of the curium sources should not have a significant impact on APXS use over the course of the mission.

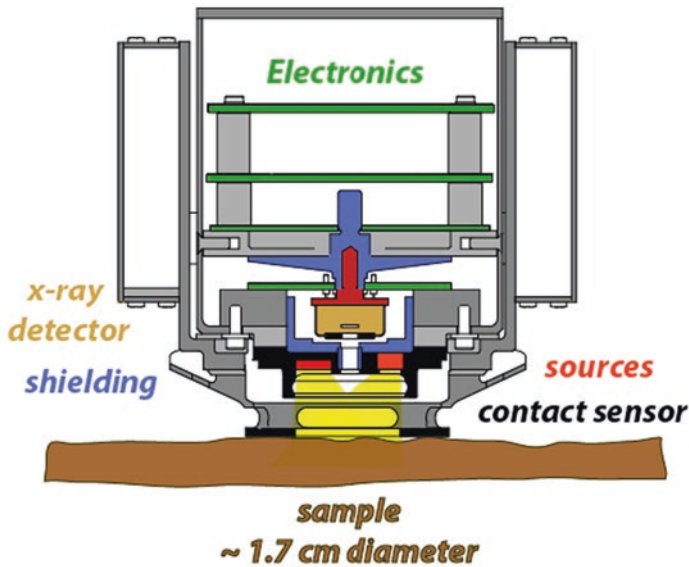


Figure 9.10. Cross-section of the APXS sensor head. University of Guelph.

APXS “sees” deeper into a target for heavy elements (to depths of 50 microns or greater) than for light elements (for which APXS may only be measuring the topmost 5 microns). The energy of X-ray emission depends on the element, so by measuring the amount of X-ray emission with respect to wavelength, APXS can detect the elements that are present (see Figure 9.11).²¹ Employing an analysis derived from observations of samples of known composition on Earth, the APXS team can convert these X-ray spectra into

²¹Dickinson et al. (2012)

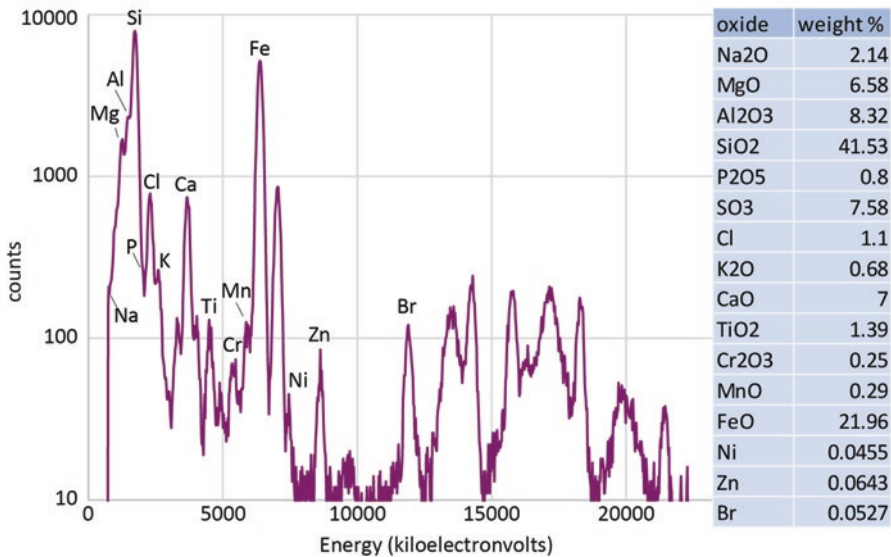


Figure 9.11. Example APXS data. Analyzing the height of peaks in the spectrum (left) allows the APXS team to measure the composition of the rock, expressed as oxides (right). This sample data comes from the John Klein drill target, the location APXS was measuring in Figure 9.8.

elemental abundances. Using the dust removal tool to brush off a measurement site improves APXS's ability to sense the abundances of lighter elements in the rock rather than the dust. For a list of all spots brushed for APXS analysis, see Table 5.2. The brush can still leave as much as 30% of the original dust covering behind.²² The most dust-free targets that APXS examines are dumped drill fines.

Curiosity's APXS has two main improvements over the ones on Spirit and Opportunity. It has a cooler for its detector that can reduce its temperature by 30°C, which allows APXS to operate at ambient temperatures up to -5°C. For comparison, the Mars Exploration Rover APXS works only at temperatures below -40°C, which means it mostly has to be used at night. The cooler allows Curiosity's APXS to be used during the daytime, although it is more frequently used overnight because data quality is better, especially during the summer. (The APXS team performed regular characterizations of instrument performance at different times of day during the summer after sol 1600 to better characterize its performance over a range of temperatures.) The cooler also improves the Curiosity APXS resolution over that of the Spirit and Opportunity APXS.²³

²²Perrett et al. (2017)

²³Slavney (2013)

There is also no alpha channel on Curiosity's APXS (that is, unlike Spirit and Opportunity, Curiosity does not detect backscattered alpha particles). Throwing out the alpha channel allowed the instrument to be designed with the X-ray detector much closer to the surface; the closest range of 19 millimeters compares to 30 for the Spirit and Opportunity APXS. That, in turn, increases the sensitivity of the Curiosity APXS by a factor of 3; reduces the spot size of an APXS measurement; and speeds up data acquisition by a factor of 5. Curiosity's APXS can get a "quick look" measurement of the major elements in only 20 minutes, and high-quality results in only 2 hours.²⁴

APXS and ChemCam both measure elemental compositions. Initially, APXS and ChemCam measurements of target compositions did not match very well, but the match has improved over time, especially as the ChemCam team has improved its calibration (see section 9.2.2.3).

The APXS calibration target, like the MAHLI calibration target (see section 7.4.2), was covered with dust kicked up during the landing. That complicated the use of the calibration target for its intended purpose, but the APXS team adjusted their calibration about 6 months after landing to account for the presence of the dust.²⁵ Another calibration adjustment around sol 1200 improved estimation of manganese abundances.²⁶

9.3.2 Using APXS

APXS was first deployed on the rock Jake Matijevic on sol 46. It can be particularly difficult to find time for APXS observations when Curiosity's goal is long-distance driving, because arm activities can't take place at a new location until post-drive data are received on Earth. Initially, contact science days and driving days were mostly distinct. But on sol 102, the rover drivers performed the first "touch-and-go" observation, where the rover deploys the APXS on a target for a short integration in the morning before stowing the arm and driving away. Touch-and-goes allow the APXS team to track changes in major-element rock composition during long traverses without major impact on drive durations. One advantage to APXS over other instruments is that it consumes negligible data volume, using only 32 kilobytes of memory to store several spectra. It is also cheap in terms of power, especially if used overnight, when its detector doesn't need to be cooled.

APXS can be used either in a contact mode (where the arm is commanded to move APXS toward a target until the contact sensor is triggered) or in a hover mode of 5 to 20 millimeters from the target. When APXS is used in contact mode on unconsolidated materials, it may leave a print of the contact sensor in the soil (Figure 9.12). For unconsolidated materials, it is only used in contact mode in locations where the rover wheel has driven over the soil, compacting it. Touching unconsolidated materials can make the contact plate of APXS dirty, so the rover cleans it after every time it is used on soil. Cleaning APXS involves holding it down, then turning it sideways, then rotating it 180°, using CHIMRA vibration to gently shake it for 20 seconds in each pose.²⁷

²⁴Dickinson et al. (2012)

²⁵Ralf Gellert, personal communication, email dated May 10, 2016

²⁶Mariek Schmidt, personal communication, email dated April 17, 2017

²⁷Ashwin Vasavada, personal communication, email dated March 28, 2017



Figure 9.12. The APXS “nose print” in the fine sand at Gobabeb as seen from Mastcam. The inner, open circle of the APXS contact plate is 29 millimeters in diameter. Mastcam image 1234MR0057070010603445E01. Credit: NASA/JPL-Caltech/MSSS.

When examining fluffy targets or irregular surfaces on which it can't be used in contact mode, APXS is often deployed using a technique called proximity mode, “proxmode” for short. APXS takes very short (10-second) integrations as it is brought closer to a target, signaling the arm to stop when it senses that it has reached the optimal distance of about 5 millimeters of standoff.²⁸ When the sensor head is in contact with the target, the sources are only about 19 mm from the surface, and the sampled area has a diameter of 17 millimeters – similar in size to the diameter of a drill hole. When it is 20 millimeters from the target, the sampled area is larger, with a diameter of at most 31 millimeters. For comparison, the brush clears an area 45 millimeters or more in diameter. MAHLI images with a toolframe distance of 2 centimeters (a standard close-up observation distance) cover an area 33 millimeters wide, comparable to the APXS field of view.

APXS is used heavily at drill sites. Typically, they brush a site near the drill location and use APXS to measure the composition of the rock to be drilled. They also perform an APXS analysis on the drill tailings (which come from the top 15 millimeters of the drill hole) as well as on the dumped pre- and post-sieve fractions of the drill powder (which represent the fine and coarse fractions of the drilled rock from 15 millimeters to the full drill depth). APXS integrations of dump sites taken before dumping can be compared to the post-dump analyses. In general, analysis of drill dump piles has yielded similar results to the pre-drill brushed spots.²⁹

²⁸ Ralf Gellert, personal communication, email dated May 10, 2016

²⁹ Gellert et al. (2015)

Curiosity APXS's rapid integration has allowed the team to regularly perform APXS raster observations. The APXS team most commonly uses rasters when examining a target that contains objects smaller than the field of view, like veins, concretions, and pebbles. Rasters are either a line of 3 observations in a row, or a 2-by-2 array with a central point for a total of 5 observations. Typically, APXS integrates for 20 minutes at each point, and then integrates overnight over the center point. The rasters help the APXS team to separate the signal of the small target of interest from the background signal.³⁰

The observation tray was specifically designed to be used for APXS analyses of sample material (see section 5.7). However, the observation tray has not seen heavy use. The amount of sample that CHIMRA drops on it is small relative to the diameter and depth of the APXS sampling region, so for heavy elements like iron and magnesium in particular, the sample being tested is thin and APXS calibrations do not apply, meaning that samples can't be directly compared to each other.³¹ An unforeseen problem was the behavior of particulate material after it is dropped to the observation tray; vibrations within CHIMRA get transferred to the rover and bounce the sample away from the center of the tray almost as soon as it is emplaced. The mission has found it more useful to measure samples dumped from CHIMRA onto the ground than to continue use of the observation tray. One unforeseen use of the observation tray was a convenient location for APXS to measure the composition of airfall dust.³²

9.3.3 APXS rock compositional classes

The APXS team classifies rocks along different compositional trends, and then uses those classifications to look for correlations between compositional variance and changes in location, elevation, and terrain types.³³ They also look for correlations with rock types and compositional trends observed on Spirit and Opportunity traverses.

Scientists who work with the APXS instruments on Curiosity and previous rovers have devised their own method of classifying rocks. The APXS team looks for clusters in major-element composition, and also for “co-variations,” patterns of groups of major elements occurring together in rocks (Figure 9.13).³⁴ Each time the APXS team encounters a new rock that is compositionally distinct from previous observations, they name a new class for the first, best-described target. Sometimes, the APXS team identifies subclasses within larger groupings. Figure 9.13 shows two ways in which APXS-defined rock classes cluster in composition along different axes. The top chart shows relative abundance of iron and silicon in the rocks; the bottom chart shows sodium and potassium.

Because Mars dust is rich in sulfur and chlorine, the APXS team subtracts those elements from their analyses and renormalizes the remaining elements to make up 100% of the rock before comparing one rock to another (Table 9.3). The APXS rock classifications are not,

³⁰ Ralf Gellert, personal communication, email dated May 10, 2016

³¹ Berger et al. (2014)

³² Berger et al. (2016)

³³ Thompson et al. (2016)

³⁴ Schmidt et al. (2016)

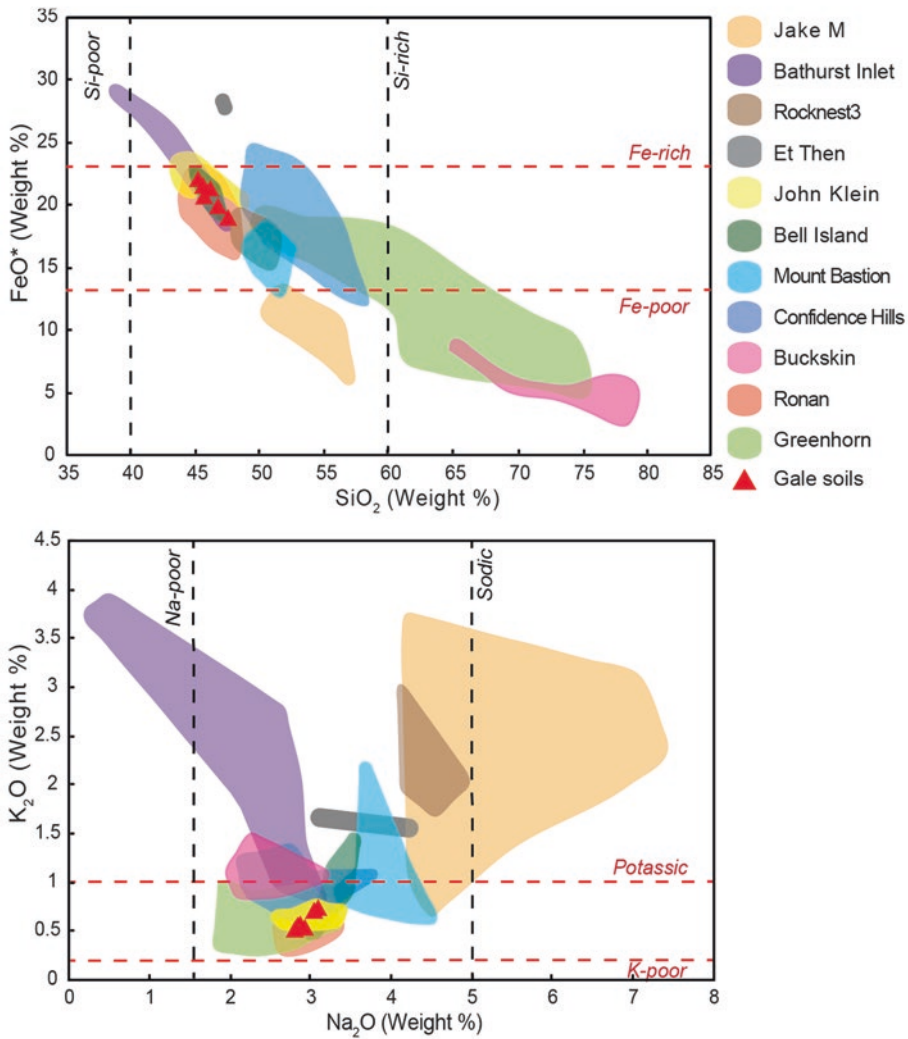


Figure 9.13. Two examples of charts used to identify clusters in APXS rock classifications. Top: rocks analyzed with APXS generally trend from silicon-poor and iron-rich (mafic rocks, like basalt) to silica-rich and iron-poor (like the very silica-rich Buckskin site). Gale soils (red triangles) are similar to the average Mars crust composition. Bottom: The association of potassium to sodium abundance in Gale rocks is more complex. Again, Gale soils are similar to average Mars crust composition, but most rocks that APXS has examined are richer in potassium; some of those are very sodium-rich, and some are very sodium-poor. Note that rock classes that overlap in one of these two diagrams may be entirely separate in the other. Graphs courtesy Mariek Schmidt.

Table 9.3. Example APXS results from sites of different APXS team-defined compositional classes. From Thompson et al. (2016).

Class	Jake M	Bathurst	Rocknest 3	Et Then	John Klein	Bell Island	Mount Bastion	Confidence Hills	Buckskin	Ronan	Greenhorn
Target	Lowerre	Oswego	Thimble	Secure	Wernecke	Eqaltulik	Heimdall	Mojave	Buckskin	Big Sky	Greenhorn
Sol	570	472	706	560	169	323	399	809	1057	1114	1130
SiO2	51.2	43.0	47.3	45.4	46.9	42.0	45.8	51.8	68.1	43.4	56.2
TiO2	0.54	0.89	0.66	0.67	0.91	0.85	0.94	1.07	1.51	0.93	1.00
Al2O3	16.2	8.0	12.0	8.6	8.9	8.8	10.8	12.4	6.1	9.7	5.5
Cr2O3	0.07	0.54	0.21	0.05	0.41	0.65	0.19	0.39	0.10	0.42	0.34
FeOT	11.5	22.4	16.9	27.2	20.5	20.6	13.2	13.5	4.4	17.4	9.4
MnO	0.2	0.5	0.1	0.3	0.3	0.4	0.3	0.3	0.1	0.4	0.1
MgO	3.08	8.71	6.37	4.03	9.80	8.26	7.17	4.47	3.45	8.52	4.77
CaO	5.71	6.13	5.23	3.67	5.40	6.54	7.46	4.29	3.87	6.87	5.98
Na2O	5.4	2.7	5.0	4.1	3.0	3.0	3.3	2.8	2.2	2.8	2.5
K2O	2.23	1.96	2.16	1.47	0.62	0.78	0.97	0.65	0.82	0.47	0.44
P2O5	0.6	0.8	0.7	0.7	1.0	0.8	0.9	1.4	1.3	0.9	1.2
SO3	2.1	3.3	2.2	3.2	0.9	6.1	7.8	5.8	7.2	6.9	10.8
Cl	0.89	0.95	0.71	0.64	1.13	1.15	0.97	0.52	0.71	1.27	1.54
Total	98.90	98.78	98.84	99.87	98.63	98.68	98.87	99.07	99.84	99.94	99.76
Ni ppm	97	360	316	194	694	276	214	839	110	411	160
Zn ppm	617	1214	680	232	794	963	782	1737	206	273	107
Br ppm	33	176	40	183	401	167	10	85	58	205	336
K2O/Na2O	0.41	0.73	0.43	0.36	0.20	0.26	0.29	0.23	0.38	0.17	0.17
Same as above, renormalized to remove sulfate and chlorine											
SiO2	52.8	44.9	48.7	47.3	47.8	45.3	50.2	55.4	74.1	47.3	64.3
TiO2	0.56	0.93	0.68	0.70	0.93	0.92	1.03	1.14	1.64	1.01	1.14
Al2O3	16.7	8.3	12.4	8.9	9.1	9.4	11.9	13.3	6.6	10.6	6.3
Cr2O3	0.07	0.56	0.22	0.05	0.42	0.70	0.21	0.42	0.11	0.46	0.39
FeOT	11.8	23.3	17.4	28.3	20.9	22.2	14.5	14.4	4.8	19	10.8
MnO	0.2	0.5	0.1	0.3	0.3	0.4	0.3	0.4	0.1	0.4	0.1
MgO	3.18	9.10	6.56	4.20	10.00	8.90	7.86	4.77	3.75	9.28	5.46
CaO	5.89	6.40	5.38	3.82	5.51	7.05	8.18	4.58	4.21	7.49	6.84
Na2O	5.6	2.8	5.1	4.3	3.1	3.2	3.6	3.0	2.4	3.1	2.9
K2O	2.30	2.05	2.22	1.53	0.63	0.84	1.06	0.69	0.89	0.51	0.50
P2O5	0.6	0.8	0.7	0.7	1.0	0.9	1.0	1.5	1.4	1.0	1.4

directly, identifications of rock type; instead, they help the science team identify trends in the data and group rocks of similar composition together. Combined with ChemCam elemental compositions, CheMin mineralogy, and observations of rock textures from Mastcam and MAHLI, the APXS rock classifications can help tell the stories of Gale's rocks.

9.3.4 Anomalies

In general, APXS has been a healthy and productive instrument with one minor technical issue. Since launch, Curiosity's APXS has exhibited an unusual behavior that has never been seen in any other instrument from previous generations. Occasionally, in the middle of acquiring data, it stops counting real X-ray events, instead counting only spurious X-ray counts at the lowest detectable energy. The APXS team calls this behavior "lockup." The ultimate cause of the behavior is unknown; it happens randomly. To prevent loss of data, the team splits long APXS integrations into two parts and reboots the instrument in between them, reducing the risk that early lockup would cause the loss of all the data from a single integration.³⁵ This mitigation strategy has prevented any loss of observations. If it happens early in an integration, lockup can affect the signal-to-noise ratio of observations, but these effects have been minimal in practice.³⁶

9.4 CHEMIN: CHEMISTRY AND MINERALOGY

CheMin brings two powerful analytical laboratory techniques to Mars: X-ray diffraction and X-ray fluorescence, allowing direct measurement of mineral composition on Mars for the first time. On Earth, X-ray diffraction and X-ray fluorescence require refrigerator-sized pieces of equipment. Developing Curiosity's miniaturized version was the result of more than two decades of work. The development of the CheMin instrument for Curiosity enabled the development of a portable X-ray diffraction/X-ray fluorescence CheMin-like instrument for use in the field on Earth.³⁷ At the start of the mission, the principal investigator of CheMin was David Blake of NASA Ames Research Center; Tom Bristow (also of Ames) has taken over the role in the second extended mission.

CheMin agitates a finely powdered sample of rock or loose sediment in front of a beam of X-rays. The X-rays diffract through the lattice structures of the minute crystals, generating a diffraction pattern of concentric rings that is recorded by a detector – actually a charge-coupled device, the same kind of detector that is at the heart of a digital camera. The angles at which the X-rays diffract are diagnostic of the minerals present. The impinging X-rays can also produce X-ray fluorescence in the sample, allowing measurement of the elemental composition of the sample, complementing APXS measurements. It is the CheMin instrument that drives the requirement for CHIMRA to prepare small samples of powder of less than 150 micrometers in diameter. CheMin has 27 sample cells, and cells can be reused for up to a total of 74 sample measurements over the course of the mission.

³⁵ Slavney (2013)

³⁶ Ralf Gellert, personal communication, email dated May 10, 2016

³⁷ The main reference for the description of the CheMin instrument is Blake et al. (2012); a useful summary of how it has worked on Mars is in Downs (2015)

9.4.1 Scientific background

While ChemCam and APXS identify the elements present in a target, CheMin identifies how those elements are assembled into minerals. Minerals can give clues to the environment in which a rock formed. Here is a brief summary of the minerals that CheMin has found in Mars rocks:

- Olivine. A magnesium-iron silicate common in basaltic rocks that is generally dark or green in color. The magnesium-rich endmember is called forsterite (Mg_2SiO_4), the iron-rich endmember fayalite (Fe_2SiO_4).
- Pyroxene. A large group of magnesium-iron-calcium silicates, with lesser amounts of other elements such as sodium, aluminum, chromium, manganese and titanium; common in basaltic rocks. Pyroxenes come in different crystal structures called clinopyroxenes and orthopyroxenes, and are usually dark or green in color. CheMin has detected several specific pyroxenes including the orthopyroxene enstatite and the clinopyroxenes augite and pigeonite.
- Feldspar. Another large group of silicate minerals which contain silicon and aluminum with variable amounts of sodium, potassium, and calcium. Feldspars are common in all rock types. Feldspars are further divided into plagioclase feldspars (sodium to calcium mixtures) and alkali feldspars (sodium to potassium mixtures). Feldspar tends to be lighter in color than olivine and pyroxene and can be gray to white to pink depending on composition. CheMin has detected plagioclase feldspars, and the alkali feldspar sanidine.
- Quartz. This is the most common crystalline form of pure silicon dioxide on Earth. There are other crystal forms of silicon dioxide, and in addition to quartz, CheMin has detected tridymite, which forms under conditions of high temperature and low pressure on Earth, as well as cristobalite, which can form at a range of conditions. All have a white color when powdered.
- Magnetite. An iron oxide in which some of the iron is reduced ($\text{Fe}^{2+}\text{Fe}^{3+}_2\text{O}_4$). It has a black color when powdered. Magnetite is a common trace or minor component of basaltic rocks.
- Hematite. An iron oxide in which all of the iron is oxidized. It indicates an oxidizing environment and has a red color when powdered.
- Iron sulfides, including pyrite and pyrrhotite, which indicate reduced environments and have a black color when powdered.
- Akaganeite. An iron oxyhydroxide with chloride that has a rusty yellow color when powdered. It may represent altered pyrrhotite.³⁸
- Jarosite. An iron sulfate with potassium, sodium, and/or hydronium. It has a yellow color when powdered. On Earth, it commonly forms when iron sulfide (pyrite) is altered by water.³⁹

³⁸ Vaniman et al. (2014)

³⁹ L evell e et al. (2015)

- Calcium sulfates. These can occur with or without water molecules incorporated into their crystal structure. Anhydrite is pure calcium sulfate, without water. Gypsum has significant water in its crystal structure. Bassanite is intermediate between the two. All have a white color. When rocks containing calcium sulfates are drilled and introduced into the warm CheMin instrument, gypsum or bassanite can dehydrate into anhydrite within a few sols.

9.4.2 How CheMin works

CheMin is located inside the body of the rover, occupying the front center. An articulated inlet cover, part of the Sample Acquisition, Processing, and Handling (SA/SPaH) system (see section 5.8) protects its inlet from infalling dust. Samples pass through a 1-millimeter sieve over a funnel and into one of 27 sample cells located on a wheel. Once analysis is complete, the wheel is rotated 180° to dump the samples into a sump at the bottom of the instrument. An X-ray source generates the X-rays that CheMin directs through the sample, and a CCD detects the diffracted and fluoresced X-rays. Components of the CheMin instrument are shown in Figure 9.14.

9.4.2.1 The CheMin Sample Handling System

CheMin's funnel is equipped with a mesh screen with wires spaced 1 millimeter apart, to protect the instrument from too-large particles. When CHIMRA delivers a sample, CheMin vibrates three piezoelectric actuators around the funnel to encourage all of the sample to pass through without sticking. The sample cells are mounted in pairs on a wheel. The wheel holds 27 sample cells and 5 reference standards. Fourteen of the sample cells have Kapton windows, and 13 have Mylar windows. The Mylar-windowed cells provide cleaner results, having little observable effect on the diffraction patterns produced by CheMin. But Mylar scratches easily and can be damaged by acidic samples. The Kapton-windowed cells will last longer, but Kapton produces a peak in the diffraction patterns that could interfere with the detection of some clay minerals.

MAHLI routinely images the CheMin inlet and mesh screen to make sure that all delivered material has passed through. When MAHLI observes any material clumping on the screen, CheMin can be commanded to run the piezoelectric actuators on its funnel to encourage any sticking material to drop. See Table 5.4 for a summary of MAHLI CheMin inlet imaging.

CHIMRA delivers a maximum of 76 cubic millimeters of sample to a sample cell. Each sample cell has a miniature funnel-shaped reservoir with a volume of 400 cubic millimeters, directing sample into a 10-cubic-millimeter active cell. The space within the active part of the cell is a very thin disk 8 millimeters in diameter and 175 micrometers deep. That depth is optimal for the 150-micrometer limit of sample powder size. The requirement of <150 micrometer powder is defined as the maximum crystal size that provides good diffraction.

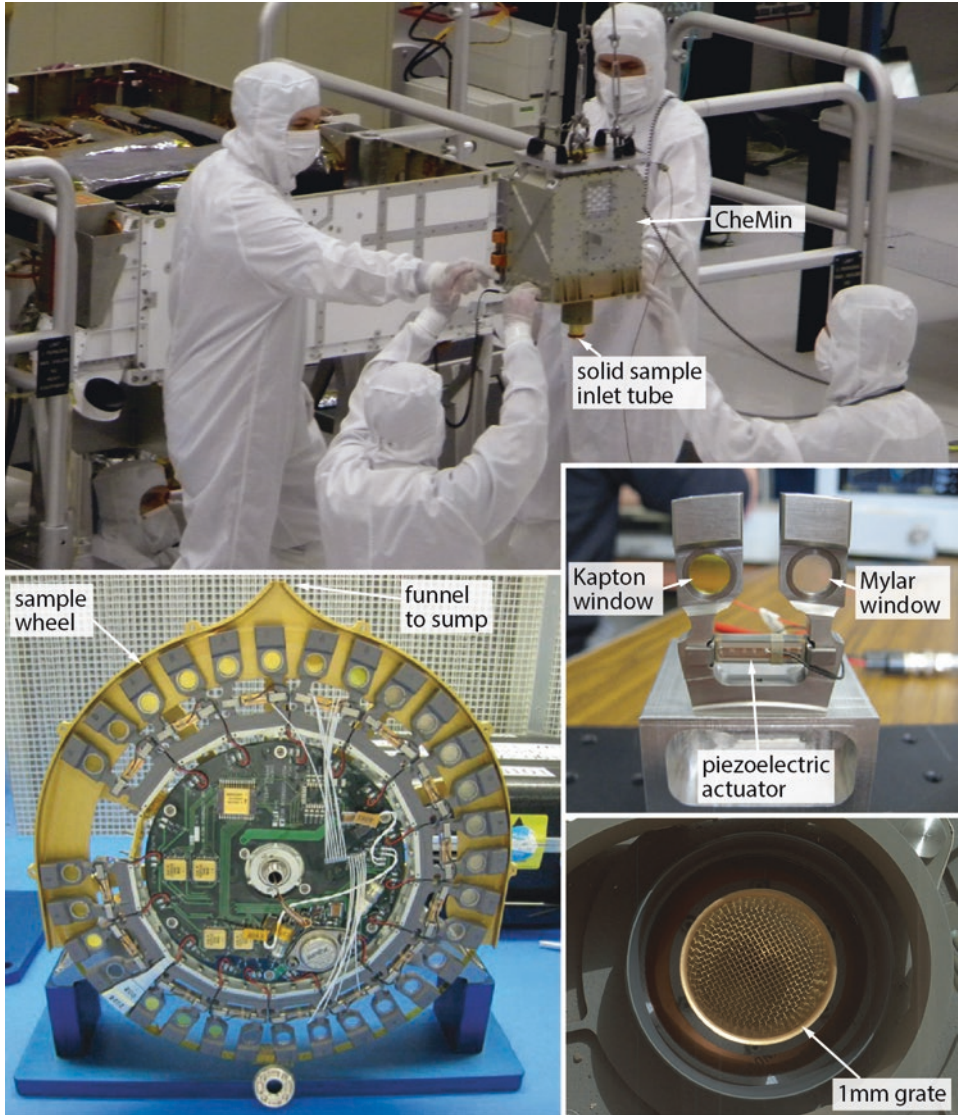


Figure 9.14. Components of the CheMin instrument. Top: installation of CheMin, June 15, 2010 (NASA/JPL-Caltech release PIA13231). The rover body and CheMin are upside down. Middle: dual-cell assembly, otherwise known as a “tuning fork,” showing both Kapton and Mylar window materials (from Blake et al. 2012). Bottom left: sample wheel assembly (Blake et al. 2012). Bottom right: Sample inlet with inlet cover opened, showing 1 mm mesh (NASA/JPL-Caltech/MSSS release PIA16163).

Each pair of sample cells has a piezoelectric actuator, referred to as a “piezo.” To get the grains inside a sample cell moving, CheMin uses the piezos to vibrate them at a range of frequencies, with the goal of getting the sample cell to vibrate at its resonant frequency, like a tuning fork. The vibrations of the two tines of the fork – the two sample cells in each pair – balance each other out so that little of the vibratory energy gets transmitted to the rest of the instrument. The intense vibration makes the mineral grains circulate like a boiling liquid, tumbling them randomly to present all orientations of all minerals to the X-ray beam. The dynamics of the vibration are extremely important. If the vibration happens at too low an intensity, grains could separate by density. It's also possible for grains to agglomerate into immobile masses wedged between the two sides of the cell; once formed, such agglomerations tend to grow. To prevent both of these from occurring, CheMin periodically shakes the cells at very high intensity for a few seconds, breaking up the agglomerations and mixing up the grains that may have separated by density. Vibration of the powdered sample in the cells had to be tested out at Mars gravity, tests that the CheMin team performed, 3 to 4 seconds at a time under microgravity created in a Piper Cherokee aircraft performing parabolic flights over the Pacific Ocean. Occasionally, the vibration turns out to be too intense, encouraging sample to bounce up and out of the cell, so CheMin is sometimes commanded to vibrate one of the cells next to the one that actually contains the sample in order to move the sample around more gently, a method that the CheMin team calls “kumbayatic” mode. (Seriously.)

Samples are usually analyzed for 20 to 40 hours over many sols, although usable data can be obtained in about 2 to 3 hours. Longer analysis times improve detection of minor minerals and improve the quality of the data. Once analysis is complete, the wheel rotates 180° to dump the sample into an internal sump, vibrating the cell to encourage the sample to fall out. The reusable sample cells have no covers, so dumping happens automatically as a result of rotating the wheel. The reference standard sample cells are covered with high-efficiency particulate air filters to prevent their powdered contents falling out with wheel rotation.

There are five standards. One is amphibole, an iron-rich silicate mineral sourced from Gore Mountain, New York, selected because it has a range of intense peaks in its X-ray diffraction pattern, as well as several closely-spaced peaks that allow the CheMin team to monitor how well they are resolving close peaks. Two other standards are mixtures of synthetic beryl and quartz in different proportions, selected because beryl has clearly defined widely-spaced peaks, allowing the team to monitor the crispness of individual peak profiles; the intermixed quartz helps them check how well they can determine relative mineral abundances, especially for minor minerals. One standard is synthetic arcanite, a potassium sulfate that also has well-defined diffraction and is strongly X-ray fluorescent, with precisely known sulfur and potassium content. Finally, a doped ceramic standard was made from a mix of the clay mineral nontronite with numerous salts, providing a standard with a wide variety of fluorescence peaks.

9.4.2.2 *The CheMin X-Ray Source*

CheMin's X-ray tube emits a cone of X-radiation using a cobalt anode. The X-rays have an energy of 6.925 keV. A pinhole plate allows only a 70-micrometer-wide beam of radiation to exit the source and pass through the center of the sample cell. The narrow beam

illuminates just 0.02% of the volume of material in the sample cell, but by vibrating the sample cell, different grains move in and out of the analysis area at different, random orientations. After passing through the cell, the direct beam falls onto a beam trap on the detector. The X-ray source has a power supply that is pressurized with a mixture of sulfur hexafluoride and nitrogen gas.

9.4.2.3 *The CheMin Detector, X-Ray Diffraction, and X-Ray Fluorescence*

The detector is a 600-by-1182-pixel CCD, of which 600-by-582 pixels is an active area. The pixels are unusually large for a CCD (40 micrometers square). An impinging X-ray photon deposits thousands of electrons in the CCD in a cloud that is tens of microns in diameter; the large size of the pixels means that almost all of this charge is usually captured in one pixel, rather than being spread across several pixels, so that each time an X-ray photon hits the detector, the detector records not only the position but also the energy of the photon. A filter in front of the detector prevents it from being exposed to visible-wavelength photons. A cryocooler brings the temperature of the detector down to at least 48°C below the interior of the rover, thereby minimizing dark current on the CCD.

X-ray diffraction happens when X-rays interact with crystalline lattices of atoms and constructively interfere, producing diffraction spikes at certain angles away from the direction of the X-ray beam. The angle of diffraction, the sum of the theta angle of incidence and the equal theta angle of reflection (hence 2-theta), depends on the wavelength of the X-ray and the spacing between atoms in the crystal lattice. The CheMin detector can record diffracted X-rays at 2-theta angles ranging from 5–50°, with an angular resolution of 0.30–0.35°.

When CheMin is operating, the CCD typically records 30-second exposures, called “frames.” In that short period, any given pixel on the detector usually records at most one incident X-ray; therefore, a single CheMin frame records not only the position but also the intensity of individual events. CheMin can store up to 2730 such images in memory (or about 22 hours of data). But that would be too much data to transmit to Earth, so the rover’s main computer can stack 10 to 200 individual exposures into a single image, called a “minor frame.” Only pixels whose values correspond to the 6.925-keV energy of the X-ray source are selected for inclusion in the minor frame. On Earth, some or all of the minor frames from a single sample can be stacked into a “major frame.” Then the pixel values can be summed around the concentric circles of the 2-D diffractogram, producing a 1-D diffractogram (see figure 9.15 for examples). The CheMin team uses these 1-D patterns for analysis of mineral composition, but they also downlink the 2-D diffractograms to diagnose problems, such as blobs caused by mineral grains that became stuck during vibration. Individual peaks in the diffractogram can be diagnostic of specific minerals, but each mineral has a set of peak positions and intensities that reveal the crystal structure. The team uses all the peaks to determine mineral abundances. If there are non-crystalline (amorphous) materials present in the sample, they show up in the diffractogram as a very broad hump upon which the narrower diffraction spikes are superimposed. The team can use the shape and height of the hump to quantify the amount of amorphous materials present, but with larger analytical error than for crystalline minerals.

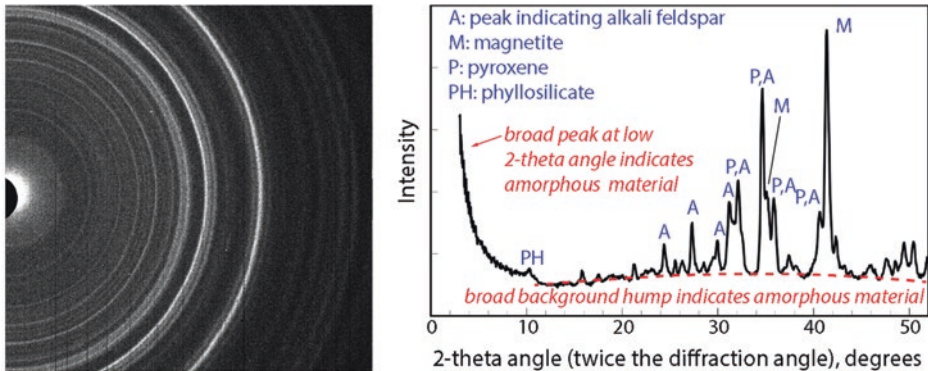


Figure 9.15. Example CheMin data from the Windjana sample. Left: A CheMin 2-D diffractogram. Black semicircle at center of the left edge is the CheMin beam stop. Light circles are from diffraction in lattice planes in minerals. Right: CheMin 1-D diffractogram produced by summing all the values of the pixels with diffracted cobalt radiation at a given distance (angle) from the X-ray beam. Sharp peaks identify specific crystalline minerals. Broad hump (dashed red line) indicates the presence of amorphous (noncrystalline) material. After Treiman et al. (2016).

The CheMin CCD can also function as an X-ray fluorescence detector. The pixel energy values in each frame serve as a measure of the energy of the X-rays that hit the detector. Many of these X-rays are diffracted ones with the same energy as the cobalt source, but other, lower-energy X-rays come from X-ray fluorescence. The energy of the fluoresced X-rays depends on the elements present. CheMin is not sensitive to elements lower in mass than potassium. CheMin reports this data in the form of a histogram (counts of pixel energy values). As with the diffractograms, to conserve downlink volume, the rover computer merges information from many CheMin CCD frames to produce histograms before transmitting the results to Earth. While mineral abundances from diffraction are quantitative (with mineral detection limits of 1 to 2% by weight) chemical composition from X-ray fluorescence is qualitative.

Over time, the CCD will accumulate damage from cosmic rays as well as from the neutrons emitted by the MMRTG. The effects of this damage can be reduced by shortening exposure times or by binning the data before processing it. CCD health is checked periodically (about every 18 months), and as of 2017 there has been no detectable degradation in CCD performance.⁴⁰

9.4.3 Using CheMin

CheMin analysis is usually performed overnight, at a time when the rover operates at cooler temperatures. A typical overnight analysis takes 10 hours. The analysis is usually repeated over multiple nights to improve counting statistics, so most samples are analyzed

⁴⁰David Vaniman, personal communication, email dated April 5, 2017

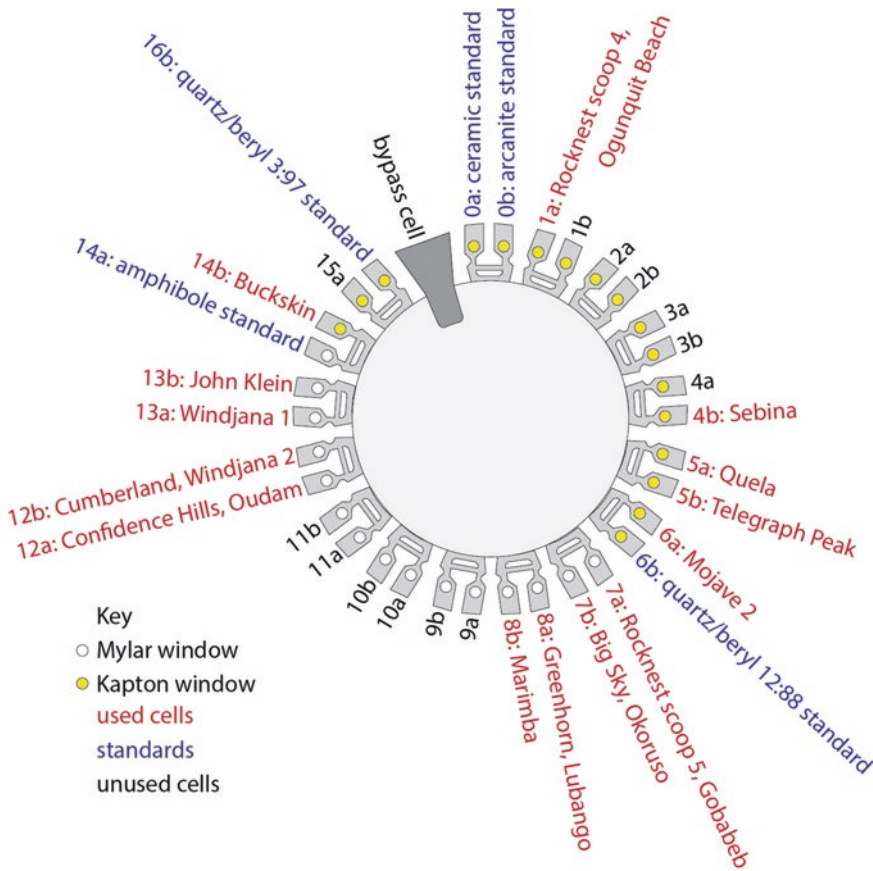


Figure 9.16. Schematic diagram of the CheMin sample wheel showing which cells have been used as of sol 1800. Information courtesy David Vaniman and Elizabeth Rampe.

for a total of 20 to 40 hours. CheMin can continue to analyze a sample in this way until a new sample is ready for delivery, at which point the instrument usually dumps the old sample in order to receive the new one. Occasionally, CheMin accepts two samples in adjacent “tuning forks,” permitting it to continue analyses on both. CheMin kept both John Klein and Cumberland in adjacent cells for about 200 sols, and also stored the Mojave2/Telegraph Peak, Greenhorn/Big Sky, and Lubango/Okoruso sample pairs in this way. As the mission has proceeded, the team has begun to reuse Mylar-windowed cells, keeping unused cells in reserve against a future date when the rover will encounter different rock types (e.g. Vera Rubin Ridge and the clay- and sulfate-rich rocks beyond it).⁴¹ Sol 640 was the first test of re-using a sample cell. Figure 9.16 is a schematic of the CheMin sample wheel showing sample cell use.

⁴¹David Vaniman, personal communication, email dated March 8, 2017

Table 9.4. Summary of CheMin sample analyses, organized approximately in order of stratigraphy, from stratigraphically highest to lowest (as in a stratigraphic column). Data are from the CheMin releases to NASA's Planetary Data System.

Group	Sample sol	CheMin delivery	CheMin analysis start	CheMin cell	Name	olivine	pyroxene	plagioclase feldspar	alkali feldspar	silica	magnetite	iron sulfide	hematite	calcium sulfate	akaganeite	jarosite	apatite	clay	amorphous
Modern basaltic sand	74	77	79	1a	Rocknest (scoop 4)	13	22	33	0	1	2	0	0	2	0	0	0	0	27
	93	94	95	7a	Rocknest (scoop 5)	16	20	29	1	1	1	0	1	1	0	0	0	0	29
	1224	1226	1236	7a	Gobabeb (scoop 1)	18	21	24	0	0	2	0	0	1	0	0	0	0	34
Stimson formation	1321	1323	1325	8a	Lubango**	0	4	11	0	1	3	0	1	6	0	0	0	0	75
	1332	1334	1335	7b	Okoruso	0	21	27	2	1	11	0	1	1	0	0	1	0	35
	1137	1139	1140	8a	Greenhorn*	0	6	21	0	51	9	0	3	10	0	0	0	0	0
	1119	1121	1122	7b	Big Sky	0	26	37	0	3	10	0	2	1	0	0	0	0	20
Murray formation	1495	1496	1496	4b	Sebina	1	2	12	2	0	0	0	6	7	0	1	0	51	19
	1464	1466	1470	5a	Quela	2	2	14	2	0	0	0	6	5	0	0	0	52	16
	1422	1425	1425	8b	Marimba	2	1	17	3	0	0	0	6	7	0	1	0	40	23
	1361	1362	1363	12a	Oudam	0	5	28	0	8	0	0	14	6	0	0	0	3	36
	1060	1061	1062	14b	Buckskin	0	0	21	4	70	3	0	0	1	0	0	0	0	0
	908	922	923	5b	Telegraph Peak	1	7	25	5	23	8	0	1	0	0	1	2	0	27
	882	884	885	6a	Mojave2	0	7	23	0	1	3	0	3	0	0	3	2	9	49
759	765	766	12a	Confidence Hills	1	12	18	5	1	3	0	6	0	0	1	1	13	39	
Bradbury group	621	623	624	13a	Windjana	4	34	4	15	0	10	1	1	1	2	0	0	8	20
	279	282	283	12b	Cumberland	1	16	22	2	0	4	1	1	2	2	0	0	18	31
	182	195	196	13b	John Klein	4	18	32	2	1	5	2	1	5	2	0	0	0	28

Gray shading denotes the second uses of those CheMin cells. Orange shading is darker when the mineral is more abundant.

* Greenhorn is an alteration halo within Big Sky type rock.

** Lubango is an alteration halo within Okoruso type rock.

The experiment has been highly successful, although as of sol 1800 it had not received a sample since the sol 1536 drill feed anomaly (see Section 5.3.4.3). Minerals detected by CheMin are mostly those associated with basalt. The first sample CheMin ingested, at the Rocknest sand shadow, has the mineralogy of basalt: plagioclase feldspar, pyroxene, and olivine, with minor amounts of other minerals, like anhydrite (a calcium sulfate) and quartz. But the rocks that Curiosity has drilled have much less olivine. Instead, there are minerals like clays, which speak of alteration by water. There is also a surprising amount of potassium feldspar in Windjana and of tridymite in Buckskin, which suggest source volcanic rocks with unexpected compositions for Mars.⁴² Some minerals form under particular conditions of temperature, pressure, humidity, acidity, and so on, so the CheMin

⁴² See, for example, Treiman et al. (2016) and Morris R et al (2016)

team use the mineral assemblages to interpret the history of the environments that the rock has experienced since its source rock formed. The CheMin analyses that have been delivered to NASA's Planetary Data System to date are summarized in Table 9.4.

9.4.4 Anomalies and issues

No serious problems have occurred with the CheMin instrument, only minor issues with individual experiments. The Buckskin sample appeared to suffer from poor grain motion and particle clumping, resulting in on-ring and off-ring diffraction spots.⁴³ The subsequent sample, Big Sky, appeared to be slightly contaminated by the presence of Buckskin material in the system (either from CHIMRA or the CheMin inlet), diagnosed by the presence of tridymite. Tridymite, an unusual high-temperature, low-pressure polymorph of quartz, was abundant in the Buckskin sample but not observed in previous or later samples.

9.5 SAM: SAMPLE ANALYSIS AT MARS

Like CheMin, SAM is a sophisticated laboratory analysis instrument that has been miniaturized to fit inside the belly of the rover. It is multiple instruments in one. Its two spectrometers analyze the chemical and isotopic composition of gases. SAM can either ingest those gases directly from the atmosphere, or create gases by slowly heating solid samples in an oven to drive off volatile materials. SAM doesn't directly measure mineral composition, but the SAM team can deduce the presence of specific minerals by observing the temperature at which gases are driven off from the sample. SAM also has a gas chromatograph that can help it identify organic compounds preserved in rocks. SAM performs atmospheric analyses frequently (typically once every two weeks) and bakes solid samples more rarely. Although SAM is not the first gas chromatograph mass spectrometer (GCMS) sent to Mars, it is the first successful one since the Viking landers.⁴⁴ (The failed Beagle 2 lander carried a GCMS.)

On Mars, SAM's work has been complicated by two problems, both of which happened prior to landing. A leaky wet chemistry cup contaminated the interior of SAM's solid sample manipulation system with an organic solvent, making it challenging to detect Martian organic materials. And "Florida air" leaked into one chamber of the instrument designed to measure atmospheric methane abundance, swamping the methane signal. Over time, the SAM team has developed workarounds for both problems, increasing their confidence in their results.

SAM was supplied to the mission by NASA's Goddard Space Flight Center, but components were built at several different institutions. The tunable laser spectrometer was built at JPL. The gas chromatograph was provided by the University of Paris and CNRS. Honeybee Robotics built the sample manipulation system. The mass spectrometer and the gas processing system were developed at Goddard. It all came together at Goddard before being delivered to JPL. The principal investigator for SAM is Paul Mahaffy.

⁴³Morris et al. (2016)

⁴⁴The SAM instrument description paper is Mahaffy et al. (2012); useful summaries of post-landing performance are in Millan et al. (2016) and Franz et al. (2017)

9.5.1 How SAM works

SAM is a large gold-plated aluminum box occupying a substantial portion of Curiosity's interior (Figure 9.17; see Figure 4.3 for its location inside the rover). SAM's two detectors are a Quadrupole Mass Spectrometer (QMS) and a Tunable Laser Spectrometer (TLS). It can also use a Gas Chromatograph (GC) in concert with its mass spectrometer to perform GC-MS experiments. Other subsystems include two solid sample inlet tubes; two atmospheric inlets; a Sample Manipulation System with 74 sample cups on a carousel; a Gas Processing System that collects and moves gases around the interior of SAM; and an electronics box. Analyzing atmospheric samples requires use of only the gas processing system, TLS, and QMS. Analyzing solid samples requires those as well as the sample inlets, carousel, and ovens. Use of the GC is an option for both solid and atmospheric samples.

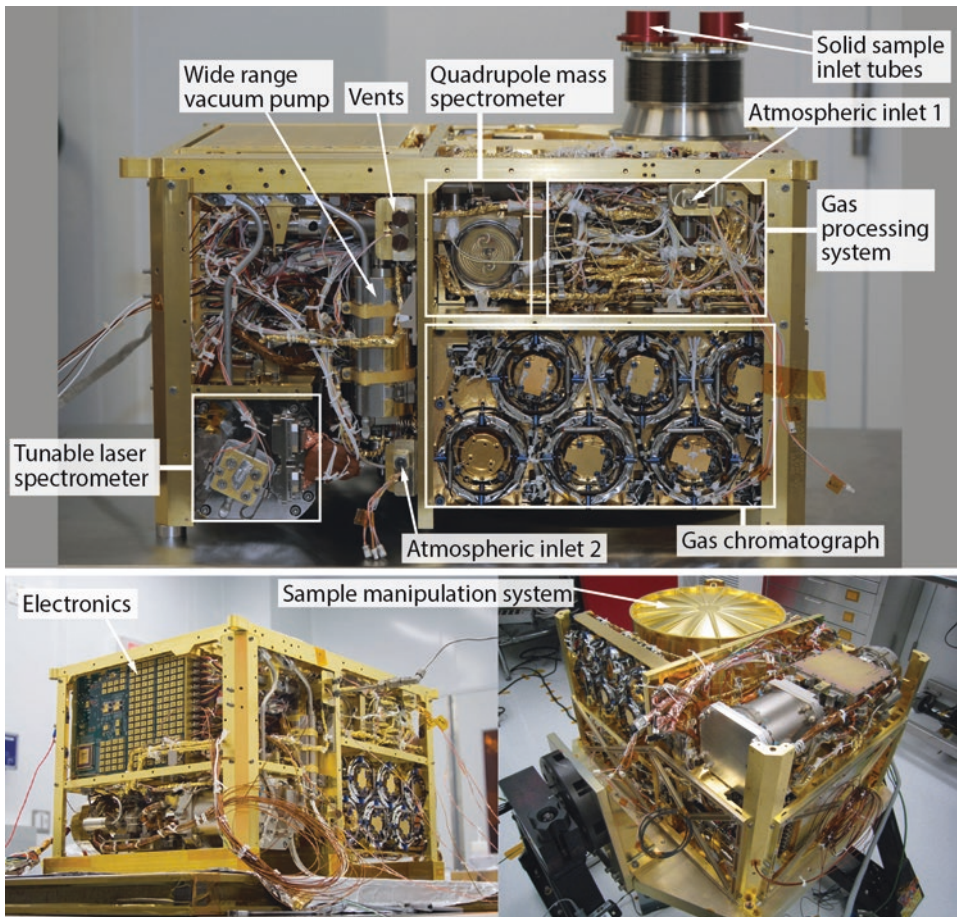


Figure 9.17. Components of the SAM instrument. Top and lower left images courtesy Paul Mahaffy. Bottom right NASA/JPL-Caltech release PIA13463.

9.5.1.1 Gas Processing System

The Gas Processing System is a spaghetti of tubing, valves, manifolds, heaters, pumps, and gas reservoirs. It includes:

- 2 helium reservoirs: These contain a nonrenewable supply of helium, which is used as a carrier gas, adding pressure to move sample gases through the gas chromatograph. The reservoirs have a volume of 180 cubic centimeters each; when launched, the helium they contained was at a pressure of 14,000 kilopascals. The helium launched with SAM would fill about four large (30-centimeter) party balloons.
- 1 low-pressure oxygen gas reservoir, used for combustion experiments.
- 1 low-pressure calibration gas reservoir.
- 2 turbomolecular vacuum pumps (“wide-range pumps”), to move gases through the system.
- 14 manifolds with 1 to 10 valves each (manifolds are chambers, junctions of many tubes; by selectively opening valves at manifolds, the SAM team can steer gases in myriad ways through the system).
- 2 high-conductance valves (that is, large valves).
- 52 micro-valves (that is, tiny valves; these are welded directly to the manifolds to save mass).
- Many transfer tubes, a lot of them wrapped with heaters.
- A hydrocarbon trap, which can be cooled to collect organic compounds and heated to release them to the gas chromatograph; it also separates heavier from lighter noble gases.
- A scrubber system that can remove carbon dioxide, which is the most abundant gas in Mars’ atmosphere, therefore enriching other gases; the scrubber can also trap water, which can later be released by heating it.
- 2 getters that can remove all except some noble gases.

Figure 9.18 is a diagram of the gas processing system. In section 9.5.2 we’ll see how gases move through this system.

9.5.1.2 Quadrupole Mass Spectrometer (QMS)

A mass spectrometer uses electric and magnetic fields to separate charged particles according to their mass-to-charge ratio (m/z). Curiosity’s mass spectrometer (Figure 9.19) is sensitive to molecular masses from 1.5 to 535.5 daltons, with a resolution of 0.1 dalton. The quadrupole design is very similar to the one that was on the Galileo Jupiter atmospheric probe; its ion source and detector are based on ones used by the ill-fated comet mission CONTOUR.

The QMS can operate continuously, taking readings of the number of ions that reach the detector every 0.02 seconds. It measures a single mass-to-charge ratio at a time. To use the QMS, the SAM team chooses a mass range of interest and sweeps through the range by changing the voltage of the power supplied to the spectrometer. If they want to focus on a very small mass range to tease apart interesting compounds with slightly different masses, they can take small voltage steps each time to achieve their maximum resolution.

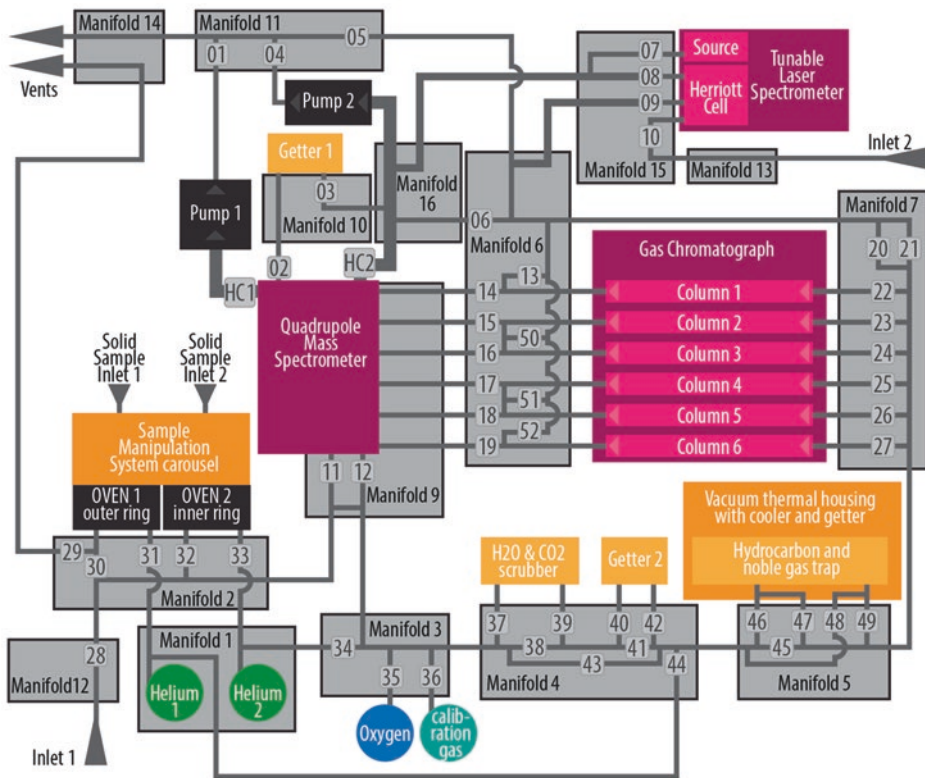


Figure 9.18. Schematic diagram of the SAM gas processing system. Tiny gray numbered squares are the micro-valves. HC = High-capacity valve. After Mahaffy et al. (2012).

Alternatively, they can sweep across their entire mass range using larger steps. Sweeping through the range in smaller steps takes longer; the choice of range and steps depends on what the SAM team is looking for in their experiment.

9.5.1.3 Tunable Laser Spectrometer

The tunable laser spectrometer was designed to measure only three specific gases: methane, carbon dioxide, and water. It can make very precise measurements of the ratios of deuterium to hydrogen; carbon-12 to carbon-13; and ratios among oxygen-16, -17, and -18. It can directly measure the atmospheric abundance of methane and water to a precision of 2 parts per billion by volume. On Mars, the TLS has been able to detect a few other compounds with absorption features in its wavelength range, including hydrogen fluoride and “a mystery chlorine compound that we are working to identify.”⁴⁵

⁴⁵Paul Mahaffy, personal communication, email dated April 8, 2017

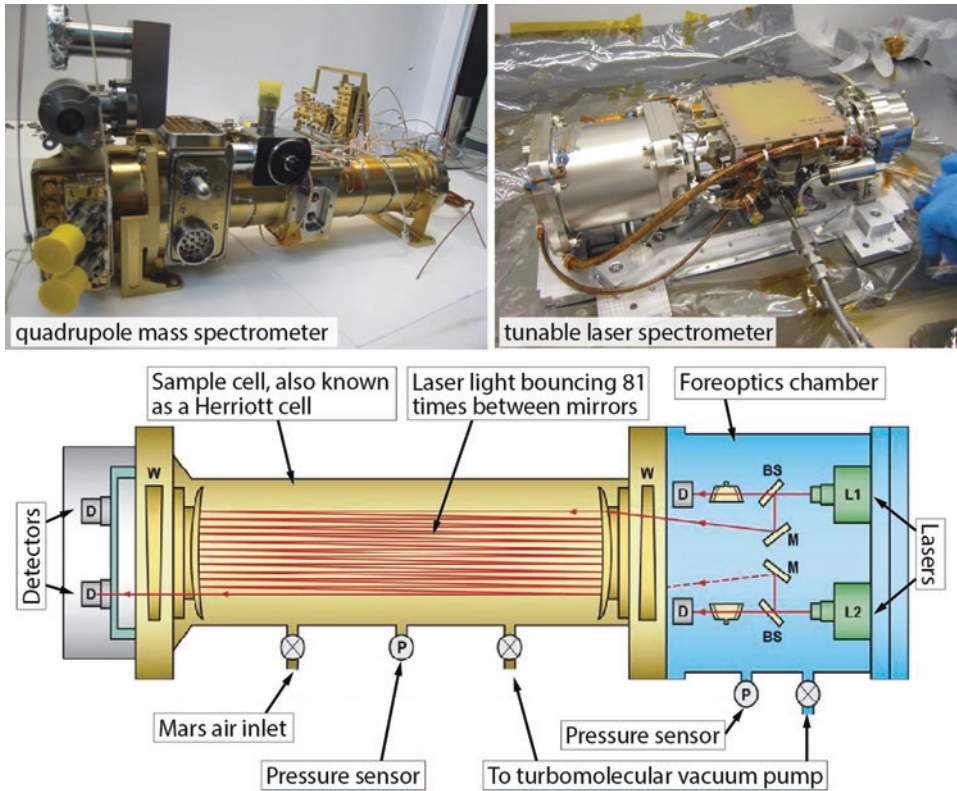


Figure 9.19. Top left: the quadrupole mass spectrometer. Top right: the tunable laser spectrometer. Bottom: diagram of the tunable laser spectrometer. The red lines show the light path as it is bounced repeatedly between two mirrors to make the laser light take a long path through the sample gas. Images courtesy Paul Mahaffy.

TLS has three components: a foreoptics chamber containing lasers and mirrors; a sample cell; and a detector chamber. The three chambers are separated by windows. TLS works by filling a cylindrical sample cell with gas, and then shooting an infrared laser into the sample cell (Figure 9.19). The sample cell is 20 centimeters long and 5 centimeters wide. Mirrors at both ends of the cylinder bounce the laser back and forth through the cell multiple times. A 2.78-micron laser, used for carbon dioxide and water, bounces through the cell 43 times, for a path length of 8.93 meters; a 3.27-micron laser, for methane, bounces 81 times, for a path length of 16.8 meters. Gases in the sample chamber absorb some of the infrared light at wavelengths specific to each gas. Bouncing it back and forth so many times gives trace gases more opportunity to absorb light before it reaches the detector. Cooling the 2.78-micron laser can tune its wavelength to 2.785 microns to access a carbon dioxide absorption line, and 2.783 microns for water. By measuring the intensity of the laser light after it exits the cell, TLS can measure the abundance of gases to part-per-billion sensitivity.

The tunable laser spectrometer doesn't operate continuously, unlike the QMS. SAM waits until the TLS chamber is filled to some desired pressure, and then performs a TLS reading. Then it usually will pump out some of the gas and perform another reading at a lower pressure. It usually repeats this a few times. Reading at multiple different pressures makes sure that there will be at least one reading for each gas at which the detector is not saturated.

At some time prior to launch, the tunable laser spectrometer's foreoptics chamber leaked, introducing Earth atmosphere into it, to a pressure of 76 millibars.⁴⁶ The SAM team refers to this as "Florida air" although it probably contains air from Maryland and California as well. The Florida air contained 10 parts per million of methane, way above the part-per-billion levels that exist in the Martian atmosphere. Because the lasers pass through the foreoptics chamber on their way to the sample cell, the methane in the foreoptics chamber swamps the signal from methane in the Martian sample. When they discovered the problem, shortly after landing, the SAM team changed how they operated the TLS. They now pump the foreoptics chamber down to a pressure of 11 millibars before running a methane experiment. Then they make measurements both before and after introducing the Martian sample into the chamber, and a third time after venting the Martian sample. They subtract the empty-cell spectrum from the full-cell spectrum, leaving them with a contribution only from the full cell.

Used in concert with the GC and QMS, the tunable laser spectrometer can help determine the abundances of gases that can be hard to pull out of mass spectrometer measurements, such as methane and the different isotopes of oxygen present in water.

9.5.1.4 Gas Chromatograph (GC)

Gas chromatography helps a mass spectrometer distinguish among different compounds by separating a gas mixture into its individual constituents, spreading out their arrivals at the mass spectrometer over time. It is particularly focused on compounds made of light elements: hydrocarbons and atmospheric gases. There are actually six different gas chromatograph "columns." Originally, only one of the columns could be used at a time. Each of the six columns is a tube 30 meters long but only a quarter of a millimeter in diameter. The tubes are wound into coils to pack them inside the instrument. The coils are visible on the side of the instrument in Figure 9.17.

Each of the columns is designed to work on different ranges of molecular weights (Table 9.5). The inside surface of each column is coated with a different substance. The substances grab hold of gas molecules and release them. Different gas molecules have more or less affinity for each column's coating. The less sticky molecules exit the column first, the stickiest last. In addition, large molecules tend to move more slowly down the column than small molecules. One of the columns (column 4) can compare abundances of

⁴⁶Webster et al. (2014)

Table 9.5. SAM's gas chromatograph columns. After Mahaffy *et al.* (2012).

Column	Injection trap?	Gases targeted
1	no	Medium molecular weight organics (organics having 5 to 15 carbon atoms)
2	no	High molecular weight volatile organic compounds, including derivatives of organics having more than 15 carbons
3	no	Volatile gases, including low-weight organics (1–2 carbons)
4	yes	Medium molecular weight organics and enantiomers (left- versus right-handed) of specific classes of organics
5	yes	Medium molecular weight organics
6	yes	Volatile organic compounds having 1 to 4 carbons, ammonia, and sulfur-containing compounds

left- versus right-handed enantiomers of organic compounds – an experiment that's actually related to astrobiology – but SAM has not yet identified any enantiomers.⁴⁷

Three of the six columns have injection traps that adsorb interesting gas species as they arrive at the start of the column, in order to concentrate them. Flash heating of the traps releases the gas molecules within a span of 4 to 10 seconds, boosting the chromatograph's ability to cleanly separate them into different constituents. Later in the mission, the SAM team has experimented with splitting the gas collected on the hydrocarbon trap into two columns by using one column that lacks a trap and one that has one. After the experiment with the trapless column is complete, SAM can heat the trap and analyze the same gas with the other column. For columns 2 through 6, as gas molecules exit the tube, they pass across a thermal conductivity detector (TCD), which can detect the major species in the gas down to the part-per-million level. From the GC, the separated gases go into the QMS.

9.5.1.5 Solid Sample Inlet Tubes

SAM has two solid sample inlet funnels and tubes, one each to access the outer and inner rings of the sample manipulation system carousel. The tubes are 4.1 millimeters in diameter, amply large to accommodate any particle that may have passed through the 1-millimeter sieve in CHIMRA. From the top of the funnel to the bottom of the inlet tube, the sample falls a distance of 25.4 centimeters. When SAM is ready to accept a solid sample, it positions a sample cup under an inlet tube. The rover opens an inlet cover (part of the Sample Acquisition, Processing, and Handling (SA/SPaH) system, see section 5.8) and vibrates the solid sample inlet tubes using piezoelectric actuators to prevent the incoming sample from sticking to the tubes. The system is designed to ensure that at least 98% of the delivered sample makes it into the waiting sample cup. The inlet tubes have heaters that allow them to be warmed to up to 120°C in case hydrated minerals build up on the inlet funnel; heating and vigorous shaking would hopefully loosen the material.

⁴⁷Paul Mahaffy, personal communication, email dated April 8, 2017

9.5.1.6 Sample Manipulation System (SMS)

The Sample Manipulation System is a double-ringed carousel with 74 sample cups (Figure 9.20). It has two motors. A carousel actuator can both rotate the carousel and move the elevator into position. An elevator actuator can raise a sample cup to pierce a foil seal, accept a new sample, or place the sample cup in an oven.

When SAM is not in use, both carousel and elevator are locked. A component called the “trash can” is parked under the solid sample inlets. Any sample material temporarily stuck to an inlet tube will fall into the trash can during driving and thereby not contaminate the rest of the instrument. To accept a sample, the carousel rotates to place a sample cup under an inlet tube. After the sample falls in, the carousel rotates to place the cup underneath one of two pyrolysis ovens. While this is happening, the elevator is still locked to the carousel, so it rotates with the carousel. Once the sample cup is in place, a latch releases the elevator from its locked position, and the carousel actuator rotates the elevator around the ring until it is positioned underneath the sample cup. Operating the elevator disengages the sample cup from the carousel and then slowly raises the sample cup into the pyrolysis oven. The elevator pushes a copper ring fused to the stem of the sample cup hard against a knife-sharp titanium ring at the bottom opening of the oven, creating a hermetic seal. SAM cups can be reused multiple times; each time a cup is reused, the elevator has to push the cup harder against the titanium knife-edge to maintain the seal.

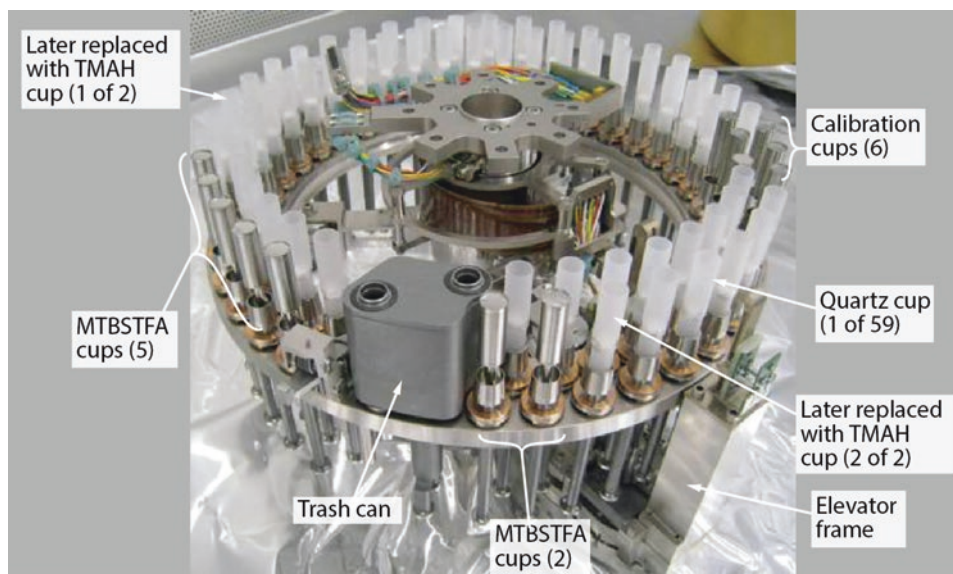


Figure 9.20. The SAM sample manipulation system with its 74 sample cups. MTBSTFA cups are for wet chemistry; quartz cups are for evolved gas analysis; and trash can is placed under the sample inlet tubes to catch any wayward sample material when SAM is not in use. After this photo was taken, two of the quartz cups were replaced with wet-chemistry TMAH cups (see text for explanation of the acronyms). Image courtesy Paul Mahaffy.

9.5.1.7 *Sample cups*

There are three types of sample cups: 59 quartz cups, 9 foil-capped wet chemistry cups, and 6 foil-capped metal cups containing calibration samples. Inside each quartz cup is a “frit,” a porous disk made of powdered quartz, on which the sample rests. The quartz disk is positioned to hold the sample in the hottest part of the oven, and its pores permit helium gas to flow through the sample, quickly carrying evolved gases away, to minimize chemical reactions between evolved gases and the remaining sample.

SAM carries wet chemistry cups because the Martian samples could potentially contain organic molecules that would decompose into simpler molecules instead of entering a gaseous state, meaning that they would not be easy to detect by high-temperature pyrolysis and gas chromatograph mass spectrometry. When samples containing perchlorate are heated, the perchlorate rapidly oxidizes the organics to carbon dioxide, water, and other simple compounds. The organic substances can potentially be kept whole if they are first “derivatized” – made more volatile by reactions with other chemicals. These reactions have to happen in a solvent, so nine of the sample cups are wet chemistry cells. Seven of them contain a mixture of two solvents called N-methyl-N-(tert-butyltrimethylsilyl) trifluoroacetamide (MTBSTFA) and dimethylformamide (DMF), designed to be used at relatively low temperatures (75–300°C). When organic molecules react with MTBSTFA, they turn into compounds that are more volatile – making them amenable to gas chromatography – and also more stable, making them less likely to decompose when heated in the SAM oven in the presence of perchlorate. The remaining two wet cells are targeted at the most complex types of organic molecules: they contain a mixture of tetramethylammonium hydroxide (TMAH) and methanol, which can break up complex organics like lipids and proteins at moderate oven temperatures of more than 340°C.

9.5.1.8 *SAM oven*

There are two ovens, one each for the outer and inner rings of the carousel. One can heat samples to 900°C, the other to 1100°C. SAM heats the oven with a heater wire, only half a millimeter thick, made of a platinum-zirconium alloy. At lower temperatures, volatile materials in rocks (such as bound water) are driven off. More volatile organics are released at temperatures between 300°C and 600°C; these may have existed in the rock as smaller organic molecules, or may come from larger organic molecules that break down upon heating. At temperatures above 500°C, carbonates may release carbon dioxide and sulfates may release sulfur dioxide. The temperature at which these gases appear can be diagnostic of the minerals originally present in the sample.

As the oven temperature slowly ramps up, QMS can detect how the composition of evolved gases changes with temperature, helping to identify the minerals that are decomposing to give off the gas. Because QMS only measures one mass-to-charge ratio at a time, the SAM team usually selects a narrow range to focus on in these ramping experiments. This narrow range can be changed mid-experiment.

9.5.1.9 Thermal considerations

Many of SAM's components require heating to relatively high temperatures for operation, not only the ovens. The tubes and manifolds operate at a temperature of 135°C in order to prevent organic molecules from sticking to them. When it's time to release hydrocarbons from the trap, the trap has to be flash-heated to 350°C. The traps in front of the GC columns must be flash-heated to 100–250°C. These temperatures are all quite high, yet other components (like the electronics, pumps, and trap coolers) need to operate at more typical spacecraft temperatures. SAM manages all these temperatures with the help of heat pipes internal to SAM as well as the rover heat rejection system for cooling, and a large number of tiny heaters wrapped around tubes, manifolds, and traps for heating. SAM has more than 60 temperature sensors.

9.5.1.10 SAM testbeds

A vital component of the SAM experiment are several duplicates of the instrument or its components in different laboratories. The most elaborate one of these is a duplicate of the SAM instrument in a laboratory at Goddard Space Flight Center. The duplicate lives inside a chamber that is designed to simulate the temperature and pressure conditions of Mars and the interior of the rover. There is even a high-fidelity duplicate of the part of the rover avionics mounting plate and all of its heat rejection system tubing that keeps SAM cool as it operates. The SAM team uses the testbed to develop new scripts and procedures.

In order to understand the results of QMS and GCMS experiments conducted on Mars, the SAM team attempts to reproduce the results in the testbed. Based on results from Mars, SAM scientists hypothesize what materials may have been present in the original sample before heating, combustion, and/or derivatization. They prepare a sample of the hypothesized composition, and run it through the SAM testbed using the same settings as the experiment on Mars to see if they can reproduce the results. In this way, laboratory experimentation is a critical element of the SAM solid sample experiments; obtaining the data from Mars is only the beginning of the experiment.

9.5.1.11 Electronics

SAM has 8 electronics modules. It can operate autonomously while the rover is otherwise asleep, powering itself off after finishing an experiment. Total data volume for a single SAM experiment is about 30 megabytes. SAM stores data in a 64 megabyte flash memory array. SAM is programmed in a BASIC-like language that allows the science team to construct new experiments, manipulating the many pathways through SAM and the many combinations of possible actions, with simple combinations of commands.

9.5.1.12 *Organic Check Material*

Five pucks of silica glass doped with fluorinated hydrocarbons are located inside hermetically sealed cans on a stand mounted to the front of the rover and can be used by the SAM team as an end-to-end calibration test, to make sure that the sample acquisition process does not alter samples acquired on Mars. Curiosity can test a sample of organic check material by positioning the drill on one of the pucks and acquiring a sample of it just as it would acquire a sample of Martian rock. None of them has yet been drilled on Mars. The loss of the drill feed mechanism means they cannot be drilled in the future unless a new process is developed that does not rely on drill stabilizers to align the drill. See section 5.6 for more about the organic check material.

9.5.2 Types of SAM experiments

There are nine basic types of SAM sequences: four for atmospheric gases, and five for solid samples.

9.5.2.1 *Direct atmospheric measurement*

SAM performs a direct atmospheric experiment about once every two weeks. See Figure 9.21 for a diagram. With a direct atmospheric measurement, SAM QMS can measure the mixing ratios of carbon dioxide, argon, nitrogen, oxygen, and carbon monoxide, the ratio of argon-40 to argon-36, and isotopes of carbon in carbon dioxide. TLS can measure carbon and oxygen isotopes in carbon dioxide.

SAM begins by heating all the tubes and manifolds that will carry gas, and also heats the chosen atmospheric inlet, in order to drive off any water that may have adsorbed onto the cold surface. It pumps down the spectrometers and takes background spectra. Then it shuts the valves connecting the pumps to the manifolds, and opens the valve connected to the inlet. Gas enters the inlet and fills the interior of several manifolds until it's stopped at valves 20 and 21 within manifold 7, where there is a pressure sensor. Finally, SAM opens one of the two valves connecting the manifold to the QMS (valves 11 or 12, see Figure 9.21). These are capillary valves that only allow a tiny amount of gas into the QMS at a time. Because the composition of the atmosphere won't change over the period of the measurement, the QMS can take tiny voltage steps to get the highest precision possible.

For TLS, SAM fills the sample chamber with Martian atmosphere and then shuts all the valves. TLS takes a reading at full pressure and then at lower pressure steps, with a pump removing sampled atmosphere at intervals, in order to make sure there will be at least one observation that doesn't saturate the detector. SAM can do both QMS and TLS in a single sol, or one or the other. Initial experiments used both, but most experiments since have used only one or the other spectrometer in order to increase the integration time and therefore the sensitivity of the measurement.⁴⁸

⁴⁸Mahaffy et al. (2013)

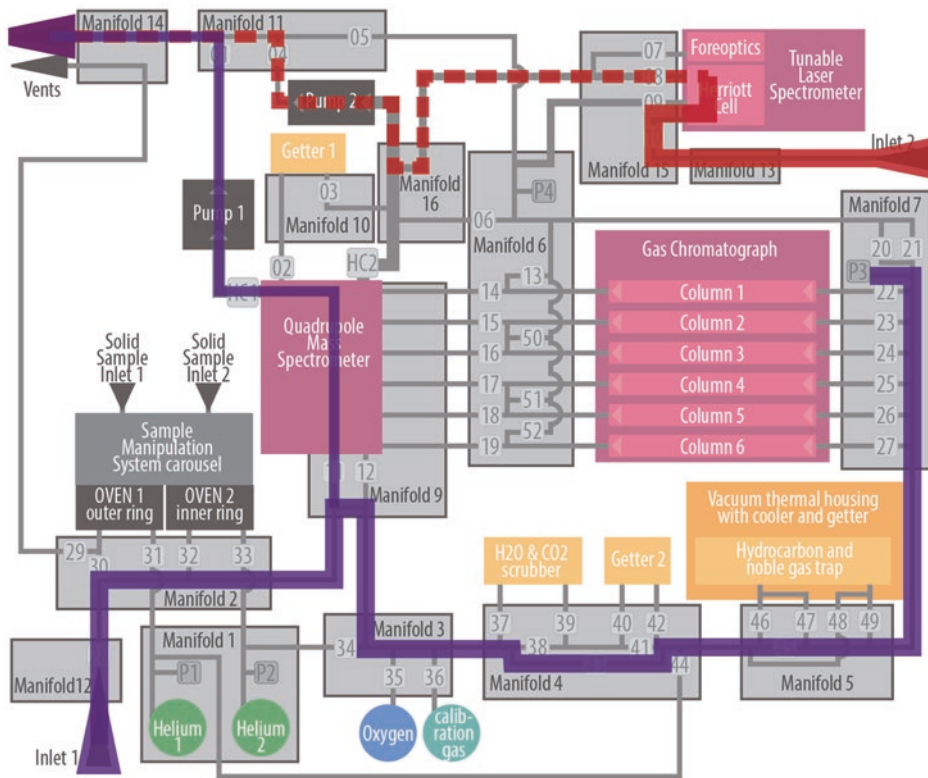


Figure 9.21. Example sample pathways through the gas processing system for atmospheric measurements. Purple line shows a path from atmospheric inlet 1 through the QMS. The ingested atmosphere fills several manifolds (3, 4, 5, and 7) while only a small amount leaks through valve 10 into the QMS. The red line shows a path from atmospheric inlet 2 through the TLS. The TLS is evacuated first (dashed red line), then air is introduced (solid line), a measurement taken, and some of the gas is vented (dashed red line), the measurement is repeated, and so on. Either spectrometer can ingest a sample from either inlet.

9.5.2.2 Noble gas enrichment

Noble gases (argon, krypton, and xenon) make up a very small fraction of the Martian atmosphere. Some of the noble gas atoms have been present since Mars formed, while others exist because of the radioactive decay of Martian materials. Depending on when Mars formed, when it was geologically active, and when it lost its atmosphere, there will be more or less of different noble gases in the atmosphere, so atmospheric isotopes can provide clues to the history of Martian geologic history. But the abundance of each isotope is tiny; except for the three isotopes of argon, SAM cannot detect them without concentrating them.

There are three different types of noble gas enrichment experiments: dynamic, semi-static, and static. The names refer to how quickly gas exits the QMS. Dynamic mode is used for more abundant gases. In semi-static and static modes, SAM's pumps work differently to maintain higher pressure in the QMS to improve the detection of trace gases.⁴⁹

The purple line in Figure 9.22 shows a dynamic mode noble gas enrichment experiment. It works like a direct atmospheric measurement, except that SAM passes the Mars air over a chemical scrubber that removes 95% of all carbon dioxide and water from the air, as well as some of the other non-noble gases. What is left behind in the manifold is mostly nitrogen and argon. After the scrubber has been allowed to work on the gas in the manifold for a while, valve 12 opens to let it flow into the QMS. QMS scans the mass range of the argon isotopes and can sensitively measure the argon-40/argon-36 and argon-38/argon-36 ratios.⁵⁰ SAM has performed this experiment once, on sol 231.

To measure argon-38, they operate SAM in semistatic mode. Semistatic mode works like dynamic mode, except that SAM also employs a getter attached to the QMS in order to remove methane, and the valve between the QMS and pump is partially shut in order to increase the pressure inside QMS. Semistatic experiments have allowed SAM to measure the abundance of argon-38 compared to the more common argon-40 and argon-36 isotopes, and also krypton isotope abundances.⁵¹ SAM performed semistatic experiments on sols 341, 364, and 976.

Finally, there is static mode (not shown in Figure 9.22). After passing the Mars air over the scrubber, SAM sends it past a hydrocarbon trap, which also traps xenon. What's left (mostly nitrogen, argon, and krypton) passes into TLS, which acts as a reservoir for this experiment. There is so little xenon that SAM continues to ingest Mars air and trap xenon for 90 minutes. Then SAM closes the valves to TLS and the hydrocarbon trap, and vacuums out the tubing and manifolds. Finally, SAM opens the valves between the hydrocarbon trap and QMS, warms the hydrocarbon trap, and pumps gently to slowly fill QMS with xenon while letting as little of it escape as possible. In this experiment, QMS scans only that range relevant to the masses of xenon isotopes. When most of the xenon has been released, the pump stops, and QMS finishes the xenon analysis by scanning what's left in its sample chamber. Then SAM goes on to analyze the krypton that's left in the sample held in TLS: it evacuates the QMS and then performs an experiment in semi-static mode with the gas from the TLS. Unfortunately, because xenon and krypton analysis happens sequentially, SAM can't directly measure isotopic ratios of krypton to xenon.⁵² SAM performed static experiments on sols 915 and 976.

⁴⁹ Charles Malespin, personal communication, email dated April 12, 2017

⁵⁰ Atreya et al. (2013)

⁵¹ *ibid.*

⁵² Conrad et al. (2016)

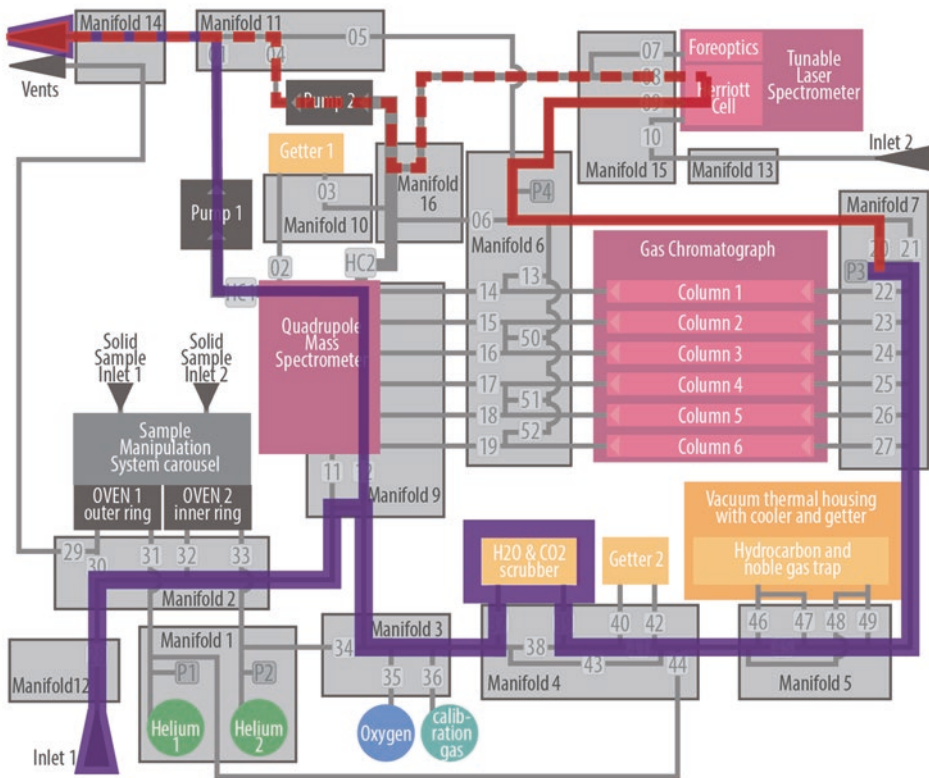


Figure 9.22. Example pathway for noble gas enrichment (purple line) and methane enrichment (red line) experiments. In a dynamic mode noble gas experiment, the pump moves atmospheric gas past the scrubber to remove water and carbon dioxide and then sends it into the QMS. The same scrubber can also prepare enriched gas to be sent to the TLS for methane measurement.

9.5.2.3 Methane enrichment

The atmospheric abundance of methane is usually too low for it to be measured precisely in a direct atmospheric experiment. To detect methane, SAM uses the same scrubber as for the noble gas experiment to remove carbon dioxide and water from the atmospheric gas, then employs the adjacent getter to remove the nitrogen from the atmospheric gas, leaving behind argon with trace amounts of methane. After two hours of scrubbing and getting, SAM sends what's left in the manifold to TLS (the red line in Figure 9.22). After the TLS measurement is complete, SAM empties TLS and performs an empty-cell measurement. Finally, SAM introduces atmosphere directly into TLS to perform a direct, non-enriched atmosphere experiment. Methane enrichment experiments were performed on sols 572, 683, 865, 964, 1086, 1168, 1321, 1450, 1527, 1578, and 1708.

9.5.2.4 Atmospheric enrichment

To study the deuterium-to-hydrogen ratio in TLS with more precision, or to search for trace higher-weight atmospheric molecules using QMS, SAM can use its scrubber to collect those gases from the atmosphere, evacuate the instrument, and then release the collected gas. Although SAM has attempted this experiment, there is not enough water in the atmosphere for it to measure isotopes. It has done better at measuring atmospheric water from solid samples.

9.5.2.5 Solid sample pyrolysis with evolved gas analysis (EGA)

Because of the MTBSTFA contamination (see section 9.5.1.7), the procedure now used for sample analysis on Mars is different from the one described in papers published before landing.⁵³ First, SAM performs a blank analysis run, going through the motions of a complete evolved gas experiment with no sample in the cup, to provide a measurement of the experimental background. When it's ready to receive a sample, SAM "conditions" (bakes) one of the 59 quartz cells in the analysis oven in order to remove any hydrocarbon material that may have stuck to its walls, then allows it to cool. SAM works the pumps hard to remove as much gas from the system as possible. The rover delivers three portions of sample material that passed through the 150-micron sieve, each portion about 75 cubic millimeters in volume. By keeping the pre-baked cup in a clean protected environment in the oven, pumping out the system, and using a triple portion, the SAM team dramatically reduces MTBSTFA contamination. SAM ramps the temperature up to 900–1100°C (depending on which oven is being used) at a rate of about 35°C per minute, although the rate of heating slows above 800°C. SAM directs helium gas through the sample as it is being heated, sending any evolved gases to QMS for monitoring the chemical composition as the temperature changes (the purple line in Figure 9.23).

9.5.2.6 Gas chromatograph mass spectrometry (GCMS)

While conducting an evolved gas experiment, SAM can send the evolved gas past the hydrocarbon trap on its way to the QMS. After the evolved gas analysis is over and the manifolds are evacuated, SAM purges a GC column, pressurizes the manifold to 100 kilopascals with stored helium, flash-heats the hydrocarbon trap, and then directs the gas through the GC column (the red line in Figure 9.23). SAM can only use one GC column at a time, but the team has developed a mode where gas can be trapped on the injection trap of a second column for subsequent analysis later in the experiment.⁵⁴

⁵³Lakdawalla (2013)

⁵⁴Charles Malespin, personal communication, email dated April 12, 2017

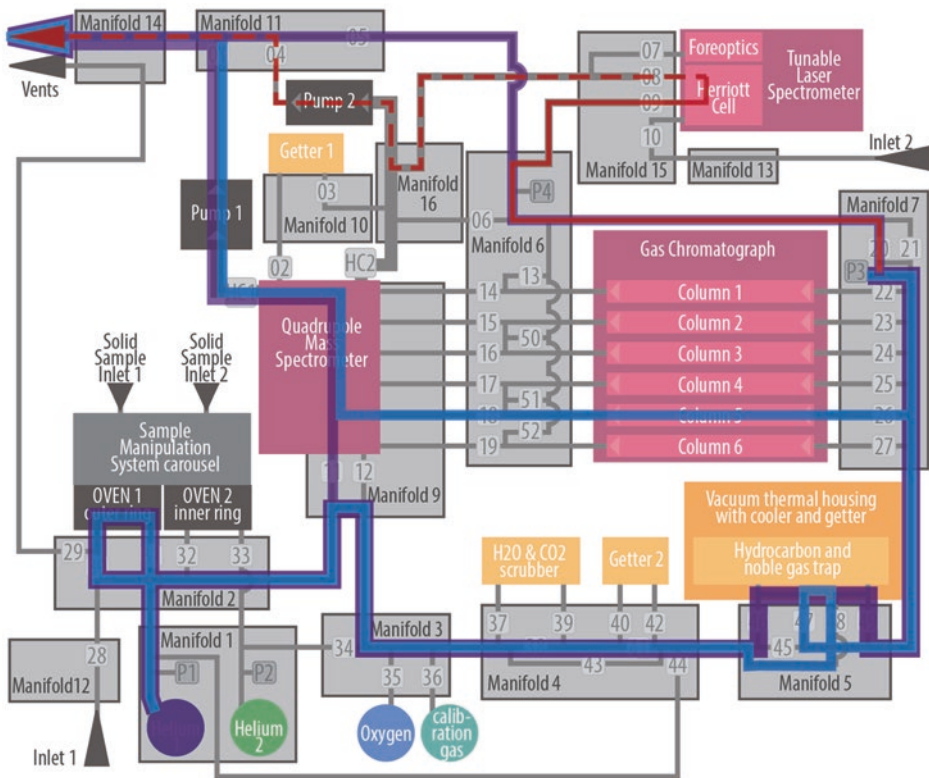


Figure 9.23. Example pathway for a solid sample evolved gas analyses (EGA). The simplest EGA pathway is shown in purple: helium gas runs through the sample cell in the oven and then through the QMS. In this diagram, the sample gas is also being directed past the hydrocarbon trap. In an evolved gas experiment, some of the gas can be sent to the TLS (red line). To perform GCMS on the trapped hydrocarbons, after the EGA run is complete, SAM purges the instrument and then uses helium carrier gas to move hydrocarbons from the flash-heated trap through a GC column into the QMS (blue line).

9.5.2.7 Tunable laser spectrometry (TLS)

To measure isotopic ratios of methane, carbon dioxide, and/or water evolved from solid samples, SAM scientists select a particular “cut” of the temperature ramp that they want to send to TLS. As the oven passes through that temperature range, all the evolved gas is sent to TLS. TLS then performs its experiments on the collected gas. Because there might be enough of any given gas to saturate the detector, TLS pumps out some of the collected gas at intervals and repeats the observation several times.

9.5.2.8 *Combustion*

Some carbon compounds are not volatile even at the highest temperatures that the SAM ovens can achieve. To search for these compounds, SAM can add oxygen from an onboard reservoir to a solid sample and then heat it to a high temperature. Any carbon compounds in the sample will combust, turning into carbon dioxide. After the combustion has had some time to take place, SAM sends the evolved gas to TLS to measure the isotopic ratio of the carbon and hydrogen in the sample. SAM has performed this experiment once, on the Cumberland sample. The experiment took three days, on sols 555, 556, and 558.

9.5.2.9 *Wet chemistry and opportunistic derivatization*

SAM can detect of amino acids and other organic compounds with one of the nine derivatization cups, which would be punctured before delivery of a solid sample and evolved gas analysis. The leak of MTBSTFA into the interior of SAM provided an opportunity to do a long-term “opportunistic derivatization” experiment on one sample (from the Cumberland drill hole) without employing any of the cups. Sample dropoffs can be made to a cup that is then not analyzed for a long time, a procedure the team calls “doggy bagging”. Over time, organics in the sample react with the MTBSTFA vapor inside SAM, and GCMS analysis can reveal derivatization products. Curiosity analyzed Cumberland samples in this way on sols 822, 823, 837, and 839, and a full Mars year later on sols 1543, 1546, 1591, and 1593.

9.5.3 SAM on Mars

The SAM experiment has been highly successful. SAM has measured the composition of past and present Martian air and monitored it over time. It has successfully measured isotopes of even the rarest noble gas, xenon. It has detected low-molecular-weight organic compounds of Martian origin. It has detected methane and observed rapid changes in atmospheric methane abundance. SAM has been used for an experiment never before conducted in space, to perform potassium-argon dating to measure the ages of drilled rocks. Even the problem of the MTBSTFA contamination has been turned into a benefit, with the performance of long-term derivatization experiments.

The complexity of SAM experiments and the amount of power they require drive a lot of the supratactical planning on Curiosity. A typical evolved-gas analysis can take three sols (one for preconditioning, one for sample preparation and delivery, and one for heating and evolved gas analysis). The evolved gas analysis usually takes 4 to 6 hours to run to completion, depending on the selected options, and it can leave the rover with a relatively low state of battery charge. For that reason it is common to conduct SAM experiments over weekends and use one weekend sol to recharge batteries.

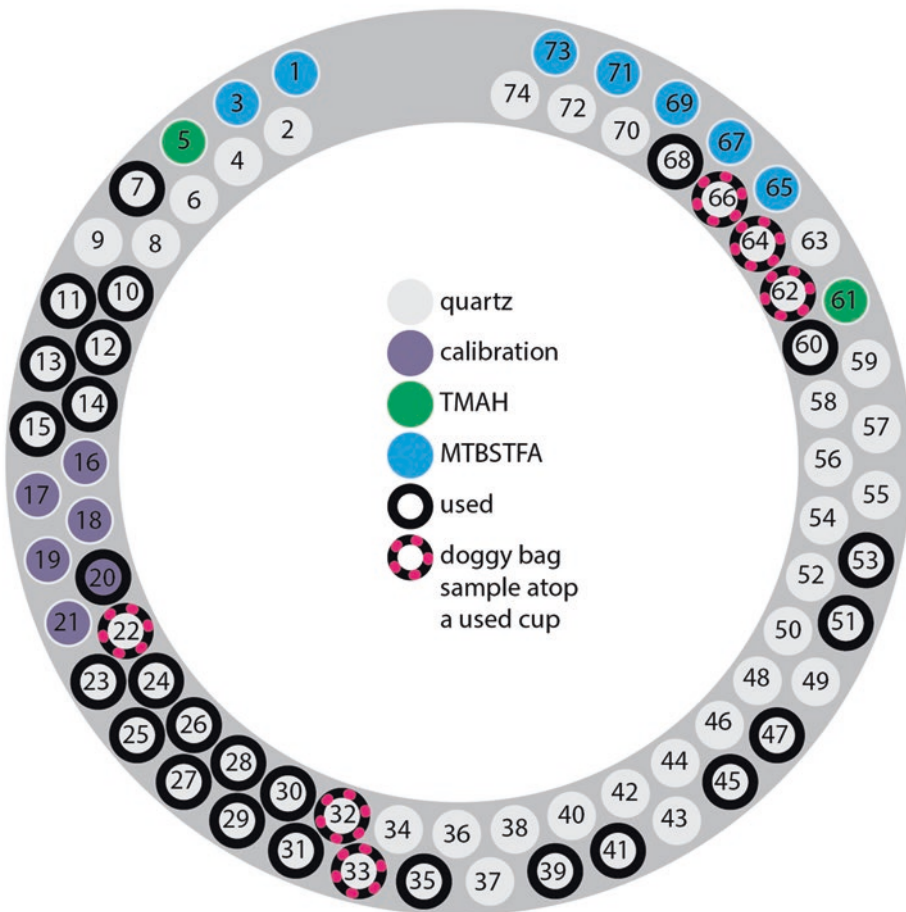


Figure 9.24. Schematic diagram of the SAM sample carousel, showing the locations of the numbered cups of different types, and which ones have been used as of sol 1800. For the identities of samples in each used cup, refer to Table 9.6. Data courtesy Charles Malespin.

As of the time of Curiosity's second extended mission proposal in January 2016, SAM had 75% of its helium supply left, but the pumps were nearing their design lifetime. Duplicates of the pumps on Earth have been tested to survive twice their design lifetime. So, barring any unforeseen events, SAM should have considerable life left. The SAM team is carefully rationing use of the pumps to ensure that they will still be working when the rover reaches the clay-rich layers beyond Vera Rubin Ridge. Usage of the cups and experiments run to date are summarized in Figure 9.24 and Table 9.6, respectively.

Table 9.6. Summary of the SAM solid sample experiments.

Type of run	Sample	Sol #	Cup #	GC Hydrocarbon temp cut(°C)
GCMS	Blank (Rocknest)	88	15	145 - 529
GCMS	Rocknest	93	15	145 - 529
GCMS	Rocknest	96	13	97 - 422
GCMS	Rocknest	99	11	529 - 816
GCMS	Rocknest	171	7	242 - 383
GCMS	Blank (John Klein)	177	23	311 - 816
GCMS	John Klein	196	23	311 - 816
GCMS	John Klein	199	25	242 - 639
GCMS	John Klein	224	27	242 - 639
GCMS	John Klein	227	29	570 - 792
GCMS	Blank (Cumberland)	276	33	442 - 569
GCMS	Cumberland	281	33	442 - 569
GCMS	Cumberland	286	35	571 - 792
GCMS	Cumberland	290	39	226 - 347
NG geochronology	Cumberland	353	41	n/a
GCMS	Cumberland	367	51	226 - 347
GCMS	Cumberland	381	45	226 - 347
GCMS	Cumberland	394	45	226 - 347
NG geochronology	Blank (Cumberland)	408	47	n/a
GCMS	Cumberland	415	47	247 - 620
GCMS	Blank (Cumberland)	421	31	247 - 620
NG geochronology	Blank (Cumberland)	428	53	n/a
GCMS	Blank (Windjana)	602	10	20 - max
GCMS	Windjana	624	10	20 - max
NG geochronology	Windjana	653	12	n/a
NG geochronology	Windjana reheat	685	12	n/a
NG geochronology	Windjana doggy bag	763	14	n/a
GCMS	Blank (Confidence Hills)	769	60	386 - max
GCMS	Confidence Hills	773	60	386 - max
GCMS	Cumberland doggy bag (opportunistic derivatization)	822	51	20 - max
GCMS	Cumberland doggy bag (opportunistic derivatization)	823	51	20 - max
GCMS	GC clean	835	51	n/a
GCMS	Blank (Cumberland)	837	45	20 - 550
GCMS	Blank (Cumberland)	839	45	20 - max
GCMS	Mojave	887	62	200 - max
EGA	Telegraph Peak	928	66	n/a
GCMS	GC clean	981	n/a	n/a
GCMS	GC clean	998	n/a	n/a
GCMS	GC clean	1071	n/a	n/a
GCMS	Buckskin	1076	24	150 - 300, 450 - 550, 650 - max
GCMS	GC clean	1117	n/a	n/a
EGA	Big Sky	1130	26	n/a
EGA	Greenhorn	1147	26	n/a
GCMS	Blank (Greenhorn)	1171	68	560 - 713, 780 - 830

(continued)

Table 9.6. (continued)

Type of run	Sample	Sol #	Cup #	GC Hydrocarbon temp cut(°C)
GCMS	Greenhorn	1178	68	376 - 562, 714 - 921
EGA	Gobabeb <150um	1224	28	n/a
EGA	Gobabeb >150um	1237	30	n/a
GCMS	GC clean	1246	n/a	n/a
GCMS	Calibration cup	1286	20	n/a
EGA	Oudam	1382	22	n/a
NG geochronology	Mojave stepped heating part 1	1402	64	n/a
NG geochronology	Mojave stepped heating part 2	1403	64	n/a
NG geochronology	Mojave doggy bag stepped heating part 1	1429	62	n/a
NG geochronology	Mojave doggy bag stepped heating part 2	1430	62	n/a
EGA	Marimba	1443	32	n/a
GCMS	GC clean	1539	n/a	n/a
GCMS	Cumberland doggy bag (opportunistic derivatization)	1543	39	20 - 500
GCMS	Cumberland doggy bag (opportunistic derivatization)	1546	39	20 - max
GCMS	GC clean	1580	n/a	n/a
Doggy bag	Oudam	–	22	n/a
Doggy bag	Marimba	–	32	n/a
Doggy bag	Cumberland	–	33	n/a
Doggy bag	Quela	–	62	n/a
Doggy bag	Quela	–	64	n/a
Doggy bag	Telegraph Peak	–	66	n/a

9.6 REFERENCES

- Atreya S et al (2013) Primordial argon isotope fractionation in the atmosphere of Mars measured by the SAM instrument on Curiosity and implications for atmospheric loss. *Geophys. Res. Lett.* 40:5605–5609, DOI: 10.1002/2013GL057763
- Berger J et al (2014) MSL-APXS titanium observation tray measurements: Laboratory experiments and results for the Rocknest fines at the Curiosity field site in Gale Crater, Mars. *J Geophys Res* 119:1046–1060, DOI: 10.1002/2013JE004519
- Berger J et al (2016) A global Mars dust composition refined by the Alpha-Particle X-ray Spectrometer in Gale Crater. *Geophys Res Lett* 43:67–75, DOI: 10.1002/2015GL066675
- Blake D et al (2012) Characterization and calibration of the CheMin mineralogical instrument on Mars Science Laboratory. *Space Sci Rev* 170:341–399, DOI: 10.1007/s11214-012-9905-1
- Campbell et al (2012) Calibration of the Mars Science Laboratory Alpha Particle X-ray Spectrometer. *Space Sci Rev* 170:319–340, DOI 10.1007/s11214-012-9873-5
- Conrad P et al (2016) In situ measurement of atmospheric krypton and xenon on Mars with Mars Science Laboratory. *Earth Planet Sci Lett* 454:1–9, DOI: 10.1016/j.epsl.2016.08.028

- Cousin A et al (2014) ChemCam blind targets: a helpful way of analyzing soils and rocks along the traverse. Paper presented at the 45th Lunar and Planetary Science Conference, The Woodlands, Texas, 17–21 Mar 2014
- Dickinson C S et al (2012) APXS on Mars Science Laboratory - First results from post-landing checkout. Presentation to the International Workshop on Instrumentation for Planetary Missions, Greenbelt, Maryland, USA 10–12 Oct 2012
- Downs R and the MSL Science Team (2015) Determining mineralogy on Mars with the CheMin X-ray diffractometer. *Elements* 11:45–50, DOI: 10.2113/gselements.11.1.45
- Farley K et al (2014) In situ radiometric and exposure age dating of the Martian surface. *Science*, DOI: 10.1126/science.1247166
- Francis R et al (2016) AEGIS intelligent targeting deployed for the Curiosity rover's ChemCam instrument. Paper presented at the 47th Lunar and Planetary Science Conference, The Woodlands, Texas, 21–25 Mar 2016
- Francis R et al (2017) AEGIS autonomous targeting for ChemCam on MSL: Results from the first 220 sols of routine science operations. Paper presented at the 48th Lunar and Planetary Science Conference, The Woodlands, Texas, 20–24 Mar 2017
- Franz H et al (2017) Initial SAM calibration gas experiments on Mars: Quadrupole mass spectrometer results and implications. *PL Space Sci* 138:44–54, DOI: 10.1016/j.pss.2017.01.014
- Gellert R et al (2009) The Alpha-Particle-X-ray-Spectrometer (APXS) for the Mars Science Laboratory (MSL) rover mission. Paper presented at the 40th Lunar and Planetary Science Conference, The Woodlands, Texas, 23–27 Mar 2009
- Gellert R et al (2015) In Situ Compositional Measurements of Rocks and Soils with the Alpha Particle X-ray Spectrometer on NASA's Mars Rovers. *Elements* 11:39–44, DOI: 10.2113/gselements.11.1.39
- JPL (2009) Sample Analysis at Mars. <https://mssl-scicorner.jpl.nasa.gov/Instruments/SAM/> Accessed 29 Apr 2016.
- Lakdawalla E (2013) DPS 2013: Confusing Curiosity SAM results. <http://www.planetary.org/blogs/emily-lakdawalla/2013/10151336-dps-2013-confusing-curiosity.html> Article dated 15 Oct 2013, accessed 12 Apr 2017
- Lanza N et al (2016) Oxidation of manganese in an ancient aquifer, Kimberley formation, Gale crater, Mars. *Geo. Res. Lett.* 43:7398–7407, DOI: 10.1002/2016GL069109
- Léveillé et al (2015) Jarosite in Gale crater, Mars: The importance of temporal and spatial variability and implications for habitability. Paper presented at the 46th Lunar and Planetary Science Conference, The Woodlands, Texas, 16–20 Mar 2015
- Mahaffy P et al (2012) The Sample Analysis at Mars investigation and instrument suite. *Space Sci Rev* 170:401–478, DOI: 10.1007/s11214-012-9879-z
- Mahaffy P et al (2013) Abundance and isotopic composition of gases in the Martian atmosphere from the Curiosity rover (supplementary materials). *Science* DOI: 10.1126/science.1237966
- Maurice S et al (2012) The ChemCam instrument suite on the Mars Science Laboratory (MSL) rover: science objectives and mast unit description. *Space Sci Rev* 170:95–166, DOI: 10.1007/s11214-012-9902-4
- Maurice S et al (2016) ChemCam activities and discoveries during the nominal mission of the Mars Science Laboratory in Gale crater, Mars. *J. Anal. At. Spectrom.* 31:863–889, DOI: 10.1039/C5JA00417A

- Millan M et al (2016) In situ analysis of Martian regolith with the SAM experiment during the first Mars year of the MSL mission: Identification of organic molecules by gas chromatography from laboratory measurements. *PL Space Sci* 129:88–102, DOI: 10.1016/j.pss.2016.06.007
- Morris R et al (2016) Silicic volcanism on Mars evidenced by tridymite in high-SiO₂ sedimentary rock at Gale crater. *PNAS* 113:7071–7076, DOI: 10.1073/pnas.1607098113
- Ollila A et al (2014) Trace element geochemistry (Li, Ba, Sr, and Rb) using Curiosity's ChemCam: Early results for Gale crater from Bradbury Landing Site to Rocknest. *J. Geophys. Res. Planets* 119:255–285, DOI: 10.1002/2013JE004517
- Peret L et al (2016) Restoration of the autofocus capability of the ChemCam instrument onboard the Curiosity rover. Paper presented at the 14th International Conference on Space Operations, Daejeon, Korea, 16–20 May 2016
- Perrett G et al (2017) Dust modelling on Martian rock surfaces studied by the Mars Science Laboratory Alpha Particle X-ray Spectrometer. Paper presented at the 48th Lunar and Planetary Science Conference, The Woodlands, Texas, 20–24 Mar 2017
- Peters S et al (2016) Celestial aspects of Mars Science Laboratory ChemCam sun-safety. Paper presented at the 39th Annual AAS Guidance & Control Conference, Breckenridge, Colorado, 5–10 Feb 2016.
- Schmidt M et al (2016) APXS classification of lower Mount Sharp bedrock: Silica enrichment and acid alteration. Paper presented at the 47th Lunar and Planetary Science Conference, The Woodlands, Texas, 21–25 Mar 2016
- Slavney S (2013) Alpha Particle X-ray Spectrometer instrument information. In Mars Science Laboratory (MSL) APXS EDR Data Archive.
- Thompson L et al (2016) Potassium-rich sandstones within the Gale impact crater, Mars: The APXS perspective. *J. Geophys. Res.* 121:1981–2003, DOI: 10.1002/2016JE005055
- Treiman et al (2016) Mineralogy, provenance, and diagenesis of a potassic basaltic sandstone on Mars: CheMin X-ray diffraction of the Windjana sample (Kimberley area, Gale Crater). *J. Geophys. Res. Planets*, 121:75–106, DOI: 10.1002/2015JE004932
- Vaniman D et al (2014) Mineralogy of a mudstone at Yellowknife Bay, Gale Crater, Mars. *Science*, DOI: 10.1126/science.1243480
- Webster C et al (2014) Mars methane detection and variability at Gale crater (supplementary materials). *Science* DOI: 10.1126/science.1261713
- Wiens R et al (2012) The ChemCam Instrument Suite on the Mars Science Laboratory (MSL) Rover: Body Unit and Combined System Tests. *SSR* 170:167–227, DOI: 10.1007/s11214-012-9912-2

Epilogue: Back on Earth

That Curiosity is still operating on Mars more than 5 years after landing is testament to the dedication and focus of a huge human team that keeps it safe and productive. The science team has over 500 members scattered around the world. Nearly 100 people are “on shift” on any given day of mission operations, including the engineering teams at JPL and the external scientists (Figure 10.1). Over the course of its development, launch, cruise, landing, and surface operation, more than 7000 different people from at least 33 of the United States and in 11 other countries have been involved in the mission.

Since landing, numerous members of the engineering and operations teams at JPL have moved on to other projects. Many of the people who were key to development are now working on the mission’s descendant, currently known as Mars 2020, which will reuse the designs of the cruise stage and entry, descent, and landing architecture to deliver a Curiosity-like rover (though with a different science package) to collect samples on Mars for a hypothetical future sample return mission.

Like most robotic missions sent to Mars, the gargantuan effort summarized in this book has one purpose: science. As of October 2017, the mission counts 250 peer-reviewed publications by team members and 157 by non-team members using mission data. The pace of publication of scientific results appeared slow to outsiders, especially to people accustomed to the rapid work of the Mars Exploration Rovers, but Curiosity’s science has much more in common with NASA’s other flagship exploration missions like Cassini and Galileo than it does with Spirit and Opportunity.

Curiosity performs long “cruises” from science field site to field site, interspersed with weeks-long periods of intensive data gathering. While at the field site, there is only time to verify data quality. The analytical laboratory instruments actually do most of their work while traversing from site to site. The SAM team, in particular, has to do significant lab work on Earth to understand results from Mars. Initial scientific analysis of data and publication of results happens mostly within instrument teams, so the first papers typically focus on results from one instrument at one site. Comparison across sites and



Figure 10.1. A portion of the Curiosity team at JPL on October 11, 2016, with the testbed rover. JPL-Caltech/Dutch Slager.

instrument teams takes more time, and synthesizing all of that into coherent geologic history takes longer yet. For all these reasons, publication of papers addressing the geologic history and habitability of each field site may happen years after Curiosity has left it. And it's only as Curiosity crosses major geologic boundaries that the science team is beginning to get a picture of the evolution of the whole Gale crater system over time. The payoff from the environmental instruments REMS and RAD increases, the longer that they gather data.

Understanding how the rover and mission work is a necessary prerequisite to understanding the mission's science results. Those have been the focus of this book. The scientific story of the Curiosity mission – the geologic setting, traverse, field sites, and science results – is beyond the scope of this book. You may read that story in the next book, *Curiosity and Its Science Mission: A Mars Rover Goes to Work*.

When this book was submitted for publication in late 2017, the rover had just climbed onto Vera Rubin Ridge, seeing for the first time into the valley beyond. It paused to take a self-portrait on sol 1943 (Figure 10.2). The ridge and valley represent new rocks and new history for Curiosity, embodying a 500-member science team, to explore.

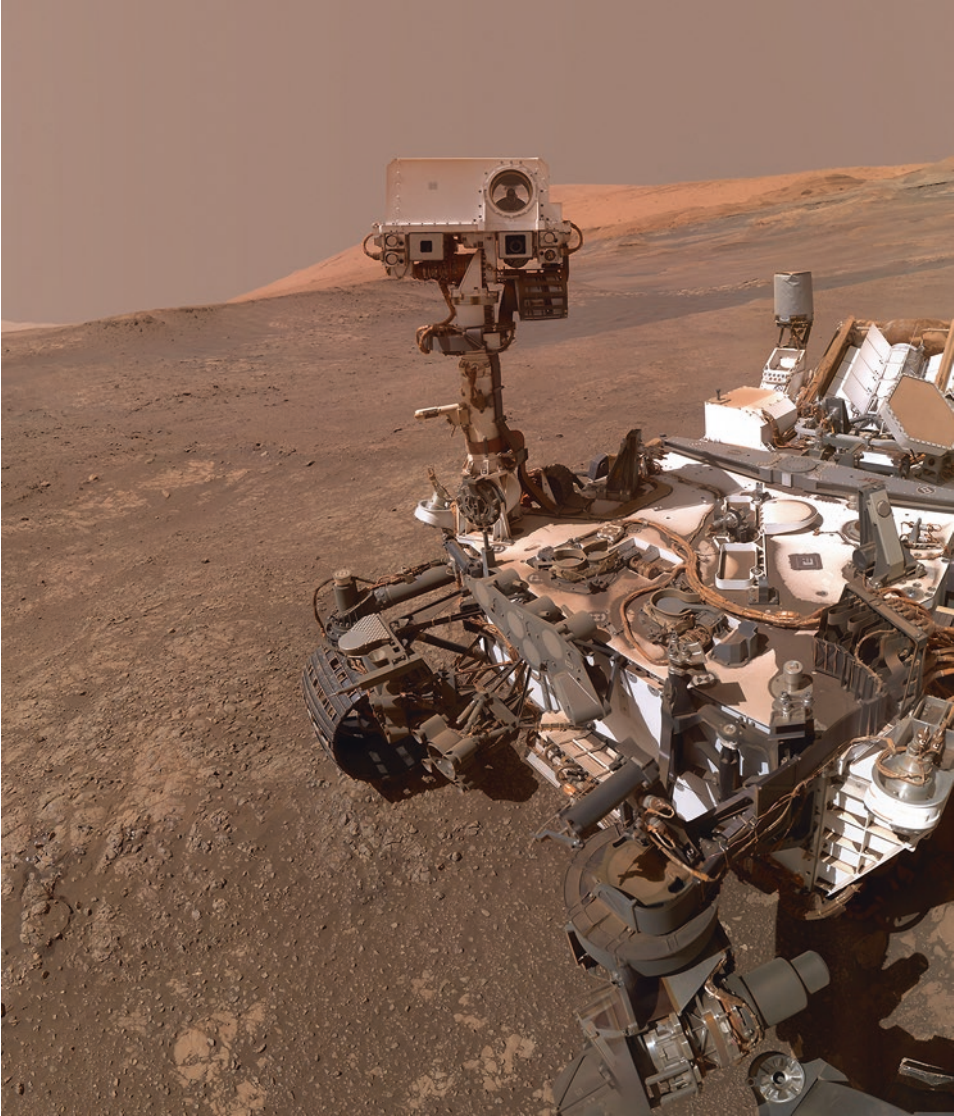


Figure 10.2. Curiosity self-portrait atop Vera Rubin Ridge, sol 1943, or January 23, 2018. Behind the rover is Mount Sharp. Credit: NASA/JPL-Caltech/MSSS.

Appendix: Curiosity Activity Summary

Following is a condensed historical summary of the Curiosity mission from sol 0-1648. Columns include:

- **Area:** A general descriptor of the mission phase, color coded: drives (white), engineering activities (orange), contact science (blue), scooping (pink), drilling (purple). These are not formally identified; rather, they were categorized by the author.
- **Noon UTC:** Time UTC corresponding to Curiosity noon LMST for the given sol. Calculated using the Mars equation of time by Joe Knapp.
- **Sol:** elapsed Martian day of mission.
- **RS:** Indicates if remote sensing activities were performed with science instruments, where C = ChemCam and M = Mastcam, with lowercase indicating fewer observations and uppercase indicating more. Based on Planetary Data System Geosciences Node records of numbers of data products per sol for these instruments. Intended to provide a qualitative estimate of how intense was the remote sensing activity on a given sol.
- **Arm:** Contains one-letter codes summarizing most arm activities, organized alphabetically roughly in the order in which they are typically performed at sample sites: **A** = APXS measurement; **B** = Brush; **C** = sCoop; **D** = mini-Drill; **F** = Full drill; **I** = Inspection of pre- and post-sieve sample volume; **P** = self-Portrait; **S** = dump pre-Sieve sample; **U** = dUmp post-sieve sample; **X** = CHIMRA cleanout; **W** = Wheel imaging. Cells for sols during which drill or CHIMRA contain sample are colored in gray. MAHLI activities other than self-portraits or wheel imaging are not included in this column for clarity, because there are too many. Based on rover activities as recorded in spacecraft images, SOWG and Mission Manager reports and Historical Overview notes from the Planetary Data System Geosciences Node; MAHLI Principal Investigator's Notebooks; and APXS team records of activities courtesy Mariek Schmidt and Lucy Thompson.

- **Activity summary:** includes one-sol drive distance; rover site/drive, change in elevation (in meters) from landing site, and total odometry (in meters) at end of drive; and comments on engineering activities, contact science targets, and other notable events. The column's account of contact science targets is complete, but it is not complete as to mobility or arm faults or runout sols because of a lack of public information. Sols known to have been lost to runouts or anomalies are colored in gray. Same sources as for Arm column.
- **Ls:** Solar longitude, a proxy for season (0 = autumnal equinox, 90 = winter solstice, 180 = vernal equinox, 270 = summer solstice.) From the "Historical Overview" summaries available at the Planetary Data System Geosciences Node.
- **T:** Minimum daily temperature from REMS ground temperature sensor, in kelvins. Obvious outliers have been removed, but these data are noisy. Color coded from blue (relatively cold) through white to red (relatively warm). Intended to allow you to tell, at a glance, through cell color, whether the season is warm or cold. Raw data courtesy Mark Lemmon.
- **P:** Maximum daily pressure from REMS pressure sensor, with same warnings as for temperature data. Color coded from dark green (relatively low pressure) to white (relatively high). Raw data courtesy Mark Lemmon.
- **Tau:** atmospheric opacity calculated by Mark Lemmon based on Mastcam solar imaging. Where multiple measurements exist for a sol, they have been averaged. Color coded from yellow (clear skies) to smoggy brown (dusty).

354 Appendix: Curiosity Activity Summary

Area	Noon UTC	Sol	RS	Arm	Activity Summary	LS	T	P	Tau	
Bradbury Landing	06 Aug 02:09	0	c		Landing!	150.1				
	07 Aug 02:49	1			HGA deploy	151.2				
	08 Aug 03:28	2			HGA point to Earth, Mast deploy	151.7				
	09 Aug 04:08	3	M		HGA test, instrument checkouts, FSW transition prep	152.2				
	10 Aug 04:48	4			FSW transition prep	152.7				
	11 Aug 05:27	5			FSW transition	153.3				
	12 Aug 06:07	6			FSW transition	153.8				
	13 Aug 06:46	7			FSW transition	154.3				
	14 Aug 07:26	8			FSW transition	154.9				
	15 Aug 08:06	9			Instrument checkouts	155.4				
	16 Aug 08:45	10	C		Instrument checkouts	155.9	197	776		
	17 Aug 09:25	11			Instrument checkouts	156.5	197	779		
	18 Aug 10:04	12	C		Instrument checkouts	157.0	197	778		
	19 Aug 10:44	13	cM		Instrument checkouts	157.6	199			
	20 Aug 11:24	14	cm		Arm unstow, sampling system checkouts	158.1	197	781		
	21 Aug 12:03	15	c		Steer wheels	158.6	196	783		
	22 Aug 12:43	16			Dr 7m to 03/0050 - el+0m - 00007m - for first drive! Drill feed retraction	159.2	197	786		
	Begin drive to Glenelg, complete commissioning	23 Aug 13:22	17	M		RCE maintenance	159.7	197	786	
		24 Aug 14:02	18			RCE maintenance, SAM atmos	160.3	198		
		25 Aug 14:41	19	CM		Mastcam checkout	160.8			
		26 Aug 15:21	20	M		Mastcam checkout, APXS atmos overnight	161.4			
		27 Aug 16:01	21	m		Dr 5m to 03/0084 - el-1m - 00011m - toward Goulburn Scour	161.9	198	788	
28 Aug 16:40		22	C		Dr 15m to 03/0106 - el-2m - 00027m - toward Glenelg, autonav checkouts	162.5	199	787		
29 Aug 17:20		23	M		Mastcam checkout, ChemCam anomaly	163.0	198	788		
30 Aug 17:59		24	M		Dr 22m to 03/0266 - el-2m - 00048m - toward Glenelg	163.5	200	788		
31 Aug 18:39		25	M		Chemcam anomaly cleared, HRS maintenance	164.1	198	790		
01 Sep 19:19		26			Dr 30m to 03/0378 - el-2m - 00078m - toward Glenelg, visodom & drill checkouts, CheMin empty cell analysis	164.7	199	790		
02 Sep 19:58		27	Cm		SAM atmos	165.2	198	789		
03 Sep 20:38		28			SAM atmos	165.8	198	790		
04 Sep 21:17		29			Dr 31m to 03/0536 - el-3m - 00108m - toward Glenelg, APXS FSW update	166.3	198	793		
05 Sep 21:57		30	Cm		Arm & drill checkouts	166.9	202	793		
06 Sep 22:36		31			ANOMALIES PRECLUDE SCIENCE (concern about arm temperature)	167.4	199	794		
07 Sep 23:16		32	CM	P	Turret checkout, MAHLI close cover selfie, CHIMRA closed loop vibe	168.0				
08 Sep 23:56		33	Cm		MAHLI cover inspection	168.5	199	796	0.72	
10 Sep 00:35		34	c	W	Arm teach point checkout: MAHLI organic check material, wheels, cal	169.1	199	795		
11 Sep 01:15		35	m		Arm retract, Mastcam video test, APXS cal	169.7	199	798		
12 Sep 01:54	36	cM		Arm teach point checkout: MAHLI REMS UV, CheMin inlet, drill bit box; ChemCam recovery	170.2		798			
13 Sep 02:34	37	M		Arm teach point & CHIMRA checkouts, Phobos transit	170.8	200	800	0.77		
Drive toward Glenelg	14 Sep 03:14	38	M		Dr 32m to 04/0006 - el-4m - 00141m - toward Glenelg	171.3	200	800		
	15 Sep 03:53	39	m		Dr 22m to 04/0410 - el-4m - 00162m - toward Glenelg	171.9	199	802		
	16 Sep 04:33	40	cm		Dr 37m to 04/0474 - el-4m - 00200m - toward Glenelg, SAM heater checkout	172.5	198	804		
	17 Sep 05:12	41	m		Dr 27m to 04/0922 - el-4m - 00227m - toward Glenelg	173.0	199	804		
	18 Sep 05:52	42	M		Dr 32m to 04/1244 - el-7m - 00259m - toward Jake Matijevic, SAM heater checkout, Phobos & Deimos transits	173.6	199	802	0.68	
	19 Sep 06:32	43	Cm		Dr 30m to 04/1638 - el-7m - 00289m - toward Jake Matijevic	174.2	200	804		

Area	Noon UTC	Sol	RS	Arm	Activity Summary	Ls	T	P	Tau
Rocknest	20 Sep 07:11	44	M		MAHLI plaque & flag, rover sag checkout	174.7	200	805	0.68
	21 Sep 07:51	45	CM		Dr 5m to 04/2008 - el-7m - 00293m - toward Jake Matijevic, Phobos night	175.3		805	
	22 Sep 08:30	46	c	A	In-situ Jake Matijevic	175.9		806	
	23 Sep 09:10	47	c	A	toward Glenelg after in-situ Jake Matijevic	176.5		806	
	24 Sep 09:49	48	CM		Dr 42m to 04/2106 - el-10m - 00335m - toward Glenelg	177.0		805	0.83
	25 Sep 10:29	49	cM		Dr 31m to 04/2650 - el-11m - 00366m - toward Glenelg	177.6		806	
	26 Sep 11:09	50	CM		Dr 49m to 04/2784 - el-15m - 00414m - toward Glenelg	178.2	203	806	
	27 Sep 11:48	51	M		Sample processing dry run, CHIMRA clean, SAM atmos	178.8		807	
	28 Sep 12:28	52	M		Dr 36m to 04/2962 - el-16m - 00451m - toward Glenelg after in-situ sky	179.3		806	
	29 Sep 13:07	53	M		Dr 2m to 04/3206 - el-16m - 00453m - toward Bathurst & Cowles	179.9	200	806	
	30 Sep 13:47	54	m	A	In-situ Bathurst & Cowles	180.5	200	809	
	01 Oct 14:27	55	cM		Dr 24m to 04/3238 - el-17m - 00476m - toward Rocknest	181.1	199	809	
	02 Oct 15:06	56	cM		Dr 6m to 04/3422 - el-17m - 00482m - toward Rocknest	181.7	200	812	0.72
	03 Oct 15:46	57	cm		Dr 2m to 04/3480 - el-17m - 00484m - scuffing Rocknest	182.2	200	811	
	04 Oct 16:25	58		A	In-situ Rocknest scuff & unscuffed	182.8	198	811	
	05 Oct 17:05	59	cM		Dr 6m to 05/0006 - el-17m - 00490m - toward Rocknest sample site	183.4	198	813	
	06 Oct 17:45	60	M	W	MAHLI range finding activity, future scoop targets, wheel stability	184.0	198	815	
	07 Oct 18:24	61	CM	C	MAHLI range finding activity, Scoop Rocknest 1	184.6	199	815	
	08 Oct 19:04	62	cm		MAHLI CHIMRA fall site, foreign object debris assessment	185.2	199	816	
	09 Oct 19:43	63			Foreign object debris assessment	185.8	198	817	
	10 Oct 20:23	64	M	U	Mastcam portion drop video	186.3	200	817	
	11 Oct 21:02	65	M	X	CHIMRA clean, in-situ foreign object debris	186.9	199	818	
	12 Oct 21:42	66	cM	C	Scoop Rocknest 2, MAHLI scoop 1 site & range finding activity	187.5	198	817	0.70
	13 Oct 22:22	67	M	U	Scoop dump, MAHLI foreign object debris & future scoop sites	188.1	198	820	
	14 Oct 23:01	68	C		Runout (concern over foreign object debris)	188.7	199	820	
	15 Oct 23:41	69	M	C	Scoop Rocknest 3, MAHLI foreign object debris	189.3	199		
	17 Oct 00:20	70	CM		CHIMRA Rocknest 3, Drop to O-tray	189.9	200	823	
	18 Oct 01:00	71	CM	S	Drop to CheMin, CheMin Rocknest 3	190.5	199	824	0.74
	19 Oct 01:40	72	CM		CheMin Rocknest 3	191.1	199	826	
	20 Oct 02:19	73	M	UX	MAHLI O-tray & CHIMRA fall site, CHIMRA clean, SAM atmos	191.7	201	828	
	21 Oct 02:59	74	CM	C	Scoop Rocknest 4, MAHLI CheMin funnel, range-finding, undisturbed drift	192.3	200	830	
	22 Oct 03:38	75	cM		CHIMRA Rocknest 4, CheMin cell dump, CheMin empty	192.9	198	830	
	23 Oct 04:18	76	CM		Drop to O-tray	193.5	202	833	0.76
24 Oct 04:58	77	CM	S	Drop to CheMin & O-tray, SAM atmos	194.1	200	833		
25 Oct 05:37	78	M		Drop to O-tray, CheMin Rocknest 4	194.7	200	833		
26 Oct 06:17	79	CM	I	CHIMRA sample inspection, SAM atmos	195.3	200	835		
27 Oct 06:56	80	M		CheMin Rocknest 4	195.9	201	836		
28 Oct 07:36	81	M	UX	CHIMRA clean, CheMin Rocknest 4, MAHLI REMS UV & CHIMRA fall site, SAM atmos	196.5	200	836		
29 Oct 08:15	82	CM		CheMin Rocknest 4, MAHLI Burwash, Et Then, scoops 3&4	197.1		838		
30 Oct 08:55	83			SAM preconditioning	197.7	199	840		
31 Oct 09:35	84	CM	P	MAHLI selfie, Burwash, Et Then, scoops 3&4	198.3	200	839		
01 Nov 10:14	85	CM	P	MAHLI selfie (stereo, +Mt Sharp), SAM EGA blank run	199.0	200	841		
02 Nov 10:54	86	m	A	In-situ Et Then, MAHLI sky, CheMin Rocknest 4	199.6	199	845		
03 Nov 11:33	87	cM		RCE maintenance, ChemCam cal, CheMin Rocknest 4	200.2	201	843	0.66	

356 Appendix: Curiosity Activity Summary

Area	Noon UTC	Sol	RS	Arm	Activity Summary	Ls	T	P	Tau	
	04 Nov 12:13	88	CM		MAHLI Portage & La Bine, SAM EGA blank run	200.8	202	846		
	05 Nov 12:53	89	M	A	In-situ Portage, MAHLI range finding future scoop 5 site, CheMin cell dump	201.4	199	851		
	06 Nov 13:32	90	CM		MAHLI Et Then, ChemCam decon, SAM dropoff dry run	202.0	200	850		
	07 Nov 14:12	91	c	A	APXS O-tray, ChemCam cal, SAM preconditioning	202.6	200	853		
	08 Nov 14:51	92			ANOMALIES PRECLUDE SCIENCE (ChemCam sick)	203.2	199	856		
	09 Nov 15:31	93	cm	CS	Scoop Rocknest 5, drop to SAM, SAM Rocknest 5 sample 1, MAHLI O-tray & SAM inlet & dump, ChemCam recovery	203.9	199	855		
	10 Nov 16:11	94	M	S	Drop to CheMin, CheMin Rocknest 5	204.5	203	860		
	11 Nov 16:50	95	m	A	Drop to O-tray, in-situ Rocknest 5 on O-tray, SAM preconditioning	205.1	202	862		
	12 Nov 17:30	96	m	S	Drop Rocknest 5 sample 2 to SAM, MAHLI SAM inlet, SAM Rocknest 5 sample 2	205.7	202	864		
	13 Nov 18:09	97	C		CheMin Rocknest 5, SAM preconditioning	206.3	203	872	0.85	
	14 Nov 18:49	98		S	CheMin Rocknest 5, ChemCam decon, drop to SAM, MAHLI SAM inlet	207.0	203	871		
	15 Nov 19:28	99			SAM Rocknest 5 sample 3	207.6	204	870		
	16 Nov 20:08	100	cM		Dr 2m to 05/0110 - el-17m - 00491m - to Rocknest 3, ChemCam cal	208.2	206	866	1.23	
	17 Nov 20:48	101	M		CheMin Rocknest 5, drill preheat checkout	208.8	205	872	1.18	
	18 Nov 21:27	102		A	Dr 25m to 05/0184 - el-18m - 00517m - toward Point Lake after APXS Rocknest 3	209.4	205	869		
	Drive to Yellowknife Bay	19 Nov 22:07	103			ChemCam decon, drill battle short checkout	210.1	206	870	
		20 Nov 22:46	104	Cm		CheMin Rocknest 5	210.7	205	883	
		21 Nov 23:26	105			SAM atmos	211.3	206	895	
23 Nov 00:06		106	M			212.0	208	897		
24 Nov 00:45		107	M			212.6	208	899		
25 Nov 01:25		108	M			213.2	206	899		
26 Nov 02:04		109	M			213.8	208	893		
27 Nov 02:44		110	M			214.5	207	897		
28 Nov 03:23		111	CM		Dr 2m to 05/0394 - el-18m - 00519m - to Bell Island, CheMin Rocknest 5	215.1	206	896	1.20	
29 Nov 04:03		112	CM		ChemCam decon, SAM preconditioning	215.7	207	898		
30 Nov 04:43		113	CM		Drill checkout	216.4	206	901		
01 Dec 05:22		114	CM		Attempt SAM delivery	217.0	206	904		
02 Dec 06:02		115				217.6	206	906		
03 Dec 06:41		116	CM	S	Drop to Rocknest 5 sample 4 to SAM	218.3	206	907		
04 Dec 07:21		117	C	A	APXS Bell Island, SAM Rocknest 5 sample 4	218.9	206	907		
05 Dec 08:01		118	M			219.5	207	907		
06 Dec 08:40		119	Cm		CheMin Rocknest 5, ChemCam cal & decon	220.2	206	912	1.08	
07 Dec 09:20		120	cM		Dr 35m to 05/0438 - el-18m - 00553m - toward Shaler, ChemCam cal, SAM recovery	220.8	207	913		
08 Dec 09:59	121	CM		Dr 24m to 05/0748 - el-18m - 00577m - toward Yellowknife Bay, CheMin Rocknest 5	221.4	207	916			
09 Dec 10:39	122	cM		Dr 1m to 05/0932 - el-18m - 00578m - toward Yellowknife Bay	222.1	208	916	1.10		
10 Dec 11:19	123	Cm		Dr 19m to 05/0944 - el-19m - 00598m - toward Yellowknife Bay	222.7	207	919			
11 Dec 11:58	124	Cm		Dr 14m to 05/1076 - el-19m - 00612m - toward Yellowknife Bay	223.4	208	920			
Explore Yellowknife Bay	12 Dec 12:38	125	Cm		Dr 26m to 05/1222 - el-20m - 00638m - toward Yellowknife Bay	224.0	206	921		
	13 Dec 13:17	126	CM		ChemCam decon	224.6	205	926		
	14 Dec 13:57	127	Cm		Dr 33m to 05/1404 - el-21m - 00671m - toward Yellowknife Bay, SAM electrical baseline test	225.3	206	926		
	15 Dec 14:36	128	m	UX	Dump sample & CHIMRA thwackless clean	225.9	206	929		
	16 Dec 15:16	129	Cm	A	In-situ Costello, Flaherty	226.6	210	932	1.23	
	17 Dec 15:56	130	Cm		Dr 6m to 05/1582 - el-20m - 00676m - toward Yellowknife Bay	227.2	209	935		
	18 Dec 16:35	131	c			227.9	208	934		

Appendix: Curiosity Activity Summary 357

Area	Noon UTC	Sol	RS	Arm	Activity Summary	Ls	T	P	Tau
John Klein	19 Dec 17:15	132	cm	A	In-situ Gillespie Lake	228.5	206	937	
	20 Dec 17:54	133	CM		Dr 22m to 05/1668 - el-20m - 00698m - toward Grandmothers House	229.1	207	937	
	21 Dec 18:34	134	Cm		ChemCam decon	229.8	206	939	1.14
	22 Dec 19:14	135	CM			230.4	206	937	
	23 Dec 19:53	136	M			231.1	208	940	
	24 Dec 20:33	137	M			231.7	207	938	
	25 Dec 21:12	138	M		Runout (planned holiday break)	232.4	206	940	
	26 Dec 21:52	139			Runout (planned holiday break)	233.0	206	940	
	27 Dec 22:32	140			ChemCam decon	233.7	207	941	
	28 Dec 23:11	141	M		Runout (planned holiday break)	234.3	205	946	
	29 Dec 23:51	142			Runout (planned holiday break)	235.0	207	944	
	31 Dec 00:30	143			Runout (planned holiday break)	235.6	208	951	
	01 Jan 01:10	144			Runout; HAPPY NEW YEAR 2013	236.3	208	946	
	02 Jan 01:49	145			Runout (planned holiday break)	236.9	207	952	
	03 Jan 02:29	146			Runout (planned holiday break)	237.5	207	946	
	04 Jan 03:09	147	cM		Dr 3m to 05/1864 - el-20m - 00701m - to Snake River	238.2	207	955	1.06
	05 Jan 03:48	148	c		CheMin Rocknest 5, ChemCam decon	238.8	207	955	
	06 Jan 04:28	149	Cm	A	In-situ Snake River, Ekwir1, Ekwir2	239.5	208	958	
	07 Jan 05:07	150	M	AB	Brush Ekwir1, In-situ Ekwir1, Grit	240.1	208	960	
	08 Jan 05:47	151	Cm		Dr 1m to 05/1908 - el-20m - 00702m - to Unit 1/Unit 2 contact, CheMin cell dump, CheMin empty	240.8	208	959	
	09 Jan 06:27	152	C		Dr 2m to 05/1922 - el-20m - 00704m - to Unit 1/Unit 2 contact	241.5	207	961	
	10 Jan 07:06	153	CM			242.1	207	958	1.11
	11 Jan 07:46	154	CM	A	In-situ Ungava, Persillion, MAHLI REMS UV	242.8	207	961	
	12 Jan 08:25	155	cm		SAM atmos	243.4	207	958	
	13 Jan 09:05	156			ChemCam decon, arm fault	244.1	207	962	
	14 Jan 09:45	157	Cm			244.7	208	959	1.07
	15 Jan 10:24	158	m	A	In-situ Mavor, Nastapola, MAHLI Tindir	245.4	206	962	
	16 Jan 11:04	159	CM		Dr 1m to 05/1960 - el-20m - 00705m - to Bonnet Plume after MAHLI Twitya	246.0	208	957	
	17 Jan 11:43	160	CM		MAHLI Tintina, Tindir Lip	246.7	208	960	
	18 Jan 12:23	161		A	In-situ Bonnet Plume, Yukon, Hudson Bay	247.3	210	966	
	19 Jan 13:02	162	CM	A	Dr 9m to 05/1992 - el-20m - 00714m - toward John Klein after in-situ Hay Creek	248.0	206	965	1.07
20 Jan 13:42	163	M		Dr 2m to 05/2188 - el-20m - 00716m - toward John Klein, attempting vein crush	248.6	207	968		
21 Jan 14:22	164	CM		Dr 3m to 05/2206 - el-20m - 00720m - toward John Klein, do wheel wiggle, ChemCam decon	249.3	208	968		
22 Jan 15:01	165	Cm	A	In-situ Sayunei	249.9	207	969		
23 Jan 15:41	166	CM		Dr 3m to 05/2276 - el-20m - 00723m - to John Klein after in-situ Sayunei	250.6	208	968		
24 Jan 16:20	167			Runout (X-band uplink failure)	251.2	208	964		
25 Jan 17:00	168	cm	A	In-situ drill target & Wernecke	251.9	206	967	1.17	
26 Jan 17:40	169	Cm	AB	Brush & in-situ Wernecke, in-situ Brock Inliner	252.5	206	963	1.15	
27 Jan 18:19	170	M		Drill preload test part 1: MAHLI "before" imaging	253.2	206	969		
28 Jan 18:59	171	cM		Drill preload test part 2: MAHLI "after" imaging, ChemCam decon	253.8	206	963	1.09	
29 Jan 19:38	172	CM		CheMin empty cell analysis	254.5	206	964	1.08	
30 Jan 20:18	173	M	AX	In-situ Wernecke 3, MAHLI Autridge, CHIMRA thwackless clean	255.1	206	960		
31 Jan 20:57	174	cM	D	Drill divot attempt w/MAHLI before, drill fault	255.8	206	963	1.03	
01 Feb 21:37	175			Runout (drill fault on sol 174)	256.4	205	963		

358 Appendix: Curiosity Activity Summary

Area	Noon UTC	Sol	RS	Arm	Activity Summary	Ls	T	P	Tau	
	02 Feb 22:17	176	Cm	D	Drill divot w/MAHLI before & after	257.1	206	964		
	03 Feb 22:56	177	m	PW	In-situ O-tray, MAHLI selfie & wheels, SAM EGA blank run	257.8	207	965		
	04 Feb 23:36	178			Mini-drill attempt, MAHLI "after" (but no hole)	258.4	207	965		
	06 Feb 00:15	179	m		MAHLI distance test Fort Confidence, in-situ cal	259.1	207	964		
	07 Feb 00:55	180		D	Mini-drill w/MAHLI after	259.7	206	965		
	08 Feb 01:35	181	CM	A	In-situ Divot 2, MAHLI McLeary, McNaughton, & McGrath; SAM electrical baseline test	260.4	206	961		
	09 Feb 02:14	182	m	F	Drill John Klein w/MAHLI before & after	261.0	206	964		
	10 Feb 02:54	183	CM			261.7	208	964	0.96	
	11 Feb 03:33	184	CM		CHIMRA John Klein(partial)	262.3	207	965		
	12 Feb 04:13	185	CM			263.0	208	965		
	13 Feb 04:53	186	CM			263.6	206	963		
	14 Feb 05:32	187	C		CHIMRA John Klein(partial)	264.3	206	961		
	15 Feb 06:12	188	CM			264.9	205	957	0.84	
	16 Feb 06:51	189	Cm		CHIMRA John Klein(partial)	265.6	205	960		
	17 Feb 07:31	190			Science runout	266.2	207	958		
	18 Feb 08:10	191			ANOMALIES PRECLUDE SCIENCE (problem with sample transfer)	266.9	204	960		
	19 Feb 08:50	192	CM			267.5	204	959	0.89	
	20 Feb 09:30	193	CM	I	CHIMRA John Klein(partial), CHIMRA sample inspection	268.1				
	21 Feb 10:09	194	cM	I	CHIMRA John Klein(partial), CHIMRA sample inspection	268.8				
	22 Feb 10:49	195	C	S	Drop to CheMin, MAHLI CheMin inlet, CheMin John Klein, SAM preconditioning	269.4				
	23 Feb 11:28	196		S	Drop to SAM, SAM John Klein	270.1	206	956		
	24 Feb 12:08	197			CheMin John Klein	270.7	205	953		
	25 Feb 12:48	198	M		FSW transition prep, SAM preconditioning	271.4	205	954	0.94	
	26 Feb 13:27	199		S	Drop to SAM, SAM John Klein 2	272.0	205	955		
	Sol 200 anomaly and recovery	27 Feb 14:07	200	M		ANOMALIES PRECLUDE SCIENCE (sol 200 anomaly)	272.7	205	956	
		28 Feb 14:46	201			ANOMALIES PRECLUDE SCIENCE (sol 200 anomaly)	273.3			
01 Mar 15:26		202			ANOMALIES PRECLUDE SCIENCE (sol 200 anomaly)	274.0				
02 Mar 16:06		203			ANOMALIES PRECLUDE SCIENCE (sol 200 anomaly)	274.6				
03 Mar 16:45		204			ANOMALIES PRECLUDE SCIENCE (sol 200 anomaly)	275.2				
04 Mar 17:25		205			ANOMALIES PRECLUDE SCIENCE (sol 200 anomaly)	275.9				
05 Mar 18:04		206			ANOMALIES PRECLUDE SCIENCE (sol 200 anomaly)	276.5				
06 Mar 18:44		207			ANOMALIES PRECLUDE SCIENCE (sol 200 anomaly)	277.2				
07 Mar 19:23		208			ANOMALIES PRECLUDE SCIENCE (sol 200 anomaly)	277.8				
08 Mar 20:03		209			ANOMALIES PRECLUDE SCIENCE (sol 200 anomaly)	278.5				
09 Mar 20:43		210			ANOMALIES PRECLUDE SCIENCE (sol 200 anomaly)	279.1				
10 Mar 21:22		211			ANOMALIES PRECLUDE SCIENCE (sol 200 anomaly)	279.7				
11 Mar 22:02		212			ANOMALIES PRECLUDE SCIENCE (sol 200 anomaly)	280.4				
12 Mar 22:41	213			ANOMALIES PRECLUDE SCIENCE (sol 200 anomaly)	281.0					
13 Mar 23:21	214			FSW transition prep	281.6					
15 Mar 00:01	215	c		Instrument checkouts	282.3					
16 Mar 00:40	216	c		FSW transition	282.9					
17 Mar 01:20	217			FSW transition	283.6					
18 Mar 01:59	218			ANOMALIES PRECLUDE SCIENCE (sol 200 anomaly)	284.2					
19 Mar 02:39	219			ANOMALIES PRECLUDE SCIENCE (sol 200 anomaly)	284.8					

Area	Noon UTC	Sol	RS	Arm	Activity Summary	Ls	T	P	Tau
	20 Mar 03:19	220			ANOMALIES PRECLUDE SCIENCE (sol 200 anomaly)	285.5			
	21 Mar 03:58	221			ANOMALIES PRECLUDE SCIENCE (sol 200 anomaly)	286.1			
	22 Mar 04:38	222	c		Instrument checkouts	286.7			
	23 Mar 05:17	223	c		RCE-B SUROM update, SAM preconditioning	287.4	203	933	
	24 Mar 05:57	224	m	S	Drop to SAM, SAM John Klein 3	288.0	204	933	
	25 Mar 06:36	225			RCE-B SUROM commit	288.6	204	931	
John Klein	26 Mar 07:16	226	CM		CheMin John Klein, SAM preconditioning	289.2	204	928	0.74
	27 Mar 07:56	227	Cm	S	Drop to SAM, SAM John Klein 4	289.9	203	929	
	28 Mar 08:35	228			Runout ("due to late breaking problem compiling integrated sol plan")	290.5	204	930	
	29 Mar 09:15	229	M	U	CheMin John Klein, CHIMRA cleanup	291.1	204	930	
	30 Mar 09:54	230	C	A	CheMin John Klein, in-situ drill hole, MAHLI mini-drill, tailings, dump piles	291.8	205	924	
	31 Mar 10:34	231			MAHLI Katherine & Dolly, SAM atmos	292.4	203	928	
Solar Conjunction	01 Apr 11:14	232	CM		CheMin John Klein	293.0	204	927	
	02 Apr 11:53	233	M		MAHLI REMS UV	293.6	206	928	0.72
	03 Apr 12:33	234	CM		RSM stow (conjunction prep)	294.2	208	931	
	04 Apr 13:12	235			Environmental science	294.9	205	923	
	05 Apr 13:52	236			Conjunction environmental science	295.5	204	926	
	06 Apr 14:31	237			Conjunction environmental science	296.1	203	923	
	07 Apr 15:11	238			Conjunction environmental science	296.7	204	926	
	08 Apr 15:51	239			Conjunction environmental science	297.4	202	926	
	09 Apr 16:30	240			Conjunction environmental science	298.0	204	925	
	10 Apr 17:10	241			Conjunction environmental science	298.6	203	923	
	11 Apr 17:49	242			Conjunction environmental science	299.2	203	920	
	12 Apr 18:29	243			Conjunction environmental science	299.8	204	922	
	13 Apr 19:09	244			Conjunction environmental science	300.4	204	918	
	14 Apr 19:48	245			Conjunction environmental science	301.0	204	917	
	15 Apr 20:28	246			Conjunction environmental science	301.7	202	920	
	16 Apr 21:07	247			Conjunction environmental science	302.3	204	910	
	17 Apr 21:47	248			Conjunction environmental science	302.9	205	924	
	18 Apr 22:27	249			Conjunction environmental science	303.5	204	916	
	19 Apr 23:06	250			Conjunction environmental science	304.1	204	919	
	20 Apr 23:46	251			Conjunction environmental science	304.7	203	919	
	22 Apr 00:25	252			Conjunction environmental science	305.3	203	915	
	23 Apr 01:05	253			Conjunction environmental science	305.9	203	919	
	24 Apr 01:44	254			Conjunction environmental science	306.5	204	914	
	25 Apr 02:24	255			Conjunction environmental science	307.1	204	922	
	26 Apr 03:04	256			Conjunction environmental science	307.7	204	916	
	27 Apr 03:43	257			Conjunction environmental science	308.3	204	916	
	28 Apr 04:23	258			Conjunction environmental science	308.9	204	916	
	29 Apr 05:02	259			Conjunction environmental science	309.5	203	918	
	30 Apr 05:42	260			Conjunction environmental science	310.1	207	927	
	01 May 06:22	261			Conjunction environmental science	310.7	204	915	
FSW update	02 May 07:01	262	c		ChemCam cal & decon	311.3	205	922	
	03 May 07:41	263			FSW transition	311.9			

360 Appendix: Curiosity Activity Summary

Area	Noon UTC	Sol	RS	Arm	Activity Summary	LS	T	P	Tau
	04 May 08:20	264			FSW transition	312.5			
	05 May 09:00	265			FSW transition	313.1			
	06 May 09:40	266			FSW transition	313.7			
	07 May 10:19	267	m		FSW transition	314.3			1.01
John Klein	08 May 10:59	268			Navcam stare test, CheMin John Klein	314.9	204	920	
	09 May 11:38	269	CM		Navcam & ChemCam checkout	315.5	205	925	
Cumberland	10 May 12:18	270	M	AP	In-situ McGrath, MAHLI drill hole walls, selfie+, CheMin John Klein	316.1	207	920	1.29
	11 May 12:57	271	CM		CheMin John Klein	316.7	205	916	
	12 May 13:37	272	m		Dr 3m to 06/0006 - el-20m - 00726m - to Cumberland, CheMin John Klein	317.3	204	917	
	13 May 14:17	273	C			317.8	204	909	
	14 May 14:56	274	C		Dr 1m to 06/0074 - el-20m - 00727m - to Cumberland, MAHLI stowed infinity-focus test	318.4	203	910	
	15 May 15:36	275	Cm	W	MAHLI Cumberland & wheels, SAM preconditioning	319.0	205	909	1.10
	16 May 16:15	276	A		In-situ Cumberland, drill preload w/MAHLI after, SAM EGA blank	319.6	206	905	
	17 May 16:55	277	Cm	A	CheMin empty, in-situ Cumberland after ChemCam LIBS	320.2	205	904	
	18 May 17:35	278	C		SAM QMS atmos	320.8	207	902	
	19 May 18:14	279	m	FI	Drill Cumberland w/MAHLI before & after, MAHLI drill hole, CHIMRA sample	321.3	206	903	
	20 May 18:54	280	m		SAM preconditioning	321.9	205	901	1.06
	21 May 19:33	281	CM	S	Drop to SAM, SAM Cumberland 1	322.5	206	901	
	22 May 20:13	282		S	Drop to CheMin, CheMin Cumberland, MAHLI inlets & REMS UV	323.1	206	901	
	23 May 20:53	283	Cm	A	In-situ drill tailings, MAHLI drill hole bottom, ChemCam autofocus laser light	323.7	205	900	
	24 May 21:32	284	CM		Portion drop videos, drop to O tray, SAM QMS atmos	324.2	203	898	1.02
	25 May 22:12	285	Cm		SAM preconditioning	324.8	204	897	
	26 May 22:51	286		S	Drop to SAM, SAM Cumberland 2, place APXS	325.4	203	898	
27 May 23:31	287		A	APXS drill tailings, CheMin Cumberland	326.0	204	899		
29 May 00:10	288	Cm		ChemCam decon, SAM preconditioning	326.5	205	895		
30 May 00:50	289	CM		Portion drop video, drop to O tray, CheMin Cumberland, APXS retract checkout	327.1	203	896		
31 May 01:30	290	Cm	S	Drop to SAM, SAM Cumberland 3	327.7	204	895	0.98	
01 Jun 02:09	291		AB	Brush & in-situ Cumberland, MAHLI Narrows 3, SAM QMS atmos	328.2	203	892		
02 Jun 02:49	292			MAHLI drill hole and tailings, SAM atmos	328.8	203	891		
03 Jun 03:28	293	C		CheMin Cumberland	329.4	205	890		
04 Jun 04:08	294	Cm			329.9	205	893		
Point Lake	05 Jun 04:48	295	m		Dr 6m to 06/0088 - el-20m - 00733m - toward Point Lake	330.5	204	893	0.96
	06 Jun 05:27	296	C			331.1	202	889	
	07 Jun 06:07	297	M		Dr 20m to 06/0122 - el-20m - 00753m - toward Point Lake	331.6	202	886	
	08 Jun 06:46	298	CM			332.2	201	888	
	09 Jun 07:26	299			Dr 8m to 06/0230 - el-19m - 00761m - toward Point Lake	332.8	203	885	
	10 Jun 08:06	300	cm		CheMin Cumberland	333.3	202	889	0.87
	11 Jun 08:45	301	cM		Dr 12m to 06/0314 - el-19m - 00773m - toward Point Lake	333.9	202	889	
	12 Jun 09:25	302	CM		Dr 3m to 06/0416 - el-18m - 00776m - to Point Lake	334.4	204	889	
	13 Jun 10:04	303	CM		MAHLI Point Lake mosaic, Katsao, Measles Point, & Hurwitz	335.0	203	888	
	14 Jun 10:44	304	C	A	In-situ Dismal Lakes, Measles Point, M3, Hurwitz	335.5	205	886	
	15 Jun 11:23	305	cM		SAM atmos	336.1	206	884	
Shaler	16 Jun 12:03	306	CM			336.7	205	883	
	17 Jun 12:43	307	Cm		Dr 32m to 06/0456 - el-19m - 00808m - toward Shaler	337.2	206	887	0.89

Appendix: Curiosity Activity Summary 361

Area	Noon UTC	Sol	RS	Arm	Activity Summary	LS	T	P	Tau	
	18 Jun 13:22	308	CM		Dr 22m to 06/0566 · el-18m · 00830m · toward Shaler	337.8	202	886		
	19 Jun 14:02	309	CM		Dr 2m to 06/0652 · el-17m · 00832m · toward Shaler	338.3	202	887		
	20 Jun 14:41	310	C		CheMin Cumberland	338.9	201	887		
	21 Jun 15:21	311	CM			339.4	202	885		
	22 Jun 16:01	312	CM			340.0	203	882	0.99	
	23 Jun 16:40	313	M		Dr 9m to 06/0664 · el-18m · 00841m · toward Shaler, SAM atmos	340.5	201	886		
	24 Jun 17:20	314	CM			341.1	201	883	0.96	
	25 Jun 17:59	315	CM		CheMin dark frame	341.6	201	884		
	26 Jun 18:39	316	CM			342.1	201	889		
	27 Jun 19:18	317	CM		Dr 7m to 06/0708 · el-17m · 00848m · toward Shaler	342.7	202	888		
	28 Jun 19:58	318	cM			343.2	201	889		
	29 Jun 20:38	319	CM			343.8	201	887		
	30 Jun 21:17	320	M			344.3	201	885	0.88	
	01 Jul 21:57	321	C		SAM atmos	344.8	200	886		
	02 Jul 22:36	322	C	A	In-situ Ailik	345.4	201	886		
	03 Jul 23:16	323	CM	A	In-situ Equaluik & Howells, MAHLI REMS UV & Gudrid	345.9	200	882		
	Drive to Darwin (Waypoint 1)	04 Jul 23:56	324	Cm		Dr 18m to 06/0810 · el-18m · 00866m · toward Mt Sharp, SAM FSW update	346.5	200	884	
		06 Jul 00:35	325	CM			347.0	200	886	
		07 Jul 01:15	326	Cm		SAM FSW update	347.5	199	890	0.84
		08 Jul 01:54	327	Cm		Dr 40m to 07/0006 · el-16m · 00906m · toward Mt Sharp, ChemCam decon	348.1	199	889	
		09 Jul 02:34	328	C			348.6	197	886	
		10 Jul 03:14	329	CM		Dr 41m to 07/0142 · el-15m · 00947m · toward Mt Sharp, SAM preconditioning	349.1	201	884	
		11 Jul 03:53	330	Cm			349.7	202	883	0.74
		12 Jul 04:33	331	CM		Dr 28m to 07/0276 · el-13m · 00975m · toward Mt Sharp, SAM high-conductance valve test	350.2	201	885	
		13 Jul 05:12	332	Cm			350.7	198	889	
		14 Jul 05:52	333	cM		Dr 16m to 07/0374 · el-12m · 00990m · toward Mt Sharp	351.2	198	888	
		15 Jul 06:31	334	C			351.8	200	890	
		16 Jul 07:11	335	Cm		Dr 38m to 08/0006 · el-10m · 01029m · toward Mt Sharp	352.3	198	889	0.72
		17 Jul 07:51	336	Cm		Dr 33m to 08/0138 · el-8m · 01062m · toward Mt Sharp	352.8	199	889	
		18 Jul 08:30	337	Cm		Dr 38m to 08/0240 · el-6m · 01099m · toward Mt Sharp	353.3	198	892	
19 Jul 09:10		338	CM		Dr 34m to 08/0500 · el-4m · 01133m · toward Mt Sharp	353.9	197	887		
20 Jul 09:49		339	Cm		SAM atmos	354.4	197	890		
21 Jul 10:29		340	m		Dr 100m to 08/0616 · el-3m · 01234m · toward Mt Sharp	354.9	198	888	0.75	
22 Jul 11:09		341	C		SAM atmos	355.4	197	888		
23 Jul 11:48		342	CM		Dr 62m to 09/0006 · el0m · 01296m · toward Mt Sharp	356.0	197	888		
24 Jul 12:28		343	Cm		Dr 34m to 09/0242 · el+1m · 01330m · toward Mt Sharp	356.5	198	887		
25 Jul 13:07		344	M		Dr 70m to 09/0372 · el+1m · 01400m · toward Mt Sharp	357.0	198	889		
26 Jul 13:47		345	M		Dr 70m to 10/0006 · el+1m · 01470m · toward Mt Sharp	357.5	198	896	0.80	
27 Jul 14:27		346	CM			358.0	197	890		
28 Jul 15:06		347	m		Dr 60m to 10/0294 · el+1m · 01530m · toward Mt Sharp	358.5	198	890		
29 Jul 15:46		348	M			359.1	199	888	0.78	
30 Jul 16:25		349	CM		Dr 70m to 10/0514 · el+0m · 01600m · toward Mt Sharp	359.6	199	888		
31 Jul 17:05		350	C			0.1	199	894		
01 Aug 17:44	351	M		Dr 85m to 11/0006 · el-1m · 01685m · toward Mt Sharp, coordinated THEMIS observation, Phobos occultation of Deimos	0.6	199	892			

362 Appendix: Curiosity Activity Summary

Area	Noon UTC	Sol	RS	Arm	Activity Summary	Ls	T	P	Tau
Darwin (Waypoint 1)	02 Aug 18:24	352	CM		SAM preconditioning	1.1	198	891	0.81
	03 Aug 19:04	353	Cm	S	Drop to SAM, SAM Cumberland 4	1.6	202	891	
	04 Aug 19:43	354	m		Dr 57m to 11/0308 · el+0m · 01742m · toward Mt Sharp	2.1	201	893	
	05 Aug 20:23	355	c			2.6	201	894	
	06 Aug 21:02	356	CM		Dr 50m to 11/0528 · el0m · 01792m · toward Mt Sharp	3.1	197	892	0.79
	07 Aug 21:42	357	Cm			3.7	198	897	
	08 Aug 22:22	358	Cm		Dr 35m to 11/0754 · el+0m · 01827m · toward Mt Sharp	4.2	198	895	
	09 Aug 23:01	359	C			4.7			
	10 Aug 23:41	360	Cm	A	In-situ Matthew, MAHLI REMS UV	5.2			0.78
	12 Aug 00:20	361	m		Dr 73m to 12/0006 · el-1m · 01900m · toward Mt Sharp	5.7			
	13 Aug 01:00	362				6.2			
	14 Aug 01:40	363	CM		Dr 85m to 12/0250 · el-1m · 01985m · toward Mt Sharp, Phobos transit	6.7			
	15 Aug 02:19	364	cM		SAM atmos	7.2			
	16 Aug 02:59	365	CM		Dr 27m to 12/0566 · el-1m · 02012m · toward Mt Sharp	7.7			0.79
	17 Aug 03:38	366	C			8.2	198	897	
	18 Aug 04:18	367		S	SAM preconditioning, drop to SAM	8.7	197	899	
	19 Aug 04:57	368	CM		SAM Cumberland 5, Phobos transit	9.2	198	900	
	20 Aug 05:37	369	M		Dr 70m to 12/0696 · el-3m · 02082m · toward Mt Sharp, Phobos transit	9.7	197	903	0.81
	21 Aug 06:17	370	Cm		Dr 82m to 13/0006 · el-3m · 02163m · toward Mt Sharp	10.2	196	901	
	22 Aug 06:56	371	CM		Dr 110m to 13/0298 · el-3m · 02273m · toward Mt Sharp	10.7	199	901	
	23 Aug 07:36	372	cm		Dr 40m to 13/0980 · el-1m · 02313m · toward Mt Sharp	11.2	198	901	
	24 Aug 08:15	373	CM	A	In-situ Maya, MAHLI Dover	11.7	196	903	
	25 Aug 08:55	374	Cm		Dr 43m to 14/0006 · el-1m · 02356m · toward Mt Sharp	12.2	196	905	0.71
	26 Aug 09:35	375	M			12.7	197	909	
	27 Aug 10:14	376	cm		Dr 43m to 14/0162 · el-3m · 02399m · toward Mt Sharp	13.2	196	909	
	28 Aug 10:54	377	cM		Dr 61m to 14/0460 · el-2m · 02461m · toward Mt Sharp	13.6	199	906	
	29 Aug 11:33	378	M		Dr 90m to 14/0806 · el-3m · 02551m · toward Mt Sharp, Phobos-Deimos together	14.1		905	
	30 Aug 12:13	379	CM		Dr 15m to 14/1138 · el-2m · 02566m · toward Mt Sharp	14.6	199	906	
	31 Aug 12:52	380	C			15.1	196	906	
	01 Sep 13:32	381		S	SAM preconditioning, drop to SAM	15.6	197	907	
	02 Sep 14:12	382	CM		SAM Cumberland 6	16.1	196	905	
	03 Sep 14:51	383	m		Dr 42m to 14/1268 · el-3m · 02608m · toward Mt Sharp	16.6	199	907	
	04 Sep 15:31	384	CM			17.1	198	909	
	05 Sep 16:10	385	M		Dr 142m to 15/0006 · el0m · 02750m · toward Panorama Point	17.6	197	908	
	06 Sep 16:50	386	C		ChemCam cal & decon	18.0	197	907	
07 Sep 17:30	387	CM	A	In-situ Ruker, MAHLI Spurs	18.5	197	910		
08 Sep 18:09	388	M		Dr 24m to 15/1004 · el-1m · 02774m · toward Panorama Point	19.0	196	907		
09 Sep 18:49	389	CM			19.5	197	908		
10 Sep 19:28	390	Cm		Dr 75m to 15/1236 · el-5m · 02849m · toward Darwin Position 1	20.0	197	908		
11 Sep 20:08	391	C			20.5	197	908		
12 Sep 20:48	392	CM		Dr 3m to 16/0006 · el-5m · 02852m · to Darwin Position 1	20.9	197	911		
13 Sep 21:27	393	M		SAM preconditioning, SAM blank, Phobos eclipse, Phobos-Deimos together	21.4	197	913		
14 Sep 22:07	394		A	In-situ Bardin Bluffs pebble, MAHLI Altar Mountain, SAM EGA blank	21.9	196	910		
15 Sep 22:46	395	M	A	APXS Bardin Bluffs matrix	22.4	197	911		

Area	Noon UTC	Sol	RS	Arm	Activity Summary	LS	T	P	Tau
Drive to Cooperstown (Waypoint 2)	16 Sep 23:26	396	Cm		Dr 10m to 16/0056 · el-4m · 02862m · to Darwin Position 2	22.9	197	913	
	18 Sep 00:05	397	CM			23.3	197	913	
	19 Sep 00:45	398	C		MAHLI vein mosaic, McMurdo, Taylor, Shackleton	23.8	196	917	
	20 Sep 01:25	399	C	A	In-situ Mount Bastion, Dragons Teeth, Kerguelen, Heimdall, Glossopteris Gully	24.3	197	917	
	21 Sep 02:04	400		A	In-situ McMurdo, Taylor, Shackleton, MAHLI vein mosaic	24.8	196	917	
	22 Sep 02:44	401	CM			25.3	198	916	
	23 Sep 03:23	402	m		Dr 23m to 16/0154 · el-4m · 02885m · toward Mt Sharp	25.7	199	917	
	24 Sep 04:03	403	m		Dr 68m to 16/0334 · el-4m · 02953m · toward Mt Sharp	26.2	196	917	
	25 Sep 04:43	404	CM		Dr 64m to 16/1058 · el-2m · 03017m · toward Mt Sharp	26.7	194	918	
	26 Sep 05:22	405			ANOMALIES PRELUDE SCIENCE (HGA blocked after short drive, uplink failed)	27.2	194	919	
	27 Sep 06:02	406	Cm		Dr 73m to 16/1590 · el-3m · 03089m · toward Mt Sharp	27.6	194	918	0.67
	28 Sep 06:41	407	Cm		ChemCam decon, SAM preconditioning, SAM triple portion blank	28.1	194	919	
	29 Sep 07:21	408	CM		SAM EGA blank	28.6	197	919	
	30 Sep 08:01	409	m		Dr 71m to 17/0006 · el-2m · 03160m · toward Mt Sharp	29.1	195	919	
	01 Oct 08:40	410	M		Dr 33m to 17/0682 · el-1m · 03193m · toward Mt Sharp	29.5	194	920	0.66
	02 Oct 09:20	411	m	W	In-situ cal, MAHLI wheels, CheMin inlet	30.0	194	918	
	03 Oct 09:59	412	m		Dr 97m to 17/0826 · el-2m · 03290m · toward Mt Sharp	30.5	194	919	
	04 Oct 10:39	413	M		Dr 80m to 18/0006 · el+0m · 03370m · toward Mt Sharp	30.9	194	920	
	05 Oct 11:18	414		S	Drop to SAM	31.4	195	921	
	06 Oct 11:58	415			SAM Cumberland 7	31.9	193	921	
	07 Oct 12:38	416	Cm			32.4	194	921	
	08 Oct 13:17	417	M		Dr 59m to 18/0428 · el+2m · 03429m · toward Mt Sharp, RCE maintenance	32.8	193	922	
	09 Oct 13:57	418	C		CheMin Cumberland, MAHLI REMS UV	33.3	193	922	
	10 Oct 14:36	419	m		Dr 126m to 18/0792 · el+3m · 03554m · toward Mt Sharp	33.8	193	923	
	11 Oct 15:16	420			SAM preconditioning, RCE maintenance	34.2	194	925	
	12 Oct 15:56	421	CM		SAM EGA blank	34.7	194	923	
	13 Oct 16:35	422	m		Dr 70m to 19/0006 · el+3m · 03624m · toward Mt Sharp	35.2	194	924	
	14 Oct 17:15	423			CheMin Cumberland	35.6	194	925	
	15 Oct 17:54	424	CM		Dr 94m to 19/0326 · el+3m · 03719m · toward Mt Sharp	36.1	194	925	
	16 Oct 18:34	425	CM		CheMin Cumberland	36.6	193	927	0.66
	17 Oct 19:14	426	CM		Dr 48m to 19/1072 · el+4m · 03767m · toward Cooperstown	37.0	194	927	
	18 Oct 19:53	427	C		SAM getter/scrubber cleanup	37.5	194	926	
	19 Oct 20:33	428			SAM preconditioning/blank	37.9	193	926	
	20 Oct 21:12	429	CM		Dr 46m to 20/0006 · el+4m · 03813m · toward Cooperstown	38.4	193	926	
	21 Oct 21:52	430	C			38.9	193	926	
22 Oct 22:31	431	M		Dr 72m to 20/0262 · el+5m · 03884m · toward Cooperstown	39.3	193	926		
23 Oct 23:11	432	Cm		CheMin/ODY interaction test	39.8	195	929		
24 Oct 23:51	433	cM		Dr 93m to 20/0770 · el+8m · 03978m · toward Cooperstown	40.3	194	927		
26 Oct 00:30	434	Cm		SAM atmos	40.7	194	930		
27 Oct 01:10	435	Cm			41.2	194	930		
28 Oct 01:49	436			Dr 94m to 21/0006 · el+8m · 04071m · toward Cooperstown	41.6	194	931		
29 Oct 02:29	437	M		Dr 32m to 21/0652 · el+9m · 04103m · toward Cooperstown	42.1	193	930		
30 Oct 03:09	438	CM		Dr 49m to 21/1034 · el+7m · 04152m · toward Cooperstown	42.6	196	930	0.66	
31 Oct 03:48	439	CM		Dr 26m to 21/1368 · el+6m · 04178m · toward Cooperstown	43.0	194	931		

364 Appendix: Curiosity Activity Summary

Area	Noon UTC	Sol	RS	Arm	Activity Summary	LS	T	P	Tau
Cooperstown	01 Nov 04:28	440	CM		Dr 5m to 21/1578 - el+7m - 04182m - toward Cooperstown	43.5	194	930	
	02 Nov 05:07	441	CM		SAM electrical baseline test	43.9	194	932	
	03 Nov 05:47	442	m	A	In-situ Pine Plains & Rensselaer, MAHLI outcrop mosaic	44.4	194	931	
	04 Nov 06:27	443	cm			44.9	194	931	
FSW trans & anomaly	05 Nov 07:06	444			FSW transition	45.3	195	931	
	06 Nov 07:46	445			FSW transition	45.8			
	07 Nov 08:25	446			FSW transition and safing event	46.2			
	08 Nov 09:05	447			ANOMALIES PRECLUDE SCIENCE (safe mode event during FSW transition)	46.7			
	09 Nov 09:44	448			ANOMALIES PRECLUDE SCIENCE (safe mode event during FSW transition)	47.1			
	10 Nov 10:24	449			ANOMALIES PRECLUDE SCIENCE (safe mode event during FSW transition)	47.6			
	11 Nov 11:04	450			ANOMALIES PRECLUDE SCIENCE (safe mode event during FSW transition)	48.0			
	12 Nov 11:43	451			ANOMALIES PRECLUDE SCIENCE (safe mode event during FSW transition)	48.5			
	13 Nov 12:23	452			ANOMALIES PRECLUDE SCIENCE (safe mode event during FSW transition)	49.0			
Drive	14 Nov 13:02	453	CM		Dr 47m to 22/0006 - el+9m - 04229m - toward Mt Sharp	49.4			0.56
	15 Nov 13:42	454	m		Dr 103m to 22/0490 - el+8m - 04333m - toward Mt Sharp	49.9			
	16 Nov 14:22	455	m		Dr 87m to 23/0006 - el+8m - 04420m - toward Mt Sharp	50.3	192	933	
Soft short anomaly	17 Nov 15:01	456	m			50.8	192	932	
	18 Nov 15:41	457			ANOMALIES PRECLUDE SCIENCE (MMRTG soft short)	51.2	191	933	
	19 Nov 16:20	458			ANOMALIES PRECLUDE SCIENCE (MMRTG soft short)	51.7			
	20 Nov 17:00	459			ANOMALIES PRECLUDE SCIENCE (MMRTG soft short)	52.1			
	21 Nov 17:39	460			ANOMALIES PRECLUDE SCIENCE (MMRTG soft short)	52.6			
	22 Nov 18:19	461			ANOMALIES PRECLUDE SCIENCE (MMRTG soft short)	53.0			
Drive to the Kimberley (Waypoint 3)	23 Nov 18:59	462				53.5			
	24 Nov 19:38	463	m	SW	Drop to SAM (doggy bag Cumberland), MAHLI wheels	54.0	191	933	
	25 Nov 20:18	464		IS	Drop to SAM (doggy bag Cumberland), CHIMRA sample volume inspection	54.4	190	935	
	26 Nov 20:57	465	CM		Dr 50m to 23/0622 - el+8m - 04470m - toward Mt Sharp	54.9	190	933	
	27 Nov 21:37	466	C		ChemCam decon, SAM atmos	55.3	190	935	
	28 Nov 22:17	467	CM		SAM helium commissioning	55.8	191	935	0.45
	29 Nov 22:56	468	M		ChemCam decon	56.2	191	936	
	30 Nov 23:36	469	CM	W	MAHLI wheels	56.7	191	937	
	02 Dec 00:15	470	m		Dr 74m to 23/0896 - el+10m - 04544m - toward Mt Sharp	57.1	190	936	
	03 Dec 00:55	471	C		ChemCam decon	57.6	191	933	
	04 Dec 01:35	472	m	AW	Dr 50m to 24/0006 - el+11m - 04594m - toward Mt Sharp after in-situ Oswego	58.0	190	935	
	05 Dec 02:14	473	C		CheMin John Klein reanalysis	58.5	190	935	0.47
	06 Dec 02:54	474	CM		Dr 9m to 24/0198 - el+11m - 04603m - toward better wheel imaging terrain, SAM atmos	58.9	190	933	
	07 Dec 03:33	475	CM			59.4	191	931	
	08 Dec 04:13	476		W	MAHLI wheels & REMS UV	59.8	190	932	
09 Dec 04:52	477	m		Dr 5m to 24/0318 - el+11m - 04608m - to sample drop location, CheMin John Klein reanalysis, drill callibration	60.3	191	934		
FSW transition	10 Dec 05:32	478	CM		FSW transition prep	60.7	190	932	0.43
	11 Dec 06:12	479			FSW transition	61.2			
	12 Dec 06:51	480			FSW transition	61.6			
	13 Dec 07:31	481			FSW transition	62.1			
	14 Dec 08:10	482			FSW transition	62.5			
	15 Dec 08:50	483			FSW transition	63.0			

Area	Noon UTC	Sol	RS	Arm	Activity Summary	Ls	T	P	Tau
Drive to the Kimberley (Waypoint 3) and wheel imaging	16 Dec 09:30	484			FSW transition	63.4			
	17 Dec 10:09	485		A	In-situ sample dump location	63.9			
	18 Dec 10:49	486	cM	UX	Dump sample, CHIMRA thwackless clean, MAHLI dump pile	64.3	192	930	0.47
	19 Dec 11:28	487	M	A	In-situ dump pile	64.8	191	930	0.45
	20 Dec 12:08	488	CM	W	Dr 1m to 24/0372 · el+11m · 04609m · for 2 of 6 MAHLI full wheel after MAHLI dump pile; CheMin John Klein renalysis	65.2	189	929	
	21 Dec 12:48	489	CM			65.7	190	929	0.47
	22 Dec 13:27	490	M	W	Dr 1m to 24/0384 · el+11m · 04610m · for 4 of 6 MAHLI full wheel	66.1	189	927	
	23 Dec 14:07	491	C			66.6	189	927	
	24 Dec 14:46	492	C			67.0	190	927	0.47
	25 Dec 15:26	493	CM		ChemCam wheel imaging	67.5	191	927	0.43
	26 Dec 16:05	494	M		Dr 20m to 24/0414 · el+12m · 04630m · toward Mt Sharp	67.9	189	927	
	27 Dec 16:45	495			ENV science	68.4	189	924	
	28 Dec 17:25	496			ENV science	68.8	189	923	
	29 Dec 18:04	497			ENV science	69.2	189	924	
	30 Dec 18:44	498			ENV science	69.7	190	924	
	31 Dec 19:23	499			ENV science	70.1	190	922	
	01 Jan 20:03	500			ENV science; HAPPY NEW YEAR 2014!	70.6	189	922	
	02 Jan 20:43	501			ENV science	71.0	189	921	
	03 Jan 21:22	502	CM		ChemCam wheel imaging	71.5	189	922	0.47
	04 Jan 22:02	503	C	A	In-situ Nedrow & Morehouse	71.9	189	921	
	05 Jan 22:41	504	m	W	Dr 24m to 25/0006 · el+11m · 04653m · toward Mt Sharp, MAHLI wheels, SAM atmos	72.4	190	918	
	06 Jan 23:21	505	Cm			72.8	189	917	
	08 Jan 00:01	506	m	AW	Dr 25m to 25/0160 · el+12m · 04679m · toward Mt Sharp, in-situ Oneida, MAHLI wheels	73.3	189	916	
	09 Jan 00:40	507	C			73.7	189	917	
	10 Jan 01:20	508	M	W	Dr 10m to 25/0248 · el+12m · 04688m · toward Mt Sharp, MAHLI wheels, CheMin amphibole standard	74.2		915	
	11 Jan 01:59	509	CM			74.6	189	914	0.45
	12 Jan 02:39	510		AW	in-situ Lowerre & Larrabee, MAHLI wheels	75.1	190	914	
	13 Jan 03:18	511	m		Dr 29m to 25/0318 · el+13m · 04717m · to contact science targets	75.5	190	914	
	14 Jan 03:58	512	Cm	AW	In-situ Kodak & Clinton, MAHLI full wheel 1 of 6	76.0	189	914	
	15 Jan 04:38	513	M	W	Dr 1m to 25/0516 · el+13m · 04718m · for 2-5 of 6 MAHLI full wheel	76.4	188	911	
	16 Jan 05:17	514	CM		Drive fault	76.9	188	910	
17 Jan 05:57	515	m	W	Dr 30m to 25/0546 · el+14m · 04748m · toward Mt Sharp, complete MAHLI full wheel	77.3	188	911		
18 Jan 06:36	516	C	A	In-situ Oscar, MAHLI sky	77.8	189	909	0.40	
19 Jan 07:16	517	Cm			78.2	189	910		
20 Jan 07:56	518	m	W	Dr 16m to 25/0756 · el+13m · 04764m · toward Mt Sharp, MAHLI wheels	78.7	189	908		
21 Jan 08:35	519	m	W	Dr 25m to 25/0892 · el+11m · 04789m · toward Mt Sharp, MAHLI wheels	79.1	190	908		
22 Jan 09:15	520	Cm	W	Dr 26m to 25/1076 · el+11m · 04815m · toward Mt Sharp, MAHLI wheels	79.6	190	906		
23 Jan 09:54	521	M	W	Dr 11m to 25/1244 · el+11m · 04826m · to King, MAHLI full wheel	80.0	188	906		
24 Jan 10:34	522	cM		SAM electrical baseline test	80.5	189	905		
25 Jan 11:13	523	Cm	A	In-situ King	80.9	189	904		
26 Jan 11:53	524	m	W	Dr 24m to 25/1302 · el+14m · 04850m · toward Mt Sharp, MAHLI wheels	81.4	188	902		
27 Jan 12:33	525	C		SAM atmos	81.8	188	901	0.42	
28 Jan 13:12	526	m	AW	Dr 15m to 25/1502 · el+13m · 04865m · toward Mt Sharp, in-situ Reedy, MAHLI wheels & REMS boom 1 & UV	82.3	188	901		

Dingo Gap

366 Appendix: Curiosity Activity Summary

Area	Noon UTC	Sol	RS	Arm	Activity Summary	Ls	T	P	Tau
Dive surge to the Kimberley (Waypoint 3) and wheel imaging	29 Jan 13:52	527	CM	W	Dr 28m to 25/1644 · el+13m · 04894m · toward Mt Sharp, MAHLI wheels	82.7	189	899	
	30 Jan 14:31	528	cM	W	Dr 16m to 26/0006 · el+14m · 04909m · to and scuff Dingo Gap dune, MAHLI wheels	83.2	189	898	
	31 Jan 15:11	529	CM	W	MAHLI full wheel 1 of 5	83.6	189	898	
	01 Feb 15:51	530	CM			84.1	188	895	0.42
	02 Feb 16:30	531		A	In-situ Barker, MAHLI Argyle, Dampier & Crossland	84.5	188	895	
	03 Feb 17:10	532	m	AW	Dr 1m to 26/0190 · el+14m · 04910m · to complete MAHLI full wheel	85.0	188	894	
	04 Feb 17:49	533	M		Dr 7m to 26/0214 · el+14m · 04918m · up face of Dingo Gap Dune	85.4	188	893	
	05 Feb 18:29	534	m			85.9	189	890	
	06 Feb 19:09	535	m		Dr 7m to 26/0296 · el+13m · 04925m · over Dingo Gap Dune	86.3	189	890	
	07 Feb 19:48	536			Runout (planned)	86.8	192	890	
	08 Feb 20:28	537	cm	AW	In-situ Fitzroy, MAHLI Halls & wheels	87.2	191	890	
	09 Feb 21:07	538	cM	A	Dr 41m to 26/0372 · el+11m · 04966m · toward Kimberley, SAM atmos	87.7	191	887	
	10 Feb 21:47	539				88.1	190	886	0.43
	11 Feb 22:26	540	M	W	Dr 73m to 26/0714 · el+13m · 05039m · toward Kimberley, MAHLI wheels	88.6	192	885	
	12 Feb 23:06	541	M		ChemCam decon	89.0	190	883	
	13 Feb 23:46	542	M	W	Dr 23m to 26/1108 · el+14m · 05061m · toward Kimberley, MAHLI wheels	89.5	190	882	
	15 Feb 00:25	543	CM			89.9	192	883	0.43
	16 Feb 01:05	544	CM		MAHLI wheels, cal, SAM TLS inlet, arm clearance & O-tray, goniometer expt & Mastcam cal target	90.4	191	880	
	17 Feb 01:44	545	cm		Dr 47m to 26/1280 · el+12m · 05109m · toward Kimberley	90.8	191	879	
	18 Feb 02:24	546	M	W	Dr 1m to 27/0006 · el+12m · 05110m · toward Kimberley, MAHLI full wheel 1-4 of 5	91.3	190	879	
	19 Feb 03:04	547	M	W	Dr 100m to 27/0030 · el+10m · 05210m · toward Kimberley, MAHLI full wheel complete	91.8	190	877	
	20 Feb 03:43	548	M	W	Dr 100m to 27/0526 · el+13m · 05310m · toward Kimberley, MAHLI wheels	92.2	189	877	
	21 Feb 04:23	549	M	W	Dr 7m to 27/0974 · el+13m · 05317m · toward Bungle Bungle, MAHLI full wheel	92.7	189	874	
	22 Feb 05:02	550	CM	A	Dr 16m to 27/1010 · el+14m · 05333m · toward Kimberley, in-situ Jum Jum, MAHLI Bungle Bungle	93.1	190	873	
	23 Feb 05:42	551	M			93.6	190	871	0.40
	24 Feb 06:22	552	M	W	Dr 79m to 27/1130 · el+13m · 05412m · toward Kimberley, MAHLI wheels	94.0	190	870	
	25 Feb 07:01	553	CM	W	Dr 55m to 28/0006 · el+13m · 05467m · toward Kimberley, MAHLI wheels	94.5	191	870	
	26 Feb 07:41	554	cM	W	Dr 1m to 28/0270 · el+13m · 05468m · for MAHLI full wheel 1-4 of 5	94.9	189	867	
	27 Feb 08:20	555	m	W	Dr 47m to 28/0304 · el+16m · 05515m · toward Kimberley, MAHLI full wheel complete, SAM combustion experiment	95.4	189	866	
	28 Feb 09:00	556			SAM combustion experiment	95.9	189	865	
	01 Mar 09:39	557			SAM combustion experiment	96.3	189	863	
	02 Mar 10:19	558	C	A	In-situ Johnny Cake, MAHLI CheMin inlet	96.8	189	864	0.45
	03 Mar 10:59	559	m	W	Dr 57m to 28/0640 · el+17m · 05572m · toward Kimberley, MAHLI wheels	97.2	189	862	
04 Mar 11:38	560	m	AW	Dr 26m to 28/0920 · el+19m · 05599m · toward Kimberley, in-situ Secure, MAHLI wheels	97.7	189	860		
05 Mar 12:18	561	m	W	Dr 31m to 28/1128 · el+20m · 05629m · toward Kimberley, MAHLI wheels	98.1	190	859		
06 Mar 12:57	562	cM	W	Dr 1m to 28/1356 · el+20m · 05630m · for MAHLI full wheel 1-4 of 5	98.6	190	859		
07 Mar 13:37	563	cm	W	Dr 20m to 28/1380 · el+20m · 05651m · toward Kimberley, MAHLI full wheel complete	99.1	189	856		
08 Mar 14:17	564	cm	AW	Dr 42m to 29/0006 · el+17m · 05692m · toward Kimberley after in-situ Monkey Yard, MAHLI wheels, Crowhurst, CheMin inlet	99.5	190	855	0.45	
09 Mar 14:56	565	M		Dr 33m to 29/0304 · el+20m · 05726m · toward Kimberley	100.0	191	852		
10 Mar 15:36	566	M	W	Dr 1m to 29/0542 · el+20m · 05727m · toward Kimberley, MAHLI full wheel 1 of 5	100.4	190	852		
11 Mar 16:15	567	CM			100.9	191	850		
12 Mar 16:55	568	M	W	Dr 68m to 29/0572 · el+20m · 05795m · toward Kimberley, MAHLI full wheel complete	101.4	191	849		
13 Mar 17:35	569	M	W	Dr 103m to 29/1026 · el+19m · 05898m · toward Kimberley, MAHLI wheels	101.8	190	849		

Area	Noon UTC	Sol	RS	Arm	Activity Summary	LS	T	P	Tau
Explore the Kimberley	14 Mar 18:14	570			Runout (planned end of drive surge sols)	102.3	191	846	
	15 Mar 18:54	571	M	AW	In-situ O-tray, MAHLI wheels	102.7	191	846	
	16 Mar 19:33	572	m		Dr 89m to 30/0006 · el+22m · 05988m · toward Kimberley, MAHLI O-tray, SAM methane enrichment	103.2	191	844	
	17 Mar 20:13	573	C			103.7	192	842	0.41
	18 Mar 20:52	574	CM	W	Dr 38m to 30/0490 · el+22m · 06026m · toward Kimberley, MAHLI wheels	104.1	191	841	
	19 Mar 21:32	575	C		CheMin sample dump, SAM electrical baseline test	104.6	191	840	
	20 Mar 22:12	576	CM	X	CHIMRA clean interrupted by arm fault	105.1	191	839	
	21 Mar 22:51	577			Runout (arm fault)	105.5	191	837	
	22 Mar 23:31	578	cm	X	CHIMRA clean interrupted by arm fault	106.0	191	835	
	24 Mar 00:10	579	cm			106.5	191	834	
	25 Mar 00:50	580	CM			106.9	191	834	
	26 Mar 01:30	581	CM	X	Dr 3m to 30/0746 · el+22m · 06029m · to Square Top after CHIMRA thwackless clean	107.4	190	831	0.45
	27 Mar 02:09	582	CM		SAM oven commissioning	107.9	193	831	0.50
	28 Mar 02:49	583	CM	A	In-situ Square Top	108.3	192	831	0.48
	29 Mar 03:28	584	cm		MAHLI dog's-eye view Square Top, Sally Downs, Sophie Downs, Pandanus Yard	108.8	192	828	
	30 Mar 04:08	585	C	A	In-situ Virgin Hills, APXS Pandanus Yard, MAHLI Square Top & REMS UV	109.3	192	827	
	31 Mar 04:48	586	C		Dr 2m to 30/0792 · el+22m · 06030m · to back up, CheMin empty cell analysis	109.7	192	827	
	01 Apr 05:27	587	M	W	Dr 22m to 30/0826 · el+24m · 06053m · toward Kimberley, MAHLI full wheel, Mastcam sunset	110.2	191	823	
	02 Apr 06:07	588	CM	W	Dr 46m to 30/0944 · el+23m · 06098m · toward Kimberley, MAHLI wheels	110.7	191	823	
	03 Apr 06:46	589	cm	W	Dr 30m to 30/1260 · el+22m · 06128m · toward Kimberley, MAHLI wheels	111.1	191	820	0.43
	04 Apr 07:26	590	CM		SAM GC1 commissioning	111.6	193	819	0.39
	05 Apr 08:05	591		AW	In-situ cal, MAHLI zenith, wheels & Tickalara	112.1	193	818	
	06 Apr 08:45	592	CM			112.5	193	819	
	07 Apr 09:25	593	CM		Dr 31m to 31/0006 · el+22m · 06159m · to investigate Kimberley	113.0	193	819	
	08 Apr 10:04	594	CM			113.5	191	815	
	09 Apr 10:44	595	M	W	Dr 56m to 31/0222 · el+21m · 06215m · to investigate Kimberley, MAHLI wheels	114.0	192	815	
	10 Apr 11:23	596			Runout (X-band uplink failure due to too many files on system)	114.4	193	814	
11 Apr 12:03	597	CM	W	Dr 28m to 31/0544 · el+20m · 06243m · to investigate Kimberley, MAHLI wheels	114.9	192	814	0.37	
12 Apr 12:43	598			Runout (X-band uplink failure due to too many files on system)	115.4	192	812		
13 Apr 13:22	599			Runout (X-band uplink failure due to too many files on system)	115.9	191	812		
14 Apr 14:02	600			Runout (X-band uplink failure due to too many files on system)	116.3	192	811		
15 Apr 14:41	601	CM	AW	In-situ Liga, MAHLI Speewah, ChemCam window & fiber optic cable, wheels, SAM preconditioning	116.8	192	808		
16 Apr 15:21	602	CM		SAM blank	117.3	192	809		
17 Apr 16:00	603	M		Dr 51m to 31/0730 · el+21m · 06294m · to investigate Kimberley	117.8	192	807		
18 Apr 16:40	604	CM			118.2	191	804	0.40	
19 Apr 17:20	605	C	AW	In-situ Lagrange, MAHLI wheels	118.7	191	806		
20 Apr 17:59	606	CM		Dr 19m to 31/1100 · el+21m · 06313m · to Windjana	119.2	191	805		
21 Apr 18:39	607	C			119.7	191	803	0.35	
22 Apr 19:18	608	CM			120.2	191	803		
23 Apr 19:58	609	CM		Dr 5m to 31/1262 · el+22m · 06318m · to Windjana	120.6	190	801		
24 Apr 20:38	610	CM			121.1	191	800		
25 Apr 21:17	611	CM			121.6	190	799	0.36	
26 Apr 21:57	612	cm	AB	Brush & in-situ Windjana	122.1	191	797		
27 Apr 22:36	613		P	MAHLI selfie, drill preload w/MAHLI before & after	122.6	191	798		

Explore the Kimberley

Windjana

368 Appendix: Curiosity Activity Summary

Area	Noon UTC	Sol	RS	Arm	Activity Summary	Ls	T	P	Tau
	28 Apr 23:16	614	CM			123.1	191	797	
	29 Apr 23:56	615	Cm	D	MAHLI Windjana brush post-LIBS, mini-drill Windjana w/MAHLI before & after, MAHLI cover open fault	123.5	192	796	
	01 May 00:35	616			Runout (MAHLI fault)	124.0	191	795	
	02 May 01:15	617	CM		MAHLI diagnostics	124.5	192	795	0.35
	03 May 01:54	618	CM		MAHLI diagnostics	125.0	191	793	
	04 May 02:34	619	CM			125.5	193	792	
	05 May 03:13	620	CM			126.0	192	791	
	06 May 03:53	621	m	F	Drill Windjana	126.5	192	790	
	07 May 04:33	622	C	A	APXS Windjana, SAM preconditioning	127.0	192	790	
	08 May 05:12	623		IS	CHIMRA Windjana, drop to CheMin, CheMin Windjana 1	127.4	192	789	
	09 May 05:52	624	m	S	Drop to SAM, SAM Windjana 1	127.9	193	790	
	10 May 06:31	625			CheMin Windjana	128.4	193	789	
	11 May 07:11	626	CM			128.9	193	787	0.35
	12 May 07:51	627	C	AP	In-situ Stephen, MAHLI drill hole & tailings, selfie+	129.4	193	787	0.38
13 May 08:30	628	Cm		MAHLI drill hole	129.9	192	788	0.35	
14 May 09:10	629		A	In-situ Stephen	130.4	191	787		
Drive toward Mt Sharp with wheel imaging	15 May 09:49	630	Cm		Dr 25m to 31/1336 · el+21m · 06342m · toward Mt Sharp, CheMin Windjana 1	130.9	192	784	
	16 May 10:29	631	M	W	Dr 27m to 31/1478 · el+22m · 06369m · toward Mt Sharp, MAHLI wheels, CheMin Windjana 1	131.4	194	783	0.35
	17 May 11:09	632	CM		CheMin Windjana 1	131.9	194	783	
	18 May 11:48	633	m	AW	In-situ Wift, MAHLI wheels	132.4	193	780	0.43
	19 May 12:28	634	m		Dr 69m to 32/0006 · el+25m · 06437m · toward Mt Sharp	132.9	193	780	
	20 May 13:07	635	CM	W	Dr 75m to 32/0484 · el+25m · 06512m · toward Mt Sharp, MAHLI wheels, Phobos night	133.4	193	780	
	21 May 13:47	636	Cm	W	Dr 59m to 32/0800 · el+26m · 06572m · toward Mt Sharp, MAHLI wheels	133.9	193	778	
	22 May 14:26	637	CM	W	Dr 40m to 32/1026 · el+26m · 06612m · toward Mt Sharp, SAM atmos, MAHLI wheels	134.4	195	779	
	23 May 15:06	638	C		SAM atmos	134.9	194	778	
	24 May 15:46	639	C			135.4	194	777	0.33
	25 May 16:25	640	CM	SW	Dr 1m to 33/0006 · el+26m · 06613m · for MAHLI full wheel 1-4 of 5, Drop to CheMin, CheMin Windjana 2	135.9	194	774	
26 May 17:05	641	cM	W	Dr 40m to 33/0040 · el+26m · 06654m · toward Mt Sharp, MAHLI full wheel complete	136.4	194	774		
Drive toward Mt Sharp	27 May 17:44	642	C			136.9	195	775	
	28 May 18:24	643	cM		Dr 85m to 33/0314 · el+22m · 06739m · toward Mt Sharp	137.4	195	775	
	29 May 19:04	644	m		Dr 104m to 33/0666 · el+25m · 06843m · toward Mt Sharp	137.9	195	774	
	30 May 19:43	645	C			138.4	193	772	0.34
	31 May 20:23	646	CM	W	Dr 31m to 33/1042 · el+27m · 06874m · toward Mt Sharp, MAHLI wheels	138.9	194	771	
	01 Jun 21:02	647	M			139.4	195	773	0.38
	02 Jun 21:42	648	C			139.9	195	776	
	03 Jun 22:22	649	m	A	Dr 57m to 34/0006 · el+26m · 06931m · toward Mt Sharp, in-situ Furnace Flats	140.5	196	776	
	04 Jun 23:01	650	M		SAM getter/scrubber cleanup, Mercury transit	141.0	194	774	0.50
	05 Jun 23:41	651	M		Dr 32m to 34/0292 · el+27m · 06963m · toward Mt Sharp with MARDI sidewalk mode test, CheMin Windjana 2	141.5	194	776	
	07 Jun 00:20	652	C		SAM preconditioning	142.0	195	779	0.42
08 Jun 01:00	653	m	SW	Drop to SAM, SAM Windjana 2, MAHLI wheels & sky	142.5	195	779		
09 Jun 01:39	654	Cm			143.0	196	776		
10 Jun 02:19	655	cM		Dr 86m to 34/0422 · el+28m · 07048m · toward Mt Sharp	143.5	197	771		
11 Jun 02:59	656	Cm		Dr 46m to 34/0780 · el+27m · 07094m · toward Mt Sharp, CheMin Windjana 2	144.0	196	769		

Area	Noon UTC	Sol	RS	Arm	Activity Summary	Ls	T	P	Tau
	12 Jun 03:38	657	Cm		Dr 121m to 34/1126 · el+28m · 07215m · toward Mt Sharp	144.6	196	769	0.52
	13 Jun 04:18	658	CM		Dr 34m to 35/0006 · el+27m · 07249m · toward Mt Sharp	145.1	196	768	
	14 Jun 04:57	659	CM			145.6	196	768	0.64
	15 Jun 05:37	660	m	W	Dr 1m to 35/0244 · el+27m · 07250m · for MAHLI full wheel, CheMin dark frame, MAHLI REMS UV	146.1	196	764	
	16 Jun 06:17	661	m		Dr 138m to 35/0268 · el+26m · 07388m · toward Mt Sharp	146.6	199	763	0.74
	17 Jun 06:56	662	cm		Dr 133m to 35/1004 · el+31m · 07521m · toward Mt Sharp, Phobos night	147.2	199	763	
	18 Jun 07:36	663	CM		Dr 25m to 36/0006 · el+32m · 07546m · toward Mt Sharp	147.7	196	761	
	19 Jun 08:15	664	CM		Dr 67m to 36/0184 · el+32m · 07613m · toward Mt Sharp	148.2	196	758	
	20 Jun 08:55	665	cM		Dr 143m to 36/0422 · el+30m · 07755m · toward Mt Sharp	148.7	197	764	0.83
	21 Jun 09:34	666	CM		MAHLI CheMin inlet	149.2	197	769	
	22 Jun 10:14	667	m	W	Dr 1m to 36/1152 · el+30m · 07756m · for MAHLI full wheel	149.8	198	771	
	23 Jun 10:54	668	cm		Dr 105m to 36/1176 · el+29m · 07862m · toward Mt Sharp	150.3	199	770	0.73
	24 Jun 11:33	669	Cm		Dr 39m to 37/0006 · el+33m · 07900m · toward Mt Sharp	150.8	197	772	
	25 Jun 12:13	670	cm		Dr 107m to 37/0298 · el+31m · 08008m · toward Mt Sharp	151.4	196	778	
	26 Jun 12:52	671	Cm		Dr 117m to 37/1076 · el+28m · 08124m · toward Mt Sharp	151.9	197	779	
	27 Jun 13:32	672	CM		Dr 82m to 37/1548 · el+27m · 08206m · toward Mt Sharp, embedding in ripple, exiting landing ellipse	152.4	196	777	0.69
	28 Jun 14:12	673	M	A	In-situ Sourdough, SAM scrubber cleanup	152.9	195	778	
	29 Jun 14:51	674	m		Dr 5m to 38/0006 · el+27m · 08212m · to back out of ripple after MAHLI Sourdough	153.5	194	779	
	30 Jun 15:31	675			SAM cleaning activities	154.0	195	782	
	01 Jul 16:10	676	cM		Dr 16m to 38/0064 · el+27m · 08228m · toward Mt Sharp	154.5	195	780	
	02 Jul 16:50	677	cM		Dr 20m to 38/0208 · el+28m · 08248m · toward Mt Sharp	155.1	196	776	
	03 Jul 17:30	678	M		Dr 67m to 38/0344 · el+29m · 08314m · toward Mt Sharp	155.6	198	775	
	04 Jul 18:09	679	M	W	Dr 1m to 38/0798 · el+29m · 08315m · for MAHLI full wheel	156.1	199	777	
	05 Jul 18:49	680			Runout (planned for Independence Day holiday)	156.7	199	780	
	06 Jul 19:28	681			Runout (planned for Independence Day holiday)	157.2	197	782	
	07 Jul 20:08	682			Runout (planned for Independence Day holiday)	157.8	197	786	
	08 Jul 20:47	683	m		Dr 52m to 38/0822 · el+30m · 08368m · toward Mt Sharp, sand ripple crossing test, SAM atmos	158.3	197	784	
	09 Jul 21:27	684			Recharge batteries, SAM getter/scrubber cleanup	158.8	198	781	
	10 Jul 22:07	685	Cm		Dr 60m to 38/1272 · el+33m · 08428m · toward Mt Sharp, SAM sample reheat	159.4	199	780	0.70
	11 Jul 22:46	686	C		Rear Hazcam thermal characterization activity	159.9	198	779	
	12 Jul 23:26	687	c	A	In-situ Nova, CheMin Windjana 2, MAHLI video of ChemCam plume	160.5	197	781	
	14 Jul 00:05	688	m		Dr 82m to 39/0006 · el+36m · 08511m · toward Mt Sharp	161.0	197	786	
	15 Jul 00:45	689	cm		Dr 10m to 39/0450 · el+37m · 08520m · toward Mt Sharp	161.6	198	785	
	16 Jul 01:25	690	cm		Dr 30m to 39/0522 · el+39m · 08550m · toward Mt Sharp	162.1	198	784	
	17 Jul 02:04	691	cm		Dr 24m to 39/0732 · el+40m · 08574m · toward Mt Sharp with MARDI sidewalk mode	162.7	198	782	
	18 Jul 02:44	692	cM		Dr 31m to 39/0930 · el+41m · 08605m · toward Mt Sharp, SAM preconditioning	163.2	199	783	
	19 Jul 03:23	693			Runout (planned for battery charging)	163.8	198	782	
	20 Jul 04:03	694	CM	AS	In-situ South Park, CheMin Windjana 2, triple drop to SAM	164.3	198	782	
	21 Jul 04:43	695	m	W	Dr 23m to 39/1182 · el+41m · 08628m · toward Mt Sharp, MAHLI wheels	164.9	198	780	
	22 Jul 05:22	696	M	A	Dr 20m to 39/1402 · el+43m · 08648m · toward Mt Sharp after in-situ Wildrose, MAHLI Surprise; RCE maintenance	165.4	198	784	0.84
	23 Jul 06:02	697			Runout (RCE-A anomaly)	166.0	200	785	
	24 Jul 06:41	698			Runout (RCE-A anomaly)	166.5	198	785	
	25 Jul 07:21	699			Runout (RCE-A anomaly)	167.1	199	787	

Area	Noon UTC	Sol	RS	Arm	Activity Summary	LS	T	P	Tau
Confidence Hills (Pahrump drill campaign 1)	09 Sep 13:02	744	CM	W	Dr 32m to 41/1336 · el+42m · 09198m · through Amargosa Valley with MAHLI full wheel	193.1		827	
	10 Sep 13:42	745	C		Rear Hazcam thermal characterization, CheMin dump, CheMin empty cell	193.7	204	827	0.75
	11 Sep 14:21	746	CM		Dr 8m to 41/1576 · el+42m · 09206m · through Amargosa Valley	194.3	204	829	
	12 Sep 15:01	747	M		Dr 92m to 41/1648 · el+40m · 09298m · through Amargosa Valley	194.9	202	831	
	13 Sep 15:41	748	M		Dr 23m to 42/0006 · el+41m · 09321m · through Amargosa Valley	195.5	201	831	
	14 Sep 16:20	749			Runout (planned)	196.1	201	832	
	15 Sep 17:00	750			Runout (planned)	196.7	202	836	
	16 Sep 17:39	751	cM		Dr 114m to 42/0192 · el+41m · 09435m · through Amargosa Valley	197.4	204	838	
	17 Sep 18:19	752	cM		Rear Hazcam thermal characterization, CheMin dump	198.0	202	840	0.82
	18 Sep 18:59	753	M		Dr 22m to 42/0858 · el+40m · 09458m · through Amargosa Valley, SAM atmos	198.6	201	841	
	19 Sep 19:38	754	Cm		ChemCam cal	199.2	201	841	0.73
	20 Sep 20:18	755	m	AB	Brush & in-situ Maturango	199.8	201	845	
	21 Sep 20:57	756	m	D	Mini-drill Confidence Hills w/MAHLI before & after	200.4	202	845	
	22 Sep 21:37	757			Runout (planned)	201.0	201	845	
	23 Sep 22:17	758	CM	AB	Brush & in-situ Moenkopi, in-situ Mammoth, MAHLI wheels	201.6	201	851	0.77
	24 Sep 22:56	759		AF	Drill Confidence Hills w/MAHLI before & after, in-situ mini-drill tailings	202.2	203	854	
	25 Sep 23:36	760			Runout (inertial measurement unit sick)	202.9	202	852	
	27 Sep 00:15	761			Engineering activities (cold patch), SAM getter/scrubber cleanup	203.5	201	856	
	28 Sep 00:55	762	CM	AI	CHIMRA Confidence Hills, APXS Paradox (Confidence Hills drill tailings)	204.1	203	853	
	29 Sep 01:34	763			SAM noble gas analysis	204.7	204	855	
	30 Sep 02:14	764			Runout (planned)	205.3	203	860	
	01 Oct 02:54	765		Su	Drop Confidence Hills to CheMin, dump pre-sieve, MAHLI Paradox & dump pile, arm fault	206.0	203	863	
	02 Oct 03:33	766	CM		CheMin Confidence Hills	206.6	202	862	0.91
	03 Oct 04:13	767	Cm	AB	Brush & in-situ Morrison, in-situ pre-sieve dump	207.2	202	866	
	04 Oct 04:52	768			SAM preconditioning & blank, MAHLI drill hole & tailings, arm fault (MAHLI cover open)	207.8	203	864	
	05 Oct 05:32	769			SAM EGA blank	208.4	204	871	
	06 Oct 06:12	770			SAM preconditioning	209.1	204	868	
	07 Oct 06:51	771	CM		CheMin Confidence Hills, MAHLI cover close recovery	209.7	202	879	
	08 Oct 07:31	772	cM		Engineering activities (cold patch), prepare for Siding Spring, Deimos night	210.3	203	881	
	09 Oct 08:10	773	CM	S	Drop to SAM, SAM Confidence Hills 1	210.9	203	879	
10 Oct 08:50	774		A	APXS Morrison, MAHLI CheMin inlet, arm fault (MAHLI cover open)	211.6	204	880		
11 Oct 09:30	775				212.2	204	880		
12 Oct 10:09	776	CM		CheMin Confidence Hills	212.8	203	882	0.89	
13 Oct 10:49	777	cm		CheMin Confidence Hills, prepare for Siding Spring, Deimos night, MAHLI cover close recovery & drill hole	213.4	202	881		
14 Oct 11:28	778	CM		CheMin Confidence Hills	214.1	203	888		
15 Oct 12:08	779	Cm	A	APXS Morrison	214.7	203	885	0.88	
16 Oct 12:47	780	CM		Dr 22m to 43/0006 · el+42m · 09480m · toward Book Cliffs, MARDI sidewalk	215.3	205	892		
Pahrump walkabout 1	17 Oct 13:27	781	CM	UX	Siding Spring, dump sample, CHIMRA thwackless clean	216.0	206	894	1.02
	18 Oct 14:07	782	CM	A	Siding Spring, APXS Confidence Hills dump, SAM electrical baseline test	216.6	206	898	
	19 Oct 14:46	783	cM		Siding Spring	217.2	204	900	
	20 Oct 15:26	784	m		Siding Spring	217.9	205	904	
	21 Oct 16:05	785	Cm		Dr 6m to 44/0006 · el+42m · 09486m · toward Book Cliffs, CheMin Confidence Hills, MARDI sidewalk	218.5	205	901	
	22 Oct 16:45	786	Cm		Thermal characterization	219.1	205	900	1.32
	23 Oct 17:25	787	CM		Dr 19m to 44/0042 · el+43m · 09504m · toward Gilbert Peak, MARDI sidewalk	219.8	207	901	

372 Appendix: Curiosity Activity Summary

Area	Noon UTC	Sol	RS	Arm	Activity Summary	LS	T	P	Tau
Ripple scuff	24 Oct 18:04	788	C			220.4	206	904	1.42
	25 Oct 18:44	789	CM			221.1	206	902	
	26 Oct 19:23	790	m		Dr 7m to 44/0196 · el+44m · 09511m · toward Alexander Hills, MARDI sidewalk	221.7	206	896	
	27 Oct 20:03	791	c			222.3	207	907	
	28 Oct 20:43	792	CM		Dr 16m to 44/0262 · el+45m · 09527m · toward Chinle, MARDI sidewalk	223.0	206	911	
	29 Oct 21:22	793	CM			223.6	208	917	1.36
	30 Oct 22:02	794	CM		Dr 30m to 44/0376 · el+47m · 09557m · toward Whale Rock, MARDI sidewalk, CheMin dump, CheMin standard	224.2	207	915	
	31 Oct 22:41	795	c			224.9	207	916	
	01 Nov 23:21	796	CM			225.5	208	917	1.48
	03 Nov 00:00	797	M		Dr 53m to 44/0574 · el+40m · 09610m · toward Whale Rock, MARDI sidewalk	226.2	207	921	
	04 Nov 00:40	798			Runout (planned)	226.8	206	925	
	05 Nov 01:20	799	cm		Dr 11m to 44/0926 · el+39m · 09621m · to and scuff Pahrump sand	227.5	207	922	1.51
	06 Nov 01:59	800			MAVEN relay test	228.1	206	925	
	07 Nov 02:39	801	CM	A	APXS Kelso	228.7	205	924	1.51
08 Nov 03:18	802		A	In-situ Dumont, MAHLI Kelso & Garlock	229.4	205	930		
Shoemaker	09 Nov 03:58	803	M	W	Dr 10m to 44/1146 · el+40m · 09631m · toward Shoemaker with MAHLI full wheel	230.0	205	930	1.46
	10 Nov 04:38	804				230.7	206	931	1.45
	11 Nov 05:17	805	m	AB	Brush & in-situ Pelona, in-situ Ricardo	231.3	207	933	
	12 Nov 05:57	806	m	AB	Brush & in-situ Ricardo, MAHLI Pelona	232.0	206	936	1.39
Pink Cliffs	13 Nov 06:36	807	M		Dr 17m to 44/1288 · el+41m · 09648m · toward Pink Cliffs	232.6	206	936	
	14 Nov 07:16	808	m	AB	Brush & in-situ Rosamond, MAHLI ChemCam & REMS UV	233.3	206	937	1.46
	15 Nov 07:55	809	m	AB	Brush & in-situ Mojave	233.9	206	939	
	16 Nov 08:35	810	M	A	In-situ Potatoe, MAHLI Pilot Knob Valley	234.6	207	939	1.42
	17 Nov 09:15	811			RCE characterization activity	235.2	207	943	
	18 Nov 09:54	812	M		Dr 12m to 44/1438 · el+42m · 09660m · to Book Cliffs	235.9	206	944	
Book Cliffs	19 Nov 10:34	813	m	AB	Brush & in-situ Punchbowl, MAHLI Old Dad Mountain, Afton Canyon	236.5	207	948	
	20 Nov 11:13	814	m	AB	Brush & in-situ Afton Canyon, MAHLI Afton Canyon, Anaverde, Topanga	237.2	205	945	1.30
	21 Nov 11:53	815	Cm	AB	Brush & in-situ Topanga, MAHLI Jail Canyon, Goblin Valley, Topanga	237.8	205	945	
	22 Nov 12:33	816	CM			238.5	205	947	
Alexander Hills	23 Nov 13:12	817	CM		Dr 36m to 44/1552 · el+44m · 09695m · toward Alexander Hills	239.1	206	956	1.19
	24 Nov 13:52	818			Battery and thermal characterization, SAM electrical baseline test	239.8	206	955	
	25 Nov 14:31	819	CM	AB	Brush & in-situ Mescal, MAHLI Cajon & Puente	240.4	207	956	
	26 Nov 15:11	820	C	A	APXS Mescal	241.1	206	952	1.29
	27 Nov 15:51	821	cM		SAM preparation activity	241.7	206	954	
	28 Nov 16:30	822	M		SAM derivatization activity part 1	242.4	207	950	
	29 Nov 17:10	823	C		SAM derivatization activity part 2	243.0	206	950	
	30 Nov 17:49	824	m	AB	Brush & in-situ Puente	243.7	206	958	
	01 Dec 18:29	825		A	In-situ cal	244.3	206	957	
	02 Dec 19:08	826	CM		Dr 26m to 44/1834 · el+45m · 09721m · toward Chinle, MAHLI cal	245.0	206	955	
	Chinle	03 Dec 19:48	827				245.6	207	954
04 Dec 20:28		828	CM	AB	Brush & in-situ Pickhandle, MAHLI Chinle mosaic, Goldstone, sky	246.3	206	954	
05 Dec 21:07		829	c		ChemCam diagnostics	246.9	206	950	
06 Dec 21:47		830	m	AB	Brush & in-situ Goldstone, MAHLI Pickhandle & Goldstone, SAM atmos	247.6	205	954	
07 Dec 22:26		831		A	APXS Goldstone	248.2	205	954	

Appendix: Curiosity Activity Summary 373

Area	Noon UTC	Sol	RS	Arm	Activity Summary	LS	T	P	Tau
Whale Rock	08 Dec 23:06	832	CM		Battery characterization	248.9	205	959	
	09 Dec 23:46	833	C	A	In-situ Tropic, MAHLI Tropic & Coachella	249.5			
	11 Dec 00:25	834	m	W	CheMin empty cell analysis, MAHLI wheels	250.2	204	956	1.03
	12 Dec 01:05	835	Cm		Dr 32m to 44/2068 · el+47m · 09753m · toward Whale Rock, SAM hydrocarbon trap cleaning	250.8	204	957	
	13 Dec 01:44	836			SAM gas chromatograph cleaning	251.5	205	955	
	14 Dec 02:24	837	CM		Dr 5m to 44/2342 · el+48m · 09758m · to Whale Rock, SAM EGA blank	252.1	205	956	
	15 Dec 03:04	838	Cm			252.8	205	961	1.12
	16 Dec 03:43	839			SAM EGA blank	253.5	205	958	1.13
	17 Dec 04:23	840	CM	XW	MAHLI San Andreas, Tecoya, San Bernardino, Gem Hill, wheels; CHIMRA clean	254.1	205	957	
	18 Dec 05:02	841			Runout (DSN failure to uplink command load)	254.8	205	957	
	19 Dec 05:42	842	CM	AW	In-situ San Andreas, MAHLI Santa Ana & wheel stability	255.4	204	955	
	20 Dec 06:21	843	CM			256.1	205	955	1.10
	21 Dec 07:01	844	M	AB	Brush & APXS Santa Ana	256.7	205	959	
	22 Dec 07:41	845	M			257.4	205	961	
	23 Dec 08:20	846			Runout (planned holiday break)	258.0	206	964	
	24 Dec 09:00	847			Runout (planned holiday break)	258.7	204	958	
	25 Dec 09:39	848			Runout (planned holiday break)	259.3	204	958	
	26 Dec 10:19	849			Runout (planned holiday break)	260.0	204	961	
	27 Dec 10:59	850			Runout (planned holiday break)	260.6	205	957	
	28 Dec 11:38	851			Runout (planned holiday break)	261.3	206	960	
	29 Dec 12:18	852			Runout (planned holiday break)	261.9	205	957	
	30 Dec 12:57	853	Cm	AB	Brush & APXS Tecoya, MAHLI focus merge test	262.6	207	960	
	31 Dec 13:37	854	C	A	APXS Sierra Nevada	263.2	206	957	1.38
	01 Jan 14:17	855	M		SAM electrical baseline test, HAPPY NEW YEAR 2015!	263.9	205	956	
	02 Jan 14:56	856			Runout (planned holiday break)	264.5	205	954	
	03 Jan 15:36	857			Runout (planned holiday break)	265.2	208	950	
	04 Jan 16:15	858			Runout (planned holiday break)	265.8	207	954	
	05 Jan 16:55	859			Runout (planned holiday break)	266.5	207	958	
	06 Jan 17:34	860			MAHLI Sierra Nevada, Santa Ana, Tecoya	267.1	204	956	
	07 Jan 18:14	861	Cm			267.8	204	956	
	08 Jan 18:54	862	M		Dr 69m to 44/2420 · el+41m · 09827m · toward Pink Cliffs	268.4	204	957	
09 Jan 19:33	863	C			269.1	203	957	0.93	
10 Jan 20:13	864	CM		Dr 4m to 44/2964 · el+41m · 09832m · to Mojave, SAM trap cleanup	269.7	203	955		
11 Jan 20:52	865			SAM methane experiment	270.4	203	952		
12 Jan 21:32	866	C			271.0	203	951	0.86	
13 Jan 22:12	867	m	AD	Mini-drill Mojave w/MAHLI before & after, APXS after	271.7	203	951		
14 Jan 22:51	868	M	P	MAHLI selfie	272.3	204	951		
15 Jan 23:31	869	C		MAHLI Mojave Chunk	272.9	203	947		
17 Jan 00:10	870			Runout (planned)	273.6	206	946		
18 Jan 00:50	871	C	A	APXS Mojave Chunk, RCE maintenance	274.2	204	945		
19 Jan 01:29	872	CM			274.9	203	943	0.91	
20 Jan 02:09	873			Runout (planned)	275.5	203	946		
21 Jan 02:49	874			FSW transition	276.2				
22 Jan 03:28	875			FSW transition	276.8				

FSW transition

374 Appendix: Curiosity Activity Summary

Area	Noon UTC	Sol	RS	Arm	Activity Summary	LS	T	P	Tau
	23 Jan 04:08	876			FSW transition	277.4			
	24 Jan 04:47	877			FSW transition	278.1			
	25 Jan 05:27	878			FSW transition	278.7			
	26 Jan 06:07	879			Runout (planned)	279.4			
Mojave	27 Jan 06:46	880	m	AB	Brush & in-situ Mojave 2, MAHLI pre-brush, post-brush, & Chunk, drill preload	280.0			
	28 Jan 07:26	881		AD	Mini-drill Mojave 2 w/MAHLI before & after, APXS drill hole, MAHLI full drill location & REMS UV	280.6	202	934	
	29 Jan 08:05	882		FP	Drill Mojave 2 w/MAHLI before & after, MAHLI selfie+	281.3	204	942	
	30 Jan 08:45	883	CM		MAHLI Mojave 2 drill hole & tailings	281.9	203	934	
	31 Jan 09:25	884		AIPS	CHIMRA Mojave, drop to CheMin, CheMin Mojave, in-situ drill hole, MAHLI selfie+	282.6	202	934	
	01 Feb 10:04	885			Runout (planned)	283.2	203	933	
	02 Feb 10:44	886	CM		SAM preconditioning	283.8	204	932	0.86
	03 Feb 11:23	887		S	Dump pre-sieve sample, drop to SAM, SAM Mojave 1	284.5	203	931	
	04 Feb 12:03	888		A	In-situ Mojave pre-sieve dump, MAHLI San Francisquito	285.1	204	934	
	05 Feb 12:42	889	CM	Au	In-situ San Francisquito, MAHLI pre-sieve dump	285.7	203	933	
	06 Feb 13:22	890	CM		CheMin Mojave	286.4	202	931	0.77
	07 Feb 14:02	891		S	Triple drop to SAM (doggy bag Mojave)	287.0	202	930	
	08 Feb 14:41	892	CM	S	Triple drop to SAM (doggy bag Mojave)	287.6	203	933	0.97
	09 Feb 15:21	893		C		288.3	203	928	
Dhive	10 Feb 16:00	894	CM	AUX	Dump Mojave, APXS dump pile, CheMin Mojave, CHIMRA clean	288.9	204	930	
	11 Feb 16:40	895	CM		MAHLI dump pile, drill hole, CheMin inlet	289.5	202	927	
	12 Feb 17:20	896	CM		Dr 17m to 45/0006 · el+42m · 09849m · toward Telegraph Peak	290.1	203	928	
	13 Feb 17:59	897		C	CheMin empty cell analysis	290.8	202	924	0.78
	14 Feb 18:39	898	CM			291.4	202	923	
	15 Feb 19:18	899	CM			292.0	203	922	
	16 Feb 19:58	900	CM			292.6	204	923	
	17 Feb 20:38	901	CM		Dr 28m to 45/0156 · el+47m · 09876m · toward Telegraph Peak	293.3	204	921	
	18 Feb 21:17	902				293.9	204	921	
	19 Feb 21:57	903	CM		Dr 7m to 45/0372 · el+47m · 09883m · to Telegraph Peak, SAM cleanup	294.5	203	918	
	20 Feb 22:36	904	CM			295.1	204	915	0.77
	21 Feb 23:16	905	CM	AB	Brush & in-situ Telegraph Peak, MAHLI future drill site, MAHLI dust cover focus test, SAM engineering test	295.8	202	917	
	22 Feb 23:55	906	CM			296.4	202	914	
	24 Feb 00:35	907		M		297.0	203	912	0.74
Telegraph Peak	25 Feb 01:15	908		F	Drill Telegraph Peak w/MAHLI before & after	297.6	203	920	
	26 Feb 01:54	909	CM		SAM QMS atmos	298.2	204	915	
	27 Feb 02:34	910		C	MAHLI drill hole & tailings	298.9	202	914	
	28 Feb 03:13	911			ANOMALIES PRECLUDE SCIENCE (battle short in drill percussion)	299.5	202	910	
	01 Mar 03:53	912			ANOMALIES PRECLUDE SCIENCE (battle short in drill percussion)	300.1	204	910	
	02 Mar 04:33	913			ANOMALIES PRECLUDE SCIENCE (battle short in drill percussion)	300.7	202	908	
	03 Mar 05:12	914	CM		Mars Express relay demonstration	301.3	203	908	0.79
	04 Mar 05:52	915	CM		Drill battle short checkout	301.9	202	912	
	05 Mar 06:31	916	CM		Drill battle short checkout, SAM electrical baseline test	302.5	202	912	0.74
	06 Mar 07:11	917	CM		Mastcam focus characterization test, HRS maintenance	303.1	202	907	0.92
Battle short anomaly	07 Mar 07:51	918	CM		Mastcam focus characterization test, prime RCE parameter dump, drill diag	303.8	203	901	0.77
	08 Mar 08:30	919	CM			304.4	203	906	0.76

Area	Noon UTC	Sol	RS	Arm	Activity Summary	LS	T	P	Tau	
	09 Mar 09:10	920			Thermal characterization of RPAM	305.0	202	905		
	10 Mar 09:49	921	CM			305.6	203	900		
	11 Mar 10:29	922	Cm	AIS	CHIMRA Telegraph Peak, drop to CheMin, CheMin Telegraph Peak, APXS tailings	306.2	201	907		
	12 Mar 11:08	923	m		Dr 10m to 45/0456 · el+49m · 09893m · away from Pahrump Hills	306.8	203	909		
Dive	13 Mar 11:48	924	CM		Dr 9m to 45/0564 · el+49m · 09902m · toward Garden City	307.4	202	905	0.80	
	14 Mar 12:28	925	CM		CheMin Telegraph Peak	308.0	202	900	0.79	
	15 Mar 13:07	926	CM		Dr 6m to 45/0780 · el+50m · 09907m · to Garden City	308.6	202	902	0.79	
	16 Mar 13:47	927	m			309.2	202	900	0.75	
	17 Mar 14:26	928	m	S	SAM preconditioning, drop to SAM, SAM EGA Telegraph Peak 1	309.8	203	899		
	18 Mar 15:06	929	CM			310.4	203	903	0.70	
	19 Mar 15:46	930	C	Au	In-situ Coalville, MAHLI Indianola & arm motion damping expt, dump pre-sieve sample	311.0	203	903		
	20 Mar 16:25	931	M		Arm fault	311.6	203	900	0.79	
Garden City	21 Mar 17:05	932			Limited due to arm fault discovered late	312.2	203	891		
	22 Mar 17:44	933			Limited due to arm fault discovered late	312.8	202	898		
	23 Mar 18:24	934			Limited due to arm fault discovered late	313.4	203	892		
	24 Mar 19:04	935	CM	A	In-situ Alvord Mountain, MAHLI Indianola	314.0	203	896	0.75	
	25 Mar 19:43	936	Cm	AB	APXS Indianola, brush & MAHLI Hyrum	314.6	203	906		
	26 Mar 20:23	937	Cm	A	In-situ Live Oak Canyon, APXS Alvord Mountain & Hyrum, MAHLI back of Coalville	315.2	203	898	0.92	
	27 Mar 21:02	938	CM		MAHLI Alvord Mountain	315.8				
	28 Mar 21:42	939	CM	W	Dr 1m to 45/0858 · el+50m · 09908m · for MAHLI full wheel 1-3 of 5	316.3				
	29 Mar 22:21	940	M	W	Dr 14m to 45/0870 · el+50m · 09922m · to Kanosh, completing MAHLI full wheel, CheMin Telegraph Peak	316.9	202	913		
	30 Mar 23:01	941	Cm		SAM diagnostics	317.5	203	913	0.90	
	31 Mar 23:41	942	Cm	A	In-situ Little Devil, MAHLI Devils Punchbowl (both on Kanosh cobble)	318.1	203	910		
	02 Apr 00:20	943	CM			318.7	203	904		
	03 Apr 01:00	944	CM		Dr 13m to 45/1002 · el+50m · 09935m · to Garden City, CheMin Telegraph Peak, HRS maintenance	319.3	203	900		
	04 Apr 01:39	945	Cm			319.9	202	899	0.99	
	05 Apr 02:19	946	CM		MAHLI Kern Peak, vein mosaic	320.4	202	896		
	06 Apr 02:59	947	CM			321.0	204	897	0.90	
	07 Apr 03:38	948	C	A	In-situ Amboy & Kern Peak, MAHLI vein mosaic, CheMin Telegraph Peak	321.6	203	901		
	Drive toward Logan Pass	08 Apr 04:18	949	M		Dr 23m to 45/1114 · el+51m · 09958m · along Artist's Drive	322.2	203	895	
		09 Apr 04:57	950	M		Dr 37m to 45/1282 · el+51m · 09995m · along Artist's Drive, thermal characterization RPAM	322.8	202	894	0.89
10 Apr 05:37		951	cM		Dr 18m to 45/1564 · el+50m · 10013m · toward Logan Pass	323.3	201	890		
11 Apr 06:16		952	cM		Dr 90m to 45/1702 · el+48m · 10103m · around ripple field, rear Hazcam thermal characterization	323.9	202	887		
12 Apr 06:56		953	CM		ChemCam focus test	324.5	202	887	0.87	
13 Apr 07:36		954	m	ASUX	Drop to SAM (doggy bag Telegraph Peak), dump sample, in-situ dump pile, MAHLI REMS UV, CHIMRA thwackless clean	325.1	203	886	0.84	
14 Apr 08:15		955	CM	AW	In-situ La Brea, MAHLI wheels	325.6	203	886		
15 Apr 08:55		956	CM		Dr 65m to 46/0006 · el+49m · 10168m · toward Logan Pass, Mastcam sunset & Mercury transit	326.2			0.93	
16 Apr 09:34		957	CM		Dr 64m to 46/0478 · el+46m · 10231m · toward Logan Pass, SAM electrical baseline test	326.8				
17 Apr 10:14		958	CM	W	Dr 22m to 46/0940 · el+47m · 10253m · toward Logan Pass, MAHLI wheels, SAM cleaning	327.4	199	888		
18 Apr 10:54		959	CM		Rear Hazcam thermal characterization	327.9	200	885		
19 Apr 11:33		960	m		Dr 102m to 46/1168 · el+44m · 10356m · toward Logan Pass	328.5	200	884		
20 Apr 12:13		961	Cm			329.1	202	890	0.89	
21 Apr 12:52		962	M	W	Dr 1m to 46/1682 · el+44m · 10357m · for MAHLI full wheel 1-4 of 5	329.6	201	885	0.86	

376 Appendix: Curiosity Activity Summary

Area	Noon UTC	Sol	RS	Arm	Activity Summary	LS	T	P	Tau
	22 Apr 13:32	963	Cm	W	Dr 17m to 46/1716 · el+45m · 10374m · toward Logan Pass, completing MAHLI full wheel	330.2	202	891	
	23 Apr 14:12	964	CM		Dr 32m to 46/1818 · el+45m · 10406m · toward Logan Pass after Phobos eclipse & Phobos-Deimos together	330.8	201	889	
	24 Apr 14:51	965	C		SAM atmos	331.3	202	889	
	25 Apr 15:31	966	Cm			331.9	203	902	0.98
	26 Apr 16:10	967			Dr 89m to 47/0006 · el+44m · 10496m · toward Logan Pass, CheMin sample dump, CheMin empty cell analysis	332.4	202	894	
	27 Apr 16:50	968	C			333.0	201	901	
	28 Apr 17:29	969	M			333.6	202	898	
	29 Apr 18:09	970	CM		HRS maintenance, Phobos eclipse	334.1	201	898	
	30 Apr 18:49	971	Cm	W	Dr 6m to 47/0528 · el+44m · 10502m · to Big Fork, MAHLI wheels, CheMin empty cell analysis	334.7	204	894	1.23
	01 May 19:28	972	C		SAM getter/scrubber cleanup	335.2	202	888	
	02 May 20:08	973	C		CheMin cleaning & blank	335.8	202	882	
	03 May 20:47	974	A		In-situ Big Fork, MAHLI Albert	336.3	202	883	
	04 May 21:27	975	Cm	AB	Brush & in-situ Albert	336.9	202	884	1.24
	Drive to & about Logan Pass	05 May 22:07	976	M		Dr 74m to 47/0604 · el+46m · 10576m · toward Jocko Butte, SAM noble gas analysis	337.5	202	886
06 May 22:46		977	Cm		SAM data transfer	338.0	203	884	
07 May 23:26		978	CM		Dr 2m to 47/1172 · el+46m · 10578m · toward Logan Pass, CheMin empty	338.6	202	883	
09 May 00:05		979	CM		Phobos eclipse	339.1	202	884	
10 May 00:45		980	Cm			339.6	200	883	
11 May 01:25		981	cM		Dr 28m to 47/1206 · el+49m · 10606m · toward Logan Pass, SAM gas chromatograph cleaning	340.2	201	884	1.18
12 May 02:04		982			Thermal characterization of RPAM-A	340.7	201	879	
13 May 02:44		983	Cm		Dr 21m to 47/1458 · el+50m · 10626m · toward Stimson Unit, ChemCam focus checkout part 1	341.3	201	879	1.09
14 May 03:23		984	M		Dr 18m to 47/1638 · el+52m · 10644m · toward Stimson Unit, CheMin cal standards	341.8	200	878	
15 May 04:03		985	CM		ChemCam focus checkout part 2	342.4	200	876	1.08
16 May 04:42		986	CM		Dr 9m to 48/0006 · el+51m · 10653m · toward Jocko Butte	342.9	200	877	
17 May 05:22		987	cM		Dr 43m to 48/0088 · el+46m · 10696m · toward Jocko Butte, battery thermal characterization, Phobos eclipse	343.5	200	876	
18 May 06:02		988	m		Battery thermal characterization, CheMin dark frame	344.0	200	876	1.06
19 May 06:41		989	Cm	AW	In-situ Spokane & cal, MAHLI REMS UV, wheels, sky	344.5	200	877	
20 May 07:21	990	CM		Dr 53m to 48/0464 · el+47m · 10749m · toward Jocko Biutte	345.1	201	876		
Drive to Marias Pass	21 May 08:00	991	CM		Dr 24m to 48/0882 · el+53m · 10773m · toward Marias Pass, backup radio checkout	345.6	200	875	
	22 May 08:40	992	CM		Dr 6m to 48/1152 · el+54m · 10779m · toward Marias Pass	346.2	200	877	
	23 May 09:20	993	M		Thermal characterization of RPAM	346.7	200	877	
	24 May 09:59	994	CM		CheMin dump	347.2	201	878	1.10
	25 May 10:39	995	M		Dr 34m to 48/1200 · el+54m · 10813m · toward Stimson-Pahrump contact at Missoula, Deimos eclipse	347.8	201	877	
	26 May 11:18	996			Runout (planned for Memorial Day)	348.3	201	877	
Missoula	27 May 11:58	997	CM		Dr 3m to 48/1536 · el+54m · 10816m · toward Stimson-Pahrump contact at Missoula	348.8		881	
	28 May 12:38	998	CM	AB	Brush & in-situ Ronan, Phobos eclipse	349.4	202	881	
	29 May 13:17	999	M	AB	Brush & in-situ Wallace, MAHLI Big Arm, HRS maintenance	349.9	200	881	1.00
Solar conjunction	30 May 13:57	1000	CM			350.4	200	876	1.01
	31 May 14:36	1001	CM		Stow arm for conjunction	350.9	200	876	0.97
	01 Jun 15:16	1002	M		Phobos eclipse, home cameras for conjunction	351.5	201	879	0.95
	02 Jun 15:55	1003	M		Home cameras for conjunction	352.0	201	877	0.94
	03 Jun 16:35	1004			Conjunction environmental science	352.5	200	876	
	04 Jun 17:15	1005			Conjunction environmental science	353.1	200	879	

Area	Noon UTC	Sol	RS	Arm	Activity Summary	Ls	T	P	Tau	
	05 Jun 17:54	1006			Conjunction environmental science	353.6	202	878		
	06 Jun 18:34	1007			Conjunction environmental science	354.1	202	879		
	07 Jun 19:13	1008			Conjunction environmental science	354.6	201	878		
	08 Jun 19:53	1009			Conjunction environmental science	355.1	200	882		
	09 Jun 20:33	1010			Conjunction environmental science	355.7	200	883		
	10 Jun 21:12	1011			Conjunction environmental science	356.2	200	880		
	11 Jun 21:52	1012			Conjunction environmental science	356.7	202	881		
	12 Jun 22:31	1013			Conjunction environmental science	357.2	202	882		
	13 Jun 23:11	1014			Conjunction environmental science	357.7	202	881		
	14 Jun 23:50	1015			Conjunction environmental science	358.3	200	885		
	16 Jun 00:30	1016			Conjunction environmental science	358.8	200	884		
	17 Jun 01:10	1017			Conjunction environmental science	359.3	200	886		
	18 Jun 01:49	1018			Conjunction environmental science	359.8	202	887		
	19 Jun 02:29	1019			Conjunction environmental science	0.3	202	886		
	20 Jun 03:08	1020			Conjunction environmental science	0.8	202	884		
	21 Jun 03:48	1021			Conjunction environmental science	1.3	200	888		
	22 Jun 04:28	1022			Conjunction environmental science	1.8	200	888		
	23 Jun 05:07	1023			Conjunction environmental science	2.4	200	888		
	24 Jun 05:47	1024			Conjunction environmental science	2.9	201	886		
	25 Jun 06:26	1025			Conjunction environmental science	3.4	201	885		
	26 Jun 07:06	1026			Post-conjunction engineering activities	3.9	201	886		
	27 Jun 07:46	1027	Cm		Post-conjunction engineering activities	4.4	199	886	0.94	
	Missoula	28 Jun 08:25	1028		A	In-situ Big Arm, MAHLI Stimson/Murray contact goniometer expt, CheMin inlet	4.9	199	887	
		29 Jun 09:05	1029	CM		ChemCam passive cal	5.4	199	891	0.90
		30 Jun 09:44	1030	CM		Dr 4m to 48/1576 - el+54m - 10820m - toward Missoula	5.9	198	888	
		01 Jul 10:24	1031	CM		MAHLI Missoula	6.4	199	887	0.94
		02 Jul 11:03	1032	CM	A	In-situ Lumpry, MAHLI Clark & Seeley, Phobos transit	6.9	199	888	0.91
03 Jul 11:43		1033	CM		SAM electrical baseline test	7.4	199	890	0.95	
04 Jul 12:23		1034	CM			7.9	198	894	0.90	
Drive east	05 Jul 13:02	1035	M		Dr 35m to 48/1606 - el+54m - 10855m - toward Elk, CheMin empty cell analysis	8.4	199	896	0.91	
	06 Jul 13:42	1036			Runout (planned for Independence Day holiday)	8.9	198	889		
	07 Jul 14:21	1037	CM		Dr 6m to 48/1912 - el+53m - 10861m - toward Elk, CheMin empty cell re-analysis, battery characterization	9.4	201	890	0.93	
08 Jul 15:01	1038	c		ChemCam cal, Mastcam sunspot, battery characterization	9.9	199	891	0.92		
Elk	09 Jul 15:41	1039	CM		Dr 0m to 48/1970 - el+53m - 10861m - toward Elk	10.4	199	893	0.92	
	10 Jul 16:20	1040	m			10.9	198	893	0.87	
	11 Jul 17:00	1041	CM	A	In-situ Lamoose, MAHLI Mosquito & REMS UV, motor control software update part 1	11.4	198	896	0.85	
12 Jul 17:39	1042	m		Dr 17m to 48/1976 - el+53m - 10878m - toward Marias Pass, SAM calibration cell	11.9	197	894	0.84		
West and east again toward Lion	13 Jul 18:19	1043	c		CheMin empty cell	12.4	200	894	0.83	
	14 Jul 18:59	1044	CM		Dr 9m to 48/2128 - el+53m - 10887m - toward Marias Pass, motor control software update part 2	12.9	199	896	0.83	
	15 Jul 19:38	1045	c			13.4	197	895	0.83	
	16 Jul 20:18	1046	CM	W	Dr 1m to 48/2206 - el+53m - 10888m - for MAHLI full wheel	13.9	198	897	0.86	
	17 Jul 20:57	1047	cM			14.3	197	898	0.83	
	18 Jul 21:37	1048	CM	X	CHIMRA dean, percussion checkout	14.8	197	897		
	19 Jul 22:16	1049	M		Dr 21m to 48/2230 - el+54m - 10909m - toward Lion	15.3	198	898	0.81	

378 Appendix: Curiosity Activity Summary

Area	Noon UTC	Sol	RS	Arm	Activity Summary	LS	T	P	Tau	
Buckskin	20 Jul 22:56	1050	C			15.8	197	897	0.77	
	21 Jul 23:36	1051	CM		Dr 6m to 48/2428 · el+54m · 10915m · toward Lion	16.3	197	899	0.79	
	23 Jul 00:15	1052	Cm		Engineering maintenance activities	16.8	197	897	0.80	
	24 Jul 00:55	1053	CM		Dr 4m to 48/2476 · el+54m · 10919m · toward Lion	17.3	197	901		
	25 Jul 01:34	1054	C			17.8	197	898		
	26 Jul 02:14	1055	C			18.3	197	899		
	27 Jul 02:54	1056	m		Dr 1m to 48/2524 · el+54m · 10920m · to Buckskin	18.7	198	901		
	28 Jul 03:33	1057	CM	ABW	Brush & in-situ Buckskin, MAHLI future mini-drill and drill sites, wheel stability	19.2	198	898	0.80	
	29 Jul 04:13	1058			HGA occlusion test	19.7	197	901		
	30 Jul 04:52	1059	CM	AD	Mini-drill Buckskin w/MAHLI before & after, APXS mini-drill site, MAHLI future drill site	20.2	197	905		
	31 Jul 05:32	1060		F	Drill Buckskin w/MAHLI before & after	20.7	196	904		
	01 Aug 06:12	1061	cm	AIS	APXS Pellow, CHIMRA Buckskin, drop to CheMin, CheMin Buckskin	21.2	197	906		
	02 Aug 06:51	1062	CM		SAM electrical baseline test	21.6	198	905		
	03 Aug 07:31	1063	M		Thermal characterization activity	22.1	197	905	0.74	
	04 Aug 08:10	1064	Cm	Au	Dump pre-sieve, MAHLI drill hole, tailings, & CheMin inlet	22.6	197	906		
	05 Aug 08:50	1065	CM	AP	In-situ dump pile, MAHLI selfie	23.1	196	905		
	06 Aug 09:29	1066	CM		Dr 25m to 48/2548 · el+53m · 10946m · toward Missoula	23.6	196	907		
	Drive toward Bagnold Dunes	07 Aug 10:09	1067	Cm		Dr 18m to 48/2800 · el+54m · 10964m · toward Missoula	24.0	196	907	0.71
		08 Aug 10:49	1068			Runout (DSN failure to uplink command load)	24.5	198	906	
		09 Aug 11:28	1069			Runout (DSN failure to uplink command load)	25.0	196	909	
		10 Aug 12:08	1070			Runout (DSN failure to uplink command load)	25.5	196	910	
		11 Aug 12:47	1071	C		Test of sun-safety software upgrade	25.9	196	910	0.70
		12 Aug 13:27	1072	Cm		Dr 35m to 49/0006 · el+56m · 10999m · toward Bagnold Dunes	26.4	196	911	0.70
		13 Aug 14:07	1073	M		Dr 47m to 49/0300 · el+58m · 11046m · toward Bagnold Dunes, CheMin Buckskin	26.9	198	910	
		14 Aug 14:46	1074	cm		Dr 21m to 49/0648 · el+59m · 11067m · toward Bagnold Dunes	27.4	195	910	0.69
		15 Aug 15:26	1075		S	SAM preconditioning, drop to SAM	27.8	195	912	
16 Aug 16:05		1076		W	Organic Check Material arm positioning checkout w/MAHLI images, MAHLI wheels, SAM Buckskin	28.3	195	914		
17 Aug 16:45		1077	CM			28.8	196	913	0.71	
18 Aug 17:25		1078	cm		Dr 29m to 49/0820 · el+61m · 11096m · toward Bagnold Dunes, CheMin Buckskin	29.3	194	912		
19 Aug 18:04		1079	C			29.7	195	912	0.64	
20 Aug 18:44		1080	CM		Dr 27m to 49/1024 · el+63m · 11123m · toward Bagnold Dunes	30.2	196	915		
21 Aug 19:23		1081	CM			30.7	196	914	0.68	
22 Aug 20:03		1082	CM	A	In-situ Ravalli	31.1	196	913	0.72	
23 Aug 20:42		1083	Cm		Dr 22m to 49/1222 · el+62m · 11145m · toward Bagnold Dunes	31.6	195	914		
24 Aug 21:22		1084	C		ChemCam cal, SAM getter/scrubber cleanup	32.1	195	913		
25 Aug 22:02		1085	CM		Dr 39m to 49/1426 · el+63m · 11184m · toward Bagnold Dunes, SAM methane experiment	32.6	195	915		
26 Aug 22:41		1086	C			33.0	196	914	0.68	
27 Aug 23:21		1087	CM	W	Dr 6m to 49/1804 · el+63m · 11190m · toward Bagnold Dunes, MAHLI wheels	33.5	196	915		
29 Aug 00:00		1088	m		Battery thermal characterization	34.0	196	915	0.62	
30 Aug 00:40		1089	CM	AUX	Drop to SAM (doggy bag Buckskin), dump sample, in-situ dump pile w/MAHLI before & after, CHIMRA clean	34.4	196	916		
31 Aug 01:20		1090	CM			34.9	196	916		
01 Sep 01:59		1091		A	In-situ Devon & dump pile, MAHLI Pentago, Lebo, Ivanhoe, Ledger, CheMin inlet, cal with UV	35.4	196	918		
02 Sep 02:39		1092	CM	AB	Brush & in-situ Ledger, in-situ Ivanhoe, MAHLI Lebo, Ivanhoe, Ledger	35.8	197	917		
03 Sep 03:18	1093	CM		Dr 16m to 49/1882 · el+64m · 11206m · toward Bagnold Dunes, battleshort checkouts, thermal	36.3	196	920	0.68		

Area	Noon UTC	Sol	RS	Arm	Activity Summary	LS	T	P	Tau
Big Sky					checkout RPAM				
	04 Sep 03:58	1094	CM		Dr 26m to 49/2032 · el+66m · 11231m · toward Bagnold Dunes, battleshort checkouts, ChemCam focus test	36.7	194	921	
	05 Sep 04:37	1095	CM		CheMin dump & empty cell analysis, SAM diagnostics	37.2	195	920	
	06 Sep 05:17	1096			Runout (planned for battery charging)	37.7	196	918	
	07 Sep 05:57	1097	CM	A	In-situ Connipion, MAHLI REMS UV & Connipion	38.1	197	921	
	08 Sep 06:36	1098	CM		Dr 13m to 49/2242 · el+67m · 11244m · toward Bagnold Dunes, battleshort checkouts	38.6	197	922	0.66
	09 Sep 07:16	1099	CM		Dr 34m to 49/2380 · el+67m · 11279m · toward Bagnold Dunes	39.1	197	922	0.61
	10 Sep 07:55	1100	CM		Dr 35m to 49/2632 · el+68m · 11313m · toward Bagnold Dunes, battleshort checkouts, SAM diagnostics	39.5	195	923	
	11 Sep 08:35	1101	CM		Battleshort checkouts	40.0	194	922	
	12 Sep 09:15	1102		AW	In-situ Badlands, MAHLI wheels	40.5	195	922	
	13 Sep 09:54	1103	C		MAHLI ChemCam window	40.9	195	925	
	14 Sep 10:34	1104	CM		Dr 21m to 49/2908 · el+66m · 11334m · toward Cody	41.4	196	923	
	15 Sep 11:13	1105	CM	AB	Brush & in-situ Winnipeg, MAHLI Sacajawea	41.8	195	921	0.64
	16 Sep 11:53	1106	CM		Dr 11m to 50/0006 · el+67m · 11345m · toward Cody	42.3	195	920	
	17 Sep 12:33	1107	CM		Dr 17m to 50/0120 · el+66m · 11362m · toward Cody	42.8	196	920	0.68
	18 Sep 13:12	1108	CM		Dr 5m to 50/0256 · el+65m · 11366m · to Cody	43.2	196	923	
	19 Sep 13:52	1109	CM	AB	Brush & MAHLI Cody, in-situ Ferdig	43.7	195	924	
	20 Sep 14:31	1110	CM	A	Dr 15m to 50/0328 · el+65m · 11382m · toward Big Sky, APXS Cody	44.1	196	925	
	21 Sep 15:11	1111	CM			44.6	195	925	0.65
	22 Sep 15:50	1112	CM		Dr 14m to 50/0454 · el+66m · 11396m · toward Big Sky	45.0	196	926	
	23 Sep 16:30	1113	C			45.5	195	926	
	24 Sep 17:10	1114	CM	AB	Brush & in-situ Big Sky, drill preload test w/MAHLI after	46.0	195	929	
	25 Sep 17:49	1115	CM			46.4	194	929	
	26 Sep 18:29	1116	m	AD	Mini-drill Big Sky w/MAHLI before & after, APXS mini-drill, MAHLI future full drill	46.9	195	928	
	27 Sep 19:08	1117	CM		RAD FSW update, SAM gas chromatograph column 4 commissioning	47.3	194	928	
	28 Sep 19:48	1118	CM			47.8	195	928	0.61
	29 Sep 20:28	1119		BF	Drill Big Sky w/MAHLI before & after, brush Big Sky 2	48.2	194	928	
	30 Sep 21:07	1120	CM		RAD FSW activation	48.7	194	930	0.63
	01 Oct 21:47	1121	cm	IS	CHIMRA Big Sky, drop to CheMin, CheMin Big Sky	49.2	193	928	
	02 Oct 22:26	1122	C			49.6	194	930	
	03 Oct 23:06	1123	CM	Au	Dump pre-sieve, in-situ tailings, MAHLI drill hole & CheMin inlet	50.1	194	928	0.57
	04 Oct 23:46	1124		A	In-situ dump pile, SAM atmos	50.5	194	928	
06 Oct 00:25	1125			Runout (planned for battery charging)	51.0	193	927		
07 Oct 01:05	1126	CM	AP	In-situ dump pile, MAHLI selfie, CheMin Big Sky	51.4	193	927		
08 Oct 01:44	1127	M	W	Dr 8m to 50/0598 · el+66m · 11403m · toward Greenhorn with MAHLI full wheel	51.9	193	928		
09 Oct 02:24	1128	CM		MAHLI Greenhorn & Pilgrim, thermal characterization RPAM	52.3	195	929	0.56	
10 Oct 03:03	1129		S	SAM preconditioning, drop to SAM	52.8	194	929		
11 Oct 03:43	1130	m	AB	Brush & in-situ Greenhorn, drill preload w/MAHLI after, SAM Big Sky	53.2	194	928		
12 Oct 04:23	1131			CheMin Big Sky	53.7	193	928		
13 Oct 05:02	1132	m	AUX	MAHLI dump site, dump sample, in-situ dump pile, MAHLI future drill site, CHIMRA thwackless clean	54.1	193	928		
14 Oct 05:42	1133	CM	X	CheMin dump, CHIMRA clean	54.6	193	925		
15 Oct 06:21	1134	m	AD	Mini-drill Pilgrim w/MAHLI before & after, APXS Pilgrim, MAHLI future drill site	55.0	195	928		
16 Oct 07:01	1135			Runout (DSN failure to uplink command load)	55.5	193	929		

Big Sky

Greenhorn

380 Appendix: Curiosity Activity Summary

Area	Noon UTC	Sol	RS	Arm	Activity Summary	Ls	T	P	Tau
Drive toward Bagnold Dunes	17 Oct 07:41	1136	CM		MAHLI CheMin inlet, CheMin empty cell	56.0	192	928	
	18 Oct 08:20	1137		F	Drill Greenhorn w/MAHLI before & after, battery thermal characterization	56.4	193	928	
	19 Oct 09:00	1138	CM		Battery thermal characterization	56.9	193	928	0.51
	20 Oct 09:39	1139	CM	IS	CHIMRA Greenhorn, drop to CheMin, CheMin Greenhorn	57.3	195	926	
	21 Oct 10:19	1140	CM		SAM atmos	57.8	194	926	
	22 Oct 10:59	1141	Cm		AEGIS software installation, SAM cleanup	58.2	193	927	
	23 Oct 11:38	1142	CM	Au	Dump pre-sieve, MAHLI drill hole, tailings, dump pile, CheMin inlet, APXS tailings	58.7	193	928	
	24 Oct 12:18	1143		A	In-situ pre-sieve dump pile & Vandalia	59.1	192	927	
	25 Oct 12:57	1144	M		Dr 19m to 50/0682 · el+67m · 11422m · to Meeteetse Overlook, CheMin Greenhorn	59.6	192	927	
	26 Oct 13:37	1145			SAM atmos	60.0	195	928	
	27 Oct 14:16	1146	CM		SAM preconditioning	60.5	195	926	0.51
	28 Oct 14:56	1147		S	Drop to SAM, SAM Greenhorn 1	60.9	192	924	
	29 Oct 15:36	1148	M		Dr 32m to 50/0854 · el+67m · 11454m · toward Bagnold Dunes, CheMin Greenhorn	61.4	193	926	
	30 Oct 16:15	1149	C			61.8	192	925	0.50
	31 Oct 16:55	1150	CM	A	In-situ Ennis, Ellis Canyon, Exshaw	62.3	192	925	
	01 Nov 17:34	1151	CM	A	Dr 9m to 50/1122 · el+68m · 11463m · toward Bagnold Dunes after APXS Ennis	62.7	191	925	
	02 Nov 18:14	1152	Cm		SAM electrical baseline test	63.2	193	924	0.47
	03 Nov 18:54	1153	CM		Dr 54m to 50/1228 · el+66m · 11516m · toward Bagnold Dunes, SAM engineering diagnostics	63.6	190	923	
	04 Nov 19:33	1154	CM			64.1	191	923	
	05 Nov 20:13	1155	CM		Dr 39m to 50/1630 · el+67m · 11556m · toward Bagnold Dunes	64.5	191	922	
	06 Nov 20:52	1156	m			65.0	192	923	0.51
	07 Nov 21:32	1157	cM	ABW	Brush & in-situ Augusta, in-situ cal, MAHLI sky & wheels	65.4	192	923	
	08 Nov 22:11	1158	M		Dr 68m to 50/1934 · el+68m · 11624m · toward Bagnold Dunes	65.8	194	920	
	09 Nov 22:51	1159	cm			66.3	191	921	0.45
	10 Nov 23:31	1160	CM		Dr 56m to 50/2444 · el+67m · 11680m · toward Bagnold Dunes	66.7	193	921	
12 Nov 00:10	1161	Cm			67.2	192	920		
13 Nov 00:50	1162	CM		Dr 38m to 50/2778 · el+68m · 11718m · toward Bagnold Dunes, REMS dune campaign	67.6	191	920		
14 Nov 01:29	1163	M		REMS dune campaign	68.1	191	919	0.49	
15 Nov 02:09	1164			Runout (DSN failure to uplink command load)	68.5	190	918		
16 Nov 02:49	1165			Runout (DSN failure to uplink command load)	69.0	191	918		
17 Nov 03:28	1166	CM	AB	Brush & in-situ Swartkloofberg, MAHLI Swakop & REMS UV, SAM getter/scrubber cleanup	69.4	192	917		
18 Nov 04:08	1167	CM		Dr 39m to 50/3082 · el+71m · 11758m · toward Bagnold Dunes, REMS dune campaign	69.9	191	917		
19 Nov 04:47	1168	cm		Dr 37m to 51/0006 · el+73m · 11795m · toward Bagnold Dunes, REMS wind calibration, SAM atmos	70.3	191	917	0.50	
20 Nov 05:27	1169	CM			70.8	191	916		
21 Nov 06:07	1170	C		SAM preconditioning	71.2	191	917	0.44	
22 Nov 06:46	1171	Cm		CheMin dump, SAM EGA blank	71.7	191	916		
23 Nov 07:26	1172	m		Dr 51m to 51/0274 · el+75m · 11846m · toward Bagnold Dunes	72.1		915		
24 Nov 08:05	1173	M		Dr 46m to 51/0598 · el+76m · 11892m · toward Bagnold Dunes, RCE maintenance activity	72.6	190	914	0.52	
High Dune	25 Nov 08:45	1174	cm		Dr 28m to 51/0880 · el+76m · 11919m · toward Bagnold Dunes, CheMin dump, CheMin empty cell	73.0	191	914	
	26 Nov 09:24	1175	C		CheMin empty cell	73.5	189	913	0.49
	27 Nov 10:04	1176	cM		CheMin empty cell	73.9		912	0.46
	28 Nov 10:44	1177	Cm		SAM preconditioning	74.4	190	910	
	29 Nov 11:23	1178	m	SW	Drop to SAM, SAM Greenhorn 2, MAHLI full wheel 1 of 5	74.8	189	909	
30 Nov 12:03	1179	M	W	Dr 1m to 51/1108 · el+76m · 11921m · to complete MAHLI full wheel	75.3	189	908		

Area	Noon UTC	Sol	RS	Arm	Activity Summary	Ls	T	P	Tau
Drive	01 Dec 12:42	1180			Runout (DSN failure to uplink command load)	75.7	189	908	
	02 Dec 13:22	1181	cm		Dr 9m to 51/1132 · el+76m · 11929m · to test dune mobility with MARDI sidewalk, RTG short clearing activity	76.2	189	907	
	03 Dec 14:02	1182	CM	AW	In-situ Warsaw & Weissrand, MAHLI wheels	76.6	189	906	0.42
	04 Dec 14:41	1183	cM		Dr 9m to 51/1304 · el+77m · 11938m · to test dune mobility	77.1	189	904	
	05 Dec 15:21	1184	CM	A	In-situ Kibnas & Barby, MAHLI CheMin inlet	77.5	188	905	
	06 Dec 16:00	1185	m		Dr 35m to 51/1436 · el+78m · 11973m · toward Namib Dune	78.0	190	903	
	07 Dec 16:40	1186				78.4	190	903	
	08 Dec 17:20	1187	CM		Dr 29m to 51/1806 · el+78m · 12002m · toward Namib Dune, RCE maintenance activity	78.9	191	901	0.47
	09 Dec 17:59	1188	C		SAM electrical baseline test	79.3	190	901	0.48
	10 Dec 18:39	1189	CM			79.8	190	899	
	11 Dec 19:18	1190	cM		Thermal characterization of RPAM	80.2	190	898	
	12 Dec 19:58	1191	C	A	In-situ Pomona & Elizabeth Bay, battleshort checkout	80.7	189	899	
	Namib Dune	13 Dec 20:37	1192	M		Dr 42m to 51/2010 · el+79m · 12044m · toward Location C, battleshort checkout	81.1	190	897
14 Dec 21:17		1193	C			81.6	190	896	
15 Dec 21:57		1194	CM		Dr 47m to 51/2328 · el+81m · 12091m · toward Location C	82.0	190	894	0.49
16 Dec 22:36		1195	C			82.5	191	893	0.45
17 Dec 23:16		1196	cM		Dr 33m to 51/2710 · el+81m · 12124m · toward Location C	82.9	190	893	
18 Dec 23:55		1197	CM			83.4	190	891	0.49
20 Dec 00:35		1198	cM	U	MAHLI future dump location, arm fault (overspeed error) during Greenhorn sample dump	83.8	191	891	
21 Dec 01:15		1199	C			84.3	191	889	0.57
22 Dec 01:54		1200	CM		Check if sample dumped	84.7	191	887	
23 Dec 02:34		1201	CM		Arm diagnostics	85.2	190	888	0.51
24 Dec 03:13		1202	CM	AX	In-situ Greenhorn dump pile (MAHLI cover closed), CHIMRA clean, battery thermal characterization	85.6	190	886	
25 Dec 03:53		1203	CM		MAHLI dump pile (cover closed), battery thermal characterization	86.1	190	883	
26 Dec 04:33		1204	CM		SAM calibration	86.5	189	883	0.44
27 Dec 05:12		1205			ENV science	87.0	191	881	
28 Dec 05:52		1206	M		ENV science	87.4	191	881	
29 Dec 06:31		1207	m		ENV science	87.9	190	881	
30 Dec 07:11		1208			ENV science	88.3	191	879	
31 Dec 07:50	1209			ENV science	88.8	191	880		
Anomaly	01 Jan 08:30	1210	M		ENV science; HAPPY NEW YEAR 2016!	89.2	190	876	
	02 Jan 09:10	1211	m		ENV science	89.7	191	875	
	03 Jan 09:49	1212			ENV science	90.1	191	874	
	04 Jan 10:29	1213			ENV science	90.6	191	872	
	05 Jan 11:08	1214	cM	W	MAHLI wheels	91.0	190	871	0.47
	06 Jan 11:48	1215			Dr 68m to 52/0010 · el+79m · 12193m · toward dune Location D (Gobabeb)	91.5	190	870	
	07 Jan 12:28	1216	Cm		Dr 43m to 52/0620 · el+77m · 12236m · toward dune Location D (Gobabeb)	91.9	190	868	0.47
	08 Jan 13:07	1217			ANOMALIES PRECLUDE SCIENCE (single bit error in RMC-A prevented any motion)	92.4	189	867	
	09 Jan 13:47	1218			Runout (due to previous sol anomaly)	92.9		866	
	10 Jan 14:26	1219	cm		RMC-A diagnostics, remote sensing without mast motion	93.3	189	866	
Gobabeb	11 Jan 15:06	1220			Remote sensing without mast motion	93.8	189	864	
	12 Jan 15:46	1221	cM		Dr 10m to 52/0942 · el+77m · 12245m · to and scuff Gobabeb, battleshort checkout, SAM atmos	94.2	188	863	
	13 Jan 16:25	1222	CM			94.7	189	862	0.54
	14 Jan 17:05	1223		A	In-situ scuff, MAHLI future scoop locations	95.1	189	861	

382 Appendix: Curiosity Activity Summary

Area	Noon UTC	Sol	RS	Arm	Activity Summary	LS	T	P	Tau
Drive west, skirting High Dune	15 Jan 17:44	1224	m	CIS	Scoop Gobabeb 1, CHIMRA sample, drop to SAM, SAM Gobabeb	95.6	189	858	
	16 Jan 18:24	1225	Cm	A	APXS future scoop 2 site	96.0	190	858	
	17 Jan 19:03	1226	M	ASLUX	Drop to CheMin, dump A (post-sieve) & B (pre-sieve), MAHLI future scoop sites, scuff, & B, in-situ A, CHIMRA clean w/2ndary thwack only	96.5	189	858	
	18 Jan 19:43	1227			CheMin Gobabeb, MAHLI dump A	97.0	188	856	
	19 Jan 20:23	1228	m	CIPU	MAHLI selfie, scoop 1 site, & dumps A&B, scoop Gobabeb 2, CHIMRA 1mm sieving, dump C (pre-sieve & <1mm), D (>1mm)	97.4	189	856	
	20 Jan 21:02	1229	CM		Thermal characterization of RPAM	97.9	190	855	0.48
	21 Jan 21:42	1230		S	MAHLI dump sites A, B, C, D; SAM preconditioning, drop 1mm portion to SAM	98.3	190	853	
	22 Jan 22:21	1231	m	ACX	CHIMRA clean w/2ndary thwack only, Scoop Gobabeb 3, attempt 1mm sieving, primary thwack anomaly	98.8	189	852	
	23 Jan 23:01	1232			ANOMALIES PRECLUDE SCIENCE (CHIMRA primary thwack actuator)	99.3	188	849	
	24 Jan 23:41	1233	cM			99.7	188	850	
	26 Jan 00:20	1234	CM			100.2	188	847	0.47
	27 Jan 01:00	1235	Cm		Arm diagnostics	100.6	189	847	0.47
	28 Jan 01:39	1236	Cm			101.1	191	844	
	29 Jan 02:19	1237	cM		CHIMRA diagnostics, SAM 1mm portion Gobabeb	101.6	189	843	0.51
	30 Jan 02:58	1238	Cm			102.0	190	842	0.48
	31 Jan 03:38	1239	Cm		CheMin Gobabeb, arm diagnostics	102.5	188	841	
	01 Feb 04:18	1240	Cm		SAM electrical baseline test	102.9	189	838	
	02 Feb 04:57	1241	cm	AP	In-situ dump C, MAHLI scoops, dump piles, Otavi, selfie+	103.4	193	837	0.46
	03 Feb 05:37	1242	cm	A	In-situ dumps B & C, MAHLI dump D & Otavi, CHIMRA diagnostics	103.9	192	837	
	04 Feb 06:16	1243	m		Dr 13m to 52/1168 · el+77m · 12258m · to DAN active position, CheMin Gobabeb, CHIMRA diagnostics	104.3	192	835	
	05 Feb 06:56	1244	CM		Dr 2m to 52/1318 · el+77m · 12260m · to scuff	104.8	189	835	
	06 Feb 07:36	1245	m	ABW	Brush & in-situ Kudis, in-situ Tinkas	105.3	189	833	
	07 Feb 08:15	1246	CM		SAM cleaning	105.7	189	835	0.46
	08 Feb 08:55	1247	m		Attempted drive faulted because arm failed to stow	106.2	190	830	
	09 Feb 09:34	1248	cm		Dr 46m to 52/1376 · el+78m · 12306m · toward Naukluft plateau	106.7	190	829	
	10 Feb 10:14	1249	m		Dr 71m to 52/1728 · el+74m · 12376m · toward Naukluft plateau	107.1	191	829	
	11 Feb 10:54	1250	cm		Dr 17m to 52/2268 · el+74m · 12393m · to Kuiseb	107.6	191	827	
12 Feb 11:33	1251	CM	ABU	Brush & in-situ Kuiseb, dump Gobabeb 3 to piles E (post-sieve) & F (pre-sieve), MAHLI dump piles	108.1	191	825		
13 Feb 12:13	1252	CM		In-situ cal	108.5	192	824		
14 Feb 12:52	1253	CM	A	In-situ Bergsig & dump piles, MAHLI Kuiseb, CHIMRA diagnostics	109.0	191	822	0.47	
15 Feb 13:32	1254	CM		CheMin Gobabeb, MAHLI Bergsig, Kuiseb, dump F (pre-sieve)	109.5	193	822	0.45	
16 Feb 14:11	1255	m		Dr 15m to 52/2394 · el+74m · 12408m · toward Naukluft plateau	109.9	192	819		
17 Feb 14:51	1256	cm		Dr 25m to 52/2506 · el+73m · 12433m · toward Naukluft plateau, battleshort checkout	110.4	191	819		
18 Feb 15:31	1257	Cm		Dr 0m to 52/2674 · el+73m · 12433m · to turn for comm	110.9	190	817		
19 Feb 16:10	1258	Cm			111.3	192	818	0.47	
20 Feb 16:50	1259	CM	AB	Brush & in-situ Gorob, in-situ Groot Aub, MAHLI CheMin inlet & REMS UV	111.8	191	815		
21 Feb 17:29	1260	M	W	Dr 7m to 52/2684 · el+73m · 12440m · toward Naukluft plateau with full MAHLI wheel imaging	112.3	192	814		
22 Feb 18:09	1261	cm			112.7	194	813		
23 Feb 18:49	1262	Cm		Dr 70m to 52/2778 · el+71m · 12510m · toward Naukluft plateau, CheMin Gobabeb	113.2	194	812		
24 Feb 19:28	1263	Cm			113.7	193	814	0.45	
25 Feb 20:08	1264	CM		Dr 25m to 53/0006 · el+69m · 12535m · toward Naukluft plateau	114.2	193	810		
26 Feb 20:47	1265	m			114.6	196	809	0.42	
27 Feb 21:27	1266	Cm	AB	Brush & in-situ Stockdale, in-situ Waterberg	115.1	195	809		

Area	Noon UTC	Sol	RS	Arm	Activity Summary	Ls	T	P	Tau
Drive across Naukluft Plateau	28 Feb 22:07	1267	M		Dr 24m to 53/0192 · el+67m · 12559m · toward Naukluft plateau; drive fault (stall right rear motor)	115.6	194	809	
	29 Feb 22:46	1268	Cm			116.1	191	808	0.41
	01 Mar 23:26	1269	cm	W	Dr 36m to 53/0378 · el+68m · 12595m · toward Naukluft plateau, MAHLI wheels before & after bump, SAM calcite cup	116.5	191	806	
	03 Mar 00:05	1270	CM		Battery conditioning	117.0	192	804	
	04 Mar 00:45	1271	Cm		CheMin Gobabeb, arm thermal characterization	117.5	193	803	
	05 Mar 01:24	1272	CM		Arm thermal characterization	118.0	193	803	0.40
	06 Mar 02:04	1273	CM	AB	Brush& in-situ Schwarstrand, in-situ Kleinberg	118.5	194	802	
	07 Mar 02:44	1274	M		Dr 46m to 53/0642 · el+73m · 12641m · toward Naukluft plateau	118.9	193	800	
	08 Mar 03:23	1275	CM	AB	In-situ Mirabib & Palmwag, MAHLI Palmhorst	119.4	192	798	0.41
	09 Mar 04:03	1276	CM		Dr 12m to 53/1062 · el+74m · 12653m · toward Sperrgebiet	119.9	192	797	
	10 Mar 04:42	1277	CM	A	In-situ Sperrgebiet, MAHLI Khomas, Maieberg, Klein Aub	120.4	193	796	0.42
	11 Mar 05:22	1278	CM	A	In-situ Sperrgebiet, MAHLI Konigstein, Maieberg, & nodules	120.9	195	797	
	12 Mar 06:02	1279	m	AB	Brush & in-situ Khomas, MAHLI Etendeka & Maieberg	121.3	193	797	
	13 Mar 06:41	1280	CM	A	APXS Khomas, CheMin Gobabeb	121.8	192	794	0.36
	14 Mar 07:21	1281	m		Dr 14m to 53/1188 · el+74m · 12667m · toward Naukluft plateau with MARDI sidewalk across Stimson contact	122.3	192	794	
	15 Mar 08:00	1282	CM		Dr 27m to 53/1290 · el+74m · 12694m · toward Naukluft plateau	122.8	192	792	
	16 Mar 08:40	1283	CM		Dr 39m to 53/1476 · el+73m · 12733m · toward Naukluft plateau	123.3	195	791	
	17 Mar 09:20	1284	CM		Dr 28m to 53/1762 · el+74m · 12761m · toward Naukluft plateau	123.8	195	792	
	18 Mar 09:59	1285	CM		Attempted drive faulted because of soft short	124.2	195	791	
	19 Mar 10:39	1286	CM		CheMin piezo vibrate, SAM calcite cup experiment	124.7	194	790	0.39
	20 Mar 11:18	1287	m	ABW	Brush & MAHLI Sesriem Canyon, in-situ Rossing, MAHLI wheels & CheMin inlet	125.2	195	792	
	21 Mar 11:58	1288	m	A	Attempted drive failed due to arm fault	125.7	195	789	
	22 Mar 12:37	1289	CM		Dr 15m to 53/2000 · el+74m · 12776m · toward Naukluft plateau	126.2	194	787	
	23 Mar 13:17	1290	cM		Dr 23m to 53/2144 · el+74m · 12798m · across Naukluft plateau	126.7	193	787	0.39
	24 Mar 13:57	1291	Cm		Thermal characterization of RPAM	127.2	196	784	0.38
	25 Mar 14:36	1292	CM		Dr 7m to 53/2304 · el+74m · 12805m · across Naukluft plateau	127.7	195	784	0.41
	26 Mar 15:16	1293	CM	BX	Brush & MAHLI Brukkaros, MAHLI Gobabis, CHIMRA clean	128.1	195	783	
	27 Mar 15:55	1294	M	A	Dr 17m to 53/2412 · el+73m · 12822m · across Naukluft plateau after APXS Brukkaros	128.6	197	783	
	28 Mar 16:35	1295	c		CheMin sample dump & empty cell analysis	129.1	194	782	
	29 Mar 17:15	1296	CM		Dr 4m to 53/2584 · el+73m · 12826m · across Naukluft plateau (short drive due to hitting suspension limit)	129.6	195	781	
	30 Mar 17:54	1297	c			130.1	197	781	0.38
	31 Mar 18:34	1298	CM		Dr 38m to 53/2650 · el+71m · 12865m · across Naukluft plateau	130.6	195	781	
	01 Apr 19:13	1299	Cm			131.1	194	779	0.40
02 Apr 19:53	1300	Cm	AB	Brush & in-situ Bero, in-situ Gudaus	131.6	196	779		
03 Apr 20:32	1301	M		Dr 5m to 53/2986 · el+71m · 12869m · across Naukluft plateau (short drive due to soft short)	132.1	196	781	0.40	
04 Apr 21:12	1302	CM			132.6	196	779	0.33	
05 Apr 21:52	1303	CM		Failed drive due to soft short	133.1	197	780	0.41	
06 Apr 22:31	1304	c			133.6	195	777		
07 Apr 23:11	1305	CM		Failed drive due to soft short	134.1	195	777		
08 Apr 23:50	1306	Cm		CheMin empty cell	134.6	196	775	0.40	
10 Apr 00:30	1307			Runout (DSN failure to uplink command load)	135.1	196	776		
11 Apr 01:10	1308			Runout (DSN failure to uplink command load)	135.6	195	774		
12 Apr 01:49	1309	CM		Dr 7m to 54/0016 · el+72m · 12877m · across Naukluft plateau	136.1	195	773	0.41	

384 Appendix: Curiosity Activity Summary

Area	Noon UTC	Sol	RS	Arm	Activity Summary	Ls	T	P	Tau
Lubango	13 Apr 02:29	1310	CM		Dr 21m to 54/0094 · el+70m · 12897m · across Naukluft plateau	136.6	197	772	
	14 Apr 03:08	1311	Cm		Dr 17m to 54/0244 · el+69m · 12914m · across Naukluft plateau	137.1	197	774	
	15 Apr 03:48	1312	CM			137.6	196	774	0.37
	16 Apr 04:28	1313	C	AW	In-situ Onesi & Uau, MAHLI Kasane & full wheel 1 of 5	138.1	197	773	0.37
	17 Apr 05:07	1314	CM	A	APXS Kasane, MAHLI REMS UV, SAM scrubber cleanup	138.6	198	770	0.36
	18 Apr 05:47	1315	M	W	Dr 1m to 54/0394 · el+69m · 12915m · to complete MAHLI full wheel	139.1	198	771	
	19 Apr 06:26	1316	Cm		Dr 25m to 54/0418 · el+71m · 12940m · toward Lubango, CheMin empty cell analysis	139.6	195	773	
	20 Apr 07:06	1317	CM		Dr 7m to 54/0674 · el+72m · 12948m · toward Lubango	140.2	194	771	
	21 Apr 07:45	1318	m	AB	Brush & in-situ Lubango, in-situ Cangulo & future drill site, MAHLI Swartbank	140.7	196	773	
	22 Apr 08:25	1319	Cm	A	Brush & in-situ Swartbank, drill preload w/ MAHLI after, SAM atmos	141.2	197	771	0.38
	23 Apr 09:05	1320		F	Drill Lubango w/MAHLI before, battery thermal characterization	141.7	197	771	
	24 Apr 09:44	1321	CM		MAHLI drill site, SAM atmos	142.2	198	771	0.38
	25 Apr 10:24	1322	C		Thermal characterization of RPAM	142.7	197	771	
	26 Apr 11:03	1323	Cm	IS	CHIMRA Lubango, drop to CheMin, CheMin Lubango	143.2	197	769	
	27 Apr 11:43	1324	C	u	Dump pre-sieve, MAHLI drill hole, tailings, dump pile, CheMin inlet	143.7	197	771	
	28 Apr 12:23	1325	C	A	APXS tailings, MAHLI Rubikon, Lianshulu	144.3	197	769	
	29 Apr 13:02	1326	CM	A	In-situ dump pile, MAHLI tailings, Nara Valley, Lorelei	144.8	197	766	0.50
	30 Apr 13:42	1327	Cm	AUX	Dump sample w/MAHLI before & after, APXS dump, CHIMRA clean	145.3	200	765	
	01 May 14:21	1328	CM		CheMin Lubango, MAHLI dump pile	145.8	198	764	0.54
	02 May 15:01	1329	m		Dr 13m to 54/0752 · el+71m · 12961m · toward Okoruso	146.3	199	764	
Okoruso	03 May 15:41	1330	Cm	AB	Brush & in-situ Okoruso, drill preload test w/MAHLI after, CheMin Lubango	146.9	198	764	
	04 May 16:20	1331	Cm			147.4	198	762	0.54
	05 May 17:00	1332		F	Drill Okoruso w/MAHLI before	147.9	198	762	
	06 May 17:39	1333	CM			148.4	200	762	0.59
	07 May 18:19	1334	cm	IS	CHIMRA Okoruso, drop to CheMin, CheMin Okoruso	148.9	198	763	
	08 May 18:58	1335	C		CheMin Okoruso	149.5	199	762	
	09 May 19:38	1336	Cm			150.0	199	764	0.65
	10 May 20:18	1337	Cm	Au	Dump pre-sieve, in-situ tailings, MAHLI dump pile, drill hole, CheMin inlet, & Ubib	150.5	202	765	
	11 May 20:57	1338	CM	P	CheMin Okoruso, MAHLI tailings & selfie	151.0	199	769	
	12 May 21:37	1339		A	In-situ pre-sieve dump pile	151.6	200	769	
	13 May 22:16	1340	Cm		MAHLI Kwakwas, pre-sieve dump pile, cal, sky	152.1	198	771	0.79
	14 May 22:56	1341	CM	AB	Brush & in-situ Kwakwas, MAHLI Rooilepel & Okoruso	152.6	198	771	
	15 May 23:36	1342	M		Dr 6m to 54/0944 · el+71m · 12967m · across Naukluft plateau, CheMin Okoruso	153.2	200	773	
	17 May 00:15	1343	Cm			153.7	201	769	0.74
	Drive across Naukluft Plateau	18 May 00:55	1344	cm		Dr 28m to 54/0998 · el+69m · 12995m · across Naukluft plateau after MAHLI Impalila, Swartmodder, Narubris, Stampriet	154.2	200	767
19 May 01:34		1345	C			154.8	201	770	0.73
20 May 02:14		1346	CM		Dr 17m to 54/1244 · el+67m · 13011m · toward Meob, CheMin Okoruso	155.3	200	773	
21 May 02:54		1347	Cm		CheMin piezo vibe	155.8	198	773	0.62
22 May 03:33		1348	CM	AB	Brush & in-situ Meob, in-situ Nomeib, MAHLI CheMin inlet	156.4	198	773	
23 May 04:13		1349	CM		Dr 12m to 54/1496 · el+66m · 13023m · across Naukluft plateau	156.9	199	774	
24 May 04:52		1350	Cm		CheMin Okoruso	157.4	200	777	0.76
25 May 05:32		1351	Cm	A	In-situ Groendraai, MAHLI Nauaspoort & mosaic	158.0	200	775	
26 May 06:11		1352	cm	A	Dr 17m to 54/1616 · el+66m · 13040m · toward Inamagando after APXS Nauaspoort	158.5	200	775	
27 May 06:51		1353	CM		Dr 52m to 54/1784 · el+66m · 13092m · toward Inamagando	159.1	198	779	

Area	Noon UTC	Sol	RS	Arm	Activity Summary	Ls	T	P	Tau
	28 May 07:31	1354	cm		HRS maintenance, thermal characterization of RPAM	159.6	199	783	0.71
	29 May 08:10	1355	CM	ABW	Brush & in-situ Inamagando, in-situ Horingbai, MAHLI wheels	160.2	199	782	
	30 May 08:50	1356	CM		MAHLI arm thermal characterization activity, SAM atmos	160.7	200	779	0.72
	31 May 09:29	1357	M		Dr 9m to 54/2208 · el+65m · 13101m · toward Oudam, MAHLI arm thermal characterization activity	161.2	200	778	
Oudam	01 Jun 10:09	1358	cm	ABU	Dump Okoruso sample w/MAHLI before & after, Brush & in-situ Oudam	161.8	201	782	
	02 Jun 10:49	1359	CM	AX	In-situ Okoruso dump, CHIMRA clean, drill preload test w/MAHLI after, MAHLI Oniguati	162.3	199	785	
	03 Jun 11:28	1360	C		MAHLI Oudam & dump pile, CheMin empty cell analysis	162.9	199	784	
	04 Jun 12:08	1361	cm	F	Drill Oudam, MAHLI after	163.4	202	781	0.76
	05 Jun 12:47	1362	cm	IS	CHIMRA Oudam, drop to CheMin, CheMin Oudam 1	164.0	201	782	
	06 Jun 13:27	1363	CM			164.5	202	785	
	07 Jun 14:06	1364	C	Au	Dump pre-sieve sample, in-situ tailings, MAHLI drill hole & CheMin inlet	165.1	200	785	
	08 Jun 14:46	1365	cm		CheMin Oudam 1	165.6	200	782	
	09 Jun 15:26	1366	CM	AB	Brush & in-situ Aubures, MAHLI tailings & REMS UV	166.2	200	783	0.78
	10 Jun 16:05	1367	M		SAM electrical baseline test	166.7	201	785	
	11 Jun 16:45	1368	CM	A	In-situ dump pile, battery thermal characterization	167.3	201	786	
	12 Jun 17:24	1369	CM		Dr 32m to 54/2286 · el+67m · 13133m · south after MAHLI dump pile, CheMin Oudam 1	167.9	202	784	
Drive south through Hartmann's Valley	13 Jun 18:04	1370	cm		Battery thermal characterization	168.4	199	788	0.73
	14 Jun 18:44	1371	CM		Dr 32m to 54/2514 · el+70m · 13165m · south after MAHLI Berg Aukas	169.0	199	788	0.75
	15 Jun 19:23	1372				169.5	201	789	
	16 Jun 20:03	1373	CM		Dr 32m to 54/2790 · el+71m · 13197m · south	170.1	200	792	
	17 Jun 20:42	1374	C			170.7	199	794	
	18 Jun 21:22	1375	CM	A	In-situ Andara, drop to CheMin, CheMin Oudam 2, MAHLI CheMin inlet	171.2	201	797	
	19 Jun 22:02	1376	cm	A	Dr 17m to 54/3042 · el+71m · 13214m · south after APXS Andara	171.8	199	798	
	20 Jun 22:41	1377			CheMin Oudam 2	172.4	199	797	
	21 Jun 23:21	1378	cm		Dr 44m to 55/0006 · el+72m · 13258m · south	172.9	199	796	
	23 Jun 00:00	1379	cm			173.5	198	795	0.70
	24 Jun 00:40	1380	cm	ABW	Brush & in-situ Koes, MAHLI wheels, SAM preconditioning	174.1	199	797	
	25 Jun 01:19	1381	CM		HRS maintenance	174.6	201	795	
	26 Jun 01:59	1382	CM	S	Drop to SAM, SAM EGA Oudam	175.2	199	796	
	27 Jun 02:39	1383	cm		Dr 31m to 55/0316 · el+73m · 13289m · south	175.8	199	795	0.66
	28 Jun 03:18	1384	cm		Dr 65m to 55/0544 · el+74m · 13354m · south	176.3	199	794	0.67
	29 Jun 03:58	1385	cm		Dr 68m to 55/0946 · el+79m · 13422m · south	176.9	200	793	
	30 Jun 04:37	1386	CM	AW	Dr 1m to 55/1318 · el+79m · 13424m · for full MAHLI wheels, in-situ Trekkopje, SAM getter/scrubber cleanup	177.5	200	794	0.73
	01 Jul 05:17	1387	CM		Dr 12m to 55/1342 · el+80m · 13436m · south	178.1	200	794	
	02 Jul 05:57	1388	c		CheMin Oudam 2	178.6	199	794	
Anomaly (FSW/Issue)	03 Jul 06:36	1389			ANOMALIES PRECLUDE SCIENCE (safe mode upon file error)	179.2			
	04 Jul 07:16	1390			ANOMALIES PRECLUDE SCIENCE	179.8			
	05 Jul 07:55	1391			ANOMALIES PRECLUDE SCIENCE	180.4			
	06 Jul 08:35	1392			ANOMALIES PRECLUDE SCIENCE	180.9			
	07 Jul 09:15	1393			ANOMALIES PRECLUDE SCIENCE	181.5			
	08 Jul 09:54	1394			ANOMALIES PRECLUDE SCIENCE	182.1			
	09 Jul 10:34	1395			ANOMALIES PRECLUDE SCIENCE	182.7			
	10 Jul 11:13	1396			ANOMALIES PRECLUDE SCIENCE	183.3			
	11 Jul 11:53	1397			ANOMALIES PRECLUDE SCIENCE	183.9			

386 Appendix: Curiosity Activity Summary

Area	Noon UTC	Sol	RS	Arm	Activity Summary	Ls	T	P	Tau	
Dive south through Hartmann's Valley	12 Jul 12:32	1398	cM		Dr 66m to 55/1426 · el+81m · 13502m · south, cheMin Oudam 2	184.4			0.68	
	13 Jul 13:12	1399	CM		Dr 32m to 55/1870 · el+80m · 13534m · south	185.0	201	807		
	14 Jul 13:52	1400	CM		Dr 14m to 55/2104 · el+80m · 13547m · toward Bimbe, CheMin funnel vibration cleaning	185.6	200	809	0.68	
	15 Jul 14:31	1401	CM		Dr 26m to 55/2228 · el+83m · 13574m · south	186.2	199	808		
	16 Jul 15:11	1402	CM		MAHLI CheMin inlet, SAM geochronology test	186.8	200	808	0.64	
	17 Jul 15:50	1403		AW	In-situ Uku, MAHLI wheels, SAM geochronology test	187.4	201	808		
	18 Jul 16:30	1404	C		MAHLI ChemCam window	188.0	202	811	0.66	
	19 Jul 17:10	1405	CM	A	Dr 30m to 55/2450 · el+83m · 13603m · south after in-situ Guri	188.6		813		
	20 Jul 17:49	1406	C		CheMin dump	189.2	201	810		
	21 Jul 18:29	1407	CM	AW	In-situ Sonneblom, MAHLI Zambezi, Tumba, Funda, mosaic, wheel stability; SAM electrical baseline test	189.8	200	813		
	22 Jul 19:08	1408	CM		CheMin empty cell, backup HRS maintenance	190.4	200	813	0.72	
	23 Jul 19:48	1409	Cm	A	In-situ Funda & Zambezi, MAHLI Tumba	191.0	201	819		
	24 Jul 20:28	1410	cm		Dr 68m to 56/0006 · el+85m · 13671m · south	191.6	202	819		
	25 Jul 21:07	1411				192.2	202	818		
	26 Jul 21:47	1412	Cm		Dr 45m to 56/0468 · el+89m · 13717m · south	192.8	201	818		
	27 Jul 22:26	1413	CM			193.4	201	819	0.72	
	28 Jul 23:06	1414	Cm		Dr 45m to 56/0780 · el+90m · 13761m · toward Marimba	194.0	201	819		
	29 Jul 23:45	1415			Thermal characterization of RPAM	194.6	201	822	0.69	
	31 Jul 00:25	1416	Cm	ABW	Brush & MAHLI Chibia, in-situ Dondo, MAHLI wheels & organic check material w/cover closed	195.2	202	830	0.72	
	01 Aug 01:05	1417	CM	A	Dr 15m to 56/1128 · el+90m · 13776m · toward Marimba after APXS Dondo	195.8	203	829	0.80	
	Marimba	02 Aug 01:44	1418	Cm	ABUX	Dump Oudam w/MAHLI before & after, CHIMRA thwackless clean, brush & in-situ Marimba, drill preload w/MAHLI after	196.4	202	831	
		03 Aug 02:24	1419	CM	A	In-situ dump pile, CHIMRA clean	197.0	202	832	
		04 Aug 03:03	1420	M	D	Attempt full drill Marimba w/MAHLI before, only mini-drill achieved; MAHLI dump pile	197.6	203	831	0.71
		05 Aug 03:43	1421	CM		SAM getter/scrubber cleanup	198.2	203	834	0.79
		06 Aug 04:23	1422	m	F	Drill Marimba w/MAHLI before & after	198.8	203	836	0.78
		07 Aug 05:02	1423	c		Drill percussion fault	199.4	206	835	
		08 Aug 05:42	1424	Cm			200.0	203	841	
		09 Aug 06:21	1425	CM	IS	CHIMRA Marimba (without drill percussion), drop to CheMin, CheMin Marimba	200.6	203	840	
		10 Aug 07:01	1426	m	Au	Dump pre-sieve, in-situ tailings, MAHLI dump pile, drill hole, & CheMin inlet	201.3	203	838	0.73
		11 Aug 07:41	1427	CM		Dr 11m to 56/1242 · el+91m · 13787m · south after MAHLI tailings	201.9	203	842	
	Dive through Murray Buttes	12 Aug 08:20	1428	cm		Dr 46m to 56/1332 · el+93m · 13833m · south, CheMin Marimba	202.5	202	844	0.69
13 Aug 09:00		1429	CM		SAM geochronology experiment	203.1	205	845	0.76	
14 Aug 09:39		1430			SAM geochronology experiment	203.7	205	847		
15 Aug 10:19		1431	m		Dr 53m to 56/1638 · el+95m · 13886m · south	204.3	206	850		
16 Aug 10:58		1432	cM		Dr 52m to 56/2040 · el+97m · 13937m · south	205.0	203	847		
17 Aug 11:38		1433	cM		Dr 55m to 56/2434 · el+99m · 13992m · south, CheMin Marimba	205.6	204	852	0.78	
18 Aug 12:18		1434	CM	W	Dr 1m to 57/0006 · el+4501m · 13993m · for 1-4 of 5 MAHLI full wheel, RCE and HRS maintenance	206.2	204	852		
19 Aug 12:57		1435	cm	W	Dr 63m to 57/0030 · el+102m · 14056m · south after complete MAHLI full wheel	206.8	205	854		
20 Aug 13:37		1436	Cm	AB	Brush & in-situ Conda, MAHLI Biula, CheMin Marimba	207.4	203	860		
21 Aug 14:16		1437	C		MAHLI REMS UV, CheMin funnel vibration cleaning, MAHLI CheMin inlet	208.1	203	856	0.96	
22 Aug 14:56		1438	M		Dr 42m to 57/0468 · el+104m · 14098m · south	208.7	205	859		
23 Aug 15:36		1439	CM		Dr 34m to 57/0780 · el+107m · 14132m · south	209.3	204	866		
24 Aug 16:15		1440	C			209.9	203	863	0.90	

Area	Noon UTC	Sol	RS	Arm	Activity Summary	Ls	T	P	Tau
Quela	25 Aug 16:55	1441	CM		Drive failed (problem with CheMin software interaction)	210.5	205	863	
	26 Aug 17:34	1442	C			211.2	205	863	
	27 Aug 18:14	1443	CM	S	SAM preconditioning, drop to SAM, SAM EGA Marimba	211.8	203	866	0.96
	28 Aug 18:53	1444	Cm	ABW	Brush & in-situ Ganda, in-situ Andulo, MAHLI wheels	212.4	204	866	
	29 Aug 19:33	1445	CM		Thermal characterization of RPAM	213.1	203	869	
	30 Aug 20:13	1446	Cm		Dr 53m to 57/1026 · el+112m · 14185m · south, CheMin empty cell	213.7	203	870	
	31 Aug 20:52	1447	m			214.3	206	874	0.98
	01 Sep 21:32	1448	CM		Dr 78m to 57/1398 · el+117m · 14263m · south, SAM getter/scrubber cleanup	215.0	204	876	
	02 Sep 22:11	1449	C			215.6	203	873	0.98
	03 Sep 22:51	1450	CM		SAM atmos	216.2	204	871	
	04 Sep 23:31	1451	M		Rover memory maintenance activity	216.8	205	874	
	06 Sep 00:10	1452	m		Dr 45m to 57/1948 · el+122m · 14308m · south	217.5	205	882	
	07 Sep 00:50	1453				218.1	205	879	
	08 Sep 01:29	1454	CM		Dr 41m to 57/2302 · el+121m · 14348m · toward Quela, MAHLI Eheke, CheMin funnel vibration cleaning	218.7	204	883	0.88
	09 Sep 02:09	1455	CM		Dr 28m to 57/2588 · el+121m · 14376m · toward Quela	219.4	204	890	0.94
	10 Sep 02:49	1456	Cm	S	Drop to SAM (doggy bag Marimba), SAM atmos	220.0	207	891	0.96
	11 Sep 03:28	1457	m	AUX	Dump sample w/MAHLI before & after, CHIMRA thwackless clean, brush & in-situ Quela, drill preload w/MAHLI after	220.7		899	0.98
	12 Sep 04:08	1458	CM			221.3	207	897	1.06
	13 Sep 04:47	1459	CM	AXW	In-situ dump pile, CHIMRA clean w/2ndary thwack only, MAHLI dump pile, CheMin inlet, wheels	221.9	208	902	1.02
	14 Sep 05:27	1460	CM	X	MAHLI dump pile, CHIMRA clean, sample cross-contamination expt	222.6	207	906	
	15 Sep 06:06	1461			MAHLI pre-drill, drill activity faulted due to soft short	223.2	207	913	
	16 Sep 06:46	1462	CM		drill diag	223.9	206	913	
	17 Sep 07:26	1463	CM	P	MAHLI Ombomboli & selfie	224.5	207	913	1.07
	18 Sep 08:05	1464		F	Drill Quela w/MAHLI before & after	225.1	207	912	
	19 Sep 08:45	1465	CM	I	CHIMRA Quela, transfer pre-sieve to scoop, inspect	225.8	208	910	
	20 Sep 09:24	1466	Cm	AIPSu	Dump pre-sieve & MAHLI, inspect post-sieve in scoop, drop to CheMin, in-situ tailings, MAHLI selfie+, CheMin inlet, drill hole; RCE maintenance	226.4	207	913	
	21 Sep 10:04	1467	CM		CheMin funnel vibration cleaning, SAM electrical baseline test	227.1	206	919	1.05
	22 Sep 10:44	1468	m		Dr 88m to 57/2804 · el+125m · 14463m · toward Karasberg	227.7	207	919	1.13
	23 Sep 11:23	1469	CM		Dr 35m to 58/0006 · el+126m · 14498m · toward Karasberg	228.3	205	920	
	24 Sep 12:03	1470	CM		CheMin Quela, MAHLI APXS cal & CheMin inlet	229.0	205	920	
	25 Sep 12:42	1471	M	W	Dr 42m to 58/0270 · el+128m · 14540m · south with MAHLI full wheel	229.6	206	922	
	26 Sep 13:22	1472	C			230.3	205	925	1.11
	27 Sep 14:02	1473	CM		Dr 16m to 58/0648 · el+129m · 14556m · south	230.9	206	928	
28 Sep 14:41	1474	CM	AB	Brush & in-situ Jwaneng, MAHLI Koping & Utuseb	231.6	206	934		
29 Sep 15:21	1475	CM		Dr 16m to 58/0780 · el+131m · 14573m · south, CheMin Quela	232.2	205	933		
30 Sep 16:00	1476	Cm			232.9	205	930	1.14	
01 Oct 16:40	1477	CM	AB	Brush & in-situ Catumbela, in-situ Gaunula, MAHLI CheMin inlet	233.5	207	931		
02 Oct 17:19	1478	CM		Dr 13m to 58/0918 · el+132m · 14585m · south, CheMin Quela	234.2	209	938		
03 Oct 17:59	1479			Thermal characterization of RPAM	234.8	208	938		
04 Oct 18:39	1480	CM	A	Dr 35m to 58/1008 · el+134m · 14620m · south after in-situ Oodi; CheMin Quela	235.5	206	938	1.46	
05 Oct 19:18	1481	C		SAM getter/scrubber cleanup	236.1	207	932		
06 Oct 19:58	1482	CM	W	Dr 39m to 58/1254 · el+136m · 14659m · south after MAHLI Cassongue & wheels; CheMin funnel vibration cleaning	236.8	206	933		
07 Oct 20:37	1483	Cm			237.4	206	931		

Drive south

388 Appendix: Curiosity Activity Summary

Area	Noon UTC	Sol	RS	Arm	Activity Summary	Ls	T	P	Tau
Sebina	08 Oct 21:17	1484	m	ABS	Brush & in-situ Serowe, in-situ Tobane, MAHLI CheMin inlet, triple drop to SAM	238.1	204	934	
	09 Oct 21:57	1485	CM		Dr 36m to 58/1578 · el+139m · 14695m · south	238.7	204	937	1.22
	10 Oct 22:36	1486	Cm			239.4	205	932	1.08
	11 Oct 23:16	1487	CM		Dr 17m to 58/1842 · el+140m · 14713m · south, CheMin funnel vibration cleaning	240.0	207	937	
	12 Oct 23:55	1488				240.7	205	935	
	14 Oct 00:35	1489	CM		Dr 7m to 58/1992 · el+140m · 14720m · to Sebina, MAHLI CheMin inlet, backup HRS maintenance	241.3	206	936	0.93
	15 Oct 01:15	1490				242.0	205	940	
	16 Oct 01:54	1491	m	ABUX	Dump sample w/MAHLI before & after, CHIMRA thwackless clean, brush & in-situ Sebina, drill preload test w/MAHLI after	242.6	205	939	
	17 Oct 02:34	1492	CM		CheMin empty cell analysis	243.3	206	943	1.07
	18 Oct 03:13	1493	CM	AX	In-situ dump pile (it had shifted due to wind), CHIMRA clean w/2ndary thwack only	243.9	207	944	1.00
	19 Oct 03:53	1494	CM	AX	In-situ dump pile (it had shifted due to wind), CHIMRA clean, sample cross-contamination experiment	244.6	206	944	
	20 Oct 04:32	1495	cm	FI	Drill Sebina w/MAHLI before & after, MAHLI dump, CHIMRA Sebina, transfer pre-sieve to scoop, inspect	245.2	206	940	
	21 Oct 05:12	1496	CM	AlSu	Dump pre-sieve & MAHLI, inspect post-sieve in scoop, drop to CheMin, CheMin Sebina, in-situ tailings, MAHLI drill hole & CheMin inlet	245.9	205	943	0.98
	22 Oct 05:52	1497	C	A	In-situ pre-sieve dump pile, MAHLI tailings	246.5	206	948	
23 Oct 06:31	1498	CM		MAHLI pre-sieve dump pile, REMS UV, sky; SAM electrical baseline test	247.2	206	946		
24 Oct 07:11	1499	cm		Dr 11m to 58/2052 · el+141m · 14731m · south	247.8	206	943	1.06	
25 Oct 07:50	1500	CM		Dr 31m to 58/2142 · el+141m · 14762m · south	248.5	206	943		
26 Oct 08:30	1501	CM		Dr 46m to 58/2400 · el+146m · 14808m · south, CheMin Sebina	249.1	205	942		
27 Oct 09:10	1502	CM		Dr 25m to 58/2766 · el+147m · 14834m · south	249.8	204	947	0.99	
28 Oct 09:49	1503	Cm		Dr 37m to 58/2952 · el+149m · 14871m · south, CheMin Sebina	250.4	205	947		
29 Oct 10:29	1504	C	A	In-situ Thrumcap, MAHLI Wonderland	251.1	204	947		
30 Oct 11:08	1505	CM			251.7	206	943		
31 Oct 11:48	1506	m		Dr 51m to 59/0006 · el+152m · 14922m · south	252.4	206	943		
01 Nov 12:27	1507	CM		Dr 29m to 59/0378 · el+151m · 14951m · south, CheMin Sebina	253.0	205	945	0.91	
02 Nov 13:07	1508	CM		Dr 44m to 59/0618 · el+150m · 14996m · south	253.7	204	943	1.00	
03 Nov 13:47	1509	CM		Dr 40m to 59/0942 · el+151m · 15036m · south, CheMin sample dump & empty cell analysis	254.3	204	947		
04 Nov 14:26	1510	C		Thermal characterization of RPAM	255.0	203	947		
05 Nov 15:06	1511	CM	AB	Brush & in-situ Penobscot, in-situ Pematic	255.7	203	945		
06 Nov 15:45	1512	M	AW	Dr 44m to 59/1266 · el+154m · 15080m · south with full MAHLI wheel	256.3	204	944		
07 Nov 16:25	1513	Cm			257.0	202	946	0.93	
08 Nov 17:05	1514	Cm		Dr 43m to 59/1602 · el+157m · 15123m · south after MAHLI Southwest Harbor	257.6	202	947		
09 Nov 17:44	1515	C			258.3	202	947	0.92	
10 Nov 18:24	1516	CM		Dr 24m to 59/2004 · el+159m · 15148m · south	258.9	203	948		
11 Nov 19:03	1517				259.6	204	951		
12 Nov 19:43	1518	CM	A	In-situ Bald Porcupine & Sheep Porcupine, MAHLI Folly Island & CheMin inlet	260.2	204	948	0.93	
13 Nov 20:23	1519	Cm		Dr 37m to 59/2248 · el+163m · 15184m · south after MAHLI Bald Porcupine & Sheep Porcupine, MAHLI cal	260.9	202	943		
14 Nov 21:02	1520	cM			261.5	201	943		
15 Nov 21:42	1521	Cm		Dr 11m to 59/2584 · el+164m · 15196m · south	262.2	202	943		
16 Nov 22:21	1522	m			262.8	203	941	0.95	
17 Nov 23:01	1523	Cm	AB	Brush & in-situ Sutton Island, MAHLI Seawall, Manset	263.5	204	944		
18 Nov 23:40	1524	cM	A	In-situ Manset	264.1	205	943		
20 Nov 00:20	1525	CM	A	In-situ Ironbound Island, MAHLI ChemCam window, CheMin empty cell	264.8	203	942	0.93	

Appendix: Curiosity Activity Summary 389

Area	Noon UTC	Sol	RS	Arm	Activity Summary	LS	T	P	Tau
Precipice	21 Nov 01:00	1526	Cm		Dr 16m to 59/2674 · el+165m · 15212m · to Precipice, SAM atmos	265.4	202	941	
	22 Nov 01:39	1527				266.1	203	941	
	23 Nov 02:19	1528	CM			266.7	202	938	
	24 Nov 02:58	1529	CM		SAM electrical baseline test	267.4	206	940	0.93
	25 Nov 03:38	1530				268.0	206	939	
	26 Nov 04:18	1531	Cm	AB	Brush & in-situ Precipice, drill preload test w/MAHLI after, RCE matinance	268.7	205	942	
	27 Nov 04:57	1532	cM			269.3	202	941	0.84
	28 Nov 05:37	1533	m	AUX	Dump Sebina w/MAHLI before & after, in-situ dump pile, CHIMRA thwackless clean	270.0	202	936	
	29 Nov 06:16	1534	cM	X	MAHLI dump pile, CHIMRA clean w/2ndary thwack only	270.6	201	937	
	30 Nov 06:56	1535	CM	X	Sample cross-contamination expt, CHIMRA clean	271.2	204	940	
Drill feed anomaly recovery	01 Dec 07:36	1536	m		Drill feed fault upon attempted drill at Precipice w/MAHLI after	271.9	205	938	
	02 Dec 08:15	1537	CM	A	In-situ Thomas Bay, drill diag	272.5	202	938	0.80
	03 Dec 08:55	1538	c			273.2	201	937	
	04 Dec 09:34	1539	c		SAM cleaning activities	273.8	200	932	
	05 Dec 10:14	1540				274.5	201	932	
	06 Dec 10:53	1541	Cm		drill diag	275.1	203	930	0.72
	07 Dec 11:33	1542	C		drill diag	275.8	203	931	
	08 Dec 12:13	1543	Cm		drill diag, SAM opportunistic derivatization step 1	276.4	202	934	
	09 Dec 12:52	1544	CM		drill diag	277.0	203	934	0.88
	10 Dec 13:32	1545	Cm		drill diag	277.7	201	932	0.79
	11 Dec 14:11	1546	C		SAM opportunistic derivatization step 2	278.3	201	929	
	12 Dec 14:51	1547	m		drill diag	279.0	205	925	
	13 Dec 15:31	1548	C		drill diag	279.6	203	925	
	14 Dec 16:10	1549				280.2	202	926	
	15 Dec 16:50	1550	C			280.9	203	927	
	16 Dec 17:29	1551	Cm			281.5	203	924	0.79
Old Soaker	17 Dec 18:09	1552	CM	A	In-situ Beachcroft & Echo Lake, MAHLI The Anvil & REMS UV, drill diag	282.2	201	921	
	18 Dec 18:49	1553	m		Dr 18m to 59/2836 · el+165m · 15229m · south, drill diag	282.8	205	919	
	19 Dec 19:28	1554				283.4	205	922	0.76
	20 Dec 20:08	1555	CM		Dr 0m to 59/3010 · el+165m · 15229m · for stability, a very small turn in place and bump	284.1	205	922	0.70
	21 Dec 20:47	1556			Runout (planned for holiday)	284.7	202	918	
	22 Dec 21:27	1557			Runout (planned for holiday)	285.3	203	919	
	23 Dec 22:06	1558			Runout (planned for holiday)	286.0	203	917	
	24 Dec 22:46	1559	m		Runout (planned for holiday)	286.6	203	915	0.72
	25 Dec 23:26	1560			Runout (planned for holiday)	287.2	204	914	
	27 Dec 00:05	1561	m		Runout (planned for holiday)	287.9	201	911	0.67
	28 Dec 00:45	1562			Runout (planned for holiday)	288.5	201	914	
	29 Dec 01:24	1563			Runout (planned for holiday)	289.1	202	916	
	30 Dec 02:04	1564			Runout (planned for holiday)	289.7	202	913	
31 Dec 02:44	1565	m		Runout (planned for holiday); HAPPY NEW YEAR 2017!	290.4	203	908	0.75	
	01 Jan 03:23	1566	CM	A	In-situ Mill Field & Thompson Island, MAHLI Old Soaker & Bar Island	291.0	203	909	
	02 Jan 04:03	1567		A	APXS Bar Island, SAM electrical baseline test	291.6	204	906	
	03 Jan 04:42	1568	Cm			292.3	203	907	0.74
	04 Jan 05:22	1569	C	A	In-situ Beech Mountain & Eagle Lake, MAHLI Old Soaker, Hodgdon Pond, Huguenot Head, Squeaker Cove	292.9	203	910	

390 Appendix: Curiosity Activity Summary

Area	Noon UTC	Sol	RS	Arm	Activity Summary	LS	T	P	Tau
Drive south & drill feed anomaly recovery	05 Jan 06:02	1570	C	A	In-situ Fresh Meadow, MAHLI Valley Cove & Gilley Field	293.5	201	907	
	06 Jan 06:41	1571	CM	A	Dr 17m to 59/3022 · el+166m · 15246m · south after APXS Valley Cove	294.1	202	908	
	07 Jan 07:21	1572		A	In-situ Isle Au Haut, MAHLI Greenstone, MAHLI REMS booms, thermal characterization RPAM	294.8	202	904	
	08 Jan 08:00	1573	Cm		Drill diagnostics	295.4	200	906	0.67
	09 Jan 08:40	1574	Cm		Dr 26m to 60/0006 · el+167m · 15272m · south, SAM getter/scrubber cleanup	296.0	202	906	
	10 Jan 09:19	1575	cm		MAHLI Dorr Mountain, arm fault (MAHLI cover open)	296.6	202	908	
	11 Jan 09:59	1576	Cm	A	Dr 30m to 60/0186 · el+169m · 15302m · south after MAHLI cover close recovery, in-situ Dorr Mountain, Mastcam inspect MAHLI	297.2	202	910	0.88
	12 Jan 10:39	1577	Cm	A	Dr 46m to 60/0402 · el+166m · 15348m · south after in-situ Mansell Mountain	297.9	204	905	
	13 Jan 11:18	1578	cM		Dr 25m to 60/0690 · el+176m · 15373m · south after MAHLI Megunticook; SAM atmos	298.5	203	906	
	14 Jan 11:58	1579			Runout (planned for battery charging)	299.1	205	897	
	15 Jan 12:37	1580	CM		SAM cleaning	299.7	201	905	0.71
	16 Jan 13:17	1581		A	In-situ Mars Hill & Camera Hill, MAHLI Smalls Falls	300.3	200	902	
	17 Jan 13:57	1582	Cm		Dr 44m to 60/0894 · el+179m · 15418m · south	300.9	201	903	
	18 Jan 14:36	1583	Cm		Dr 16m to 60/1272 · el+180m · 15434m · south	301.5	203	904	0.72
	19 Jan 15:16	1584	Cm	A	Dr 31m to 60/1428 · el+182m · 15465m · south after in-situ Frost Pond	302.2	203	900	
	20 Jan 15:55	1585	cM		Dr 14m to 60/1656 · el+183m · 15479m · south after MAHLI Jewell	302.8	202	908	0.79
	21 Jan 16:35	1586	m	AB	Brush & in-situ Belle Lake, in-situ Bluffer Pond	303.4	200	900	
	22 Jan 17:14	1587	M		Dr 28m to 60/1758 · el+186m · 15507m · south, drill diagnostics	304.0	201	898	
	23 Jan 17:54	1588			CheMin dump & empty cell	304.6	201	899	
	24 Jan 18:34	1589	M	A	Dr 31m to 60/2016 · el+189m · 15538m · south after in-situ Cape Elizabeth	305.2	203	897	
	25 Jan 19:13	1590	m			305.8	204	903	1.08
	26 Jan 19:53	1591	M	AW	Dr 8m to 60/2262 · el+189m · 15546m · south with full MAHLI wheel after in-situ Musungun, SAM op deriv step 1	306.4	200	889	
	27 Jan 20:32	1592	M			307.0	201	897	
	28 Jan 21:12	1593	cm	A	In-situ Misery & Misery Offset, MAHLI Dead River	307.6	200	892	
	29 Jan 21:52	1594	m		Dr 26m to 60/2352 · el+190m · 15573m · south, drill diagnostics, SAM op deriv step 2	308.2	201	894	0.93
30 Jan 22:31	1595	m			308.8	897	0.73		
31 Jan 23:11	1596	cM	A	Dr 21m to 60/2580 · el+190m · 15593m · south after in-situ Isleboro	309.4	203	890		
01 Feb 23:50	1597			SAM electrical baseline test	310.0	204	900	0.93	
03 Feb 00:30	1598	cM	A	Dr 29m to 60/2736 · el+188m · 15622m · south toward Mapleton (dune stop 1) after in-situ Digdeguash	310.6	204	896	0.79	
04 Feb 01:10	1599	m		HRS maintenance, SAM atmos	311.2	202	900	1.01	
05 Feb 01:49	1600	cM	A	In-situ Rye & Whiskey, APXS thermal characterization	311.8	202	896	0.88	
Stop 1	06 Feb 02:29	1601	M		Dr 27m to 60/2934 · el+186m · 15648m · south to Mapleton wheel scuff site, APXS thermal characterization	312.4	206	894	0.89
	07 Feb 03:08	1602	cM	A	In-situ McKenny & Matagamon, MAHLI Scarboro, Flume Ridge, The Forks, West Branch	313.0	205	896	1.03
08 Feb 03:48	1603	M	A	In-situ Flume Ridge, MAHLI Matagamon, West Branch, Flume Ridge, Dry Wall, McKenny	313.6	204	890	0.96	
09 Feb 04:27	1604	cM		Dr 55m to 60/3168 · el+189m · 15704m · toward Ireson Hill after MAHLI Flume Ridge, Matagamon, McKenny	314.2	202	898		
Ireson Hill	10 Feb 05:07	1605	Cm		Dr 22m to 61/0006 · el+187m · 15725m · toward Ireson Hill after MAHLI Cary's Mills	314.8	201	887	
	11 Feb 05:47	1606	Cm	A	In-situ Quoddy & Pogy, APXS thermal characterization	315.4	202	896	
	12 Feb 06:26	1607	Cm		drill diagnostics, thermal characterization of RPAM	316.0	203	887	0.91
	13 Feb 07:06	1608	CM		Dr 9m to 61/0162 · el+187m · 15735m · to Ireson Hill, drill diagnostics, MAHLI compression tests	316.6	204	889	1.04
	14 Feb 07:45	1609	CM	A	In-situ Perry & Spurwink, MAHLI Passagassawakeag	317.2	202	891	
15 Feb 08:25	1610	CM		Dr 26m to 61/0258 · el+189m · 15761m · toward Sandy Point Beach (dune stop 2), drill diag	317.7	203	882	1.20	
Stop 2	16 Feb 09:05	1611	cm		Dr 23m to 61/0462 · el+191m · 15785m · toward Sandy Point Beach after MAHLI Patch Mountain	318.3			

Appendix: Curiosity Activity Summary 391

Area	Noon UTC	Sol	RS	Arm	Activity Summary	Ls	T	P	Tau
	17 Feb 09:44	1612	Cm		Dr 32m to 61/0654 · el+194m · 15817m · toward Sandy Point Beach, APXS thermal characterization	318.9			
	18 Feb 10:24	1613	C			319.5			
	19 Feb 11:03	1614	Cm	A	In-situ Spider Lake, MAHLI Chain Lakes & REMS UV	320.1			0.93
	20 Feb 11:43	1615			APXS cal, drill diagnostics, MAHLI compression tests	320.7			0.92
	21 Feb 12:23	1616	m		Dr 0m to 61/0930 · el+194m · 15817m · toward Sandy Point Beach	321.2	201	890	
	22 Feb 13:02	1617	CM		Dr 20m to 61/0938 · el+194m · 15837m · toward Sandy Point Beach, drill diagnostics	321.8	203	881	0.93
	23 Feb 13:42	1618	CM	AW	In-situ Tomhegan & Waweig, MAHLI Seeboomook, Cookson, wheels	322.4	203	886	0.97
	24 Feb 14:21	1619	cM		drill diagnostics, MAHLI dust cover open fault	323.0	201	888	0.89
	25 Feb 15:01	1620	CM		MAHLI diagnostics	323.6	203	886	0.85
	26 Feb 15:40	1621	Cm		SAM electrical baseline test	324.1	202	890	1.04
MAHLI dust cover recovery	27 Feb 16:20	1622	m		APXS thermal characterization	324.7	204	890	
	28 Feb 17:00	1623	Cm	W	MAHLI and drill diagnostics, MAHLI wheels (occluded by cover)	325.3	205	884	
	01 Mar 17:39	1624	M		APXS thermal characterization	325.9	206	888	
	02 Mar 18:19	1625	CM		MAHLI diagnostics, Mastcam video MAHLI cover, APXS thermal characterization	326.4	203	891	1.13
	03 Mar 18:58	1626	CM		APXS thermal characterization, HRS maintenance	327.0	203	889	1.18
	04 Mar 19:38	1627	CM		MAHLI diagnostics, Mastcam video MAHLI cover	327.6		888	
	05 Mar 20:18	1628	CM	W	Dr 25m to 61/1146 · el+195m · 15862m · toward Southern Cove (dune stop 3), MAHLI diagnostics, MAHLI wheel	328.1	203	888	1.06
	06 Mar 20:57	1629	CM		APXS thermal characterization	328.7	205	883	1.17
	07 Mar 21:37	1630	Cm	A	Dr 41m to 61/1338 · el+196m · 15903m · toward Southern Cove after in-situ Sangerville, drill diagnostics	329.3	206	886	
	08 Mar 22:16	1631	Cm			329.9	206	883	
Stop 3 (Southern Cove)	09 Mar 22:56	1632	Cm	A	Dr 29m to 61/1656 · el+197m · 15932m · toward Southern Cove after in-situ Spring Point, MAHLI cal, drill diagnostics	330.4	202	881	
	10 Mar 23:36	1633	C			331.0	202	878	
	12 Mar 00:15	1634	CM	A	In-situ Canada Falls	331.5	202	881	
	13 Mar 00:55	1635	m		Dr 29m to 61/1914 · el+197m · 15961m · toward Southern Cove	332.1	204	879	1.20
	14 Mar 01:34	1636	Cm		Dr 7m to 61/2154 · el+196m · 15967m · to Southern Cove	332.7	204	880	
	15 Mar 02:14	1637	CM	A	In-situ Spragueville & Ripogenus, MAHLI Shin Brook; drill diag	333.2	203	883	1.09
	16 Mar 02:53	1638	Cm	A	In-situ Ash Island & Greenvale Cove, MAHLI Ripogenus & Spragueville, Ash Island; drill diagnostics	333.8	202	881	
	17 Mar 03:33	1639	Cm		Dr 31m to 61/2238 · el+198m · 15998m · toward Ogunquit Beach (dune stop 4) after MAHLI Greenvale Cove & Holmes Hole; drill diagnostics	334.3	203	875	
	18 Mar 04:13	1640	C	A	In-situ Junk of Pork Island, MAHLI Uncle Steve's Point; drill thermal characterization	334.9	201	875	1.05
	19 Mar 04:52	1641	CM	A	Dr 1m to 61/2478 · el+4501m · 16000m · for full MAHLI wheel after APXS Uncle Steve's Point; drill diagnostics	335.5	203	875	
Drive to Ogunquit Beach	20 Mar 05:32	1642	m		Dr 27m to 61/2502 · el+200m · 16027m · toward Ogunquit Beach, thermal characterization of RPAM	336.0	203	873	
	21 Mar 06:11	1643	Cm		Dr 41m to 61/2746 · el+200m · 16067m · toward Ogunquit Beach	336.6	202	876	
	22 Mar 06:51	1644	Cm	A	In-situ The Hop, MAHLI The Horns; drill diagnostics	337.1	200	879	
	23 Mar 07:31	1645	CM		Dr 21m to 61/3082 · el+201m · 16088m · toward Ogunquit Beach; drill diagnostics	337.7	199	877	1.14
	24 Mar 08:10	1646	CM		Dr 31m to 61/3232 · el+201m · 16119m · toward Ogunquit Beach, SAM electrical baseline test	338.2	201	872	
	25 Mar 08:50	1647	CM	A	In-situ Halfdite Ledge	338.8	203	872	
	26 Mar 09:29	1648	M		Dr 10m to 62/0006 · el+201m · 16128m · to Ogunquit Beach, drill diagnostics	339.3	202	869	

About the Author



Emily Lakdawalla is Senior Editor and Planetary Evangelist for The Planetary Society. She is an internationally known science communicator who shares her passion for solar system exploration by writing and editing The Planetary Society's blogs at planetary.org/blog, speaking to classrooms, sharing space photos and science explanations on twitter.com/elakdawalla, and developing other space science education projects.

Emily holds a Master of Science degree in planetary geology from Brown University, where she studied tectonics on Venus and was among the first to develop Geographic Information Systems off of Earth. She began writing about space exploration for the public when Cassini arrived at Saturn in 2004, and has since covered the science and operations of robotic missions across the solar system, from MESSENGER at Mercury to Rosetta at 67P/Churyumov-Gerasimenko and New Horizons at Pluto. Emily has been an active supporter of the international community of space image processing enthusiasts as Administrator of the forum UnmannedSpaceflight.com since 2005. She is also a contributing editor to *Sky & Telescope* magazine.

Emily has been recognized by the space science community for her work in promoting space exploration to the public. She was awarded the 2011 Jonathan Eberhart Planetary Sciences Journalism Award from the Division for Planetary Sciences of the American Astronomical Society for her blog entry about the Phoebe ring of Saturn. Asteroid 274860 was formally named "EmilyLakdawalla" by the International Astronomical Union on July 12, 2014. She received an honorary doctorate from The Open University in 2017.

She is currently working on the sequel to this book, *Curiosity and Its Science Mission: A Mars Rover Goes to Work*. She resides in Los Angeles with her husband (who is not a planetary scientist) and two daughters.

Index

A

Aeolis Mons, 119
aerogel, 151
animation 46
announcement of opportunity, 10, 13
anomaly, 72, 78, 116, 121, 125, 126, 129, 133, 146, 148, 162, 195, 198, 206, 208, 209, 229, 250, 271, 280, 302, 308, 326, 354, 358, 359, 364, 369, 374, 381, 382, 385, 389, 390
argon, 308, 337–340, 343
Atlas V, 19, 48, 51, 53, 57–59
autonav, 127, 176, 230, 232, 354
autonomous navigation, 126, 147, 228–230, 232

B

Bagnold dunes, 119, 133, 255, 306, 378–380
battle short, 50, 195, 356, 374
Bayer, 236, 240–241, 243, 258
blind drive, 124, 127, 231, 232

C

calcium sulfate, 250, 304, 307, 320, 326
clast survey, 250, 255, 288
clay, 119, 301, 320, 322, 325, 326, 344
commissioning activity phase, 121
complexity, 9, 16, 17, 24, 29, 46, 110, 114, 115, 154, 242, 246, 249, 298, 343
conjunction, 126, 133, 160, 161, 213, 228, 243, 273, 280, 307, 359, 376, 377
CONTOUR, 329
cosmic ray, 276, 280–282, 284, 324
curium, 311

D

Deimos, 251, 354, 361, 362, 371, 376
derivatization, 336, 343, 345, 346, 372, 389
descope, 28–31, 239, 267
Dingo Gap, 119, 129, 130, 156, 365, 366
dream mode, 147, 148
dry-lubricated motors, 16, 25

E

epithermal, 280–282
ExoMars, 39, 157, 159, 160

F

Freon, 62, 66, 67, 149, 151

G

guarded motion, 230, 232
guided entry, 3, 16, 22, 27, 71, 78, 83, 86

H

habitability, 8, 9, 11, 21, 350
heater tables, 152, 153
hematite, 4, 119, 133, 305, 319, 326
HiRISE, 18, 29, 69, 76, 77, 93, 94, 97, 104–106, 165, 176, 252

J

JPEG, 242–246
JunoCam, 252

K

Kimberley, 119, 129–131, 147, 364–367

L

local mean solar time, 112, 113
 local true solar time, 112, 113, 153, 255
 lockup, 318

M

Maggie, 179
 magic cylinder, 187, 189
 Marias Pass, 119, 132, 161, 285, 376, 377
 Mars Express, 10, 15, 22, 47, 72, 120, 122, 157, 159, 160, 374
 Mars Reconnaissance Orbiter, 1, 15, 17, 18, 22, 29, 41, 47, 57, 66, 68, 69, 71, 76, 78, 79, 93, 101, 102, 104, 115, 119, 122, 155, 157–162, 165, 224, 252
 Mars Smart Lander, 4–7, 18, 25
 Mars time, 110, 114–116
 microbes, 9, 23, 24, 49
 Morse code, 169, 170
 MTBSTFA, 334, 335, 341, 343

O

Odyssey, 1, 8, 13, 15, 17, 18, 22, 24, 57, 66–69, 71, 72, 78, 79, 83, 93, 101, 102, 115, 120, 155, 157–159, 162, 176, 224, 280
 olivine, 319, 326

P

Pahrump Hills, 119, 131, 132, 209, 211, 213, 253, 255, 269, 270, 290, 304, 305, 370, 375
 Peace Vallis, 118, 119, 121, 306
 Philae, 298
 Phobos, 251, 298, 354, 355, 361, 362, 368–370, 376, 377
 Phoenix, 30, 31, 33, 34, 40, 158, 213, 217, 252, 286
 planetary protection, 22–24, 47–50, 193

plutonium, 7, 24, 39, 138, 139, 144, 280
 portion plus, 198, 201

R

recurring slope lineae, 50
 restricted sol, 116–118, 161, 228, 248, 285
 runout, 353, 355, 357–359, 366–374, 376–381, 383, 389, 390

S

Scarecrow, 31, 32, 163, 181
 shrinkwrap stereo, 249
 sidewalk mode, 131, 253, 255, 368–370
 Siding Spring, 251, 370, 371
 sky crane, 10, 16, 41, 69, 96
 slide sol, 116–118
 soft short, 127, 132, 144, 145, 364, 383, 387
 soliday, 116–118
 special region, 23, 24, 50
 supratactical, 114, 115, 343
 surge sol, 117, 118, 128, 131, 367

T

terrain mesh, 115, 229, 231, 232, 247
 thermo-electric cooler, 41, 295, 300
 TMAH, 334, 335
 traction control, 148, 177
 traversability, 41, 127, 232
 tridymite, 319, 326, 327

V

Vehicle System Testbed, 179, 180
 Vera Rubin Ridge, 119, 133, 161, 325, 344, 350, 351
 visodom, 230, 232, 354
 visual odometry, 124, 147, 224, 228, 230, 232

Z

Zabriskie plateau, 131
 z-stack, 147, 260, 261, 267